GEOCHEMISTRY AND PALEOCLIMATE CHANGES IN SEDIMENTS; NORTHERN ARABIAN SEA

by

ATHAR ALI KHAN

BSc (HONS), MSc, KARACHI

THESIS SUBMITTED FOR THE DEGREE OF

DOCTOR OF PHILOSOPHY

AT THE UNIVERSITY OF EDINBURGH

OCTOBER 1989

FOR VERILY IT IS THY LORD
WHO IS THE MASTER CREATOR,
KNOWING ALL THINGS.

(QURAN, S.XV.86)

TO

MY PARENTS

ABSTRACT

Four selected piston cores (i.e. CD1715, CD1730, CD1739 and CD1738) in a north-south transect from Charles Darwin Cruise CD18/86 are investigated in this study.

The northern Arabian Sea is under the influence of both variable northwesterly dust winds and seasonal upwelling. Their characteristic effects on the mineralogy and chemistry of the sediments are analysed both areally and temporally. From the accumulation rates of lithogenic and biogenic elements an attempt has been made to understand the climatic conditions of cold and warm periods of late Pleistocene time. For this purpose, an age model developed based on oxygen isotope and carbonate stratigraphy of a core RC-2761. Carbonate content variations of four cores show that southern cores CD1715 and CD1730 record a sedimentation history of last 250,000 years. Cores CD1738 and CD1739 have been dated to the base of stage 5 (i.e. 120 Kys).

These cores were sampled at 10cm intervals and sediments were subjected to mineralogical and geochemical analysis (Si, Al, Fe, Ca, Mg, K, Ti, P, Sr, Cr, Ni, Zn, Cu, Br, I, Zr, Ba, La, Ce, Nd, organic carbon, biogenic silica, $\delta^{13}C$, $\delta^{15}N$). Optical examination reveals that sediments contain various proportions of terrigenous and biogenous components. SEM examination of detrital grains shows rounded and pitted quartz grains and subhedral dolomite, indicative of aeolian transport. Biogenic components largely include, planktonic foraminiferids and diatoms.

Semi-quantitative mineralogical studies by XRD has shown that quartz, feldspar, chlorite and illite are the major minerals in the sediments. Peak intensity ratios of Qtz/Fld, Qtz/Chl and Qtz/Ill indicate that cores in north relatively contain more chlorite, and feldspar is low compared to quartz. Cores CD1715 and CD1730 are relatively impoverished in quartz and chlorite but contain more feldspar. The relative change of peak intensity ratios in different climatic stages is not very clear.

The geochemistry of major elements Si, Fe and K and their ratios to Al covary with peak ratios of specific minerals and these indicate both a textural control as well as areal and temporal variations in mineralogy of the sediments. Northern cores (i.e. CD1738 and CD1739) are relatively coarser grained as shown by higher Si/Al ratios and higher Fe/Al ratios implying more chlorite. The ratios of Si/Al, K/Al generally show contrasting trends in glacial and interglacial stages. The minor element goechemistry of the sediments shows more complex relationships. The patterns of Ti, Cr and Zr ratios to Al are different. Ti/Al and Zr/Al profiles tend to follow each other, while Cr/Al profiles show inconsistent trends. The Zr/Al ratio is invariable in cores and shows a persistent aeolian input. Cr and Cr/Al ratios are

very high and suggest derivation from local ophiolites and transport to the deep sea by pluming or by turbidity currents.

The geochemistry of the biogenic constituents include calcite, organic carbon, biogenic silica, Ex Ba (aluminosilicate free). Their causal relationship with metals (i.e. Cu, Ni, Zu) possibly suggests a genetic or diagenetic association. Biomarkers contents are higher in cores CD1715 and CD1730 than in cores CD1738 and CD1739. The changing patterns of biomarkers between cold and warm stages show increased biological production in the Holocene (stage 1), interglaical stages 3, 5 and 7. Isotopic analysis of $\delta^{13}C$ and $\delta^{15}N$ shows that organic matter is of marine origin throughout the cores.

Halogens geochemistry (iodine and bromine) and their ratios to organic carbon indicates an oxic depositional environment. Iodine relative to bromine shows preferential loss as a result of burial diagenesis. Halogens and their ratios to organic carbon in glacial/interglacial stages follow organic carbon contents and this suggests a possible association with biological productivity. However, the higher ratios in cores CD1738 and CD1739 may be a result of high sediment accumulation rates.

Sedimentation rates increase from cores CD1715 and CD1730 to cores CD1739 and CD1738. Lithogenic fluxes of quartz, aluminium, dolomite, zirconium and titanium show a marked gradient from north to south. This implies provenance from the north and northwest and aeolian transort by northwesterly winds. This source has been persistent throughout the last 250,000 years. Lithogenic flux values are higher in glacial stages and indicate change in climate. The highest lithogenic fluxes are seen in glacial stage 2, and indicates the greatest aridity during the last 250,000 years climatic history.

Biogenic fluxes (calcite, organic carbon, excess Ba and biogenic silica) decrease towards the north. Variations of biogenic fluxes between climatic stages show antipathetic trends to that observed for the lithogenic fluxes. This confirms the idea that distribution of biogenic and lithogenic components in NW Arabian Sea sediments is more controlled by the climatic patterns and the peculiar features associated with them.

The Holocene and interglacial periods (3, 5 and 7) are characterised by strong SW monsoon winds and upwelling and higher biogenic fluxes occur during these times. The lower biogenic values during the earliest interglacial stages suggests erosion of the sediment. This is evident from the comparison of productivity record of excess Ba flux from ODP core 722 (2000m water depth) and deep sea cores of this study. At stage boundaries 3/4, 5/6 and 6/7 the ridge core (ODP 722) shows high values of excess Ba flux; low values in basin cores at these boundaries are explained by the physical removal due to bottom currents.

TABLE OF CONTENTS

CHAPTER 1

INTRODUCTION

INTRODUCTION

Over the past decade significant advances have been made in palaeo-oceanographic research by improvements in our understanding of the dynamic relationship between climate and ocean. In this respect CLIMAP research group (Climate long range investigation mapping and prediction) has contributed an immense knowledge about the past climatic changes using oceanic proxy records (McIntyre et al, 1976).

Oceanic sediment cores are potentially important as they can provide continuous records of low frequency palaeoclimatic information (of the order of 10^3 years). The physical, chemical and paleontological characters of marine sediment sequences record many important features of the past climate, and sediment cores permit reconstruction of numerous aspects of oceanic and climatic variations. For instance, changes in global ice volume are reflected in the oxygen isotope ratios of foraminiferal tests. Changes in sediment character and their geochemistry reflect their host minerals and varying environmental conditions such as those related to continental erosion and biological productivity. The interacting behaviour of these indicators provides an insight to understanding the cause of oceanic and climatic changes.

Oceanic sediments mainly consist of terrigenous deposits and of biogenic sediments. Terrigenous deposits are detrital material derived from erosion of the land masses surrounding the ocean basins while biogenic sediments composed largely of accumulations of carbonates and siliceous skeletal remains of micro-organisms that formerly lived in the ocean waters. Terrigenous detritus arrives on the ocean floor by a number of different pathways, but the principal transporting agencies are turbidity currents, bottom currents, wind and ice. In the mid- and high-latitudes both coarse and fine terrigenous material appears to have been delivered to the ocean floors primarily during glacial periods (Ruddiman and McIntyre, 1977) reflecting particularly the ice-rafting of glacially-eroded debris and to a lesser extent the transport of aeolian sediments from the greatly expanded periglacial regions. Wind-blown sediments have constituted major proportions of the fine detritus input in low latitudes during glacial times (Folger, 1970). In many ocean sediment sequences a broad correlation can be detected between increased deposition of terrigenous debris and former glacial episodes. Biogenic sediments on the other hand provide a record of changes in ocean water temperature through upwelling and by implication in atmospheric circulation.

This study, the first of its kind in this part of the ocean, is an attempt to recognise both areal and temporal patterns of lithogenous input into the NW Arabian Sea by a combined study of mineralogy and major and minor element geochemistry for a longer time record, spanning the last 250 kys. The aim of this work is to reveal the influence of atmospheric fallout from different sources and the variation in intensity of these during glacial and interglacial events.

Indices of upwelling intensity for the late Pleistocene has hitherto relied on palaeontological evidence either by assessment on the relative abundance of certain foraminifera (Prell, 1984) or pollens of recognisable source. In this work an attempt will be made to assess the geochemistry of a variety of biomarker elements and their burial within the sediments.

The North Arabian Sea because of its geographical position receives a high proportion of its sediments as wind blown material from the neighbouring continents. Sirocko and Sarnthein (1988) have established a regional pattern of mineralogical variations of lithogenous constituents for the past 18,000 years B.P. and have concluded a dominant input as dust carried by north-west winds.

Further, biogenous production is also very high as a result of enhanced upwelling during south-west monsoon periods and this should be reflected in the sedimentary record. The area, which until very recently has received little attention, is of extreme importance for understanding the history of monsoon winds that affect much of Southern Asia. Previous studies on sediment cores based on either plankton abundances (Prell, 1984) or vegetation information (van Campo, 1986), have indicated an increased precipitation and higher marine biological productivity during warm interglacial periods of the late Pleistocene, due to a stronger south-west monsoon system.

For this reason emphasis is given to the geochemistry of biogenic calcite, silicon, organic matter and minor elements associated with these. An attempt has also been made to establish variations in the accumulation of these, which should shed light on the upwelling history caused by changes in monsoonal activity.

The integration of wind blown lithogenous accumulation with that of biomarker fluxes will be an important objective of this work.

During the 1986 Charles Darwin Cruise 18/86, several piston cores and box cores were collected from the northern Arabian Sea. Four cores (i.e. CD1715, CD1730, CD1738 and CD1739) in a north-south transect accumulating both terrigenous and biogenic sediments are analysed in this study. Some use has also been made of a fifth core CD1709 in the identification of sources of certain lithogenic elements.

An important pre-requisite for reliable palaeoclimatic reconstruction is dating. In the current study, stratigraphy of the cores and their correlation is based on the carbonate stratigraphy of a previously collected core RC-2761 (Lat. 16°38′N, Long. 59°52′E) which has been compared with an oxygen isotope stratigraphy.

The locations of these cores is such that the sediments within them are likely to receive very variable lithogenous and biogenic fluxes and hence should show patterns of climatic change along the southern parts of the Arabian Peninsula.

CHAPTER 2

GEOLOGY, METEOROLOGY AND HYDROGRAPHY OF THE AREA

2.1 GEOLOGY OF THE AREA

The continents surrounding the Arabian Sea are characterized by markedly different geology as they exhibit the effects of tectonic interaction of plates. To the north the Makran is an active subduction zone which has been described with trench, trench slope, trench slope break and fore-arc basins (Farhoudi and Karig, 1977). The principal rocks outcropping range from Eocene to Oligocene flysch in the north and Miocene to Pliocene shallow water clastics in the south (Jones, 1961; Ahmed, 1969). Western Makran in Iran is characterized by a folded rock sequence of Paleozoic, Mesozoic and Cenozoic limestones with evaporite, sandstones and clays.

The arcuate mountains of Oman in the northwest are characterized by a variety of lithofacies, including the Arabian platform and the Semail ophiolite, representing tectonically emplaced Oceanic Crust during the closure of the Tethyan ocean (Bailey, 1981). The four important geological units in this area are: (i) Crystalline basement rocks overlain by a thick shelf carbonate sequence, (ii) Hawasina group of deep water limestones, (iii) the Semail ophiolite consisting of peridotite, gabbro, diabase, pillow lavas and associated pelagic sedimentary rocks, and (iv) shallow marine limestones of Cenozoic age.

Along the Southeast African margin, a spectrum of rocks ranging in age from early Precambrian to Holocene are exposed. The crustal plain is underlain by rocks of Mesozoic to Holocene and comprised mainly of sedimentary rocks, mostly clastics. The rocks exposed along the northeastern boundary of the Arabian Sea and the Southern Indian coast are mainly basic igneous rocks of the Deccan Basalt.

Further inland all these bordering continents have vast areas of desert. The Thar desert of India, Rubulkhali in SW Arabia, coastal Makran of Iran and Pakistan and lowlands of Mesopotamia and Africa (Fig. 2.1) are major arid lands which are potential source areas for the sediments in the NW Arabian Sea. Main trajectories of aeolian dust shown in Fig. 2.1 originate from the surrounding deserts and transport a substantial dust load in to the NW Arabian Sea (Coude-Gausson, 1984).

2.2 PHYSIOGRAPHY

The bottom topography of the Indian Ocean north of the Equator is shown in Fig. 2.2. The Arabian Sea, the area of this study, is bounded to the west by Arabia, to the north by Iran and Pakistan and to the east by India and the Chagos-Laccadive ridge.

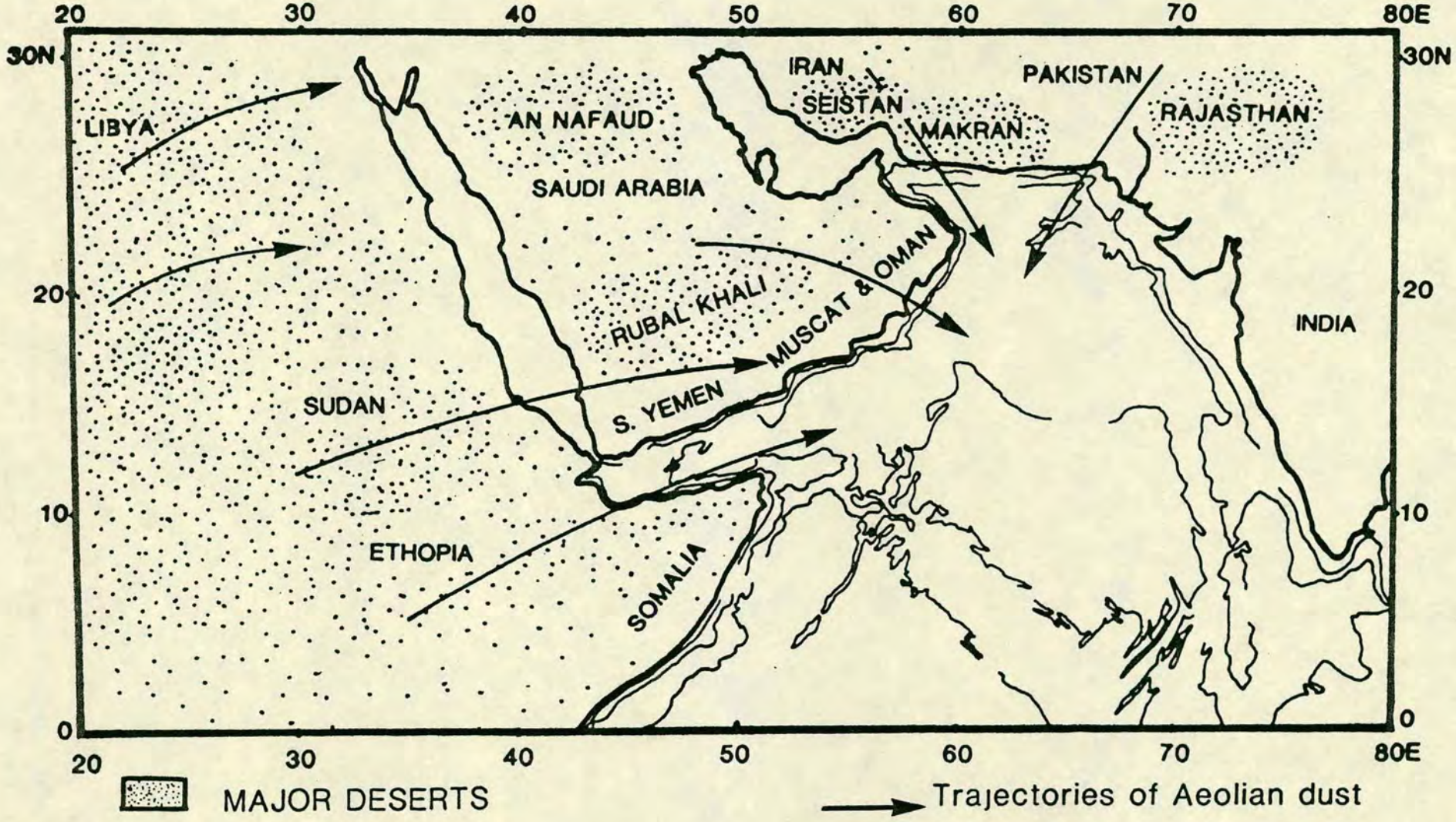

FIGURE 2.1 MAJOR DESERT AREAS BORDERING THE ARABIAN SEA. ARROWS ARE THE MAIN TRAJECTORIES OF AEOLIAN DUST AFTER COUDE-GAUSSEN, 1984.

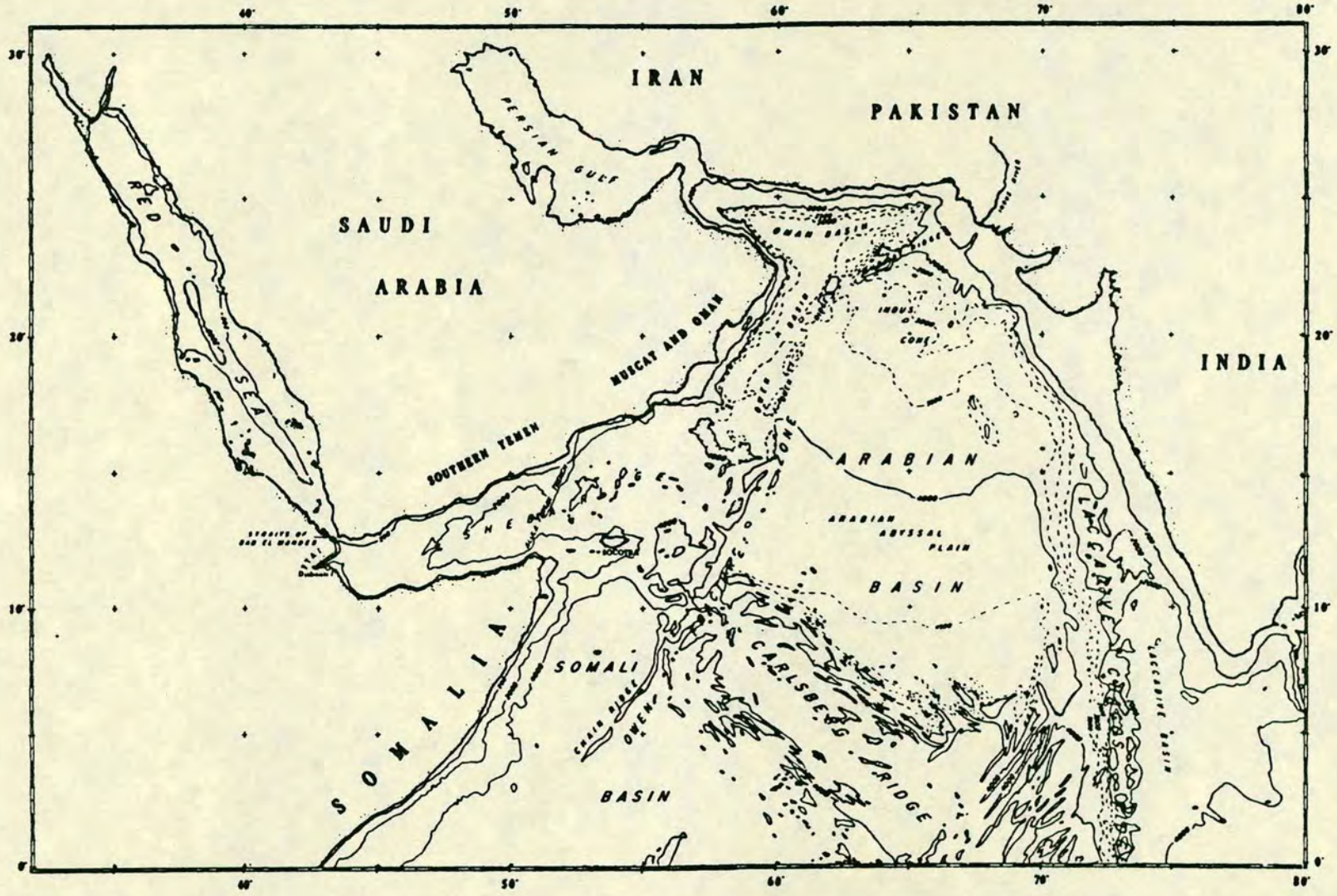

FIGURE 2.2 BATHYMETRIC MAP SHOWING MAIN PHYSIOGRAPHIC FEATURES OF N. INDIAN OCEAN (DSDP, 1974)

The continental shelf of the Arabian Sea shows variation in both width and depth. To the east, it has a monotonous width of about 100-150km and 100m depth off the Gulf of Kutch-Indus delta. The most pronounced bathymetric feature of the shelf-slope in the east is the Indus Canyon which commences around 10-20m water depth and ends at 1400m depth at the foot of the continental slope. Along the Markran margin west of Karachi, the continental shelf is narrow, ~40km wide, and shows a steep gradient. Offshore of this area, the continental margin displays terrace-like features, which are a result of the accretion of offscrapped sediments from the underlying subducting plate (White, 1982).

Along the Arabian and African coast the shelf is generally narrow. Off the Oman coast it is only about 10km wide except in the area of Masirah Island and Kuria Maria Island where the shelf is wider, ~70km. However, the continental slope in this area is steeper with a marked scarp southwest of Oman. Around Muscat, the average slope of the margin is 5 degrees (White, 1984). Further southward, along the Yamni coast, the continental shelf again decreases in width (ie. 30-40km) and the continental slope differs in that it descends smoothly and steeply to the trough of the Gulf of Aden (Fig. 2.2).

An outstanding feature of the seafloor in the northern Arabia Sea is a northeast-southwest trending graben and ridge system called the Owen Fracture Zone. This fracture zone is a continuous 2000km long structure about 2km below sea level, paralleling the continental margins of Arabia and Somalia and dividing the northern Arabian Sea into two main depositional basins: the Oman basin in the west and the Arabian basin towards the east. The Oman basin is roughly triangular in outline and occupies the central floor of the Gulf of Oman at a depth of about 3000m. The Arabian basin has a maximum depth of 4500m and merges to the north into the Indus Cone. To the west and the northwest it abuts the Owen Fracture Zone, the northern continuation of which, the Murray ridge, separates the Indus basin from the Oman basin. The Murray ridge, which starts from the south of Karachi (Pakistan), is volcanic in origin (Barker, 1966) and consists of a linear series of seamounts, scarps and small basins. It continues as the Owen ridge (~2km) to the south of the Gulf of Oman, which extends into the Owen Fracture zone to 5°N. The Owen ridge has an asymmetric cross section with a relatively gentle eastern slope in comparison to the western slope. To the west, between the Arabian continental margin and Owen ridge, an elongated narrow basin, called the Owen basin, occurs at a depth of 3500m. It is oriented in a northeast-southwest direction and extends towards the Oman basin in the north (Fig. 2.2).

The southern limits of all these basins are set by the northwest-southeast trending Carlsberg ridge which separates the Arabian Sea to the north from the eastern Somalian basin to the south. An offset extension of the Carlsberg ridge on the western side of the Owen Fracture zone in the Gulf of Aden is the Sheba ridge. The axis of the Sheba ridge is offset by a series of northeast-southwest trending fracture zones; the largest of which is the Alula-Fartak trench which runs between the Somalian and Arabian coast and displaces the ridge axis at 52°E by about 200km.

In the northwest, a shallow epicontinental sea, the Persian Gulf, with a mean depth of 25m and maximum of 90m, adjoins the Gulf of Oman at 24°.30'N, 57°.40'E through the Strait of Hormuz. Similarly, the Red Sea communicates with the Arabian Sea through the Gulf of Aden at 12°N by way of a sill at (100-110m) near Bab el Mandeb.

The various sedimentary basins comprising the Arabian Sea display a range of depositional environments and receive sediments of a wide variety of composition. In the east, the Indus basin is characterized by detritus of the Indus river and is dominated by proximal alluvial sediments, and oceanward by thick turbidite sequences displaying coarse-leveed channel systems (Kolla and Cumes, 1984; McHargue and Webb, 1986). The basins in the west and southwest, of particular interest to this study, are dominated by pelagic and hemipelagic deposits of wind blown material (Kolla et al. 1981a; Siroko and Sarnthein, 1988) and mixed with marine carbonate.

2.3 METEOROLOGY

Because of its location, the northern Indian Ocean is characterized by seasonal changes in the circulation of its tropical atmosphere. This monsoonal circulation is mainly controlled by the differential heating of land and ocean. In the summer the continents are transformed into centres of lower pressure, while in the winter they are comparatively cooler than the warm oceans and consequently are areas of high pressure. Hence, during winter a pressure gradient is established which creates a NE monsoon winds directed from India, Pakistan and Afghanistan towards the Arabian Sea (Fig. 2.3). This is recognised as a surface layer of atmosphere below 1500m (Ramage et al. 1972; Kirshnamurti et al. 1980). At such times the Indian Ocean is protected from the cold, violent Siberian anticyclones by the Himalayas. Consequently a weak pressure gradient between North India and the Arabian Sea allows gentle northwesterly winds of 2-3m/sec to occur in the Arabian Sea (Ramage, 1969). During summer (June-August) the intensive warming of the continental

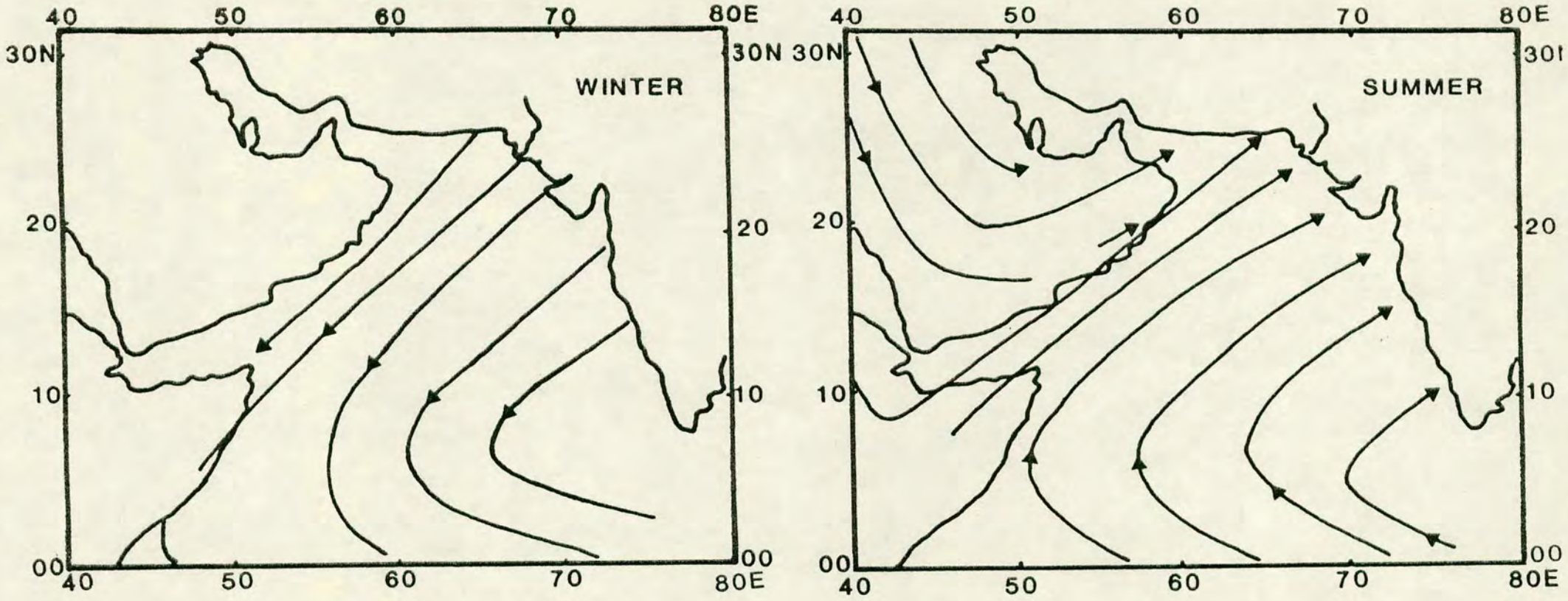

FIGURE 2.3 SEASONAL SURFACE WINDS PATTERN FOR ARABIAN SEA (HASTENRATH and LAMB, 1980)

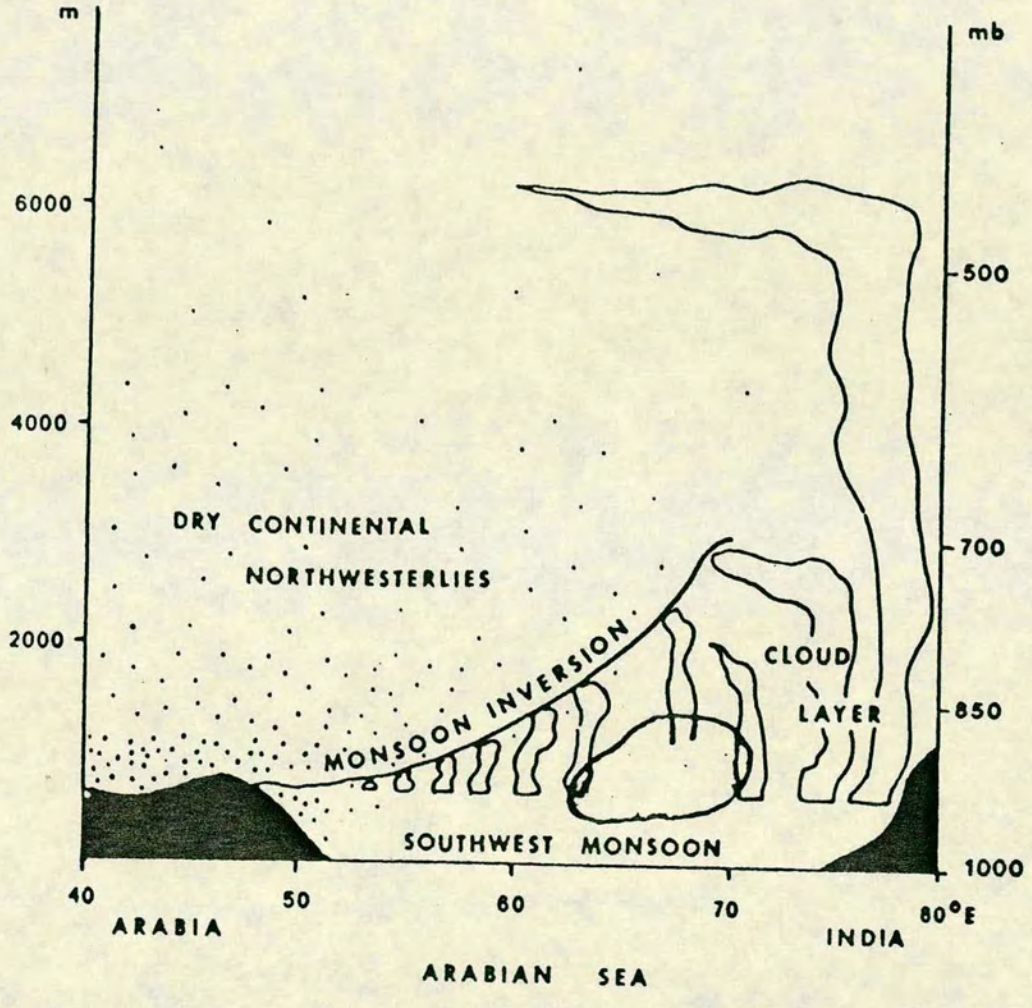

FIGURE 2.4 VERTICAL STRUCTURE OF THE LOWER AND MIDDLE TROPOSPHERE DURING JUNE AND JULY OVER ARABIAN SEA (SIROCKO and SARNTHEIN, 1988)

landmass creates a low pressure in Asia. This results in a land directed strong southwesterly monsoon over the Arabian Sea (Fig. 2.3). These winds are loaded with water vapour and cause abundant summer rain in the Indian Peninsula.

The vertical structure of summer troposphere, on the basis of temperature changes, has been established by Pant (1978) (Fig. 2.4). He divided the lower troposphere into two layers (i) a low level monsoon layer with potential dust transport; (ii) a cloud layer intensifying to the southeast where dust is rained out. This layer is relatively cool but northwestwards, near the South Arabian Coast it is marked by a temperature inversion associated with a mid-atmospheric layer, the base of which gradually rises towards the southeast (Narayanan and Rao, 1981). This inversion is caused by a mixing of a warm, dry upper atmospheric layer originating from central Arabia and regions to the north, with the cooler moist air masses of low level southwesterly monsoon.

The high level upper atmosphere (> 600m) carries dry air masses and a high dust load southward during summer (McDonald, 1938; Ackerman and Cox, 1982; Sirocko and Sarnthein, 1988). Occasional major dust storms occur in this region as a result of this transport (Foda et al., 1985; Chen, 1986; Ackerman and Cox, 1988).

2.4 HYDROGRAPHY

2.4:1 Surface Circulation

The northern Indian Ocean is different from other major oceans because of a reversal of the atmospheric and oceanic surface circulations. The monsoon winds are the dominating factor in controlling the surface currents in the Arabian Sea (Fig. 2.5). During the winter, the winds are predominately from the northwest. As a consequence, a weak southwest directed monsoon drift current flows along the Indian-Pakistan coast, then at about 10°N it turns west; one branch flows into the Gulf of Aden and the other south along the Somali Coast.

In summer, the winds change to southwest and the sea currents pattern changes in response to the southwest monsoon winds. Surface flow is directed north of the equator, to the northeast, and currents are stronger. Further, a branch of the south equatorial current now turns north between 5°S and the equator, and flows along the coast of Somalia and Arabia to affect the Arabian Sea. It is observed as a strong Somali current with speeds up to 7 knots (Swallow, 1980). East of Socotra Island, the Somali current becomes part of an anticyclonic circulation which continues to the northeast along the coast of Arabia, thence, south along the coast of

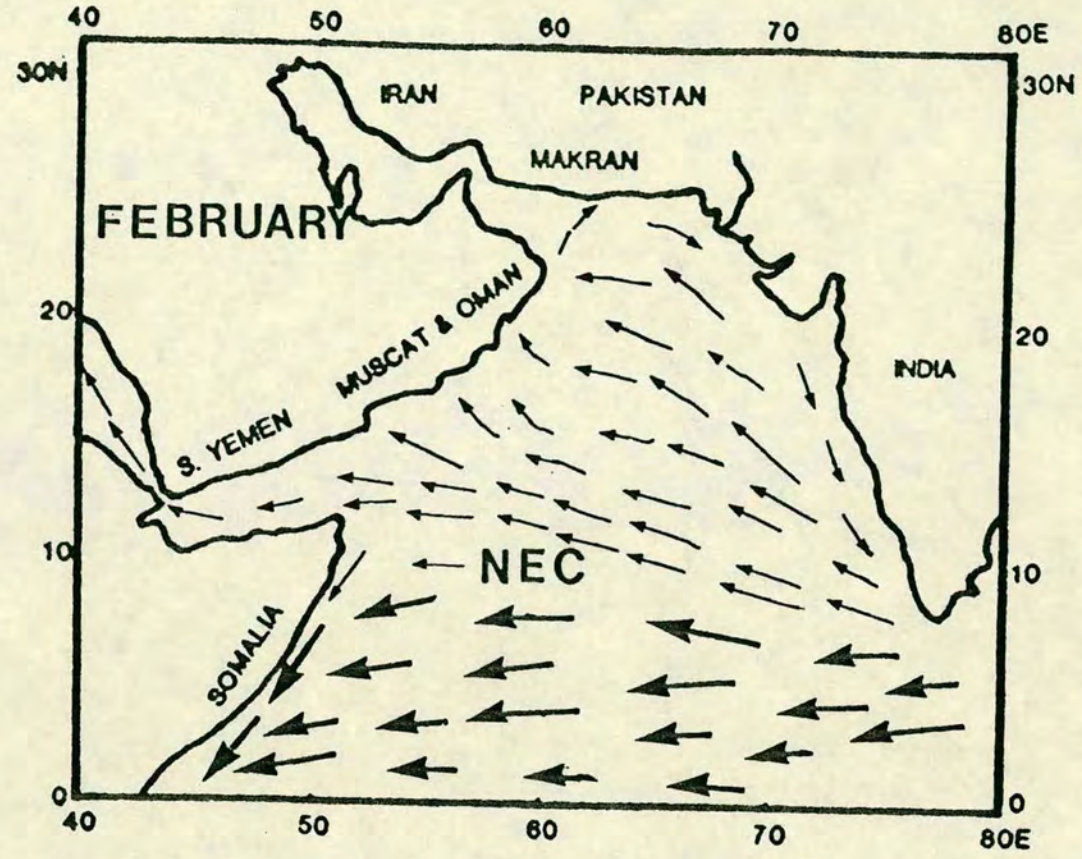

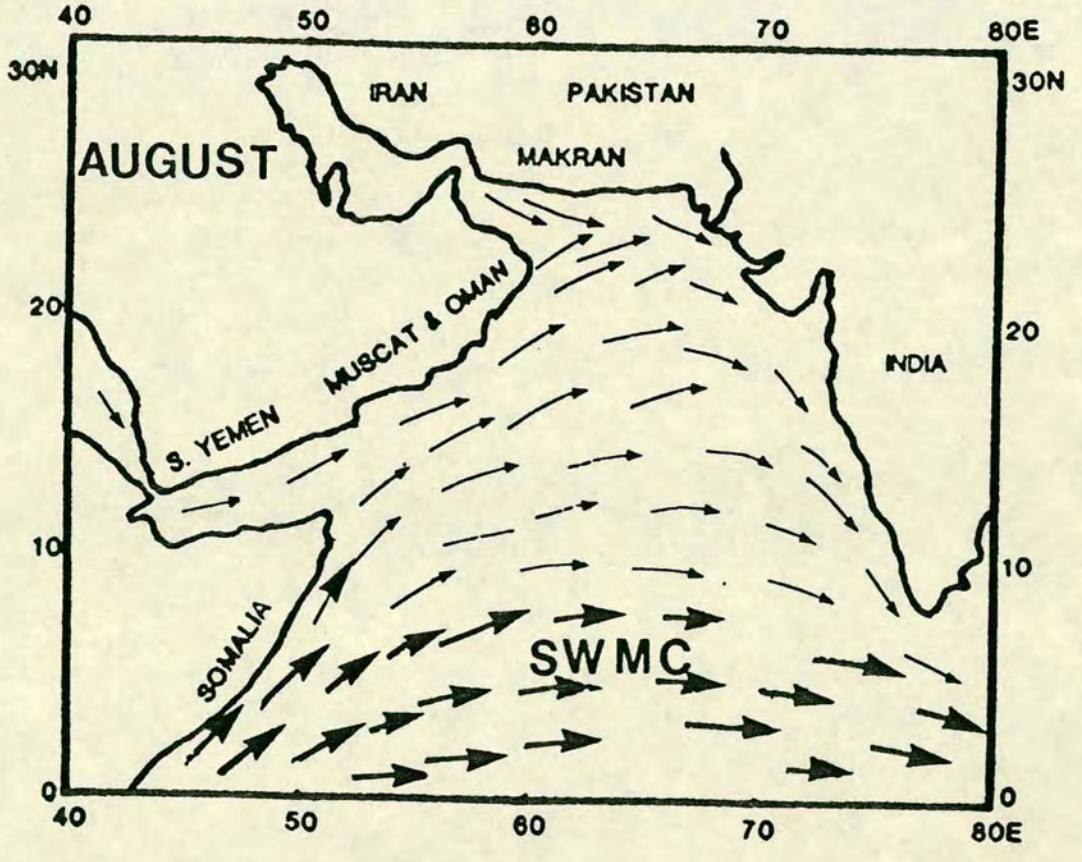

FIGURE 2.5 SURFACE CURRENTS OF NORTH ARABIAN SEA DURING NE MONSOON (NOV - FEB) AND SW MONSOON (JUN - AUG). (WYRTKI, 1973)

India to 10°N. During this transport, it joins the southwest monsoon drift current, flowing east between 5° and 10°N. These currents promote a region of pronounced upwelling along the African and Arabian coast during this period when Ekman transport of surface water is directed southward (Wyrtki, 1973; Prell and Streeter, 1981).

The Arabian Sea has high surface salinities (up to 36.5°/₀₀) due to evaporation. Surface temperature range from 22.5 to 28.5°C, increasing from north to south. Maximum difference in temperature is found during the SW monsoon.

2.4:2 Water Masses

Deeper water masses are characterized by their density, temperature, salinities and oxygen content. These are:

1. North Indian high-salinity intermediate waters (25-100m)
2. Antarctic intermediate water (2000-2500m)
3. Antarctic bottom water/Atlantic deep water (~3000m).

2.4:2a North Indian high salinity intermediate water

A relatively high-salinity subsurface water in the northern Indian Ocean spreading towards the south, north of 10°S, has been called the north Indian high-salinity intermediate water (Wyrtki, 1973). This water has a relatively uniform salinity of 34.9 to 35.5°/₀₀. Some of it is formed in the Arabian Sea but there are large components from the Red Sea and the Persian Gulf with values to 36.2°/₀₀. Rochford (1964) determined five different origins for these high-salinity waters in the upper 1000m. The major transport pathways of the high-salinity water with corresponding depths are shown in Fig. 2.6. Because of high evaporation in the Red Sea, surface salinities can be 42.5°/₀₀. Cooled in winter, particularly in the Gulf of Suez, this water reaches densities higher than that of the bottom Red Sea water (ie. T = 18°C, S = 42.0°/₀₀, δt = 30 against T = 21.6°C, S = 40.6°/₀₀, δt = 28.6) (Tchernia, 1980). After sinking, this water flow to the south-southeast and enters the Arabian Sea with a density of 27.2 through the Strait of Bab el Mandeb at a depth of 100-110m. This Red Sea water subsequently spreads between δ = 27.3 and 27.1 and sinks to 600-900m. Its salinity ranges from 36.3-34.9°/₀₀. Similarly in the Persian Gulf, surface water attains a high salinity ie. 40-41°/₀₀ owing to an excess of evaporation

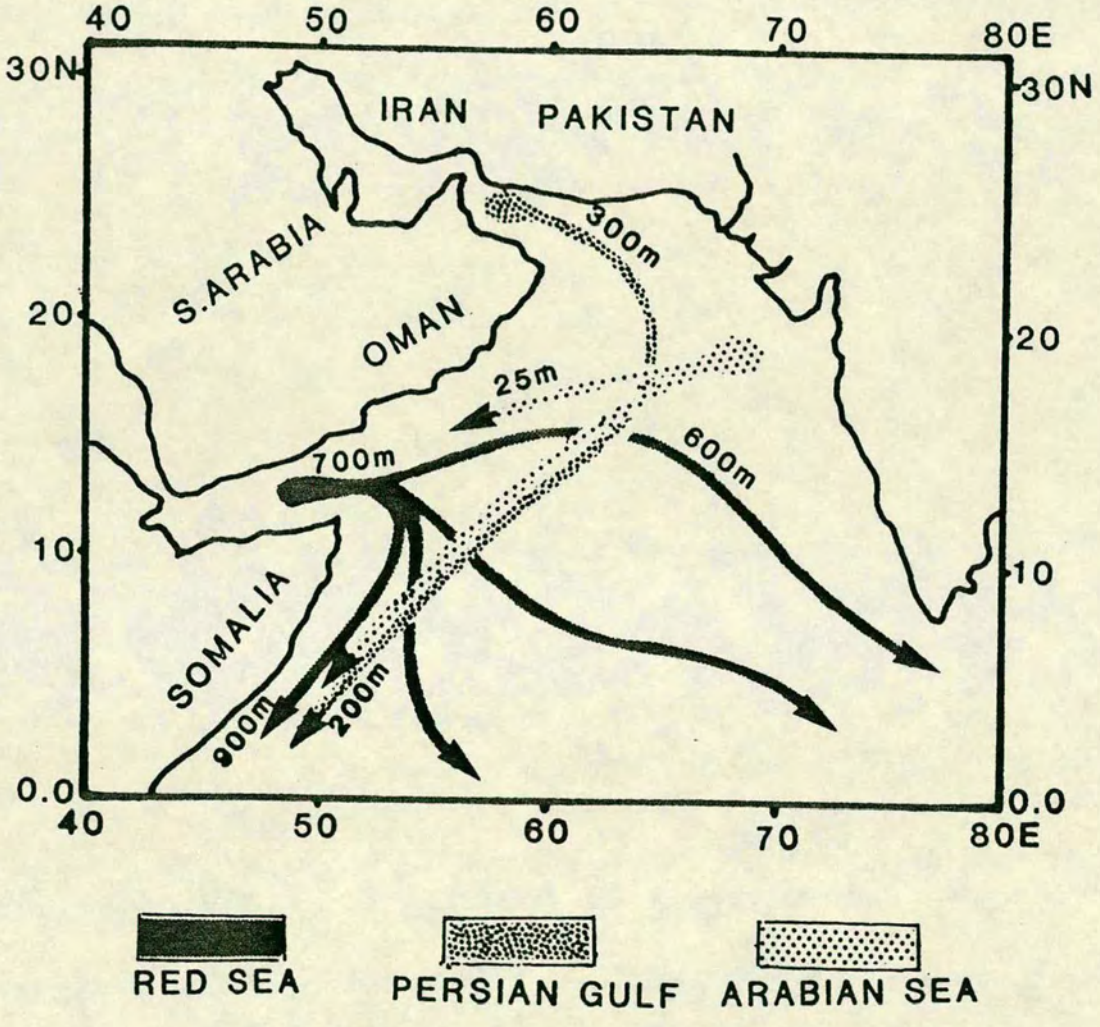

FIGURE 2.6 THE MAJOR PATHS OF HIGH SALINITY WATER MASSES OF THE NORTH INDIAN OCEAN. NUMBERS ALONG THE PATHS SHOW THE DEPTH AT THAT POINT (ROCHFORD, 1964)

over precipitation. During the cooling of the Persian Gulf in winter, vertical convection is induced, and causes formation of cool and therefore heavy bottom water. This water flows towards the Gulf of Oman through the Strait of Hormuz at a depth of 200-300m and spreads southwards as far as the Arabian Sea (Düing and Schnwill, 1967), where it tends to lose its character (Ramesbabu et al. 1980) due to mixing. The Persian Gulf water (S = 36.1-35°/₀₀) outflow has a density range between δ = 26.4 and 26.8 and is found in the north Arabian Sea at depths of 300-400m.

These two high salinity water masses and others shown in Fig. 2.6 form a thick layer of almost uniform salinity. However, the individual layers can still be recognised from their salinities.

2.4:2b Antarctic intermediate/Antarctic bottom water

In the Arabian Sea the deep bottom water of an Antarctic circumpolar origin has been recognised, and has been named North Indian deep water (Ivanenkov and Guibin, 1960). This water is transported northwards from the southern ocean through a chain of basins by deep western boundary currents (Warren 1978, 1981).

The Antarctic bottom waters originating in the Weddell Sea, is characterized by Θ = -0.7°, S = 34.66°/₀₀, O = 6ml/l and σt = 27.88 (Tchernia, 1980). In spreading to the east and north at 4000m this water penetrates into the Indian Ocean near 62°E, between Crozet Island and Kergulen. Near 40°S its potential temperature is 0°C and it passes from the Crozet basin to the Madagascar basin, the Mascarene, the Somali, and into the Arabian basin as indicated by the evolution of potential temperature from Θ=-0.7 to 1.2°C. This evolution is due mainly to slow mixing with the North Atlantic deep water (NADW) above. In the Arabian basin the Antarctic Bottom water (North Indian Deep Water) is recognised by these properties Θ = 1.23°, S = 34.73°/₀₀, O = 5ml/l, σt = 27.83 (Tchernia, 1980).

Unpublished CTD results of Charles Darwin Cruise 86/17 also confirm these earlier findings of the occurrence of Antarctic bottom water in the Arabian Sea. The Antarctic bottom water at sites CD1715 and CD1730 is recognised between 3500-4000m water depths by its low temperatures, salinity (1.7°C, 34.7°/₀₀) and high oxygen (120-130μm/kg) and silicate contents (140-150μm/kg). The North Atlantic deep water (NADW) enters the Indian Ocean in the region of Aghulas Plateau at 2500-3500m depth and spreads to the east and also, importantly, to the north into the Western Indian Ocean. Between 1500-2000m depth in the North Arabian Sea, a

water mass with relatively high temperature and salinity value (T = 3.4°C and S = 34.8-35.2°/₀₀) (unpublished results CD86/17) is probably a northern extension of North Atlantic deep water.

2.5 MONSOON CONDITIONS AND UPWELLING

In the regions dominated by eastern boundary currents eg. northeast and southwest oceanic margins, prevailing winds (Trade Winds) directed parallel or subparallel to coastlines have an effect on the ekman transport of warm surface waters towards the ocean. Subsurface water, which is colder and denser, is drawn up to replace them. This oceanographic process is known as upwelling. Normally upwelling water contains higher concentrations of nutrients (such as phosphate, silicates, nitrates) than surface water, which had been depleted as a result of biological demand. Regions of upwelling are amongst the richest biological areas of the world, and increased skeletal biogenic material is contributed to the bottom sediments.

The northern Indian Ocean, however, is unique in this respect as seasonal upwelling is a response to westerly boundary winds the southwest monsoon system. Oceanographically, characteristic gradients in the physical, chemical and biological properties have been observed. Detailed studies of these gradients in the Arabian Sea during SW monsoon have confirmed the surface effects of upwelling over almost the whole of the northern Arabian Sea (Wyrtki, 1971, 1973; Sastry and DeSouza, 1970, 71, 72; Smith and Codispoti, 1980; Qasim, 1982; Kutzbach, 1981; Sengupta et al. 1976; Prell and Kutzbach, 1987). The marked effects of upwelling in this region are briefly described below.

2.5:1 Temperature and Salinity

The response of the Arabian Sea to the monsoon winds is clearly observed in the sea-surface temperature (SST) patterns during the summer, a time of high SST. A distinct temperature gradient from coast to offshore occurs during the southwest monsoon affecting the northwestern sector of the Arabian Sea (Fig. 2.7). At this time surface water temperature is low (22-23°C) along the coasts of Africa and Arabia and gradually increases to 27-28°C in the Central Arabian Sea (Bruce, 1974; Prell and Huston, 1979). In a similar manner a highly saline surface layer (about

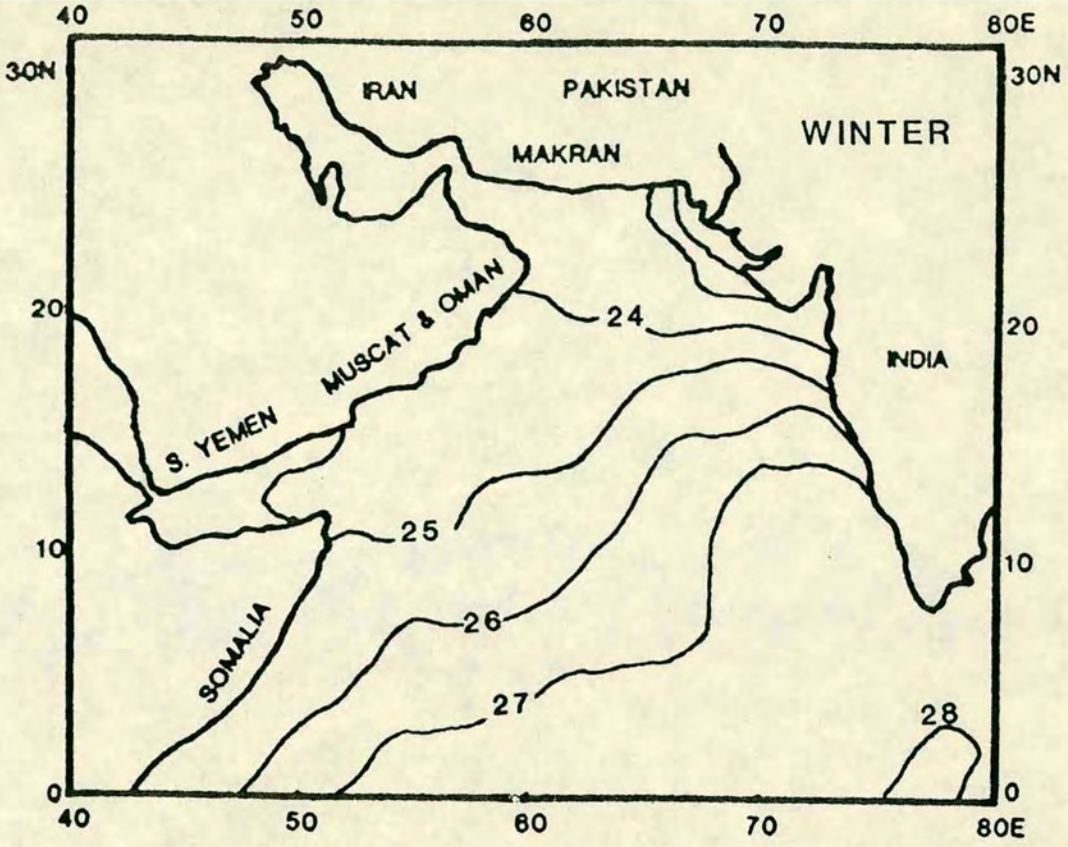

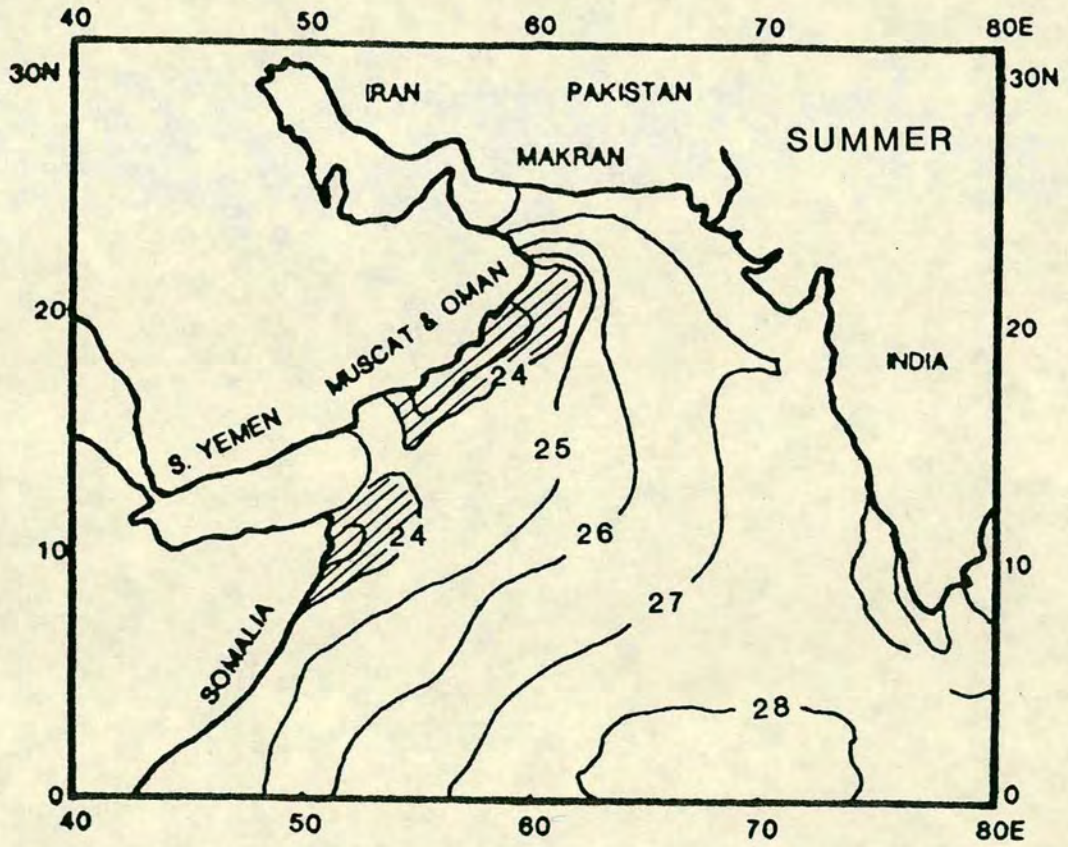

FIGURE 2.7 DISTRIBUTION OF SEA SURFACE TEMPERATURE ALONG NW ARABIAN SEA IN WINTER AND SUMMER MONTHS (PRELL and STREETER, 1981)

36.00°/₀₀) occurs offshore and differs from inshore coastal waters which have lower salinities (35.6-35.7°/₀₀). The higher salinity is characteristic of upwelled sub-surface waters.

2.5:2 Dissolved Oxygen

One of the most important chemical characteristics of upwelling areas is the oxygen minimum zone that underlies upwelled waters (Margalef and Estrada, 1981). In the Arabian Sea the concentration of dissolved oxygen decreases markedly with depth. A vertical section of dissolved oxygen distribution (Fig. 2.8) shows that the surface waters are saturated with oxygen. Values at 100m are about 2ml/l and commonly are below 1ml/l. Such low concentrations form the top of the thick oxygen minimum layer (200-1500m) which shows dissolved oxygen <0.5ml/l especially north of 15°N. The deep water is also relatively low in oxygen because of a restricted deeper bottom water flow with concentrations less than 4.0ml/l (Wyrtki, 1971).

Surface oxygen concentration shows maximum range (1.94 to 6.41ml/l) during upwelling from the southwestern monsoon (Qasim, 1982). A shallow oxygen minimum (O_2 = 0.5-1ml/l) is seen within the thermocline at 200m. The strong density stratification and sluggish deep water circulation restrict the renewal of oxygen at intermediate depths, and in the deepest waters. These features in conjunction with the degradation of a high rate of supply of organic matter from the surface result in a severe depletion of dissolved oxygen in all waters below the thermocline (Wyrtki, 1971, 1973). Additionally the inflow of waters rich in organic matter from the Red Sea and the Persian Gulf (Ryther and Menzel, 1965; Szekielda, 1970) not only increase the stratification described above, but also contribute to the depletion of oxygen.

2.5:3 Nutrients

Due to organic matter degradation the nutrient distribution is generally inversely correlated to dissolved oxygen. Such mechanisms are also indicated by the denitrification of certain waters observed by Sen Gupta et al. (1975, 1976) and Anderson et al. (1982). High concentrations of nutrients in surface coastal waters off both Somalia and Arabia occur during the SW monsoon periods (Wyrtki, 1971; Sastry and De Souza, 1971, 1972; Qasim, 1982). Their concentrations in the offshore

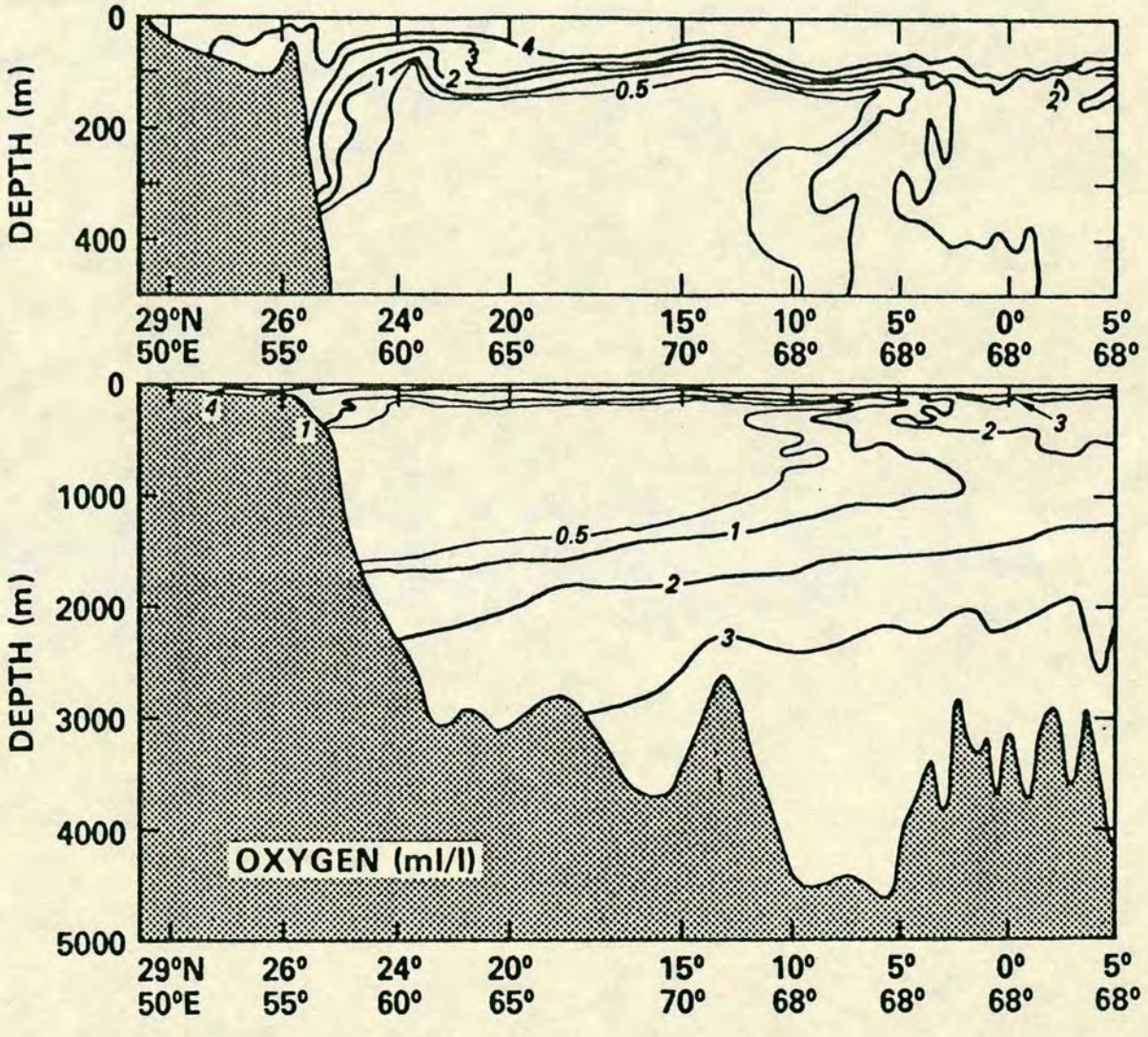

FIGURE 2.8 NORTH-SOUTH VERTICAL PROFILE OF DISSOLVED OXYGEN IN THE ARABIAN SEA (WYRTKI, 1971)

regions, however, are generally low during these times (Reddy and Sankaranarayanan, 1968) possibly indicating more consumption with increased biological production. Ryther et al. (1966) described the degradation of particulate organic matter during fallout and upwelling leads to an active recycling of nutrients with consumption in surface water and a build up of high concentration below the thermocline. The distribution of the different nutrients in the Arabian Sea are shown in Fig. 2.9.

2.5:3a Phosphate

Fig. 2.9a shows the patterns of dissolved phosphate in the Arabian Sea. In the northwest, phosphate shows a well defined increase in the upper water and at 200m shows a concentration of 2.4 per μ mol^{-1} well above that seen at an equivalent depth at the equator (~1.0 μ mol^{-1}). The oxygen minimum zone, 200-1200m, shows high concentration but the highest values according to Wyrtki (1973) occur between 1200 and 1600m (3.0 μ mol^{-1}): that is, at the base of the oxygen minimum zone. In the upper water at a depth of about 100 metres, the phosphate concentration decreases and overlying surface layers offshore showing values lower than 0.5 μg at/l have been reported (Sastry and De Souza, 1972, Smith and Codispoti, 1980).

2.5:3b Nitrate

Similar distribution patterns of nitrate concentration have been observed, decreasing from north to south and from west to east. This is consistent with a progressive increase in oxygen concentrations. Qasim (1982) has documented the maximum average value of 22.25 μg at/l and maximum range of 0.01 to 25.50 μg at/l in nitrate during the SW monsoon both at the surface and at 100m. Nitrate distribution with depth in the Arabian Sea is characterized by denitrification. Since the intermediate waters in NW Arabian Sea are depleted in oxygen, nitrate undergoes reduction and exhibits a minima at intermediate depths (Sen Gupta et al., 1976; Deuser et al., 1978; Sen Gupta and Naqvi, 1984). The intensity of denitrification decreases southward, consistent with increases in oxygen concentration and decreases in the thickness of oxygen minimum layers.

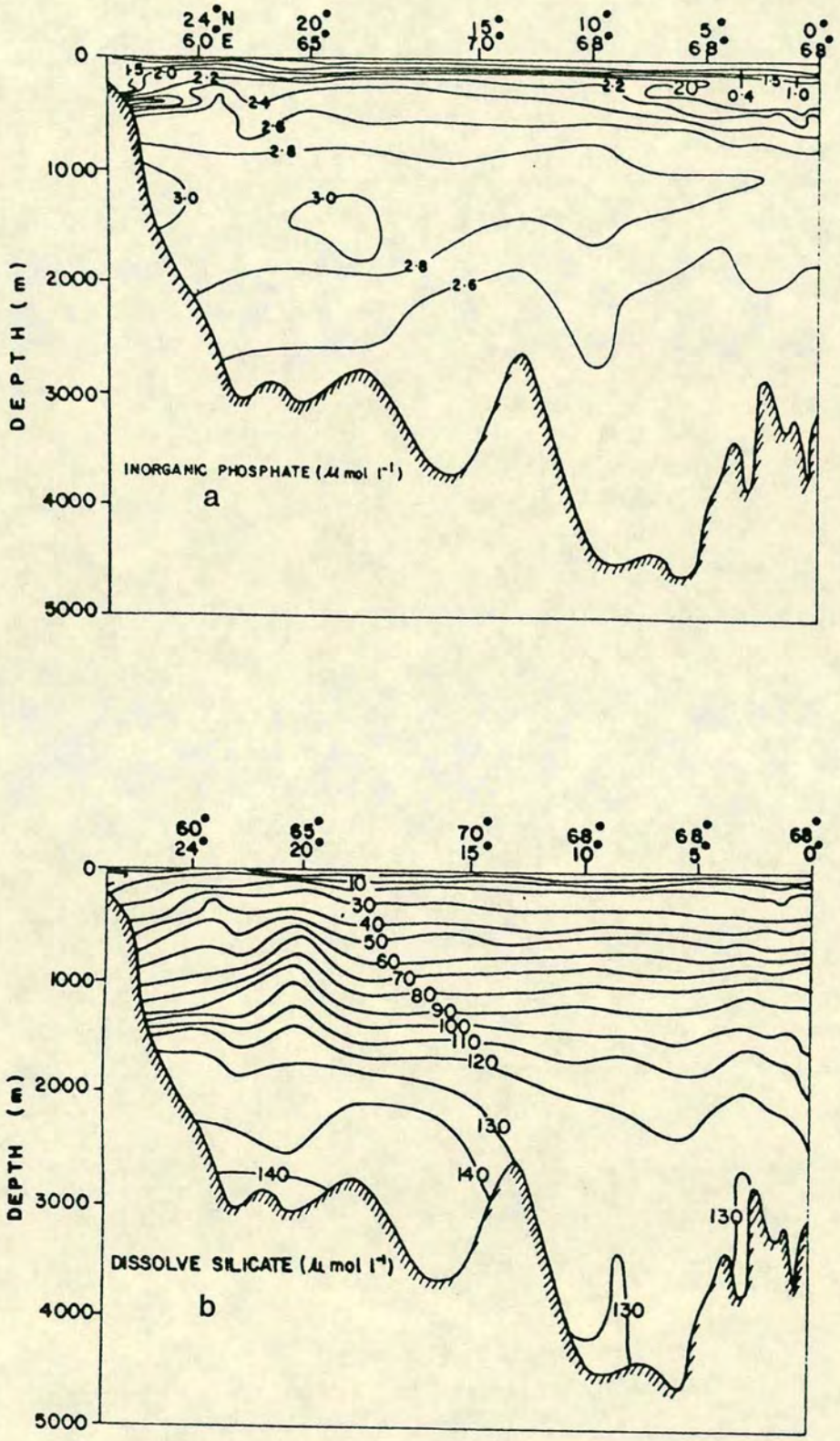

FIGURE 2.9 DISTRIBUTION OF INORGANIC PHOSPHATE (a) AND DISSOLVE SILICATE (b) ALONG A SECTION RUNNING FROM THE GULF OF OMAN THROUGH THE ARABIAN SEA TO THE EQUATOR. (WYRTKI, 1971)

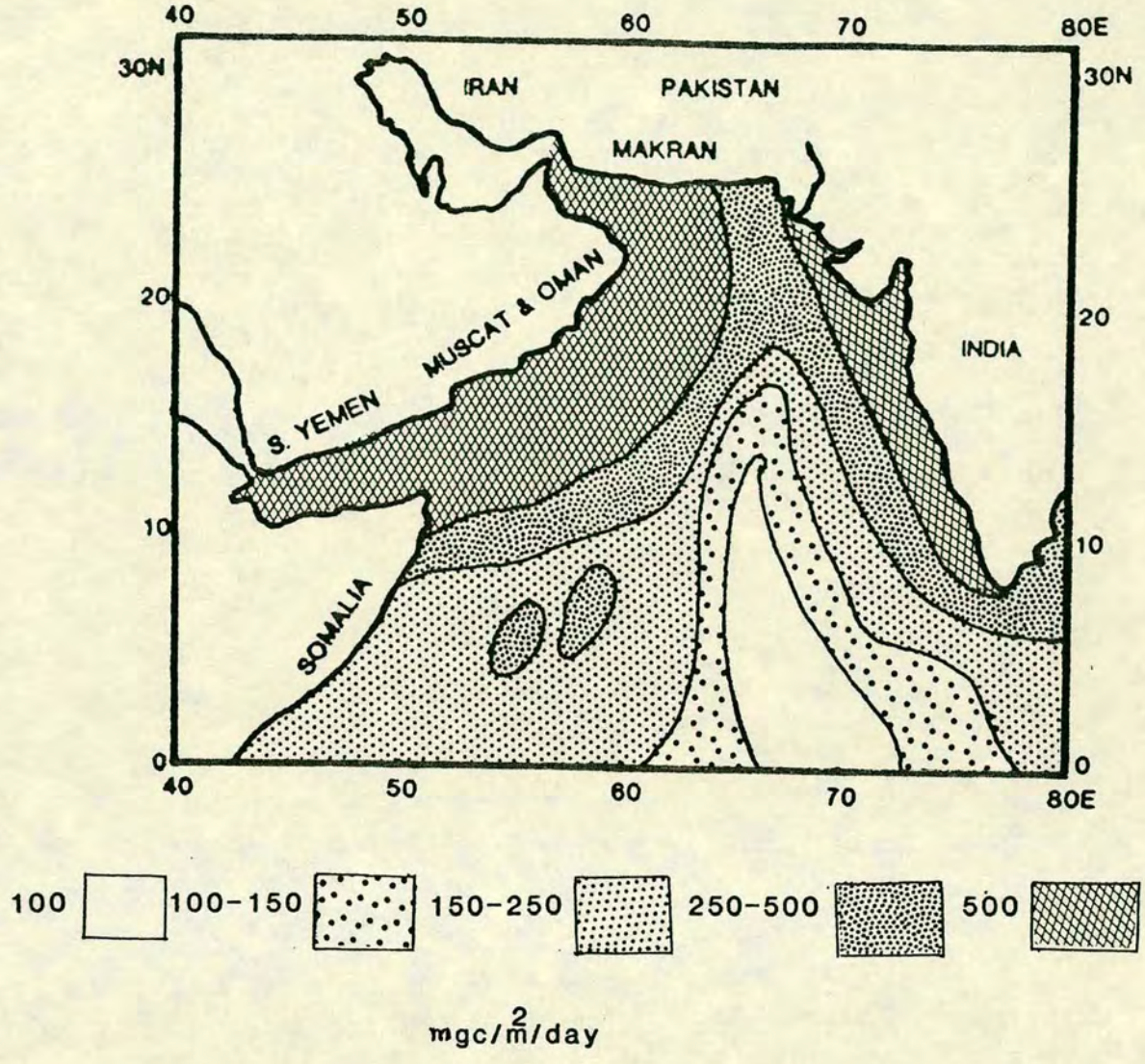

FIGURE 2.10 PRIMARY PRODUCTION IN THE NORTHERN INDIAN OCEAN (FAO DEPARTMENT OF FISHERIES, 1972)

2.5:3c Silicate

The silicate concentrations observed in the Arabian Sea (150-160 μ mol^{-1}) are much higher than those of the Atlantic but approach that of the maximum value for the Pacific (McGill, 1973). Silicate in the deep water is unusually high reaching concentrations greater than 150 μg at Si/l. Such very high silicate content seems to be characteristic of the deep water of the Arabian Sea (Sen Gupta et al. 1976; Rajendron et al. 1980). Surface values are low but tend to show increased values where a high degree of upwelling prevails. Silicate values tend to show a somewhat linear increase with water depth (Fig. 2.9b).

2.5:4 Productivity

Photosynthetic productivity in the Arabian Sea is significantly higher than average ocean water (Ryther and Manzel, 1965). The highest values occur in the north and concentrations greater than 1 g C/m^2/day are reported (Kuzmenko, 1973; Ryther et al. 1966). The high productivity of the western Arabian Sea (Fig. 2.10) has been attributed to the presence of unusually high levels of inorganic nutrients at a shallow depth, often within or in close proximity to the euphotic zone (Ryther et al., 1966). Higher concentration of nutrients during upwelling times are transported across the thermocline to the euphotic zone. The water masses entering the Arabian Sea from the south at intermediate and deep levels rise slowly, and eventually reach the near-surface layers as a result of a general, deeper water upwelling and increases the nutrient levels. This general upward movement of subsurface waters, upwelling due to winds, largely controls the high level of photosynthetic productivity in the Arabian Sea. At this time carbon uptake rates 0.5 to 1.0 g C/m^2/day and chlorophyll concentrations above 0.5 μ g/l have been measured in the upper 50m of water over wide areas (Krey and Babenerd, 1976; Qasim, 1982).

CHAPTER 3

SEDIMENTS AND CHRONOSTRATIGRAPHY

3.1 LOCATION OF CORES

In 1986, from October 15th to November 7th, the Natural Environment Research Council (NERC) UK research ship Charles Darwin undertook an Oceanographic Cruise 86/17 of the North Arabian Sea. Eleven piston cores and twenty eight box cores were collected between 15° and 25°N. Results of five selected piston cores, the location of which are shown in Fig. 3.1 and Table 3.1 are reported in this study. These cores are generally 7-8m in length and raised from a water depth of 1500-4000m. As the core sites seem to be influenced by varying contributions of biogenic and terrigenous materials, the piston cores were selected on a north-south transect in order to decipher trends of spatial and temporal variation of these materials. Cores CD 1715 and CD 1730 were chosen principally to identify the record of monsoonal upwelling affecting the northern Arabian Sea. These two sites located on the ocean side of the Owen Ridge are likely to be less affected by terrigenous input than other cores and it is anticipated that they will record a continuous history of sedimentation and will have incorporated within them a variety of upwelling signals. Core CD 1739 raised from the Murray Ridge and CD 1738 from the Oman basin (Fig. 3.1 Table 3.1) have been examined to show the temporal and spatial variation in terrigenous materials which are likely to be caused either by changes of wind patterns or by sea level fluctuation during glacial and interglacial times. Additionally, core CD 1738 from the Oman basin is likely to provide a record of the regressive and transgressive history of the Persian Gulf and its influences on sedimentation in the Gulf of Oman.

3.2 CORES DESCRIPTION

In general, the cores are mainly composed of clay to silt sized terrigenous and biogenic constituents. The colour of the sediments varies from pale yellow, pale greenish to olive green and greyish green. Red brown oxidized surface sediments 5-10cm thick have been encountered in the hemipelagic box cores. However, in the piston cores investigated, only core CD 1730 shows a surfacial 10-15cm reddish colouration. Hence it is assumed that the uppermost ~10cm of the other cores, particularly in the hemipelagic cores 1738, 1739, 1715, is missing. A summary of these for each core is reported here.

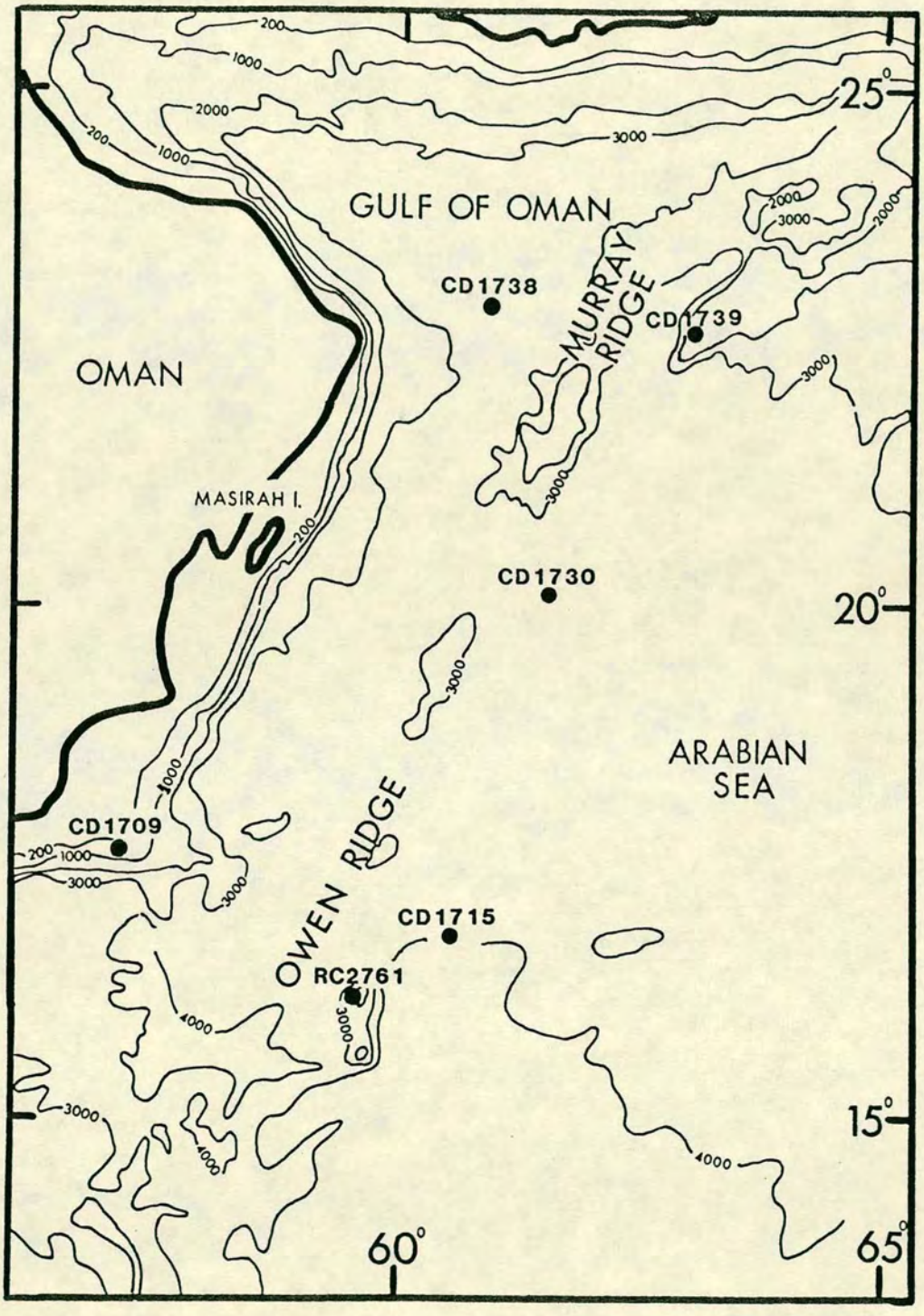

FIGURE 3.1 LOCATION MAP OF PISTON CORES.

Table 3.1 Locations and Water Depth of Cores Analysed in this study

CORES	LOCATION	CORE LENGTH (cm)	WATER DEPTH (metres)
CD 1709	17°36′.3N 57°21′.5E	475	405
CD 1715	16°37′.7N 60°40′.1E	740	4015
CD 1730	19°55′.6N 61°42′.9E	800	3580
CD 1739	22°15′.7N 63°12′.9E	800	1620
CD 1738	22°45′.1N 61°16′.7E	750	3340

CORE CD 1715

The core CD 1715 was collected from a flat plain on the distal edge of Indus cone but on the ocean side of the Owen Ridge. Sediments are pale olive 10Y 6/2 to light grey 5Y 5/2. Dark grey, green, 5GY 6/1 fine silts and clay intercalated with foram enriched layers produce a weak banding of 2-5cm interval. Clay bands are usually homogenous but the upper 100-150cm of the core appears to be mottled. The lower parts of the core tend to be light grey, and contain more silt. Diatoms are common, but are not a major constituent. Red/brown layers of sediment 2-5cm thick occur at 300cm, 250cm, 610cm and 615cm.

At least ten turbidite bands of variable thicknesses are seen in the core, particularly in the uppermost and lower sections. In the upper section of the core, two prominent fine grained turbidite bands occur at 92-95cm and 130-140cm depths. The upper and middle parts of the core are essentially free of any recognisable sandy units. In contrast, below six metres, several 1cm-10cm thick fine sandy and silty turbidite layers occur. These are dark green in colour and show grading with typical features such as scours and load structures at their bases.

CORE CD 1730

Core CD 1730 also lies in plain area, 200 miles north of core CD 1715 near the eastern boundary of the Owen-Murray ridge system. The uppermost 10-15cm of the core shows red/brown 5YR 3/4 oxidized surface sediments. Below, the interval 15-80cm displays homogenous light grey 5Y 4/2 silty clay ooze with high water content. Within the interval 100-150cm, forams seem abundant occurring as white bands, 2-3cm thick, in a sequence of light-medium green sediments. Throughout, the lithology is mostly uniform varying in colour from light olive grey 5Y 4/1, to greenish grey 5GY 6/1 and pale green 10Y 6/2. In the middle and lower sections, diatoms occur but are never abundant. The sediments seem to have a high water content. At ~170cm, 300cm and 650cm depth ~10cm thick pale brown oxidized sediments occur. A dark intense green coloured sediment occurs at 340cm displaying faecal pellets (Plate 1). This unit shows some mixing over an interval of ~20cm. In appearance this sediment is macroscopically dissimilar to the surrounding sediments, it is more indurated, and contrasts with the light green-grey carbonate rich sediments above and below it. This band is tentatively interpreted as an ash band. The only ash band reported in the Arabian Sea sediments of upper Pleistocene-Holocene age is that found during ODP leg 117 (Shimmield, pers. comm.) and is recongised as the

PLATE 1: FAECAL PELLETS IN CORE CD1730 AT DEPTH 300cm X50

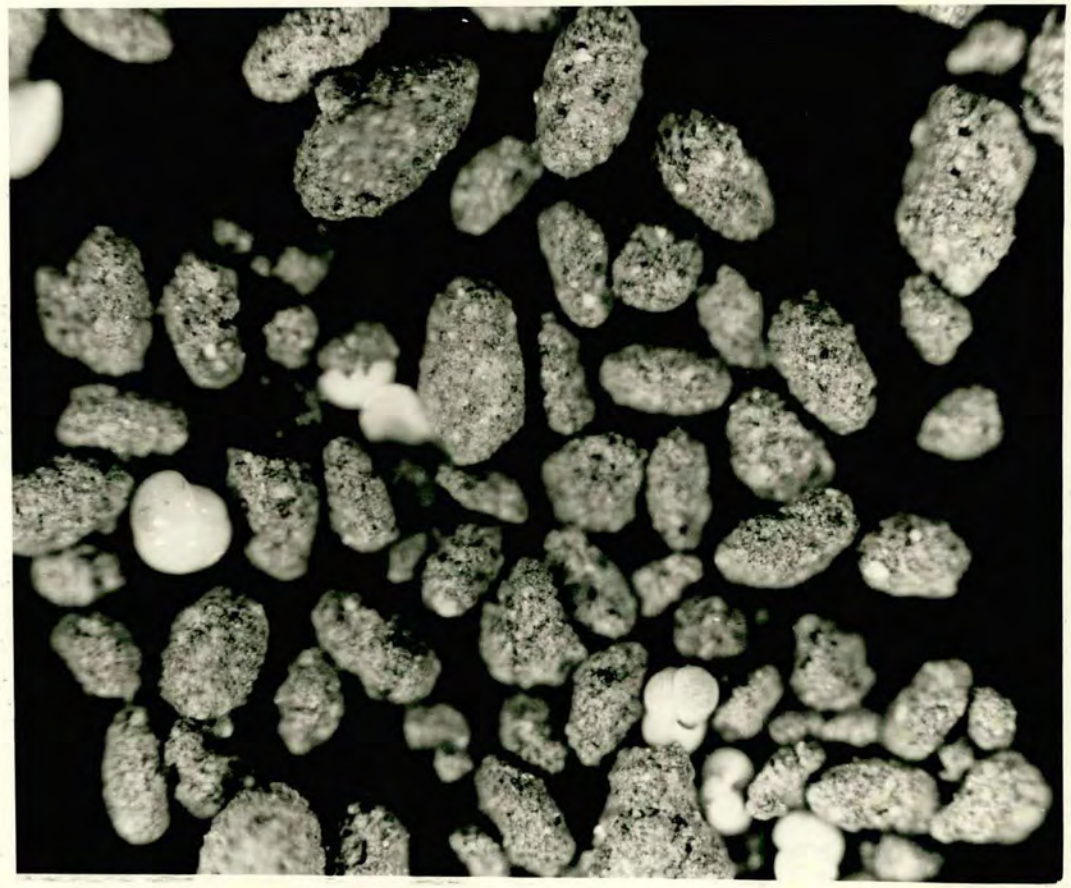

TOBRA Ash dated ~71.0 kys BP. This Ash band has also been reported in ODP core and other cores in the area collected during Charles Darwin Cruise CD 17/86 (Price, pers. comm.).

CORE CD 1739

Core CD 1739, taken from a topographic high on the Murray ridge, shows overall dark green 5GH 6/1 to olive grey 5Y/52 coarse foraminiferal silts, with rare diatoms. Biogenic constituents are abundant. At the bottom of the core complete shells of gastropod and pelcypods were recovered. The top oxidized surface is lacking in this core and the ash band is not recongised.

CORE CD 1738

This core was collected from the southern limits of Oman abyssal plain and is situated to the west of the Owen fracture zone. At least the top 10-20cm of sediment was lost during coring. The core mostly contains olive grey 5Y 4/1 coarse silts and silty clay. This core differs from other cores in that it contains very little biogenic material and displays few foraminiferids. Most of the core displays homogeneous lithology except near the bottom, where between 540cm and 700cm of the core shows alternate dark green 5GY 6/1 and light green 10Y 6/2 banding, approximately 5-10cm thick. Two ~10cm thick dark grey-green coarse grained sandy bands occur between 240-250cm and 530-540cm. The dark green ash band is absent.

CORE CD 1709

This core was collected from a shallow basin only 800m deep along southern Oman Continental margin. It contains relatively more coarse grained sediment than other cores described above. These are coarse silt and silty clay, dark green 5GY 6/1 and olive grey 5Y 4/1 colour. Dominantly a silt, with common sponge spicules. Foraminifera (Planktonic) are not as common as in other cores. Broken biogenic debris are abundant. Lithology is mostly homogeneous, and slightly indurated.

3.3 MICRO-DESCRIPTION OF SEDIMENTS

Examination of smear slides and SEM photographs shows that the terrigenous fraction of these sediments contains a significant amount of silt size quartz, feldspars and dolomite. The dolomite mostly occurs as highly corroded subhedral rhombs or anhedral grains. Euhedral dolomite is rare (Plate 2a). Quartz dominant grains are usually rounded and pitted (Plate 2b), probably indicative of an aeolian source. Other recognisable minerals are anhedral feldspar and chlorite aggregate. Cores CD 1738 and CD 1739 in the north appear to have a higher terrigenous component and show abundant quartz chlorite aggregates and occasional dolomite grains in the coarse grained fraction of the sediment. Cores CD 1730 and CD 1715 which are mainly fine silt and clays appear overall to have finer-grained terrigenous constituents than core 1738, and also appear to have less quartz and more dolomite than the northern cores. The turbidite layers of both cores, especially CD 1715 show substantial increases in both quartz and dolomite contents compared to the normal sediment of these cores. The biogenic component in the sediments is dominated by foraminiferids, diatoms and coccolithophorids. Perfect skeletons as well as broken debris of all these can be seen under the SEM (Plate 3). In core CD 1715 and CD 1730 calcareous skeletons are largely of planktonic forams ie. Globogerinids, and in cores CD 1738 and CD 1739 these are also occasionally seen (Shimmield, pers. comm.). The planktonic foram G. *bollorides* is found in abundance in this area, and is used to infer the upwelling signals (Prell, 1984).

3.4 SEDIMENT SAMPLING

The piston cores investigated in this study were brought to the Geology Department, Edinburgh University in 1m long refrigerated sections in a plastic liner. These core sections were cut into two halves with the help of a knife using the principle of electro-osmosis (Chmelik, 1967). One half is used for sampling and the other is kept for archive.

Because of the generally uniform lithology of the sediments, all the cores were continuously sampled at an interval of 10cm, to the base of each core. However, some sediment horizons of unusual colour and lithology, such as recognisable turbidites, were also sampled. The sediment samples were weighed before and after drying at 70-80°C for about 24 hours to determine their water contents. A proportion of the dried samples were ground to a fine powder ($<2\mu$) using tungsten carbide Tema mill and subsequently used for different chemical analyses. The unground fraction was used for XRD mineral identifications.

PLATE 2: SEM PHOTOGRAPHS SHOWING DETRITAL GRAINS IN SURFACE SEDIMENTS

(a) EUHEDRAL DOLOMITE (CD1722 2-3cm)

(b) PITTED ROUNDED QUARTZ (CD1722 22-24cm)


2,24KX 5KV WD:4MM S:02224 P:00013
20UM


2,63KX 5KV WD:4MM S:02224 P:00009
10UM

PLATE 3: SEM PHOTOGRAPHS SHOWING BIOGENIC COMPONENTS IN SURFACE SEDIMENTS

(a) DIATOM (CD1722 22-24cm)

(b) PLANKTON FORAMINIFERA (CD1722 2-3cm)

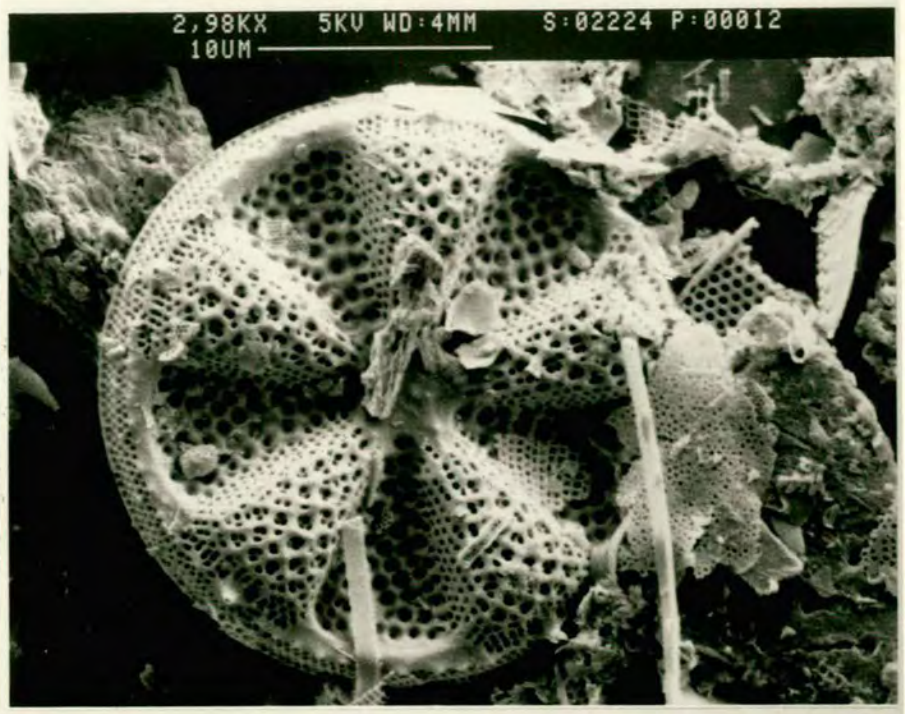
2,98KX 5KV WD:4MM S:02224 P:00012
10UM


1,94KX 5KV WD:4MM S:72223 P:00016
20UM

3.5 WATER CONTENT AND POROSITY

Porosity of oceanic sediments is largely affected by the depth, grain size and sediment composition. Coarse-grained and high carbonate rich sediments tend to have a low porosity (Pettijohn, 1975). In geochemical studies of recent sediments, porosity plays an important role as it affects the release of nutrient to the overlying waters (Berner, 1975; Martens and Klump, 1980; Reimers, 1982) and its measurement is essential for the determination of fluxes of different chemical species with sediments and across the sediment water interface. In this study sediment porosity is determined following the method of Berner (1971). That is porosity (Ø)

$$\text{Ø} = \frac{W.Ps}{W.Ps + (1-W).Pw}$$

where W = % H_2O
Ps = dry density of sediments (g cm^3) = 2.7g cm^3
Pw = density of interstitial water = 1.025g cm^3.

Water contents and porosity are presented in appendix C.1. These results are only semiquantitative as some drying of the sediment could have occurred during transport and storage. Even so, the data presented is sufficiently reliable for use in determining gross changes in the burial flux of the sediment and its components.

Profiles of water contents and porosities of the sediments for CD 1715, 1730, 1738 and 1739 are shown in Figs. 3.2 and 3.3. Water contents vary between 20% to 60% and porosities vary between 0.40 to 0.83, the highest values being found in core CD 1715. All cores show a fall in water content with depth. Surface sediments of CD 1715 sediments show the highest water content and porosity. The rapid decline in the uppermost 30-40cm is principally an effect of burial, while in the lower section the variation in water content is more indicative of changes in sediment texture and composition.

Cores CD 1715 and CD 1730 overall show higher water content and porosity (> 40% and $\geq$ 0.70) relative to CD 1738 and CD 1739. Such high values reflect their fine-grained sediments and this will be confirmed by the measurement of mineralogy (Chapter 4). Füchtbauer and Reineck (1963) have shown that clay contents and associated organic carbon generally increases porosity.

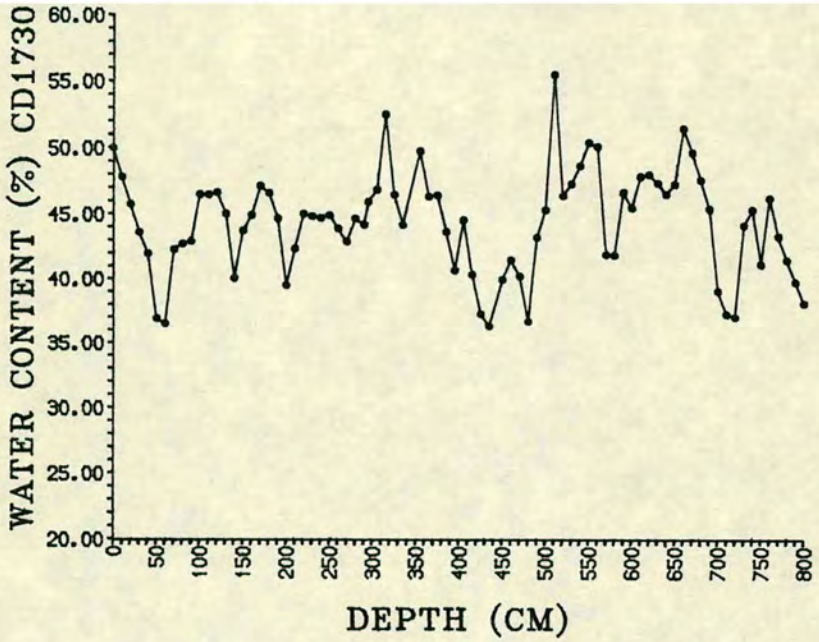

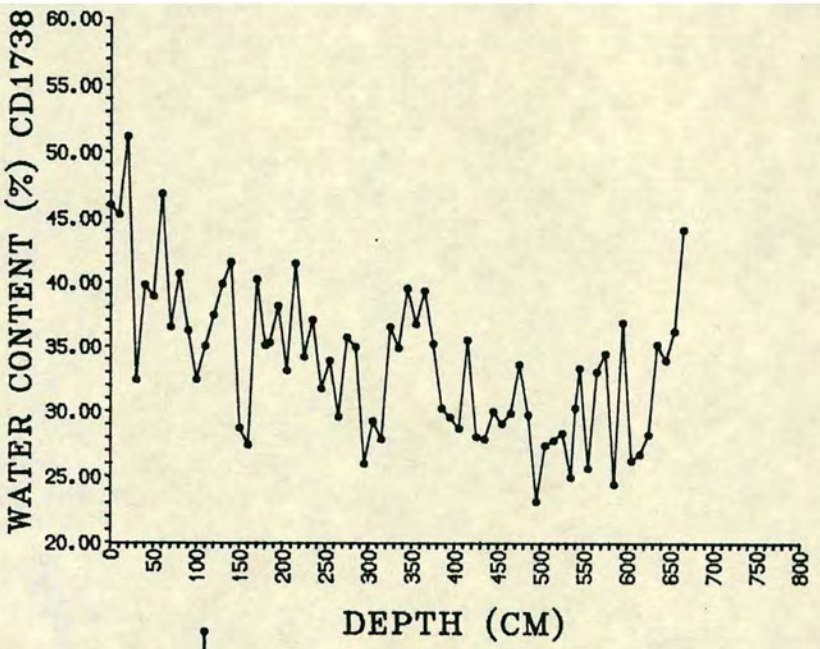

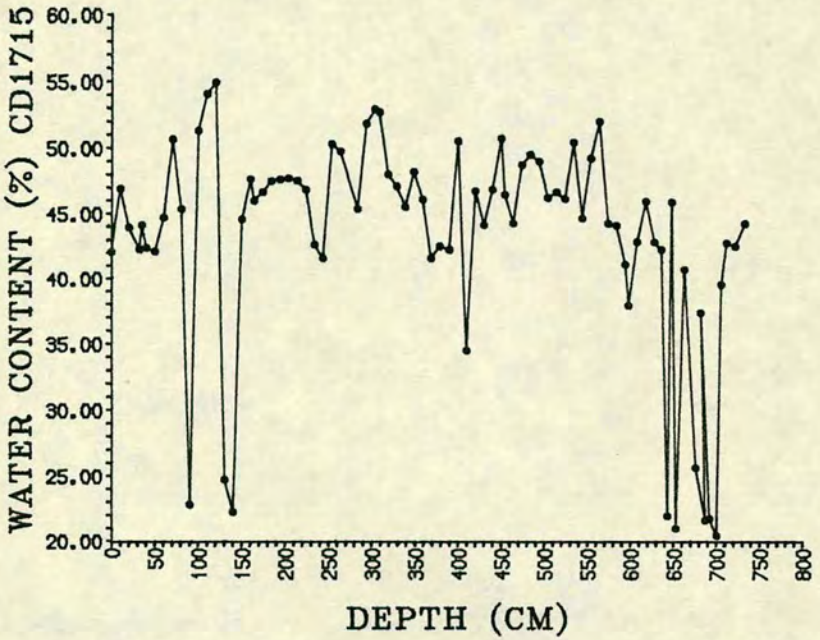

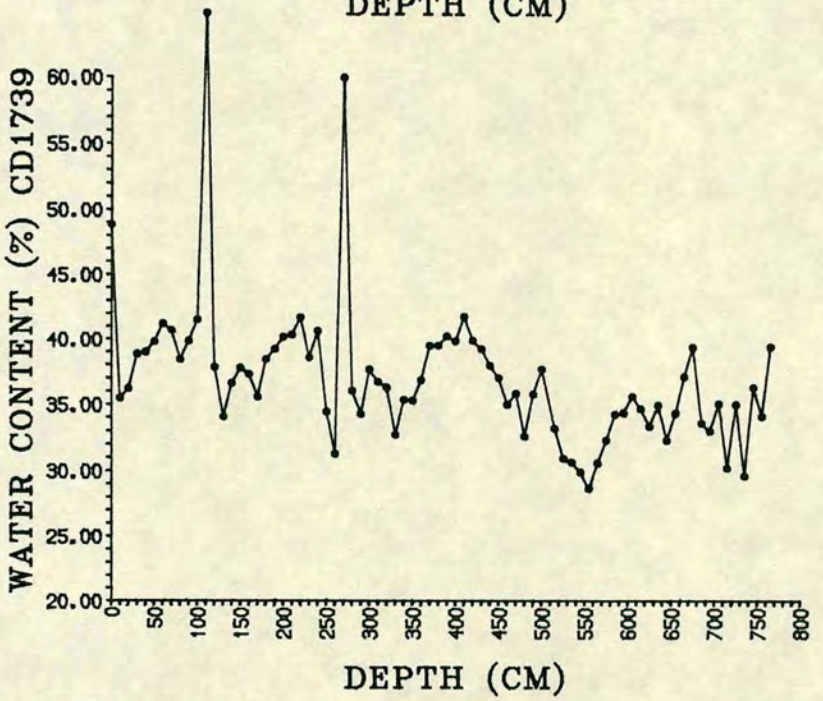

FIGURE 3.2 WATER CONTENT OF SEDIMENT CORES FROM NW ARABIAN SEA.

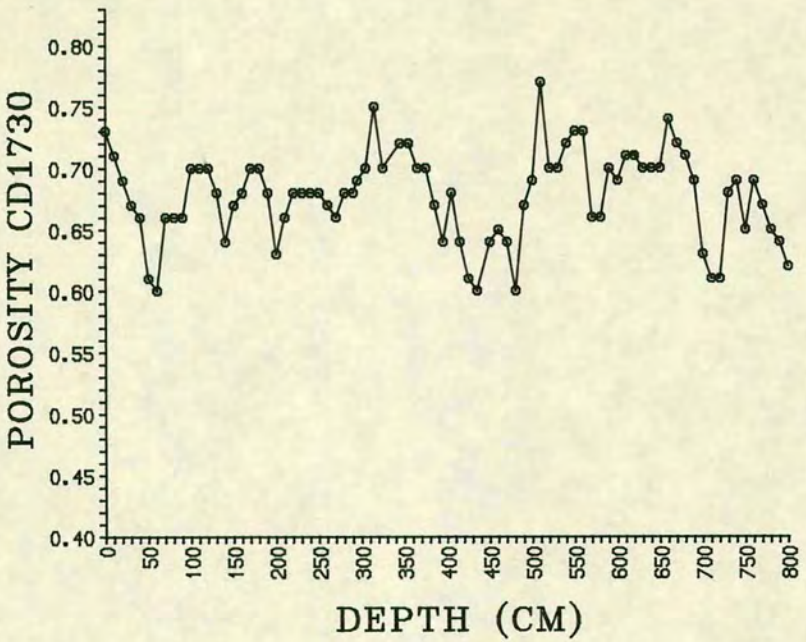

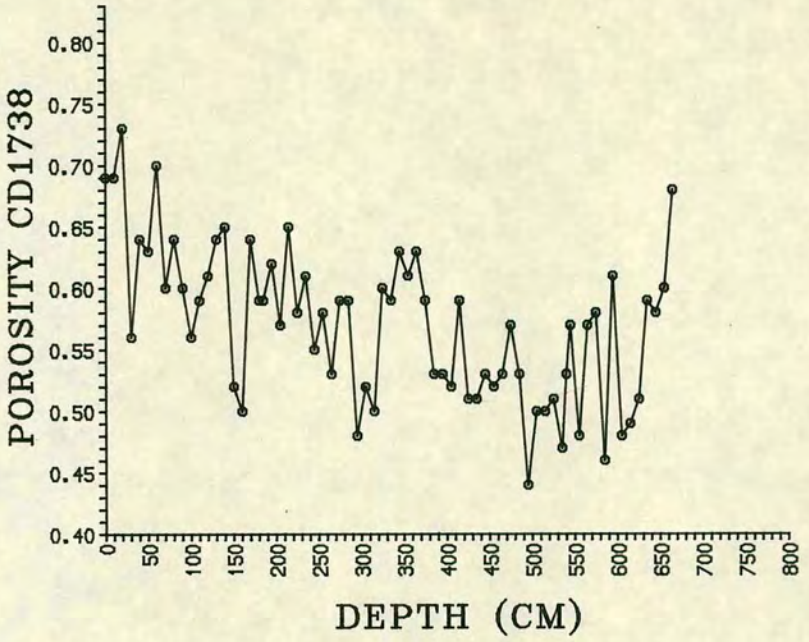

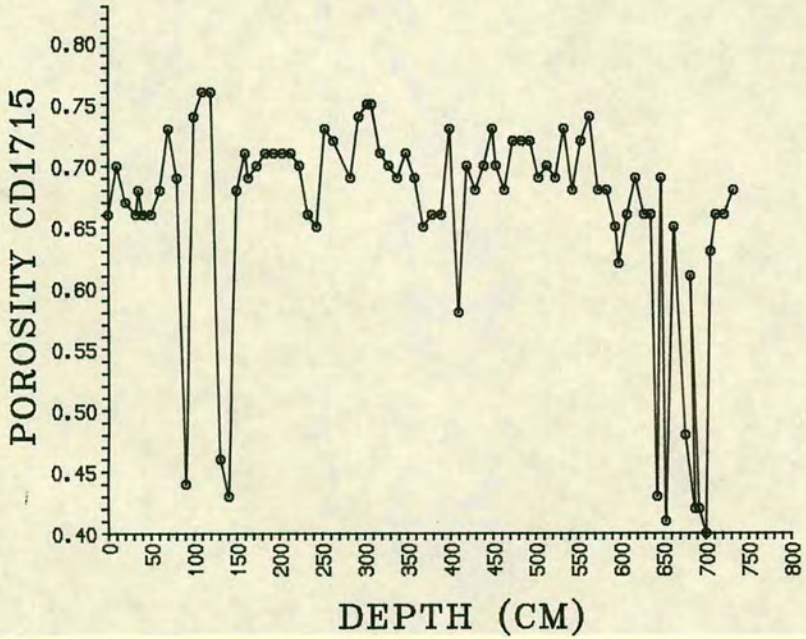

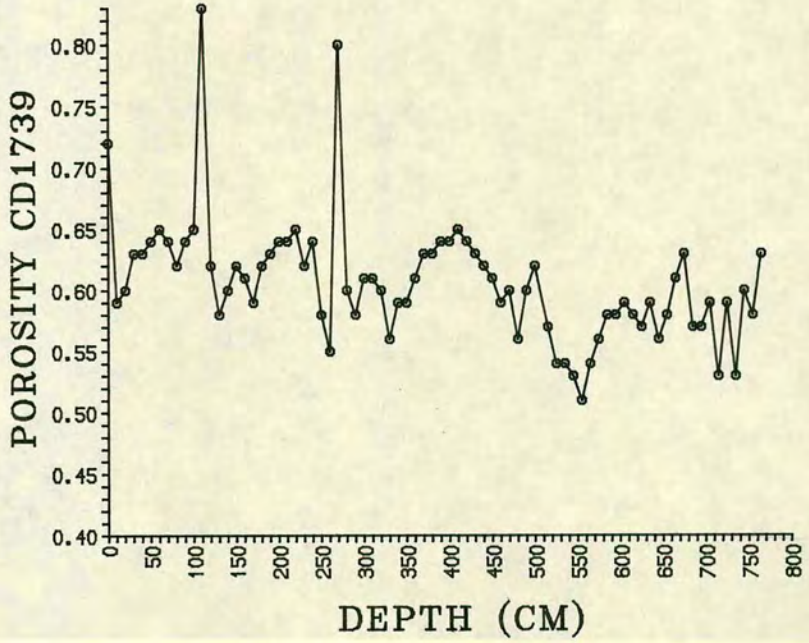

FIGURE 3.3 POROSITY CHANGES WITH DEPTH IN CORES FROM NW ARABIAN SEA

In core CD 1715 at 90cm, 130cm, 140cm and at several horizons below 500cm, water content and porosity values are anomalously low (w.c. = < 20%, porosity ~0.40) and correspond to various turbidite band of sandy texture.

If we exclude the turbidite layers in 1715 the general trend of water content and porosity in the two cores (CD 1715, CD 1730) is one of two cycles between 50 and 400cm and in 400cm to the bottom of each core with lowest water content occurring between 380cm and 430cm. It implies a subtle cyclic change in sediment texture and composition.

Water contents and porosity in cores CD 1739 and CD 1738 are considerably below those seen in CD 1715, 1730. These cores contain relatively coarse-grained sediments and the decreasing water content from 40% to 30% in the cores with depth may imply a coarsening of the grain size or changes in composition.

3.6 CHRONOSTRATIGRAPHY

The occurrence and fractionation of oxygen isotopes O^{16} and O^{18} are important parameters in the dating of deep-sea cores. When water evaporates and water vapours condensate O^{16} and O^{18} display fractionations. Since O^{16} is the lightest isotope it is fractionated relative to O^{18} in water vapours during the evaporation cycle. Transport and the consequential condensation of this water vapour as it cools towards higher latitudes allows for the precipitation of the heavier isotopes leaving the residual water vapours to become progressively enriched in O^{16}. Precipitation of snow and ice at high latitudes hence will show a very significant enrichment of O^{16} relative to that of seawater, especially tropical seawater (Broecker and Van Dok, 1970).

Ice volume changes in the Pleistocene that is between glacial and interglacial episodes is to be seen in the $\delta^{18}O$*. Values of ocean water, being positive during glacial times, when much $\delta^{18}O$ is held in the ice and negative during interglacial periods when ice melts and lowers the $\delta^{18}O$ of ocean water. The amplitude of ice volume changes is reflected in the $\delta^{18}O$ values of ocean water.

Skeleton secreting organisms broadly inherit the oxygen isotope content of the waters they inhabit. Hence planktonic and benthonic foraminiferids display $\delta^{18}O$ in their carbonate tests that reflect the isotopic compositions of surface and ocean

---

$$*\delta^{18}O = \frac{(O^{18}/O^{16}) \text{ sample} - (O^{18}/O^{16}) \text{ standard}}{(O^{18}/O^{16}) \text{ standard}} \times 1000$$

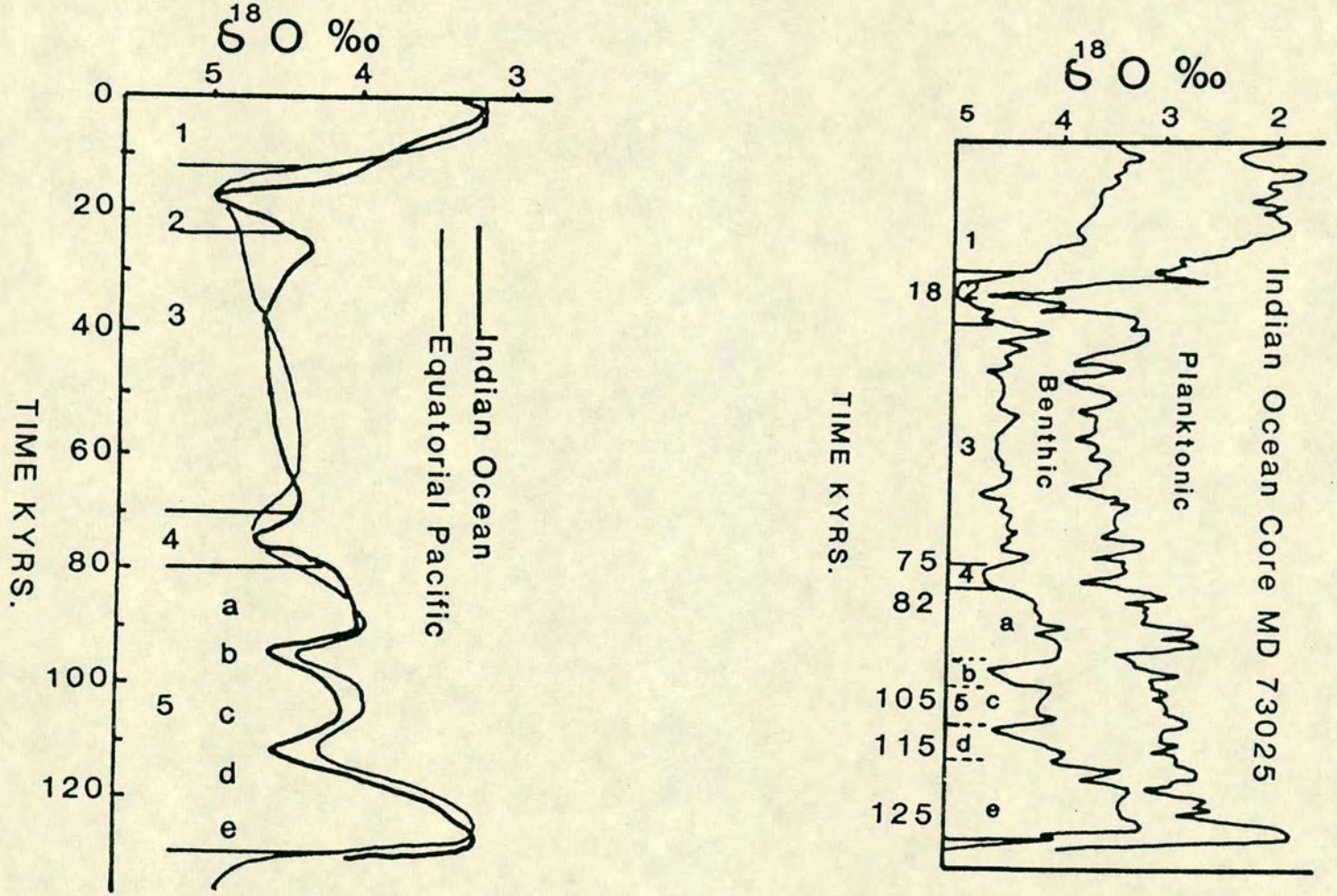

FIGURE 3.4 (a) OXYGEN ISOTOPE RECORDS FROM EQUATORIAL PACIFIC (SHACKLETON, 1977) AND SOUTHERN INDIAN OCEAN.

(b) PLANKTONIC AND BENTHIC FORAMINIFERA OXYGEN ISOTOPIC RECORD (DAANSGAARD and DUPLESSY, 1981).

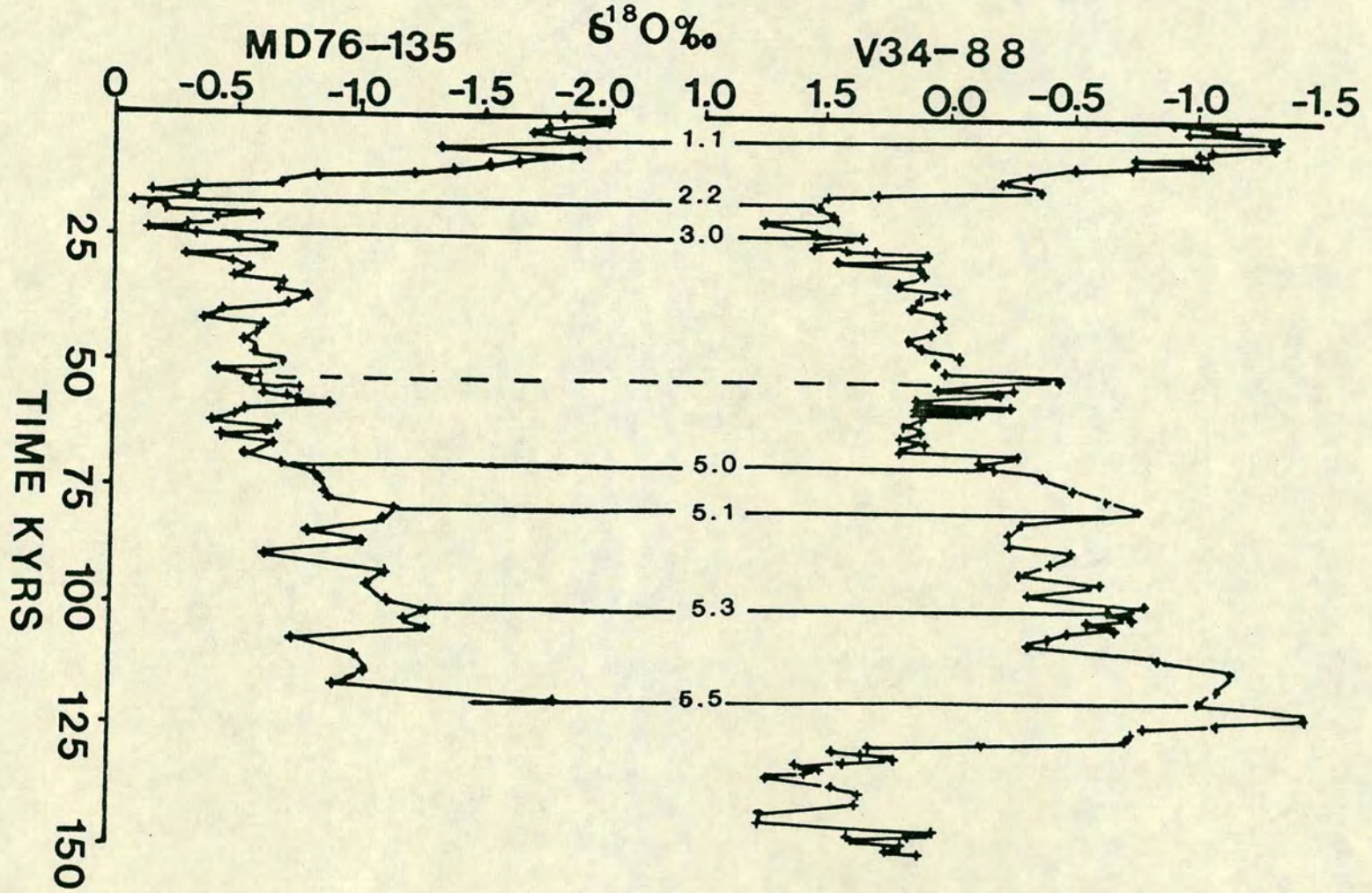

FIGURE 3.5 OXYGEN ISOTOPE STRATIGRAPHY IN ARABIAN SEA CORES. MD76-135 FROM DUPLESSY (1982) AND V34-88 FROM PRELL (1984). MD76-135 SHOWS THE $\delta^{18}O$ SIGNALS RECORDED IN G. sacculifer AND IN CORE V34-88 MEASURED IN G. rubber.

waters respectively. It is from these observations that the $\delta^{18}O$ values of specific planktonic foraminiferids in sediment cores allows for a stratigraphic framework to be established. Oxygen isotope records from sediment cores are broadly globally synchronous (Shackleton and Opdyke, 1973; Imbrie et al., 1984). Fig. 3.4 represents the isotopic record based on benthic foraminifera in sediments recovered from eastern equatorial Pacific and southern Indian Ocean. These two deep sea cores clearly indicate that changing isotopic composition of the oceans is globally consistent (Imbrie et al., 1984). Published oxygen isotope stratigraphy (Duplessy, 1982; Prell, 1984) based on different forams from separate cores collected in the NW Arabian Sea shows highly correlateable isotopic events (Fig. 3.5). This oxygen isotope record shows high negative values during the Holocene < 15kys and during the last interglacial eg. 120-127 kys.

In deep sea isotopic records, instead of glacial and interglacial terms Emliani (1955a) has designated odd and even numbers to progressive glacial and interglacial events, the Holocene has been represented by Stage 1.

3.7 DATING OF CORES

In the absence of profiles of $\delta^{18}O$ for the four cores CaCO3 stratigraphy has been used for dating sediment cores in this study. Such an approach has limitations but it has been used satisfactorily in other areas where isotope or carbon dating is unavailable (Van der Gaast et al., 1984; Lyle et al., 1988). The chronostratigraphy of published northern Arabian Sea cores is based on the oxygen isotope stratigraphy of selected planktonic foraminifera (Duplessy, 1982; Prell, 1984). For instance the isotope stratigraphy based on the analysis of G. *Sacculifer* and G. *ruber* shows trends of $\delta^{18}O$ seen in Fig. 3.5 (from Duplessy (1982) and Prell (1984)).

Given that the amplitude of $\delta^{18}O$ values is a reflection of ice volume changes, the most intense glacial episode occurs during Stage 2, while other glacial events ie. Stage 4 and 6 show only moderate intensity. Similarly while the warmest interglacial period is seen during Stage 1 (Holocene), the interglacial Stage 3 is of low intensity and considerably weaker than Stage 5. An oxygen isotope profile and the carbonate contents of a supplementary core RC-2761 (Lat. 16°38'N, Long. 59°52'E) also taken from Owen Ridge and provided by Prell (at Brown University, USA) have been used to provide means of establishing the geochronology of the piston cores to be examined in this thesis. Prell's data also includes information on the carbonate content of RC-2761. The profile of $\delta^{18}O$ for RC-2761 is shown in Fig. 3.6 and can be compared with the SPECAMP oxygen isotope record for the world oceans (Imbrie

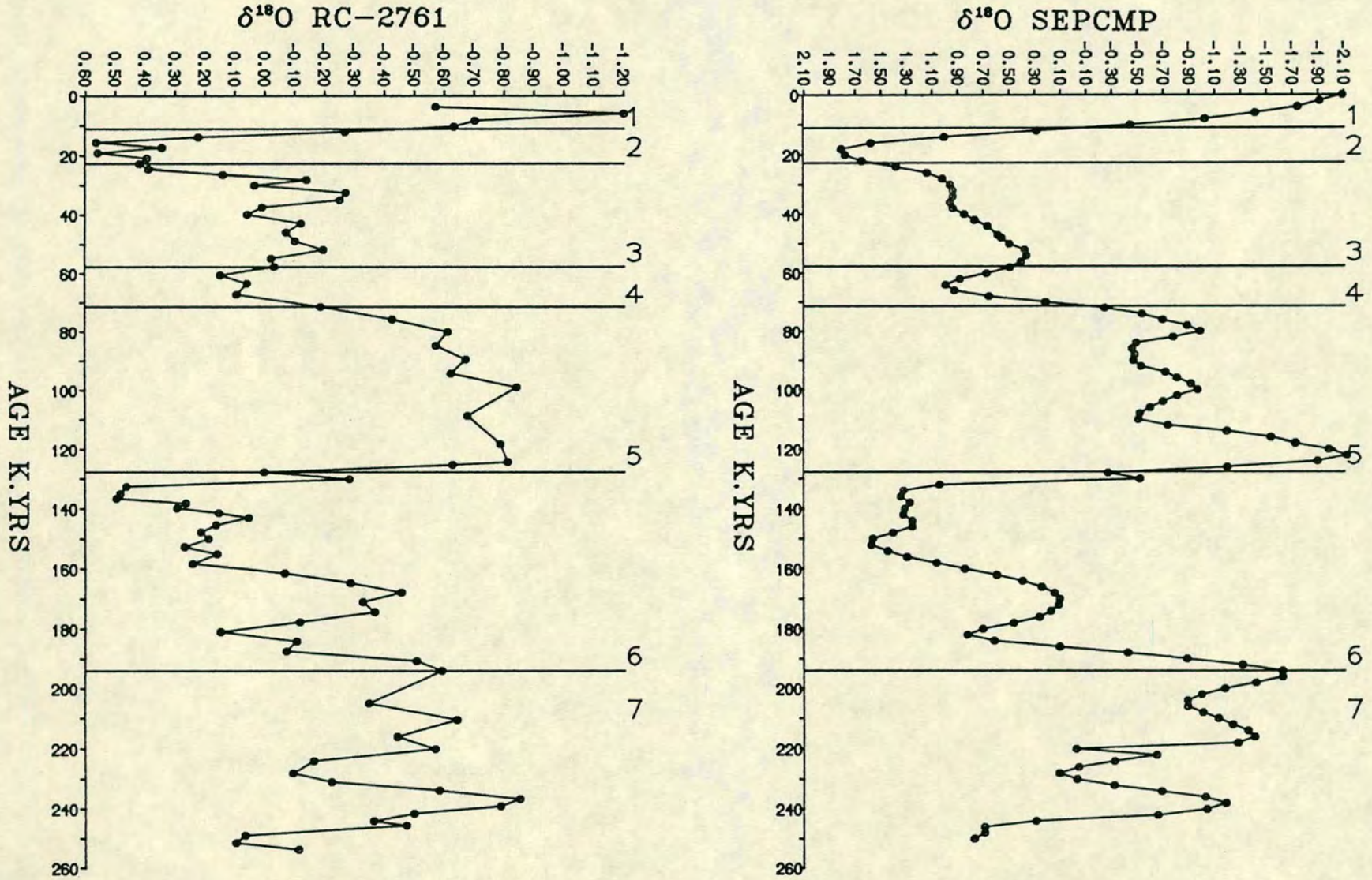

FIGURE 3.6 OXYGEN ISOTOPE RECORD IN CORE RC-2761 FROM NW ARABIAN SEA AND $\delta^{18}O$ RECORD FROM WORLD OCEAN PRODUCED BY SEPCMP (IMBRIE et al, 1984).

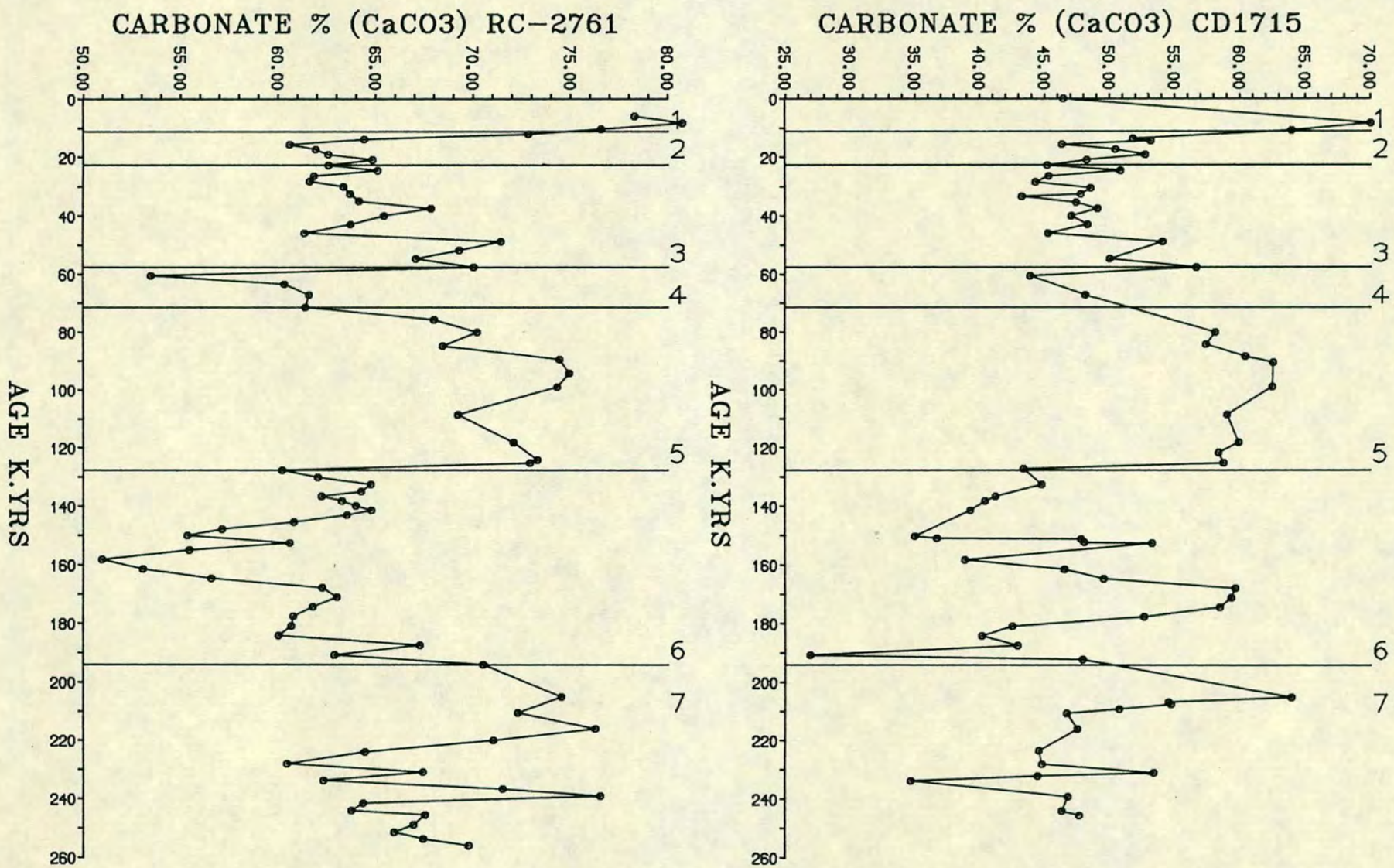

FIGURE 3.7 CARBONATE STRATIGRAPHY OF CORE RC-2761 AND ITS CORRELATION WITH CORE CD1715.

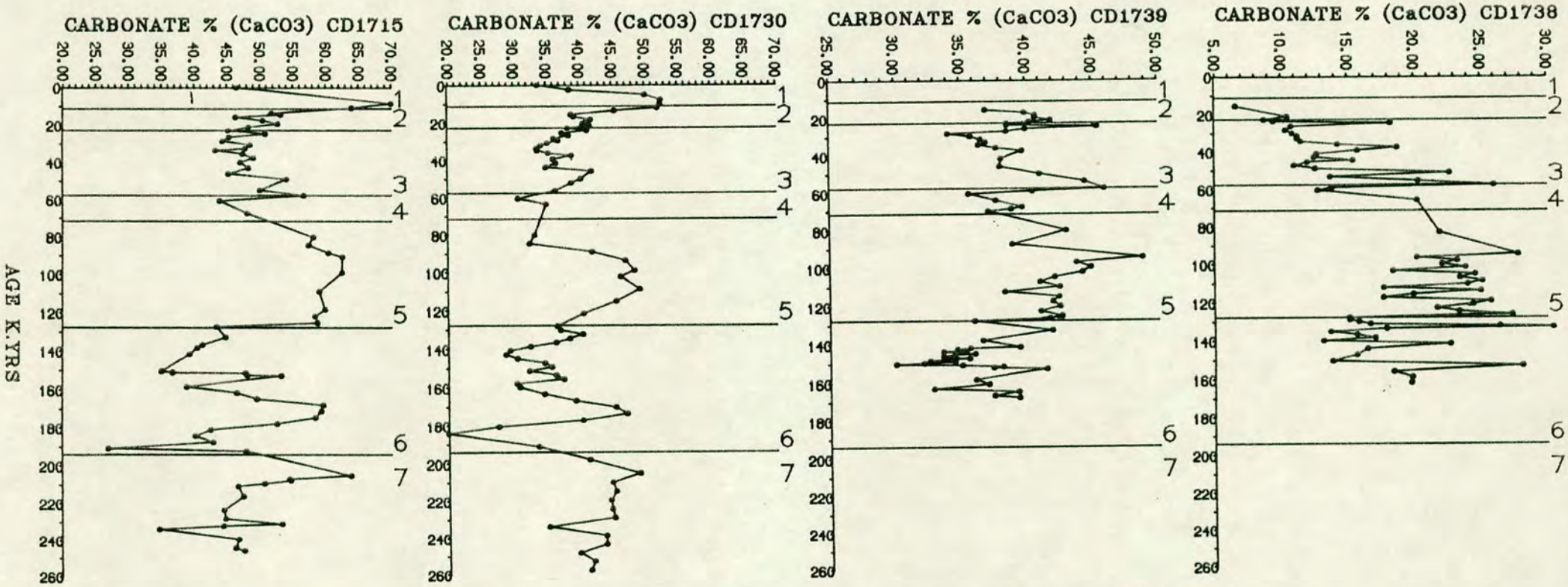

FIGURE 3.8 CARBONATE STRATIGRAPHY OF STUDIED CORES FROM NW ARABIAN SEA.

et al., 1984) to the base of Stage 7. The profiles show a very good fit and imply that there are no obvious hiatuses in accumulation of the Arabian Sea core. The $\delta^{18}O$ profile shows intense periods of ice melting during Stage 1 and 5 and a smaller melting signal during Stage 7 than as seen for SPECAMP profile. The most intense glacial events are to be seen during Stage 2 and during the uppermost Stage 6. A period of only moderate cooling is noted during Stage 4.

The calcium carbonate contents of cores CD 1715, CD 1730, CD 1738 and CD 1739 have been determined based on major element and analysis of the sediments (see chapter 5 and Appendix B and C), these contents have been corrected for dolomite in the sediments.

The profile of $CaCO_3$ for core CD 1715 has been fitted against the chronostratigraphic $CaCO_3$ profile of RC-2761 (Fig. 3.7). An extremely good fit is obtained extending to the base of Stage 7. The fit appears to be better in the young isotope stage 1-5 than below 6. Overall higher carbonate content occurs during interglacial events than glacial events. Highest carbonate occurs during the early-middle Holocene, while the surface sediments do not show well defined patterns. It is likely that the surface sediments at site CD 1715 are not represented in this piston core. In piston core CD 1730 about 10cm thick red/brown sediments were recovered at the top of core suggest that top surface sediments in core CD 1715 have been lost during coring.

On the basis of the $CaCO_3$ profiles, a reliable chronostratigraphic record can be determined for core CD 1715 and this has been extended to date core CD 1730, CD 1738 and CD 1739. Fig. 3.8 shows these profile of $CaCO_3$ for core CD 1715 and those of core CD 1730, CD 1739 and CD 1738. There is a pronounced similarity in the shape of $CaCO_3$ profiles of the four cores. However, the considerably lower $CaCO_3$ contents of CD 1739 and especially CD 1738 does hinder attempts to correlate the cores. Correlation of $CaCO_3$ content highs and lows of the four cores shows that both the more southern cores ie. CD 1715 and CD 1730 display a record of accumulation extending to ~250kys, while the northern cores which are likely to have greater terrigenous contribution, are tentatively dated to ~150kys. Unfortunately Holocene sediments of core CD 1739 and CD 1738 are largely missing, which may be due to poor piston core recovery of the surface sediments rather than non-accumulation.

CHAPTER 4

MINERALOGY OF THE SEDIMENTS

4.1 INTRODUCTION

The results of a mineralogical study of the cores from the Arabian Sea are discussed here. As the chemistry of the sediment is largely controlled by its mineralogy, this study provides the primary framework of spatial and temporal variation in the chemistry of the sediments of the Arabian Sea. Semi quantitative studies of the mineral from XRD analysis have been made using bulk sediments as well as carbonate free sediments. The methodology and instrument conditions for these analyses are given in Appendix A.1 and C.2. Essentially the mineralogical assessments are based on ratios of peak intensities to provide information on the relative changes of minerals during the late Pleistocene. The published work on the mineralogy of the surface sediments of the Northern Arabian Sea is of limited geographical extent, and does not describe the mineralogical changes down the cores over the past 250 kys.

4.2 MINERAL IDENTIFICATION

The minerals observed in this study include quartz, chlorite, illite, mixed layer clays, feldspar and dolomite (Fig. 4.1). Trace amounts of Palygorskite have also been identified. Kaolinite does not appear to be present in these sediments. This is confirmed by the persistence and retention of 7A° for chlorite after heating at 600°C. Most especially the clay minerals have been identified from their characteristic basal reflections.

4.3 CLAY MINERALS

Chlorite:- Chlorite is recognised by its 14.0, 7.0, 4.7 and 3.54A° sequence of basal reflections, although the latter reflection (3.54A° (004)) is interfered by quartz. However, as other clay minerals also have coincident reflections eg. 14.0A° montmorillonite and 3.55A° muscovite these cannot all be considered unequivocal measures of relative chlorite content. As kaolinite was confirmed to be absent, the 7A° peak here is defined as a measure for chlorite.

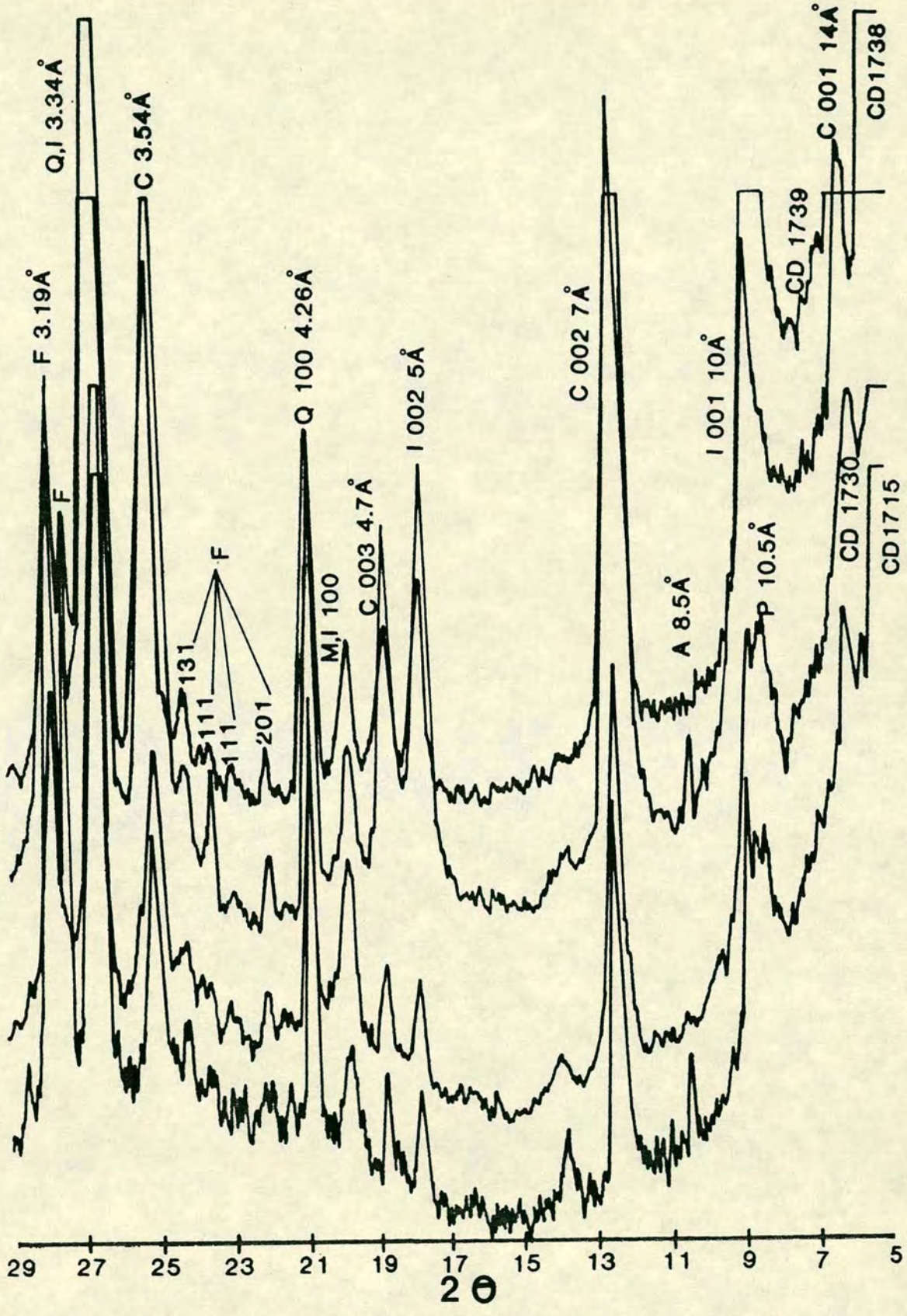

FIGURE 4.1 DIFFRACTOGRAMS OF CARBONATE FREE SEDIMENT SAMPLES FROM TOP SURFACE OF EACH CORES.

A= Amphibole, C= Chlorite, F= Feldspar, I= Illite, M= Muscovite, P= Palygorskite, Q= Quartz.

Illite:- The basal peaks at 10.0, 5.0, 3.3A° are herein defined as illite (mica). With the exclusion of 10A° (001) and 5A° (002) peaks most illite reflections coincide with other minerals. The 5A° peak intensity has been adopted as a measure of illite (mica) firstly because it is of the same order of intensity as the other clay mineral reflections and so provides more manageable clay mineral intensity ratios and secondly it is not so prone to changes of peak intensity caused by crystallographic changes as is seen in the 10A° reflection.

Mixed-layers clays:- Mixed layers clays probably consist of interlayered illite (mica) and chlorite and possibly illite/montmorillonite, which has been previously recorded in these sediments (Sirocko and Sarnthein, 1988).

Palygorskite:- A relatively small, broad diffuse to sharp reflection at 10.5A° occurs in some cores and overlaps with mica (10.0A°) (Fig. 4.1). This has been identified as palygorskite ($MgAl_5Si_8O_{20}(OH_2)_3.H_2O$). Occurrence of palygorskite in the Arabian Sea sediments has been reported (Kolla et al. 1977; Sirocko and Sarnthein, 1988). Sirocko and Sarnthein (1988) have not been able to quantitatively express the 10.5A° reflection as a measure of palygorskite because of the overlap with mica, and instead have used the 6.4A° reflection to measure its content in the sediments. However this reflection is interfered by feldspars (6.4A°), and hence no semiquantitative estimate of the mineral has been made.

4.4 NON-CLAY MINERALS

Quartz, dolomite and calcite are the most important non-clay minerals present.

Quartz:- Quartz is probably the most abundant mineral. Reflections at 4.26A° and 3.54A° correspond to the (100) and (101) peaks. The reflection at 3.34A° is coincident with a weak (003) illite peak and while former being the most intense reflection it is often too sensitive to measure as its intensity is often offscale. For this reason and following Biscay (1965), the 4.26A° peak intensity was used as the relative measure of quartz abundance.

Feldspar:- The characteristic sharp peaks at 3.19A° (28.04° 2Θ) and a less intense 4.04A° (21.98° 2Θ) reflection indicated the presence of feldspar. The 3.19A° peak represents total feldspar (Heath, 1969) and the 4.04A° peak indicates plagioclase (Peterson and Goldberg, 1962; Heath, 1969). The peak intensity at 3.19A° has been employed as a measure of feldspar content.

Amphibole:- The only selected mineral recognised is amphibole which occurs as a very weak reflection at (8.5A°) 10.42° 2Θ. This peak was not measured in the cores as it is thought that amphiboles are quantitatively unimportant in these sediments.

4.5 CARBONATE MINERALS

In the bulk sediments the carbonate minerals identified between 29.0° and 31.0° 2Θ are calcite and dolomite (Fig. 4.2). Calcite occurs as a sharp very strong peak at 29.4°2Θ (3.0°A) and is abundant in the sediments, while a peak identified at 31.0°2Θ (2.88 A°) as dolomite has similar characteristic reflection. In cores CD 1739, CD 1738 these reflections, especially that of dolomite, appear to be suppressed partially as a result of higher mass absorption of the sediment caused by higher clay contents (60-70%).

The calcite distribution will be dealt with in later chapters, the dolomite however, is being reported here because it appears as an important detrital mineral in these sediments.

Owing to the inherent problems in using the XRD method for the measurement of dolomite and calcite abundances (Tennant and Berger, 1957; Weber and Smith, 1961; Bromberger and Hayes, 1956; Royse, Weddell and Peterson, 1971; Lumsden, 1979), reliable estimates of both minerals are obtained by the chemistry. However, attempts have been made to measure the dolomite content in sediments using a calibration curve based on peak intensity measurements of calcite (3.0A°) and dolomite (2.88A°) (Equation 1) in a series of prepared standard mixes in a medium containing 40% clay:

Peak intensity Ratio = 2.88A° (Dol) I/(Dol) I 2.88A° + (Calcite) I 3.0 A°

The peak intensity ratio obtained from the above relationship is plotted against the content of dolomite in the standard mixes is shown in Fig. 4.3 and is employed as a calibration curve for unknown samples. It appears that above 5% dolomite, analytical precision is good but its determination appreciably below this

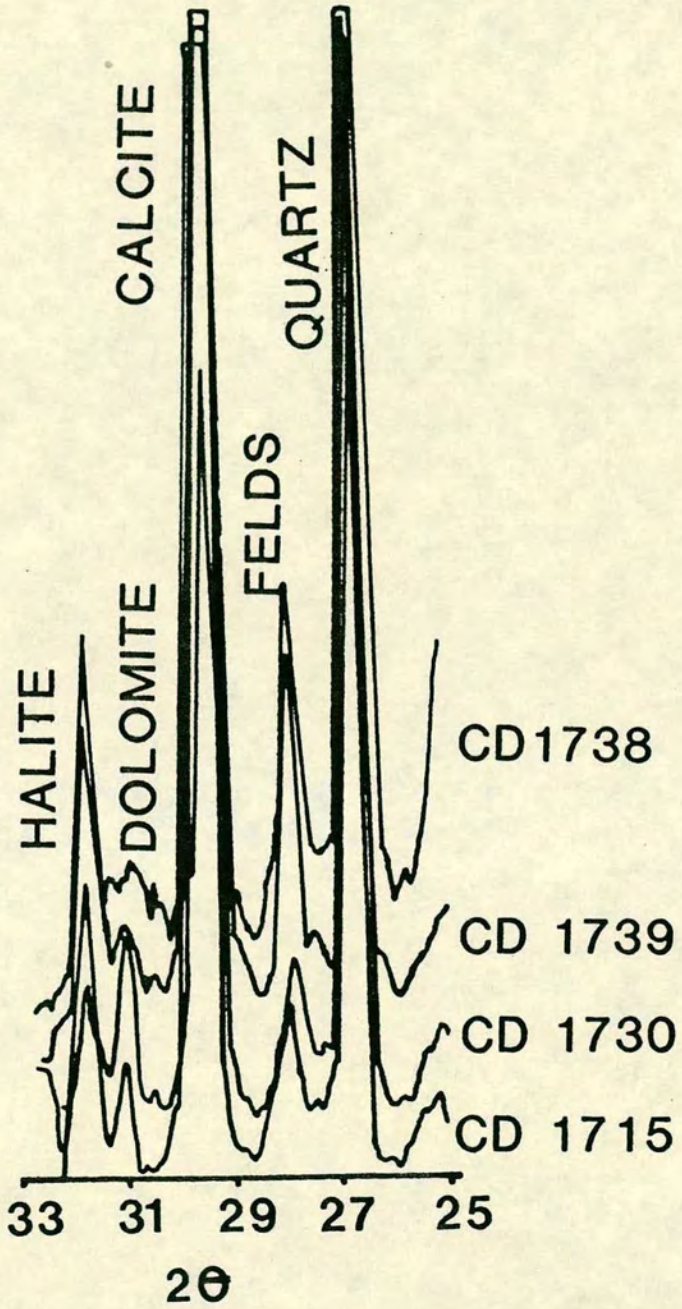

FIGURE 4.2 X-RAY DIFFRACTOMETER TRACING OF BULK SEDIMENT SAMPLES OF CORES FROM NW ARABIAN SEA. SEE CALCITE PEAK AT 29.4° 2θ AND DOLOMITE AT 31.0° 2θ.

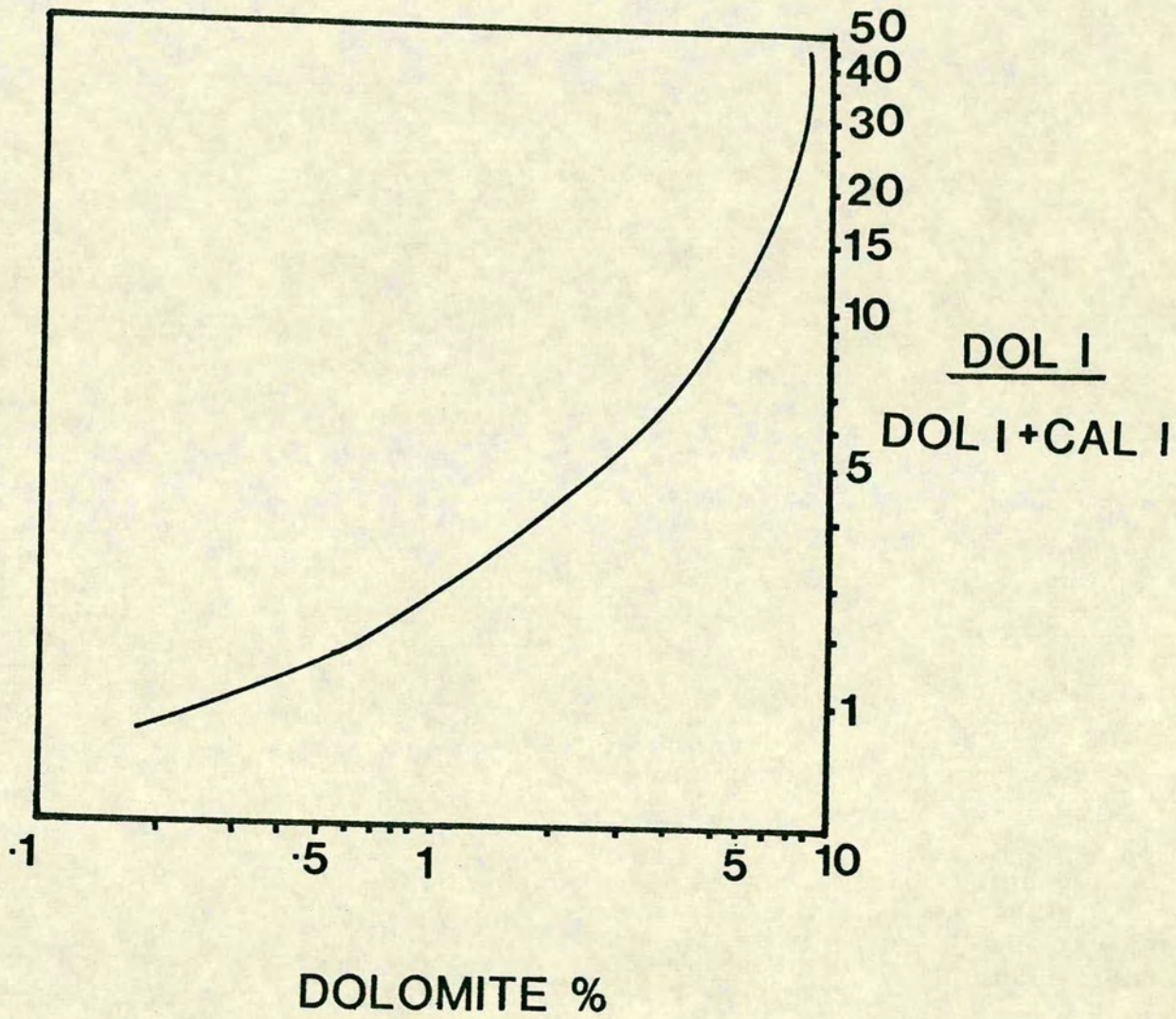

FIGURE 4.3 CALIBRATION CURVE FOR DETERMINATION OF DOLOMITE IN SEDIMENTS.

level. Nevertheless, the trends of dolomite down the cores 1715, 1730 obtained from either chemistry or XRD are broadly similar (Figs. 4.4 and 4.5). Estimates of the dolomite content in cores CD 1738, CD 1739 are less reliable. Due to the lower contents of dolomite in these cores the XRD assessment is found to have considerable error. Further, given the higher content of ferromagnesian clays in cores CD 1738 and CD 1739, the estimation of dolomite contents from the chemical composition of the sediments is also prone to unreasonable errors.

4.6 AREAL AND TEMPORAL VARIATIONS IN MINERALOGY

The four cores from the northwestern Arabian Sea show a marked variation in mineralogy over space and time. An attempt will be made to consider the areal pattern of the Holocene based on the mean analysis of Stage 1 sediments from cores CD 1715 and CD 1730 and the individual samples representing basal Holocene for CD 1739 and CD 1738. The mineralogy of the Pleistocene sediments will then be assessed and compared with surface trends from this and published studies. Turbidite layers in the Pleistocene of core CD 1715 have been omitted for this appraisal. The mineralogical variations have been assessed in terms of Quartz/Feldspar, Quartz/Illite, Quartz/Chlorite, Feldspar/Quartz, Feldspar/Chlorite peak intensity ratios and dolomite contents are measured by XRD.

Profiles of the ratios of mineral peaks are plotted in Figs. 4.6 to Figs. 4.9. The average peak ratio for Holocene and different isotopic stages in each core is given in Tables 4.1 and 4.2. The percentage of quartz calculated from the total Si content (see chapter 8) and dolomite content (carbonate free basis) calculated from the chemical composition have also been compared with the published estimates of their abundance in sediments of the Holocene and of the last glacial maximum (18,000 years BP) (Kolla and Biscay, 1977 and Sirocko and Sarnthein, 1988). The results obtained for quartz and dolomite at these times are very similar to those quoted by Kolla and Biscay (1977) and Sirocko and Sarnthein (1988). The slightly lower quartz percentages in this study are probably due to different methodology used here, which is based on the Si content of biogenic Si-free sediment not the total Si content.

Most quartz grains and all the silt size dolomite in the Arabian Sea sediments have been identified as wind blown material (Stewart et al. 1965; Kolla and Biscay, 1977 and Sirocko and Sarnthein, 1988). High percentages of these minerals in the sediments reflect contribution from the surrounding continents, and their distribution in the sediments shows the effectiveness of low tropospheric and high stratospheric

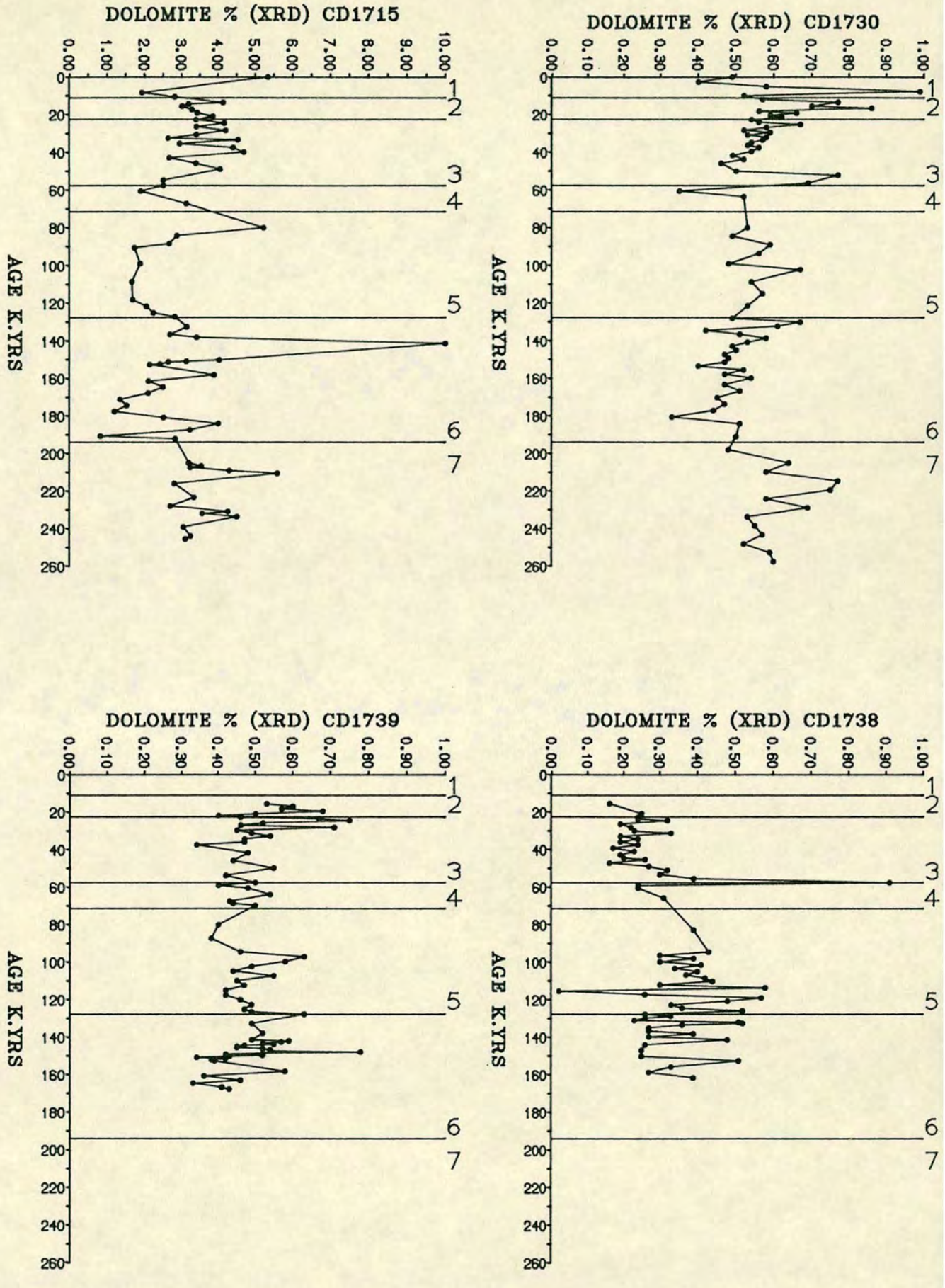

FIGURE 4.4 PROFILES OF DOLOMITE CONTENTS OBTAINED FROM XRD METHOD.

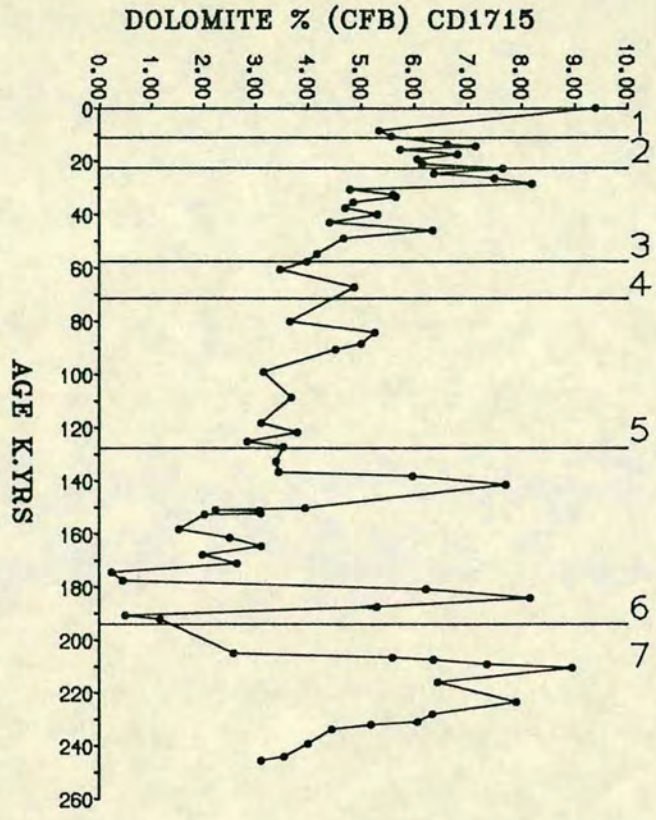

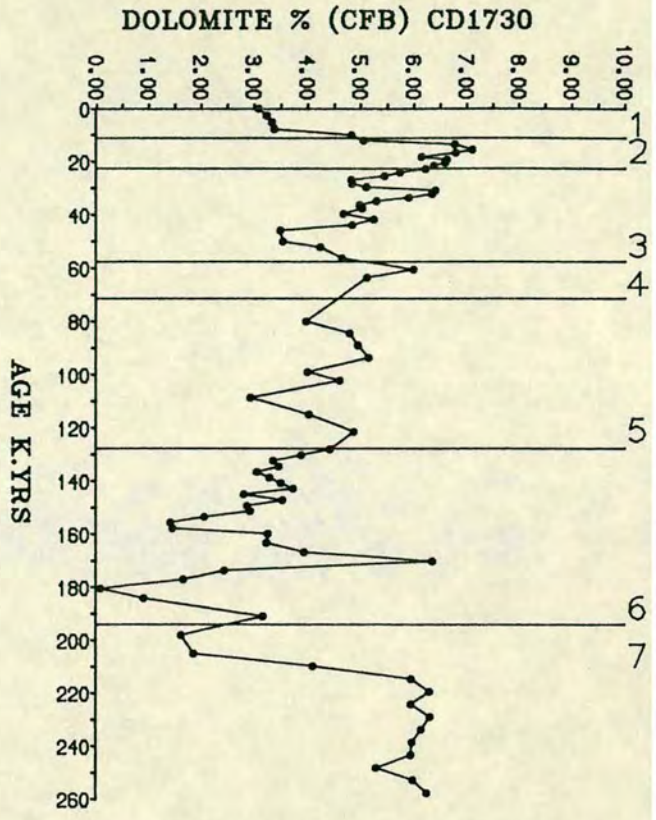

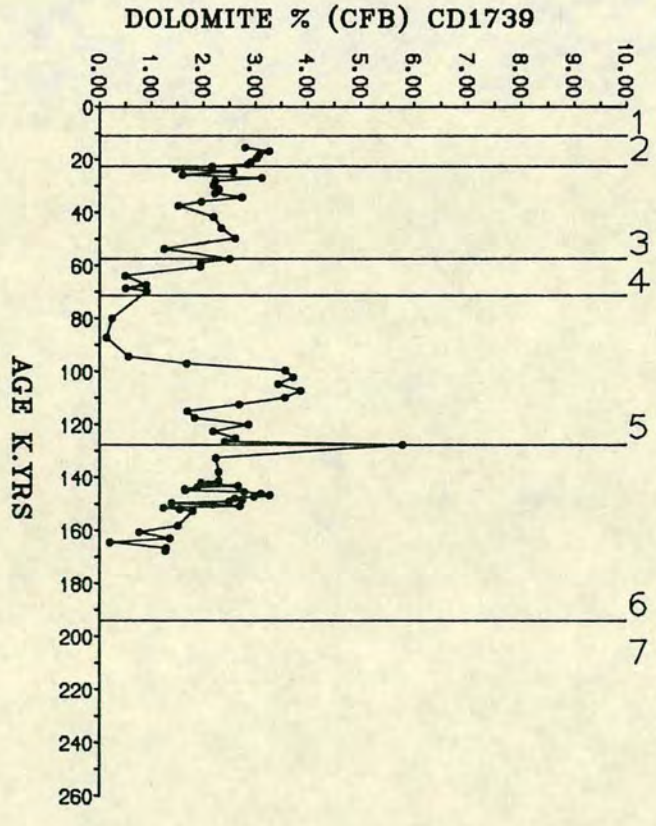

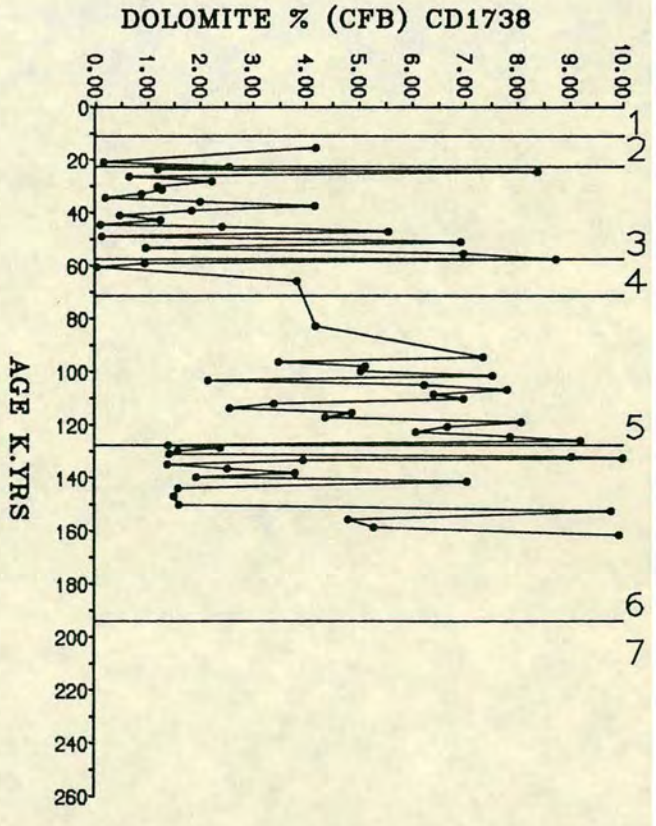

FIGURE 4.5 DOLOMITE CONTENTS CALCULATED FROM THE CHEMISTRY OF SEDIMENTS.

Table 4.1 Quartz and Dolomite contents in Holocene and last glacial maximum

	HOLOCENE (0-10,000 years B.P)		LAST GLACIAL MAXIMUM (18,000 years B.P)	
	Quartz %	Dolomite %	Quartz %	Dolomite %
Present Study				
CD 1715	5.0	6.75	4.5	6.44
CD 1730	2.5	3.55	4.0	6.13
CD 1739	4.5	3.21*	5.5	2.79*
CD 1738	5.0	1.54*	6.0	3.26*
Sirocko and Sarnthein 1988	8.0	5.0	-	-
Kolla and Biscay 1977	5-10	-	9.0	-

* Dolomite contents quoted here for cores CD 1739 and CD1738 (based on chemical composition) could be subject to considerable error.

Table 4.2 Dolomite contents and XRD minerals peak ratio in different climatic stages of studied cores

Core #	Stage	Dolomite % CFB	Qtz(I)/Fld(I)	Fld(I)/Chl(I)	Qtz(I)/Chl(I)	Qtz(I)/Ill(I)
	1	6.75	0.74	1.02	1.0	2.32
	2	6.44	0.82	1.70	1.33	3.55
	3	5.45	0.71	2.02	1.29	3.63
CD 1715	4	4.09	0.55	2.65	1.42	4.09
	5	4.02	0.78	1.75	1.27	4.0
	6	3.26	0.97	1.53	1.38	4.28
	7	5.44	1.05	1.06	1.32	4.42
	1	3.55	0.98	0.75	0.75	3.2
	2	6.13	1.17	1.31	1.59	5.18
	3	4.7	1.14	1.58	1.55	5.58
CD 1730	4	4.84	1.02	2.6	2.75	7.1
	5	4.3	1.04	1.96	2.26	6.92
	6	3.0	1.11	1.96	1.37	3.83
	7	5.0	1.15	1.63	1.81	5.0
	2	2.79	2.34	0.26	0.77	2.66
	3	2.19	2.38	0.47	1.12	3.60
CD 1739	4	1.34	2.61	0.48	1.23	3.21
	5	2.52	2.03	0.53	1.18	2.82
	6	2.12	2.16	0.30	0.71	2.23
	2	3.26	1.32	0.51	0.64	2.41
	3	2.95	1.64	0.33	0.52	1.73
CD 1738	4	2.83	1.74	0.33	0.53	1.66
	5	5.33	1.32	0.77	0.83	2.99
	6	4.25	1.21	0.83	2.00	3.02

Note: CFB = carbonate free basis.

winds in this area. The recent studies (Sirocko and Sarnthein, 1988) using both sediments and satellite records indicate that main source regions lie in Arabia and Mesopotamia, and that northwesterly winds dominate the dust trajectories. This study and that of Sirocko and Sarnthein (1988) shows that quartz, dolomite and chlorite are the dominant components of the North Arabian Sea sediments of Holocene age.

Table 4.1 shows that there is some variation in this supply from core to core. The quartz content is small in core CD 1730 showing approximately half the content of the other cores. The trend in dolomite is more obvious, its content appears to decrease northward from 6.75% in core CD 1715 through CD 1730 (3.55%) and CD 1739 (2.39%) to a low value of 1.54% in core CD 1738. The Qtz(I)/Fld(I) and Qtz(I)/Chl(I) ratios also show a significant areal trend in Holocene (Stage 1) sediments (Table 4.2). Qtz(I)/Fld(I) ratio increases from low Holocene values in core CD 1715 and CD 1730 (0.74 and 0.98) to high values in cores CD 1738, CD 1739 (1.21 and 2.0 respectively) while Qtz(I)/Chl(I) ratio decreases from 1.0 in CD 1715 to 0.51 in core CD 1738. Such trends may signify that detrital supply comes from more than one source. The higher quartz content relative to feldspar and higher chlorite content relative to quartz and feldspar in cores CD 1739 and CD 1738 (see Tables 4.2) may indicate that sediments in these cores are rich in chlorite and quartz. Further, the impoverished content of dolomite, but higher chlorite contents in the sediments from the Gulf of Oman as noted by Sirocko and Sarnthein (1988) are thought by them to be linked with a provenance of Persian Gulf outflow waters and rivers from Makran to the northeast. In contrast, Holocene sediments of cores CD 1715, CD 1730 show much higher dolomite and were probably transported here by northwesterly winds crossing the Oman because similar mineralogical compositions of the cores are noted by Sirocko and Sarnthein (1988) in this area.

Down core variation in mineralogy is most likely controlled by the climatic fluctuation as suggested by Kolla and Biscay (1977). He has shown that at about 18,000 years BP a marked increase in quartz from 5% to 9.0% (Table 4.1) is linked with the increased aridity of the climate during the last glacial maximum. Similarly around 9,000 years ago he noted a decrease in the quartz percentage to 6%, and suggested this was a result of a short humid period.

In Table 4.1 and Fig. 4.6 to Fig. 4.9 such a pattern during the last glacial maximum period (18,000 years ago) and 9,000 years ago is clearly seen by decrease in different mineral peak ratios around 10,000 years and increase at 18,000 years ago. Therefore it can be assumed that the variation in the mineralogy of cores from the Arabian Sea not only reflects different source areas, but also shows trends that seem to be related to changes in the climatic conditions.

4.6:1 Temporal trends in dolomite

The dolomite content, calculated on a carbonate free basis for the four cores has been calculated from the Mg content of the sediments (see Appendix B.3). These calculations have been made because of the poor precision of dolomite measurements by XRD for sediments containing <5% dolomite. Even so, the overall trends of dolomite content seen in Fig. 4.5 expressed from the composition of the sediments, are also seen in the XRD measurements (Fig. 4.4). The content of dolomite in cores CD 1715 and CD 1730 are similar and reach maximum values of ~8.0%. These cores show significantly higher values than are seen in cores CD 1739 and CD 1738 where highest dolomite horizons rarely exceed 4% and 3% respectively. Temporal patterns of change in dolomite in cores CD 1715 and CD 1730 are very similar and show high contents for much of Stage 7. However, towards the top of Stage 7 and especially at the base of Stage 6, minimal dolomite values occur. Both cores show a well defined increase in dolomite content from this latter position to the top of Stage 2.

In the Holocene there is some evidence of a fall in dolomite content in these cores. The pattern of dolomite variation in core CD 1739 is not so well defined. Dolomite appears as two cycles from the Stage 6 to mid Stage 5 and from mid Stage 5 to Stage 2, where dolomite contents tend to increase. The trend of dolomite in CD 1738 is probably unreliable given the high content of ferromagnesian silicates in these sediments. However XRD analyses of dolomite confirms that its content in these sediments is significantly lower than that in CD 1715 and CD 1730.

4.6:2 Quartz/Feldspar

The trends of the ratios of quartz (4.02A°) peak intensities to feldspar (3.19A°) peak intensities are shown in Fig. 4.6. The overall trend of quartz/feldspar intensity ratios shows a progressive increase from CD 1715 through CD 1730, CD 1738 to CD 1739. The latter two cores show much higher values especially in certain horizons in CD 1739 where intensity ratios show values that exceed 5.0. The relative sensitivities of the diffraction intensity peaks are not known, hence this ratio does not represent content ratios. There is a similarity in the pattern of Qtz(I)/Fld(I) ratios with time for cores CD 1715 and CD 1730 in that high ratios are seen during Stage 7; low ratios seen at the base of Stage 6. Highest ratios occur in Stage 2, while significantly lower values are to be found in Holocene sediments. These overall

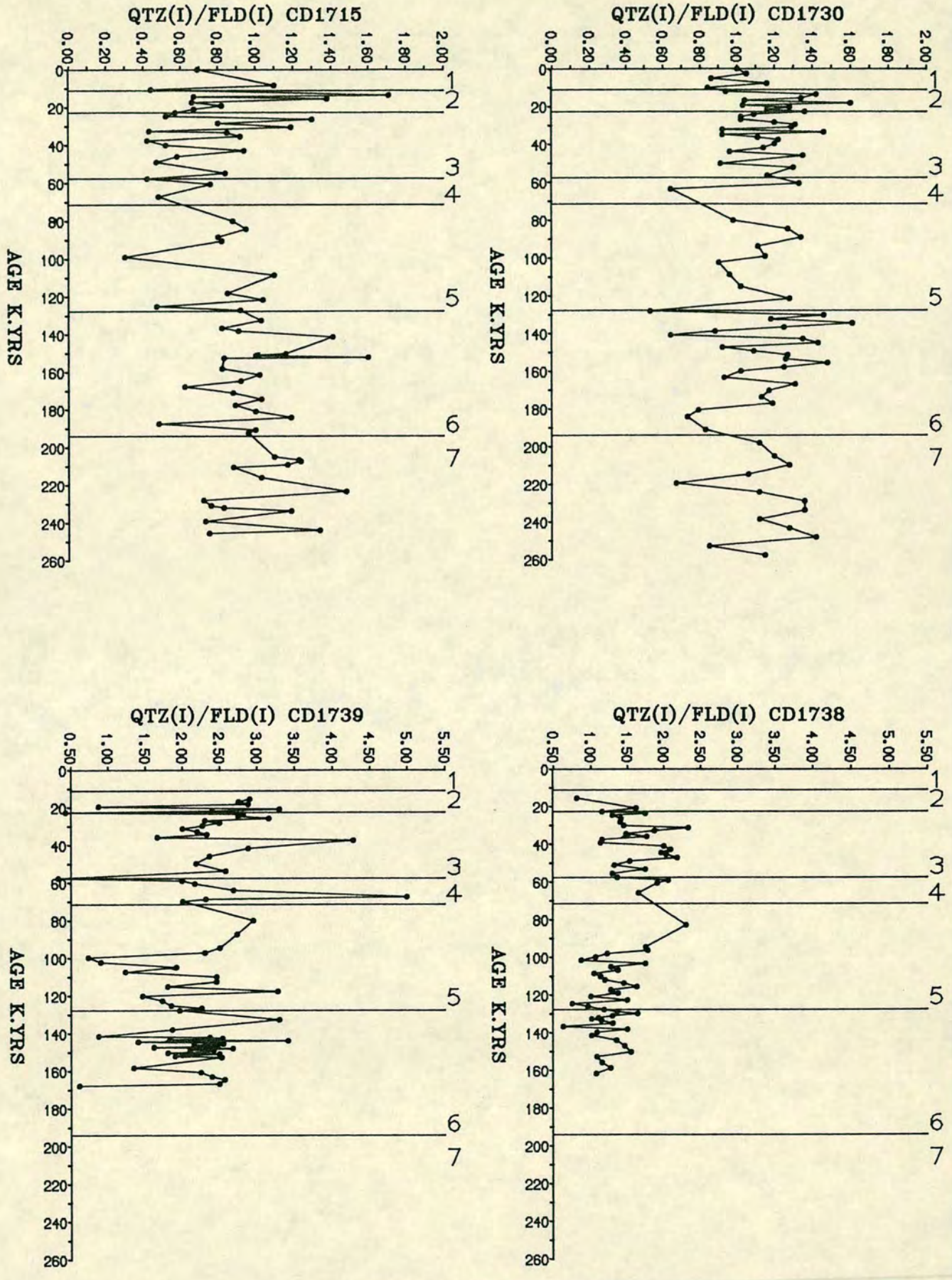

FIGURE 4.6 THE TRENDS OF QUARTZ (4.02A°)I/FELDSPAR (3.19A°)I RATIOS IN CORES FROM NW ARABIAN SEA.

trends are similar, but seem more attenuated than those of dolomite described above. For instance, the increase seen in dolomite in core CD 1715 between Stage 6 and 2 is not seen in Qtz(I)/Fld(I) ratios and is very small in CD 1730. In core CD 1738 there is no obvious trend with time although the younger section of the core (< 100 Kys) shows somewhat higher Quartz/Feldspar ratios. Such a trend also occurs in core CD 1739. The very high Qtz(I)/Fld(I) intensity ratios in this core reflect an important and local source of quartz relative to feldspar in these sediments, and the very high values in some horizons could signify aeolian dust storm events.

4.6:3 Quartz/Chlorite/Illite

The Qtz/Chl peak intensity ratios shown in Fig. 4.7 show very different trends in the four cores. The trend in core CD 1730 has certain similarities with the dolomite content and quartz/feldspar ratio trends in that they show high ratios at the base of the core (Stage 7) (Table 4.2), low ratio in Stage 6 and an increase in younger sediments except for the Holocene where ratios are low. Unlike dolomite and the Qtz(I)/Fld(I) ratio (Fig. 4.4), which show maximal values during Stage 2, the Qtz(I)/Chl(I) ratio is highest in Stage 4 (ie. 2.75 (Table 4.2)). Core 1730 shows by far the highest ratios and are appreciably higher than CD 1715 which shows no obvious temporal trends.

The trend of Qtz(I)/Chl(I) in CD 1738 is very different from that of Qtz(I)/Fld(I). The base of the core, that is > 100 ky, shows a low Qtz(I)/Fld(I) ratio while the Qtz(I)/Chl(I) ratio is high in this section of the core. Qtz(I)/Chl(I) ratios in core CD 1739 also appear to have little relation to that of Qtz(I)/Fld(I). The trends of Quartz/Illite intensity ratios (Fig. 4.8) overall show a good correlation with Quartz/Chlorite. This is especially seen in CD 1730 and like Quartz/Chlorite, shows the highest Qtz(I)/Ill(I) ratio of the four cores (Table 4.2).

4.6:4 Feldspar/Chlorite

The Fld(I)/Chl(I) ratio shown in Fig. 4.9 denotes a similar trend as seen in Qtz(I)/Chl(I) and Qtz(I)/Ill(I) (Figs. 4.7 and 4.8). This suggests that the input of feldspar to the sediments is mostly associated with quartz especially in cores CD 1715, CD 1730 and CD 1739. The low ratio of Flds(I)/Chl(I) in cores CD 1739 and CD 1738, being less than 1.0, shows that these sediments in the north are impoverished in feldspar relative to quartz and chlorite. The southern cores CD 1715

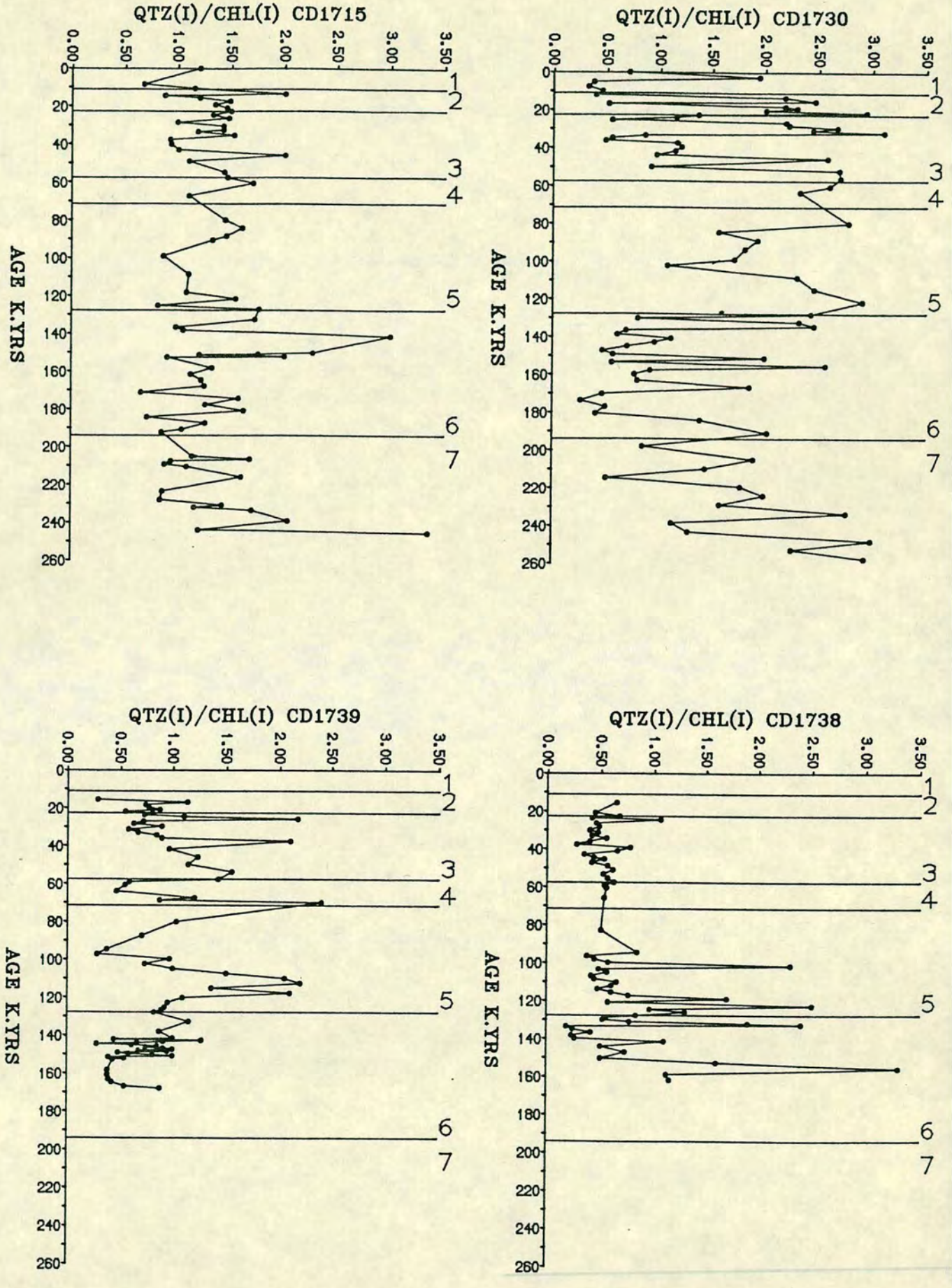

FIGURE 4.7 QUARTZ (4.02A°)I/CHLORITE (7.0A°)I RATIO PROFILES.

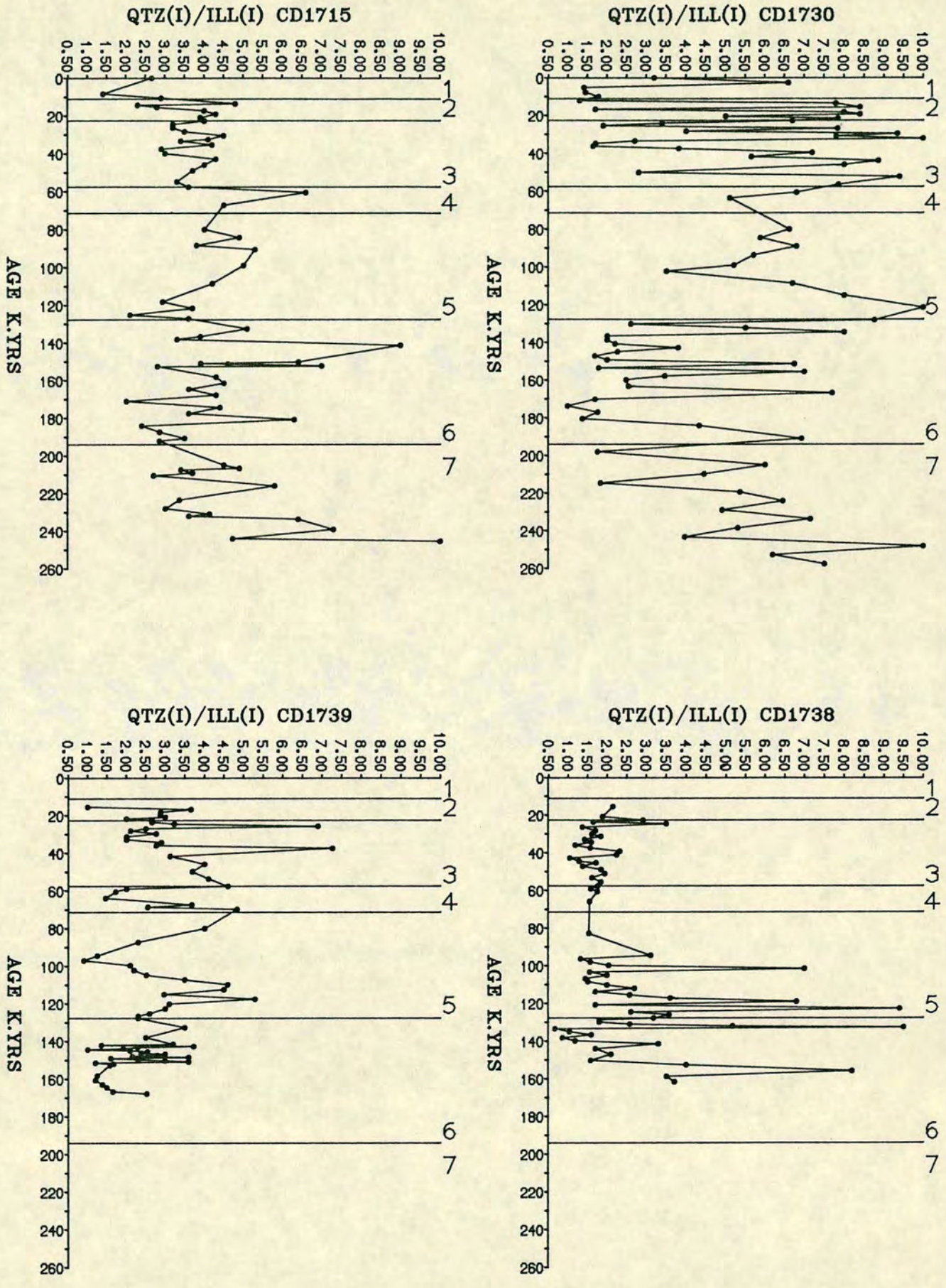

FIGURE 4.8 QUARTZ (4.02A°)I/ILLITE (5.0A°)I RATIO PROFILES.

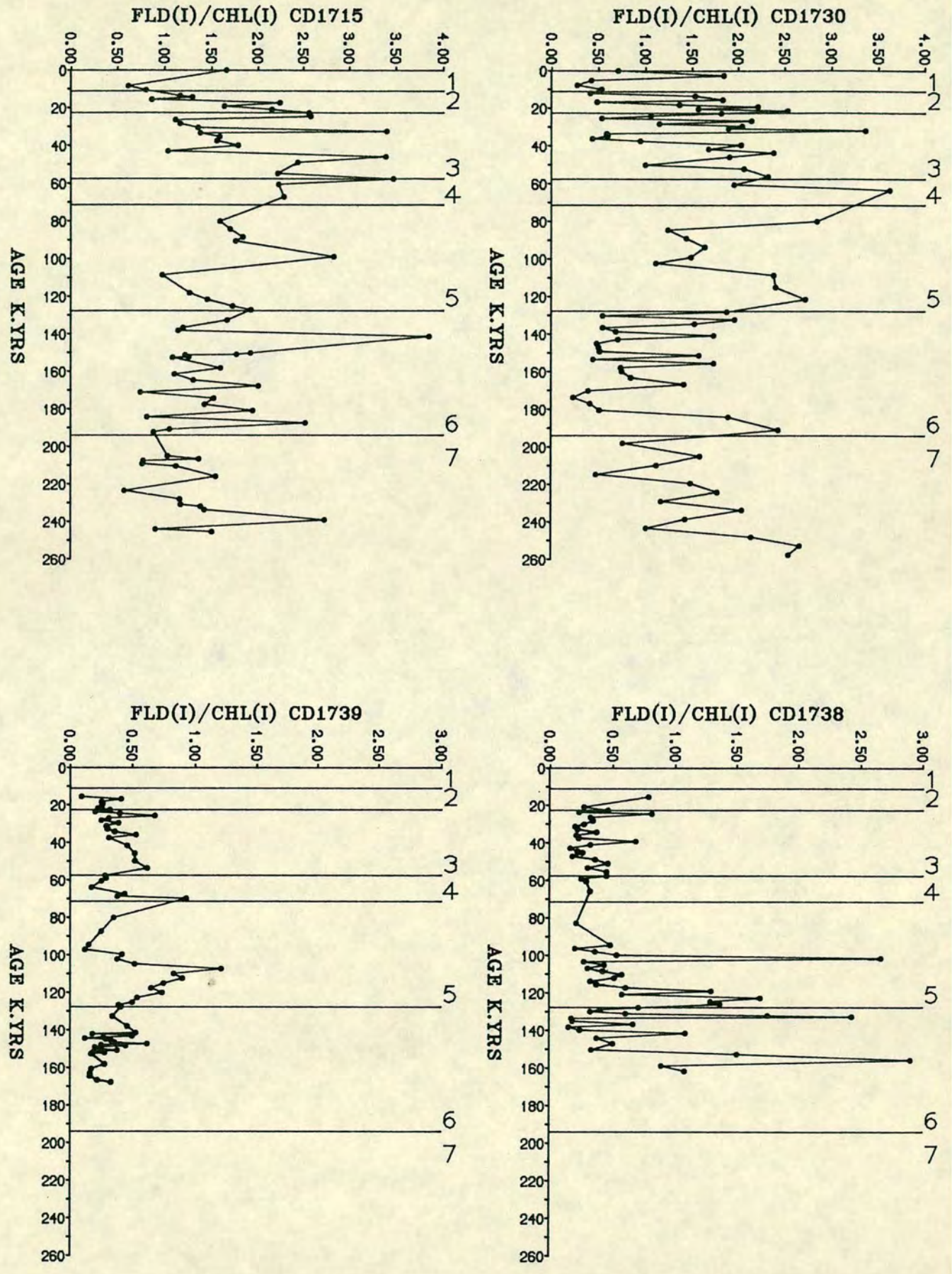

FIGURE 4.9 FELDSPAR (3.19A°)I/CHLORITE (7.0A°)I RATIO PROFILES.

and CD 1730 show high Fld(I)/Chl(I) ratios ie. ~2.0 (Table 4.2) and these ratios tend to increase especially in Stages 2, 4. Overall, this trend is consistent with profiles of Qtz(I)/Chl(I) and Qtz(I)/Ill(I) which also show an increase during Stage 2, 4. The pattern for Stages 1, 3, 5 is different, although Fld(I)/Chl(I) ratios generally show an increase at the upper and lower boundaries of Stages 3 and 5. The Stages 6 and 7 show much the same pattern as seen before in profiles of Qtz/Flds, Qtz/Chl and Qtz/Ill.

4.7 CONCLUSION

Analysis of mineral contents based on their X-ray diffraction characteristics is at best semi-quantitative and often is imprecise. Even so, the peak intensity ratios of major minerals identified in the sediments clearly show that the relative abundances of these minerals in the sediments vary from core to core and with time, and provide some indication of the spatial and temporal changes in the mineral composition of the sediments.

The four cores, based on their mineralogical affinities, can be divided into two groups. The southern cores CD 1715 and CD 1730 show overall fairly low constant quartz to feldspar intensity ratios (~1.2) suggesting a common provenance during the late Pleistocene. This source seems to be dominated by quartz and feldspar with relatively impoverished amounts of chlorite and illite as is seen by the high Qtz(I)/Ill(I) and Qtz(I)/Chl(I) ratio (Table 4.2). These cores also show a high dolomite content (~5%). In contrast the cores in the north, CD 1739 and CD 1738, are, relative to quartz, impoverished in feldspar and rich in chlorite and illite. The Qtz(I)/Fld(I) ratio in these two cores is ~2.0, except at the bottom of core CD 1738 where this ratio significantly increases. In addition the northern cores show a much lower dolomite content (2-3%) (Table 4.2). Overall these observations suggest a different source for these cores compared with the southern cores, and that the provenance may have changed with time.

In the lower sections (Stage 5 and 6) of core CD 1738 the trends of Qtz(I)/Fld(I) and Qtz(I)/Chl(I) ratios and calculated dolomite contents are broadly similar as those seen in cores CD 1730 and CD 1715. This similarity implies that until Stage 5, the source region of the cores had been the same. The high dolomite and quartz contents indicate that cores CD 1715 and CD 1730 were dominated by aeolian material. Sirocko and Sarnthein (1988), on the basis of high chlorite contents in Gulf of Oman sediments, suggested transport from the Persian Gulf and Makran margin regions. This is likely because the sediments of the Indus River, rich in

chlorite and quartz, are prevented from being transported into this basin since early Miocene because of the Murray Ridge (Jipa and Kidd, 1974). Emery (1956) discovered that feldspar in the Persian Gulf is very subordinate to quartz. Further, it seems that there is a gradient in carbonate content which decreases southwards towards the Gulf of Oman (Stoffers and Ross, 1979). Scanning Electron Microscopy of pitted quartz grains from a core in the Gulf of Oman (23°56′N, 59°14′E) led Stoffers and Ross (1979) to conclude that they had been transported by wind and also had subsequently spent time in a high energy shallow environment such as the Persian Gulf or coastal Oman. This evidence, together with high Qtz(I)/Fld(I), low Qtz(I)/Chl(I) ratio and low dolomite content in cores CD 1738 from the Gulf of Oman, support this contention that significant transport of sediments by Persian Gulf outflow waters has occurred for the last 100,000 years. Before this period in the Gulf of Oman the dominant input was aeolian from a source common to other cores. The occasional peaks in core CD 1738 showing very high ratios especially in the upper section of the core, are probably a result of dust outbreaks which are a common feature in this area (Ackermann and Cox, 1988). The similarity in trends of peak intensity ratios of different minerals shown in Figs. 4.6 to 4.9 for cores CD 1715, CD 1730 and CD 1739, indicate that their mineralogies are broadly uniform but may have slight variations in texture.

A detailed mineralogical assessment of Holocene sediments of the Northern Arabian Sea by Sirocko and Sarnthein (1988) has shown that northwesterly winds originating from the Arabian peninsula, Mesopotamian lowlands and from Iraq and Iran has been the instrument for introducing most of the lithogenic material to areas where cores CD 1715, CD 1730 and CD 1739 were collected. Such a source appears to have been dominant in the accumulation of these cores over the last 250 kyr. Kolla and Biscay (1977) have shown that at 18,000 yrs BP, the maximum glacial time, there is an increase in the quartz content of this sediment possibly due to a change in climate. The mineralogical assessment of the four cores also shows an increase in dolomite content and Qtz(I)/Fld(I) and Qtz(I)/Chl(I), Qtz(I)/Ill(I) ratios. Figs 4.5 to 4.9 show that during glacial stages 2, 4, 6, quartz and dolomite tend to increase while during interglacial stages 3, 5 there is a general decrease in these minerals. Stage 7, however, in contrast to stages 3 and 5, shows a higher quartz and dolomite loading. Quartz relative to either chlorite and/or illite is also high during glacial stages.

CHAPTER 5

GEOCHEMISTRY OF LITHOGENIC ELEMENTS

5.1 INTRODUCTION

The chemistry of major and minor elements in deep sea sediments is largely controlled by terrigenous minerals and biogenic detritus. In this chapter the geochemistry of detrital elements and their areal and temporal variations will be discussed.

In a multicomponent system, the interpretation of the geochemistry of a particular component is hindered by the dilution effects of one or the other components. Therefore, element distributions are often reported as ratios and for the terrigenous component, this is usually with respect to Al. Because Al is almost exclusively incorporated as detrital aluminosilicate, it has been used as an indicator of terrigenous input (Arrhenius, 1952; Landergren, 1964; Bostrom et al., 1969; Chester and Aston, 1976; Bischoff et al., 1979). Here the variations in the element/Al ratio have been appraised in order to interpret changes in mineralogy and texture of the sediments in the five cores described in chapter 3. The element contents of the sediments which was measured by XRF analysis (Appendix A.2), are diluted by residual sea salt. This effect is significant for several major elements, including Na, Mg, Ca and K. Contents reported in this chapter, and elsewhere in this thesis, have been corrected for the concentrations from sea salt by the method described in appendix A.3 and all data is presented on a salt free basis. The elements investigated below have been grouped and discussed separately based on their mutual relationship to Al, their interrelated geochemical nature and their origin.

5.2 GEOCHEMISTRY OF MAJOR ELEMENTS

5.2:1 Silicon

Silicon in sediments mostly occurs as quartz, aluminosilicates and biogenic silica. In areas of high productivity siliceous skeletons can make an important contribution to the total Si content of the sediments. The sediments of the northern Arabian Sea have been shown to contain high amounts of quartz, feldspar, illite, and chlorite (chapter 4). Montmorillonite has also been reported in small amounts (Stewart et al., 1965; Kolla and Biscay 1977). The positive intercept on the Si axis suggests the presence of free silica as quartz (Fig. 5.1). Cores CD 1709 and CD 1738 show intercepts of 5 and 10% silica which implies relatively higher amounts of quartz in these cores which is commensurate to the location of cores.

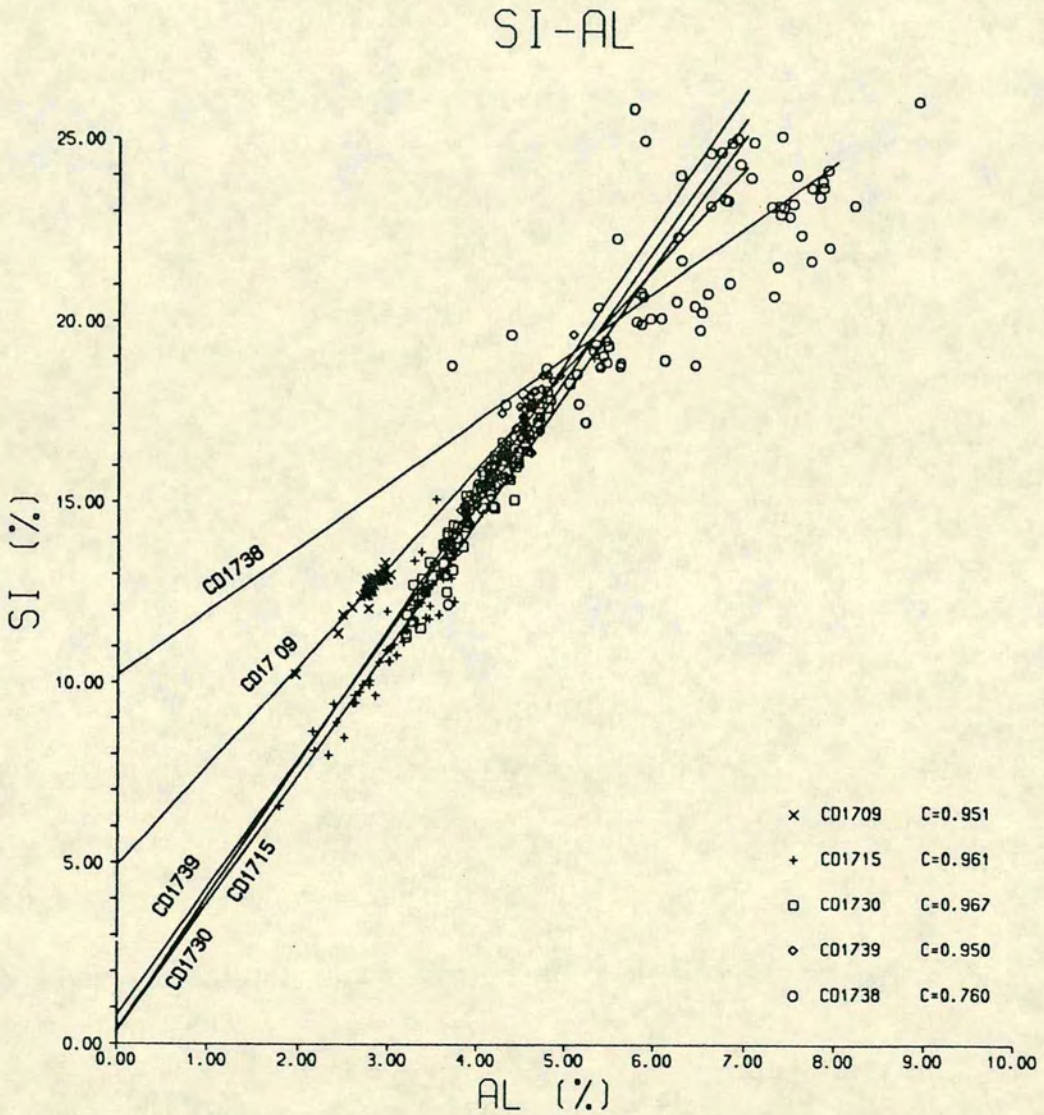

FIGURE 5.1 CORRELATION OF Si AND Al IN FIVE CORES FROM NW ARABIAN SEA.

Table 5.1 Elements/Al ratio in cores from NW Arabian Sea.

Core	Stage	Si/Al*	Fet/Al*	K/Al	Ti/Al	Cr/Al	Zr/Al
	1	3.2	0.60	0.29	0.087	0.0042	0.0027
	2	3.33	0.62	0.30	0.083	0.0035	0.0025
	3	3.35	0.63	0.32	0.089	0.0036	0.0028
CD 1715	4	3.20	0.61	0.29	0.087	0.0028	0.0025
	5	3.20	0.59	0.26	0.082	0.0027	0.0031
	6	3.28	0.60	0.31	0.088	0.0034	0.0025
	7	3.32	0.59	0.30	0.060	0.0026	0.0022
	1	3.2	0.65	0.28	0.057	0.0033	0.0025
	2	3.64	0.60	0.30	0.059	0.0035	0.0025
	3	3.67	0.59	0.30	0.061	0.0038	0.0027
CD 1730	4	3.60	0.51	0.35	0.063	0.0038	0.0027
	5	3.52	0.59	0.26	0.063	0.0036	0.0027
	6	3.45	0.69	0.30	0.060	0.0034	0.0025
	7	3.54	0.57	0.28	0.060	0.0036	0.0024
	1						
	2	3.80	0.55	0.29	0.058	0.0028	0.0029
	3	3.80	0.54	0.27	0.060	0.0028	0.0029
CD 1739	4	3.80	0.55	0.28	0.058	0.0027	0.0028
	5	3.76	0.53	0.29	0.058	0.0028	0.0030
	6	3.76	0.54	0.29	0.066	0.0029	0.0027
	1						
	2	3.32	0.58	0.28	0.054	0.0025	0.0021
	3	3.28	0.59	0.29	0.056	0.0026	0.0021
CD 1738	4	3.26	0.60	0.29	0.058	0.0030	0.0022
	5	3.42	0.57	0.29	0.065	0.0028	0.0024
	6	3.72	0.55	0.28	0.058	0.0028	0.0027
World average Turekian & Wedphol 1961		3.0	0.78	0.30	0.055	0.001	0.0018

*: Si/Al ratios in cores CD 1715 and CD 1730 are T.Si-Biog.Si ie. Si(lith).

*: Fet/Al is Fe free from authigenic iron from pyrite.

The Si/Al ratio in sedimentary aluminosilicates is generally 3.0 (Bostrom et al., 1972). Any Si in excess of this value indicates either biogenous Silica or detrital quartz. The average Si/Al ratio 3.5 (Table 5.1 and appendix C.3) in the Arabian sediments clearly reflects that Si is mainly associated with detrital alumino silicates with additional quartz and or biogenic silica.

Because of the complications of biogenic silica in assessing the lithogenous geochemistry of the cores, an attempt has been made to analyse the content of biogenic silica by sodium bicarbonate digestion method (see chapter 6 and appendix A.5 for details). The following discussion on the geochemistry of Si involves the non-biogenic silicon content of the sediments in cores CD 1715 and CD 1730 and is represented as Si(lith). Because the biogenic silica content of cores CD 1738 and CD 1739 is very low (see chapter 6) the total Si of the sediment is assumed to be detrital or lithogenous.

The Si/Al profiles of the four cores are shown in Figs. 5.2a, b. The overall low Si/Al ratio (3.2 to 3.4) in core CD 1715 suggests only a small contribution of quartz to the sediments. Cores CD 1730 and CD 1739 show a slightly higher Si/Al ratio of 3.5 and 3.8 respectively. The time variation of this ratio indicates that the Holocene sediments of CD 1715 and CD 1730 (excepting the uppermost horizons) show significantly lower Si/Al ratios than the underlying Stage 2 sediments (Fig. 5.2a). There appears to be a marked change in ratio around 10 kys.

Interpretation of the pattern of Si/Al ratio changes with depth is difficult to assess. There is no simple relationship between Si/Al ratios and glacial/interglacial intervals. In cores CD 1715 and CD 1730 low ratios occur for much of the glacial Stage 6. While high ratios occur during Stage 2 and upper Stage 3, similar values can be seen in certain interglacial intervals and especially towards the base of Stage 5. Core CD 1739 shows an overall trend similar to CD 1730 with high ratio occurring near the base of Stage 5 and low ratios in the middle horizons of Stage 6. The slightly higher overall ratio in CD 1739 (Table 5.1) implies somewhat higher quartz contributions to these sediments compared with CD 1715 and CD 1730. The Si/Al ratio of CD 1738 tends to show somewhat lower overall ratio compared with the other cores, especially CD 1739. This may be due to either lower quartz contents or probably to the very different aluminosilicate ferromagnesian mineralogy of the cores (chapter 4). While the Si/Al ratio for much of the core is ~3.40, the profile tends to be erratic, isolated horizons showing values >4.0. This is especially noticed at the junction between Stage 5 and 6 and implies a high quartz contents. These profiles of Si/Al ratio show certain similarities to certain mineralogical ratios described in chapter 4. Overall the Si/Al ratio relates to the quartz/illite and quartz/chlorite ratios of Figs. 4.7 and 4.8. For instance, the high Si/Al ratios at the base of Stage 5

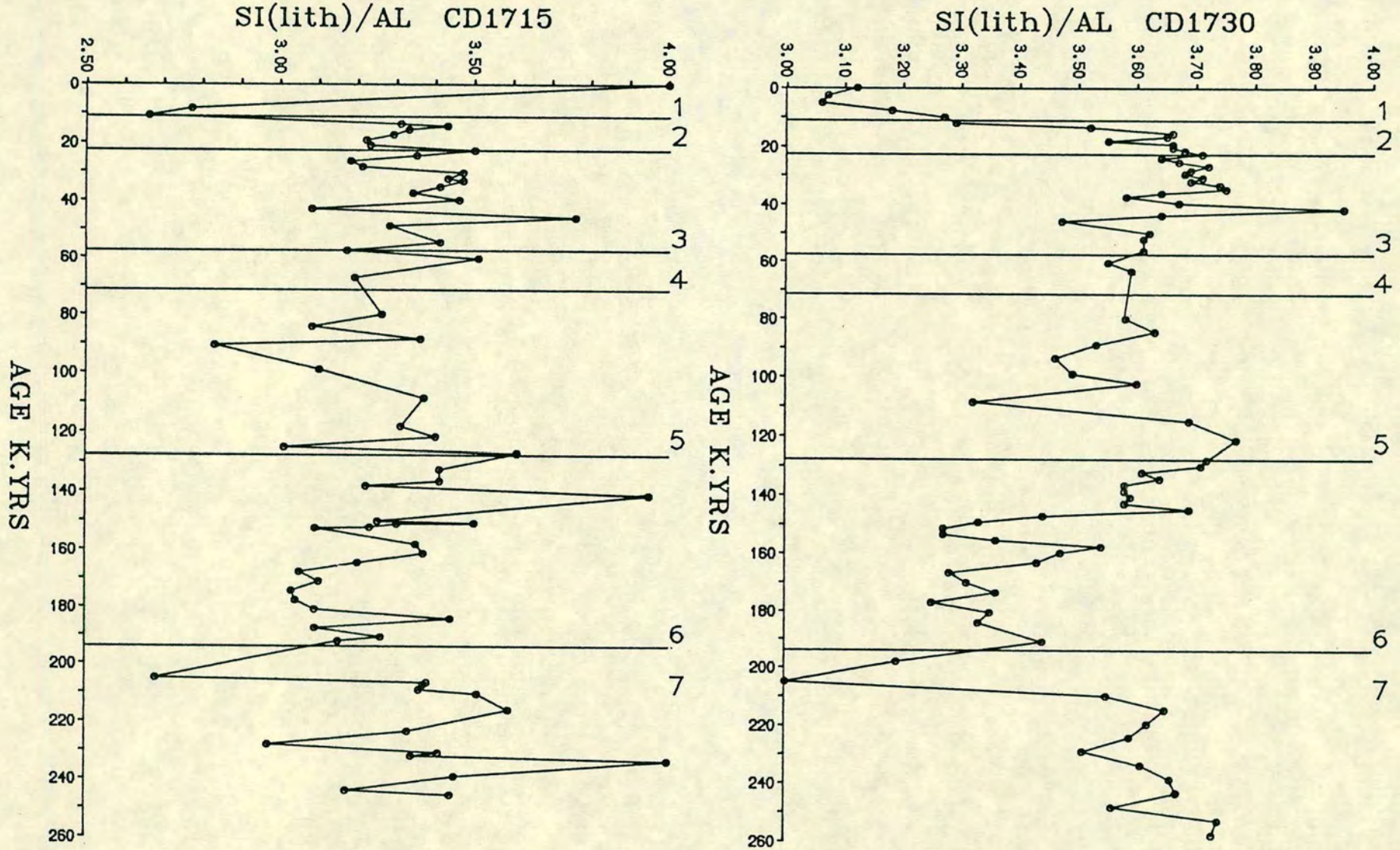

FIGURE 5.2a Si(lith)/Al RATIO VARIATIONS IN CORES CD1715 AND CD1730. NOTE THE DIFFERENCE IN SCALE.

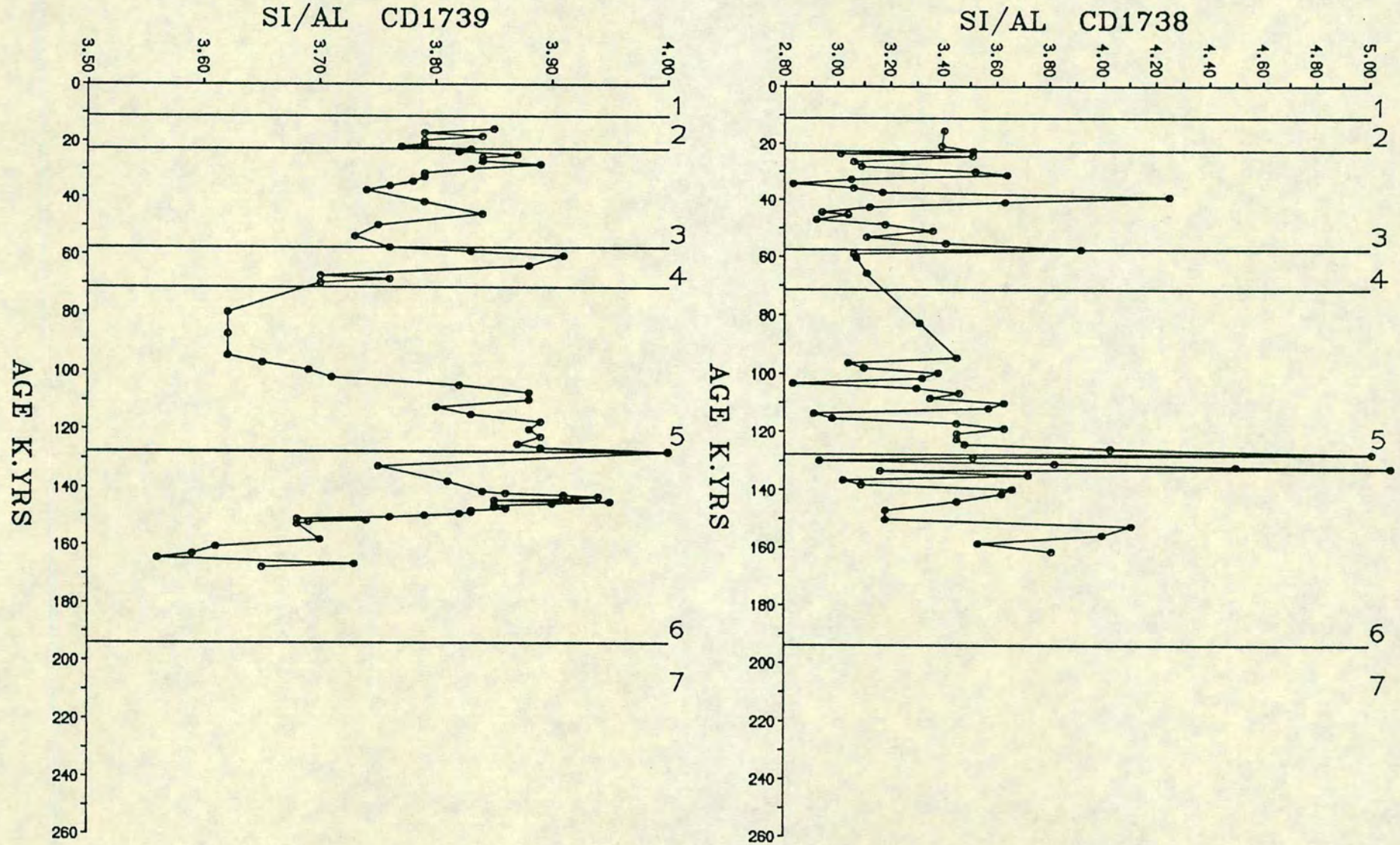

FIGURE 5.2b Si/Al RATIO VARIATIONS IN CORES CD1739 AND CD1738. NOTE THE DIFFERENCE IN SCALE.

(CD 1738) can be correlated with high quartz/illite and quartz/chlorite. The overall profiles of Si/Al in the other cores are also broadly similar to the trends of these mineral pairs. For example, the increases in Si/Al in Stage 5 and Stage 6 in CD 1715 and CD 1730 also shows increases in quartz relative to clay minerals, but this is not so apparent in core CD 1739.

5.2:2 Iron

In deep sea sediments iron is mostly associated with terrigenous material, particularly the clay minerals. Carrols (1958) has shown that iron occurs in clays as: (a) an essential constituent within the crystal lattice; (b) a minor constituent within the crystal lattice; and (c) an iron oxide coating on the surface of the clay particles. The strong coherence in Fe and Al (Fig. 5.3) indicate that aluminosilicate minerals, probably Fe-rich chlorite or Fe-rich mixed layer clays (chapter 4) host the Fe in the sediments of the Arabian Sea. A progressive increase in Fe content of the studied cores clearly indicates the relative proportion of these minerals. Core CD 1709 shows negative Fe intercept, possibly indicating a non ferro-aluminosilicate phase. Cores CD 1738 and CD 1739 show a positive incercept 0.50% Fe and a smaller Fe gradient with respect to Al compared to cores CD 1715, CD 1730 probably indicates that a different clay mineral feldspar assemblage is present in these sediments. Core CD 1709 shows the highest Fe/Al gradient and as this core appear to quartsoze and shows relatively poor contents of ferromagnesian clay minerals, such high Fe to Al gradients may indicate a high content of Fe bearing heavy minerals.

In organic rich sediments there is a possible contribution of iron from authegenic pyrite which may be in sufficient concentration to increase the Fe/Al ratio. For this reason the contribution of Fe held as sulphide, has been subtracted from the total Fe contents to define better the geochemistry of the lithogenic fraction. This adjustment has been calculated from the total sulphur in the sediments (analysed by XRF method) assuming that all the sulphur held in the sediment occurs as pyrite (FeS_2) (see appendix C.6). This resultant Fe is designated lithogenous Fet.

In chapter 3, it was shown that chlorite is a major clay mineral in all cores. Therefore, it is to be expected that Fet/Al profiles (Figs. 5.4a, b) will indicate its distribution in both time and space. Lithogenic Fet/Al ratio show a small variation between 0.50 to 0.65 (Table 5.1) and the strong geochemical relationship of the two elements is evident in all cores (Fig. 5.3).

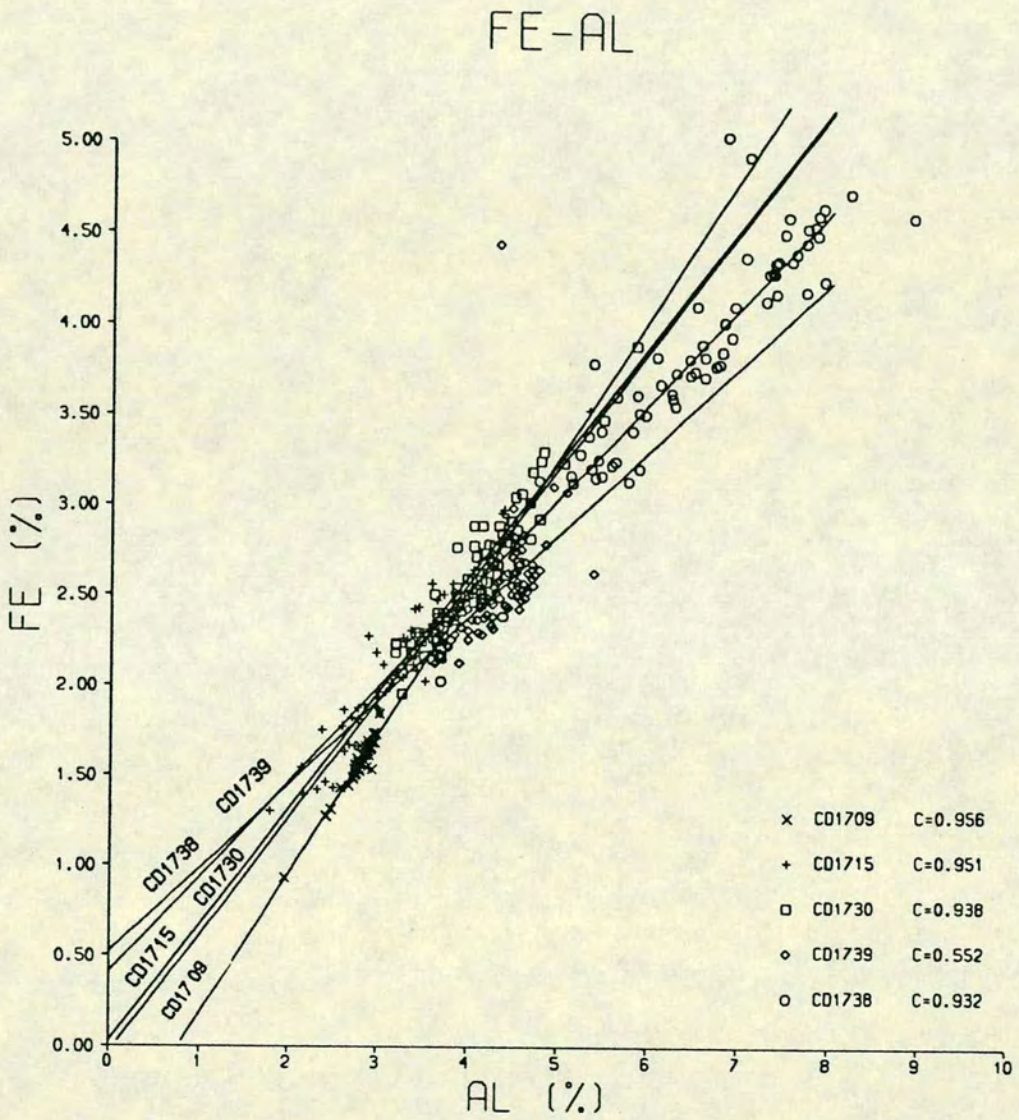

FIGURE 5.3 CORRELATION OF Fe AND Al IN SEDIMENT CORES FROM NW ARABIAN SEA

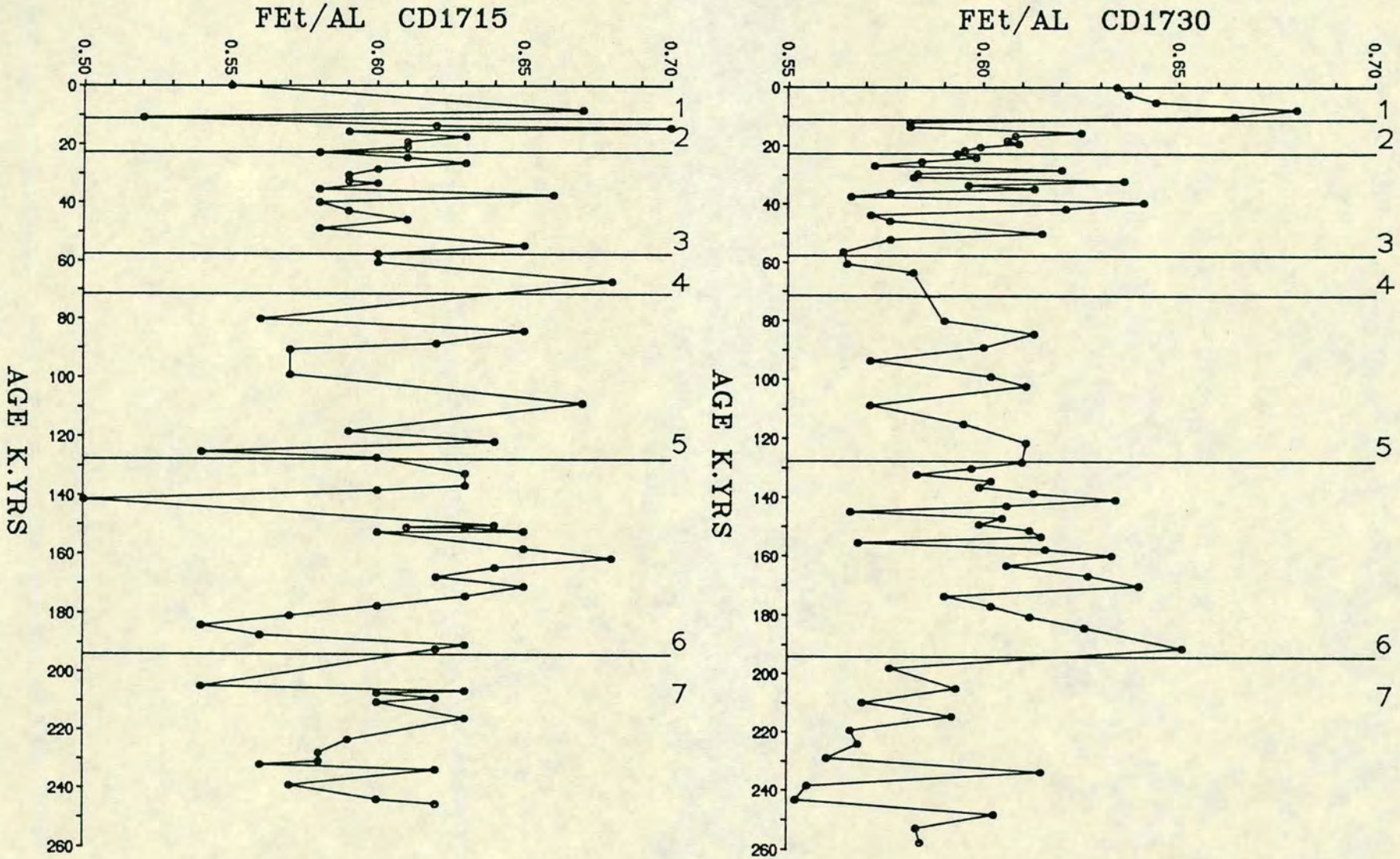

FIGURE 5.4a Fet/Al RATIO PROFILES OF CORES CD1715 AND CD1730. NOTE THE DIFFERENCE IN SCALE.

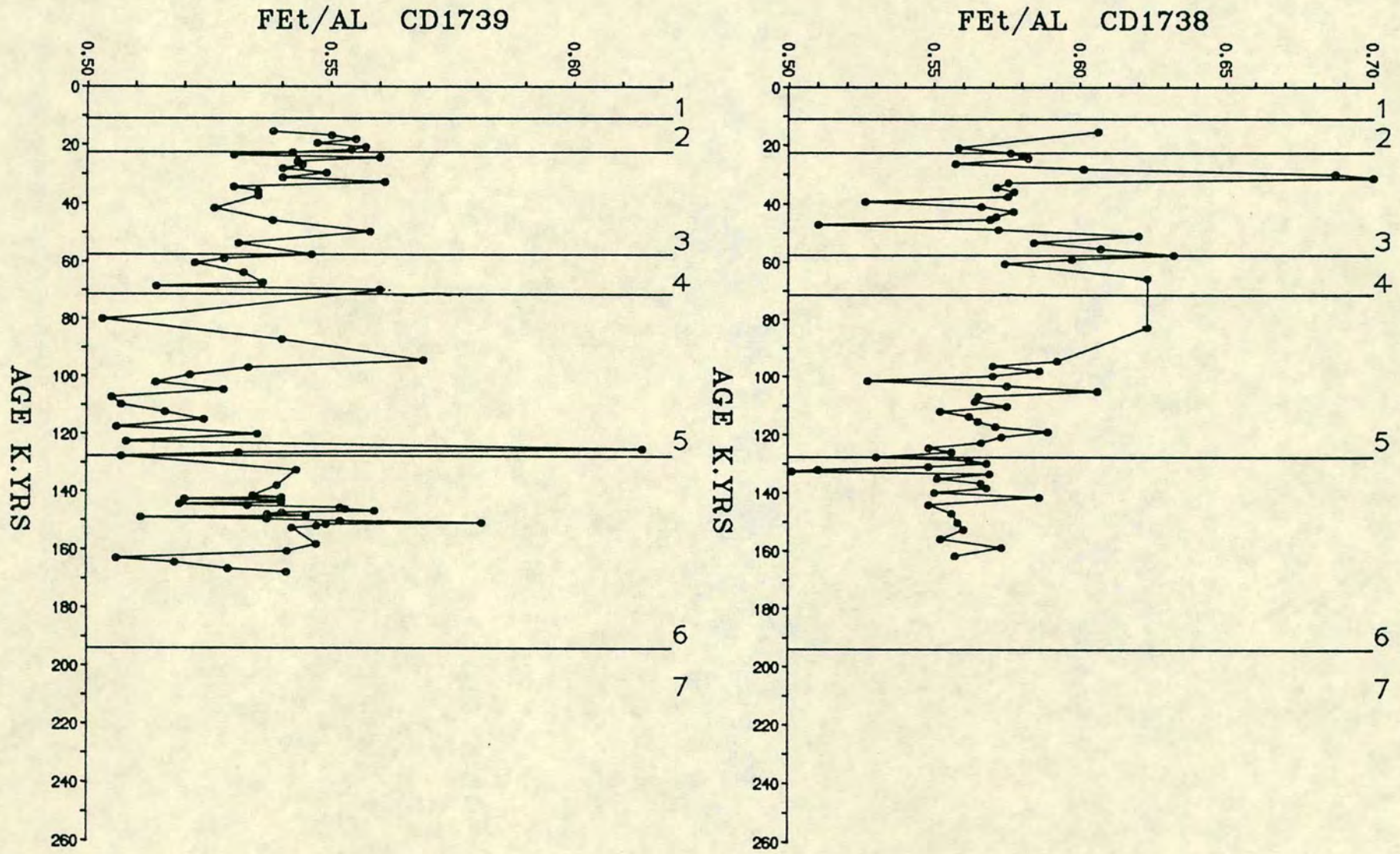

FIGURE 5.4b Fet/Al RATIO PROFILES OF CORES CD1739 AND CD1738. NOTE THE DIFFERENCE IN SCALE.

Profiles of Fet/Al ratio have been compiled and are presented in Figs. 5.4a, b. The Tobra ash layer at 71,000 yrs has been omitted from the profiles. Some cores, especially CD 1715, show a spiky Fet/Al profile with no obvious trends, some of this may be due to the contained turbidites. However, in core CD 1730, which is essentially free of turbidites, the overall trend of Fet/Al ratio is the reverse of what was observed for Si(lith)/Al, in that the Holocene has a higher ratio (ie. >0.65) which falls off dramatically in Stage 2. The Fet/Al ratios in other stages is also the reverse of that noted for Si(lith)/Al, Stage 5 and 7 showing low Fet/Al ratio, while Stage 6 has a high ratio. A similar trend is seen in Qtz(I) to Chl(I) and illite ratios (Fig. 4.7) in the sediments of these stages, which implies association of iron with chlorite. The patterns of feldspar/chlorite ratios in CD 1739 show the reverse of this trend with lower ratios, especially when compared to those of cores CD 1715, CD 1730. However, the general decrease of Fet/Al in the bottom half of core CD 1738 is accompanied by an increase in feldspar/chlorite and quartz/chlorite. It seems clear that the geochemistry of Fe relative to Al and Fe-bearing heavy minerals is complex. This may be due to variations in the composition of the chlorite between and within cores.

5.2:3 Potassium

A correlation of potassium and aluminium shown in Fig. 5.5 suggests that in Arabian Sea sediments the potassium is exclusively controlled by detrital minerals. Potassium is mainly held in illite and feldspar, therefore the variation in the K/Al ratio may reflect the variations in illite and feldspars present in the sediments (Boyle, 1983). A higher potassium content relative to Al in sediments implies a greater feldspar contribution. Fig. 5.5 shows that cores CD 1738 and CD 1739 are deficient in potassium relative to aluminium compared to that in cores CD 1715, CD 1730. This supports the earlier evidence of low feldspar contents in cores CD 1738 and CD 1739 (see chapter 4).

The ratio of K relative to Al between and down the cores shows very little variation, ranging between 0.29-0.35 (Figs. 5.6a, b). It can also be employed to decipher the mineralogical and textural differences and complements the study of Qtz(I)/Feld(I) and Si/Al, Fet/Al ratios (Figs. 4.6 and 5.2). This is best seen in core CD 1730 where the K/Al (Fig. 5.6a) ratios tend to follow Si(lith)/Al ratios (Fig. 5.2) and contrasts to Fet/Al (Fig. 5.4) ratios. The K/Al ratios in cores CD 1715 and CD 1730 are lowest (~0.27) within the Holocene and like Si(lith)/Al and Fet/Al ratios there is a marked change in K/Al ratios between Stage 1 and 2, where values

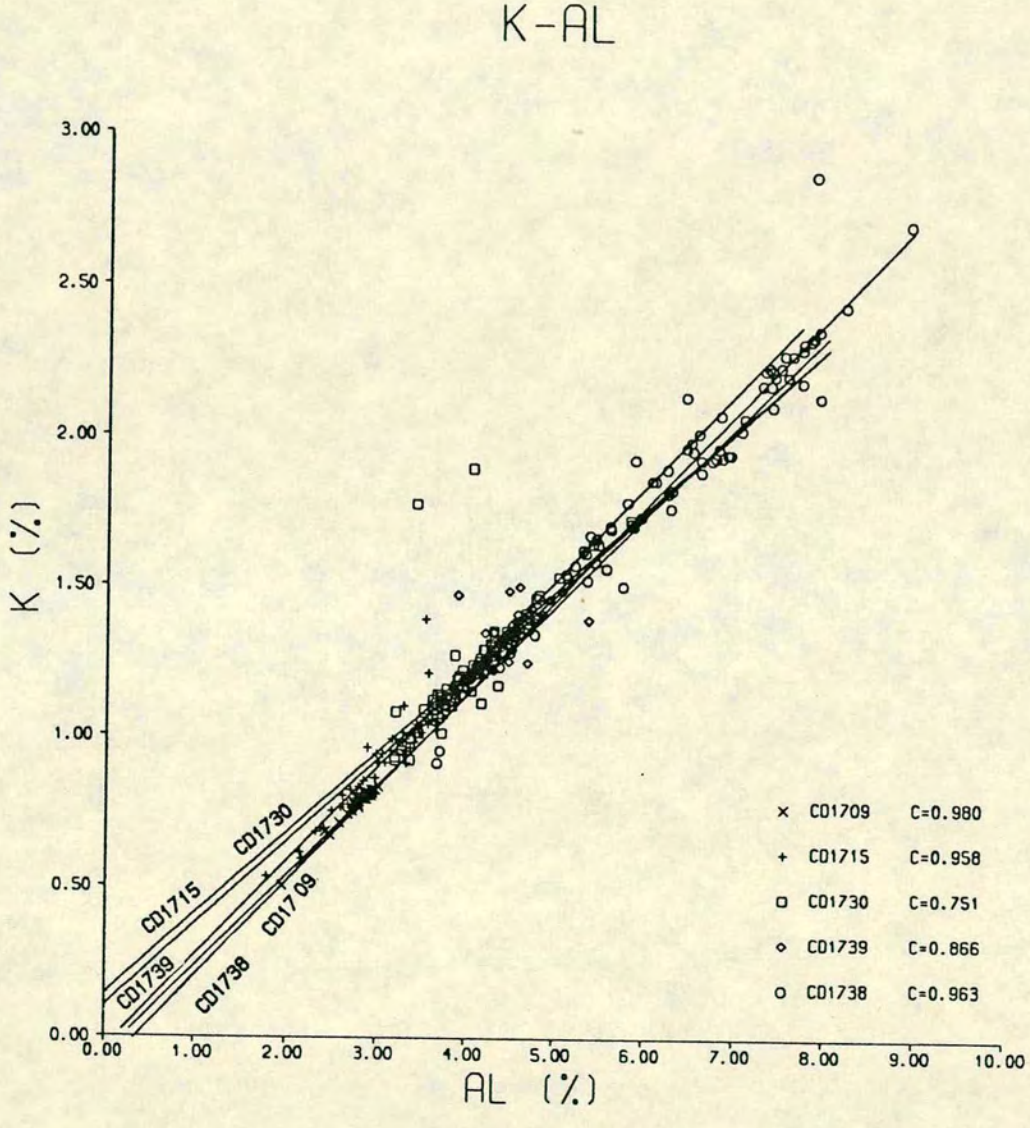

FIGURE 5.5 CORRELATION BETWEEN K AND Al IN CORES FROM NW ARABIAN SEA.

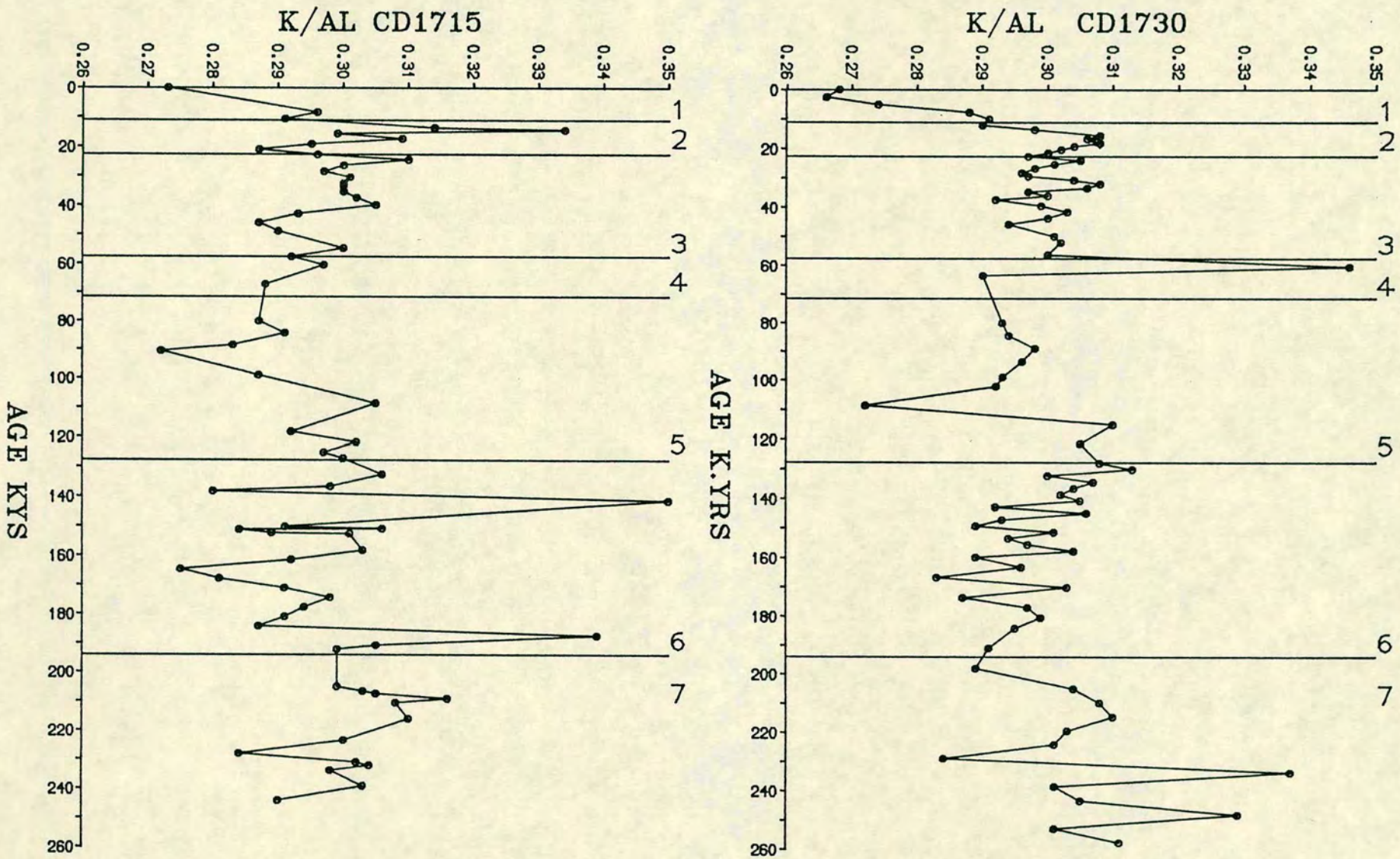

FIGURE 5.6a K/Al PROFILES OF CORES CD1715 AND CD1730.

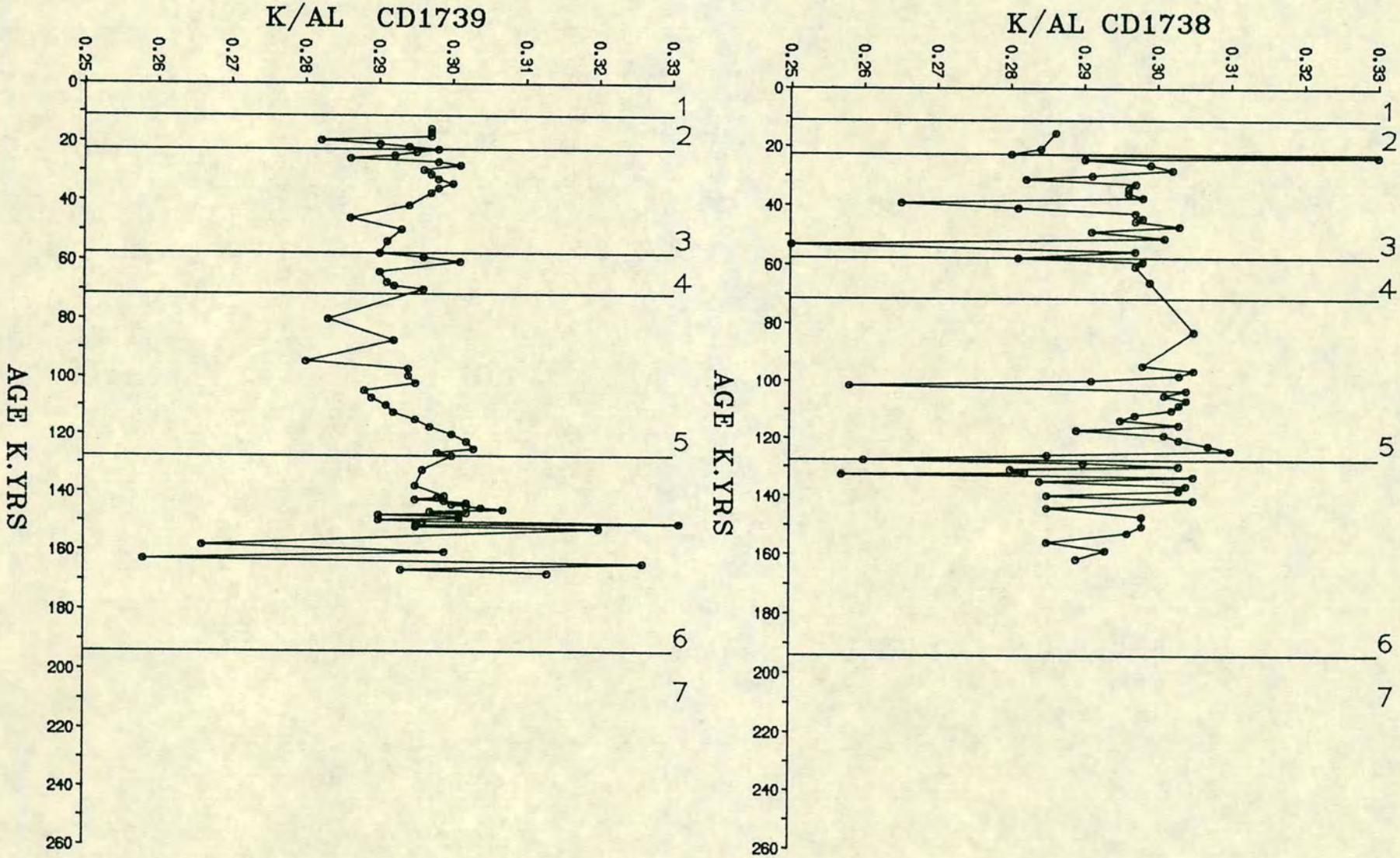

FIGURE 5.6b K/Al PROFILES OF CORES CD1739 AND CD1738.

Table 5.2 Elements/Al ratios of coarse turbidite bands in core CD 1715

Nos.	Depth cm	Si/Al	Fe/Al	K/Al	Ti/Al	Cr/Al	Zr/Al	LA/Al	CE/Al	ND/Al	Y/Al
1	90	5.30	0.51	0.28	0.11	0.0135	0.0062	3.48	14.28	6.62	5.92
2	130	6.35	0.38	0.31	0.08	0.0068	0.0029	0.00	5.32	3.27	4.91
3	140	7.35	0.33	0.34	0.08	0.0096	0.0036	0.41	7.83	6.18	4.53
4	643	5.40	0.48	0.27	0.11	0.0102	0.0043	2.41	9.99	5.85	5.85
5	653	5.90	0.45	0.28	0.11	0.0149	0.0069	3.92	9.63	4.28	6.06
6	668	5.05	0.49	0.29	0.07	0.0042	0.0019	4.21	5.84	5.19	4.54
7	676	5.73	0.42	0.28	0.07	0.0095	0.0038	4.79	7.86	3.76	5.47
8	687	3.74	0.72	0.31	0.08	0.0041	0.0025	3.74	8.81	5.07	4.80
9	692	5.16	0.52	0.28	0.11	0.0081	0.0033	4.93	11.83	4.70	5.59
10	700	6.07	0.47	0.29	0.10	0.0171	0.0065	2.64	12.85	6.04	6.42

increase from 0.27 to >0.31. The pattern of increasing K/Al in glacial intervals is probably indicative of a higher feldspar input which has higher K/Al ratios than illite and hence will be related to quartz and Si(lith)/Al ratios in these stages.

At depth, increased K/Al ratios within the lower parts of Stage 5 and upper Stage 6, especially in CD 1730, are also similar to the trend of increasing Si(lith)/Al, quartz/chlorite and quartz/illite ratios. This trend is not apparent in Stage 4 sediments. The higher K/Al ratios throughout much of Stage 7 also implies a higher feldspar content in the sediments, and this is also seen in high feldspar/chlorite ratios (Fig. 4.9).

K/Al ratios in cores CD 1738 and CD 1739 (Fig. 5.6b) are generally below 0.30 and follow the trends of Si/Al (Fig. 5.2b) and Flds(I)/Chl(I) ratios (Figs. 4.9). Such low ratios are possibly due to a relative impoverishment of feldspars compared with cores to the south. This trend may also be the cause of an intercept on the Al axis in Fig. 5.5. High K/Al ratios occurring as spikes, with values of up to 0.35, in CD 1715 and CD 1730 are probably the result of coarse-grained bands, since these horizons also show higher Qtz(I)/Ill(I) Si/Al ratios, (Figs. 4.8, 5.2). The coarse turbidite bands in core CD 1715 show high K/Al ratios of ~0.30 (Table 5.2) which is associated with high Si/Al ratios.

5.3 GEOCHEMISTRY OF MINOR ELEMENTS

5.3:1 Titanium

Titanium in deep sea sediments occurs mostly as fine particles in continental derived minerals like ilmenite, rutile and anatase (Rankama and Sahama, 1950; Chester and Aston, 1976). Since these minerals are highly resistant to weathering, and therefore largely found in the heavy minerals fraction of detrital sediments (Goldschmidt, 1954). High contents (>0.7%) in sediments often indicate that it is derived from basaltic debris (Goldberg and Arrhenius, 1958). Biogenic Ti has been found in marine organisms (Nicholls et al., 1959; Martins and Knauer, 1973; Bostrom et al., 1974). However, in the biogenic sediments of the equatorial Pacific productivity belt, convincing evidence of an organic contribution has not been found (Goldberg and Arrhenius, 1958; Pederson, 1979).

The concentrations of Ti in sediments from the NW Arabian Sea range from 0.20 to 0.40% (Appendix C.3). In Fig. 5.7 the straight line relationship between Ti and Al suggest the uniformity of incorporation of Ti with aluminosilicates. The best fit lines shown in Fig. 5.7 for all the five cores shows that in all cores, considerable

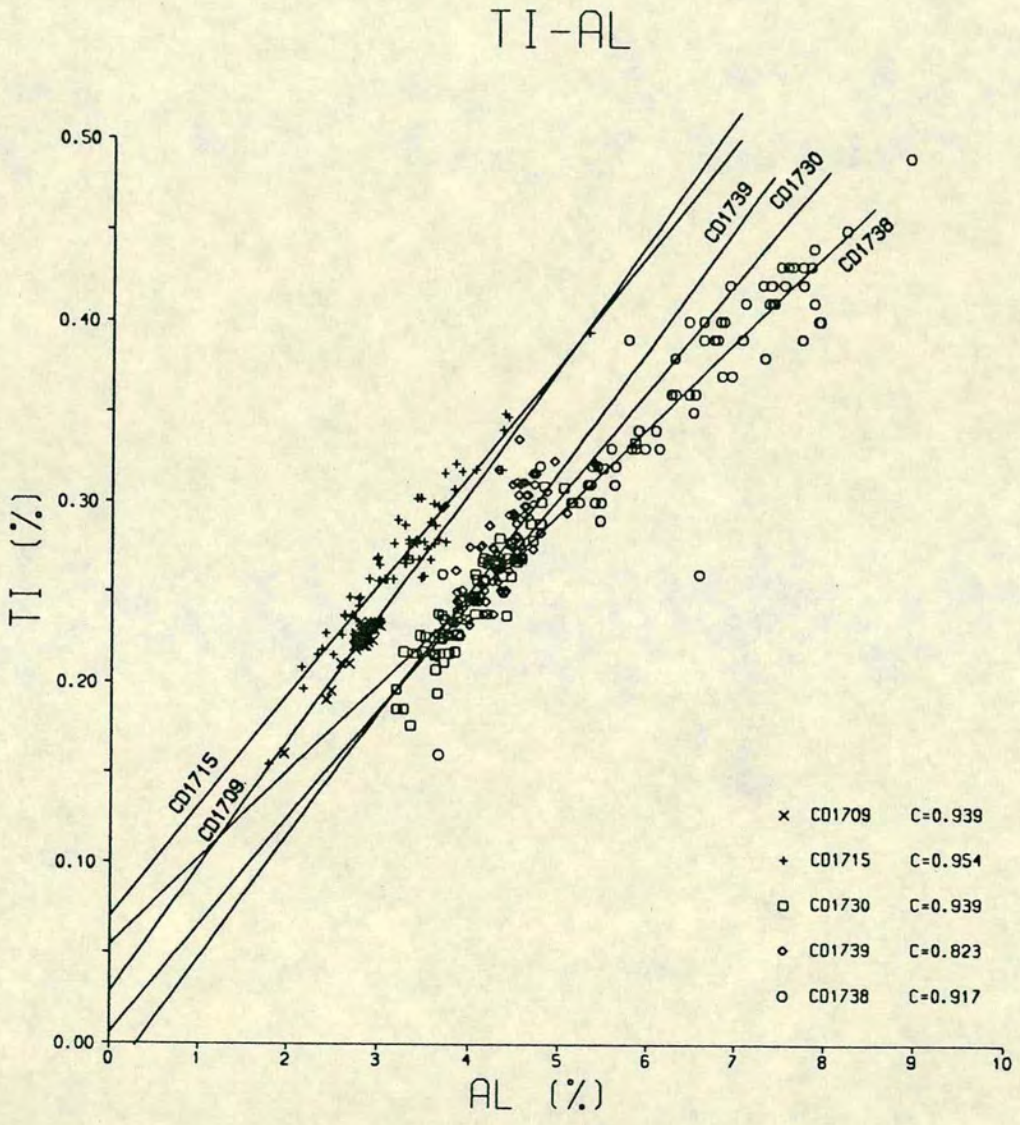

FIGURE 5.7 CORRELATION BETWEEN Ti AND Al IN SEDIMENT CORES FROM NW ARABIAN SEA

titanium occurs as Al free titanium minerals above that associated with aluminosilicates. This Fig. 5.7 also represents that cores CD 1738 and CD 1739 are relatively impoverished in this excess Ti and probably is a result of a different mineralogy.

In XRF analysis of carbonate rich sediments, for Ti there may be an interference effect of Ca (Boyle, 1983). However, in the present case such interference has not been observed and this was confirmed by analysing pure carbonate, which showed a negative count ratio for Ti. Thus the Ti results reported here are quite satisfactory, and do not show any artifact of carbonate (G. Fitton, Pers. Comm.). There may, however, be some interference of Ba (Lα) on TiO_2 (Kα); hence barium and carbonate rich sediments may show some error in Ti contents. This error is likely to be small and does not account for the Ti intercept in Fig. 5.7 especially for core CD 1709 and CD 1738 which have low Ba content.

The titanium content varies with depth and it is normalised to Al as shown in Fig. 5.8a, b. This variation may be due to either a change in the composition of the detrital input or to the bottom transport of the sediments, for instance, by winnowing of bottom currents. Ti/Al trends shown in Fig. 5.8a for core CD 1715 and CD 1730 are difficult to interpret during glacial and interglacial Stages. However, the vertical profiles of the two cores are similar. The glacial Stages 2, 4 and 6 show low Ti/Al, while interglacial Stages 3, 5 and 7 have high values. For the four cores there is a general decrease in Ti/Al ratio from core CD 1715 to CD 1738. The highest ratio occurs in core CD 1715 (ie. ~8.0 x 10^{-2}) and CD 1730 and CD 1739 are intermediate in Ti/Al showing value about ~6.5 x 10^{-2}, while the lowest values are seen in core CD 1738 ie. 5.5 x 10^{-2} (Table 5.1).

Ti contents may be related to grain size in clays and the frequent occurrence of anomalous Ti/Al values, especially in cores CD 1738 and CD 1739, indicate coarse grained sediments, as correspondingly high values have also been seen in the Si/Al, and K/Al profiles. However, the highest Ti/Al values in 8.0 x 10^{-2} in core CD 1715 observed do not match with the assumed texture of sediments in this core. Stage 5 in this core shows values of Ti/Al, very similar to that of turbidites Ti/Al ratio (Table 5.2). As in cores CD 1738 and CD 1739, the coarser sediment horizons tend to have high titanium content but the sediments in core CD 1715 appear to be relatively fine grained and accordingly should show low Ti/Al. This contrast can perhaps be explained by a different provenance and different clay mineralogy of this core. Weaver and Pullard (1973) reported that illite contains relatively more titanium ie. 0.7% than chlorite and montomorillonite, which has a Ti content in the range of 0.2-0.6%. If this is the case in the North Arabian Sea, the varied Ti/Al ratio in the

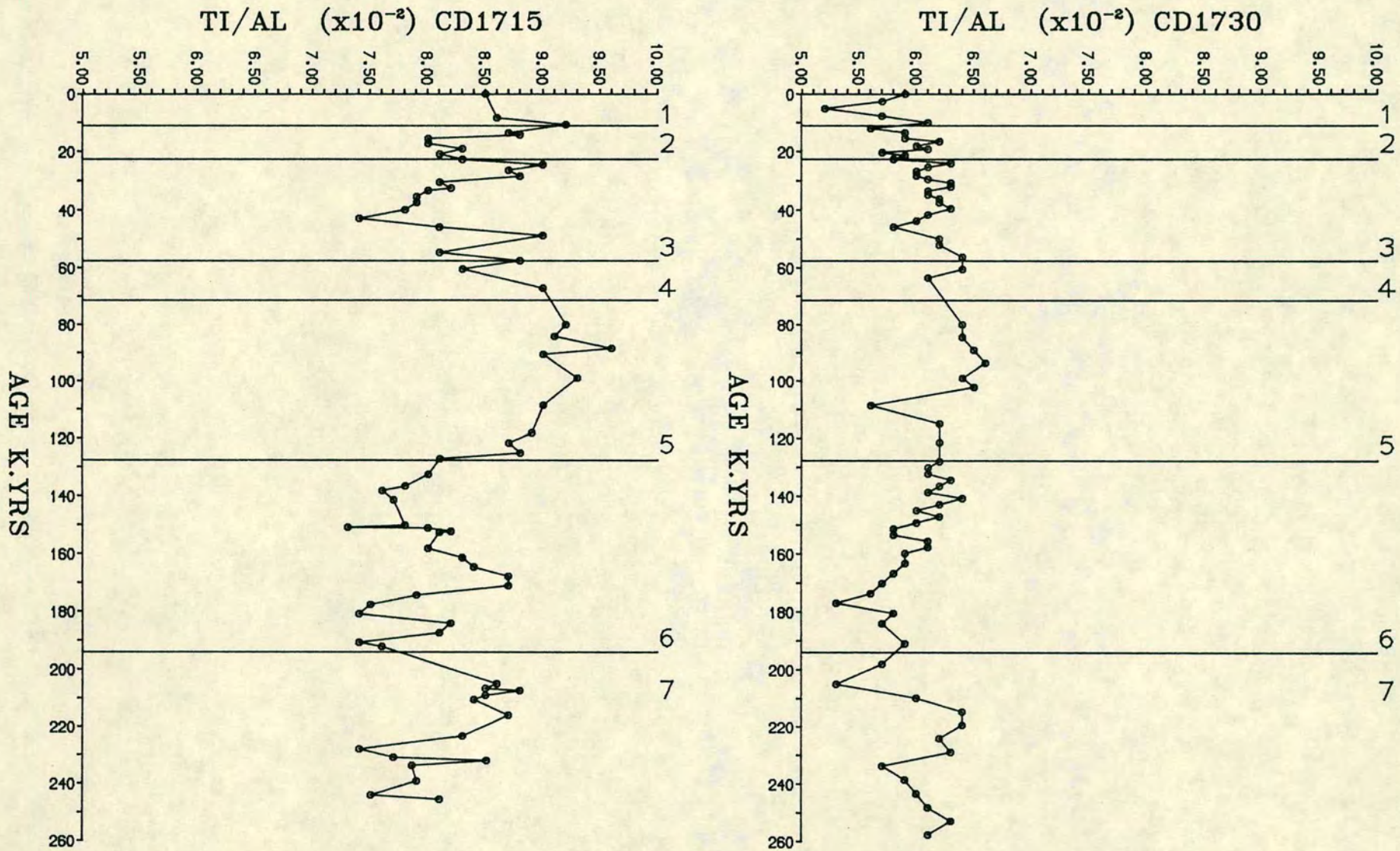

FIGURE 5.8a Ti/Al RATIO VARIATIONS IN CORES CD1715 AND CD1730.

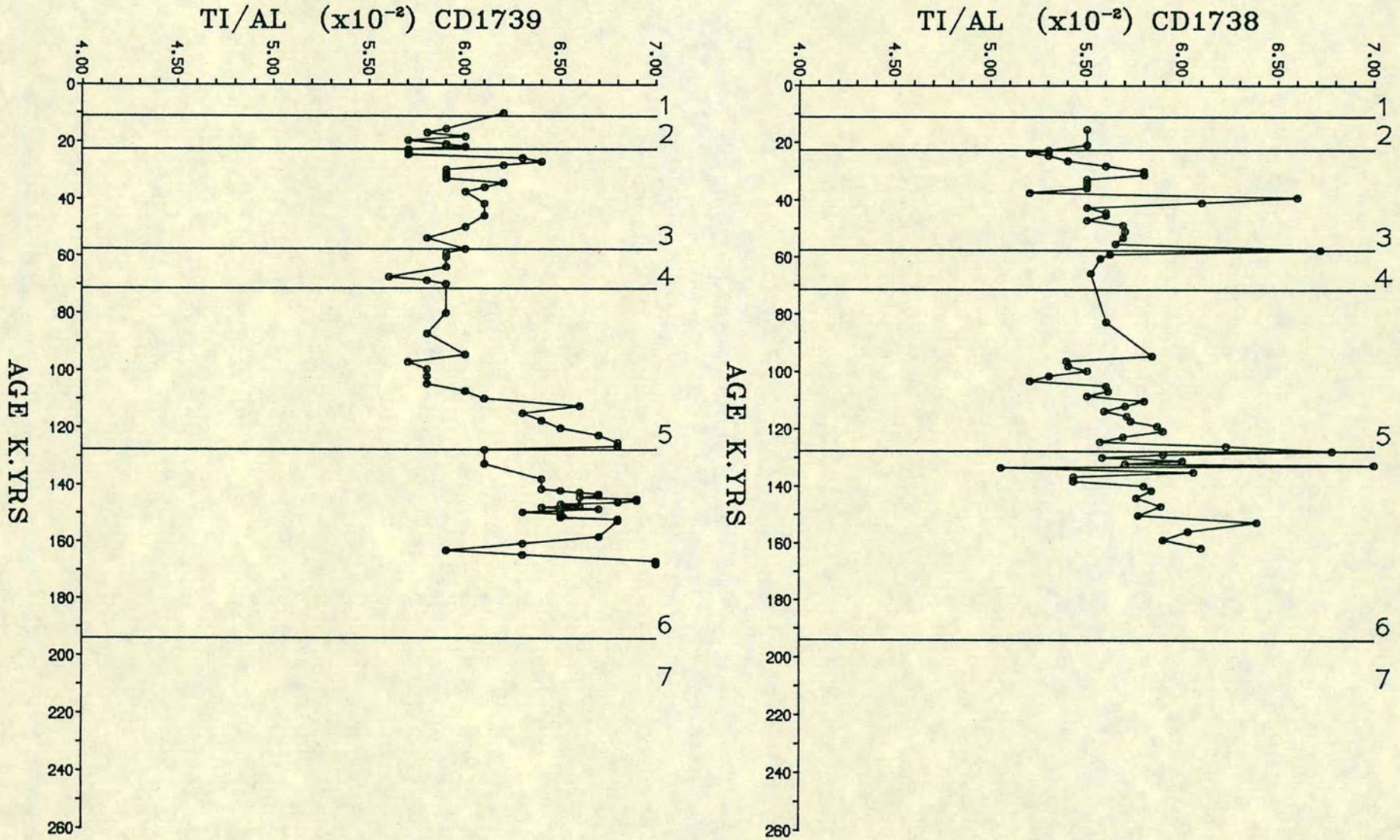

FIGURE 5.8b Ti/Al RATIO VARIATIONS IN CORES CD1739 AND CD1738.

studied cores probably indicate differences in clay mineralogy which accounts for the different Ti contents in the sediments.

In chapter 4 which describes the mineralogy of the cores, it has been shown that chlorite is relatively dominant in the northern cores. Fet/Al (Figs. 5.4b) shown in the preceding section largely reflects the Fe contribution in these sediments from chlorite. El-Wakeel and Riley (1961) have shown that a linear relationship exists between Fe and Ti content of deep sea sediments. Correlation between Fe and Ti content of the four cores shown in Fig. 5.9 also shows similar relationship. However, the different intercept at Ti line suggests that there is a progressive depletion in Ti relative to Fe from core CD 1715 to CD 1738. The high Ti intercept of core CD 1739 is probably due to the presence of more coarse-grained titanium minerals in this core, whereas in fine grained sediments of core CD 1715 the high Ti is most likely associated with, but not exclusively found in clay minerals ie. illite. This is also seen from the Fet/Ti ratio which gradually increases from cores CD 1715 to CD 1730. The Fet/Ti ratios shown in Fig. 5.10a, b therefore strengthen this view that in Arabian Sea sediments the clay mineralogy does exert some control on the titanium content. However, this cannot explain the variations in Ti/Al and Fet/Ti down the cores. These vertical changes are more likely to be due to changes in the relative detrital input. When the Ti/Al ratio profiles are compared with Zr/Al and Cr/Al profiles, a characteristic pattern emerges. The shapes of Ti/Al and Zr/Al (Fig. 5.8 and 5.12) are very similar, while Cr/Al (Fig. 5.14) profiles do not match those of Ti/Al and Zr/Al. This dissimilarity may be a result of a change from a local to distant control mechanisms, that is mechanical redistribution of elements by bottom currents or atmospheric dust fallout. To quantify the effects of either factor is not possible with the present data. However, it is important to point out that geochemistry of elements mainly associated with heavy minerals (ie. Ti, Zr, Cr) in the Arabian Sea sediments is different from normal deep sea sediments. This will be dealt with below.

5.3:2 Zirconium

Zirconium in sediments mainly occurs as detrital zircon (Erlank et al., 1978). Zircon is highly resistant to weathering and tends to occur in the coarse-grained fraction of the sediments (Goldschmidt, 1954; Hill and Parker, 1970). The changes in Zr/Al ratio thus may be interpreted as a variation in the sediment texture. This is shown in Fig. 5.11 by the various amounts of Zr as seen from the intercept of Al against Zr of examined cores. Free of turbidites, core CD 1730 shows an intercept

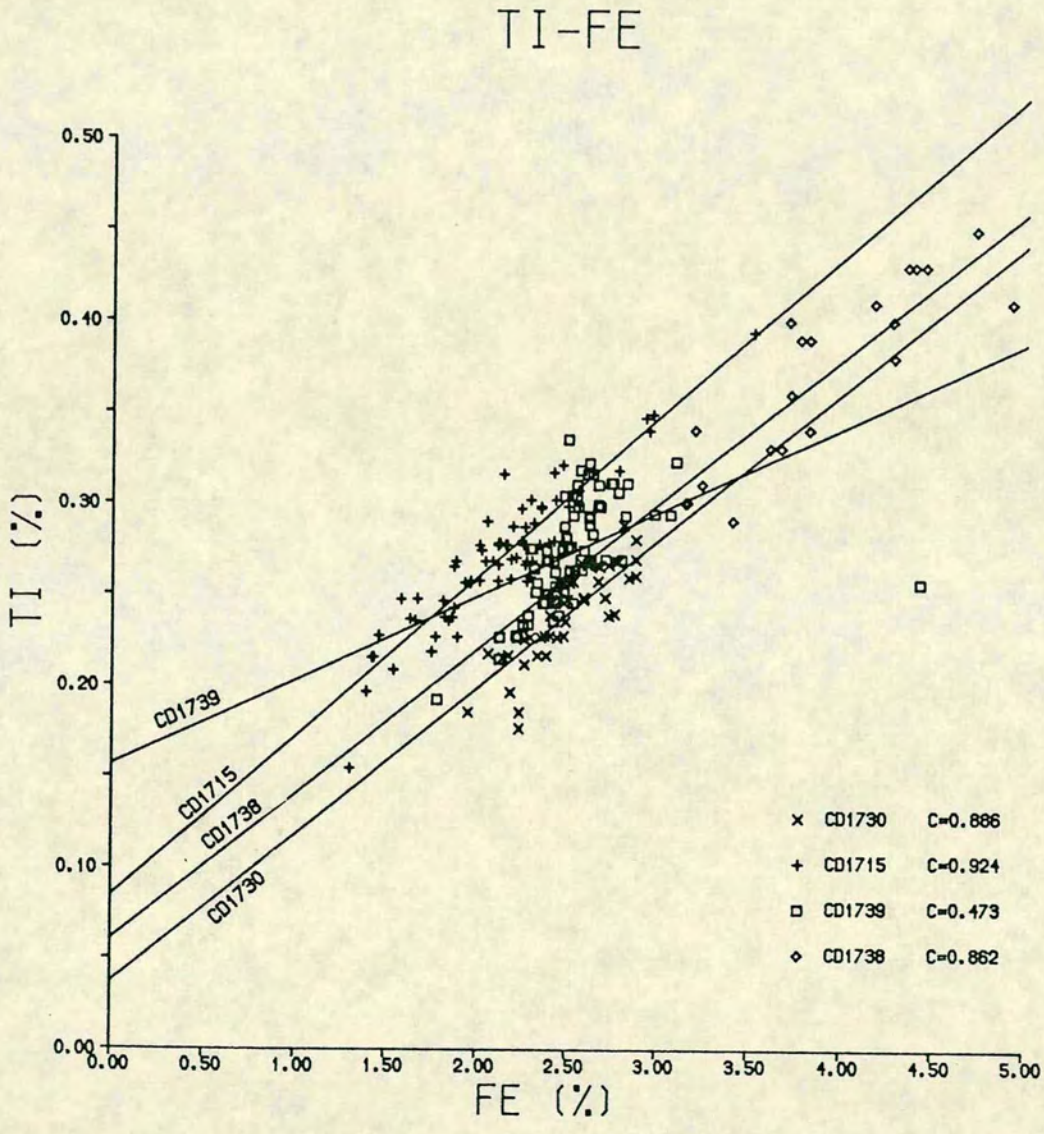

FIGURE 5.9 CORRELATION OF Ti AND Fe IN CORES FROM NW ARABIAN SEA.

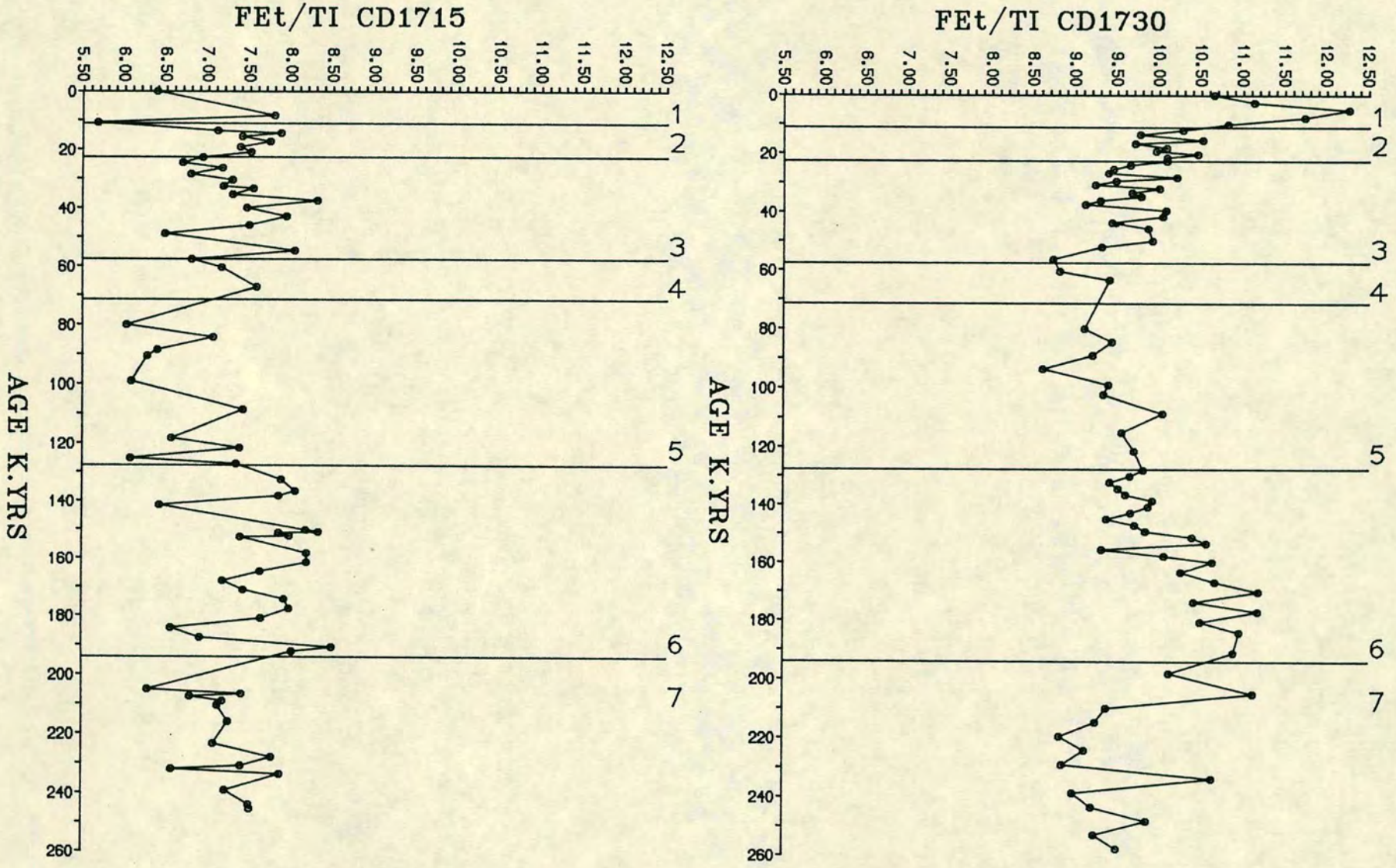

FIGURE 5.10a VARIATION OF Fet/Ti RATIOS IN SOUTHERN CORES (CD1715 AND CD1730) FROM NW ARABIAN SEA.

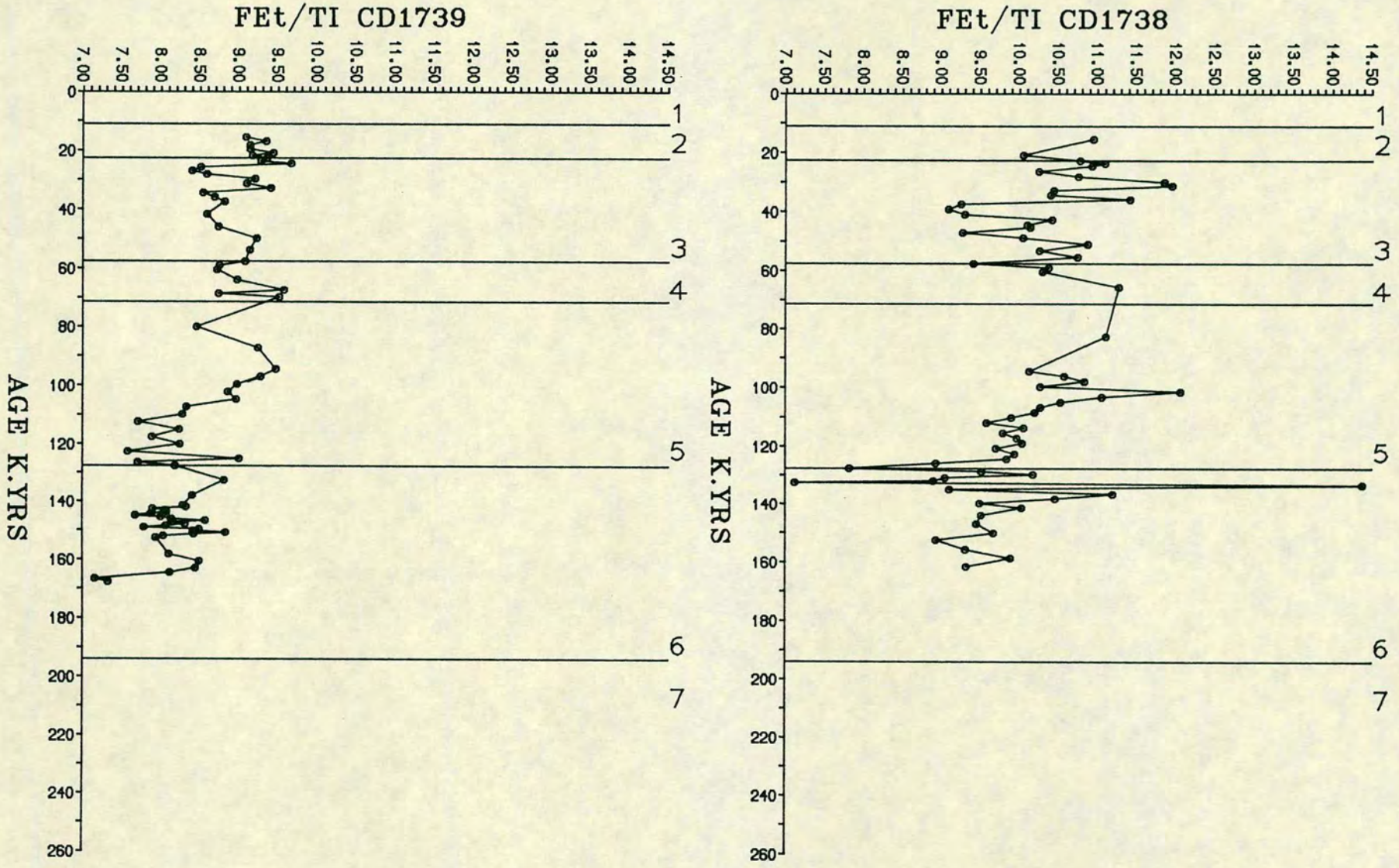

FIGURE 5.10b VARIATION OF Fet/Ti RATIOS IN NORTHERN CORES (CD1739 AND CD1738) FROM NW ARABIAN SEA.

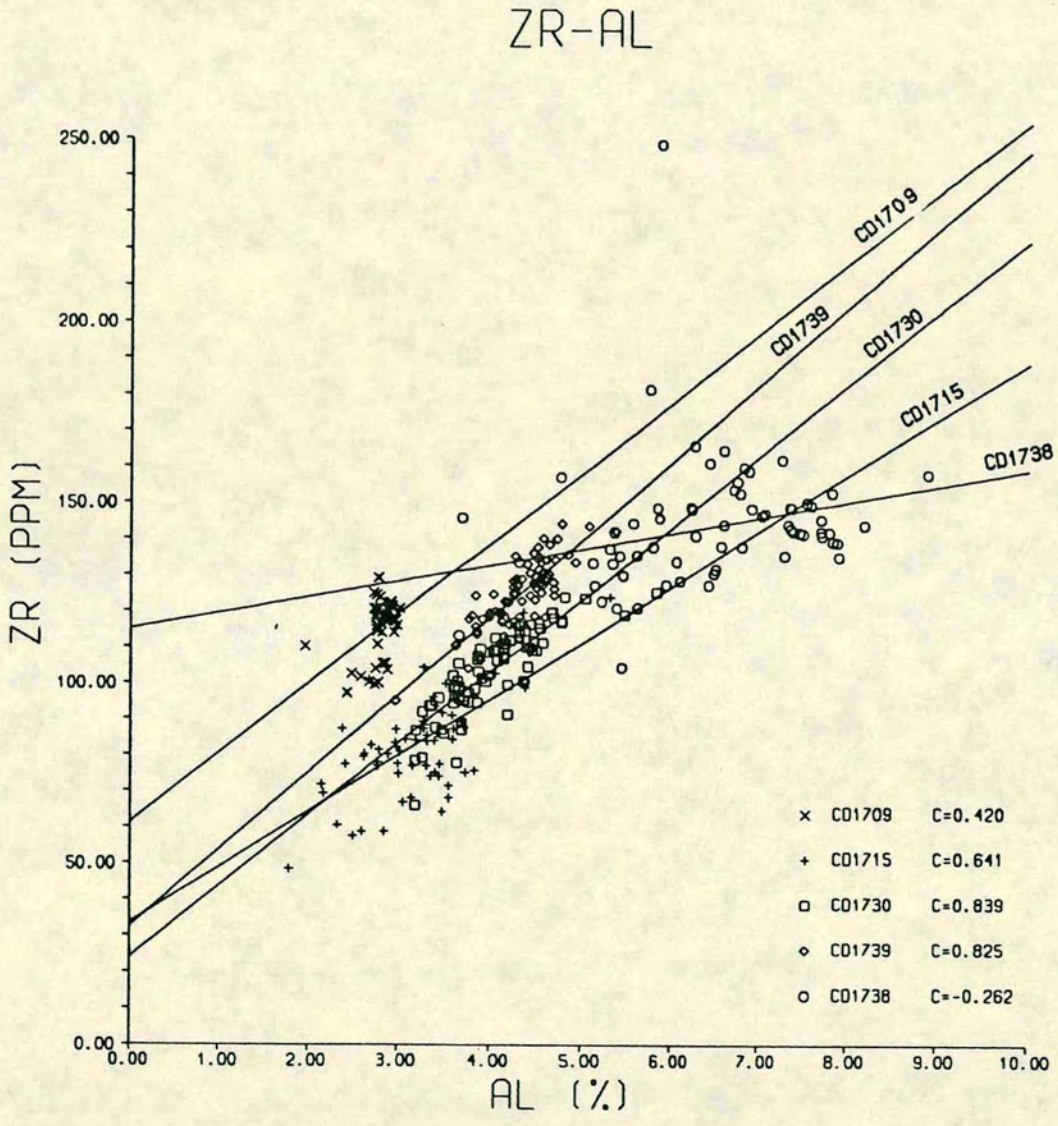

FIGURE 5.11 CORRELATION BETWEEN Zr AND Al IN SEDIMENTS FROM NW ARABIAN SEA.

of 35 ppm Zr and cores CD 1709 and CD 1738 60 and 110 ppm respectively. This imples that cores are progressively showing a coarser-grained detrital input.

The areal and temporal variation in Zr/Al ratio is shown in Fig. 5.12a, b. Zr/Al mostly shows coherent trends with Ti/Al. Generally, interglacial Stages 3 and 7 indicate lower trends with Zr/Al than glacial Stages 2, 4, 6. This pattern is best seen in core CD 1730. This indicates that during glacial times, sediments contain relatively more coarse grained heavy minerals than during interglacials. Ti/Al, Si/Al and K/Al also show consistent trends and imply that the detrital input during cold isotopic stages is relatively enriched in quartz, feldspar, zirconium and titanium.

Since the core sites are areally well separated with respect to the Arabian coast, they are likely to show the difference in the input of detrital constituents at these locations. This is evident from the Zr/Al profiles of two cores CD 1715 and CD 1730 (Fig. 5.12a). In the upper section of these cores, Zr/Al ratio trends are different. In core CD 1715, Zr/Al ratios oscillate considerably with age, showing a maximum value in the upper part of Stage 5, like Ti/Al. Despite the fact that core CD 1715 is relatively impoverished in Zr (Fig. 5.11), the highest Zr/Al ratio prior to the Holocene, like Ti/Al (Fig. 5.8a), is seen in interglacial Stage 5. This pattern is not easily discerned in core CD 1730. Zr and Ti are generally considered to reflect the coarse-grained fraction in deep sea sediments (Hill and Parker, 1970). Therefore their similarity in core CD 1715 suggests changes in the coarse-grained fraction of the sediment containing Zr and Ti. Clemens and Prell (pers. comm.), from textural analyses of core RC-2761, noted that coarse grained particles are more abundant in interglacial stages, particularly in Stage 5, and have related this to the intensity of monsoon winds. Therefore, it may be possible that the high Zr/Al and Ti/Al ratios observed during Stage 5, especially in CD 1715, are caused by a similar mechanism to that considered in the ridge core RC-2761. However, the flux changes of these elements (chapter 9) suggest that although the lithogenic input was low during interglacial time, the stronger SW winds, as opposed to the NW winds, may have transported coarse particles. This suggests that low level SW monsoon winds may have carried a dust load up to 20°N. Further to the north in cores CD 1739 and CD 1738 Zr/Al, Ti/Al are different from core CD 1715. In the case of core CD 1730 Zr/Al ratios are fairly constant between 2.5 and 2.7 x 10^{-3}.

In cores from the Gulf of Oman and adjacent areas (ie. CD 1738 and CD 1739) Zr/Al ratio profiles are similar to those of Si/Al, K/Al, Ti/Al and show an increase during Stage 5 and 6. Overall, a wide range of Zr/Al ratios occur in core CD 1738 ie. 1.8 x 10^{-3} to > 4.0 x 10^{-3}, while in core CD 1739 it varies only between 2.5 to 3.0 x 10^{-3}. The lower part of the core CD 1738 comprising of Stage 5 and

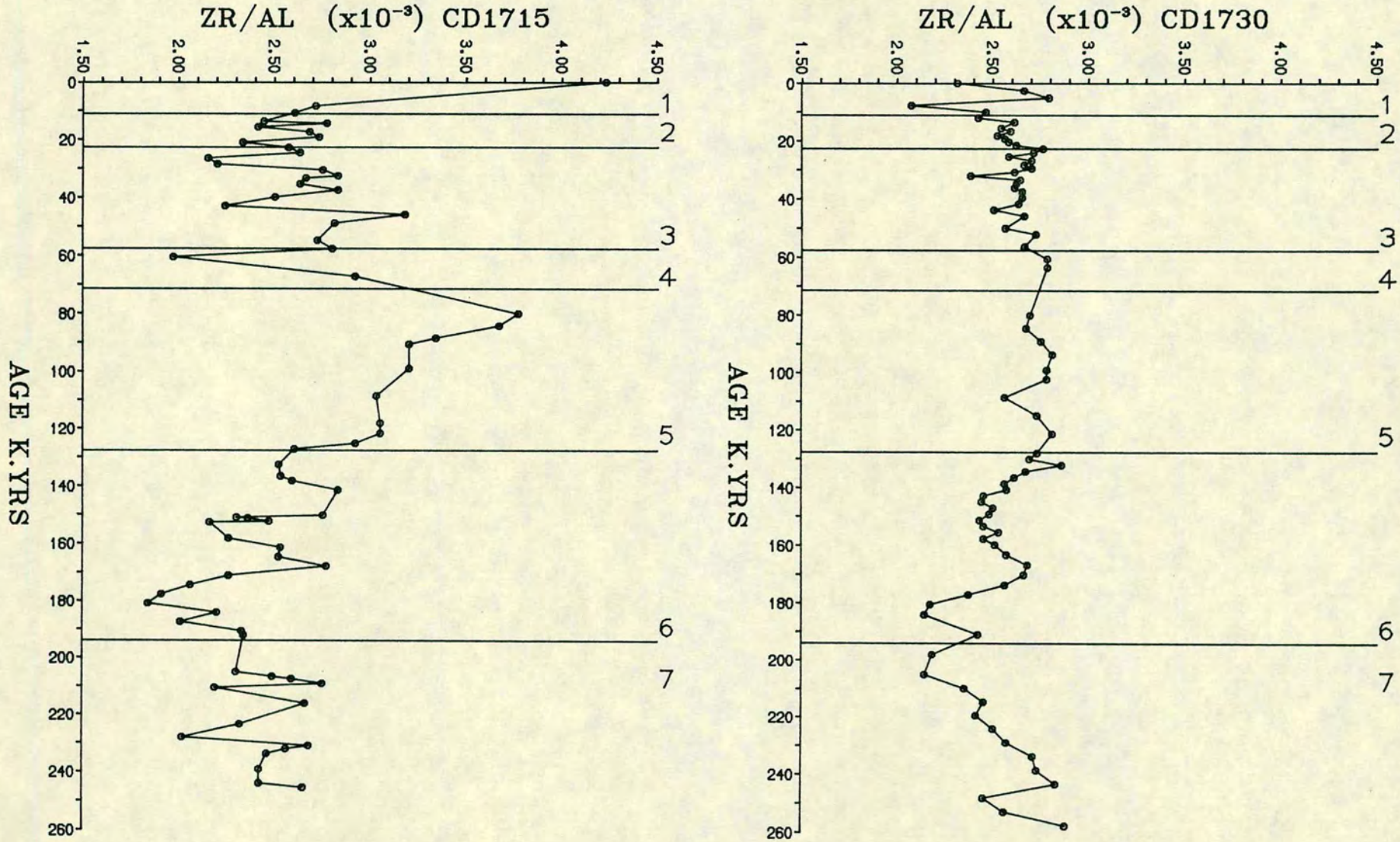

FIGURE 5.12a Zr/Al RATIO VARIATIONS IN CORES CD1715 AND CD1730

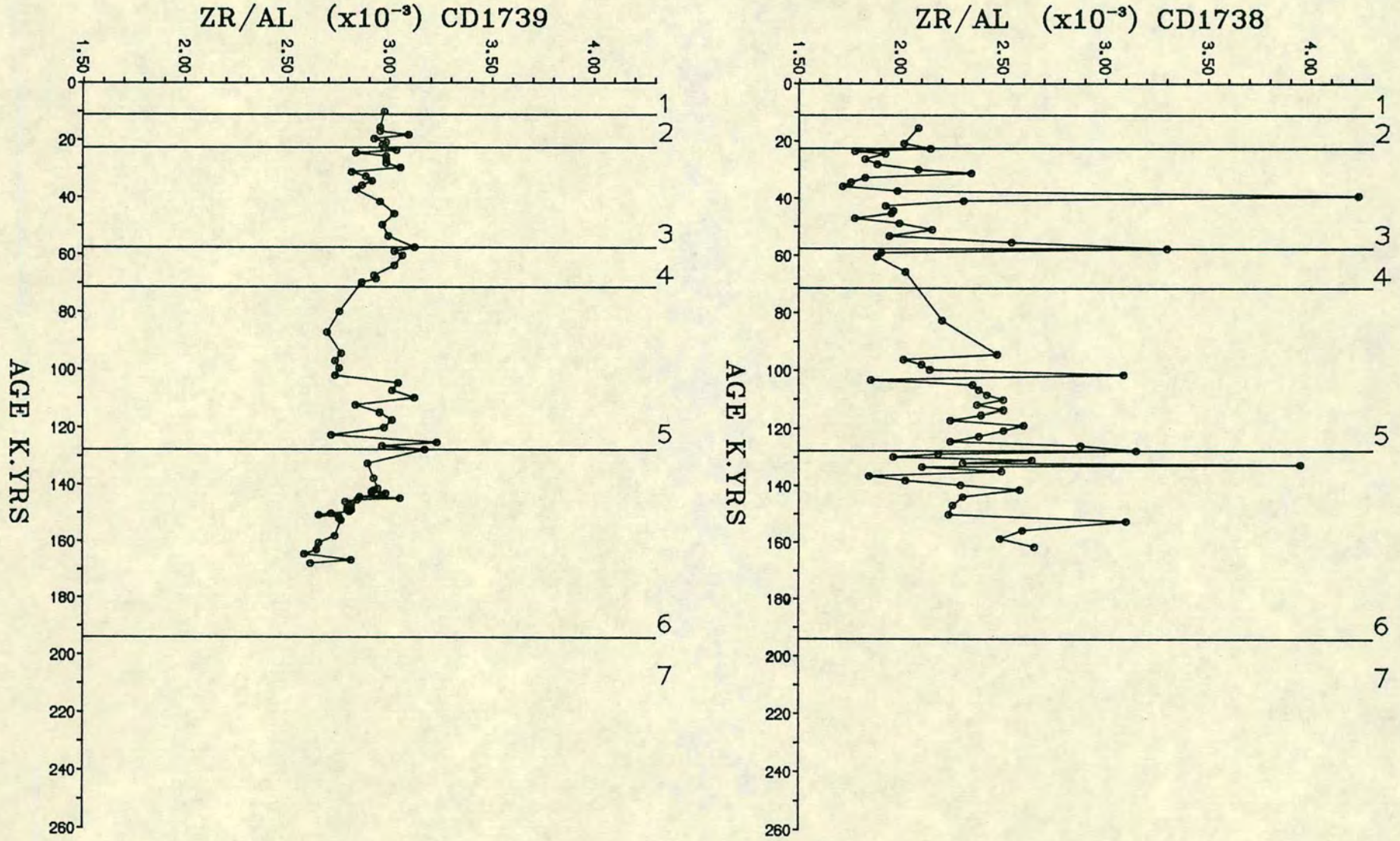

FIGURE 5.12b Zr/Al RATIO VARIATIONS IN CORES CD1739 AND CD1738.

Stage 6 show high values above which Zr/Al ratio gradually decreases. Erratic peaks in Zr/Al in these cores are synchronous with those observed for Si/Al, K/Al, and Ti/Al ratios.

5.3:3 Chromium

Sediments in near shore environments are generally higher in their chromium content, relative to that found in deep sea clays, especially if they contain volcanic detritus (Wedephol, 1960; Young, 1954). Goldberg and Arrhenius (1958) and El-Wakeel and Riley (1961) also noted that the high chromium content in some deep sea sediments is mostly associated with basaltic pyroclastics. According to Goldberg and Arrhenius (1958), more than 100 ppm of chromium in sediments indicates the presence of altered or unaltered basaltic materials. Goldberg and Arrhenius (1958) also found that chromium is concentrated in the coarse-fraction of oceanic sediments, and most of the Cr is not held in the clay mineral fraction.

Along the Oman margin, sandy sediments in core CD 1709 contain Cr up to 200 ppm (Fig. 5.13), and further inshore, surface sediments are reported to have an exceptionally high Cr contents, reaching 1000-1100 ppm (Shimmield et al., 1988). This Cr may be derived locally from the weathering or ablation of local South Oman ophiolites. Unusually high Cr was noted in many horizons of the cores CD 1709, CD 1715, CD 1730, CD 1738 and CD 1739 (Figs. 5.14a, b) (see Appendix C.4). This suggests that there must be some transport of ophiolite materials to hemipelagic areas, either: (a) transport by turbidity currents; (b) by the pluming of outer Oman shelf sediments to hemipelagic areas, or (c) by local aeolian dust inputs.

The influence of an ophiolite provenance is seen in the very high Cr or Cr/Al ratios in the relatively coarse-grained sediments of core CD 1709 situated on the Oman continental slope (Fig. 5.13). They are considerably higher than the mean oceanic sediments (Cr/Al = 0.0011) (Turekian and Wedphol, 1961) and probably indicate the presence of appreciable amounts of detrital magnetite, ilmenite and chromite. The sediments probably indicate a somewhat coarse-grained texture, possibly caused by some winnowing of fine-grained material by currents at this location.

The Cr and Cr/Al contents of turbidites (see Table 5.2) mostly associated with core CD 1715 also show unusual contents of Cr and are likely to derived from shallow water sediments to the north. The ratio of Cr/Al in all sediments of cores CD 1715, CD 1730 and CD 1738 varies from 2.0 to 5.0 x 10^{-3} and is considerably higher than the average oceanic sediments ie. 1.1 x 10^{-3} (Turekian and Wedphol, 1961). Plots of Cr against Al (Fig. 5.13) shows that all the cores have an appreciable

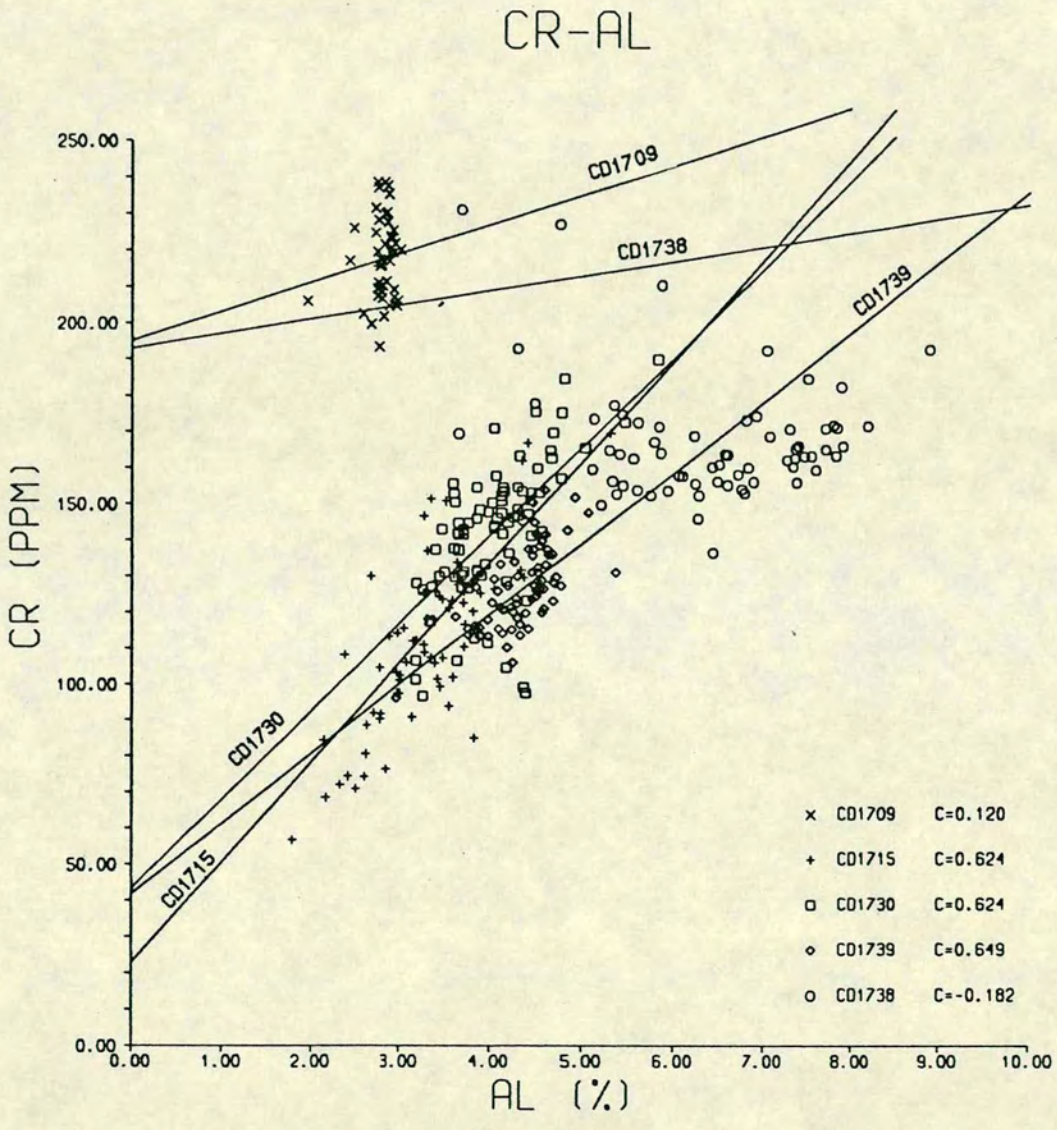

FIGURE 5.13 CORRELATION BETWEEN Cr AND Al IN SEDIMENTS FROM NW ARABIAN SEA.

Cr intercept. This suggests that all the sediments contain substantial chromium bearing non aluminosilicates, chromite, magnetite and ilmenite.

The Cr/Al profiles (Fig. 5.14a, b) of the four cores are very variable and their trends are dissimilar. For instance, Cr/Al in the younger sections of core CD 1715 (70,000 years BP to present), largely follow those of Zr/Al and Ti/Al; there is also some similarity to these elements in lower parts of this core in Stage 6 and Stage 7. However, in Stage 5, the distribution of these elements do not show any consistant trend, and suggests that Ti and Zr are more dominant than chromium. On the other hand, in core CD 1730 (Fig. 5.14a), Ti/Al and Zr/Al (Figs. 5.8, 5.12) indicate a fairly constant ratio throughout the core but in contrast secular changes are seen in Cr/Al ratios (Fig. 5.14a). In Stage 3, Cr/Al ratio is markedly low and ratio falls as low as 2.10×10^{-3} from an average Cr/Al ratio of $3.0\text{-}3.5 \times 10^{-3}$ of this core. The contrasting pattern in Cr/Al of two cores (ie. CD 1715 and CD 1730) are also observed in Stage 4 and Stage 5. The upper Stage 5 of core CD 1715 (90,000-70,000 years BP) shows the highest Cr/Al ratio (ie. 5.0×10^{-3}) while the ratio is characteristically low in the middle of Stage 4. Core CD 1730 shows invariable Cr/Al ratio values $>3.50 \times 10^{-3}$. In Stage 6 and 7 cores CD 1715 and CD 1730 are similar in Cr/Al ratios with slight differences in amplitude.

The patterns of Cr/Al profiles in cores CD 1738 and CD 1739 (Fig. 5.14b) are broadly the same as those of Ti/Al and Zr/Al (Figs. 5.8b, 5.12b). However, a difference in the trends does exist. Like core CD 1730, Cr/Al fluctuates down the core. In younger stage (ie. 3), the Cr/Al ratio is very low, $\sim 2.0 \times 10^{-3}$, and the trend differs from core CD 1739. In earlier stages (ie. 5 and 6), Cr/Al ratio trends are similar and follow those of other elements/Al ratio such as Si, K, Ti and Zr. Ratio of Cr/Al increases up to 4.0 with spasmodic events showing ratios between 5.0 and 6.0.

5.4 CHROMIUM CONTENT AND ITS ASSOCIATION WITH LOCAL SOURCES

In the north western Arabian Sea sediments, it has been found that Cr contents are much higher than normal deep sea sediments and most likely reflect derivation from local ophiolites. Further inshore, sediments are reported to contain 1000 ppm Cr, possibly in lag sediments and caused by winnowing (Shimmield et al., 1988). This evidence implies that Cr in deep sea sediments of NW Arabian Sea is transported either by pluming or by turbidity currents from local sources along the Oman margin.

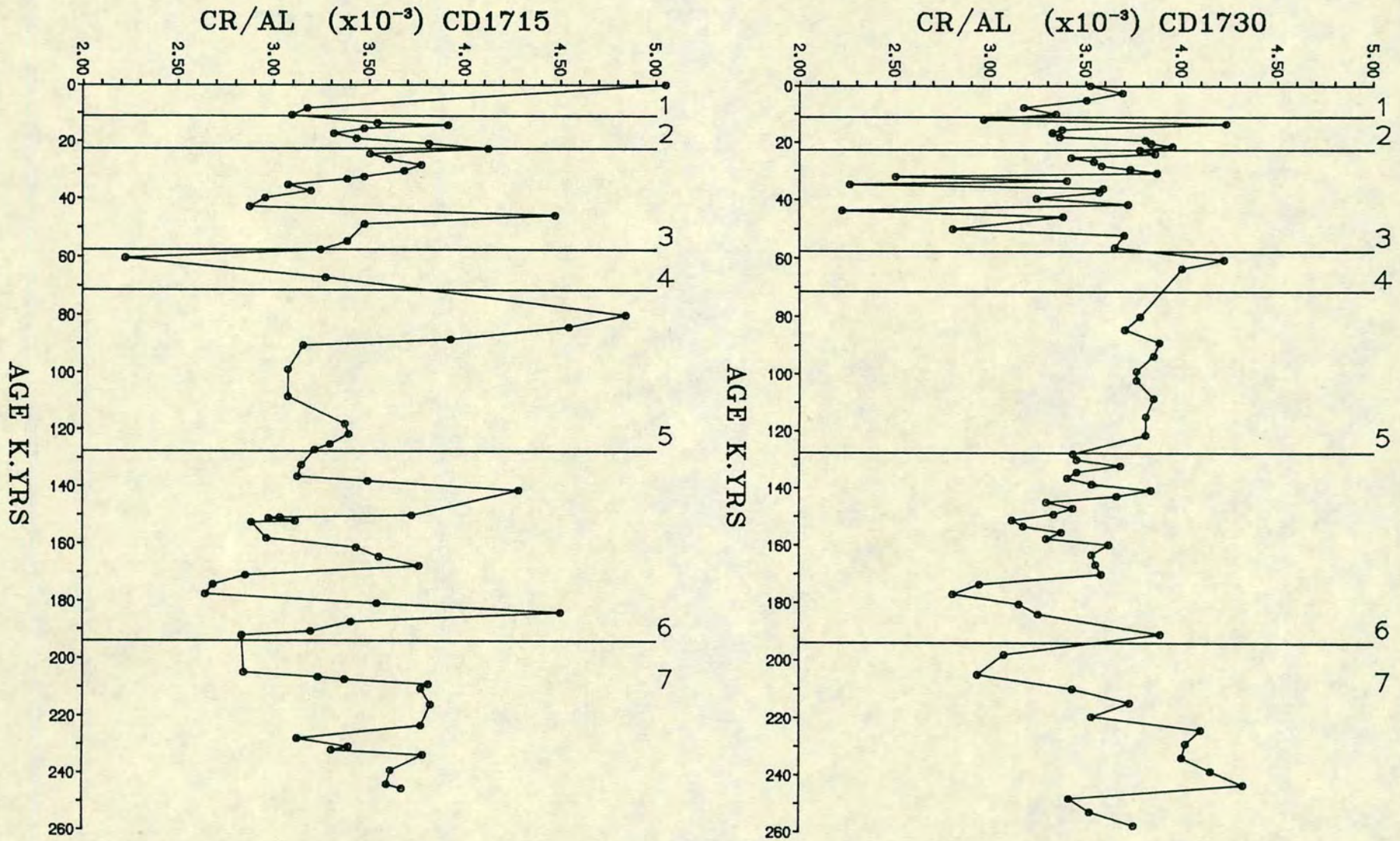

FIGURE 5.14a Cr/Al RATIO PROFILES OF CORES CD1715 AND CD1730.

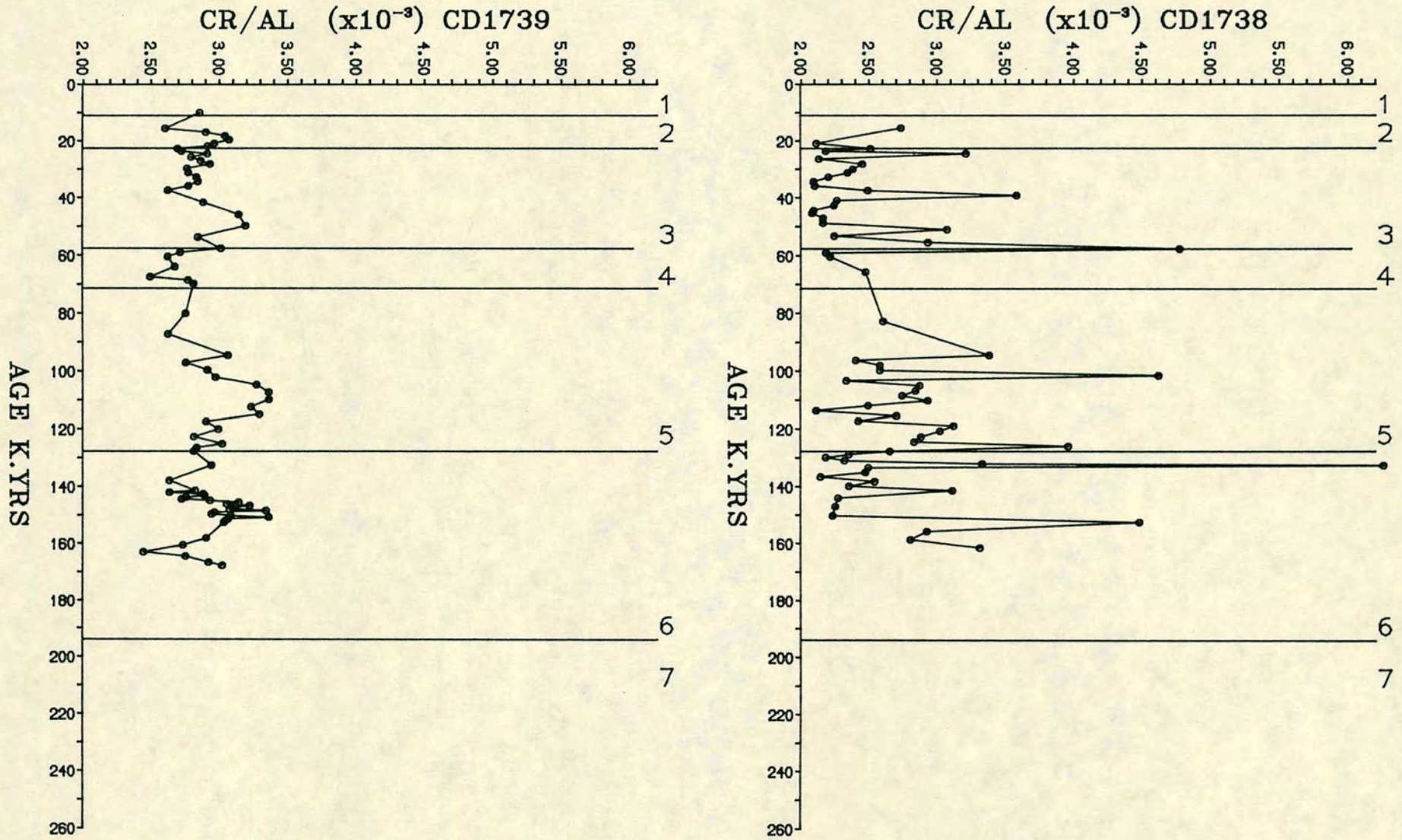

FIGURE 5.14b Cr/Al RATIO PROFILES OF CORES CD1739 AND CD1738.

The zirconium and titanium distribution in oceanic sediments is largely controlled by the presence of coarse grained heavy minerals. Similarly, the chromium content also indicates its association with heavy minerals like chromite, ilmenite, magnetite. One may expect a positive correlation between these elements in the cores. Although this occurs within coarse-grained turbidites (Table 5.2), their ratios with Al in the pelagic sediments of the cores do not always covary. For example, in core CD 1715, Ti/Al ratios (Fig. 5.8a) are highest and follow Zr/Al ratios (Fig. 5.12a). In Stage 3 of this core, Cr/Al (Fig. 5.14a) ratio is higher than in Stage 5. Core CD 1730, which is free of turbidite bands shows higher Zr/Al ratios and is vertically constant like the Ti/Al ratio (Fig. 5.8a, 5.12a). In contrast to core CD 1715, the Stage 3 sediments in core CD 1730 show lowest Cr/Al ratios and high ratios in Stage 5.

This differing behaviour of Cr in comparison to Zr and Ti in these sediments, implies a fluctuating input from a Cr rich source, in contrast to a uniform input of Zr and Ti.

5.4:1 Distant and local sources

Zirconium and quartz both in the NW Arabian Sea sediments occurs as either hydrodynamically heavy or coarse-grained constituents. Their variation with time is similar, and this relationship may indicate a distant provenance, predominantly transported by prevailing winds. Ratios of Zr to Quartz shown in Fig. 5.15, indicate a constant ratio over a period of 250,000 years, in contrast to the ratio against Cr which oscillates significantly (Fig. 5.16).

The uniform Zr/Qtz ratios down cores (Fig. 5.15) and the changing Cr/Zr ratios imply that either the sources of zirconium and chromium are different or that they were transported by different media. The higher Zr/Qtz ratios in northern cores eg. CD 1738 (>5.0) suggest that the sediments at these sites contain relatively more heavy mineral input by winds. For instance the Zr/Qtz ratios in core CD 1715 range between 1.5-2.0, while core CD 1730 shows higher ratios 2.0 to 2.5. Core CD 1739 shows a uniform ratio ~2.4.

Zr/Qtz ratios (Figs. 5.15) seen in the studied cores support the view that distribution of Zr and quartz in the Arabian Sea sediments is controlled by the fallout of dust, while the Cr as shown by Cr/Al ratios seems to have been introduced in a different way, which is illustrated in Cr/Zr ratio profiles (Figs. 5.16). Cr/Zr trends in the different isotopic stages of cores CD 1715 and CD 1730 (Fig. 5.16a), differ from cores in the Gulf of Oman area. Cores CD 1715 and CD 1730 have

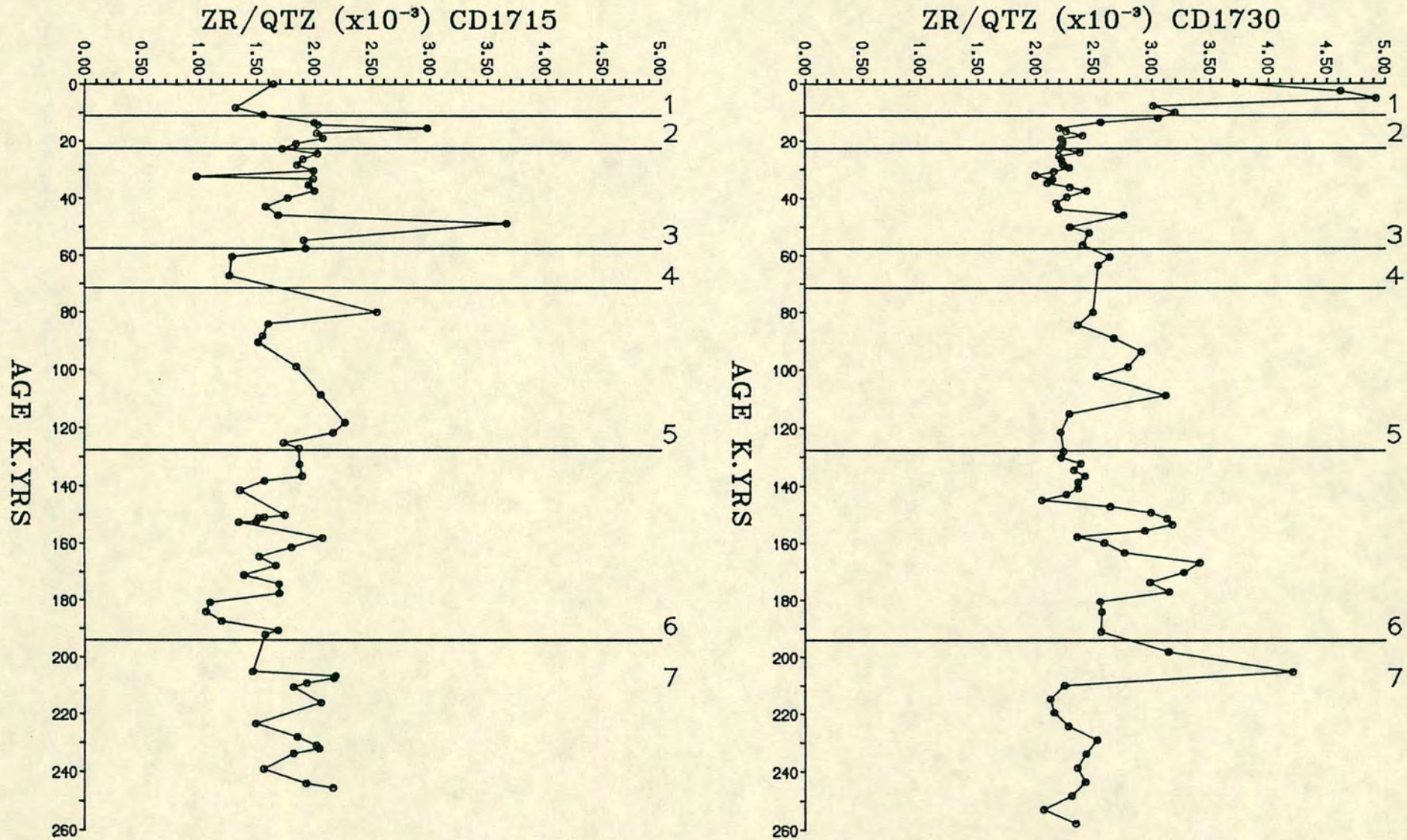

FIGURE 5.15a Zr/Qtz RATIO PROFILES OF CORES CD1715 AND CD1730.

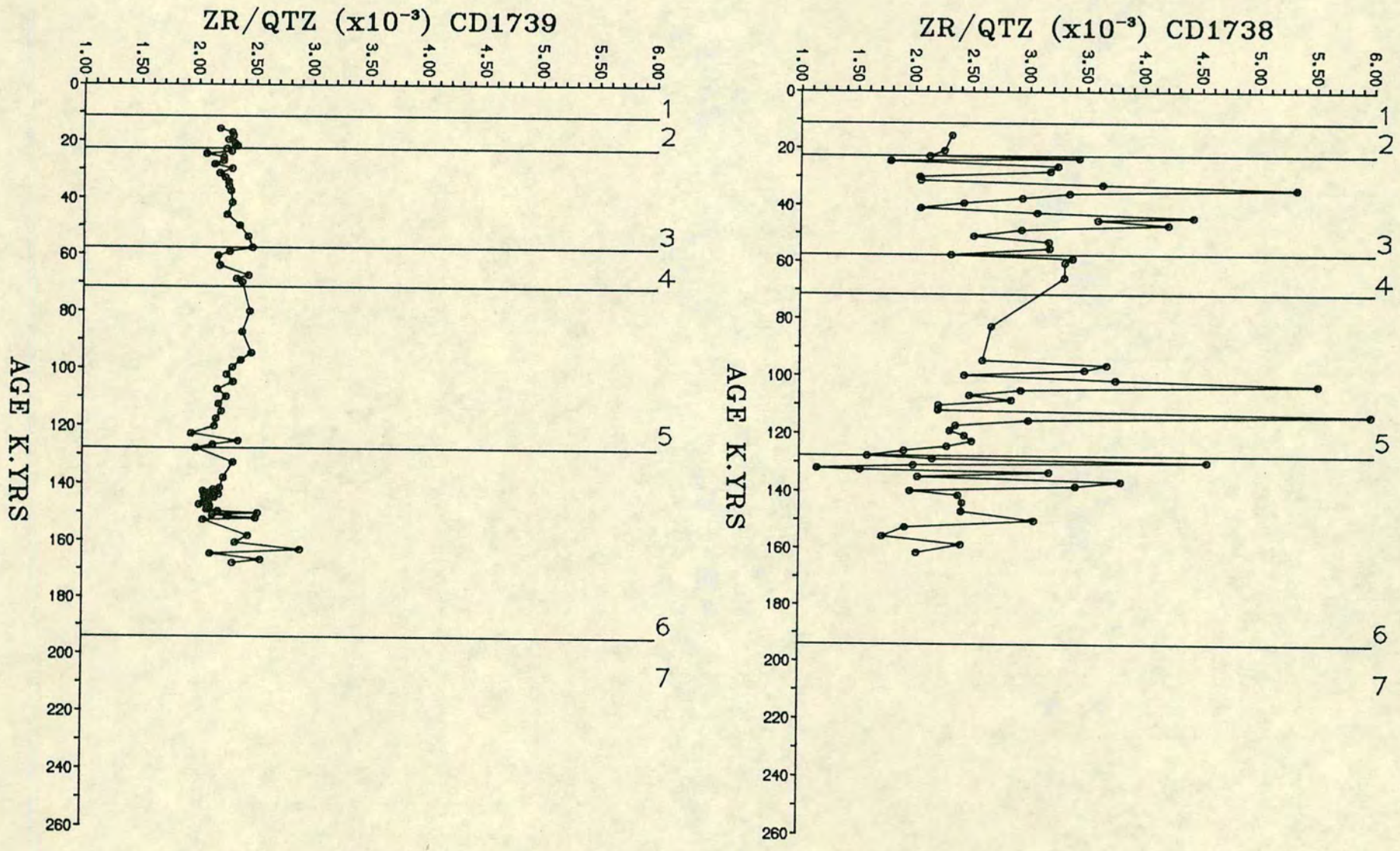

FIGURE 5.15b Zr/Qtz RATIO PROFILES OF CORES CD1739 AND CD 1738.

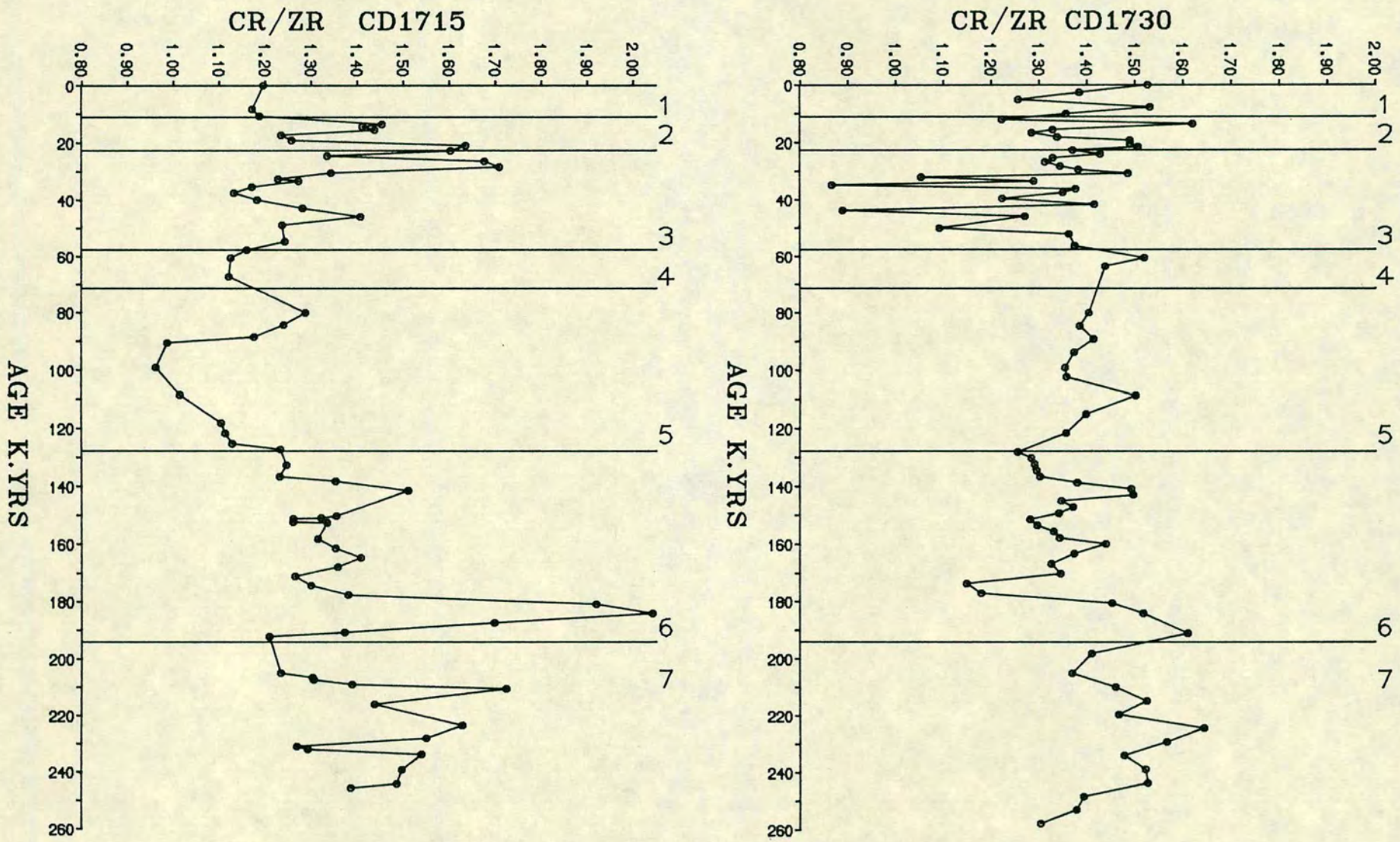

FIGURE 5.16a Cr/Zr RATIO PROFILES OF CORES CD1715 AND CD1730.

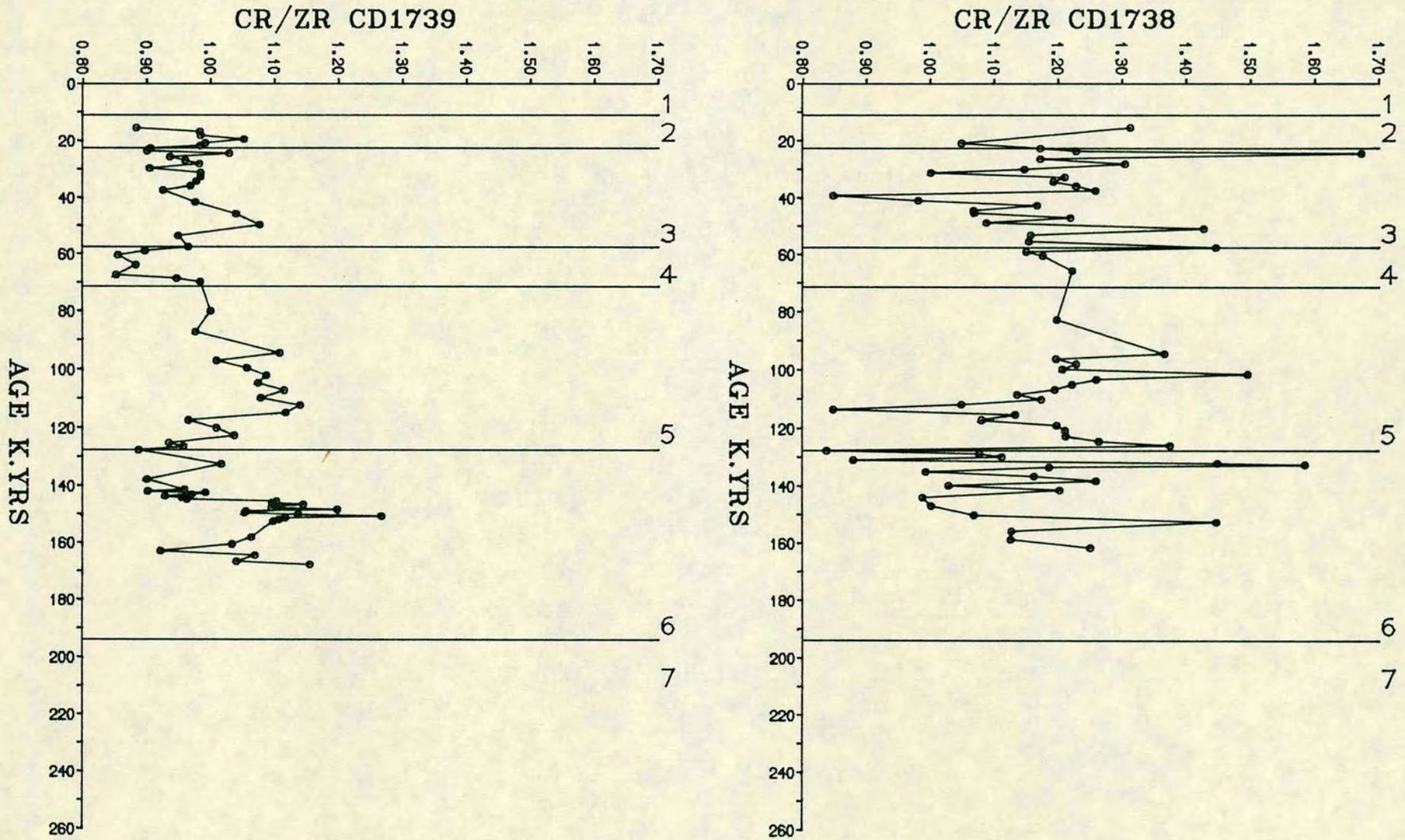

FIGURE 5.16b Cr/Zr RATIO PROFILES OF CORES CD1739 AND CD1738.

similar ratios in glacial Stages 2 and 6 and also in interglacial Stage 7. However, there is a marked difference in ratios within the period 130,000 years BP to 20,000 BP. Interglacial Stages 3, 5 and intervening glacial Stage 4 are showing antipathetic trends in that chromium in Stage 3 relative to Zr is high (>1.20) in core CD 1715 and low (<1.20) in core CD 1730. The interglacial Stage 5 shows an opposite trend to that of Stage 3 in these cores.

Enrichment and impoverishment of Cr relative to Zr in in isotopic Stages 3 and 5 of CD 1715 and CD 1730, may suggest some mechanical redistribution of Cr in these sediments. High Cr relative to Zr in Stage 3 of core CD 1715 probably indicates that currents were of insufficient strength to redistribute the Cr evenly in north western Arabian Sea sediments. The Cr/Zr ratio trend in core CD 1730 is similar to that of the general trend in core CD 1738, and it is quite possible that a high dust input has an overall diluting effect on Cr content. However, the unusually high Cr/Zr ratio in Stage 5 of core CD 1730 may be due to an unusual input of Cr from near shore sediments, and was introduced by water currents as sediment plumes.

5.5 RARE EARTH ELEMENTS

The rare earth elements (REE) within the sediments are predominantly lithophilic in nature and reflect the clay mineral content. Clay minerals, as the products of weathering of igneous minerals, tend to inherit and average the REE distribution of their sources. The low concentrations of REEs associated with quartz and the other major silicates (such as feldspar) generally cause a decrease in the REE contents of coarse-grained sediments (Haskin et al., 1966).

In this section, an attempt has been made to identify the pattern of REE distribution in the NW Arabian Sea sediments in order to ascertain the source, composition and nature of sediments in the four cores. In chapters 4 and 5, it has been noted that detrital constituents in sediments contain various proportions of quartz, chlorite, illite and feldspar. Elements like Si, Al, Fe, K, Ti and Zr are directly or indirectly related to their content in the sediments. In the four cores, the ratios of various minerals and elements change with time. The northern cores, CD 1738 and CD 1739, are rich in chlorite relative to quartz and feldspar, whilst the latter minerals are of a relatively higher concentration in cores CD 1715 and CD 1730. A similar trend is observed in the chemistry of Si, Fe, Zr and Cr of these cores. This represents a change in mineralogy, and therefore indicates some variation

of source and the intensity of the wind transport. Thus it is possible that REE distribution may help to confirm the changing character or source of the sediments.

REEs analysed by XRF techniques are listed in appendix C.7. The mean content of REEs (La, Ce, Nd, Y) in each core is given in table 5.3. They show slightly lower values than shales, which is probably caused by a greater dilution from quartz (Haskin et al., 1966). Table (5.3) also shows a general enrichment of REEs from core CD 1715 to CD 1738. This increase towards cores CD 1738 and CD 1739 may be due to a smaller content of feldspar and different proportions of clay minerals in these cores as seen in Fig. 4.6. Furthermore, the ratios of La and Nd relative to Ce change from south to north, and their patterns as element ratios are displayed in Figs. 5.17, 5.18, 5.19.

REEs ratios relative to Ce and Nd observed in cores CD 1738 and CD 1739 are very similar to the European and North American shales (Table 5.3) (Haskin and Haskin, 1966). Cores in the south (ie. CD 1715 and CD 1730) do show different ratios and the high ratios of Nd/Ce (~0.50) in cores CD 1715 and CD 1730 suggest that sediments in the south are relatively richer in Nd than Ce, than in the north (Table 5.3). This implies that Nd and Ce are differently partitioned in illite, chlorite and possibly feldspar. Since the cores CD 1715 and CD 1730 are found to contain more feldspar relative to chlorite, (chapter 4) and that feldspars can have very different REE ratios (Schnetzler and Philpotts, 1970). Therefore the low REE content in cores CD 1715 and CD 1730 and higher Nd/Ce ratios may be following the relative enrichment and depletion of feldspar and also chlorite in these sediments. Although some correlation between the type of clay mineral and REE content is known (Dypvik and Brunfelt, 1976; Chaudari and Cullar, 1979), it is not always discernable (Cullers et al., 1975). Hence, it is difficult to establish whether the clay mineral differences account for the varying REE contents and REE element ratios of NW Arabian Sea sediments.

The distribution pattern shown in Figs. 5.17, 5.18, 5.19 shows a change in REE ratios between the glacial and interglacial events of cores CD 1715 and CD 1730. Core CD 1738 and CD 1739 show no such difference, which implies a more uniform detrital input from a single source. High average REEs ratios given in Table 5.3 indicates a lower La and Ce content relative to Nd in the south, which may be coupled to the higher feldspar and poorer chlorite contents of these sediments. The profiles of REEs ratios shown in Figs. 5.17, 5.18, 5.19 are similar in trends for the different cores. This is seen especially in La/Ce, La/Nd, Ce/Nd of cores CD 1715 and CD 1730. Generally, these ratios are low in the Holocene and fluctuate considerably in a period from 70,000 years BP to 10,000 years BP, encompassing Stage 2 and Stage 3. For the most part, the profiles in these Stages are very spiky and do not show obvious trends, except for being lower in Stage 2.

Table 5.3 Mean concentration of REEs and their ratios to Ce and Nd.

Cores #	La (ppm)	Ce (ppm)	Nd (ppm)	Y (ppm)	La/Ce	Nd/Ce	La/Nd	Ce/Nd
CD 1715	9.61	32.18	17.40	18.42	0.31	0.55	0.57	1.87
CD 1730	10.99	35.01	17.31	19.19	0.31	0.50	0.64	2.06
CD 1739	15.22	37.85	18.29	18.37	0.40	0.48	0.85	2.09
CD 1738	22.48	53.57	22.27	22.21	0.43	0.42	0.98	2.38
N America Shale	32	73	33	27	0.43	0.45	0.96	2.21
European Shale	41	86	42	32	0.47	0.48	0.97	2.04

Data from Haskin and Haskin, 1966.

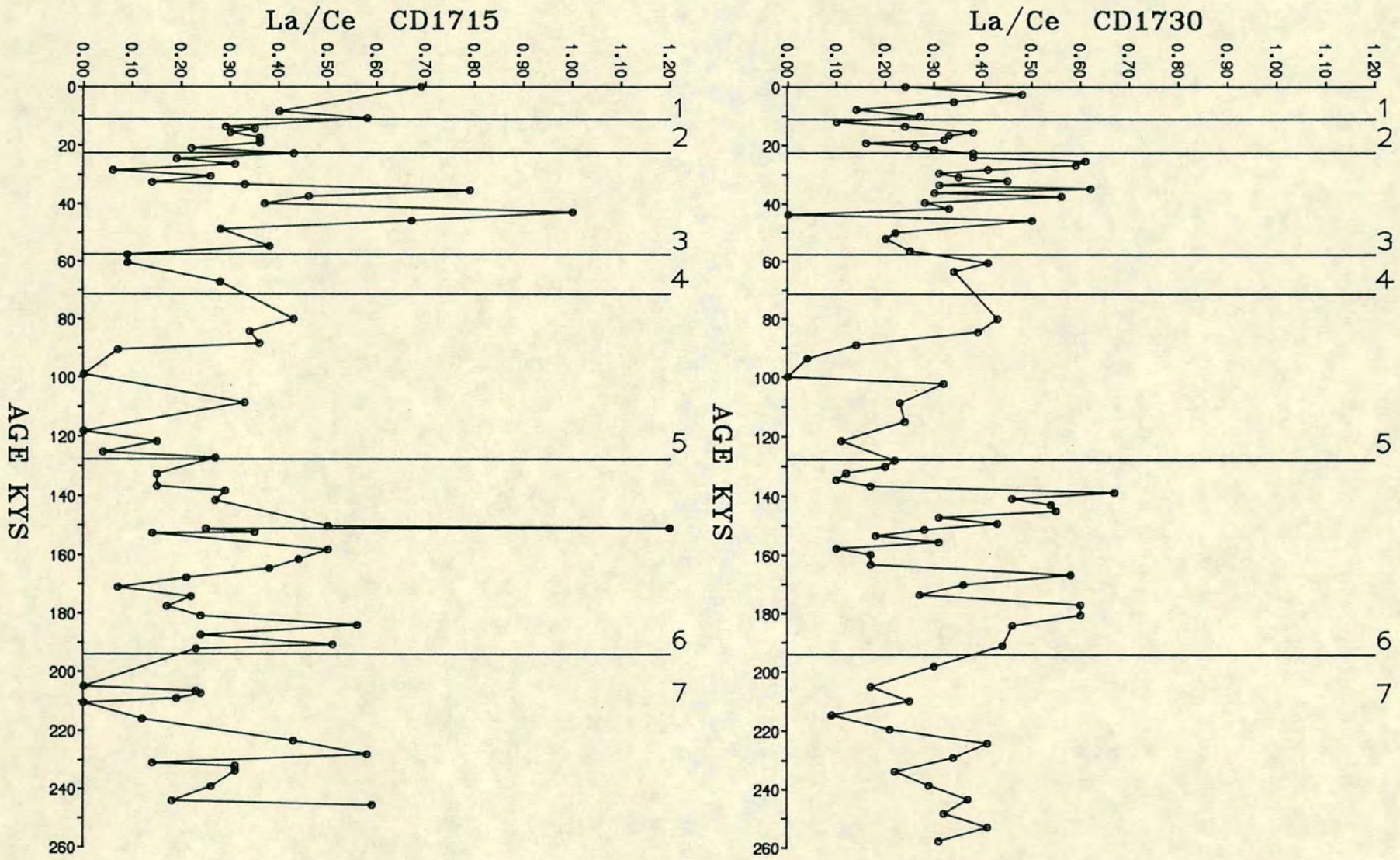

FIGURE 5.17a La/Ce RATIO VARIATIONS IN CORES CD1715 AND CD1730.

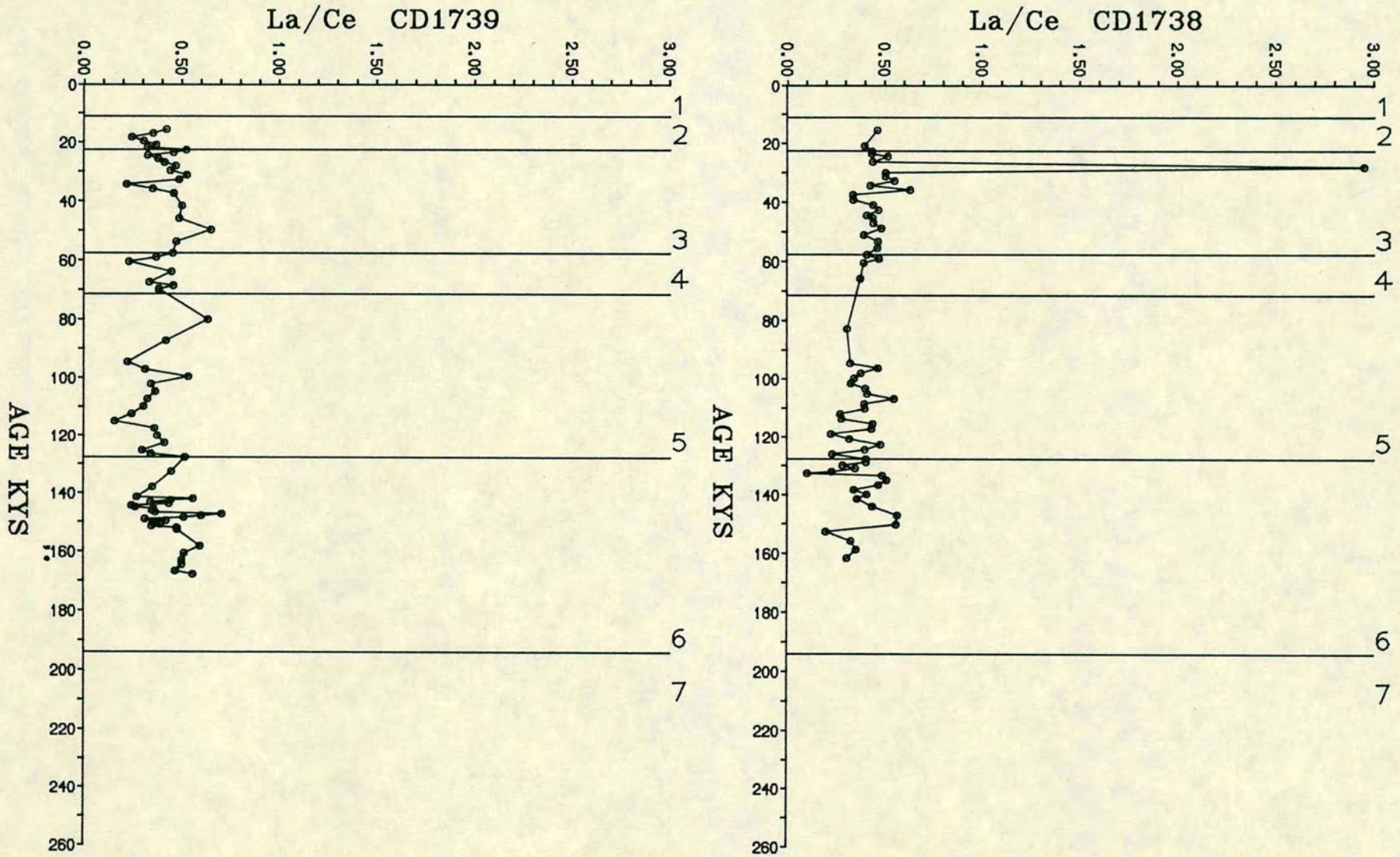

FIGURE 5.17b La/Ce RATIO VARIATIONS IN CORES CD1739 AND CD1738.

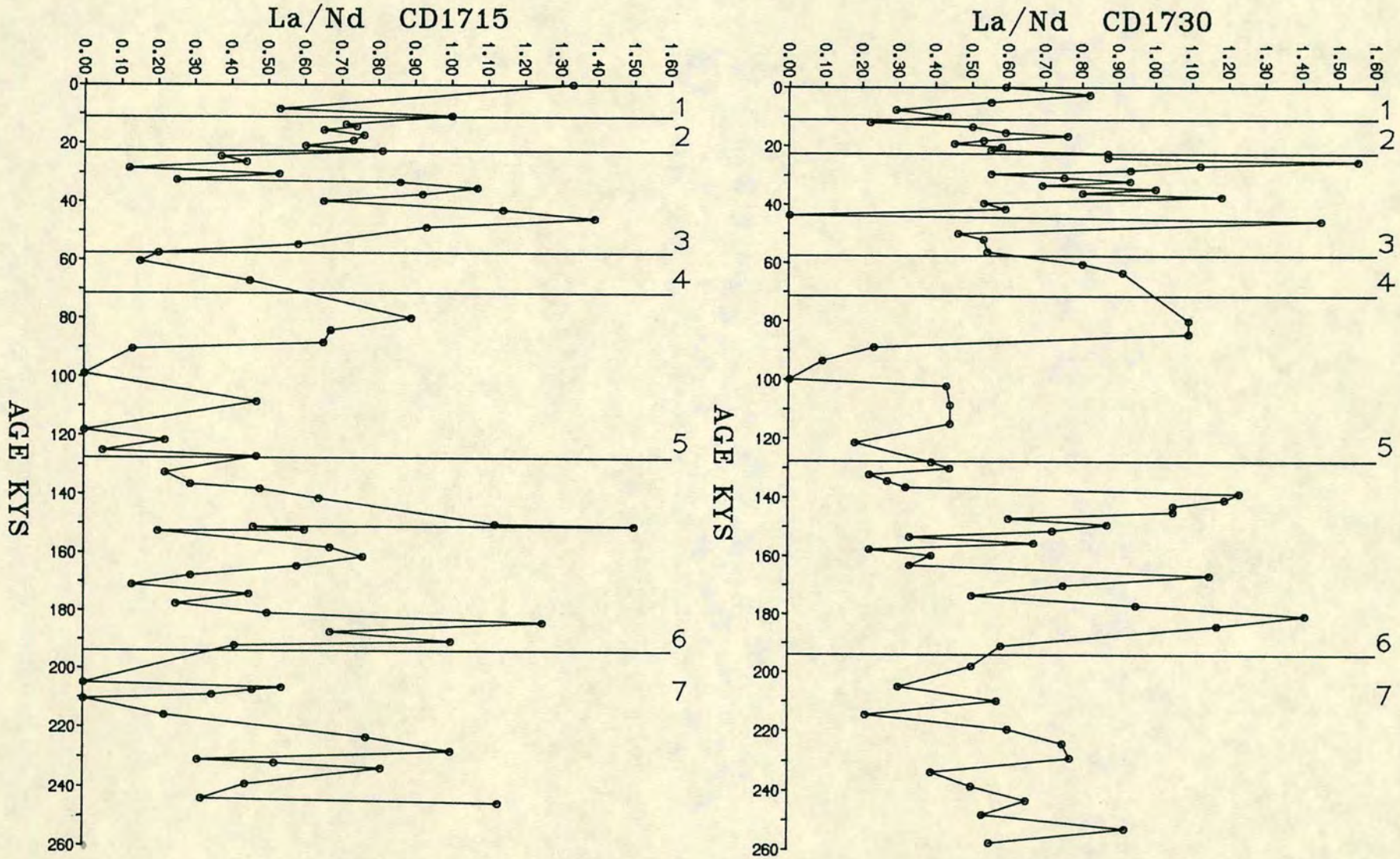

FIGURE 5.18a La/Nd RATIO VARIATIONS IN CORES CD1715 AND CD1730.

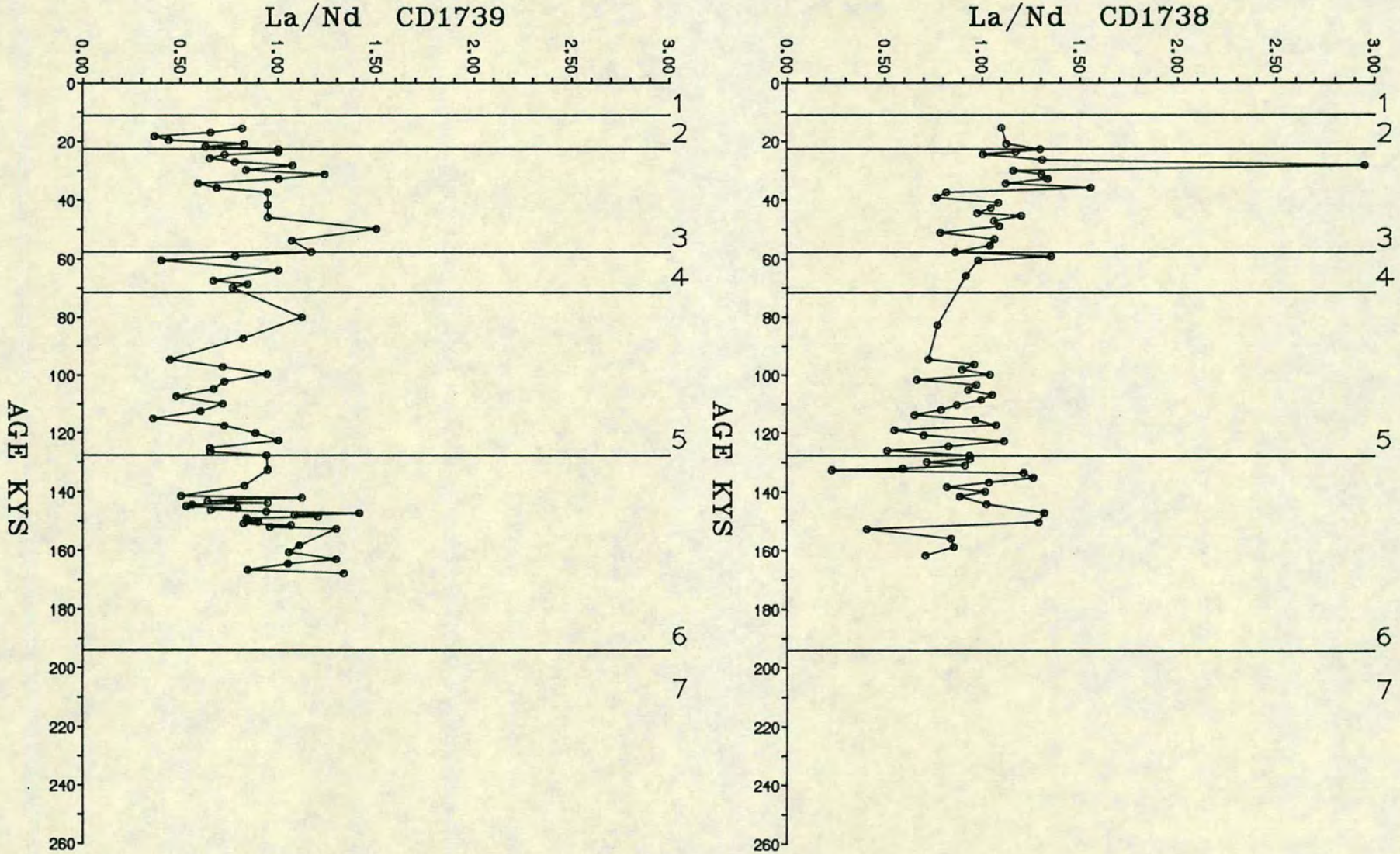

FIGURE 5.18b La/Nd RATIO VARIATIONS IN CORES CD1739 AND CD1738.

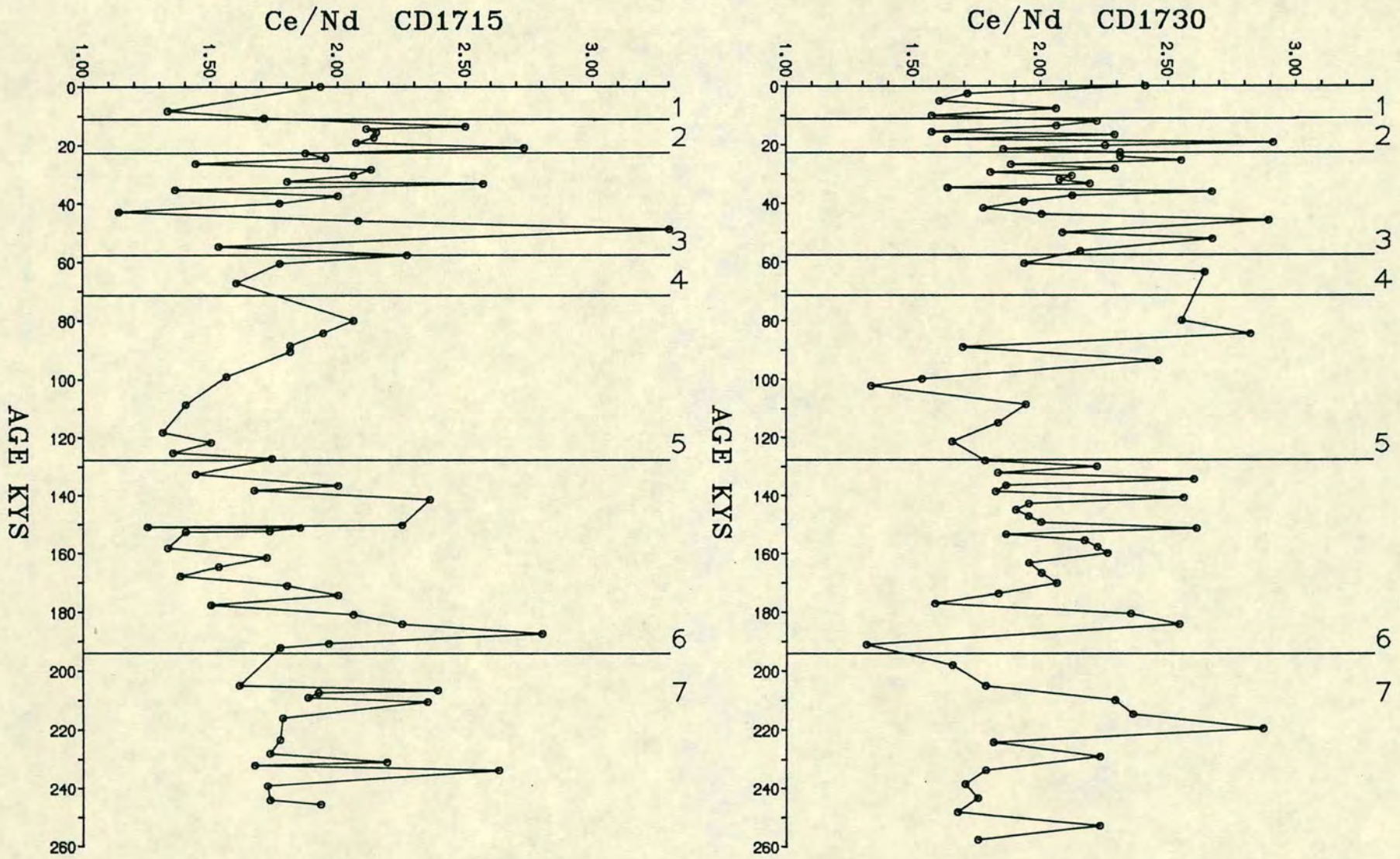

FIGURE 5.19a Ce/Nd RATIO VARIATIONS IN CORES CD1715 AND CD1730.

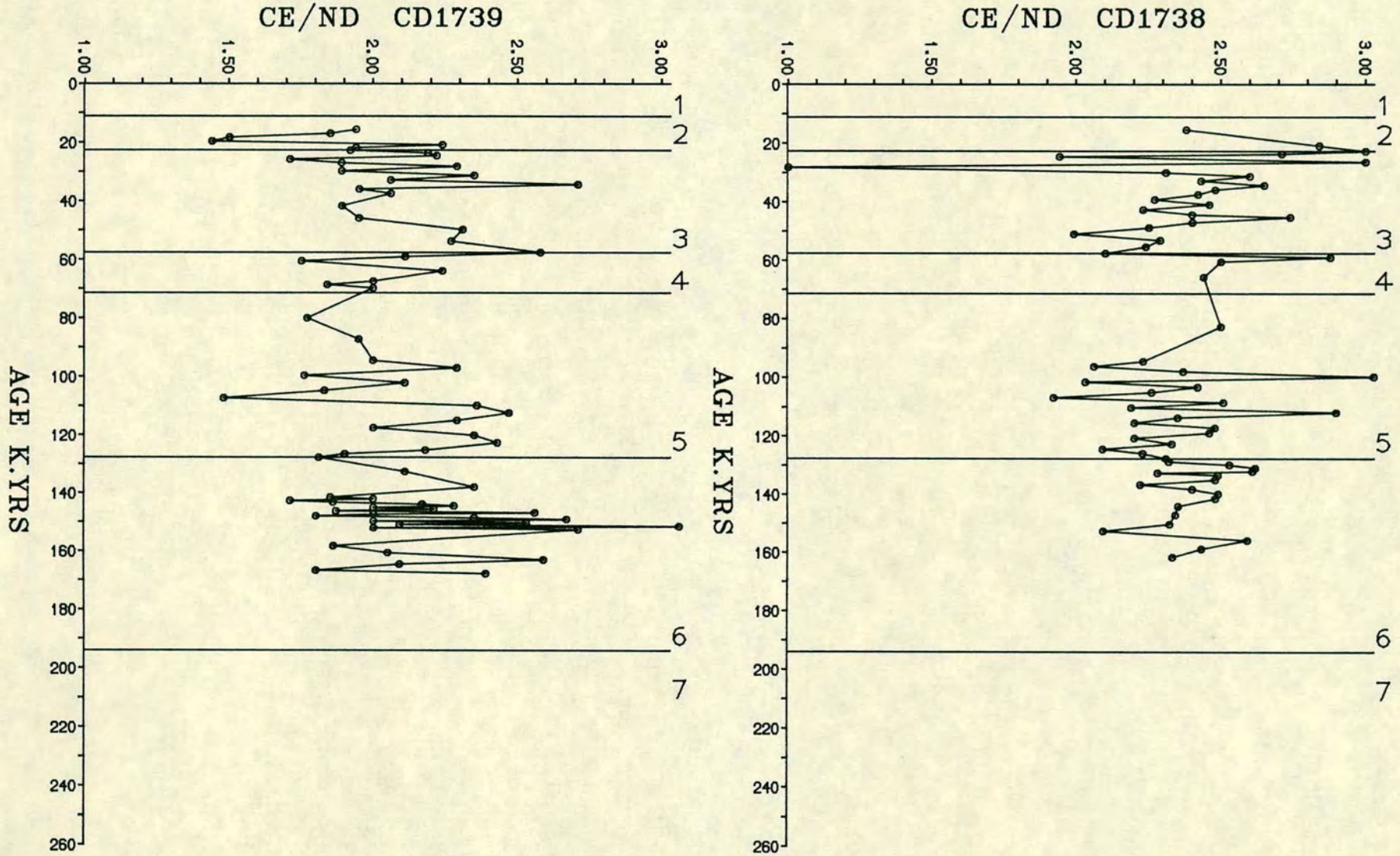

FIGURE 5.19b Ce/Nd RATIO VARIATIONS IN CORES CD1739 AND CD1738.

In the older Stages 4, 5, 6, 7 and glacial Stage 4 shows a decrease in ratio. In Stage 6, REE ratios show higher values. This is likely to be associated with chlorite/illite changes (Figs. 4.7 and 4.8) and indicates a significant increase in clays relative to feldspar in glacial Stage 6, whereas in preceding interglacial Stage 5 chlorite is impoverished relative to feldspar. Thus the trends observed in the REE ratio profiles (Fig. 5.17, 5.18, 5.19) suggest that the higher ratio in Stage 6 is a result of relatively more clay than feldspar, compared to Stage 5. Interglacial Stages 5 and 7 show sympathetic trends in core CD 1730 and CD 1715. Ratios of REEs tend to increase during these stages, especially in the upper part of Stage 5. The trends in interglacial Stages 5 and 7 imply that sediments are different in clays which host the REEs.

CHAPTER 6

GEOCHEMISTRY OF BIOMARKERS

6.1 INTRODUCTION

It is known that the distribution of calcite, barite ($BaSO_4$), opal (Biogenic SiO_2) and organic carbon in deep sea sediments largely reflects the biochemical cycles in the ocean (Bishop, 1988; Lyle et al., 1988). Generally, the sediments underlying areas of high surface water productivity, show a considerable increase in their carbonate contents but more importantly in the contents of barite, opal and organic carbon (Arrhenius, 1952; Goldberg and Arrhenius, 1958; Turekian and Tausch, 1964; Koblentz-Mishke et al., 1970; Bostrom et al., 1973; Muller and Suess, 1979; Premuzic et al., 1982; Calvert and Price, 1983; Jansen et al., 1988). A good correlation between calcite, opal and organic carbon fluxes has been shown from sediment trap data in areas of high biological production in the equatorial Pacific and Atlantic (Fisher, 1983; Dymond and Lyle, 1985).

In the north Arabian Sea the imprints of overlying water productivity have been observed (Olaussan et al., 1971; Marching, 1974; Prell, 1984; Shimmield et al., 1988) and show a high input of organic carbon, biogenic calcite and opal to the seafloor. The fertility record in the north Arabian Sea sediments is, however, dominated by calcareous skeletons, in contrast to other major upwelling areas of the world (Gulf of California: Calvert, 1966; Krissek et al. 1980; Namibin: Calvert and Price, 1983) where diatomaceous sediments are abundant. Shimmield et al. (1988) attributed this difference to a seasonal upwelling linked with the monsoon system.

In this chapter, areal and temporal distribution of the biomarkers including calcite, excess Sr (non-terrigenous), excess Ba (non-terrigenous), organic carbon and biogenic silica are described. Here it is aimed to show their geochemical association, and to correlate these with the biogenic input. Factors like dissolution, degradation and dilution by other constituents will be discussed in chapter 9, which are primarily concerned with their accumulation rates.

6.2 CALCITE ($CaCO_3$) DISTRIBUTION

Mechanisms controlling the carbonate sedimentation in deep oceans have been a subject of great discussion for the last two-three decades (Volat et al. 1980), but it is universally agreed that calcite supply is biogenic; from organisms capable of precipitating carbonate out of sea water to build their skeletons. Arrhenius (1952) proposed that the carbonate productivity associated with glacial periods in the tropical Pacific was caused by higher wind strength, and consequently more

intensified upwelling than is observed today. Later workers have supported this hypothesis although with slight reservations (Broecker et al., 1958; Hays et al., 1969; Quinn, 1971; Gardner and Hays, 1976; Valencia, 1977; Pederson, 1983).

One problem that has not been satisfactorily solved is whether total biological productivity and the calcite content of sediments are related. Upwelling of nutrient rich water is also likely to induce siliceous productivity, and hence may consequently cause some reduction of carbonate productivity. Similarly the increase in total biological productivity would increase the production of organic matter and its fall out to the seabed. Under these circumstances, the CO_2 evolved by the oxidation of organic matter during fallout may intensify carbonate dissolution (Berger, 1970; Theide, 1973; Thunnel, 1976). It is because of these observations that it is extremely difficult to quantify biological processes. Furthermore, high fluctuating total sedimentation rates tend to affect dissolution of carbonate by protecting the tests on the seabed. Nevertheless, Arrhenius (1952) and Pederson (1983), showed that a carbonate increase observed in sediments of Wisconsin age (the last glacial maximum) in the equatorial Pacific is a direct result of increased productivity. Lyle et al. (1988) in core V19-28 also taken from the eastern tropical Pacific, claim that fluctuation in the calcite record in the sediments is a direct result of calcite production within the euphotic zone. This controversy in the relationship between carbonate contents in sediments and surface total productivity seems also to apply to the sediments from the north western Arabian Sea. However, the north Arabian Sea sediments appear to differ from many other areas in the world, especially in respect of equatorial Pacific Ocean sediment profiles. Northern Arabian Sea sediments seem to show a lower carbonate content during glacial episodes, and in this are superficially similar to carbonate trends in the north Atlantic where higher terrigenous input during glacial events tends to dilute carbonate content.

6.2:1 $CaCO_3$ in Arabian Sea Sediments

Calcium carbonate contents in northern Arabian Sea sediments were determined from the Ca analysis performed by XRF spectrometry (Appendix B.3) and are given in appendix C.10.

Comparisons of the distribution of $CaCO_3$ in the examined cores from the Arabian Sea have been illustrated in Fig. 6.1 and they allow one to determine the spatial and temporal changes in $CaCO_3$ content in the different cores. A very clear pattern that the calcite record displays, is that carbonate content varies considerably from one core to another. Core CD 1715 and CD 1730 (Fig. 6.1a) show relatively

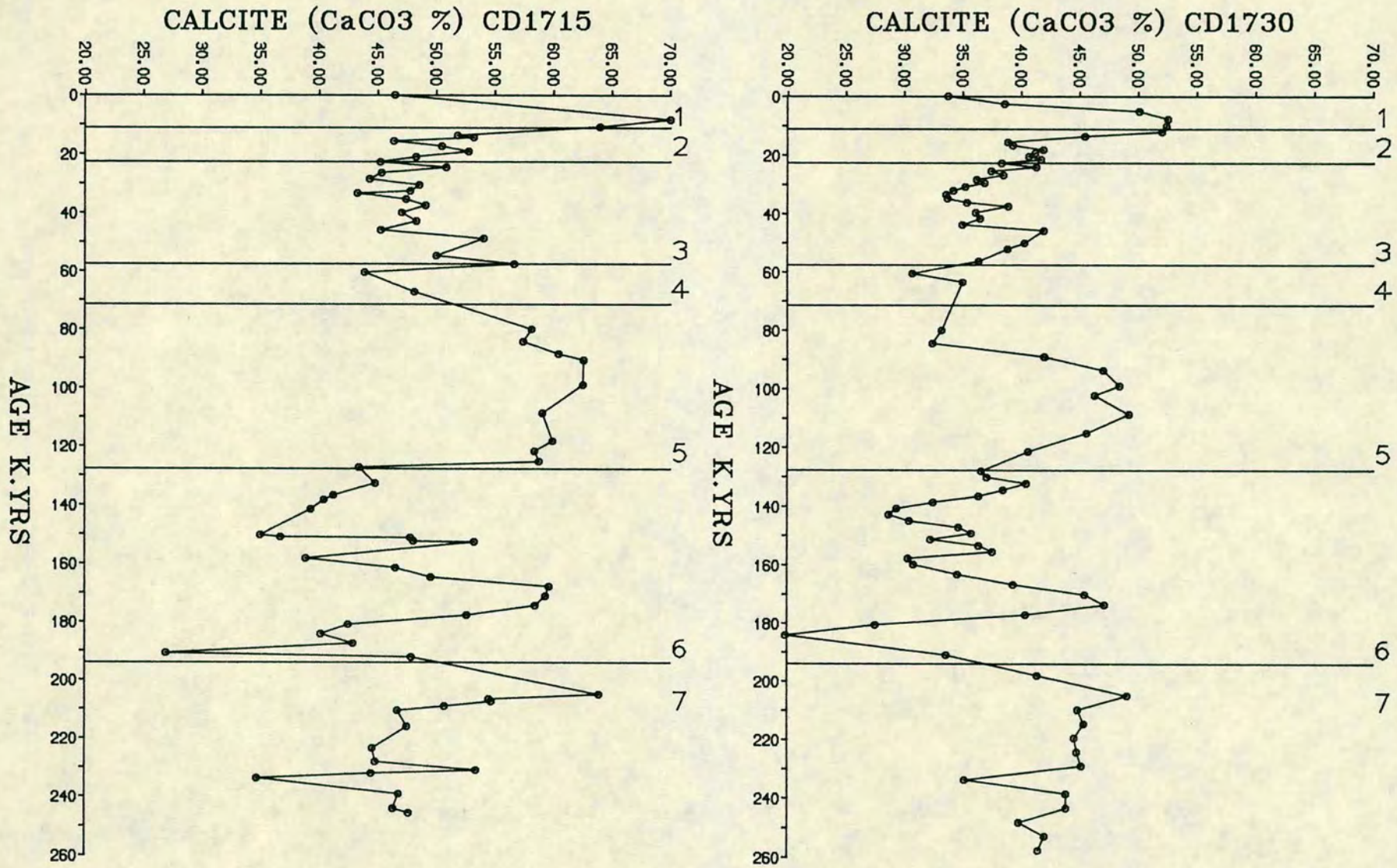

FIGURE 6.1a CALCITE ($CaCo_3$%) VARIATIONS IN GLACIAL AND INTERGLACIAL STAGES OF CORES CD1715 AND CD1730.

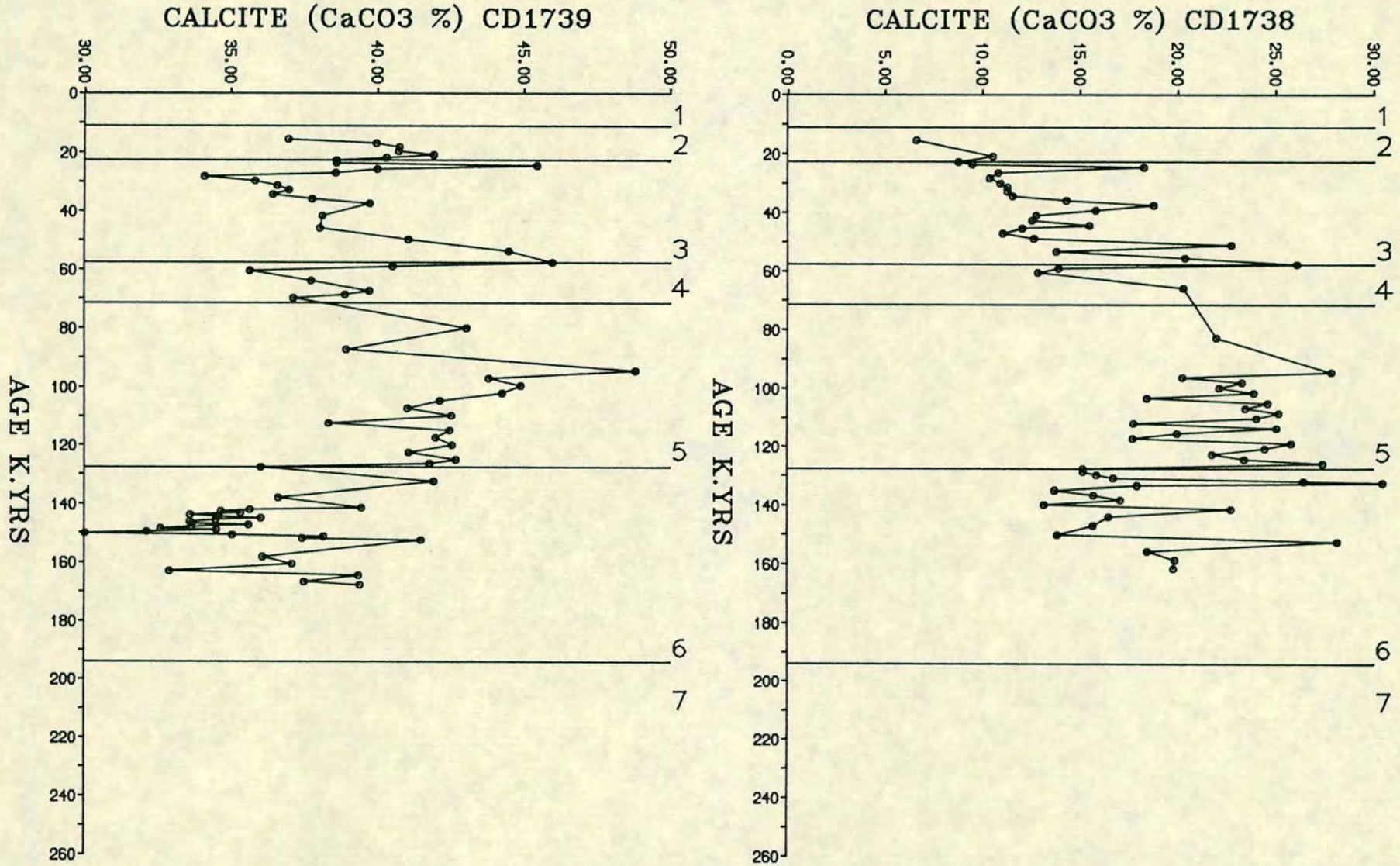

FIGURE 6.1b CALCITE ($CaCo_3$%) VARIATIONS IN GLACIAL AND INTERGLACIAL STAGES OF CORES CD1739 AND 1738.

high carbonate contents ie. ~40-50% calcite and are much higher than those of cores CD 1739 and CD 1738 which show low calcium carbonate ≤ 40.0%. Core CD 1738 is highly impoverished in calcite, especially in the upper section of the core comprising the period of the last 100,000 years, where carbonate content is only ~10.0% (Fig. 6.1b).

Down all cores, the calcite records (Figs. 6.1) extending over the last 250,000 years BP, display a pattern that is reminiscent of both the low (Atlantic type) and the high (Pacific type) carbonate content. Holocene sediments which occur in cores CD 1715 and CD 1730 (Fig. 6.1a) mark a maxima where carbonate is as high as 70.0%. Further, calcite profiles appear to exhibit the highest contents at the transitional boundary of glacial to interglacial stages, and these are very pronounced at the boundary between Stages 1-2 and Stages 3-4. Such a pattern also occurs within the upper Stage 6 but at 128,000 years, that is before the inception of the last interglacial, all the carbonate records show an abrupt decrease. Calcium carbonate contents of the interglacial and glacial stages are different from one core to another. For instance, the interglacial Stage 5 is very high in carbonate content in all cores and generally ranges between 40-50%, but in core CD 1715 calcium carbonate exceeds 62.0%. In Stage 3 carbonate contents are always low compared with Stage 5; core CD 1715 shows 35-40% calcium carbonate and in other cores CD 1730 and CD 1739 carbonate is even lower, 30-40% respectively. In contrast to interglacial Stages 3 and 5, Stage 7 is distinct in its trend of calcium carbonate and generally shows low carbonate ~45.0%. During the glacial Stages 2, 4, and 6 carbonate contents tend to be low and are generally less than 40%. However, Stage 2 is calcite rich (40%) relative to earlier glacial stages. In cores CD 1715 and CD 1730 (Fig. 6.1a), middle Stage 6 horizons also exhibit an increased carbonate content but show greatly reduced carbonate at their upper and lower boundaries, especially during an interval of 180,000-200,000 years BP where carbonate content decreases to ~25%.

The carbonate content of the core CD 1738 is low (20-30%), its trend with time, correspond to other cores only in Stages 5 and 6. As a whole, the very low carbonate content in this core, and particularly in the upper section spanning the last 100,000 years where calcite contents are 10%, suggests much dilution from higher terrigenous input. In preceeding chapters describing the mineralogy and geochemistry of lithogenic elements, it has been shown that the detrital content of core CD 1738 and in CD 1739 is high, and it also appears to have more non-clay minerals. The variation in carbonate contents of the investigated cores may also be related to the intensity of upwelling, and an increase of carbonate productivity. The effect of $CaCO_3$ dissolution has not as yet been assessed because all cores are apparently above the CCD. Kolla et al. (1976) have reported that CCD is about 4000

metres deep in the North Indian Ocean and believe that carbonate content variations are caused more by dilution from terrigenous input than carbonate dissolution.

The relative proportions of different calcareous organisms present in sediments may also produce cyclicity in carbonate contents of deep sea cores because of their differential solution and preservation. Olaussen et al. (1971) showed that in cores off the Somali coast, the foraminifera are in greater abundance relative to Coccoliths and he (1961, 1966) found that rises in productivity will increase the number of foraminifera relative to the number of coccolithophorides. To obtain some insight into the changes of carbonate secreting organisms in these cores the Sr/Ca ratio of the carbonate fraction of the sediments has been investigated. Here it is assumed that the major contributor of carbonate to the Arabian Sea sediments are foraminifera, which is also evidenced from Prell (1984) and it has been found that his results of variation in abundance of G. *bolloides* are largely correlated with the carbonate trends seen in the investigated cores. The trend in these cores (particularly CD 1715 and 1730) could be due to higher productivity, and hence carbonate fallout in the northern Arabian Sea during interglacial time. Such variation of $CaCO_3$ contents in sediments may help to establish the pattern of biological production that is likely to be related to climatic changes.

6.3 EXCESS STRONTIUM

The strontium distribution in deep sea sediments is divided between carbonate, apatite, barite and aluminosilicates (El Wakeel and Riley, 1961; Goldberg and Arrhenius, 1958; Hirst, 1962). It is evident, however, that carbonates contain a high proportion of the strontium in marine sediments (El Wakeel and Riley, 1961). In equatorial Atlantic sediments, calcium carbonate ooze is the main contributor of strontium (Turekian and Kulp, 1956). The average Sr concentration of pelagic clays is generally low about 450 ppm (Goldberg and Arrhenius, 1958). Essentially, the main contributors to the deep sea carbonates are the foraminifera and coccoliths. Data on separated foraminiferal tests from different workers are presented in Table 6.1a to show the Sr levels of forams. Generally the foraminifera occur as coarse fractions relative to coccoliths and show high concentrations of strontium (Turekian, 1964), while the strontium content of coccoliths is low (Thompson and Chow, 1956).

Strontium distribution in the surface sediments of the northern Indian Ocean indicates that it is controlled by the carbonate content (Shankar et al. 1987) and in the area of high biological activity, as off the Oman continental margin, the occurrence of calcareous biogenic sediments have been linked to the upwelling record

Table 6.1a **Sr Concentration of Pelagic Foraminefera Tests**

Area	Sr (ppm)	Reference
Equatorial Atlantic	1200	Emiliani (1955b)
Equatorial Pacific Indian Ocean	1300	Thompson and Chow (1956)
Atlantic Ocean	1200	Turekian (1957)
Atlantic Ocean	1150	Krinsley (1960)
Atlantic Ocean	1600	Turekian (1964)

Table 6.1b **Strontium in Coccolith tests**

	Sr (ppm)	Reference
Coccolith chalk - Nicobar formation (Cretaceous) Nebraska	1000	Turekian (1964)

(Shimmield et al., 1988). The Sr content in the cores CD 1715, CD 1730, CD 1739 and CD 1738 reported here is as excess strontium that Sr contents calculated to be free from the contribution of Sr in aluminosilicates based on Sr/Al (0.0021) for deep sea clays of Turekian and Wedhpol (1961). This Sr is also corrected for dolomite Sr as the sediments from Arabian Sea are found to contain ~5% dolomite ($CaMgCO_3$ is assumed to contain 700 ppm Sr) (see Appendix B.4).

Excess Sr has been ratioed against Ca associated with calcite to show the variation of excess Sr/Ca ratio between cores and to illustrate variation at depth. The values of excess Sr/Ca ratios of cores CD 1715 and CD 1730 generally range between 3.0 to 4.5 x 10^3 which is in agreement with the reported Sr/Ca ratio of globogerina and deep sea sediments (Table 6.2). Such Sr/Ca ratios suggest that Sr in Arabian Sea sediments is largely associated with foraminiferids with coccolithophorids being very subordinate.

The variation in Ex.Sr/Ca down the cores (CD 1715, CD 1730, CD 1739 and CD 1738) shown in Fig. 6.2 may also be indicative of the relative input of detrital and biogenic calcite. Generally the variation in Sr/Ca ratio in deep sea sediments has been linked with foraminiferids/coccolithophorids (Turekian, 1957; Thompson and Bowen, 1969). Thompson and Chow (1956) have shown that Sr/Ca ratios in coccolith ooze ranges from 1.6 to 1.8 and for forams from 2.2 to 3.3 (Table 6.2). The Ex.Sr/Ca ratio in the Arabian Sea sediments (~3.0-4.0) suggest that coccoliths are a minor fraction relative to forams and this has also been stated by Olaussen et al. (1971). Hence, the variation in Ex.Sr/Ca may be explained either by (a) changes in the production of forams through times or (b) dilution effects resulting from terrigenous supply.

The profiles of Ex.Sr/Ca shown in Fig. 6.2 for investigated cores are broadly similar in pattern to those of $CaCO_3$ content (Fig. 6.1) suggesting some dependency of Sr towards high Ca content horizons. The vertical trends of Ex.Sr/Ca ratios show higher values in interglacial stages, following the $CaCO_3$ content. The Holocene shows the highest values of Ex.Sr/Ca ie. ~4.0 which may indicate that the foraminiferids content is high during this time. The trend in core CD 1738 however, differs from other cores in that it is generally much lower with values <2.0 occurring in the upper 100,000 years section of the core. Such a low Sr/Ca ratio must be explained by much higher contributions of terrigenous calcite to the sediment during this time. It is known that in the Gulf of Oman and Persian Gulf areas there is considerable input of lithogenic calcite (Emery, 1956; Stoffers and Ross, 1979; Sirocko and Sarnthein, 1988). Similarly, during cold stages, higher terrigenous supply with concomitant increase in lithogenic calcite may account for a low Sr/Ca ratio in Arabian Sea sediment. The presence of detrital calcite blown off the neighbouring land masses by wind is reported in surface sediments of the Arabian Sea (Emery,

Table 6.2 **Strontium to calcium ratios reported for deep sea cores and globigerina tests**

Reference	Description	Sr/Ca x 10^3
Odum (1957)	Globigerina ooze	5.5 to 6.6
Emiliani (1955b)	Globigerina tests	2.8
Thompson and Chow (1956)	"Deep Sea Sediments" Indian Ocean	4.2
	"Globigerina ooze" Pacific Ocean	3.3
"	Coccolith	2.0
Turekian (1964)	Coccolith ooze	2.6-2.5
Present study	Deep Sea Sediments NW Arabian Sea	3 to 4.5

Note: Sr in present study is Ex.Sr and Ca is the amount of calcium incorporated in calcite.

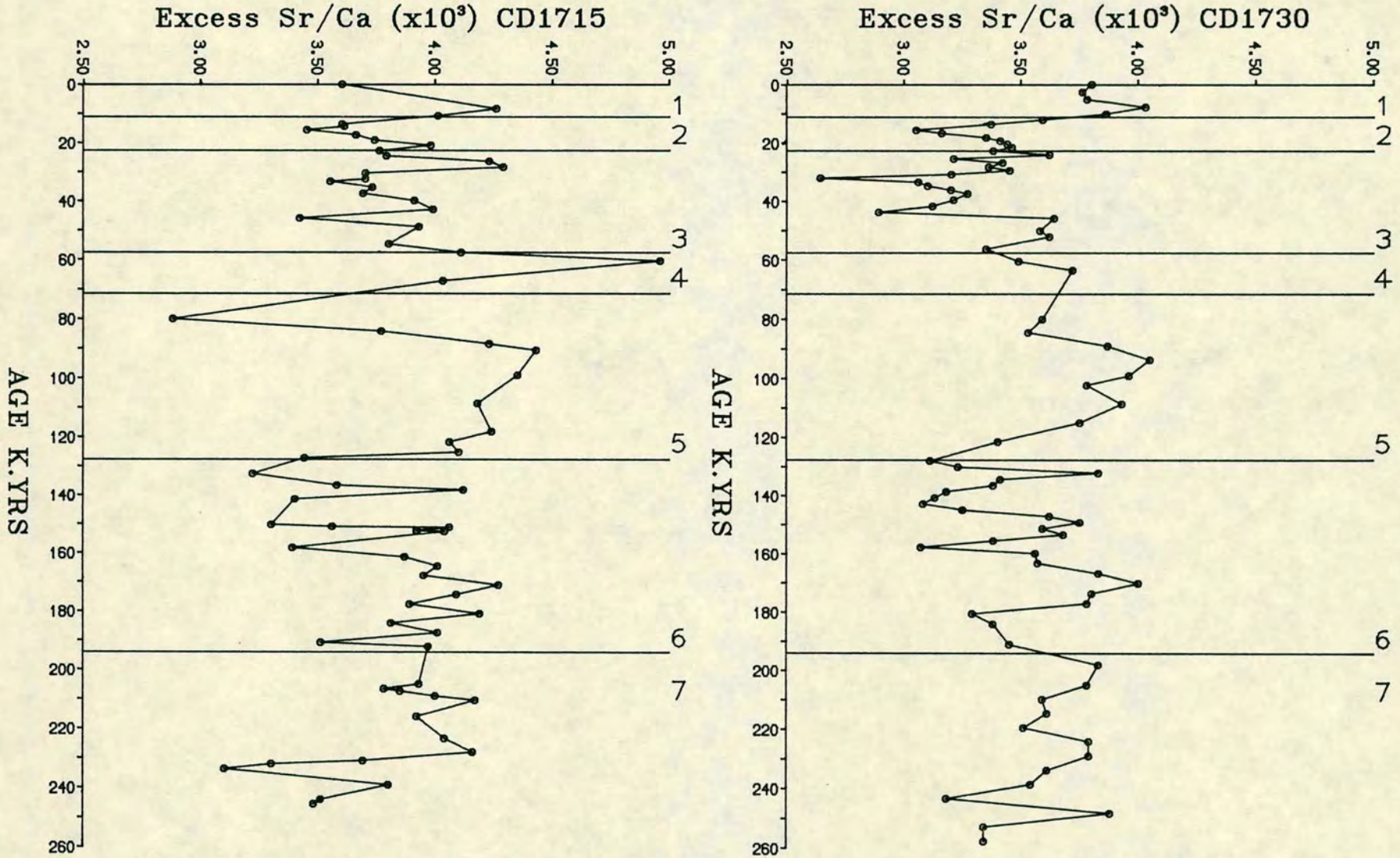

FIGURE 6.2a EXCESS Sr/Ca RATIO VARIATIONS IN GLACIAL AND INTERGLACIAL STAGES OF CORES CD1715 AND CD1730.

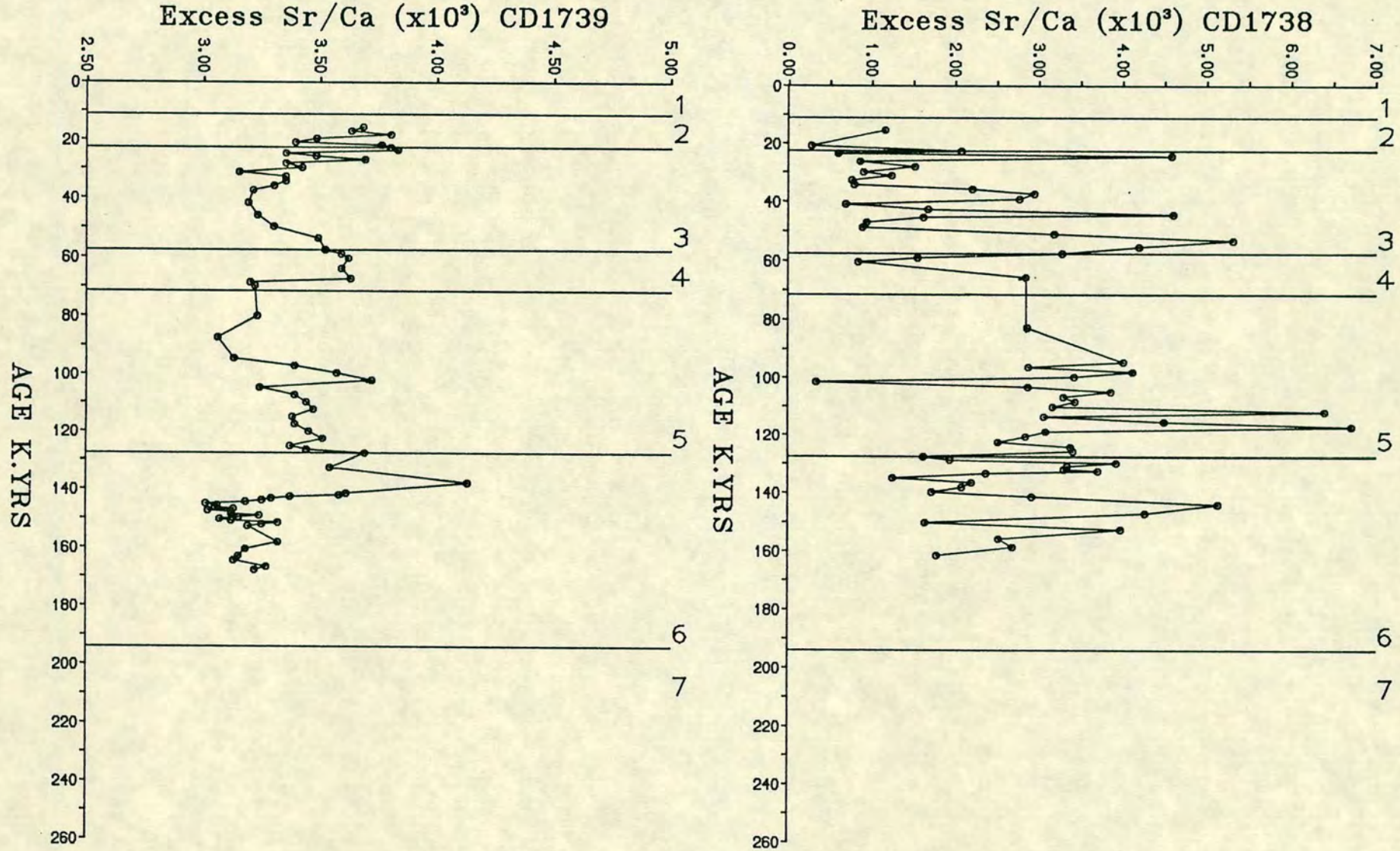

FIGURE 6.2b EXCESS Sr/Ca RATIO VARIATIONS IN GLACIAL AND INTERGLACIAL STAGES OF CORES CD1739 AND CD1738.

1956; Stoffers and Ross, 1979; Sirocko and Sarnthein, 1988). This lithogenic calcite is generally lower in Sr content (200-300 ppm) (Price, pers. comm.) than biogenic calcite (1300-1500 ppm). So the decreasing trend Ex.Sr/Ca ratio during glacial stages may be considered as a result of increased lithogenous material.

6.4 ORGANIC CARBON

The occurrence of upwelling and high primary productivity, along with a correspondingly high concentration of organic carbon in the marine sediments, is a common association found at many of the oceanic margins, especially along the western margins of bordering land masses (Sackett et al., 1973; Muller and Suess, 1979). Off California for example, sediments in the near shore basin contain up to 6% organic carbon (Emery, 1960), while off Peru, where primary production is much more intense sediments show very high organic carbon ie. ~21% (Krisseck et al., 1980). Along the Namibian Shelf, an area of pronounced upwelling, sediments are enriched in organic carbon more than 22.0% (Calvert and Price, 1983). Krissek and Scheidegger (1981) have indicated that the following are important factors in controlling organic carbon and other related upwelling signals in marine sediments.

1. Surface water productivity.
2. Strength and persistence of O_2 minimum zone and its location relative to the sediment accumulation.
3. Magnitude of terrigenous sediment input to the region.
4. Bottom current activity.

The organic carbon record in Pleistocene marine sediments often shows some cyclicity (Stevenson and Cheng, 1972; Muller and Suess, 1979; Pederson, 1983; Curry and Lohmann, 1985; Finney, 1981). Muller and Suess (1979) and Sarnthein et al. (1987) have used such records for estimating the change in paleoproductivity of the overlying waters. The general trend is for more organic carbon to accumulate in sediments associated with upwelling during the last glacial period. Most sediments showing higher organic carbon contents during glacial times are associated with either eastern boundary currents or equatorial current regimes. However, in the Indian Ocean the patterns of organic carbon are such that the northern areas, where a western boundary current prevails especially during the SW monsoons, tend to show a higher accumulation of carbon during interglacial events (Fontugne and Duplessy, 1986).

6.4:1 Organic carbon content in NW Arabian Sea Sediments

The organic carbon content in the studied cores was analysed by the leco analyser on HCl digested samples to dissolve carbonates. For method of analysis see appendix A.4 and tabulated data for each core is given in appendix C.10.

The organic carbon contents distribution and patterns of spatial and temporal variation are shown in Fig. 6.3. It usually ranges between 0.2% to 2.0% and this range is similar to most other oceanic sediments associated with high biological productivity in overlying waters (see Table 6.3). On the basis of average carbon content, the cores can be divided into two groups. Mean values of organic carbon in core CD 1715 and CD 1730 are relatively high, often in excess of 0.75% whereas low values are found in cores CD 1739 and CD 1738 at ~0.5%.

For these cores showing a good Holocene record the organic carbon content at the surface is high (1.0%) and this abruptly decreases to 0.3% in cores CD 1715 and 0.4% in core CD 1730 at stage boundary of 1 and 2 (Fig. 6.3a). At depths in different climatic stages organic carbon shows considerable variations, that could either be related to the changing fertility of overlying water, or caused by fluctuating total sediment accumulation rates. Profiles of organic carbon shown in Fig. 6.3 particularly CD 1715 and CD 1730 show that the organic carbon content in glacial stages tends to be low, while in interglacial stages, it is high. An increase from their normal value of 0.5-0.7% to more than 1.0% in cores during interglacial stages could, if all other factors were the same, be an indication of higher productivity related with upwelling. However, contrasting patterns of organic carbon distribution are also evidenced within certain isotopic stages and in cores CD 1739 and CD 1738. For instance, stages 3, 5 and 7 in cores CD 1715 and CD 1730 show a minimum organic carbon content at the stage boundaries of 3/4, 5/6 and 6/7. Organic carbon values at these boundaries tend to be about half that of the average carbon content in the upper part of the same stages. In core CD 1715, a very high value of organic carbon (2.0%) at the boundary of Stage 6/7, which is not pronounced in CD 1730 may be due to an unidentified turbidite layer.

Overall the two cores CD 1715 and CD 1730 show similar patterns with low organic carbon contents occurring during glacial stages, especially during Stage 2 and much of Stage 6. Stage 2 (18,000 years BP) is unusually poor in organic carbon; values range between 0.3% to 0.8% and are consistent with other studies in this area (Fontugne and Duplessy, 1986, See Table 6.4) have been considered to be due to a period of low productivity, linked with weak SW monsoon upwelling. In glacial Stage 4 and the middle of Stage 6, both cores ie. CD 1715 and CD 1730 (Fig. 6.3a)

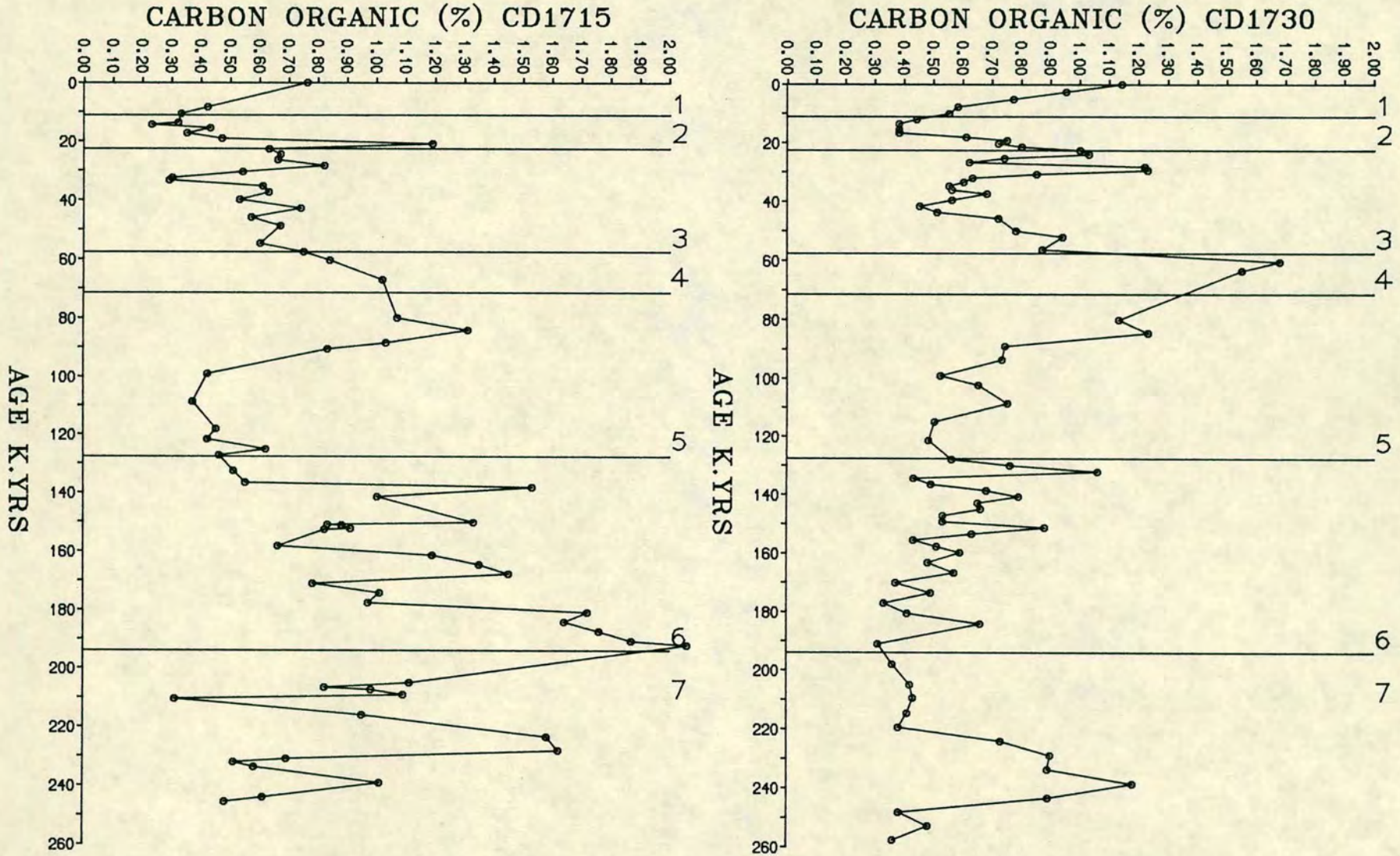

FIGURE 6.3a ORGANIC CARBON PROFILES OF CORES CD1715 AND CD1730.

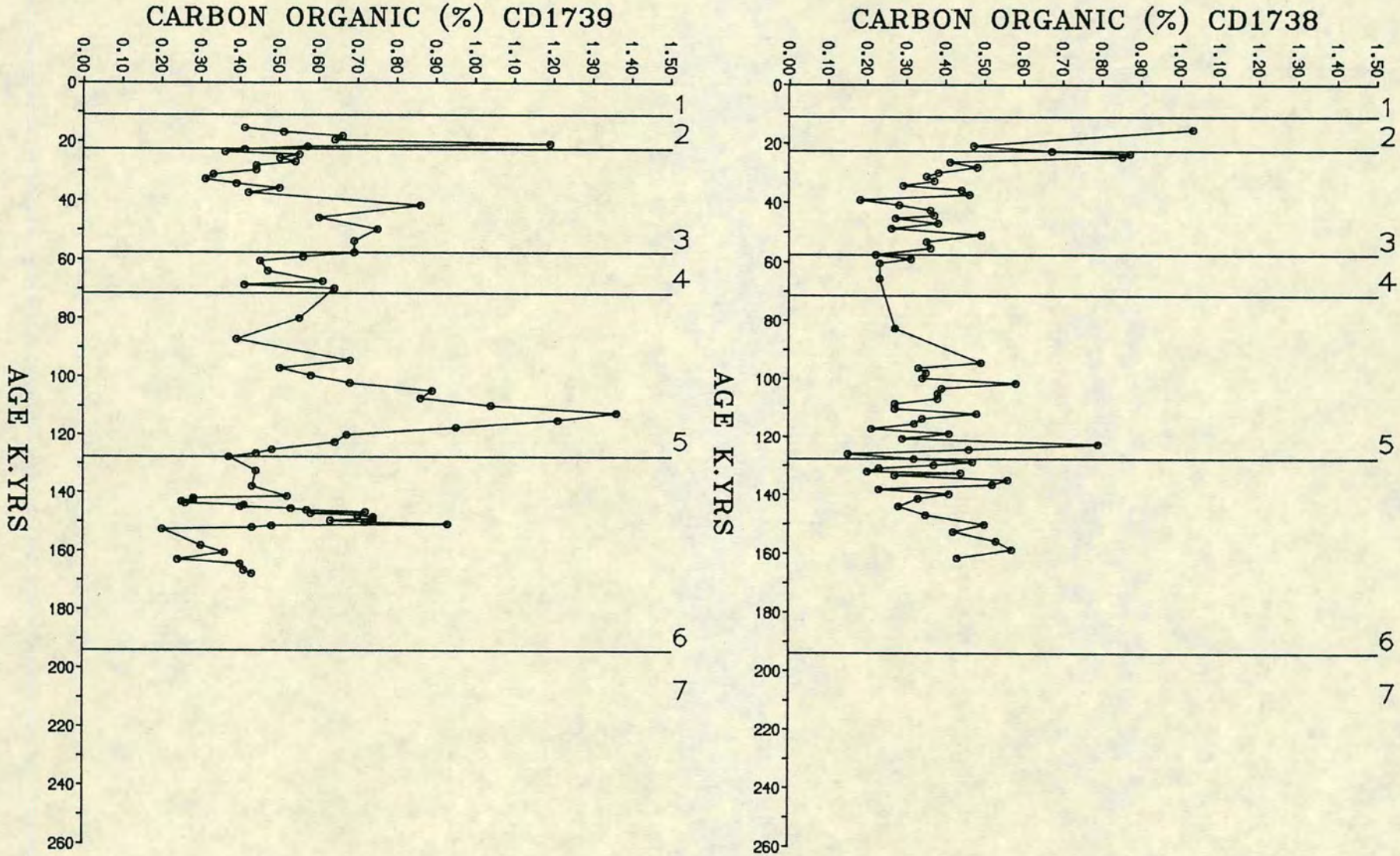

FIGURE 6.3b ORGANIC CARBON PROFILES OF CORES CD1739 AND CD1738.

Table 6.3 Organic carbon in surfacial biogenous sediments of productive areas

Location	Average C.org (%)	Reference
Marginal Seas		
SW African Continental margin	10.0	Calvert and Price (1971)
Peru Continental margin	10.0	Reimmers and Suess (1981)
Oman Continental margin	5	Shimmield et al (1988)
Oceanic Areas		
Gulf of California	3.5	Van Adel (1964)
Okhotsk Sea	1.5	Listizin (1972)
Black Sea	2	Degens and Ross (1974)
NW Arabian Sea	2	Fontagne and Duplessy (1986)
NW Arabian Sea	1.5	Present study

Table 6.4 Changes of organic carbon concentration between Holocene and Glacial Age

Location Core	Organic Carbon %		Reference
	Holocene	Last Glacial	
Argentine Basin	0.6-0.9	0.8-1.2	Stevenson & Chang (1972)
V15-142			
V15-141	0.4-0.7	0.6-1.2	
Eastern Equatorial Atlantic			
M12392-1	0.4	2.0-3.0	Muller & Suess (1979)
Eastern Equatorial Pacific	0.4-0.6	1.0-2.5	Pederson (1983)
P2, P6			
N. Indian Ocean			
MD77203	1.2-2.5	0.3-0.8	Fontugne & Duplessy (1986)
NW Arabian Sea			
CD 1715	0.3-0.8	0.2-0.5	Present study
CD 1730	0.4-1.1	0.35-0.8	

show high organic carbon (~1.0%), which in the case of Stage 4 may be caused by an abundance of faecal pellets (Plate 1). Until accumulated rates for organic carbon have been discussed, it is not possible to infer what are the main controls on the organic contents within these sediments.

The distributions of carbon organic content in core CD 1739 and CD 1738 (Fig. 6.3b) are broadly similar in that they tend to show somewhat high values in Stage 2 sediments, while Stage 3, 4 and the upper horizon of Stage 5 tend to show overall low content, ie. 0.5% or less. The lower stages of these cores show slightly elevated contents. Thus in many respects these vertical patterns differ markedly from cores CD 1715 and CD 1730 which appears to be positioned to receive less terrigenous input. It seems obvious that carbon contents are not simply controlled by the history of overlying water productivity rates, but are probably influenced by other sedimentary phenomenon such as total sediment accumulation, and especially accumulation of dilutant terrigenous material.

The carbon organic content of the four cores does show good correlation with the mineralogy, and hence the grain size texture of the sediments. This is shown in the following section.

6.4:2 Organic Carbon and Lithology of the Sediments

The variation in organic carbon content from one core to another and at depth is likely to be influenced by the textural characters of the sediments. It is known that the effects of particle size on controlling organic carbon contents of sediments are considerable (Trask, 1953; Brodovsky, 1965; Van Andel, 1964; Hunt, 1981), and that clays contain proportionally more organic matter than coarse grained sediments that are subject to the same input (Bush and Keller, 1981). In general, coarse sediments are expected to have lower organic matter contents, either through less organic input or by winnowing of the organics with fine grained detritus by erosive currents. Changes in organic carbon content seen in the four cores may be reflected in the lithological variations. Chapters 4 and 5 describing the mineralogy and lithogenic elements, have shown that the four cores progressively became more coarse grained from core CD 1715 to core CD 1738 and that this is reflected by an enrichment of quartz and other resistant minerals.

The patterns of Si/Al and Zr/Al described in chapter 5 are related to the quartzose nature of the sediments and have been plotted against the trend of organic carbon content for the four cores (Figs. 6.4). There is an antipathetic relationship showing that much of the carbon content of the cores is influenced by sediment texture especially in the more recent isotopic stages ie. 1 to 3.

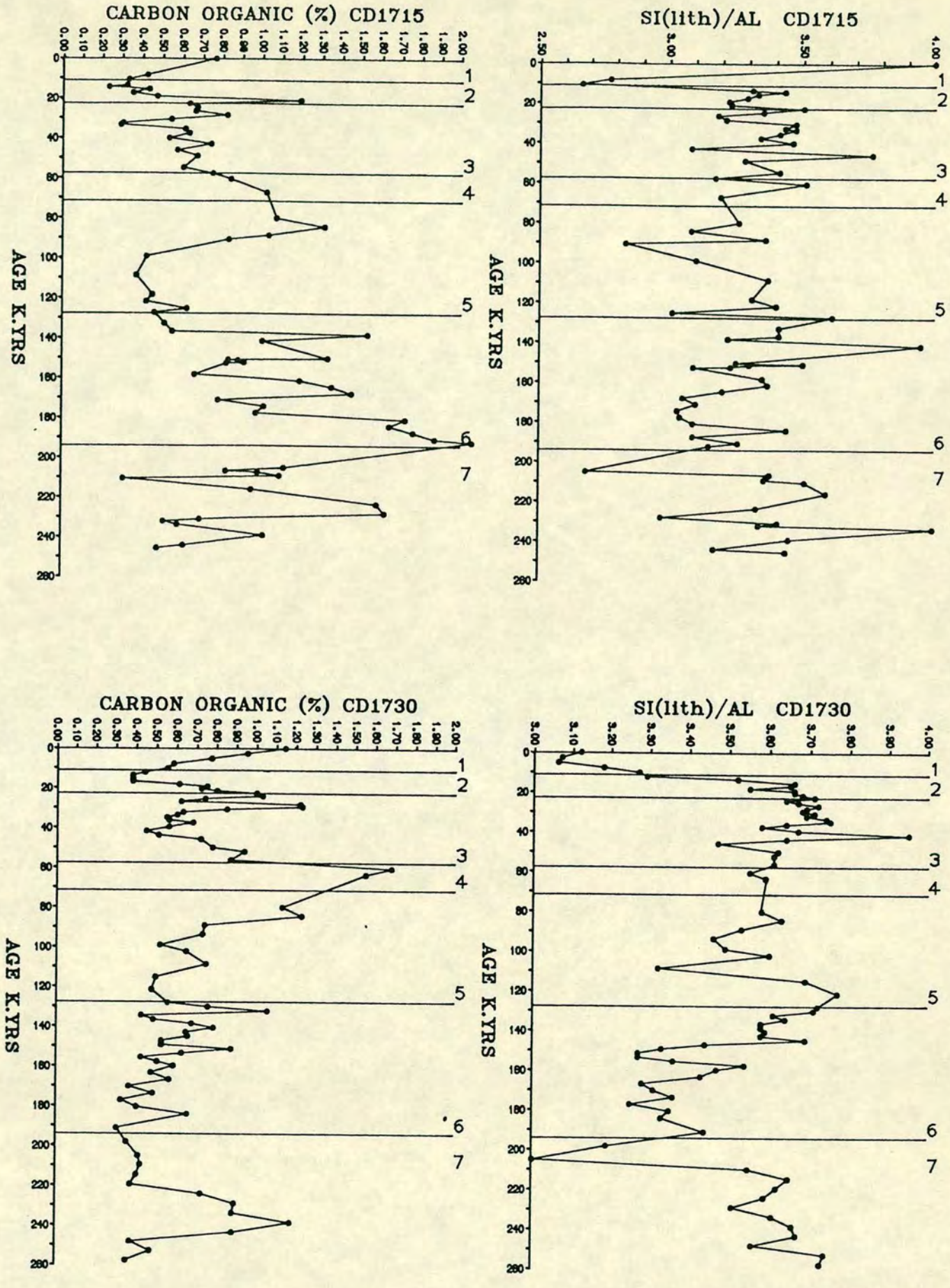

FIGURE 6.4a CARBON ORGANIC AND Si(Lith)/Al VARIATIONS IN CORES CD 1715 AND CD1730.

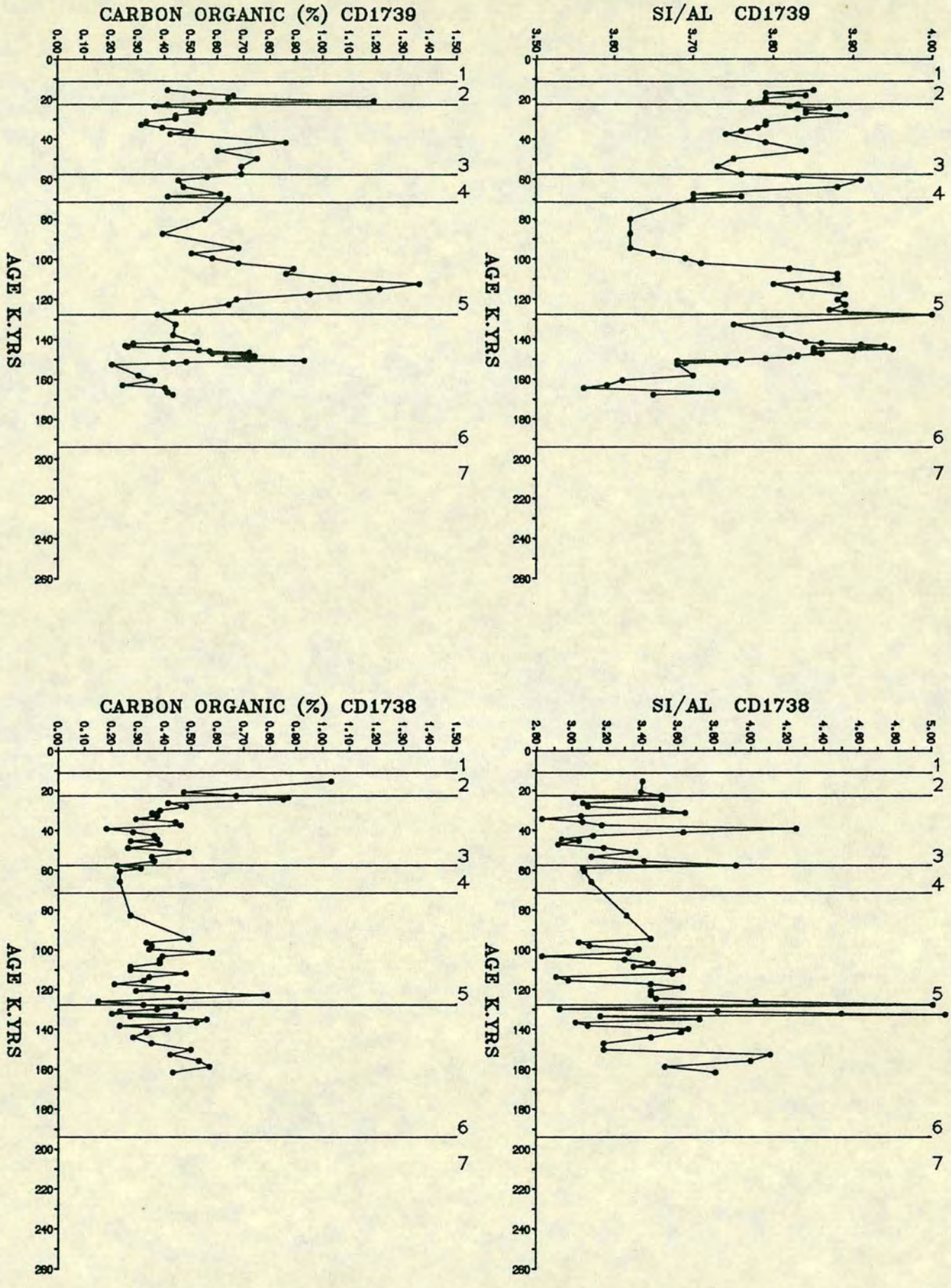

FIGURE 6.4b CARBON ORGANIC AND Si(Lith)/Al VARIATIONS IN CORES CD1739 AND CD1738.

6.5 BIOGENIC SILICA

The vertical distribution of dissolved silica in oceans is mainly controlled by the interaction of physical and biological activity. In areas of upwelling, nutrients brought to the photic zone induce high biological production. Diatoms, and to a lesser extent today, Radiolaria, extract dissolved silica incorporating it into skeletal structures, and causing a depletion in the surface waters. Since the oceans are undersaturated with silica, the majority of the diatom tests dissolve in the water column before reaching the seafloor (Calvert, 1968; Listizin, 1972; Berger, 1976; Heath, 1976; Van Bennekom and Berger, 1984). Having settled at the sea floor, considerable portions of opal dissolve in the upper sediment layer (Scharde, 1972). Nevertheless, opal concentrations in the ocean surface sediments are considered to primarily reflect surface water productivity (Lisitzin, 1972; Molina-Curz and Price, 1977; Broecker and Peng, 1982; Leinen et al. 1986). Productivity is often a climatically controlled phenomenon, and the variation of biogenic silica in sediments, even though a very small (0.05-0.15%) proportion of the biogenic silica is produced in photic zone (Hurd, 1973), may be used to reconstruct the climatic history. Van der Gasst and Jansen (1984) and Jansen et al. (1988) have shown that in the Angolan basin the fluctuation in opal records are controlled by climate and they found that dissolution effects are more significant than those of dilution with terrigenous material. Though the abundance of biogenic siliceous components reflects the surface water phenomenon (upwelling) and is controlled by both relative magnitude of biogenic and detrital input, Krissek and Scheidegger (1981) have shown that environment of deposition is also an important controlling factor. Their total assemblage is best preserved and interpreted in low energy environments (Schutte, 1981).

6.5:1 Biogenic silica (opal) in north Arabian Sea sediments

The biogenic silica in two cores CD 1715 and CD 1730 is discussed in this thesis. Since these cores are found to be less affected by terrigenous input compared with cores CD 1739 and CD 1738, they may provide a more reliable record of biological activity producing siliceous organisms. The biogenic silica in the sediments was determined by wet chemical method following Eggiman et al. (1980). The analytical method is given in appendix A.5 and data presented on a salt free basis are tabulated in appendix C.10.

The biogenic silica contents of the deep sea cores are shown in vertical profiles (Fig. 6.5) and both cores display a marked cyclicity with time. Generally the biogenic silica in cores range between 0.5% to 2.0%. The core CD 1715, which is relatively enriched in the biogenic component (both siliceous and calcareous), shows a value of biogenic silica about 1.0%. Both cores show a very similar distribution of biogenic Si with time, about 1.0%. High biogenic silica contents occur in surficial Holocene sediments, that is 2.1% in CD 1730 and 1.5% in CD 1715. Below they show a well defined decrease towards and including Stage 2 sediments. Stage 3 sediments also show importantly low Si and an abrupt increase is seen during Stage 4 and the upper parts of Stage 5. The lowest horizons of Stage 5 are characteristically extremely low in biogenic silica, and an increased value only occurs as relatively uniform in Stage 6. Stage 7 contents are somewhat lower than Stage 6.

The concept of higher productivity and hence possibly higher biogenic Si follows during interglacial periods, with uniformly low Si productivity during glacial episodes not clearly seen in the profiles. Certainly there is high Si in Holocene sediments that occurs during Stage 1, but below there is often a reverse trend. For instance, the lower horizons of the interglacial Stage 5 has less Si than the glacial Stage 6 and additionaly Stage 7 has lower Si than Stage 6.

It seems obvious that variable amounts of fallout of biogenic Si is controlled by productivity changes, and the content of biogenic Si residing in a sediment is greatly influenced by other factors such as the level of dilution of biogenic detritus, as well as possible dissolution changes over time. Given that the input of biogenic Si is governed by overlying water productivity, it is important to see if its pattern is similar to other biogenic matter.

6.5:2 Effects of dilution/production

The biogenic Si distribution down cores CD 1715 and CD 1730 must now be considered against that of organic carbon content, and also against lithogenic variations in the cores. Inspection of the distribution of biogenic silica and that of organic carbon for CD 1715 and CD 1730 (Fig. 6.3a) in particular, show very similar overall trends. These include high Holocene contents for both elements, and a sustained decrease towards and including Stage 2. A similar pattern of distribution is also seen for Stages 4 and 5. The oscillation of contents of biogenic silica during Stages 6 and 7 is also seen in organic carbon. However the overall increase in biogenic silica for much of Stage 6 and upper Stage 7 is not seen in organic carbon.

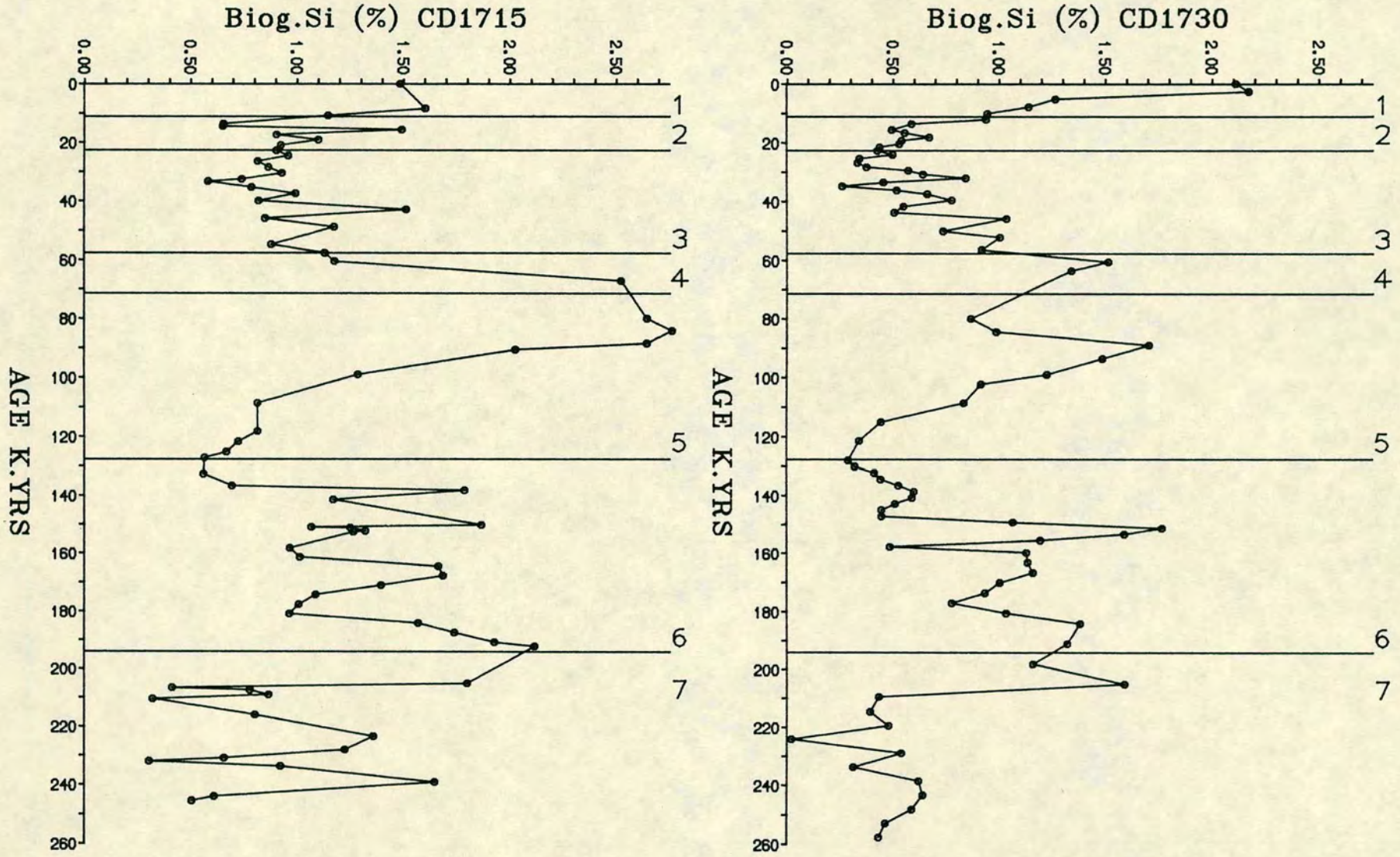

FIGURE 6.5 Biog.Si PROFILES OF CORES CD1715 AND CD1730.

It is not known until the geochemistry of the cores is considered further if such similarity of trends is due solely to a varying dilution by terrigenous detritus, or that elevated contents of both elements implies increased productivity. Certainly the patterns of biogenic silica in both cores and especially in CD 1730, which is free of turbidites, is closely related to the lithology of the sediments. The pattern of biogenic silica shows a strong antipathetic trend to that of the Si(Lith)/Al ratio (Fig. 5.2) implying less biogenic silica in more quartzose or coarse grained sediments. Schuette (1981) and Krissek et al. (1981) have shown that organic carbon and biogenic silica are best preserved in low energy environments. In the present case, it has been found that Si/Al (Fig. 5.2) shows a slight increase in ratio at the same horizons where biogenic content is low, implying higher concentrations of coarse material. This contributes to the result of scouring action, which has winnowed the fine particles, and a coarser residue of quartz and heavy minerals has been retained. This possibility will be dealt with in later chapters.

6.6 MARINE GEOCHEMISTRY OF BARIUM

The association of barium with the biogenic components of oceanic sediments has been noted by several workers. Goldberg and Arrhenius (1958) correlated the barium concentration of the Pacific Ocean with surface biological productivity. Revelle et al. (1955) have found a high concentration of barium in Pacific siliceous sediments. A similar relationship is evident for the Atlantic Ocean (Turekian and Taush, 1964). A correlation of Ba with $CaCO_3$ and organic matter has been indicated on the East Pacific rise (Church, 1970, 1979). He proposed that the Ba content in pelagic sediments is largely controlled by a biochemical cycle in the ocean. The real mechanism of barium precipitation and accumulation in sediments is as yet vague. For instance in the Namibian shelf, an area of pronounced upwelling, the biogenic sediments rich in diatom ooze do not show any Ba enrichment (Calvert and Price, 1983). However, Brongersma-Sanders (1967) has suggested that some diatoms and in particular some species of the genera Rhizosolenia and chactoceras, concentrate Ba from seawater, and thereby act as important conveyors of this metal to bottom sediments. Furthermore, Brongersma-Sanders (1967) found Ba levels up to 3660 ppm in organic-rich diatom ooze off Walvis Bay, and argue that this enrichment is due to its concentration by diatoms.

Dehairs et al. (1980) reported that particulate barite in surface water occurs as a result of biological processes and the Ba content is correlatable with the overlying biological productivity. He indicated that barite formed within the microenvironment of decaying organic debris or in the skeletons of planktonic

organisms falling directly to the sea floor, and this imparts the signature of biological activity. Recently Bishop (1988) confirmed this finding and showed that barite formed in >53μm fraction in near-surface waters and released into the 1-53μm fraction at depths below the euphotic zones. He concluded that favourable barite formation conditions are found in recently dead siliceous plankton and large aggregate particles such as faecal pelets and marine snow.

6.6:1 Excess Barium Contents

In the present study Ba distribution is reported as excess Ba which is free of the contribution held in aluminosilicates. This is calculated using the following equation and data is listed in appendix C.10.

$$Ex.Ba = Total\ Ba - (Al \times Ba/Al)$$

Total Ba and Al are the total Ba and Al contents measured in the sediments.
Ba/Al is background ratio in the sediments which in this case is (0.0066) mean Ba/Al ratio of turbidite horizons of core CD 1715.

The Ba contents in cores CD 1715, CD 1730 and CD 1739 from the Arabian Sea have been plotted in vertical profiles (Fig. 6.6). The cores CD 1715 and CD 1730 show much greater enrichment in Excess Ba (150-1000 ppm) than cores CD 1739 and CD 1738 ($\leq$100 ppm) and core CD 1738 rarely shows any enrichment at all.

Like other biogenic elements (calcite, organic carbon, biogenic silica) in cores CD 1715 and CD 1730 the trends of Excess Ba profiles for the last 250,000 years also show some cyclicity in their pattern between glacial and interglacial events. The highest concentration (>700 ppm) of Excess Ba occurs in the Holocene and in the middle of Stage 6. Generally contents are low with glacial events 2, 4 and high in interglacial stages. Furthermore, cores CD 1715, CD 1730 and CD 1739 clearly show a synchronous pattern with age, even though concentrations vary from one core to another. This may reflect either the change in the productivity of the overlying water and/or varying dilution by terrigenous constituents. Core CD 1715 is relatively higher in Ba and Excess Ba compared with the other cores, and shows values that always exceed 50 ppm whereas in other cores it does show negative values. The pattern of core CD 1730 can be considered typical for the distribution of Excess Ba with time. High Holocene values show, with time, a well defined fall in content towards and including Stage 2. Stage 3 is characteristically also low in Excess Ba

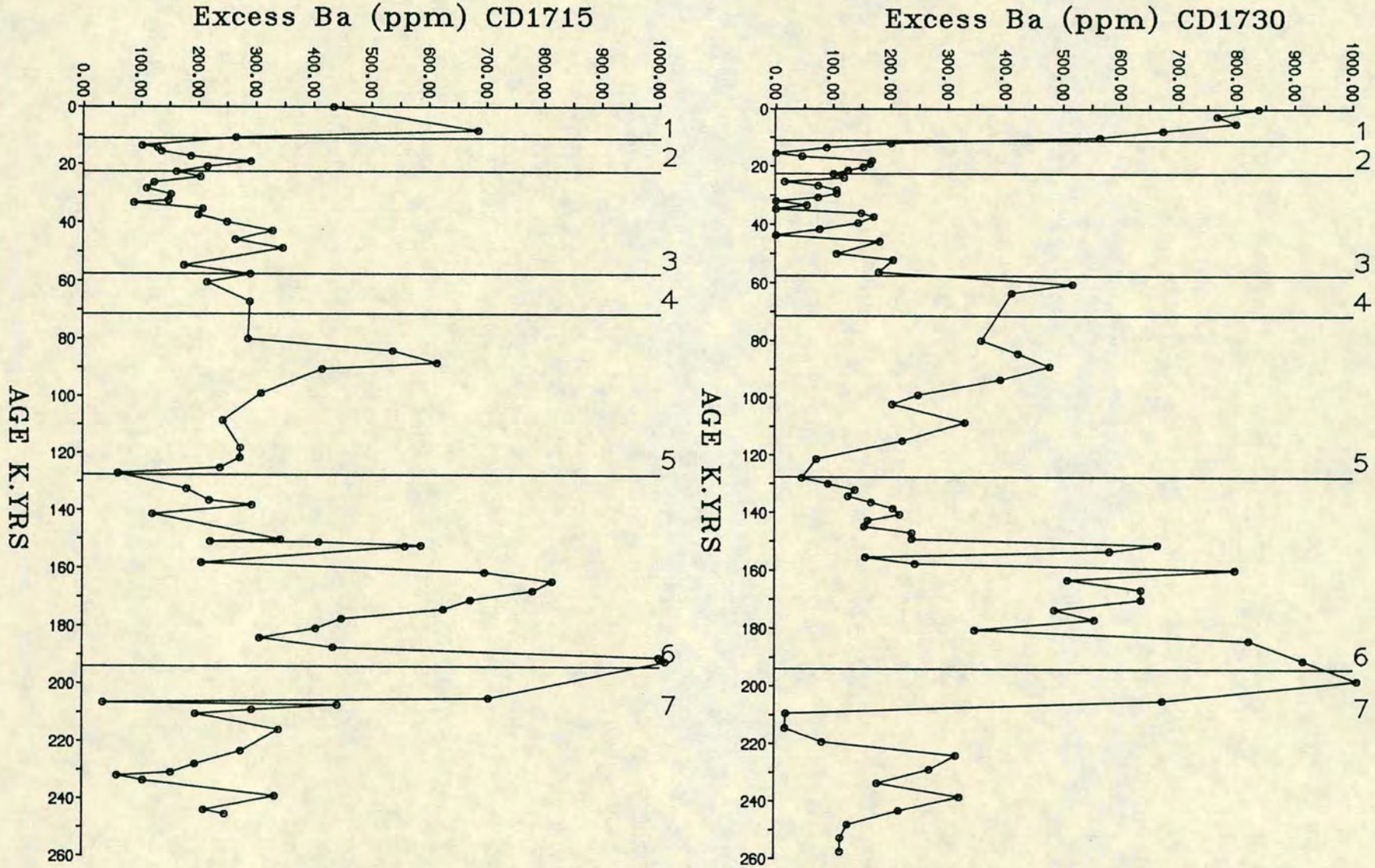

FIGURE 6.6a PATTERNS OF EXCESS Ba DURING GLACIAL AND INTERGLACIAL STAGES OF CORES CD1715 AND CD1730.

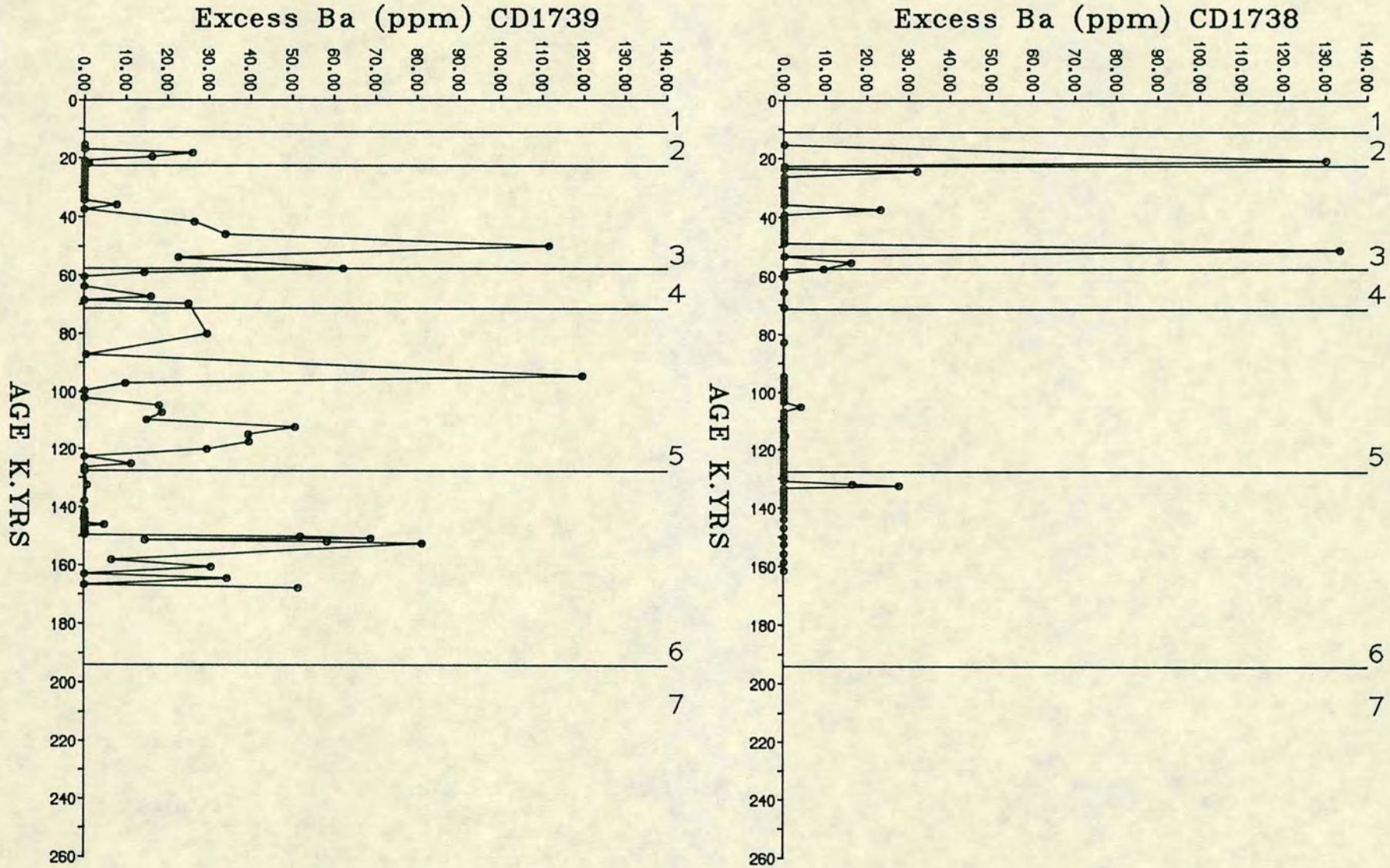

FIGURE 6.6b PATTERNS OF EXCESS Ba DURING GLACIAL AND INTERGLACIAL STAGES OF CORES CD1739 AND CD1738.

with an abrupt increase in Stage 4. Stage 5 shows a gradual fall in Excess Ba to its base and a well defined increase throughout Stage 6. Stage 7 shows much lower Excess Ba.

Overall this general pattern has similarities with biogenic silica (Fig. 6.5) and organic carbon (Fig. 6.3). However, there are some noteable differences and this can again be best seen in CD 1730. The well defined increase in Excess Ba in Stage 6 is also seen in biogenic Si, however organic carbon over this interval shows no definite increase. Furthermore, although the patterns of Excess Ba and biogenic silica in core CD 1730 are very similar, the amplitude of variation between isotopic stages does vary significantly. Excess Ba within Stage 6 and the base of Stage 7 are equal, if not higher than seen in the Holocene (Stage 1), and considerably higher than is seen in Stage 4 and upper Stage 5. However, biogenic silica is highest in the Holocene and the other two zones have equal contents of biogenic silica enrichment. In core CD 1715 the high biogenic silica seen in Stage 4 and Stage 5 is not correlateable with the generally low Excess Ba in this depth interval. It is clear that such variations are not caused by terrigenous dilution alone, but that the relative burial of biogenic markers are also important factors.

6.7 GEOCHEMISTRY OF METALS (Ni, Cu, Zn)

Contents of these elements in excess of that held in aluminosilicates have usually been ascribed to associations with organic matter, especially in upwelling areas (Curtis, 1966; Calvert and Price, 1970; Calvert, 1976; Spears and Amin, 1981). For instance, the concentration of Cu, Ni, Zn and Mo in sediments off Namibia can be positively correlated with the amount of organic carbon (Calvert and Price, 1983). Marine plankton is the most often cited source of metals and thus suggest some association with organic carbon. Brongersma-Sanders (1965, 1966) indicated a syngenetic incorporation of metals in planktons in the euphotic zone. However, it has been argued that the metal concentration in plankton material is not sufficiently high to account for the metal enrichments observed in sediments (Brumsack, 1980). Scavenging from the water column (Volkov and Famina, 1971, 1974) or postdepositional metal enrichment by sorption on organic matter, for instance, humic material (Nissenbaum and Swain, 1976; Calvert and Morris, 1977; Calvert et al., 1985) has been suggested. Moreover, organic matter content and metal concentration in sediment is invariably controlled by their textural characteristics (Trask, 1953; Van Andel, 1964; Krauskopf, 1979; Ackerman, 1980; Salomons and Forstner, 1983).

6.7:1 Excess Metal Contents in NW Arabian Sea Sediments

In the current study, metal contents in the North Arabian Sea are expressed as excess metals. The excess contents of elements, Ni, Cu, Zn have been calculated by subtracting the metal contribution held in the terrigenous components assumed to have a constant metal/Al ratio (see Appendix B) from the total concentration in the sediments. The data are tabulated in Appendix C.11. The average contents of Excess Ni, Excess Cu and Excess Zn in cores CD 1715 and CD 1730 are listed in table 6.5 and their vertical distributions are illustrated in Figs. 6.7, 6.8 and 6.9. Concentrations of Excess Ni, Cu and Zn in cores CD 1715 and CD 1730 when compared with the metal contents of different organisms (Table 6.5) show a similar value to that of planktons. Despite the fact that organic rich diatomaceous sediments show significant enrichment of metals (Calvert and Price, 1983), it is difficult without more information to relate the excess metal concentration in sediments exclusively to the genesis and fallout of plankton from the overlying water. Moreover the excess metal to carbon ratio in sediments is likely to be much higher than seen in plankton. For this reason alternative mechanisms of enrichment must be considered. During burial, diagenetic release of metals from authigenic constituents, and their uptake by organic matter either at or near the sediment/water interface is known.

Surface sediments from oceanic depths off the South Arabian shelf show an oxidising surface which is enriched in metal oxides, particularly MnO_2 (>1%) (Watson, pers. comm.). Such sediments show considerable enrichment of Cu, Zn and Ni and exist through sorption by MnO_2. Such an enrichment shows Cu, Zn, and Ni contents up to an order of magnitude higher than is within the biological mixed layer (~10cm) found in the buried sediments. Mn recycling occurs (Watson, pers. comm.) through redox reactions releasing Mn and other transition elements to the pore water within the subsurface reducing sediments. It is possible that a proportion of released Cu, Ni and Zn is sorbed by organic matter in the subsurface environment. The amount of metals held within the buried sediments is probably controlled by: (a) the contents of Mn oxides in the surface sediments which must be associated with its supply from the neighbouring continents together with the rate of total sediment accumulation. Additionally, surface sediment manganese is in effect a product of diagenetic recycling, the severity of which is controlled by organic matter degradation; (b) the amount and quality of organic matter that is surplus to the requirement for surface sediment diagenesis. Under a reasonably constant rate of manganese and other metal supply from the overlying seawater, one should expect a close relationship between buried Ni, Cu, Zn contents and organic carbon.

Table 6.5 Metal contents of marine organisms and NW Arabian Sea sediments

Organisms	Ni (ppm)	Cu (ppm)	Zn (ppm)	Reference
Plankton	65	238	-	Nicholls et al. (1959)
Plankton	36	200	2600	Vinogradova and Kovalskiy (1962)
Brown Algae	11	3	150	Bowen (1966)
Plankton	9	13	165	Presley et al. (1972)
Zoo and microplankton	8.4-11.6	11.5-57.6	180-780	Martin and Knauer (1973)
Plankton	83	340	2700	Bostrom et al. (1974)
Zooplankton	39	8.1	483	Fowler (1977)
Plankton	93	280	880	Moore and Bostrom (1978).
SEDIMENTS				
Namibian Shelf diatom ooze	108	68	68	Calvert and Price (1983)
NW Arabian Sea				
Core CD 1715*	38	33	57	Present study
Core CD 1730*	26	32	60	

*Average Excess metal contents

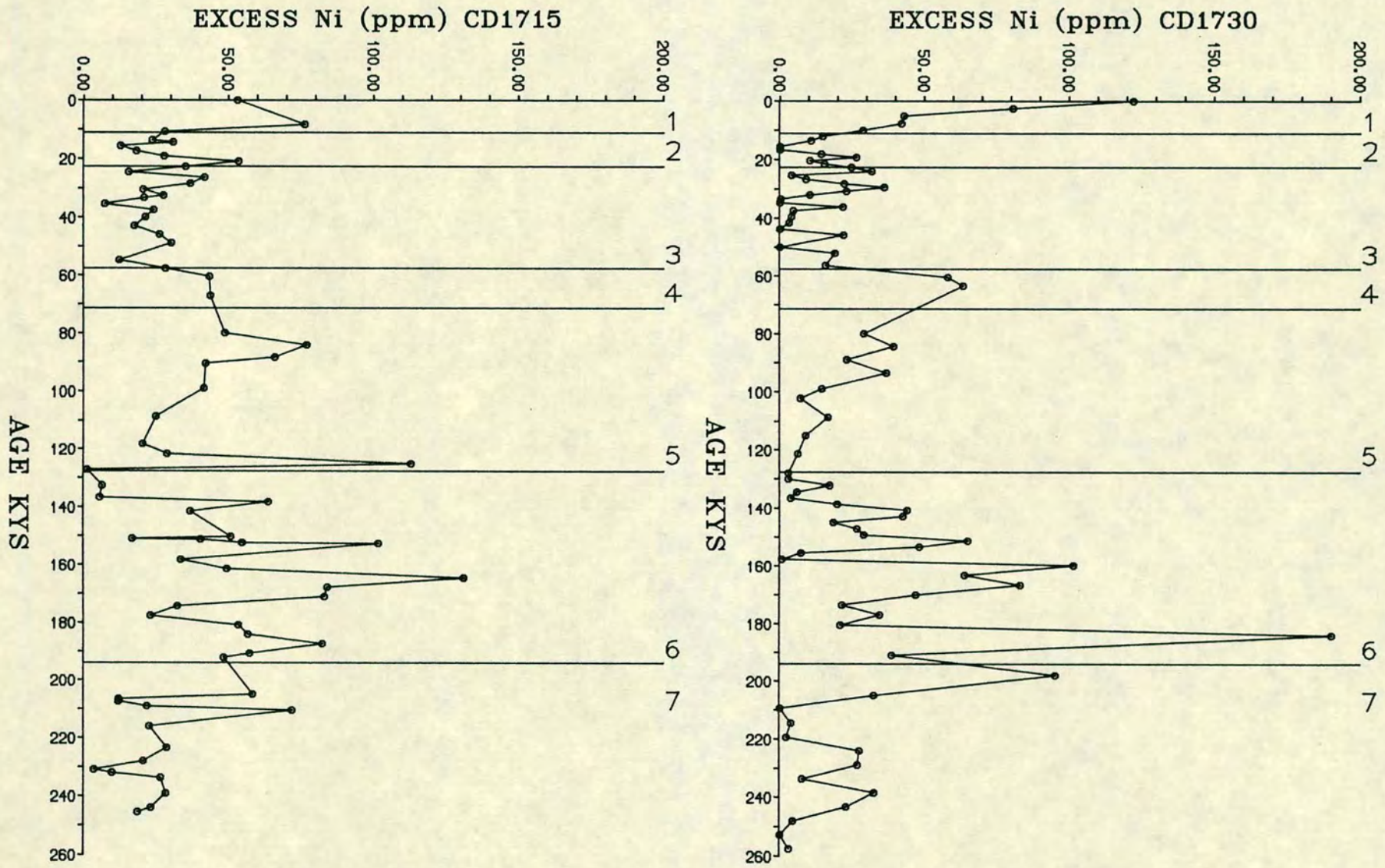

FIGURE 6.7 EXCESS Ni PROFILES OF CORES CD1715 AND CD1730.

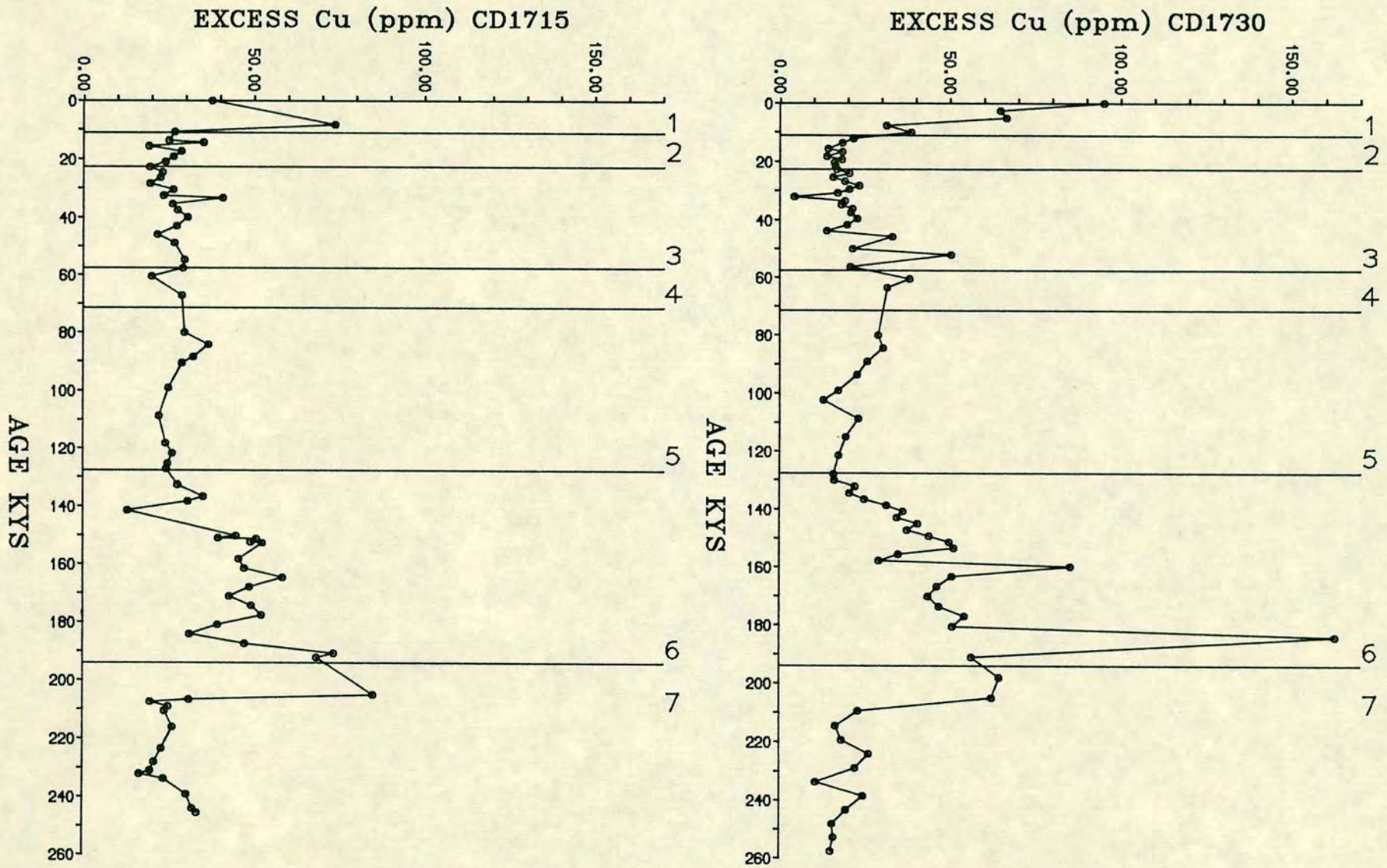

FIGURE 6.8 EXCESS Cu CONTENT VARIATIONS IN CORES CD1715 AND CD1730.

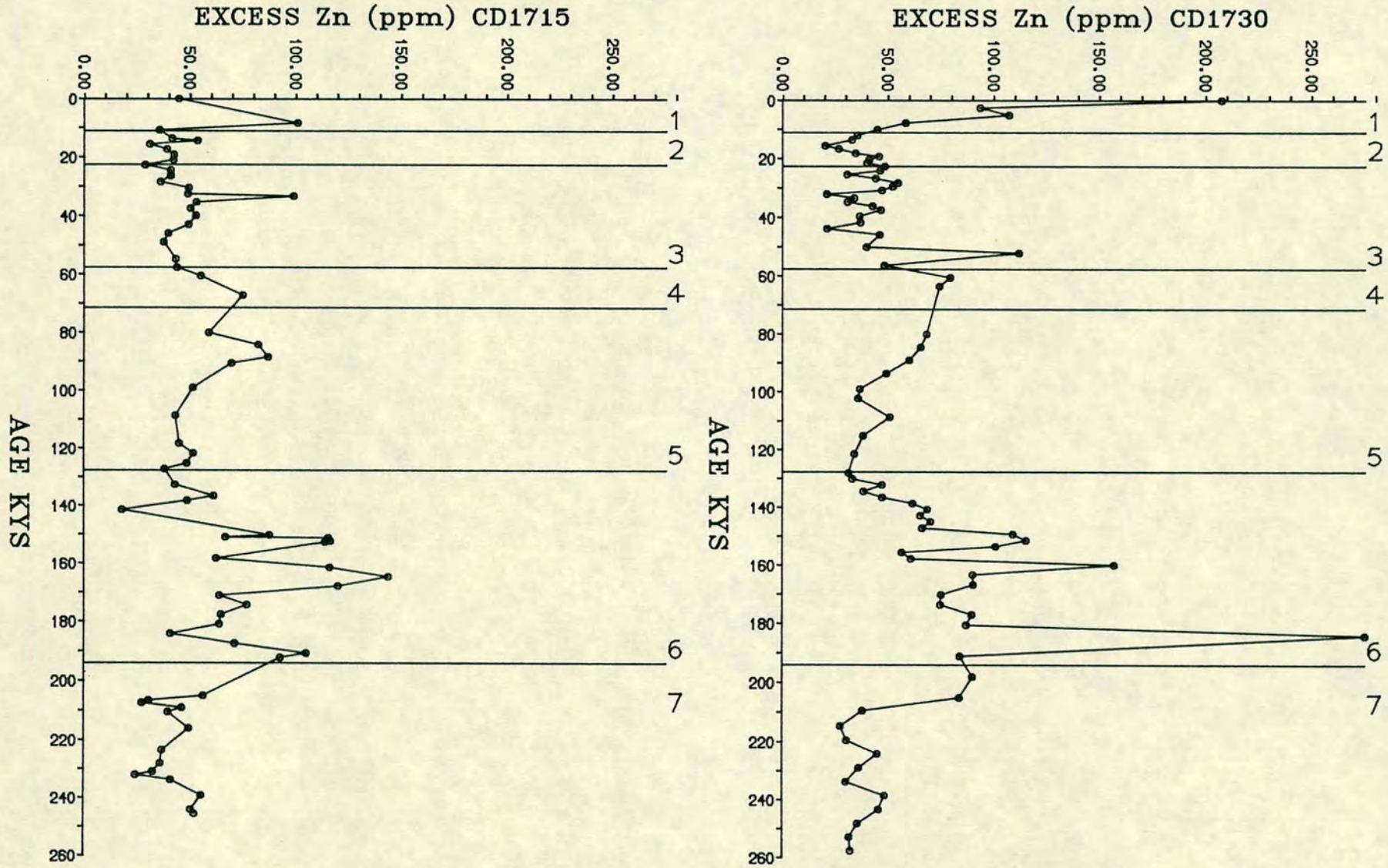

FIGURE 6.9 EXCESS Zn CONTENT VARIATIONS IN CORES CD1715 AND CD1730.

In the preceeding section, profiles of organic carbon and Excess Ba (Fig. 6.3 and 6.6) have been observed to show close relationship for much of the period of accumulation of cores CD 1715 and CD 1730. Their coherent variation down the cores in glacial and interglacial stages, except in Stage 6, CD 1730 suggest a genetic relationship. Similarly, the patterns of variations of Excess Ni, Cu and Zn shown in Figs. 6.7, 6.8 and 6.9 display positive trends with those of organic carbon and Excess Ba.

The profiles show for all these metals, higher contents in the Holocene, and for much of the duration of Stage 6. In this respect the profiles of CD 1730 differ from C.org and are more closely alike to Ba. This suggests that Cu, Ni and Zn may be biomarker elements, being obviously related to plankton production rather than being governed by sorption processes with buried carbon. However, as the controls on heavy metal uptake with oxides and carbon are essentially unknown, the suggestion that Cu, Ni and Zn represent biomarker elements can only be tentative.

CHAPTER 7

$\delta^{13}C$ AND $\delta^{15}N$ IN SEDIMENTS

7.1 INTRODUCTION

Organic matter in marine sediments may be of either marine or terrestrial origin. Land-derived organic matter includes recently biosynthesized plant debris and dissolved humic substances (Thurman, 1985, Hedges et al, 1986 a,b). Marine derived organic matter is formed almost exclusively by phytoplankton which are particularly rich in proteins. In offshore areas, marine sediments indicate that the predominant organic carbon source is plankton (Degens, 1969; Hedges and Parker, 1976). In certain marginal areas of oceans, terrigenous carbon may contribute a significant proportion of the carbon fraction of the sediments (Lee and Wakeham, 1988).

It has been seen from the distribution of organic carbon content described in the preceding chapter, that all cores show a pronounced cyclicity during glacial and interglacial stages. Generally, low organic carbon is found in glacial stages which are relatively enriched in lithogenic elements, e.g. quartz and dolomite. It is therefore likely, that glacial events may be associated with increased input of terrestrial organic matter. A number of chemical parameters have been used to distinguish between marine and terrestrial organic matter. These are C/N, C/H, Br/C.org (Bordovsky, 1965; Pocklington and Leonard, 1979; Mayer et al, 1981) and $\delta^{13}C$, $\delta^{15}N$ stable isotope ratios (Cline and Kaplan, 1975; Peters et al, 1978; Sweeny et al, 1978; Sweeny and Kaplan, 1980).

In this chapter the source of the organic matter within northwestern Arabian sediments will be discussed. C/N ratio, $\delta^{13}C$ and $\delta^{15}N$ stable isotope analysis performed on one core (CD1730) are described in order to assess the relative proportions of terrestrial and marine organic matter.

7.2 NITROGEN

The total nitrogen contents measured in sediments of core CD1730 are shown in Figure 7.1. As can be seen, they closely follow the trends shown by the organic carbon (Fig. 6.3). This suggests that these two elements possess a common source. However the small positive intercept on the carbon axis in Figure 7.2 possibly indicates the presence of small amounts of nitrogen free carbon. Organic carbon and total nitrogen content in the sediments were analysed by two different methods (Appendix A.6) and the relationship thus shown in Figure 7.2 is not due to any sample artifacts.

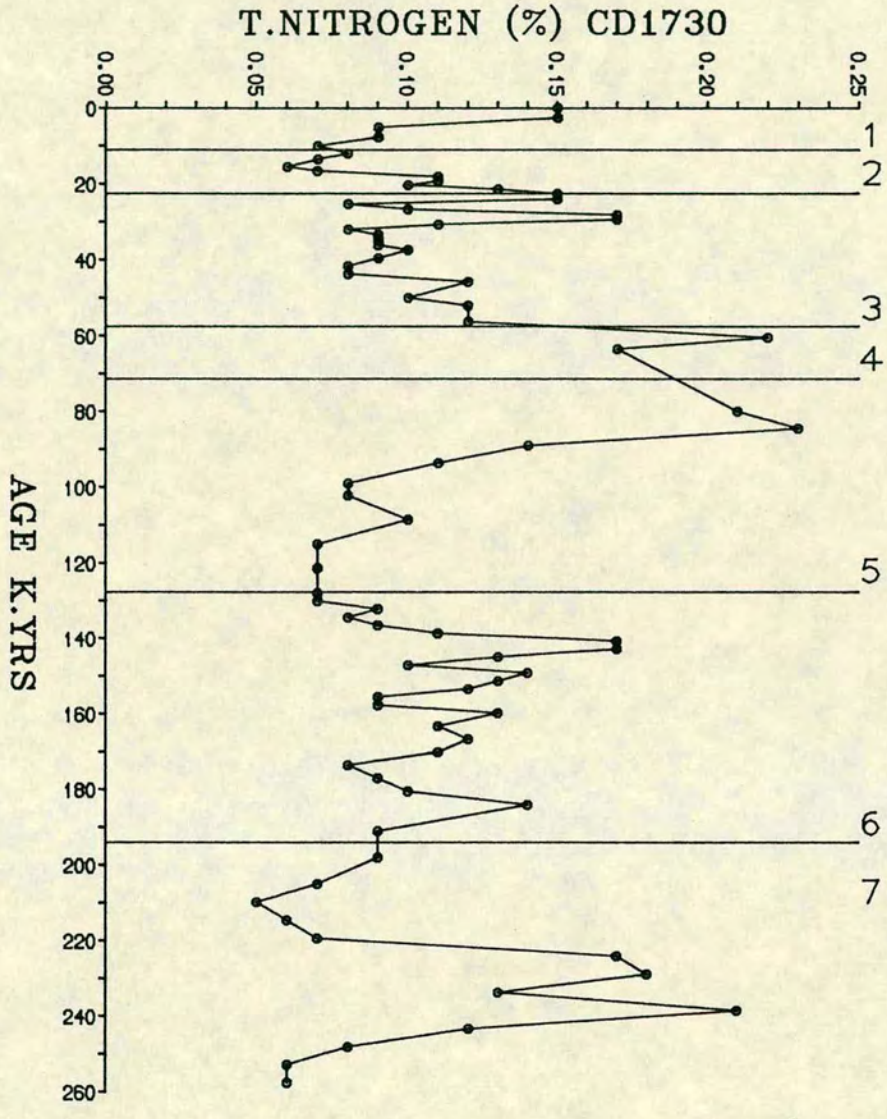

FIGURE 7.1 TOTAL NITROGEN CONTENT VARIATIONS IN GLACIAL AND INTERGLACIAL STAGES. CORE CD1730.

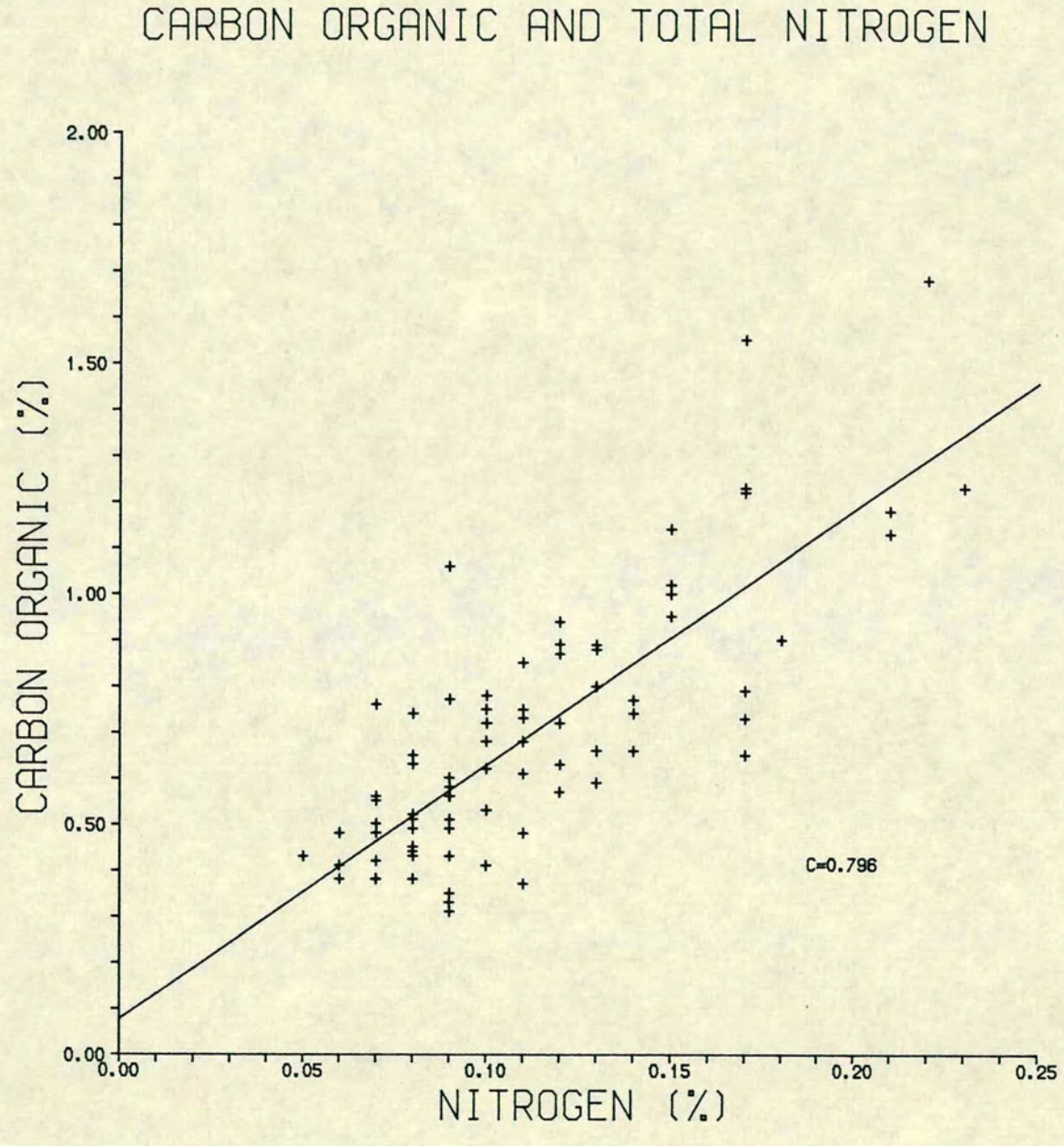

FIGURE 7.2 CORRELATION BETWEEN CARBON ORGANIC AND TOTAL NITROGEN.

Sediments in core CD1730 from the northwest Arabian Sea show nitrogen values in a range from 0.05% to 0.25%. These values are found to be much greater than the values of 0.03% to 0.08% noted by Muller (1977) for deep sea Pacific sediments. In a similar manner to organic carbon, the sediments show a pronounced decrease in nitrogen content in glacial stage 2 and in the lower parts of stages 3 and 5. The minimum nitrogen value, i.e. 0.05% occurs in the upper parts of stage 7 during the period 210-200,000 years BP. Glacial stages 4 and 6 show relatively higher nitrogen values of about 0.20% and >0.10% respectively.

7.3 C/N

The proteins are the most important contributors of organic nitrogen (Wakeham et al, 1984) and as such may be used to characterise different types of organic matter. Protein has a C/N atomic ratio of about 3.0, and so organisms rich in protein have a low C/N ratio, e.g. polychaetes (3.4), fish and fish bones (3.9) and copepods (4.3) (Beers, 1966). In contrast, other zooplankton and phytoplankton give a marginally higher atomic ratio of 6.24 and 6.97 respectively (Table 7.1). Benthic organisms are also found to be rich in protein, giving C/N ratios of 4-5 (Bordovsky, 1965 a,b). Higher land plants are low in proteins and therefore display very high C/N ratios of 25-30 (Marlett and Erdmann, 1959; Muller, 1977). Hence C/N ratios have been used to characterise the nature of the organic matter within sediments (Badar, 1955; Bordovskiy, 1965; Pocklington and Leonard, 1979; Berner, 1979). The C/N ratio for marine plankton of 6.6 given by Redfield et al (1963) forms the basis for distinguishing between terrestrial and marine organic matter.

C/N ratios in the Arabian Sea sediments of the present study range from 4-11. Variation in C/N ratios with depth in core CD1730 is shown in Fig. 7.3. A marked cyclicity is seen down the core. Variation of C/N in different stages may either indicate variation in the source of organic matter input or the breakdown of the organic matter. In glacial stage 2 the C/N ratio (~5.50) is lower than most marine C/N values and is considerably lower than stage 1 (>8.0). It is known that stage 2 witnessed an increased aridity with higher terrestrial debris input to the sediments (Kolla and Biscay, 1977). This is also seen in Si/Al profiles (Fig. 5.2). In contrast to this, the C/N ratios in stage 2 and upper stage 3 show a decrease which can be explained by the presence of inorganic nitrogen associated with clays deposited at this time. However, for much of stages 3,5 and 7 C/N values largely fall in the range 6-7 which is close to the Redfield ratio and implies that, during interglacial stages, marine organic matter is more predominant. Occasionally there is

Table 7.1 Element Composition of Marine Organisms

Organism	Author	Content % dry weight				Atomic ratios
		C	H	N	P	C/N
Diatoms	1	18.68	3.65	2.49	0.60	8.75
Peridineans	1	33.49	5.58	4.61	0.57	8.48
Copepods	1	45.52	7.22	9.96	1.03	5.33
Bacteria	1	50.40	6.78	12.30	-	4.78
Benthos	1	51.55	7.67	12.32	-	4.88
		Atomic ratios in Plankton				
Zooplankton	2	103	-	16.5	1	6.24
Phytoplankton	2	108	-	15.5	1	6.97
average	2	106	-	16.0	1	6.63

1 Data from various authors given in Bordovskiy (1965,a)

2. Fleming (1940); Redfield et al (1963).

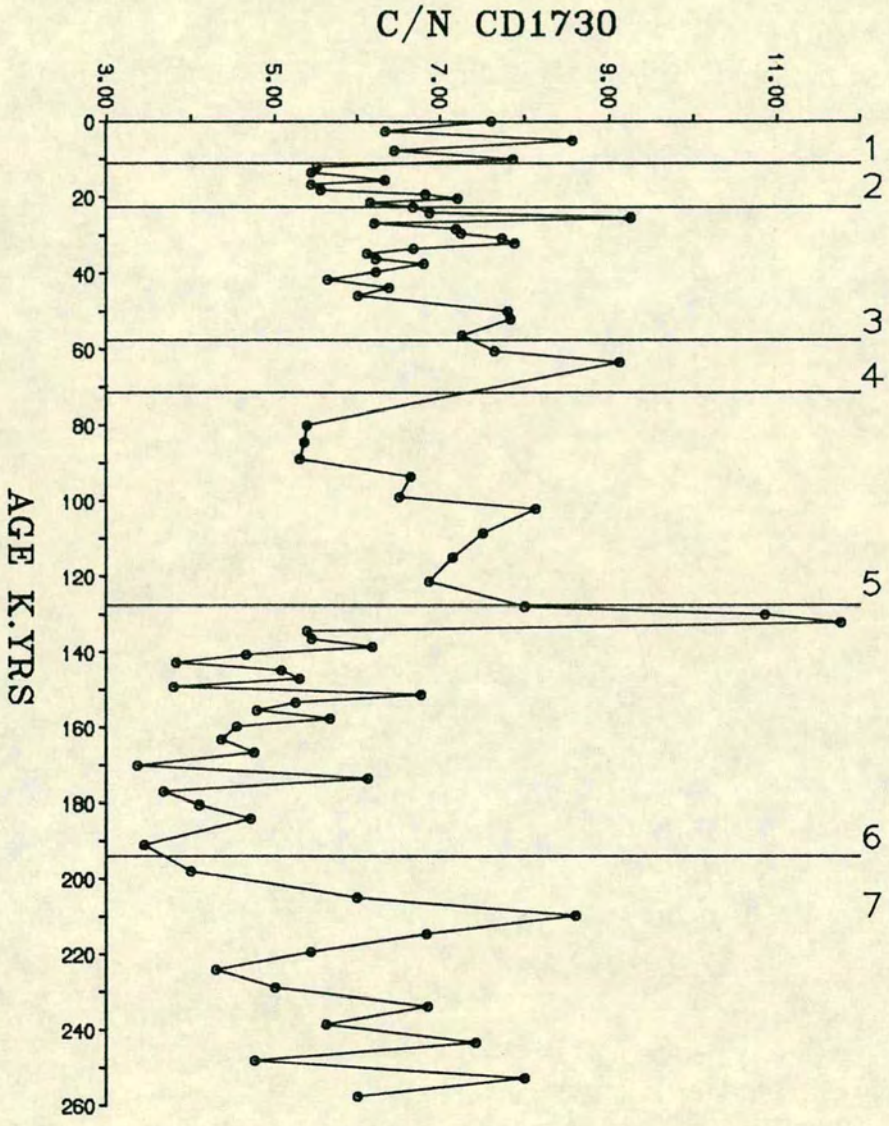

FIGURE 7.3 C/N RATIO PROFILE OF CORE CD1730.

an increase in the C/N ratio from its normal value of 6.0 to 8.0 or more. This increase suggests that organic matter may have undergone some selective mechanical sorting or chemical degradation as a consequence of bottom water erosion. This is particularly noticeable in the lower parts of stages 3 and 5, and in the upper sections of stage 7. Here values are about 8-9, higher than normal marine sediments (~6.6).

A surface sediment study of this area from numerous cores also supports this interpretation (Shimmield et al, 1988). High C/N ratios in certain core tops may be the result of mechanical winnowing and degradation and as a consequence of which, the sediments have also become greatly enriched in Cr and Si/Al (Table 7.2), compared with unwinnowed sediments. A very low C/N ratio (3-4) seen in glacial stage 6 may be tentatively attributed to the increased clay contents adsorbing N (Fig. 4.7 and 4.8). This has been postulated by several workers, and it was noted that values of C/N below 5.0 are not uncommon (Arrhenius, 1952; Bader, 1955; Bordovskiy, 1965c). Arrhenius (1952) suspected that significant amounts of $NH4^+$ may be adsorbed by clay minerals and later studies have confirmed this (Stevenson and Cheng, 1972; Muller, 1977; Rosenfeld, 1977). A fixed ammonium content has been shown to be related to clay mineral composition (Stevenson and Dhariwal, 1959; Stevenson et al, 1967). For example, illite and vermiculite minerals have the ability to retain large amounts of ammonium in a non-exchangable form; montmorillonite type minerals appear to have low ammonium fixing capacities. Thus, when a C/N profile was compared to a quartz/illite profile (Fig. 4.7) it was found that in stage 6 illite was relatively more abundant than in other parts of the core. Therefore, it is possible that the low C/N ratios in this stage indicate a significant adsorption of $NH4^+$ and could account for between 12% and 64% of the total nitrogen.

However the validity of using C/N ratios in order to identify the sources of organic matter in core CD1730 may be in question. Factors influencing the C/N ratio as shown in several diagenetic studies can alter the orginal chemical character of the organic matter. For this reason an attempt has been made to show the nature of the organic matter and its relative variation with time using stable isotope variations of $\delta^{13}C$ and $\delta^{15}N$. This is discussed in following sections.

7.4 CARBON ISOTOPES ($\delta^{13}C$)

The carbon isotopic ratio of organic matter in marine sediments primarily depends on the percentage of continental to marine carbon. Several studies have shown that the carbon in terrestrial plants is depleted in $\delta^{13}C$ compared to that of marine plants (Sackett and Thompson, 1963; Sackett, 1964; Sackett and Rankin, 1970;

Table 7.2 **C/N ratio and Cr, Si/Al of Surface Sediments from Oman Continental Margin, N.W. Arabian Sea**

Station No	Longitude E Latitude N	Depth (m)	Si/Al	Cr ppm	C/N
1704	17.°41'.7 57.°22'.3	400	5.55	731	9.6
1705	17.°36'.7 57.°21'.8	770	4.93	1116	11.1
1706	17.°33'.9 57°.22'.5	1048	5.38	694	10.3
1710	17.°32'.2 57.°21'.9	1295	4.96	638	10.2
1711	17.°16'.6 57.°26'.0	3648	5.08	180	6.7
1718	19.°20'.6 58.°14'.4	440	7.03	229	8.6
1721	19.°46'.3 58.°36'.0	645	6.59	342	8.8
1722	19.°34'.5 58.°31'.3	780	6.82	292	8.4
1723	19.°42'.2 58.°58'.7	2780	5.48	234	7.7

(From Shimmield et al, 1988)

Newman et al, 1973). Since marine sediments are reported to contain an admixture of terrestrial and marine organic matter this would be reflected in the $\delta^{13}C$ of the associated sediments.

The $\delta^{13}C$ value of typical terrestrial organic carbon is known to lie within the range, -26.0°/oo to 28.0°/oo (Hunt, 1970; Sackett and Rankin, 1970; Newman et al, 1973; Gearing et al, 1977; Fontugne and Jouaneau, 1981). This is distinct from marine organic matter which shows $\delta^{13}C$ values lying in the range of -18.0°/oo to -22°/oo (Fontugne and Duplessy, 1978; 1981; 1986). $\delta^{13}C$ values of plankton in northern Indian Ocean are stated to lie around -20°/oo (Table 7.3) (Fontugne and Duplessy, 1978; 1981).

In this thesis, $\delta^{13}C$ results from core CD1730 are described. The $\delta^{13}C$ analysis of the selected samples were made by Dr T. Pederson at the Department of Oceanography, University of British Columbia, Canada. The analytical methods are described in appendix A.7 and the results are listed in table 7.4. The purpose of this study was to ascertain whether or not land derived organic matter has influenced the organic carbon content of the sediments. During glacial episodes, stronger northerly or northwesterly winds may have transported more land derived organic matter with a high terrigenous input from surrounding land masses. Hence, the pattern of the isotopic composition of organic carbon in northwestern Arabian Sea sediments during glacial and interglacial times should reflect the relative proportions of marine and terrigenous organic matter.

The range of $\delta^{13}C$ values from the investigated sediments is -19.0°/oo to -21.6°/oo PDB (Table 7.4). This is within the range of recent marine sediments as reported in published literature (See Table 7.5). The variation in $\delta^{13}C$ values, although small and obtained from a limited number of horizons does however appear to show some cyclicity (Fig. 7.4). For instance, an increase in $\delta^{13}C$ from -21.0°/oo to -19.0°/oo occurs between the Holocene and the last glacial maximum (18,000 years BP). An increase in $\delta^{13}C$ in the Holocene has also been observed by Fontugne and Duplessy (1986) and related to a productivity change associated with SW monsoons. Surface sediment and some other Holocene horizons show a $\delta^{13}C$ of -19.0°/oo which is very similar to that of modern plankton (Table 7.3). This implies that organic carbon is of marine origin. However, the lowest $\delta^{13}C$ value (i.e. -21.6°/oo) occurs in some subsurface sediments of Holocene age. In chapter 6 it has been shown that productivity indicators (Biogenic silica and Ex. Ba) show the highest values during the Holocene (Figs 6.5 and 6.6) and suggest a very high marine organic carbon production. However a small decrease in $\delta^{13}C$ value in the upper Holocene refered to above, probably implies an occasional small contribution from land derived organic carbon. This is supported by high Cr/Al ratio of these sediments (Fig. 5.14a).

Table 7.3 **Sea surface temperature and $\delta^{13}C$ of Plankton organic Carbon from Arabian Sea upwelling and Offshore areas (Fontugne and Duplessy, 1981)**

	Latitude N Longtidue E	Temperature C°	$\delta^{13}C$ (°/₀₀)
	14°01'8N 73°01'1E	30.42	-18.76
	13°58'3N 71°53'2E	30.72	-19.01
Arabian Sea	16°32'5N 67°53'5E	31.12	-19.27
Offshore Area	17°56'7N 63°09'8E	30.47	-19.08
	19°13'3N 60°40'9E	29.77	-18.80
	16°27'0N 67°17'0E	29.03	-19.00
Upwelling	20°41'9N 59°34'1E	26.49	-20.47
Area	19°18'0N 58°26'0E	28.02	-19.68
	17°44'0N 57°40'4E	26.31	-20.15

Table 7.4 $\delta^{13}C$ **data of selected samples from Core CD1730**

Depth (cm)	Age (KYS)	$\delta^{13}C$(PDB) (°/oo)
0.00	0.00	-19.71
10.00	2.60	-21.61
20.00	5.10	-18.90
30.00	7.70	-19.62
40.00	10.00	-20.36
50.00	12.00	-20.32
70.00	15.50	-21.13
80.00	16.60	-20.78
90.00	18.10	-19.61
100.00	19.20	-19.27
110.00	20.30	n.a.*
120.00	21.40	n.a.
130.00	22.60	n.a.
140.00	24.00	n.a.
150.00	25.30	n.a.
160.00	26.70	n.a.
170.00	28.20	n.a.
180.00	29.40	n.a.
190.00	30.70	n.a.
200.00	32.00	n.a.
210.00	33.40	n.a.
220.00	34.70	n.a.
230.00	36.10	n.a.
240.00	37.40	n.a.
250.00	39.50	n.a.
260.00	41.60	n.a.
270.00	43.70	n.a.
280.00	45.80	n.a.
290.00	50.00	n.a.
295.00	52.10	-19.40
305.00	56.30	-19.88
315.00	60.50	-19.21
325.00	71.00	-20.35
345.00	80.00	-19.23
355.00	84.50	-20.02
365.00	89.00	-20.92
375.00	93.60	-20.63
385.00	99.00	-20.34
395.00	102.20	-19.80
405.00	108.60	-20.06
415.00	115.00	-20.64
425.00	121.40	-20.65

* n.a. = not analysed

Table 7.5 δ^{13} **of Total Organic Material from Upwelling Zones**

Sample and Location	$\delta^{13}C$ °/₀₀ PDB	Reference
Diatomaceous ooze Namibian Shelf	-19.5	Calvert and Morris, 1977
N. Indian Ocean	-18.0 to -20.0	Fontuge and Duplessy, 1986
NW Arabian Sea	-19.0 to -20.0	"
NW Arabian Sea	-19.0 to -21.0	Present Study

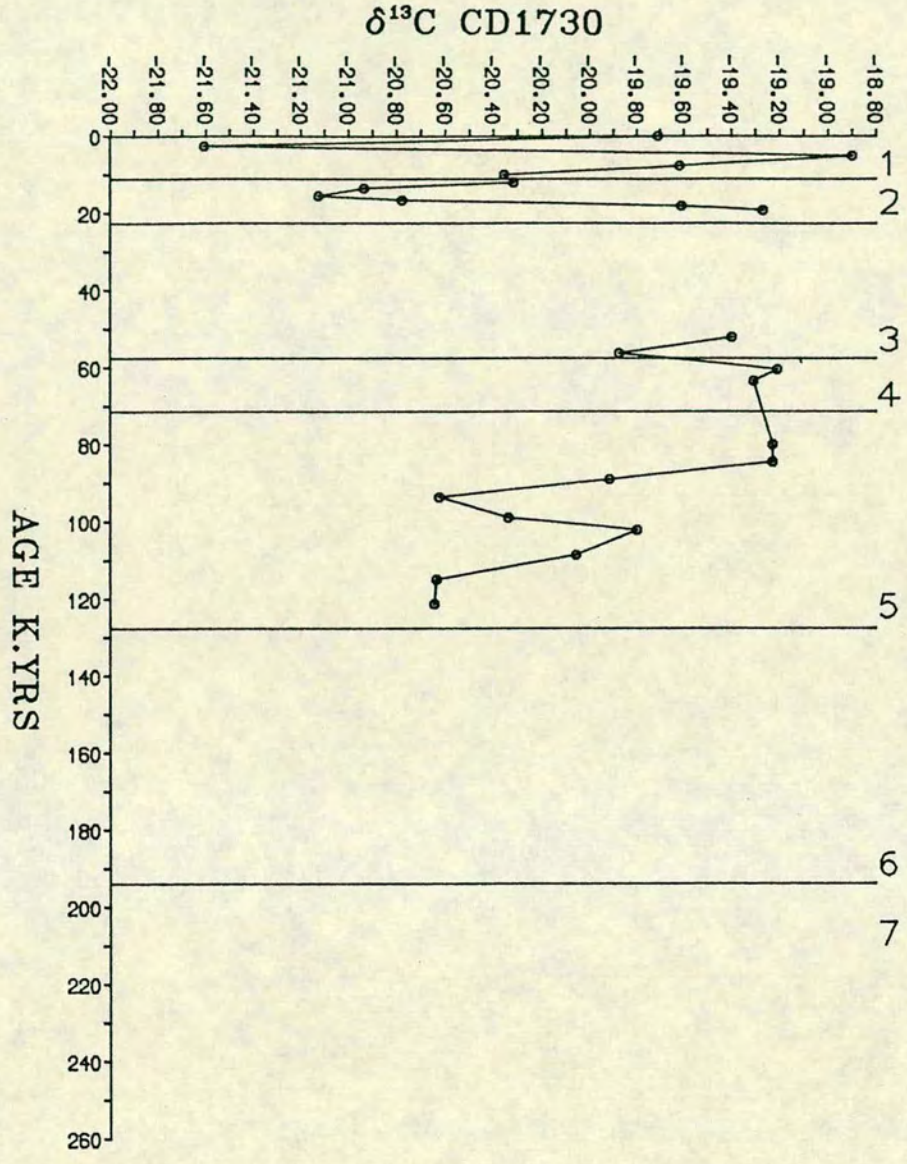

FIGURE 7.4 $\delta^{13}C$ VALUES OF ORGANIC CARBON IN SELECTED SAMPLES OF GLACIAL AND INTERGLACIAL STAGES.

In chapter 5, the evidence presented showed that Cr in the northwest Arabian sediments is largely derived from local sources as a result of pluming or other forms of transport from more marginal sediments. It is possible that with Cr, some land derived organic material of low $\delta^{13}C$ is also transported. For stages 3 and 4, the $\delta^{13}C$ is -19.4°/₀₀ implying a dominantly marine source. In stage 5 $\delta^{13}C$ values are relatively lower (-20.0°/₀₀) especially in its lower parts, again suggesting small contributions of terrigenous carbon, if any. These changes however may also indicate change in relative abundance of different planktonic species. From the very small amount of data of $\delta^{13}C$ available, it is impossible to assess the relative importance of either source (i.e. plankton type or organic source) and their change with time. However $\delta^{15}N$ analysed for the whole of core CD1730 may be more helpful in investigating the origin of organic matter.

7.5 NITROGEN ISOTOPES ($\delta^{15}N$)

Unlike $\delta^{13}C$, there has been little work on $\delta^{15}N$ variations in the marine sediments. Soil scientists and agronomists have used $\delta^{15}N$ to determine the source of organic matter and N uptake in plants (Keeny and Bremner, 1976; Kohl et al, 1971; Shearer et al, 1973, 1979). Much of the work on marine environments using $\delta^{15}N$ has been concerned with particulate organic matter (Cline and Kaplan, 1975; Saino and Hattori, 1980; Altabet and Deuser, 1985; Altabet and McCarthy, 1985, 1986). The ratio of $\delta^{15}N/NO_3$ has been used to determine the rate of denitrification (Cline and Kaplan, 1975). Recently, O'Donnell (1988) used $\delta^{15}N$ to recognise the relative proportions of marine and terrestrial organic matter, in the coastal sediments off Scotland. Despite this study and other similar work (e.g. Peters et al, 1978; Sweeny et al, 1978; Sweeny and Kaplan, 1980) the behaviour of $\delta^{15}N$ in marine sediments is not well understood.

The isotopic composition of atmospheric nitrogen is constant and ^{15}N comprises 0.37% of the total nitrogen, present in the atmosphere. The remainder is composed of the common ^{14}N isotope (Mariotti, 1983). The atmosphere is the major source of nutrient nitrogen in terrestrial organic matter. Therefore, the input of nitrogen to the terrestrial biosphere should be isotopically similar to that in the atmosphere ($\delta^{15}N$=0°/₀₀ relative to air). A slight variation, however, occurs due to the contamination by nitrogen compounds, released from rock weathering and during biogenic cycling (Hoering, 1955; Miyake and Wada, 1967; Riga et al, 1971; Bremner and Tabatabai, 1973).

In the marine environment the major nitrogen source is inorganic nitrate, which is enriched in N^{15} relative to the atmosphere (Cline and Kaplan, 1975; Sweeny and Kaplan, 1980). It has been considered that the $\delta^{15}N$ value of any sediment sample is an average of the amount of nitrogen derived from the euphotic zone of the ocean, and the amount of nitrogen from land. Peters et al (1978) have reported that terrestrial organic matter is relatively stable, and is of a refractory nature. As a consequence of this, after entering the marine system very little fractionation of terrigenous organic material occurs. However, marine organic matter is prone to fractionation especially during fallout to the sediment surface, and shows the $\delta^{15}N$ values in the range of +7.0°/oo to + 13.0°/oo (Cline and Kaplan, 1975; Wada and Hattori, 1978; Saino and Hattori, 1980). For terrigenous organic matter nitrogen, a value of $\delta^{15}N$ is between 0°/oo and +2.0°/oo. This value is very close to the $\delta^{15}N$ of standard nitrogen in the atmosphere which has been reported by many workers (Fig. 7.5) (Cline and Kaplan, 1975; Peters et al, 1978; Wada and Hattori, 1978; Sweeny et al, 1978; Saino and Hattori, 1980; Sweeny and Kaplan, 1980).

In this study $\delta^{15}N$ and total nitrogen of the Arabian Sea sediments have been analysed for one core CD1730 and an attempt has been made to understand their temporal variation in relation to marine and terrestrial organic input. The analytical methods used and the results are presented in appendix A6 and C12 respectively.

7.5.1 $\delta^{15}N$ in Arabian Sea Sediments, Core CD1730

$\delta^{15}N$ in core CD1730 from the Arabian Sea varies from 5°/oo to 16°/oo. In general, $\delta^{15}N$ values fall within the range of 8 °/oo to 13°/oo which are similar to that of marine nitrogen $\delta^{15}N$ (i.e. 7°/oo to 13°/oo) (Cline and Kaplan, 1975; Wada and Hattori, 1978; Saino and Hattori, 1978). This suggests that the origin of organic matter in the Arabian Sea sediment is predominantly marine. This conclusion is also supported by the heavy $\delta^{13}C$ value, as noted in the preceding section. Figure 7.6 shows the relationship between total nitrogen (T-N) and $\delta^{15}N$ in sediments and suggest that $\delta^{15}N$ is independent of total nitrogen. A similar relationship has been shown by O'Donnell (1988).

The $\delta^{15}N$ profile (Fig. 7.7) displays considerable fluctuation over the last 250,000 years BP. Significant trends seen are in the Holocene (stage 1), stage 3, 5 and in upper section of stage 7, and this probably indicates a climatic control affecting the production in the overlying water and deposition of organic matter at the sediment surface.

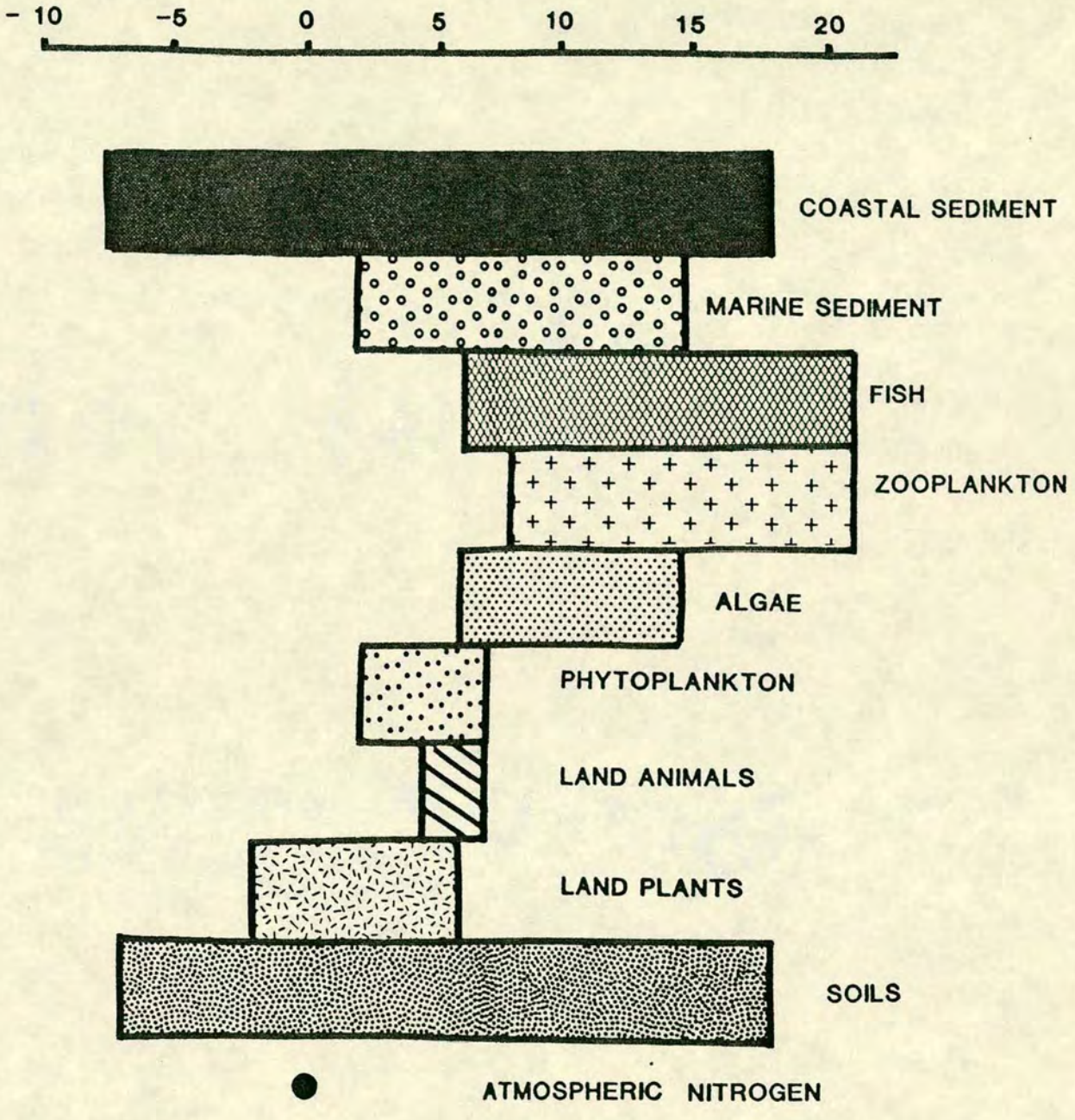

FIGURE 7.5 VARIATION IN $\delta^{15}N$ VALUES OF NATURAL SUBSTANCES. MODIFIED AFTER WLOTZKA (1972), KAPLAN (1975), MIYAKE and WADA (1967), SWEENY et al (1978).

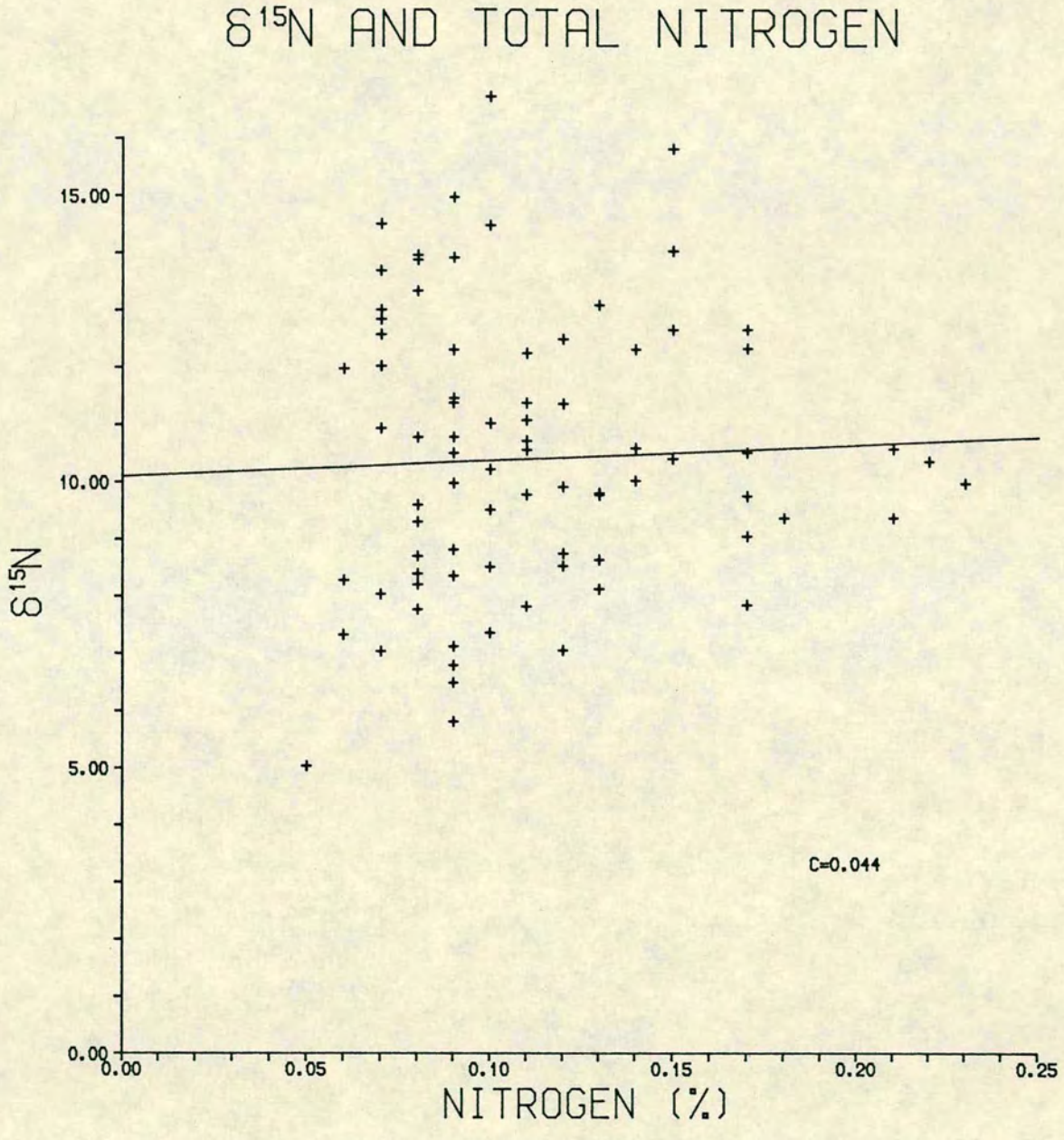

FIGURE 7.6 $\delta^{15}N$ VARIATION AGAINST TOTAL NITROGEN.

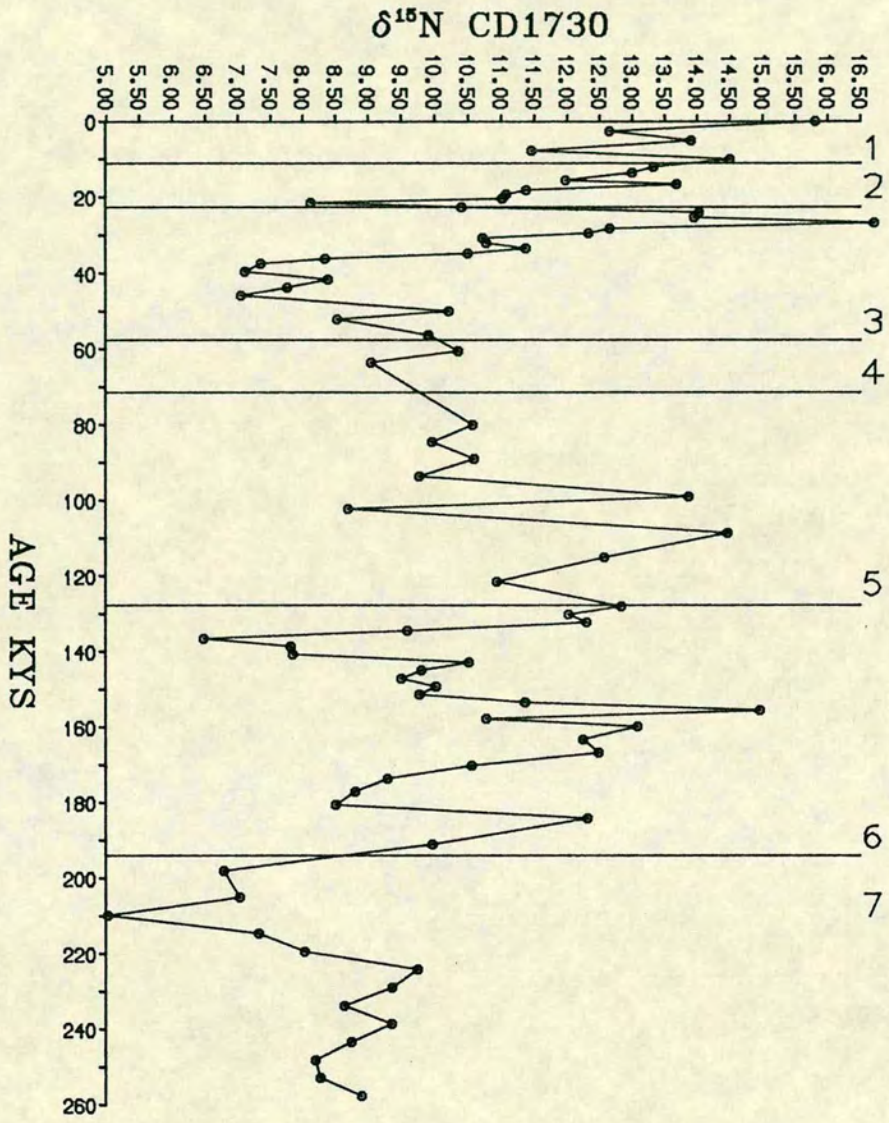

FIGURE 7.7 $\delta^{15}N$ CHANGES IN GLACIAL AND INTERGLACIAL STAGES FROM CORE CD1730.

The highest values occur at the surface, about 16°/₀₀ which sharply decreases downwards to ~11°/₀₀. This abrupt surficial change is also seen in organic carbon and T-nitrogen (Figs 6.3a and 7.1). In the middle of stage 3, the $\delta^{15}N$ is low (~7.0°/₀₀) while for most of stages 5 and 6 the $\delta^{15}N$ reassumes its Holocene character. Only in the upper stage 7, $\delta^{15}N$ are similar to the low values of stage 3.

It is possible that these $\delta^{15}N$ variations may be caused by variable supply of terrigenous (low $\delta^{15}N$) and marine (high $\delta^{15}N$) nitrogen. An attempt has been made to see if this is possible, following Sweeny and Kaplan (1980) who calculated the relative concentration of each member from the equation (See equation 7.1). Here it is assumed that terrigenous nitrogen is +2°/₀₀ and marine nitrogen is +10.0°/₀₀.

Equation (7.1) = $$Nm = \frac{\delta S - \delta T}{\delta m - \delta T} \times Ns$$

$$Nt = Ns - Nm$$

(Sweeny and Kaplan, 1980).

Nm = marine fraction %

Nt = terrestrial fraction %

Ns = total nitrogen in sediments

δs = $\delta^{15}N$ in sediments

δt = $\delta^{15}N$ in terrestrial nitrogen, i.e. +2.0°/₀₀

δm = $\delta^{15}N$ in marine nitrogen, i.e. 10.0°/₀₀

The weight percentage content of the fractions calculated in the sediments from the above relation are plotted against age and shown in Figure 7.8. These profiles can be used tentatively to ascertain the relative proportion of either component with time. From Figure 7.8 it is clear that marine rather than terrestrial nitrogen is dominant in the organic matter of Arabian Sea sediments.

The uppermost parts of interglacial stages 3,5 show relatively high marine nitrogen, ~0.20 (wt.%) while in glacial stages it is lower between 0.10 (wt.%) and 0.15 (wt.%). The profile shows that terrestrial nitrogen fraction is insignificant in the sediments, and even in glacial stages values are very low. A minor fraction of terrestrial nitrogen up to 0.05 (wt.%) is seen in the lower sections of stages 3, 5, 6 and 7. Correspondingly, a decrease is noticed in marine nitrogen at these times (Fig. 7.8). Overall, the terrestrial nitrogen fraction profile shows a broad positive relationship with Si(lith)/Al ratio profile (Fig. 7.9).

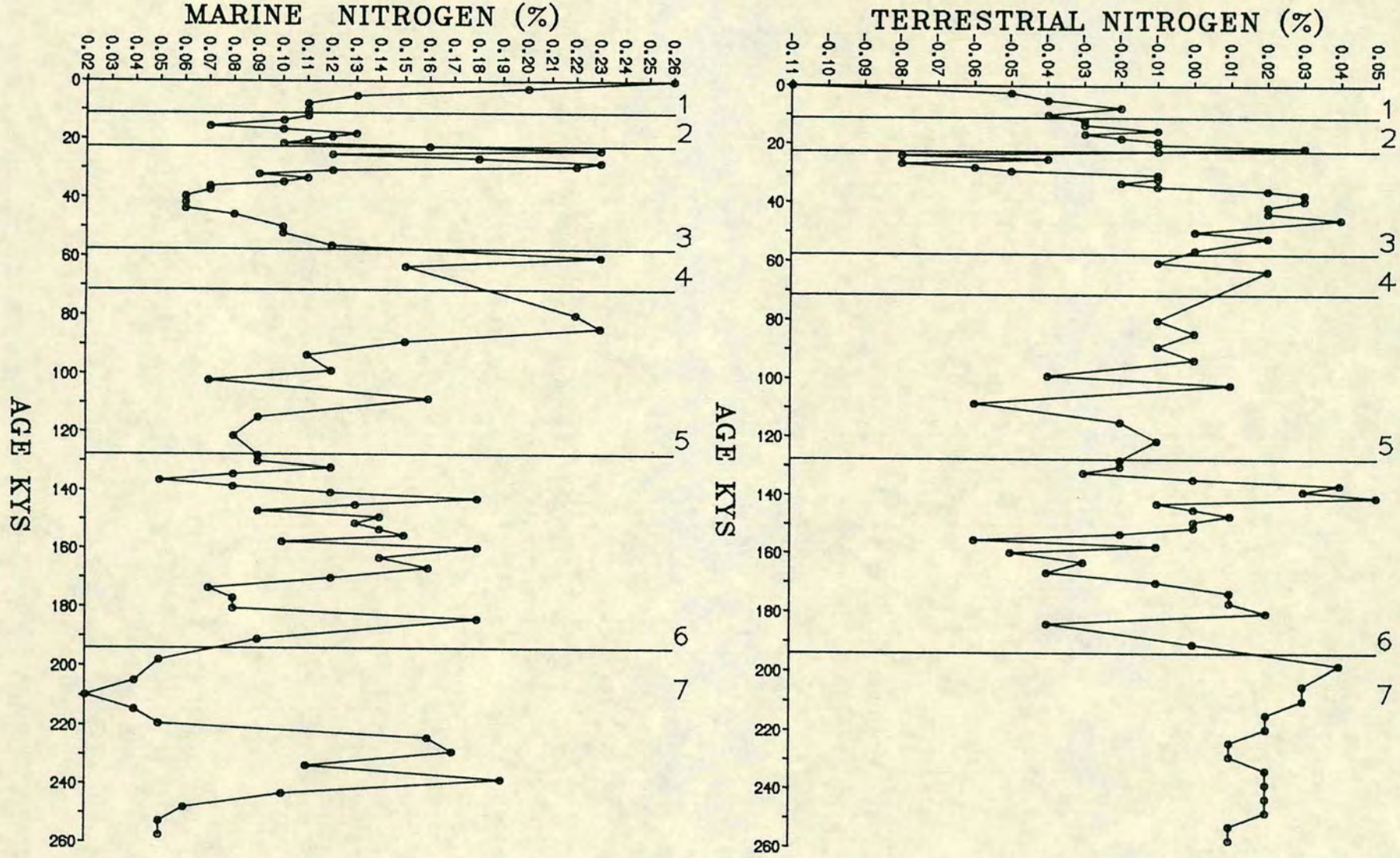

FIGURE 7.8 VARIATIONS OF MARINE AND TERRESTRIAL FRACTION OF NITROGEN IN GLACIAL AND INTERGLACIAL STAGES.

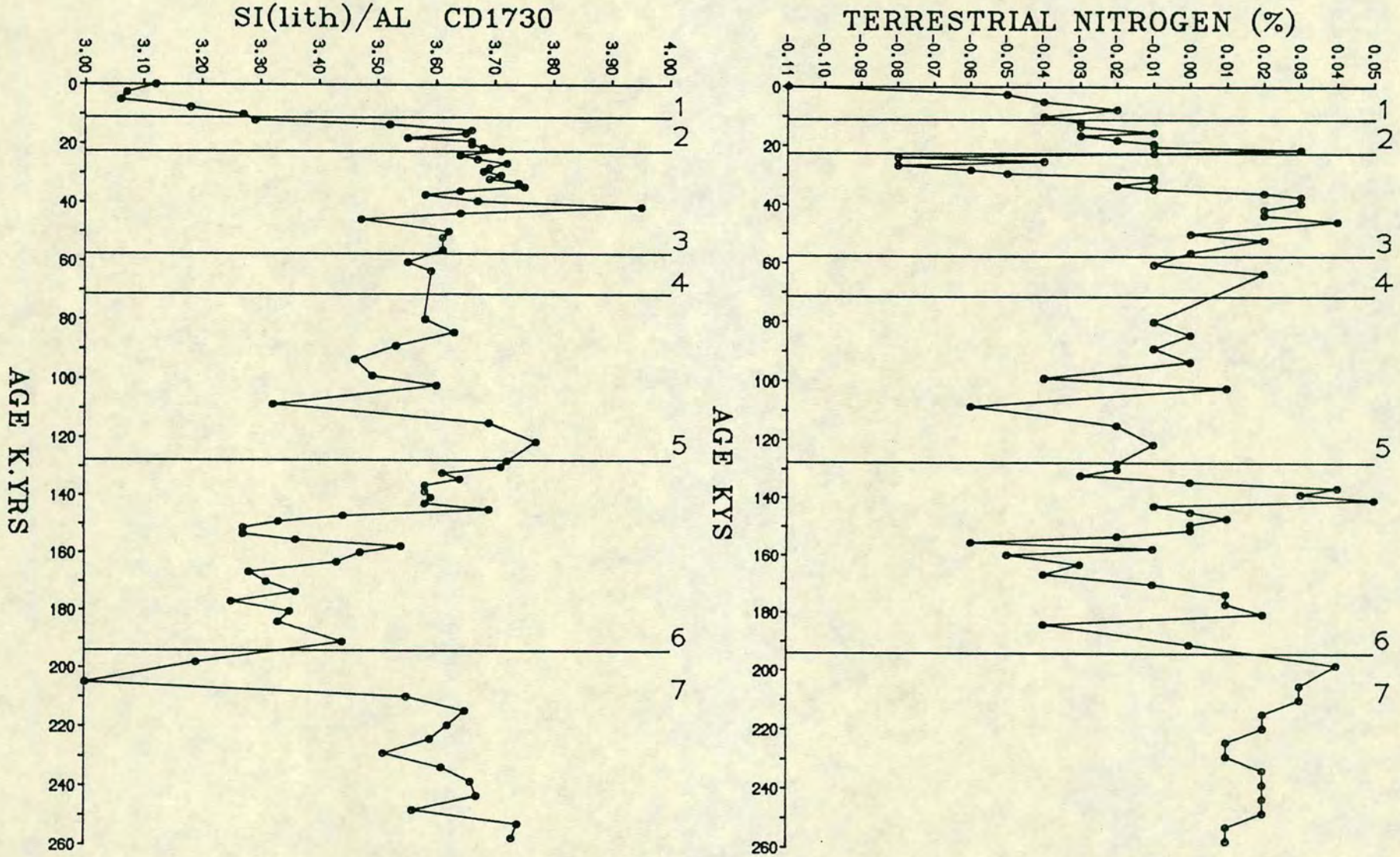

FIGURE 7.9 SYMPATHETIC TRENDS BETWEEN TERRESTRIAL NITROGEN AND Si(Lith)/Al AT LOWER BOUNDARIES OF STAGE 3 AND 5.

As with the $\delta^{13}C$ results, the $\delta^{15}N$ data is difficult to use in assessing the relative proportions of marine and terrestrial organic matter during different climatic stages in the Arabian Sea sediments. Nevertheless, the $\delta^{15}N$ values shown here in addition to $\delta^{13}C$ suggests that marine organic matter is dominant. However, when compared with C/N and Si/Al ratios some similarities are seen, and the following explanations could be possible and given to derive tentative conclusions from the trends in $\delta^{15}N$ data.

1. = Productivity
2. = Environment of Deposition

7.5.1.a *Productivity*

$\delta^{15}N$ variation shown in Figure 7.7 generally follows the biomarkers such as C.org, biogenic silica and Ex. Ba. (Figs 6.3, 6.5a and 6.6). Since these biomarkers in the sediments reflect the fertility of overlying water, the behaviour of $\delta^{15}N$ may also be associated with organic matter production. Biomarker and nitrogen isotope trends, although showing a generally consistent pattern, also display distinct horizons of disparity. For example, in the Holocene (stage 1) $\delta^{15}N$ shows high values, but the amplitude is different from Biog. Si and Ex. Ba. (Figs 6.5a and 6.6a). However, the marine nitrogen fraction trend (Fig. 7.8a) seen in this stage is similar to biomarker profiles like Biog. Si. and Ex. Ba. In upper stage 3, $\delta^{15}N$ and marine nitrogen both show high values, while Biog. Si. and Ex. Ba do not increase. Furthermore, marked dissimilarities occur at the top of stage 5 and stage 7. Here $\delta^{15}N$ values are characteristically low, whereas biomarkers are not lower.

This discrepency, in the patterns of these elements, probably reflects various mechanisms controlling the chemistry of individual elements. A stepwise increase in $\delta^{15}N$ for different trophic level of a food chain has been observed (Fig. 7.5) (Mingawa and Wada, 1984; Macko and Parker, 1984). For instance, phytoplankton are found to have a ratio of -2.5°/$_{oo}$ and 6°/$_{oo}$, while zooplankton are higher varying between +6°/$_{oo}$ and +14°/$_{oo}$. Therefore $\delta^{15}N$ results in the sediments maybe being influenced by the type and relative abundance of phytoplankton and zooplankton in overlying waters. Different species of marine diatoms have also been shown to have different $\delta^{15}N$ values (Wada and Hattori, 1978). Therefore, it is possible that the $\delta^{15}N$ profile of the investigated core may reflect variations in the biota of the overlying water.

Macko and Parker (1984) studied regional differences in the isotopic composition of biota and sediments from the continental shelf of the Gulf of Mexico. They attributed differences in $\delta^{13}C$ and $\delta^{15}N$ to the primary source (Table 7.6). They found that particulate organic matter from south Florida contained large quantities of *Tricodesmium* spp which has been associated with nitrogen fixation (Dugdale et al, 1964). This species is very similar in composition to dissolved atmospheric nitrogen. Although *Tricodesmium* is not the only primary source of nitrogen in the region, Macko and Parker (1984) observed further depletion in zooplankton, shrimps and sediments (Table 7.6) from south Florida in comparison to samples from the northwestern Gulf.

The occurrence of massive blooms of the same species, the *Trichodesmium* in the Arabian Sea is a common feature during the southwest monsoon (Qasim, 1970). According to Macko and Parker (1984) the differences in $\delta^{15}N$ values of sediments from south Florida and the northwestern Gulf is due to the abundance of *Tricodesmium* spp in the former area. The same may hold true in the northwestern Arabian Sea sediments. In the Arabian Sea, such a study has not yet been carried out to document the observed differences in $\delta^{15}N$ of the sediments. It is, therefore, not certain that *Trichodesmium* or other factors could effect the $\delta^{15}N$ variation in these sediments. This uncertainity is further supported by the occurrence of a wide range and overlap in $\delta^{15}N$ values of both marine and terrestrial matter as shown in Figure 7.5.

7.5.1b *Environment of Deposition*

O'Donnell (1988) hypothesised that erosion of fine material may decrease the $\delta^{15}N$ value by increasing the relative terrestrial portion of the organic matter. The variation in the texture of sediments generally suggests either a change in sedimentary input or an erosive phase. Shimmield et al (1988) documented surface sediments from the Oman continental margin which showed high C/N ratio in relatively coarse grained sediments, which were also enriched in Cr. They concluded that as a result of strong bottom currents the more labile organic matter shows greater loss due to the removal of fines. As a result of this, the nitrogen which represents a more labile fraction of organic matter is reduced and therefore increases the C/N ratio.

Earlier, it was noticed that most of the biomarkers in stage 3,5 and 7 show small values. The $\delta^{15}N$ profile (Fig. 7.7) in the present study largely reflects marine nitrogen in the organic matter. $\delta^{15}N$ values and percentage of marine nitrogen (Figs

Table 7.6 **Stable isotopic compositions of organic materials from the Gulf of Mexico (Macko et al., 1984).**

	Northwest Gulf		South Florida	
	$\delta^{15}N$	$\delta^{13}C$	$\delta^{15}N$	$\delta^{13}C$
Particulate organic matter (POM)	+ 7.5±0.8	-21.0±1.4	-0.9±1.4	-19.4±1.2
Zooplankton (mixed)	+ 8.9±0.9	-19.2±0.7	+5.9±0.7	-18.4±1.1
Sediment (acid residue)	+ 6.5±0.2	-20.6±0.6	+3.6±0.1	-18.5±0.7
Shrimp (*Panaeus* spp.)	+12.9±1.1	-15.6±1.1	+8.4±0.9	-14.8±0.5

Table 7.7 $\delta^{15}N$ **and C/N values of surface sediments from Oman Margin**

STATION	T.N%	at.%N	$\delta^{15}N$	Nm%	Nt%	$\delta^{13}C$	C/N
CD 1704	0.39	0.37	8.22	0.30	0.09	n.a	9.6
CD 1705	0.27	0.37	7.29	0.18	0.09	n.a	11.1
CD 1706	0.36	0.37	7.18	0.23	0.13	n.a	10.3
CD 1710	0.35	0.37	7.07	0.22	0.13	n.a	10.2
CD 1717	0.12	0.37	7.92	0.09	0.03	n.a	15.4
CD 1724	0.17	0.37	7.78	0.12	0.05	n.a	10.0

* Nm = marine nitrogen fraction
** Nt = terrestrial nitrogen fraction

7.8) show a decrease at the above mentioned stage boundaries. In contrast, the terrestrial content and Si/Al ratio indicate a synchronous increase (Fig. 7.9). This implies that much of the organic material in the interglacial stages could have been winnowed away leaving behind a concentrate rich in quartz. Stable isotopic values of $\delta^{15}N$ in interglacial stages are generally 10.0°/₀₀. A decrease from this value is observed at the lower boundaries of stage 3,5 and 6 suggests an increase in the terrestrial organic nitrogen (Fig. 7.9).

Surface samples from this area are known to have suffered a severe loss of organic matter by winnowing (Shimmield et al, 1988). These samples have also been analysed for $\delta^{15}N$ to see if current activity affects $\delta^{15}N$ values. These samples show $\delta^{15}N$ values ranging from 7°/₀₀ to 8°/₀₀ (Table 7.7), that is, close to those of the sediments which show increased Si/Al ratios at the stage boundaries of 3/4, 5/6 and 6/7. Therefore it is possible that low $\delta^{15}N$ values are associated with high Si/Al ratios.

In summary, from the isotopic data of the core CD1730 the following results can be inferred.

a. $\delta^{13}C$ and $\delta^{15}N$ in the northwestern Arabian sediments indicate a marine organic source.
b. the effect of changes in productivity on $\delta^{15}N$ values seems to be more important than the environment of deposition.
c. a slight variation in isotopic data of $\delta^{15}N$ during interglacial stages could be the result of a winnowing action, which concentrates the organic matter associated with the terrestrial material.
d. isotopic data may be used to determine the environment of deposition.

CHAPTER 8

GEOCHEMISTRY OF HALOGENS

HALOGENS

8.1 INTRODUCTION

It has been documented that iodine and bromine in marine sediments are exclusively associated with organic matter (Shishkina and Pavlova, 1965; Price et al, 1970; Price and Calvert, 1977). The ratio of I and Br relative to carbon in the open ocean sediments is generally invariable. However at depth a decrease in both relative to carbon occurs as a result of alteration of organic matter. A correlation between I and organic matter in surface sediments has been noted by Ullman and Aller (1980) and Elderfield et al (1981). A similar relationship between Br and organic matter has also been suggested (Price and Calvert, 1977; Mayer et al, 1981; Malcolm and Price, 1984). The iodine content of marine sediments varies between different marine environments (Table 8.1). Studies have shown that I is generally more enriched in shallow marine sediments (Price et al, 1970; Pavlova and Shishkina, 1973; Price and Calvert, 1973). In these sediments, due to high organic carbon contents, I has been found to be more prone to diagenetic reaction than Br (Price and Calvert, 1977). It has been suggested that the relative reactivity of the I and Br is linked with the different constituents of organic matter. Harvey (1980) noted I may be associated with nitrogenous compounds in organic matter. This material is more labile during degradation (Gordon, 1971; Suess and Muller, 1980; Grudmanis and Murray, 1982). The ratio of I relative to organic carbon has been used to distinguish oxic and anoxic sediments (Price and Calvert, 1973). Anoxic sediments are reported to show a low I/C.org ratio (i.e. 20-30 x 10^{-4}) compared to oxic sediments. In open ocean conditions oxic sediments show a higher ratio ~250 x 10^{-4} (Table 8.3).

8.2 IODINE AND BROMINE

In this thesis, the distribution of I and Br in the sediments of the northwestern Arabian Sea are discussed. Total iodine and bromine were determined by the method of x-ray flourescence. The data for both elements, on a salt free basis, are tabulated in appendix C.13. The mean contents of both I and Br for the cores examined in this study are listed in Table 8.2.

All cores show that I is predominant over Br. The concentration of the two elements within cores varies considerably (Figs 8.1 and 8.2), although the sediments' average concentration remains fairly constant (Table 8.2). A correlation between both iodine and bromine and organic carbon is shown in Figures 8.3 and 8.4 which is consistent with other studies (Price and Calvert, 1977; Pederson and Price, 1980).

Table 8.1 Published iodine contents of marine sediments

Reference	Location and Lithology	Iodine (ppm)	I/C.org ($x10^{-4}$)
Shishkina and Pavlova (1965)	Indian and Atlantic Ocean Calcareous Ooze	39	156
	Pacific Ocean Red Clay	29	106
	Pacific and Indian Ocean Grey Clays	202	348
Price et al (1970)	Barents Sea Muds and Sands	60-828	25-380
Pavlova and Shishkina (1973)	NW Pacific	21-398	70-260
	Peru	37-610	80.0-242
Price and Calvert (1973)	SW African Shelf organic rich diatomaceous ooze	96-1990	16-252
Harvey (1980)	Buzzards Bay	20	20.0
	Gulf of Maine	220	110.0
Pederson and Price (1980)	Panama Basin hemipelagic sediments	76-861	395.0

Table 8.2 Mean contents of I, Br and their ratios relative to C.org

CORES	I(ppm)		BR(ppm)		I/C.org x 10^{-4}		BR/C.org x 10^{-4}		I/BR	
Arabian Sea	Range	Mean	Range	Mean	Range	Mean	Range	Mean	Range	Mean
CD1715	10-90	52	1-94	30.77	10-84	75	2.0-213	36	0.4-21.0	3.01
CD1730	20-204	74	5.0-168	48.0	35-221	110	14-165	67	0.5-6.5	1.88
CD1739	16-116	57	3.0-88	36.0	37-235	109	7-164	64	0.6-18.0	2.05
CD1738	7-227	54	2.2-129	33.0	19-486	132	2.62-266	78	0.24-17.0	2.15
Other areas										
Barents Sea* (Price et al, 1970)	100-828	400	30-255	110	200-380	290	40-100	80	0.5-2.8	1.45
Panama Basin* (Pederson and Price, 1980)	70-400	250	30-150	-	250-400	395	-	146	2.3-2.6	2.4
Pacific Ocean* (Wakefield, 1981)	-	~50	-	-		~60.0	-	-	-	-

* Surface Sediments

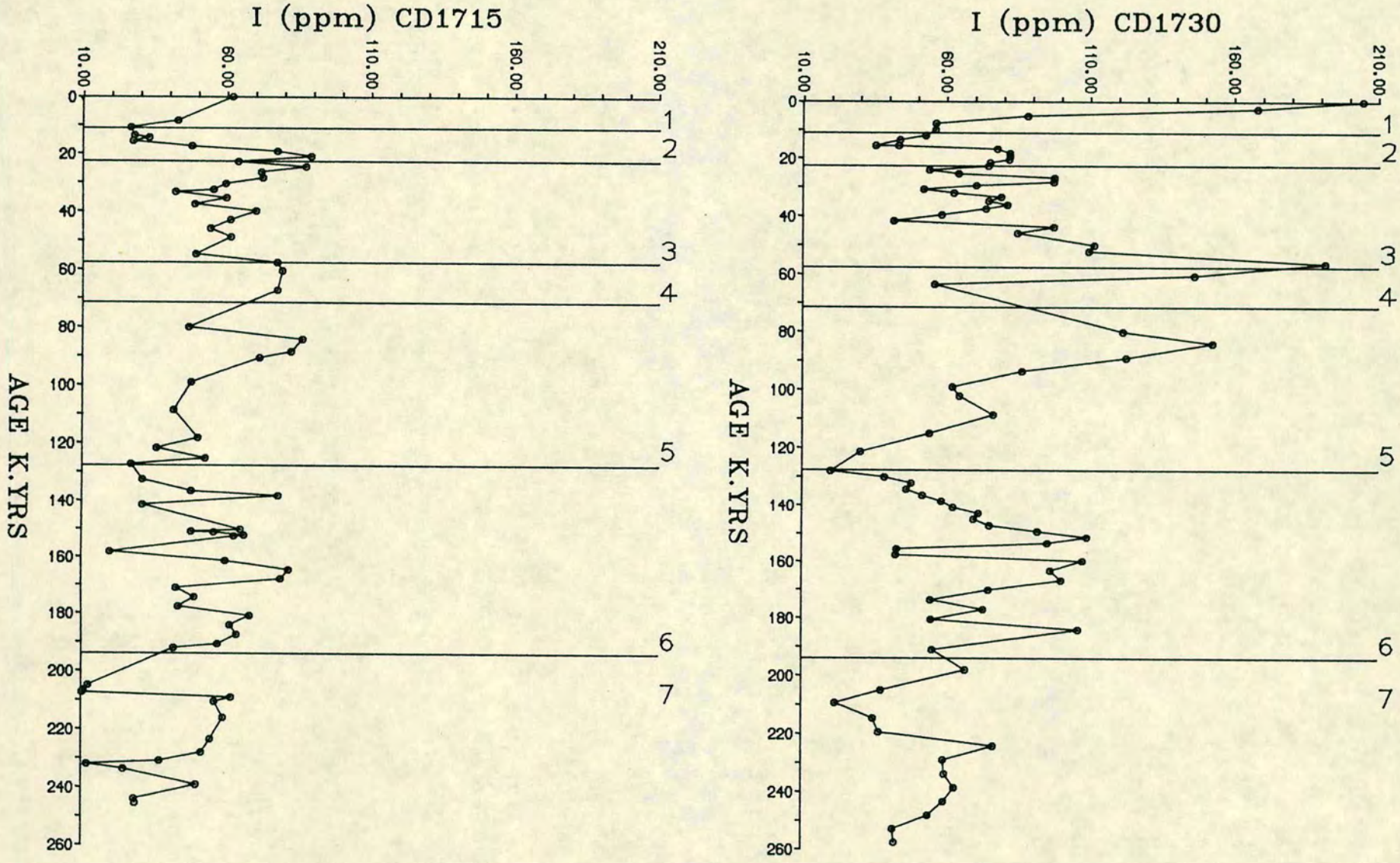

FIGURE 8.1a IODINE PROFILES OF CORES CD1715 AND CD1730.

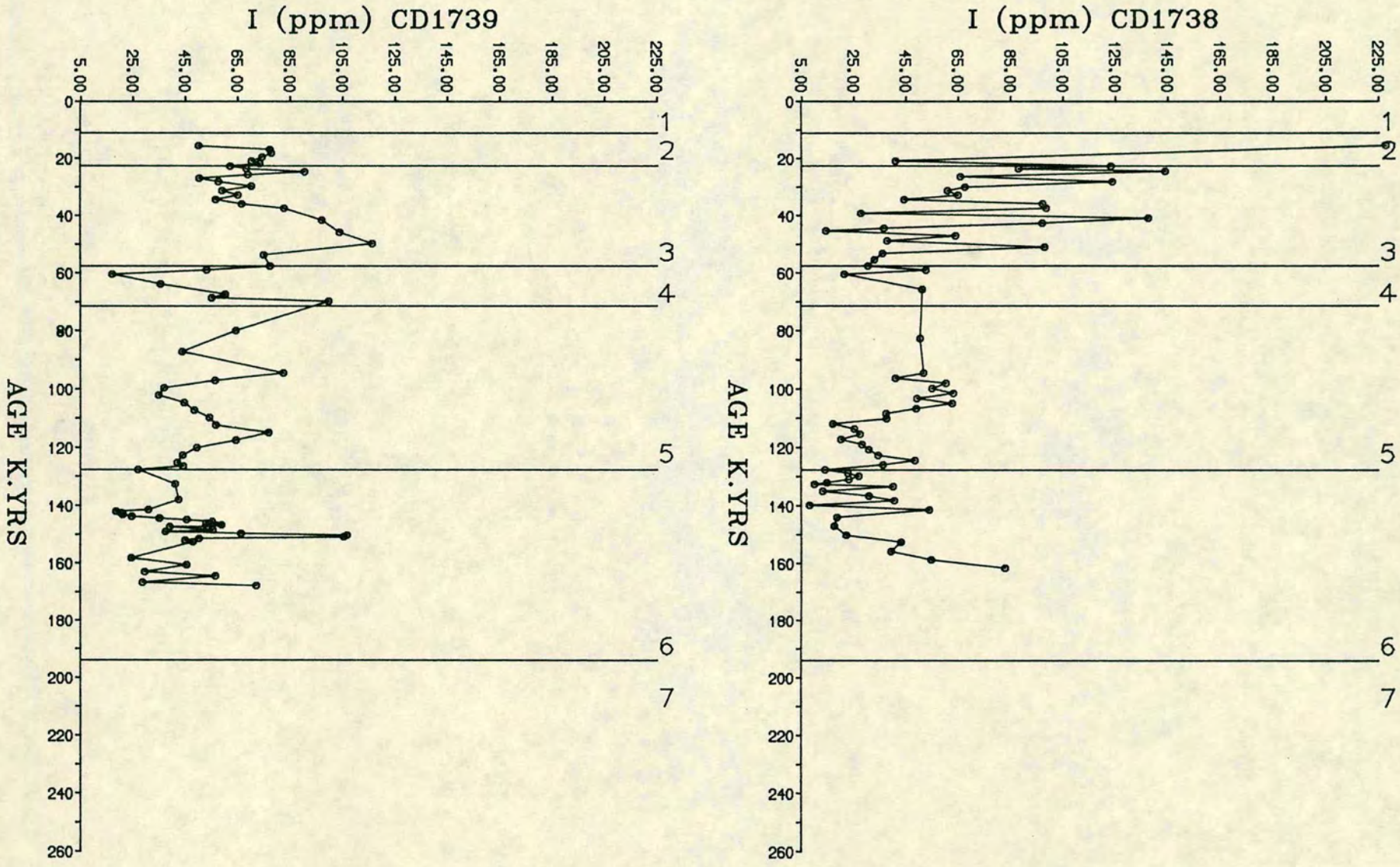

FIGURE 8.1b IODINE PROFILES OF CORES CD1739 AND CD1738.

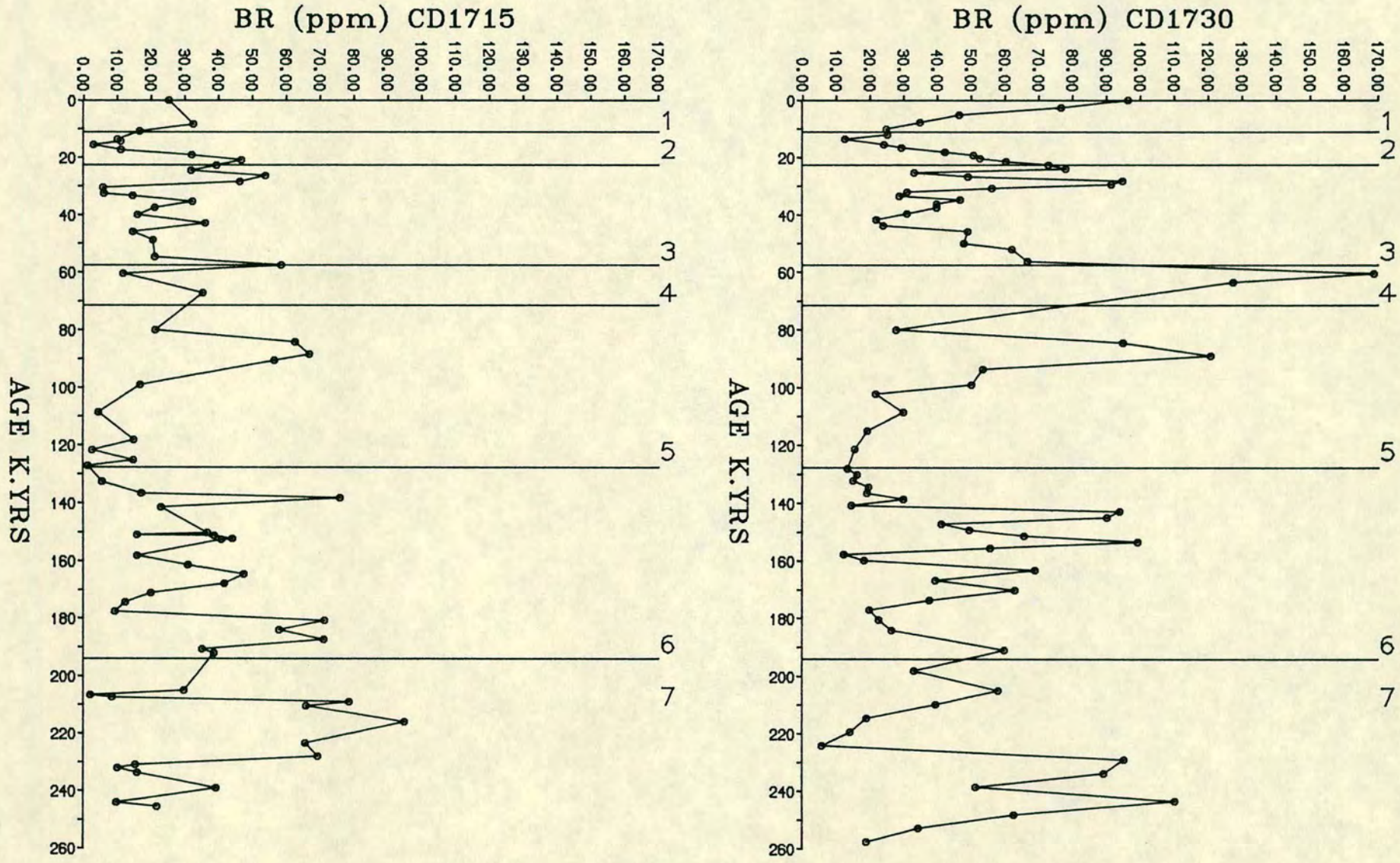

FIGURE 8.2a BROMINE PROFILES OF CORES CD1715 AND CD1730.

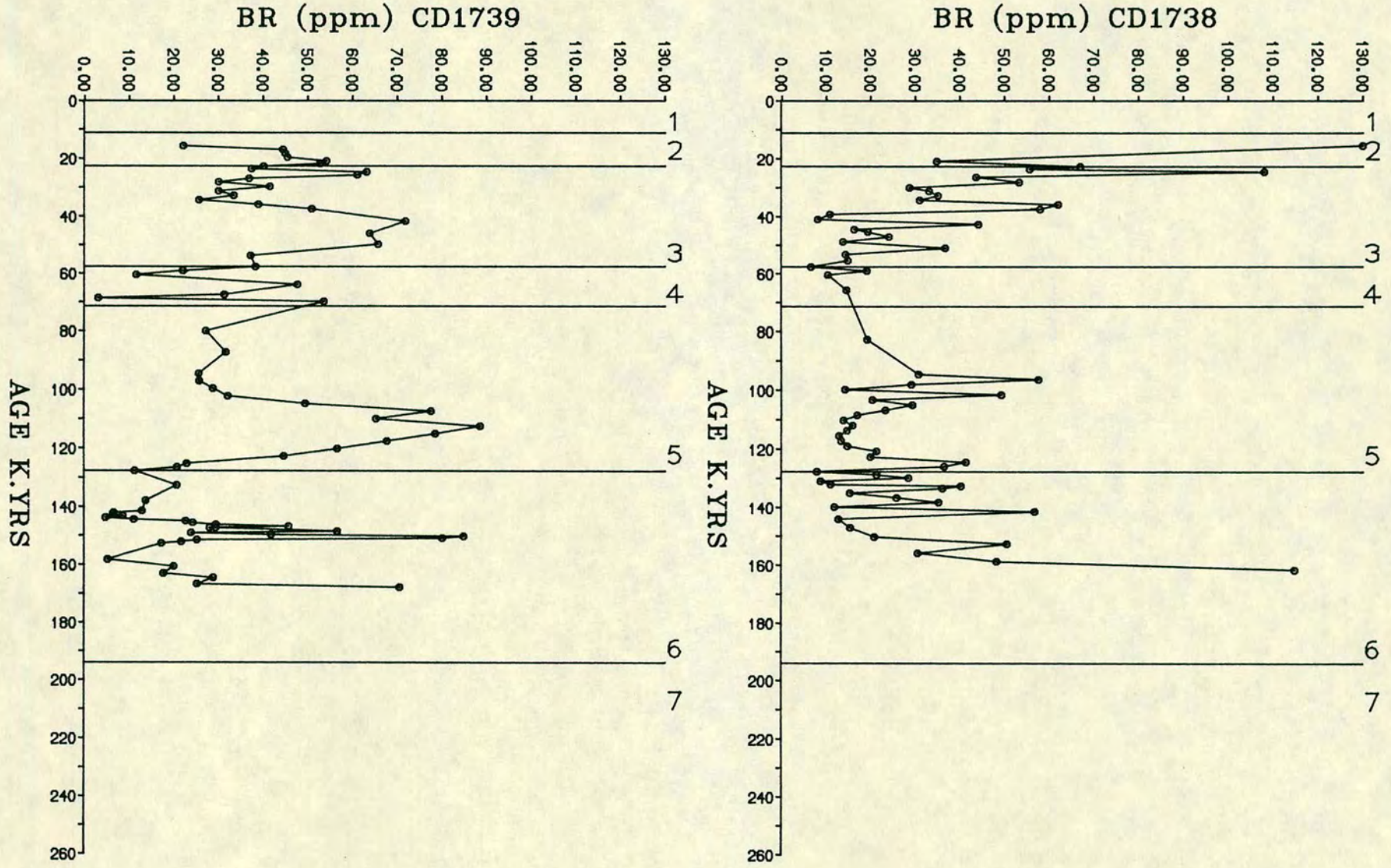

FIGURE 8.2b BROMINE PROFILES OF CORES CD1739 AND CD1738.

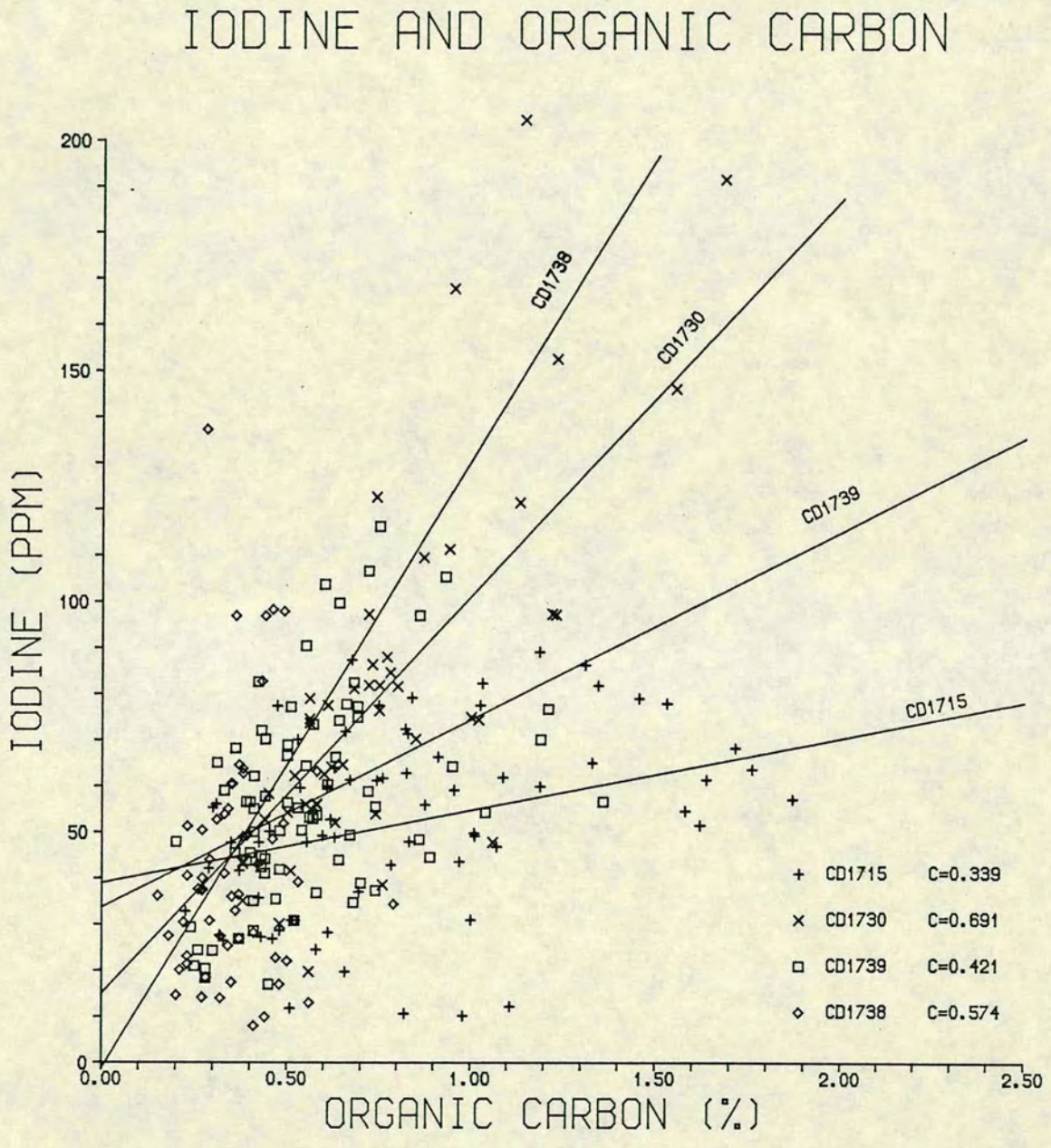

FIGURE 8.3 THE RELATIONSHIP BETWEEN IODINE AND ORGANIC CARBON IN SEDIMENTS CORES FROM NW ARABIAN SEA.

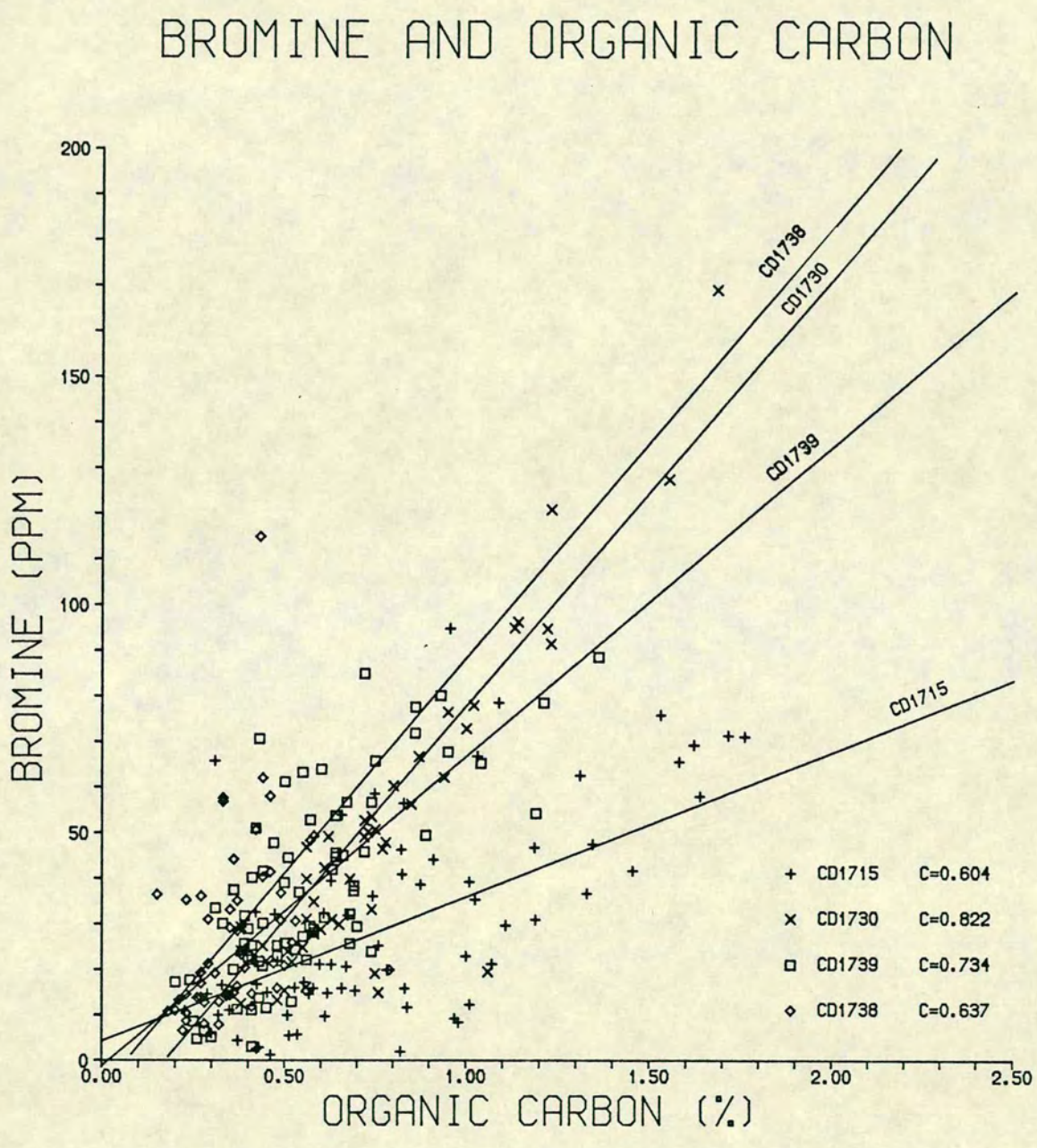

FIGURE 8.4 THE RELATIONSHIP BETWEEN BROMINE AND ORGANIC CARBON IN SEDIMENT CORES FROM NW ARABIAN SEA.

These workers have noted that under oxidising conditions, the quantity of iodine and bromine present in the surface sediments is directly proportional to the concentration of organic carbon. However, intercepts at 20,30 and 40 ppm iodine in the cores shown (Figure 8.3) imply some unusual enrichment of iodine over C.org in sediments. It is known that iodine and bromine contents in recent surface sediments have been only indirectly related to primary production sources (Price and Calvert, 1973; Mayer et al, 1981). The higher iodine in the cores (i.e. CD1715, CD1730, CD1739) may be a result of sorption of iodine by seston at the sediment/water interface, a mechanism similar to that present in macroalagae (Shaw, 1959). The relationship between Br and organic carbon (Fig. 8.4) shows a close association, but suggests that the Br uptake by organic matter is either limited in the northwestern Arabian Sea sediments or is lost during sediment burial. The vertical trends seen in iodine and bromine (Figs 8.1 and 8.2) closely follow those of organic carbon (Figs 6.3a,b).

A rapid decline in I and Br content occurs in Holocene (stage 1) may be the result of early diagenetic loss of halogens from the sediments. Since the cores CD1715 and CD1730 are found to contain red oxidised surface sediments, the marked change in I and Br together with C.organic probably indicates some diagenetic effect during burial. The similarity in the distribution of iodine and bromine (Figs 8.1 and 8.2) and that of organic carbon (Fig. 6.3a,b) in the different isotopic stages, implies a common controlling factor in the buried sediments. To understand this better, the vertical variation of I and Br with respect to organic carbon and the relative variation of I with Br are discussed in the following section. Figures 8.5, 8.6, 8.7 show the distribution of I/Br, I/C.org, and Br/C.org ratios of the four cores.

8.3 HALOGENS/C.org RATIOS

I/Br profiles shown in Figures 8.5a,b show no obvious systematic trends, except that there is an overall decrease, although small, in ratio from the top of the cores to their bases. This decrease in I/Br supports Pederson and Price's (1980) suggestion that I is lost preferentially to Br during burial diagenesis. The range in I/Br ratio however is very large with occasional spikes. This is particularly seen in cores CD1715, CD1739 and CD1738. Since these elements are associated with each other, these anomalously high values need further consideration.

The I/C.org ratios, shown in Figures 8.6a,b for the four cores, display a considerable vertical fluctuation. Their patterns are dissimilar and this is most evident in stage 6 of cores CD1715 and CD1730 (Fig. 8.6a). Unlike the trends in carbon organic (Figs 6.3) the I/C.org ratios show an overall increase from core

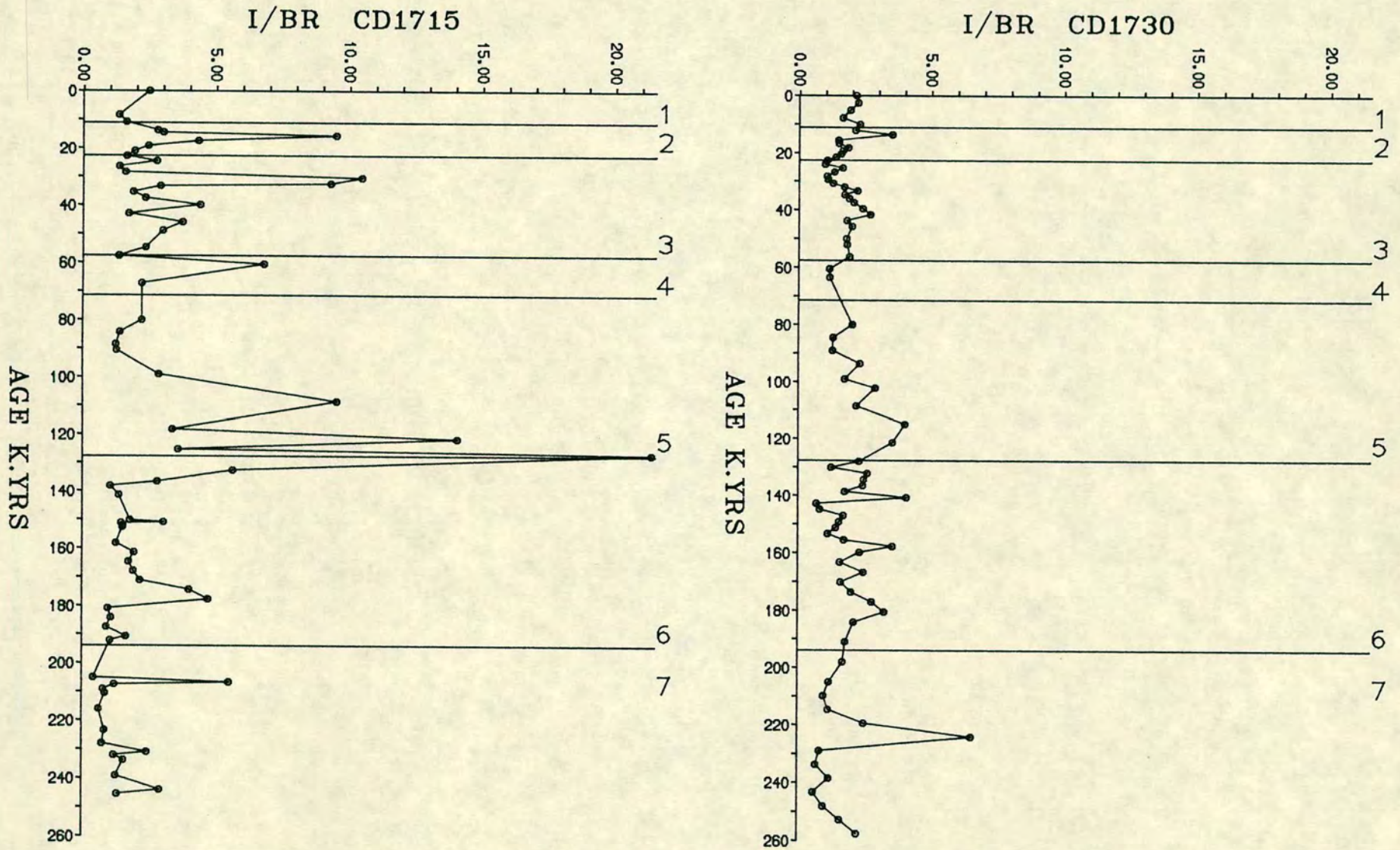

FIGURE 8.5a I/Br RATIOS IN NW ARABIAN SEA CORES CD1715 AND CD1730.

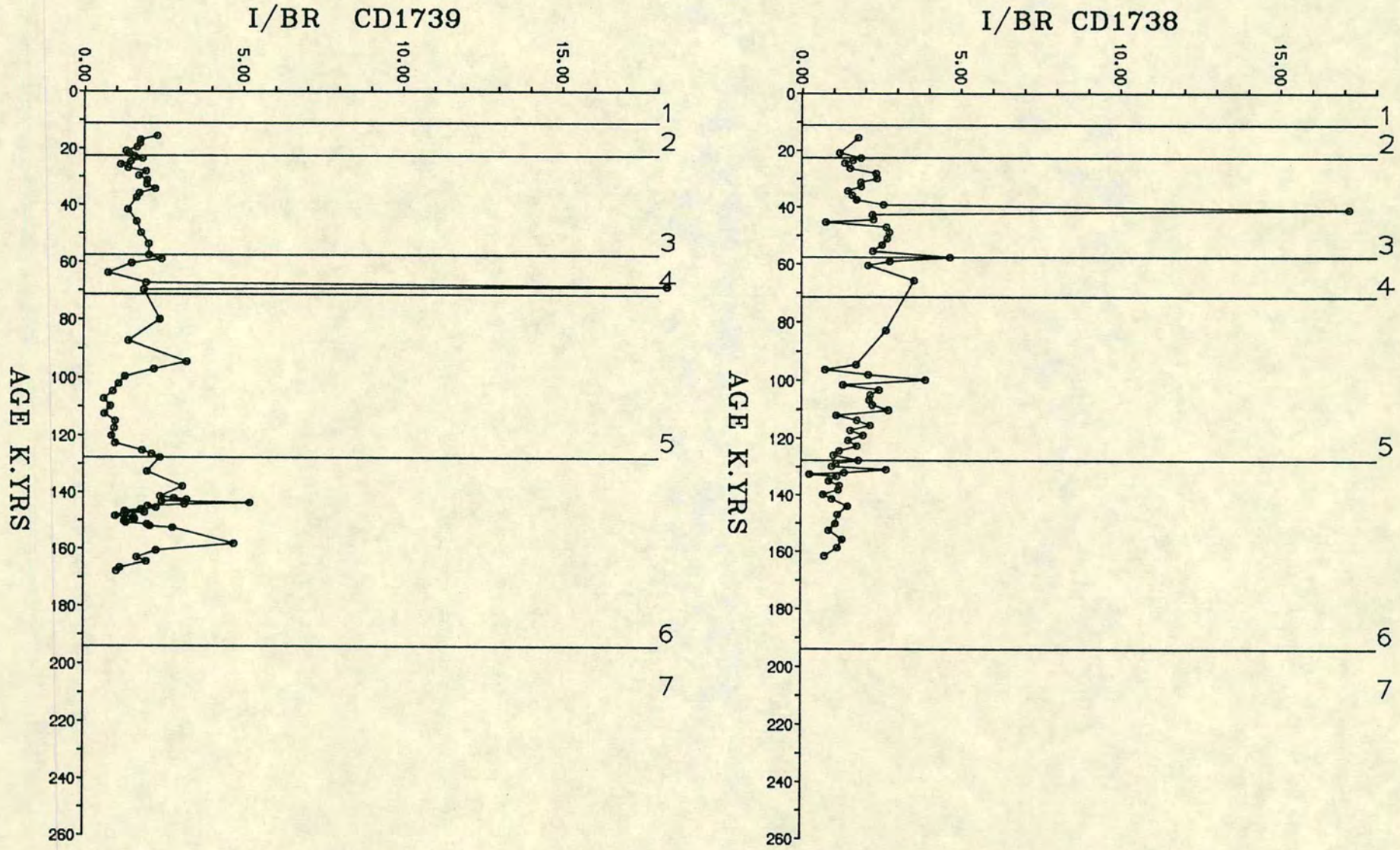

FIGURE 8.5b I/Br RATIOS IN NW ARABIAN SEA CORES CD1739 AND CD1738.

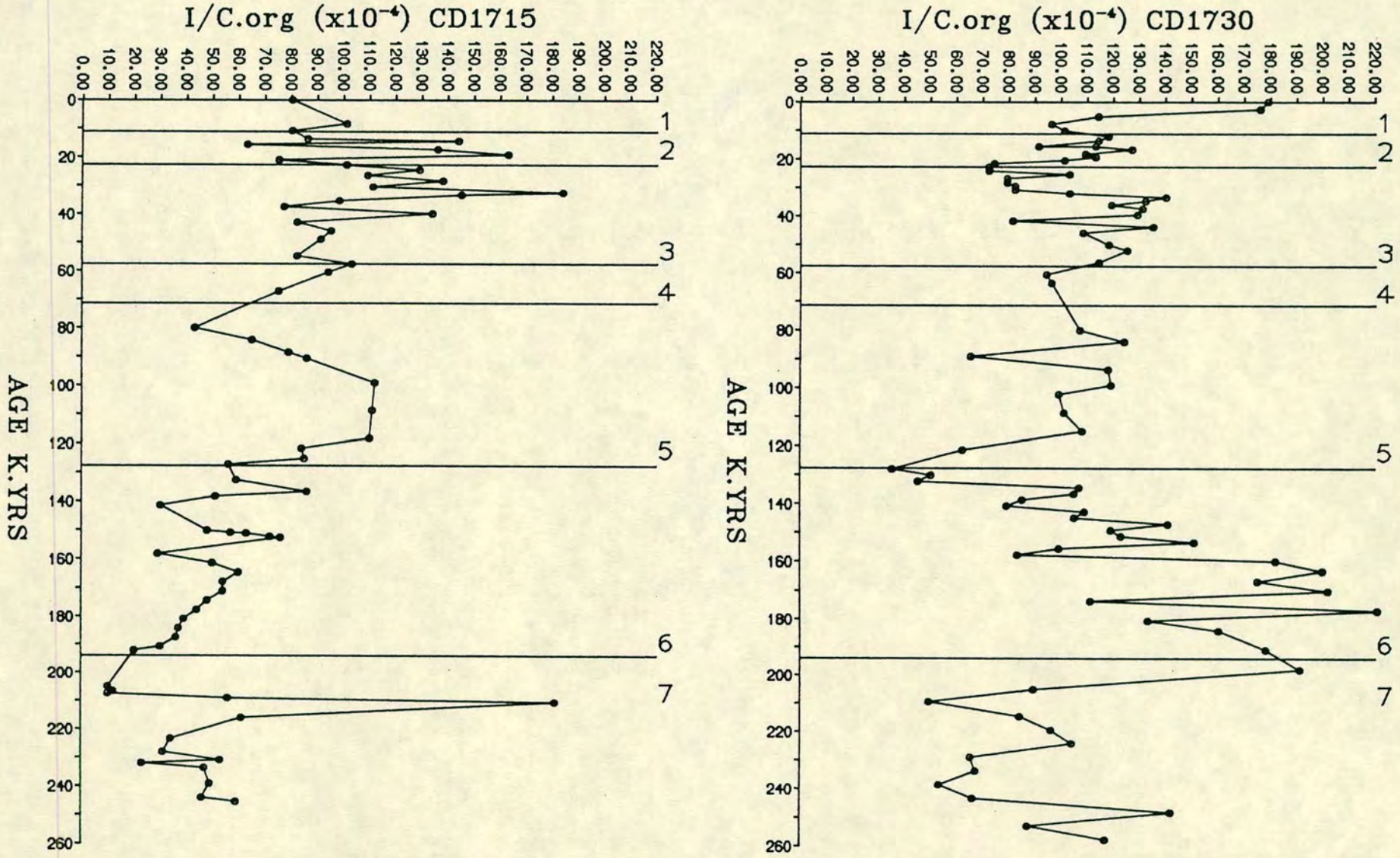

FIGURE 8.6a I/C.org RATIO PROFILES OF CORES CD1715 AND CD1730.

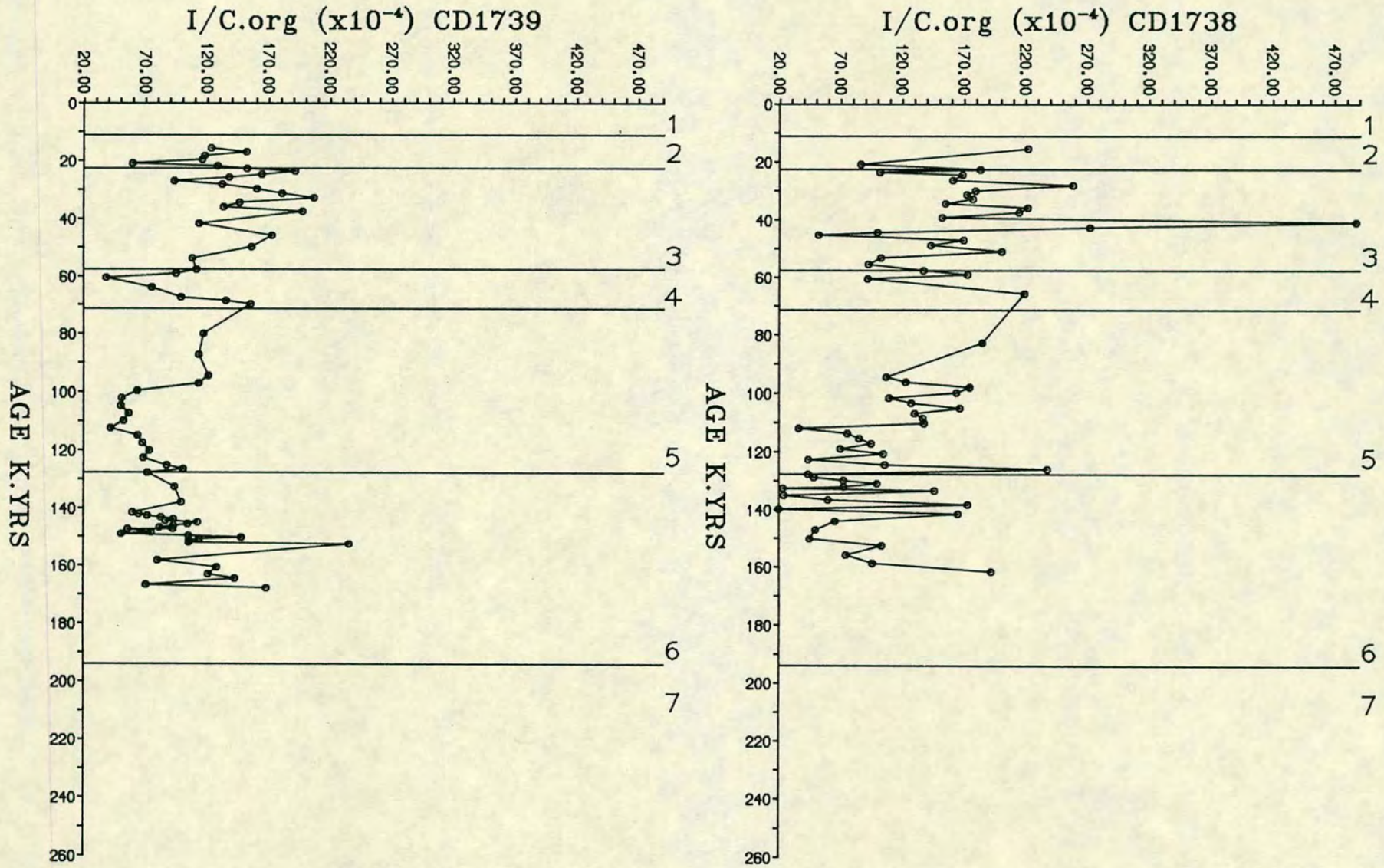

FIGURE 8.6b I/C.org RATIO PROFILES OF CORES CD1739 AND CD1738.

CD1715 to CD1738. The I/C.org ratio in core CD1715 is low (i.e. 75 x 10^{-4}) while in cores CD1738 and CD1739 I/C.org values are high more than 100 x 10^{-4} (Table 8.2).

The I/C.org ratios found at surface in core CD1715 is ~80 x 10^{-4} and that in core CD1730, ~180 x 10^{-4}. In core CD1730 there is an abrupt decrease in the order of magnitude in stage 1 (Fig. 8.6a). In core CD1715 a slightly different trend occurs within stage 1, and is probably due to a lack of surface sediment during core recovery. However around 8-9000 years BP both cores show a similar pattern. Down the cores, I/C.org ratio oscillates without any systematic trends. However, all cores tend to show a general fall in the ratio with depth, which is consistent with trends seen in other oceanic and hemipelagic sediments (Pederson and Price, 1980).

For most of stage 6 (core CD1730) I/C.org ratios range between 100-150 x 10^{-4} while the same stage in core CD1715 shows a I/C.org ratio of <100 x 10^{-4}. This contrast in I/C.org ratio in two cores may be due to the presence of coarse turbidite bands in cores CD1715. These sandy sediments are impoverished in organic matter which may be degraded, and may therefore show anomalous trends in the I/C.org ratio. The decrease in I/C.org ratio in stages 2 and 4 may be explained by the low production of organic matter in these stages. This study suggests that iodine is enriched in oxic sediments underlying areas of high primary productivity like other elements such as Ba, Biog. Si. I/C.org ratios and I in interglacial stages are higher and may represent an environment of greater uptake of I at the sediment/water interface, under more oxidising environments.

The average I/C.org ratio in core CD1738 is relatively high ~132 x 10^{-4} (Table 8.2) especially in a section comprising the last 100,000 years (Fig. 8.6b). In this younger section of core CD1738 and also in CD1739, the I/C.org ratios are >150 x 10^{-4} and may be related to the high accumulation rates. This may result in a greater uptake and better preservation of I during burial diagenesis.

The ratios of Br/C.org also increases in cores CD1715 to CD1738 (Figs 8.7a,b) (Table 8.2). In core CD1715 the mean Br/C.org ratio is 36 x 10^{-4} and progressively increases through cores CD1730, CD1739 (~65 x 10^{-4}) to core CD1738 (78 x 10^{-4}). The similarity in pattern of I and Br with respect to organic carbon illustrates their close association. The trends in the Br/C.org ratio, at depth (at least for the upper 150 kys) in cores CD1730 and CD1715 are very similar showing low ratios at the lower horizons of stage 5. Interglacial stages (i.e. 3,5 and 7) tend to show higher values than glacial stages (Figs 8.7a,b). The Br/C.org profiles for cores CD1738 and CD1739 do not show similar trends except in Stage 3 (Fig. 8 7b). Here the Br/C.org ratios are the highest in its upper part, whereas in lower parts the profiles show a decrease in ratio.

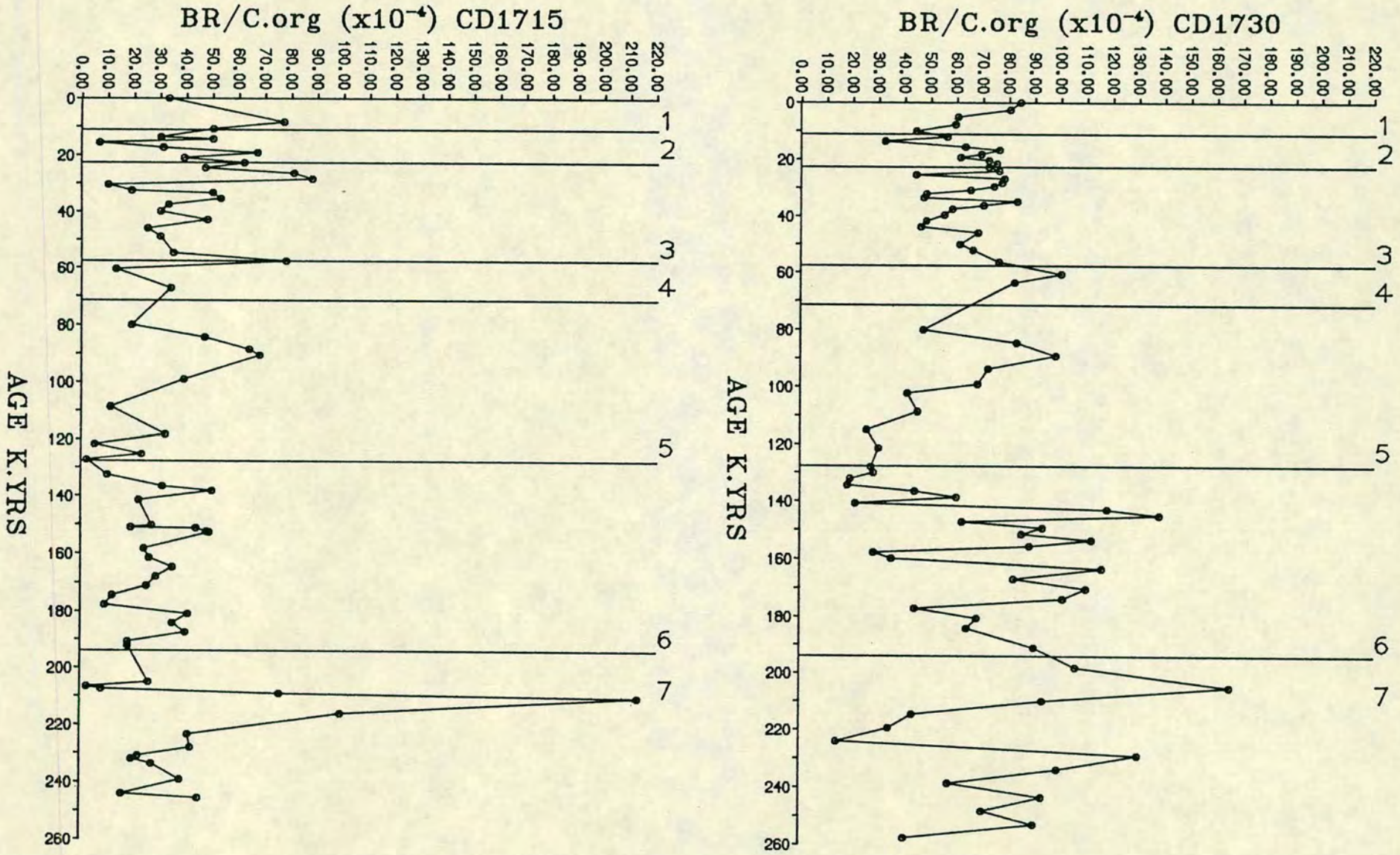

FIGURE 8.7a Br/C.org RATIOS IN CORES CD1715 AND CD1730.

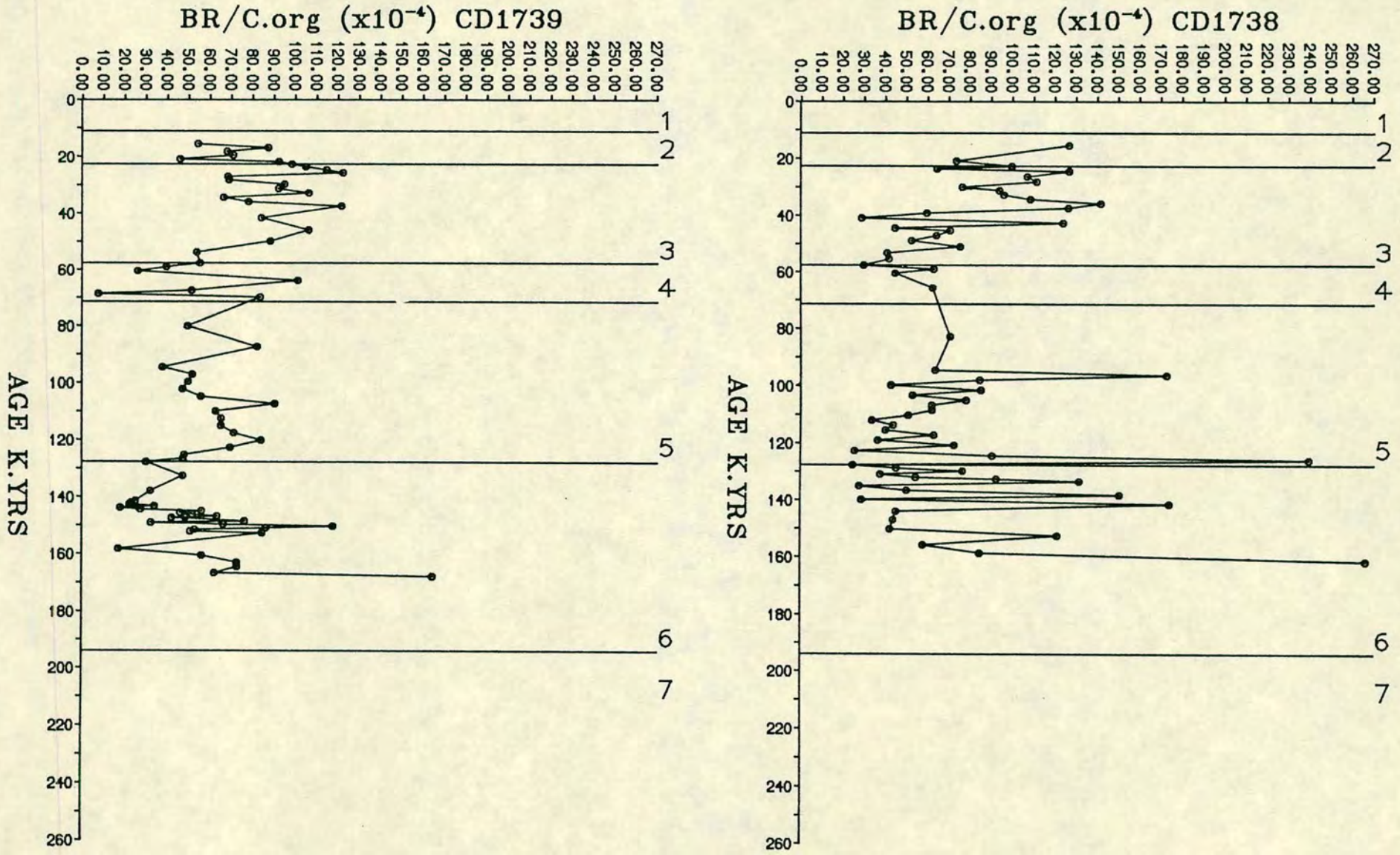

FIGURE 8.7b Br/C.org RATIOS IN CORES CD1739 AND CD1738.

The relative changes of Br/C.org and I/C.org ratios at depth are small, suggesting only small differences in geochemical behaviour during burial. The I/Br ratio shown in Figures 8.5a,b is essentially constant down the cores, except for the surface sediments. This may possibly suggest a similar mechanism for the uptake and removal observed in other oceanic sediments (Pederson and Price, 1980). Iodine enrichment has been ascribed to redox-controlled sorption of iodine by seston at the sediment/water interface, a mechanism similar to that of macroalgae described by Shaw (1959). Price and Calvert (1977) argued that the enrichment of bromine may also occur by an analogous mechanism. In contrast Mayer et al (1981) have postulated that bromine is concentrated by residual enrichment. In the present case, Mayer et al's (1981) postulation does not hold true as greater diagenetic loss of organic carbon occurs in Holocene (Chapter 6, Fig. 6.3) and the trends of I/C.org and Br/C.org are similar (Figs 8.6 and 8.7).

The isotopic values of $\delta^{13}C$ and $\delta^{15}N$ in addition to C/N ratio analysed for core CD1730 (Chapter 7) clearly indicate that organic matter in Arabian Sea sediments is predominantly marine in origin. Mayer et al (1981) suggested that Br/C.org ratio in some estuarine sediments is controlled by the input of different types of organic material with different bromine contents. Therefore the Br/C.org ratio may be used to indicate the source of the organic matter. Furthermore, in some Gulf of Maine estuarine sediments the Br contents have been shown to be related to marine primary production (Mayer et al, 1981). Similarly, in the surface sediments of Loch Etive a direct relationship between iodine, bromine and the marine organic component has been recorded (Malcolm and Price, 1984). The Br/C.org ratio in the northwestern Arabian Sea sediments is 40-80 x 10^{-4} (Table 8.2). These values are lower than Loch Etive estuarine surface sediments (i.e. 180 x 10^{-4}) and deep sea sediments of Barents Sea (120 x 10^{-4}), Panama Basin (146 x 10^{-4}). However, they are similar to the Br/C.org ratio of 60 x 10^{-4} found on the Namibian Shelf (Price and Calvert, 1977) sediments which receive a very high input of organic material from marine primary production. Hence, it is possible that Br content in the northwestern Arabian Sea sediment indicates an exclusive link with primary production, which result in the linear relationship between Br and organic carbon (Fig. 8.2).

However, secular changes of Br/C.org ratios are not easily understood. The trends are dissimilar in cores CD1715 and CD1730 but show similarities in the northern cores, CD1738 and CD1739. This probably implies either different diagenetic behaviour upon burial, or association with different types of organic matter.

Table 8.3 I/C.org ratio of oxic and anoxic sediments

Area	Oxic Sediments $x10^{-4}$		Anoxic Sediments $x10^{-4}$		Reference
	I/C.org	Br/C.org	I/C.org	Br/C.org	
Black Sea	-	-	20	-	S E Calvert, 1987 (Unpublished data)
SW Africa Inner Shelf	-	-	20-30	50-60	Price & Calvert (1973)
Near Shore Peru	-	-	16.0	-	Pavlova & Shishkina (1973)
Gulf of California	230-280	-	-	-	Price & Calvert (1973)
SW Africa Outer Shelf	250	-	-	-	Price & Calvert (1973)
Barents Sea	380	120	-	-	Price et al (1970)
Panama Basin	395	146	-	-	Pederson & Price (1980)
NW Arabian Sea					
CD1709	-	-	25	45	Present Study
CD1715	75	36	-	-	Present Study
CD1730	110	67	-	-	Present Study
CD1739	109	63	-	-	Present Study
CD1738	132	78	-	-	Present Study

Table 8.4 Iodine/Carbon atom ratios of seawater, plankton and marine sediments

Reference	Sample	I/C ($x10^{-4}$)
Elderfield & Truesdale (1980)	Seawater	1.0
	Plankton	1.0-2.8
Spencer et al, 1978	Faecal pellets from sediment traps	1.6-3.1
Wong et al, 1976	Particulate Iodine	~1.0
	Oxidised Sediments	~25
Price and Calvert, 1977	Reduced Sediments	~1.5

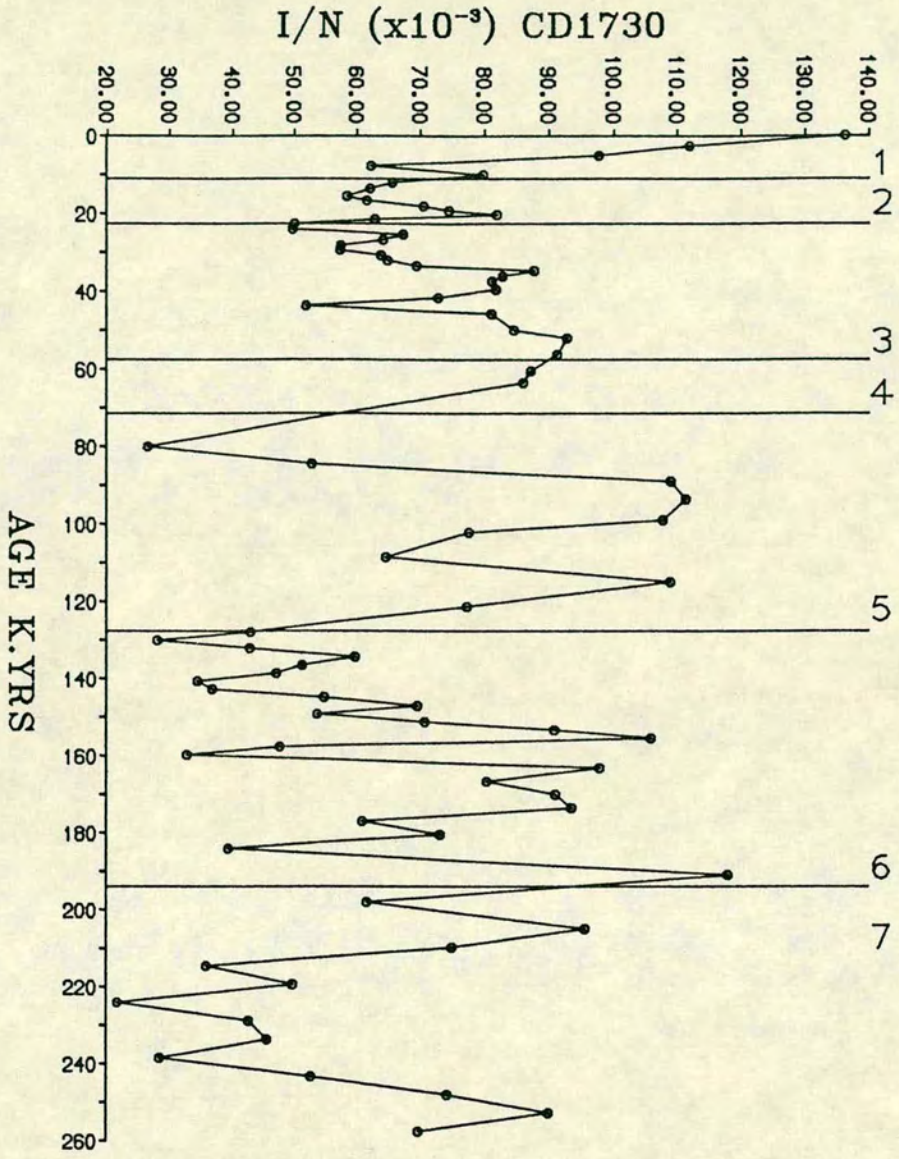

FIGURE 8.8 I/N PROFILE OF CORE CD1730.

In general, the I/C.org ratio in marine sediments has been used to indicate oxic and anoxic conditions (Table 8.3) (Price and Calvert, 1973). The I/C.org ratios in this study are found to be intermediate between those of oxic and anoxic sediment (Table 8.3). Similar values are reported from Pacific deep sea sediments (Table 8.1) (Pavlova and Shishkina, 1973; Pederson and Price, 1980; Wakefield, 1981). The I/C.org ratio (~100 x 10^{-4}) is higher than plankton I/C.org ratio, (i.e. ~20 x 10^{-4}) (Elderfield and Trusedale, 1980) and less than deep sea sediments of oxidising environments (Table 8.3).

Price and Calvert (1977) suggested that under an oxidising environment significant uptake of I occurs at the sediment/water interface by plankton seston, which subsequently accounts for the high I/C.org ratio. Much of this iodine is lost with burial diagenesis. Therefore, the vertical decrease in iodine within the sediments is reflected in the increase in pore water iodine concentrations (Shishkin and Pavlova, 1965). A rapid decrease in I/C.org ratio is seen in Holocene (stage 1) and is probably due to diagenetic effects. The I/C.org ratios shown in Figures 8.6a,b generally show different values in glacial and interglacial stages, similar to that of organic carbon (Fig. 6.3) the value of I/C.org ratio tends to decrease in glacial stages. It has been recorded earlier that I in sea water is biophilic in nature (Vinogradov, 1953; Goldschmidt, 1954). In oceanic water its' coupling with nutrients has also been noted by Elderfield and Trusedale (1980). In table 8.4, the consistent values of I/C.org ratios of various components like sea water, plankton, faecal pellets, pore water and particulate matter confirms that iodine is biophilic. Therefore, the high I content and I/C.org ratios in interglacial stages may imply increased biological productivity during warm periods. However, in stage 6 I/C.org ratio shows a contrasting trend, especially in core CD1730 (Fig.8.6a). Here the I/C.org ratio is high whereas in the same stage, in core CD1715 it is low. This difference is possibly a result of a different composition of the organic matter in two cores. Harvey (1980) noted that iodine shows a strong association with nitrogenous compounds. The total nitrogen and iodine profiles of core CD1730 (Figs 7.1 and 8.3) closely follow each other and therefore support Harvey's (1980) results. The relative variation of I and N is shown in Fig. 8.8, indicating a high value of I/N 100 x 10^{-4} in the middle of stage 6 (CD1730).

In summary, the geochemistry of iodine and bromine from Arabian Sea sediments, is largely consistent with other oceanic areas, where the sediments are depositing under oxidising conditions. However from the profiles, described in this section, it is apparent that the detail is insufficient to explain the geochemistry of Halogens.

CHAPTER 9

LITHOGENIC FLUXES

9.1 INTRODUCTION

Deep sea sediments contain a detailed record of the ocean's response to various climatic conditions. Such records may provide a relatively continuous history of climatic change over a long period. Generally, the elemental concentrations within the sediments, expressed as percentages of the dried samples, gives an idea of the relative proportions of constituent components. However, in order to obtain the effectiveness of the transporting media, and the controlling mechanisms for their distribution in the sediments before and after deposition, accumulation rates are of prime importance in order to study the sedimentary fluxes to the sea floor (Van Andel et al., 1975; Luz and Shackleton, 1975; Demaster, 1981; Boyle, 1983). Accumulation rates, expressed in units of weight per unit area and time are widely used in Paleoclimatology and Paleoceanography as a means of delineating variations in sedimentation and ocean productivity signals preserved in the deep-sea sedimentary records (Leinen and Heath, 1981; Rea and Harrsch, 1981; Rea and Janecek, 1982; Curry and Lohman, 1985). Accumulation rates are independent of dilution effects from other components and thus permit quantitative estimates of sedimentary budgets (Van Andel et al., 1975).

Arabian Sea sediments, as deciphered from the preceding discussion, comprise a two component system. These are terrigenous (lithogenic) and biogenic, the latter component largely consists of calcareous and siliceous skeletons. The western margin experiences seasonal upwelling due to the SW monsoon and has been shown to record a characteristic biological signal (Prell, 1984). The variation in the magnitude of these features, however, may have changed by the higher input of terrigenous material from the surrounding continents in a similar manner to the Atlantic Ocean. As a consequence, the study of the variation of either factor in the Arabian Sea is particularly dependent on the variation in lithogenic fluxes during the late Pleistocene.

Long-term changes in the monsoonal regime has been studied by both climatic modelling (Kutzbach, 1981; Kutzback and Guetter, 1986) and direct proxydata (Prell, 1984; Duplessy, 1982). Surface salinity patterns and sea surface temperature anomalies obtained from isotopic composition and faunal assemblage of planktonic foraminifera provided, the information about regional extent of monsoon regime and strength of wind induced upwelling (Prell and Hutson, 1979; Prell and Curry, 1981; Duplessy, 1982). Van Campo et al. (1982) and Van Campo (1986) used pollen to reconstruct the late quaternary vegetation history of East Africa and India. However, the dust input studies in the NW Arabian sediments has not yet been reported, particularly for late Pleistocene times.

Recently, Sirocko and Sarnthein (1988) studied the wind blown material in NW Arabian Sea sediments for the Holocene period. Several other studies have indicated the presence of aeolian material in the Arabian Sea sediments (Stewart et al., 1965; Olausson and Olsson, 1968; Goldberg and Griffin, 1969; Von-Stackelberg, 1972; Mattriat et al., 1973; Marching, 1974; Kolla and Biscay, 1977; Kolla et al., 1981a, b). These studies were of limited scope and mainly concentrated on the sedimentological provinces based on the mineral composition of surface sediments. Except for Sirocko and Sarnthein, (1988) all these studies are vague in delineating source areas, transport mechanisms and in estimation of relative contribution of source areas. Their detailed study of the Holocene period has clearly shown the significance of aeolian material in NW Arabian sediments, and controlling factors for its areal variation.

In this chapter, the focus of study will be the total flux and changes of different lithogenic fluxes during the last 250,000 years in the Arabian Sea. The variables which will be discussed in this chapter are aluminium, quartz, dolomite, zirconium and chromium. In chapter 5 it has been shown that these elements are detrital in nature, thus changes in their flux is anticipated to provide information regarding the efficiency of the transporting mechanism and the change in source areas through time. Moreover, the importance of climatic changes which regulate the fluxes changes, can be inferred. For quantitative description of oceanic processes in response to climatic change, an accurate time scale is necessary. A time scale developed for the investigated cores is based on correlation with the carbonate stratigraphy of a core RC-2761 provided by Prell (Brown University, USA). This core has also been dated by tuning the oxygen isotope signal recorded in the planktonic foraminifera with the SPECMAP stack (Imbrie et al., 1984). The chronostratigraphy of the examined cores is described in chapter 3 and it has been shown in Fig. 3.8 that there is reasonable age control in all four cores. It is more likely that cores CD 1739 and CD 1738 may have certain errors in dating, but overall the different isotopic stages in all cores are synchronous.

9.2 SEDIMENTATION RATES

Prior to calculating mass accumulation rates, in units of weight per unit area and time, linear deposition rates in units of thickness per unit time have been established. This was done assuming constant and continuous sedimentation between dated levels. Sedimentation rates are computed in cm/kys using both dated points and linear interpolation between these points. Since the dating of cores is not very

accurate, there is a limitation on the accuracy of the sedimentation rates reported here. Calculated sedimentation rates in cm/kys are listed in appendix C.14 and are plotted against age in Figs. 9.1a, b. Sedimentation rates for four cores shown in Fig. 9.1a, b display marked spatial and temporal variations. Average sedimentation rates in deep sea cores CD 1715 and CD 1730 is low ie. 3-5cm/1000 years while core CD 1739 and CD 1738 shows higher average sedimentation rates ~>5cm/kys. The highest sedimentation rates occur in core CD 1739 at up to 17cm/kys.

Trends of temporal variations is such that Holocene and interglacial stages tend to show low sedimentation rates, whereas even isotopic (cold) Stages 2, 4, 6 display increased sedimentation rates. Highest sedimentation rates, ie. 5-10cm/kys are seen in glacial Stage 2 in all four cores. Similarly interglacial Stage 3 in these cores also shows higher sedimentation rates, particularly in the upper part where it is almost of same magnitude as seen in Stage 2. Stage 4 is intermediate and Stage 6 displays sedimentation rates lower than Stage 2, ie. 3-4cm/kys in cores 1715 and CD 1730 while the same stage in core CD 1739 shows highest sedimentation rates ~17cm/kys. Sedimentation rates are lowest in interglacial Stages 5 and 7 (1-2cm/kys) in cores CD 1715 and CD 1730. Sedimentation rates up to 4cm/kys in Stage 7 of core CD 1715 are erroneous as a result of the turbidites mentioned in chapter 2.

9.3 BULK ACCUMULATION RATES

It is known that accumulation rates are an important factor for reconstructing Paleoclimatic and Paleoceanographic history from deep sea sediments record (Van Andel, 1975; Leinen and Heath, 1981; Rea and Harrsch, 1981; Rea and Janecek, 1982; Curry and Lohman, 1985; Sirocko and Sarnthein, 1988). Since mass accumulation rate is a product of sedimentation rate (cm/kys) and dry bulk density (g/cm^3) (Koczy, 1951; Van Andel et al., 1975), the calculation of accumulation rates require dry bulk densities for the sediments. Luz and Shackleton (1975), Lyle and Dymond (1976) and Clemens et al. (1987) have shown that the values of dry bulk densities (DBD) depend on the lithology and carbonate content of the sediments, and they derived an empirical relationship to calculate DBD from the carbonate content of sediments. The best method for DBD measurements however, is that of the water loss technique, which is more reliable if made on freshly collected cores. In the present case, dry bulk densities are obtained by measuring water content (method described in chapter 2), and dry bulk densities are calculated using the equation:

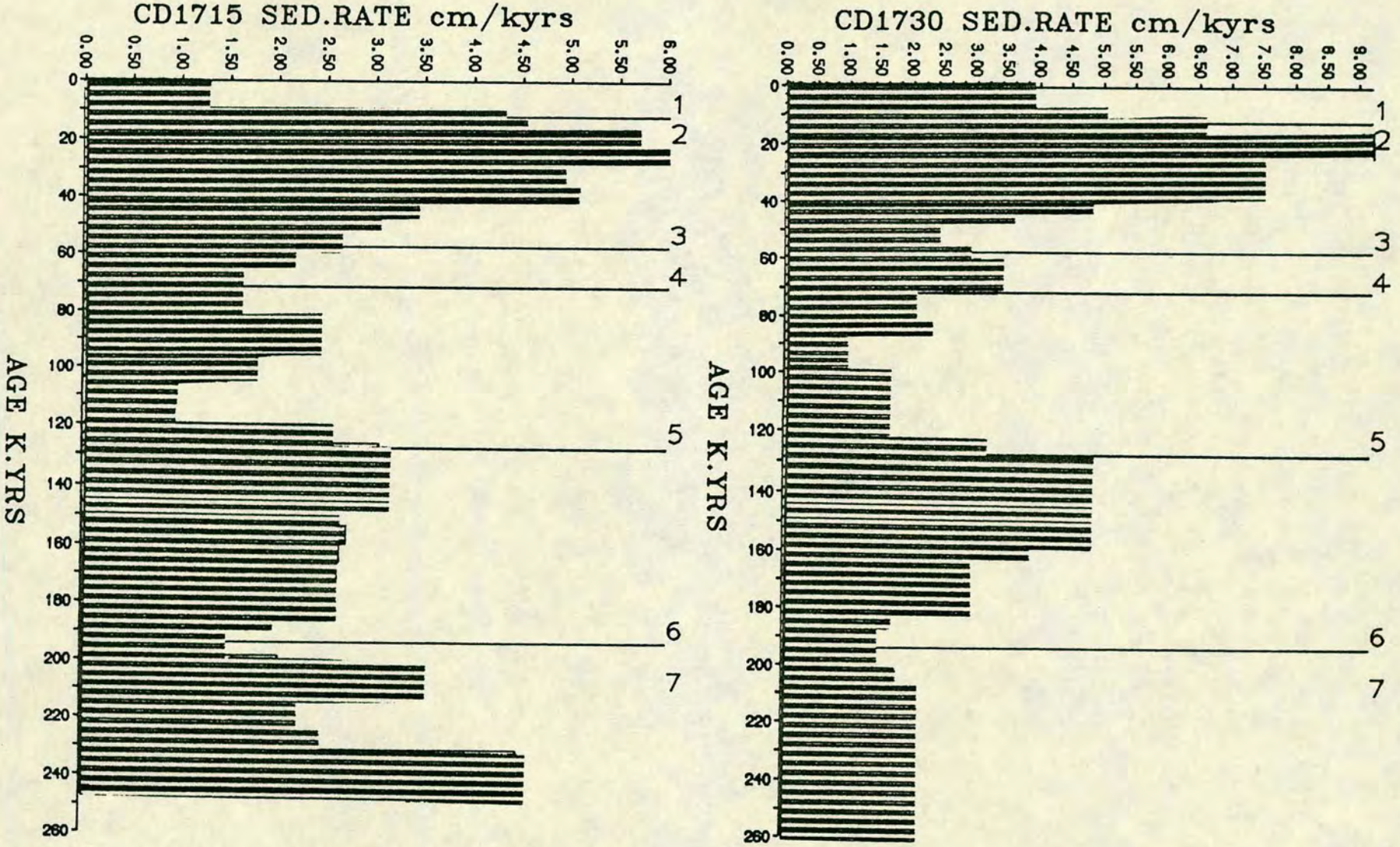

FIGURE 9.1a SEDIMENTATION RATES IN GLACIAL AND INTERGLACIAL STAGES OF CORES CD1715 AND CD1730.

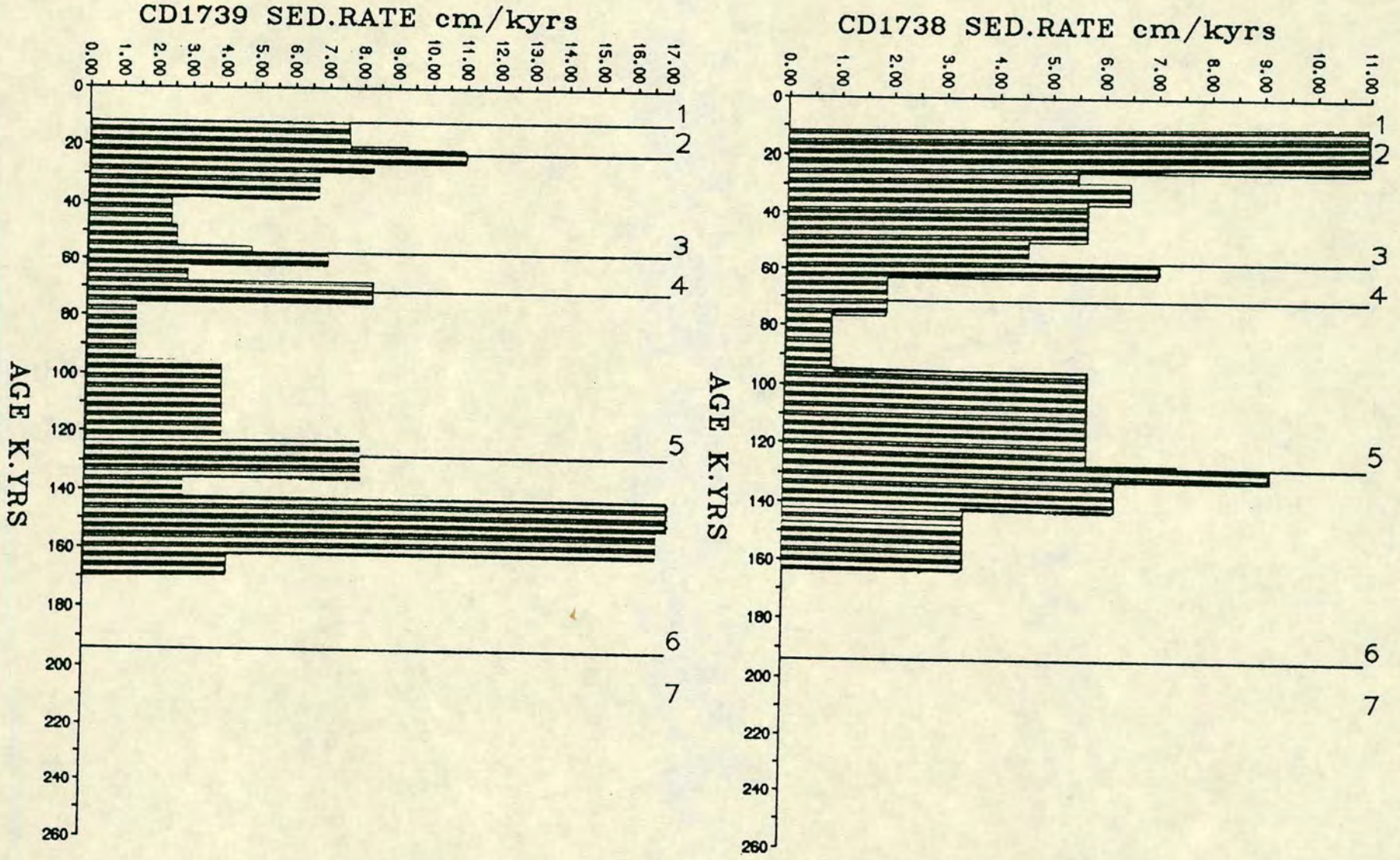

FIGURE 9.1b SEDIMENTATION RATES IN GLACIAL AND INTERGLACIAL STAGES OF CORES CD1739 AND CD1738.

$$DBD = \frac{Ms}{\frac{Ms}{ds} + \frac{Mw}{dw}}$$

Ms = dry sediment mass
Mw = water mass loss
ds = 2.7 gm/cm^3 (density of solids)
dw = 1.03 gm/cm^3 (density of water)

At the time of opening of cores very little dessication was noticed, thus it is assumed that dry bulk density data listed in appendix C.14 is satisfactory. This data was used in the calculation of bulk sediment accumulation rates and the fluxes of different components discussed in this and following chapter. The bulk accumulation rates are expressed in g/cm^2/kys, while the element accumulation rates are given in either g/cm^2/kys or mg/cm^2/kys. The flux data is presented in appendix C.15 and mass accumulation rates of each component in different cores is shown in Figs. 9.2a, b. The rates are calculated as follows.

M. acc = P.S.C
M. acc = Mass accumulation rates in g/cm^2/kys
P = dry bulk density in g-cm^3
S = sedimentation rates cm/kys
C = concentration of individual component in % or ppm.

Bulk accumulation rates as shown in Fig. 9.2 clearly suggests the patterns varying from south to north and changing over a period of 250,000 years. The bulk accumulation rates are gradually increasing from cores CD 1715 and CD 1730 (3-4 g/cm^2/kys) to cores CD 1739 and CD 1738 (>5g/cm^2/kys). The changing trend in bulk accumulation rates in different climatic stages is more significant in glacial Stages 2, 4 and 6 and shows higher bulk accumulation rates. Bulk accumulation rate during last glacial time Stage 2 is highest, ie. 5-7 g/cm^2/kys in cores CD 1715 and CD 1730, while in cores CD 1739 and CD 1738 it is higher than this value and reaches up to 13 g/cm^2/kys in core CD 1738. In Stage 6 bulk accumulation rates are lower than Stage 2, but still higher than glacial Stage 4. Interglacial Stages 5 and 7 show the lowest accumulation rates, ie. up to 2 g/cm^2/kys. Stage 3, however, shows higher trends, especially in the upper parts and bulk accumulation rates are 5-7 g/cm^2/kys.

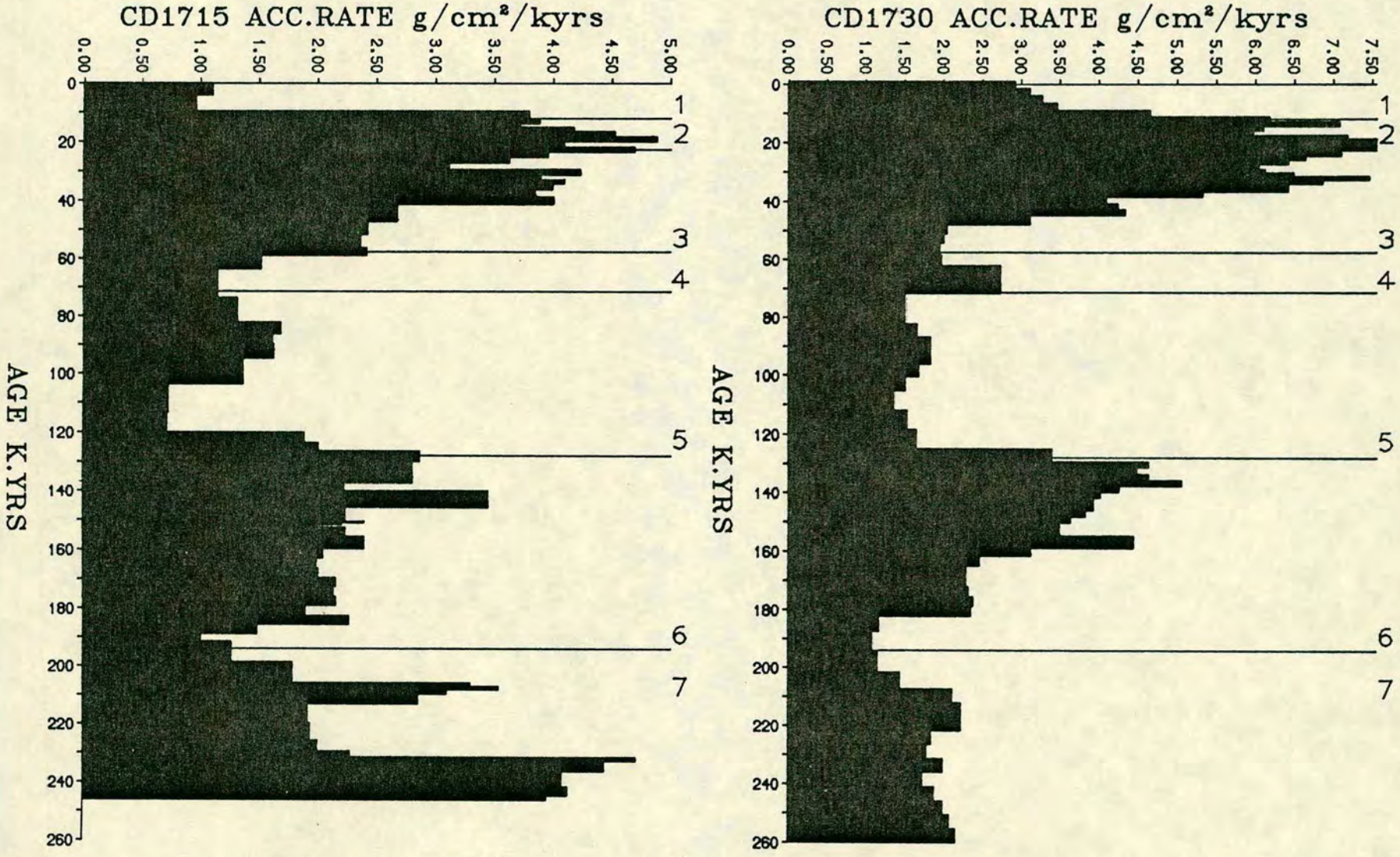

FIGURE 9.2a ACCUMULATION RATE PROFILES OF CORES CD1715 AND CD1730.

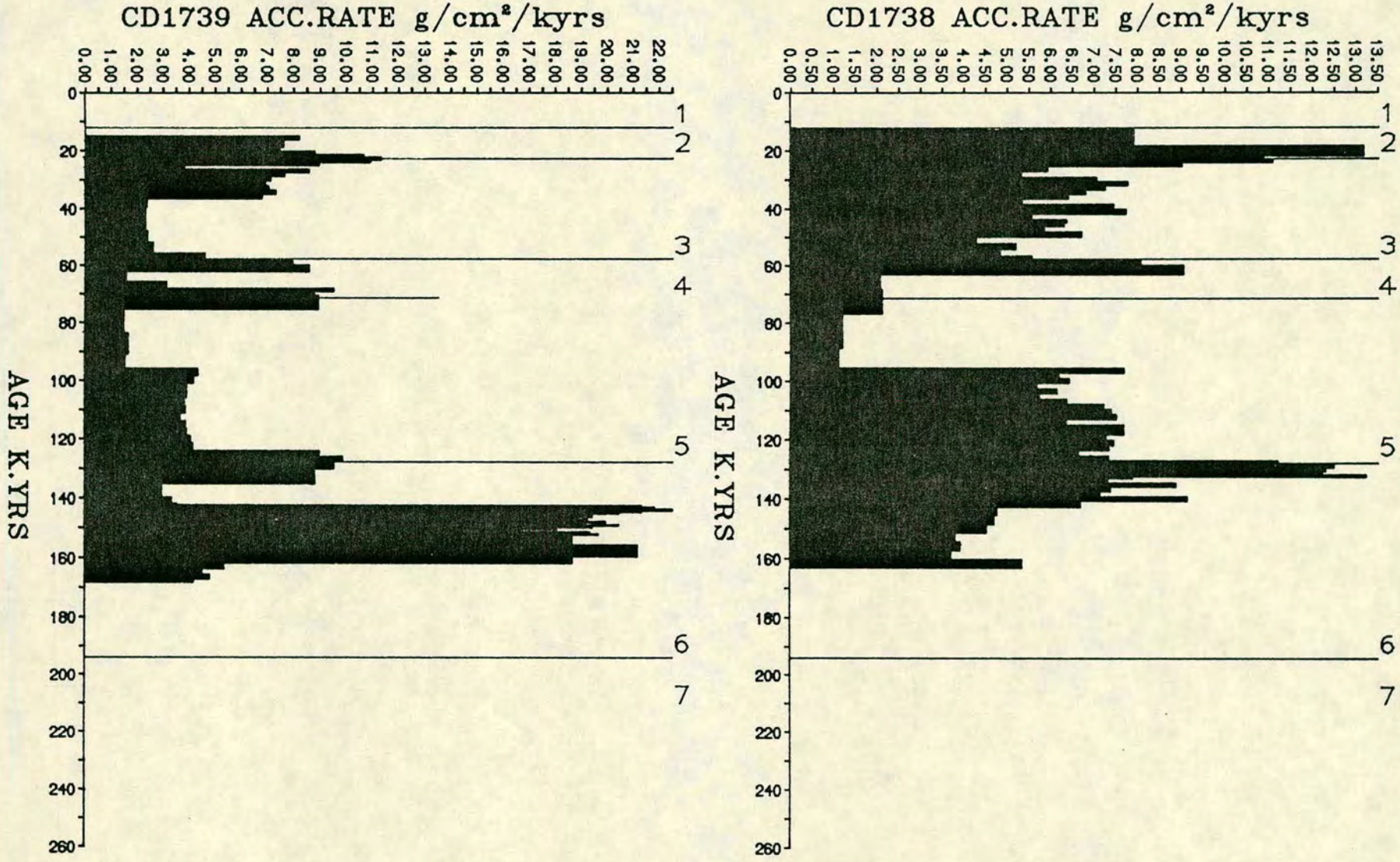

FIGURE 9.2b ACCUMULATION RATE PROFILES OF CORES CD1739 AND CD1738.

9.4 LITHOGENIC FLUXES

Key sediment components used as fluxes in this study are aluminium, quartz, dolomite, zirconium and titanium. The flux data is given in appendix C.15 and their variation with respect to time is discussed in the following section. In chapter 5 it has been shown that these components are largely derived from terrigenous sources and constitute the dominant portion of the sediment at the core sites. Since core locations are far from the influence of Indus River input, it is assumed that winds are of prime importance in transporting this material. Since the winds transport is generally controlled by the climatic patterns of source areas, the variation in detrital flux (core RC-2761) should broadly correlate with the oxygen isotope record of the same core (Fig. 9.3). This core (RC-2761) is close to the core CD 1715, and was collected from the Owen ridge (Long. 59°52′E, Lat. 16°38′N) by Prell, Brown University, USA. From unpublished results of carbonate, dry bulk density, and sedimentation rates, detrital fluxes are calculated and shown in Fig. 9.3. The oxygen isotope record shown in this Figure provides a record of the waxing and waning of ice sheets, and provide indirect information on global climate. A well marked correlation between the oxygen isotope record and detrital flux of core RC-2761 indicates higher fluxes during glacial stages, whilst low fluxes occur in the Holocene and intervening interglacial stages. A similar pattern of lithogenic fluxes of the other investigated cores show variation during cold and warm stages.

9.4:1 Aluminium Flux

Aluminium fluxes shown in Figs. 9.4a, b, clearly indicate high flux in glacial Stage 2, 4 and 6 while Holocene (Stage 1) and interglacial Stages 3, 5 and 7 are very low. It can also be seen from these figures and table 9.1 that the flux is changing as a factor of distance from source. The northern cores (CD 1739 and CD 1738) display large Al fluxes, averaging about 400-500 $mg/cm^2/kys$ whereas in cores CD 1715 and CD 1730 towards the south, the average flux is lower ranging from 80 to 150 $mg/cm^2/kys$ (Table 9.1).

Atmosphere fallout is the dominant source of aluminium to Arabian Sea sediments. In table 9.2 the atmospheric Al concentration in different marine regions are shown. It is apparent from this table that in the northern Arabian Sea, the average Al concentration in marine aerosol is 1.317 ng m^{-3} of air, which is among the highest recorded for the marine environment (Chester et al., 1985). The

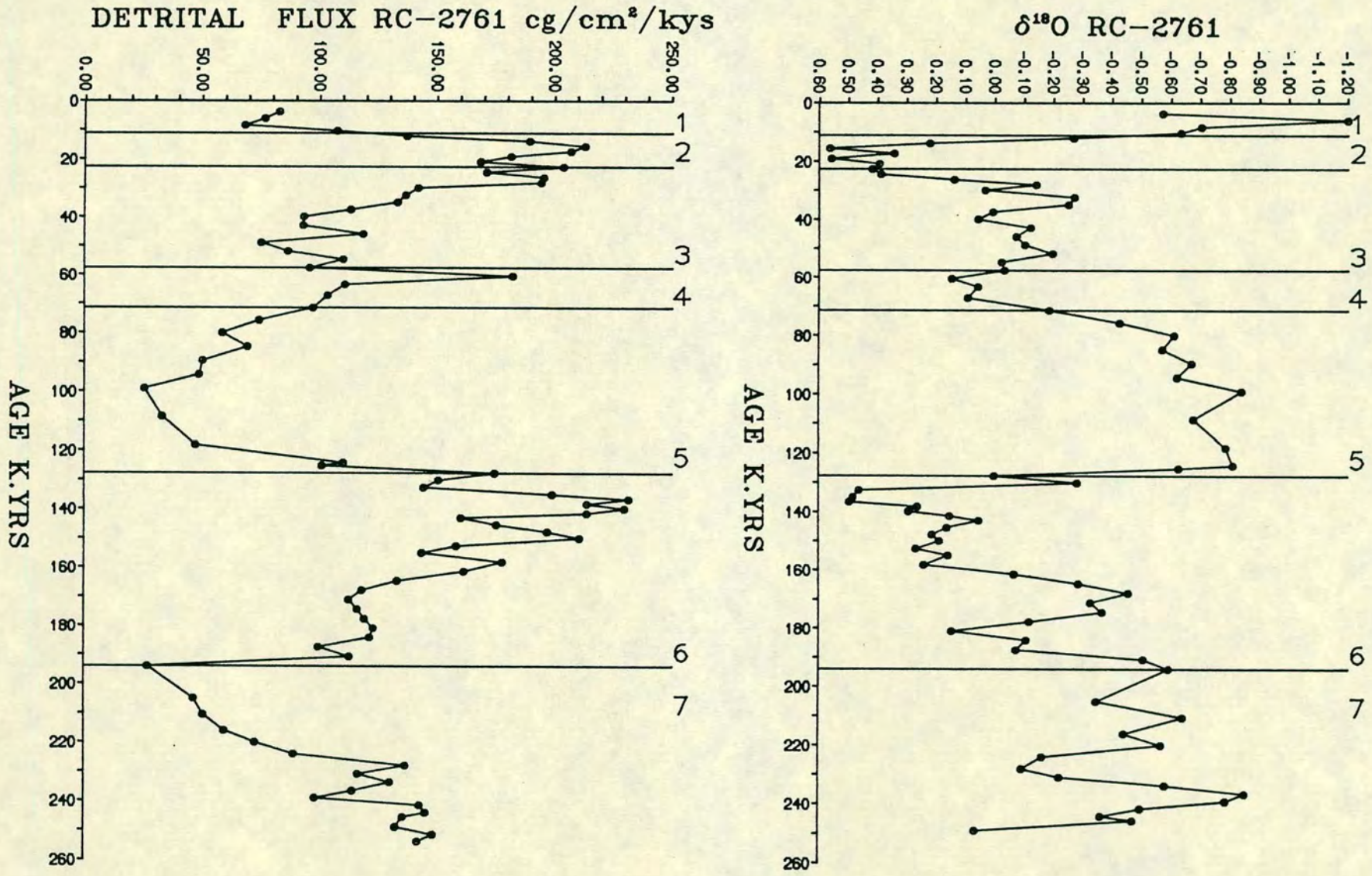

FIGURE 9.3 OXYGEN ISOTOPE RECORD AND DETRITAL FLUX (TOTAL FLUX - CALCITE FLUX) OF CORE RC-2761.

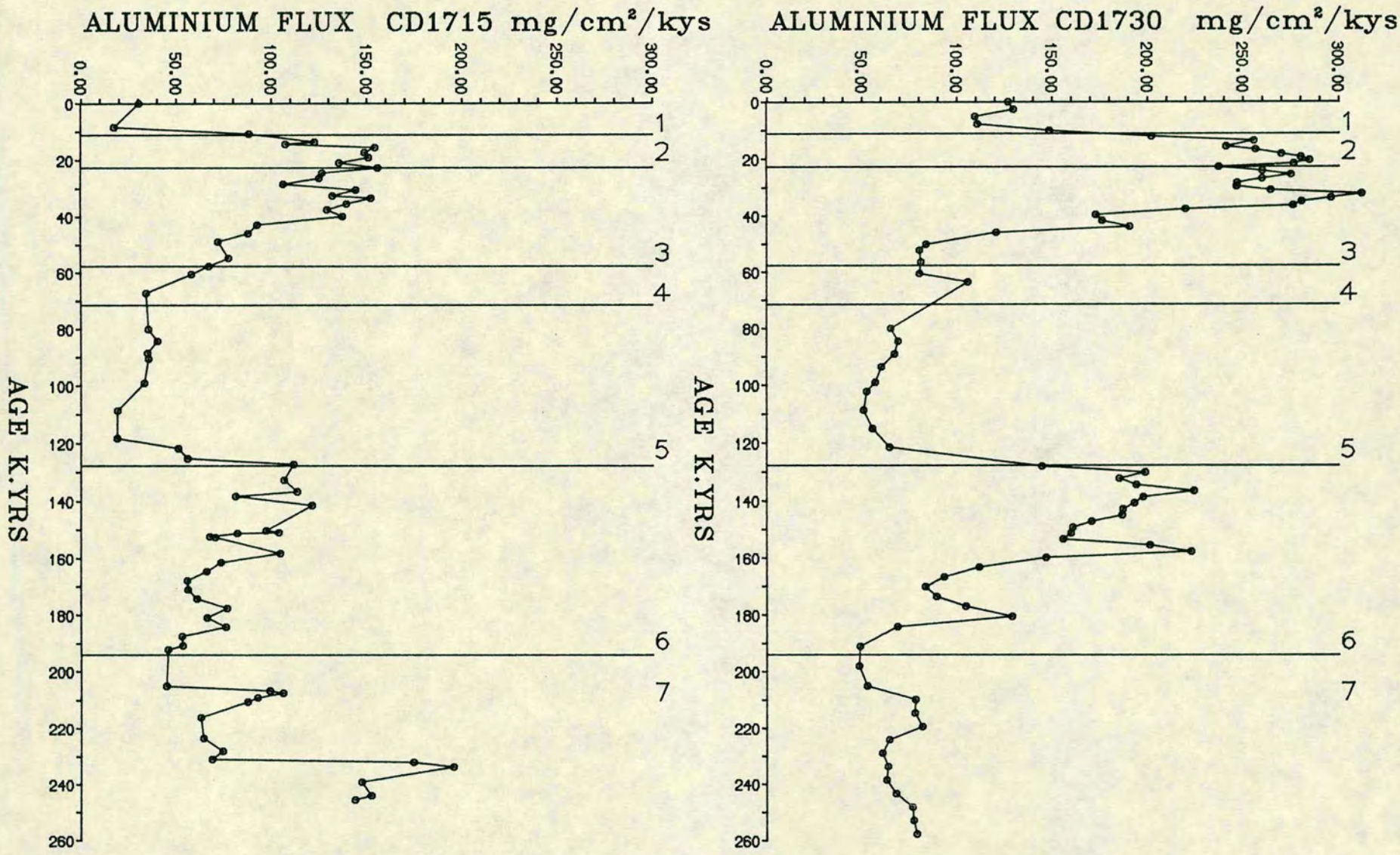

FIGURE 9.4a ALUMINIUM FLUX PROFILES. CORES CD1715 AND CD1730.

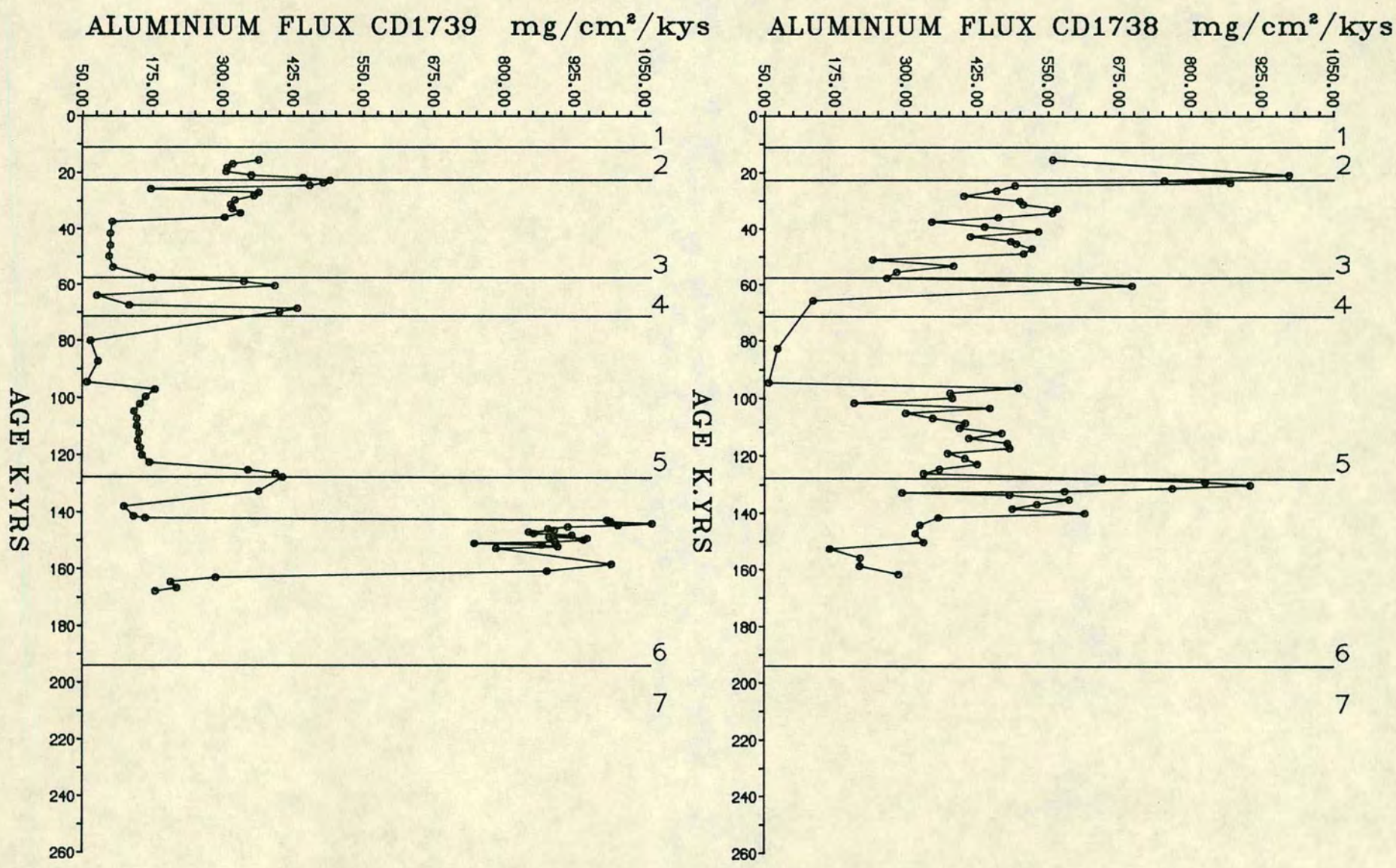

FIGURE 9.4b ALUMINIUM FLUX PROFILES. CORES CD1739 AND CD1738.

Table 9.1 **Minimum, maximum and mean values of lithogenic fluxes in glacial and interglacial Stages.**

CORES	FLUX	CD 1715		CD 1730		CD 1739		CD 1738	
	$mg/cm^2/kys$	Range	Mean	Range	Mean	Range	Mean	Range	Mean
	Quartz	35.5-148	87.2	61.9-160.7	94.4	-	-	-	-
	Aluminium	17.2-88.3	45.2	109-202	137.7	-	-	-	-
1	Dolomite	14.8-75.8	48.6	54-150	81.40	-	-	-	-
	Zirconium	0.047-0.23	0.13	0.22-0.48	0.33	-	-	-	-
	Titanium	461-14.40	7.99	5.74-11.43	7.93	-	-	-	-
	Quartz	125.1-233	171.5	160.7-329	284.60	394.5-650	480.8	449-871.9	646.1
	Aluminium	88.31-155	132.88	202-284	255.91	303.9-489	366.5	556-971	787.2
2	Dolomite	75.8-197	132.3	150.2-296	257.60	133-180	149.18	18.4-308	173.8
	Zirconium	0.23-0.41	0.34	0.49-0.73	0.66	0.88-1.45	1.08	1.15-1.95	1.56
	Titanium	13.58-48.82	29.67	11.43-17.14	15.22	15.71-26.55	21.17	30.81-54.0	42.62
	Quartz	55.2-383	172.0	88.4-373.7	253.2	121.7-650.9	354.5	183.3-764	345.5
	Aluminium	67.0-155	116.20	79.8-311	214.3	96.8-489	268.3	240.1-868	461.6
3	Dolomite	41.5-197	104.3	44.1-313	176.0	17.9-165	82.4	0.0-618	133.3
	Zirconium	0.18-0.40	0.30	0.21-0.78	0.56	0.28-1.45	0.79	0.51-1.84	0.972
	Titanium	14.87-42.68	32.79	4.94-19.84	13.23	6.10-27.28	16.04	13.70-45.43	26.17
	Quartz	79-98	88.90	70.2-115.75	89.85	103.6-554	358.6	135-697	299
	Aluminium	33-67	52.93	64.8-105.3	82.62	74.9-431.8	277.2	82.4-396	425
4	Dolomite	28-41	33.25	39.9-91.2	67.80	4.9-107.1	51.9	0.9-359	122.3
	Zirconium	0.09-0.18	0.133	0.17-0.29	0.225	0.16-1.28	0.56	0.27-1.31	0.90
	Titanium	6.38-23.86	12.64	4.20-6.5	5.26	4.02-26.86	15.62	7.45-38.87	24.69
	Quartz	25-156	73	41.5-177	75.50	64.6-648	256.1	53.9-1281	344.7
	Aluminium	18-111	42.5	50.46-144	68.32	57.5-405	191.4	56.4-644	362.4
5	Dolomite	8.8-57.2	26.42	20.26-95.2	46.63	1.3-344.6	77.1	38.9-491.9	262.9
	Zirconium	0.057-0.29	0.13	0.13-0.39	0.186	0.16-1.28	0.565	0.14-2.03	0.873
	Titanium	2.09-8.52	5.45	2.87-8.98	4.33	3.92-27.09	11.80	3.30-43.68	20.71
	Quartz	68.04-254	121.78	46-242	152.13	162.2-1437	903.2	223.5-1281	533.6
	Aluminium	45.36-121	79.04	48.6-224	152.1	123.6-1061	696.7	163.4-902.8	468.2
6	Dolomite	1.92-161	43.17	1.18-113.2	65.3	5.4-410	216.8	59.6-883	246.8
	Zirconium	0.10-0.34	0.19	0.11-0.58	0.386	0.36-3.14	1.96	0.50-2.03	1.12
	Titanium	4.24-16.25	10.01	2.91-13.99	9.24	7.79-63.37	45.77	10.26-50.43	27.24
	Quartz	68-265	136.9	266-96.75	71.19	-	-	-	-
	Aluminium	44-195	103.7	48.0-81.5	66.87	-	-	-	-
7	Dolomite	7.69-136	82.49	10.9-79.12	55.84	-	-	-	-
	Zirconium	0.10-0.48	0.25	0.10-0.22	0.16	-	-	-	-
	Titanium	4.90-17.44	9.01	2.74-5.24	4.07	-	-	-	-
	Average								
	Quartz	25.28-383	130.10	26.6-373	160.8	64.6-1437	550.1	53.9-1281	402.9
	Aluminium	17.18-195.3	89.59	48-311.8	150.31	57.5-1061	422.3	56.4-971.9	446.9
	Dolomite	1.92-196	69.55	1.18-313	107.93	13-410.4	133.5	0.0-883.1	208.9
	Zirconium	0.047-0.48	0.228	0.10-0.78	0.38	0.16-3.14	1.21	0.14-2.03	1.00
	Titanium	2.09-48.84	15.65	2.74-19.84	9.15	3.92-68.37	26.89	3.30-54.00	25.42

Table 9.2 Atmospheric Al concentrations in different oceanic areas.

AREA	Atmospheric Al Concentration (ngm^{-3} of air)		
	Range	Mean	Reference
Eastern Atlantic			
Westerlies	30-160	60	Chester et al. (1984)
NE Atlantic Trades	58-$\geq$ 50,000	3,168	
Open Ocean Atlantic			
SE Trades	3.8-498	28	Chester et al. (1984)
Westerlies	1.5-5.4	2.6	
Mediterranean Sea	60-1,602	332	Sanders (1983)
Red Sea	416-2,236	1,243	Sanders (1983)
Northern Arabian Sea	323-20,300	1,317	Chester et al. (1985)

aluminium flux recorded in sediments of the core CD 1738 taken from Gulf of Oman confirms Chester et al. (1985) findings. Since the Al flux indicates the importance of aeolian transport of crustal material in the sediments, its fluctuation through various climatic stages may be the result of changing wind intensity, aridity and general atmospheric circulation.

Mean flux and maximum and minimum ranges in Al values for each Stage are given in Table 9.1. The highest Al flux occurs in glacial Stage 2 (20,000-11,000 years BP). The values of Al flux for other glacial Stages (ie. 4 and 6) are relatively low (Table 9.1), the lowest being found in glacial Stage 4. Pronounced changes occur in the Holocene and interglacial Stage 5 and 7. In the latter two stages the magnitude of decrease is almost the same, showing Al flux 50-60 $mg/cm^2/kys$ in cores CD 1715 and CD 1730. However, in Stage 3, the Al flux for the early 10,000 years (60,000-50,000 years BP) is low, whilst progressive increase in flux is noted in younger sediments. Prior to reaching maximum values in Stage 2, a sudden decrease in aluminium flux between ~40,000-20,000 years BP can be seen in all cores. This period corresponds to high lake levels in East Africa (Kutzbach and Street, 1985; Foucault and Stanley, 1989) and thus low Al flux possibly indicates the wetter climate of the adjacent continents. This is further supported by a similar change observed in other lithogenic fluxes as discussed later.

9.4:2 Quartz Flux

Quartz is common in the marine aerosol transported by wind (Prospero and Bonatti, 1969; Prospero and Carlson, 1972; Blank et al., 1985). It has been shown that the quartz content in sediments accumulating beneath aerosol deposition is highly consistent with that of the composition of the aerosol (Blank et al., 1985). The variation of quartz with respect to other clay minerals (Bowles, 1975) and quartz accumulation rates (Theide et al., 1982) have been employed to deduce past climate. In the Arabian Sea, Kolla and Biscay (1977) were the first to show that climate has an important bearing on the distribution of quartz. Recently, in their Holocene studies of Arabian Sea sediments, Sirocko and Sarnthein, (1988) have arrived at the same conclusion. In the present study of four cores, a longer time record (~250,000 years) of quartz abundance in Arabian Sea sediment is discussed.

In order to study the quartz flux, the quartz content in this thesis is calculated from the chemistry of Si analysed by XRF. Since core CD 1715 and CD 1730 are shown to contain 1-2% biogenic silica (chapter 5), the following relationship is used for calculating the quartz content:

Quartz(Si) % = T.Si-(Si x Si/Al) - Biog. Silica

Si/Al = 2.5 (Assumed composition of aluminosilicates detritus).

In cores CD 1739 and CD 1738 a slightly different relationship was applied because these cores appear to have insignificant biogenic silica.

Quartz(Si) % = T.Si-(Si x Si/Al)

Quartz fluxes (expressed as Si) in the cores from NW Arabian Sea are presented in appendix C.15 and their oscillations are shown in Figs. 9.5a, b. Quartz fluxes show a similar distribution, both areally and temporally to aluminium. The quartz flux increases progressively from core CD 1715 to core CD 1738. Average flux in core CD 1715 is very low, ie. 130.00 mg/cm^2/kys while in north cores CD 1739 and CD 1738 show four fold increase (Table 9.1). Similar changes occur from one to another core in glacial and interglacial events (Table 9.1). Overall, the glacial events in all cores tend to show high quartz flux while in interglacial stages the flux tends to be low. The highest quartz flux seen in glacial stages occurs in Stage 2 and is 170 and 300 mg/cm^2/kys in core CD 1715 and CD 1730 respectively (Fig. 9.5a). Further north in cores CD 1739 and CD 1738 the data show the flux to be twice as high (Fig. 9.5b). In other glacial Stages (4, 6) the quartz flux is generally low and is broadly the same for all cores during Stage 4 (Figs. 9.5a, b) (Table 9.1). On the other hand the Holocene and other interglacial stages, as expected, show relatively low quartz flux compared to glacial stages. Except for the interglacial Stage 3, the other two warm Stages, ie. 5 and 7, in cores CD 1715 and CD 1730 display invariable quartz flux of about 75.0 mg/cm^2/kys. The most significant trend seen in all cores is such that flux of quartz exhibits a steady increase toward younger interglacial and younger glacial stages. The northern cores show a dramatic increase in flux during Stage 6.

It is known that fluctuation of quartz content and quartz flux in marine sediments reflects the climatic patterns of the surrounding areas (Bowles, 1975; Theide et al., 1982). Likewise, the changes in the quartz flux observed in different climatic stages recognised in this study are most likely reflecting the climatic condition prevailing at those times. In later sections of this chapter this subject will be discussed in more detail.

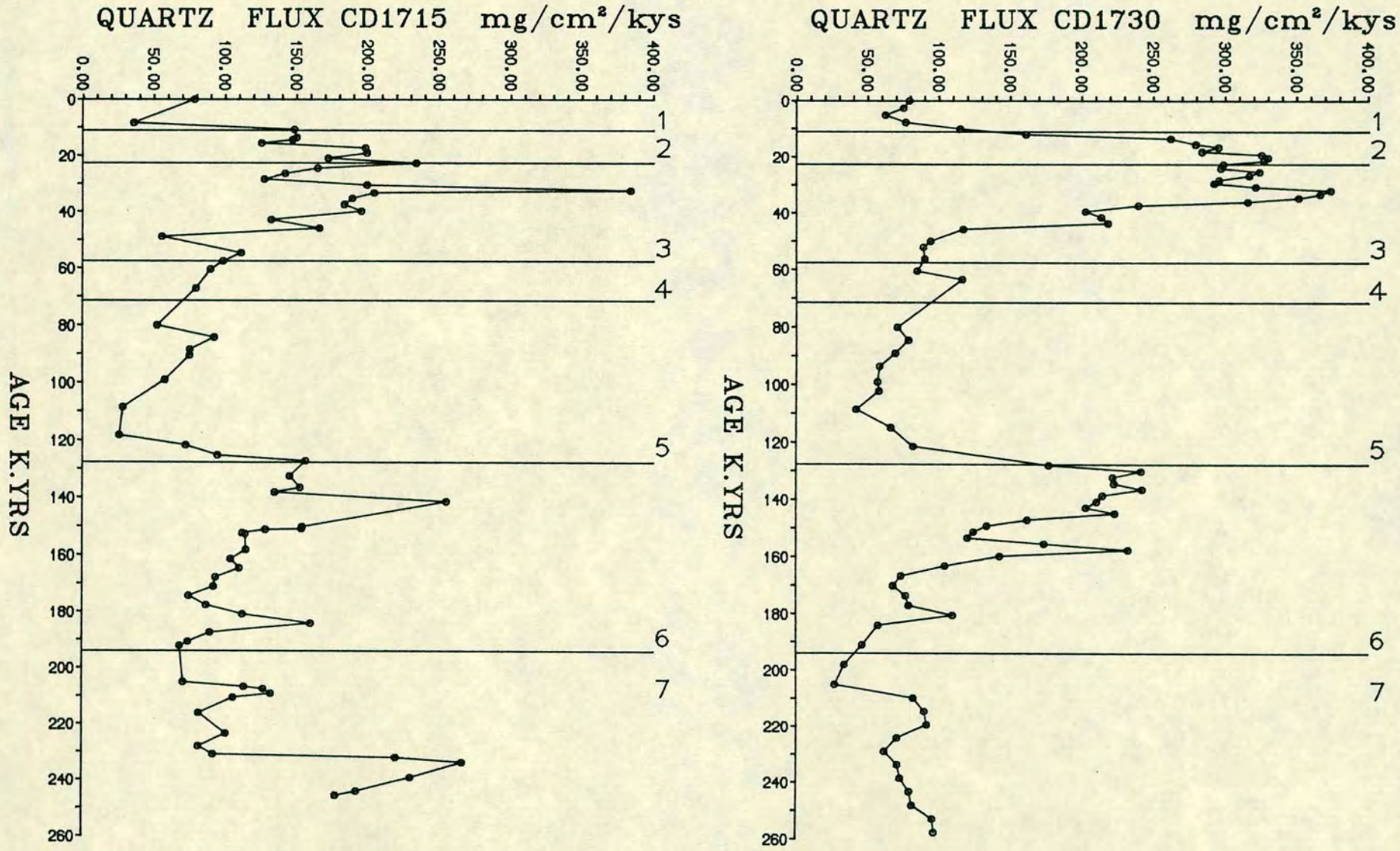

FIGURE 9.5a QUARTZ FLUX VARIATIONS DURING GLACIAL AND INTERGLACIAL STAGES OF CORES CD1715 AND CD1730.

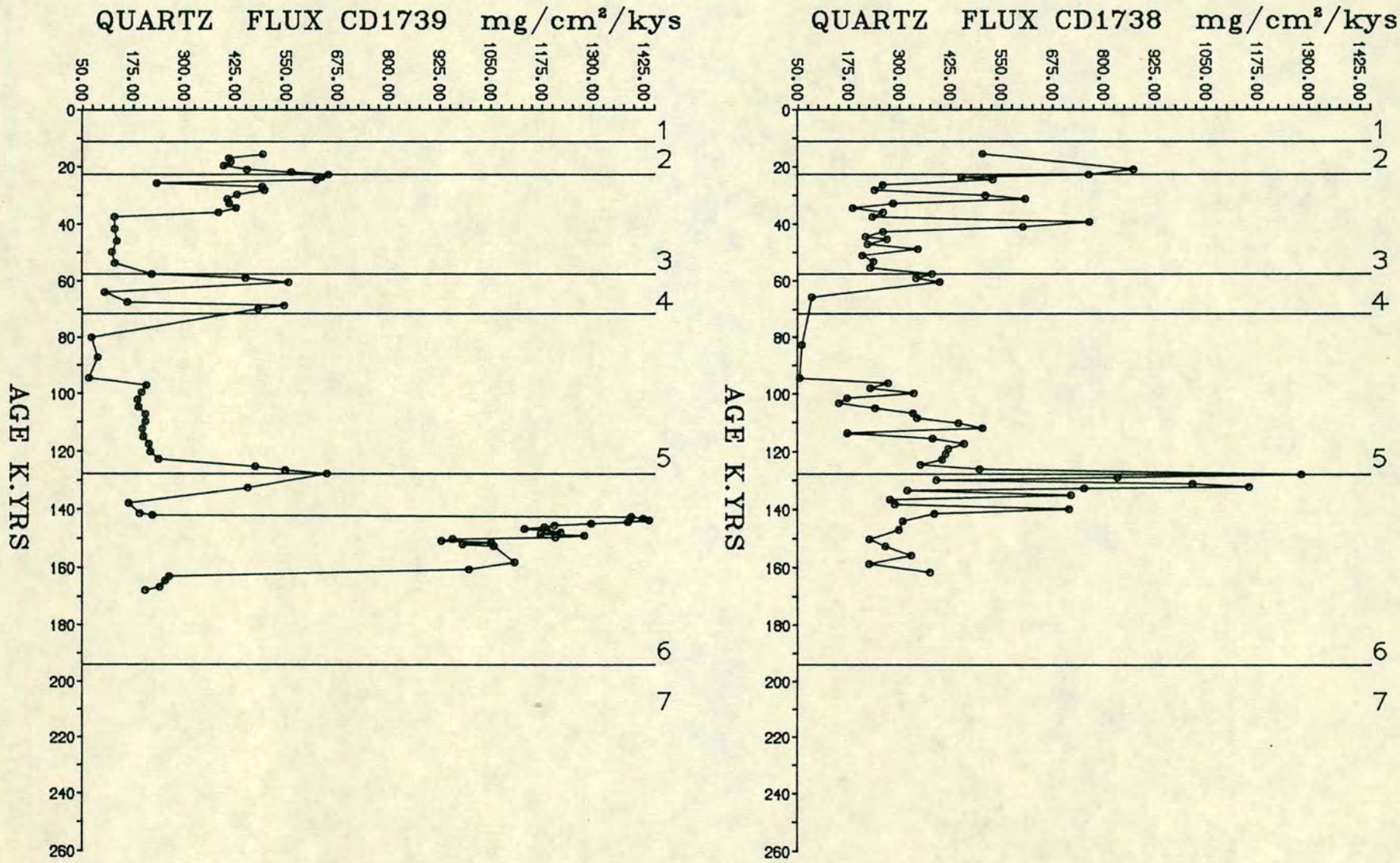

FIGURE 9.5b QUARTZ FLUX VARIATIONS DURING GLACIAL AND INTERGLACIAL STAGES OF CORES CD1739 AND CD1738.

9.4:3 Dolomite Flux

A number of studies (Stewart et al., 1965; Stoffers and Ross, 1979; Sirocko and Sarnthein, 1988) show that silt-size dolomite, along with quartz and clay minerals, occurs in Arabian Sea sediments in substantial quantities. In this area dust samples have been shown to contain significant dolomite (Stoffers and Ross, 1979). Sirocko and Sarnthein (1988) documented the accumulation rates of dolomite and outlined the transport direction from the Oman coast to the south.

In all the cores, subhedral rhombs of dolomite are recognised (SEM) (plate 2a). The dolomite content in the sediments has been calculated (Appendix B.3) from XRF data, and calculated as a flux. The quantitative flux estimates of dolomite reported by this procedure can show sizeable errors, particularly in cores CD 1739 and CD 1738 because of enrichment of chlorite, and thus may contribute significant erroneous Mg not allowed for in the assumptions given in appendix B.3, during the calculation of dolomite from the chemical analysis of the sediments. Nevertheless, the dolomite flux in all cores is remarkably similar to other lithogenic fluxes throughout the investigated time (Figs. 9.6a, b) period.

The distribution of dolomite flux both areally and temporally follows the Al and quartz flux (Figs. 9.4 and 9.5) and profiles show a trend of increases from core CD 1715 to core CD 1738. The highest dolomite occurs in core CD 1738; the average flux in this core is about four times higher than that of core CD 1715 (Table 9.1). Generally, the average dolomite flux in core CD 1715 and CD 1730 is ~50 $mg/cm^2/kys$. The very high dolomite flux in cores CD 1738 and CD 1739 > 200 $mg/cm^2/kys$, probably indicate a closeness of source. However, sporadic occurrence of very high dolomite fluxes such as 400, 500 or 800 $mg/cm^2/kys$ as seen in CD 1738 may suggest larger dust storms in this area. Fluctuation in dolomite fluxes observed in glacial and interglacial stage is similar to that of Al and quartz. Highest flux occurs in glacial Stage 2, ie. 18,000 years BP while previous glacial stages are generally low in dolomite flux (Table 9.1). In interglacial stages, flux decreases almost by a factor of 2 to 3 from the neighbouring glacial periods. Holocene and interglacial Stage 7 are extremely low showing dolomite flux (<50.0 $mg/cm^2/kys$) while Stage 3 is an exception indicating ~200 $mg/cm^2/kys$.

The overall trends seen in the oscillation of aluminium, quartz and dolomite are consistent, but a marked minima in dolomite occurred around 180,000 years BP and 120,000 years BP in cores CD 1715 and CD 1730. In cores CD 1739 and CD 1738 the trend of dolomite flux in the upper section comprising last 100,000 years is different from what is seen in other cores, and may be an artifact in the calculation

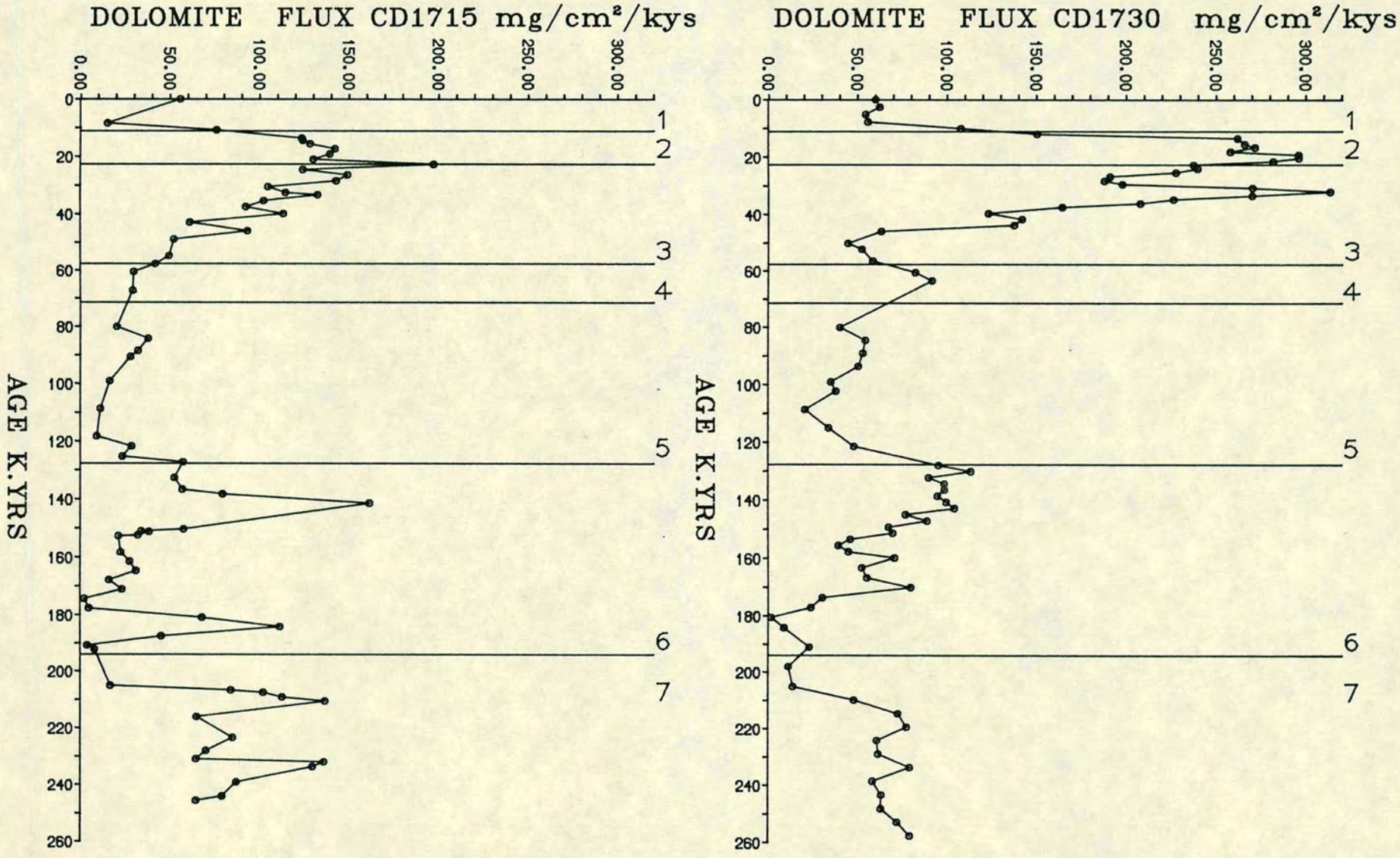

FIGURE 9.6a DOLOMITE FLUX PROFILES. CORES CD1715 AND CD1730.

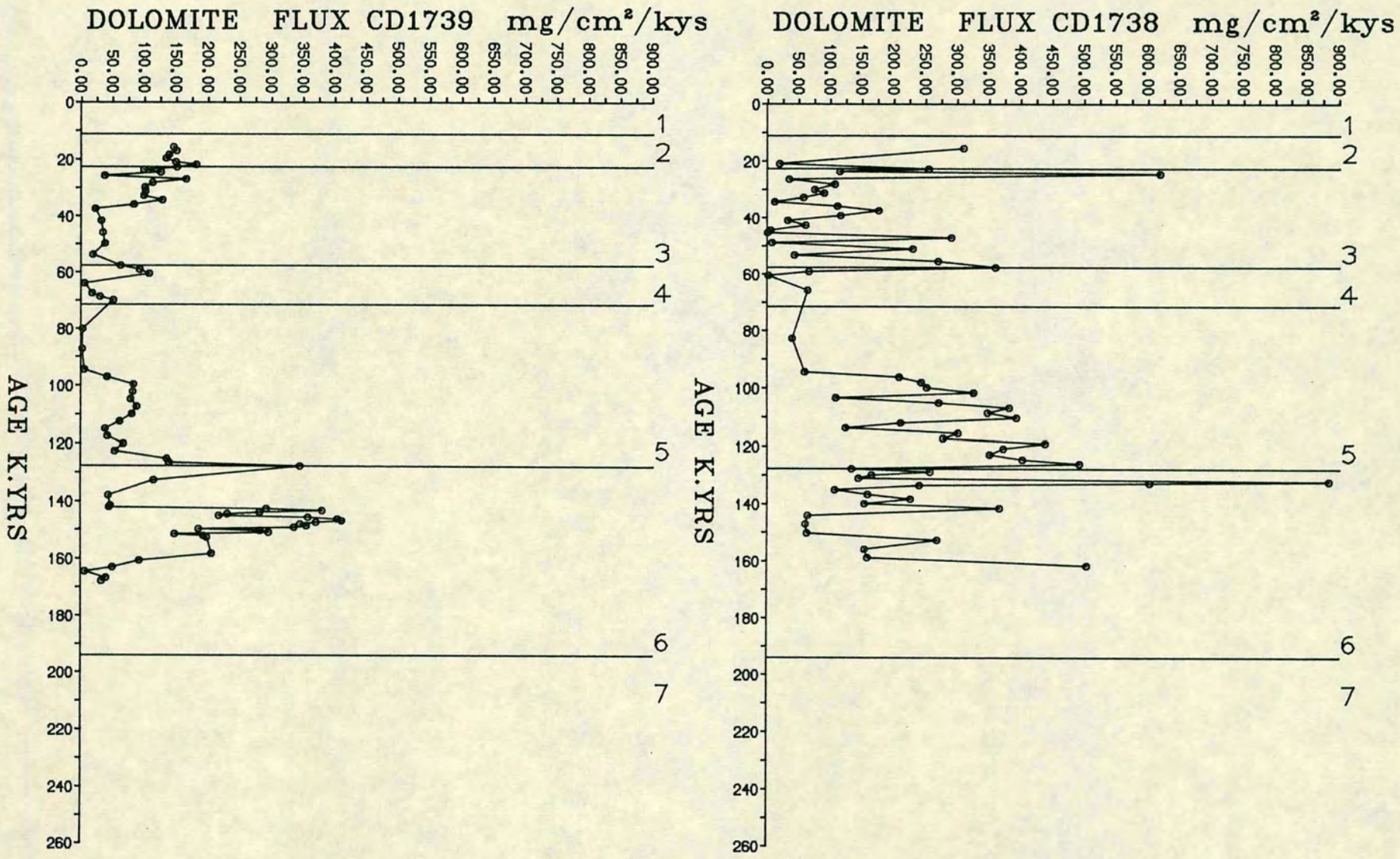

FIGURE 9.6b DOLOMITE FLUX PROFILES. CORES CD1739 AND CD1738.

of dolomite content. Even so, quartz flux also shows some similarity to dolomite over this time period and hence these trends may be the result of a local factor, such as the influence of the Persian Gulf.

9.4:4 Zirconium Flux

Zirconium flux variations shown in Figs. 9.7a, b are found to be closely associated with other lithogenic fluxes discussed earlier. The similarity in zirconium flux profiles to those of aluminium, quartz and dolomite suggest that all are exclusively controlled by the dust transport of northwesterly winds. Further, mean maximum and minimum flux values for Zr given in table 9.1 for glacial and interglacial stages show significant differences. Mean values of Zr flux increases from 0.23 mg/cm^2/kys in core CD 1715, to 0.38 mg/cm^2/kys in core CD 1730 and reaches ~1.00 mg/cm^2/kys in cores CD 1739 and CD 1738.

Regular changes in flux down cores is consistent with other lithogenic fluxes. Holocene and interglacial stages are generally 3 to 4 times lower in Zr flux compared to glacial stages. The highest flux is observed in glacial Stage 2, cores CD 1738 and CD 1739 shows about five fold increase compared to that calculated in the preceding interglacial Stage, ie. 3. However, in cores CD 1715, CD 1730, Zr flux increases in Stage 2 and Stage 3 are almost of the same magnitude, showing about 0.5-0.7 mg/cm^2/kys in last glacial stage in respective cores. cores CD 1739 and CD 1738 in last glacial stage indicate a Zr flux about 1.50 mg/cm^2/kys, which is about the same order of magnitude increase over that of Stage 2 to that of cores CD 1715 and CD 1730. However, other glacial stages (4 and 6) are relatively low in Zr flux but still show a higher flux than occurs in adjacent interglacial stages (Table 9.1).

Characteristic decreases in Zr fluxes occur in interglacial Stages 5 and 7 (Figs. 9.7a, b). This is consistent with the fluxes such as quartz, aluminium and dolomite discussed earlier. In Stage 3, although the Zr flux is low in its lower part, it increases in its middle part, and continues upward to increase to ~35,000 years BP. A short period c.~37,000-22,000 years BP in the upper part of Stage 3 shows a slight decrease in flux. This feature is common to all profiles and may be denoting an important short climatic phase occurring in this area between 37,000-21,000 years BP (Kutzbach and Street, 1985; Foucault and Stanely, 1989).

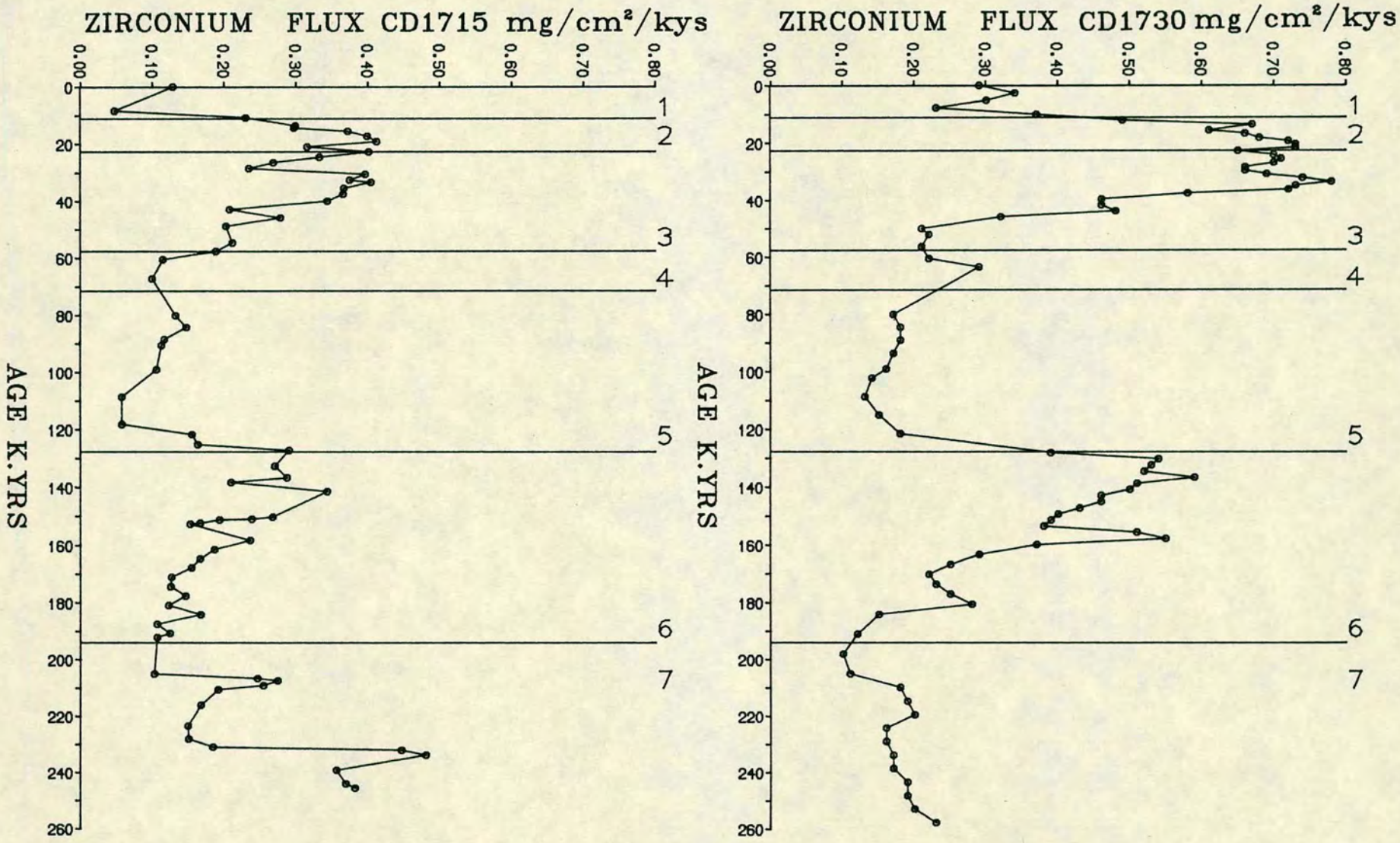

FIGURE 9.7a ZIRCONIUM FLUX PROFILES. CORES CD1715 AND CD1730.

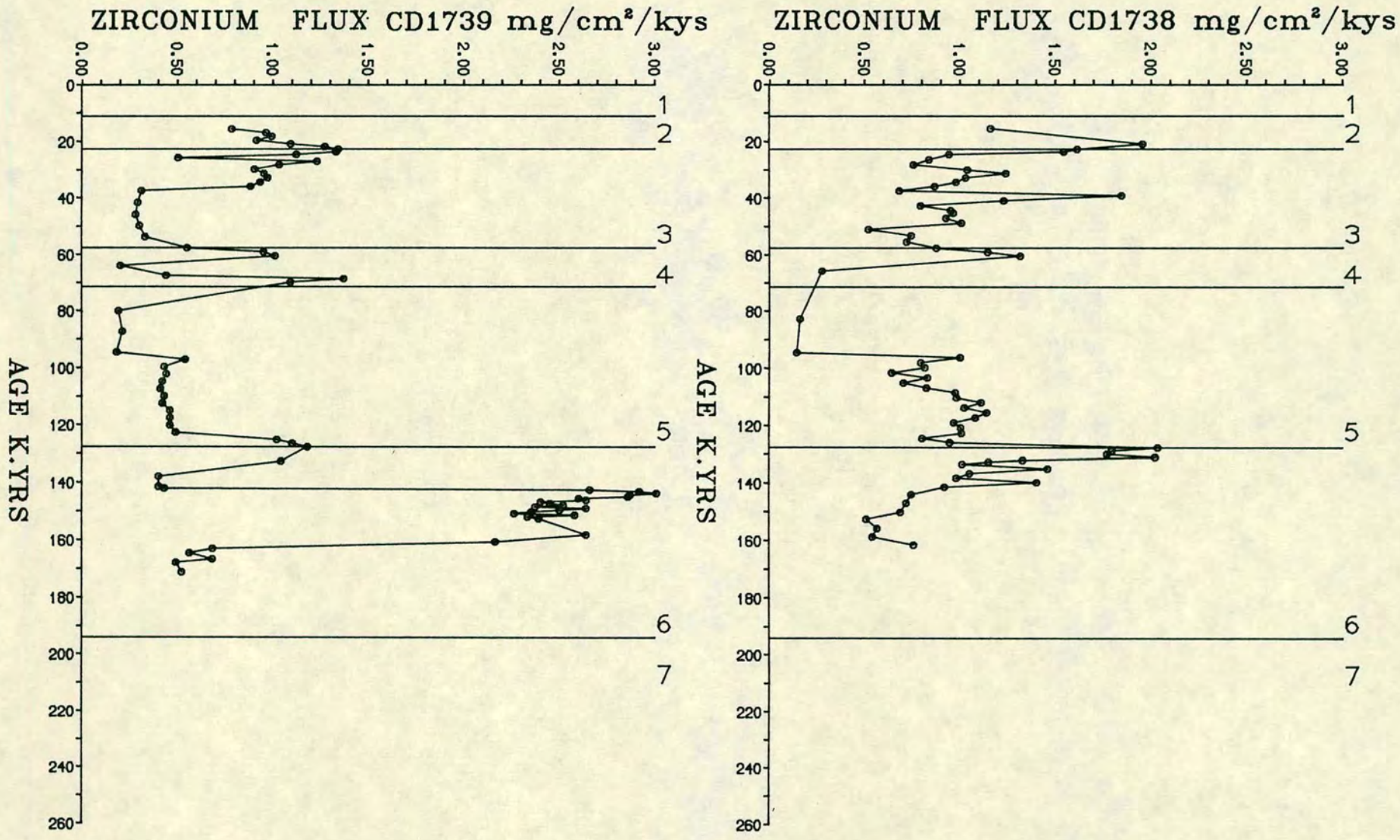

FIGURE 9.7b ZIRCONIUM FLUX PROFILES. CORES CD1739 AND CD1738.

9.4:5 Titanium Flux

Areal and temporal trends in the titanium flux (Figs. 9.8a) are again similar to other lithogenic fluxes shown earlier (Figs. 9.4 to 9.7). The mean values of flux increases towards core CD 1738 from CD 1715 (Table 9.1) and tends to increase in glacial Stages (2, 4 and 6) whereas in interglacial Stages (3, 5 and 7) and Holocene fluxes are low (Table 9.1).

Vertical changes in titanium flux shown in Figs. 9.8a, b, although similar in trends, shows a different amplitude of variation between core CD 1715 and CD 1730 (Figs. 9.8a). Relative input changes of titanium flux appears to be much higher in core CD 1715 and is especially observed in interglacial Stage 3. The titanium flux values for Stage 3 are higher (40 $mg/cm^2/kys$) in core CD 1715 compared to 15 $mg/cm^2/kys$ in core CD 1730 with higher fluxes occurring in the upper part of CD 1730 and the lower part of the stage in CD 1715. In Stage 6, these cores also show dissimilar patterns but flux values are similar. In chapter 5, which described the geochemistry of minor elements, it was found that contents of titanium in core CD 1715 and CD 1730 (Fig. 5.8a) are different in that the former core is higher. And in relation to Cr, the difference of titanium in Stage 3 and 6 of these cores probably suggests either a redistribution mechanism or a different clay mineralogy. Since the higher Cr content in NW Arabian Sea sediments suggests its derivation from local sources (ie. ophiolites), the high Cr in core CD 1730 implies more local input and therefore may dilute the more distant input of quartz and zirconium. Zr/Qtz (Figs. 5.15) generally shows invariable ratio down the cores while Cr/Zr (Figs. 5.16) ratio varies considerably in different climatic stages. Hence it is most likely that factors that control the zirconium flux in these cores (CD 1715 and CD 1730) also control the changing patterns of Ti flux. However, in northern cores (ie. CD 1739 and CD 1738) titanium flux (Figs. 9.8b) is high (Table 9.1) indicating substantial aeolian input which is commensurate to their location. Characteristically higher Ti flux has been observed in the middle of Stage 6, showing flux value of about 65 $mg/cm^2/kys$. Synchronous higher fluxes of quartz, aluminium, dolomite and zircon are also seen in these cores.

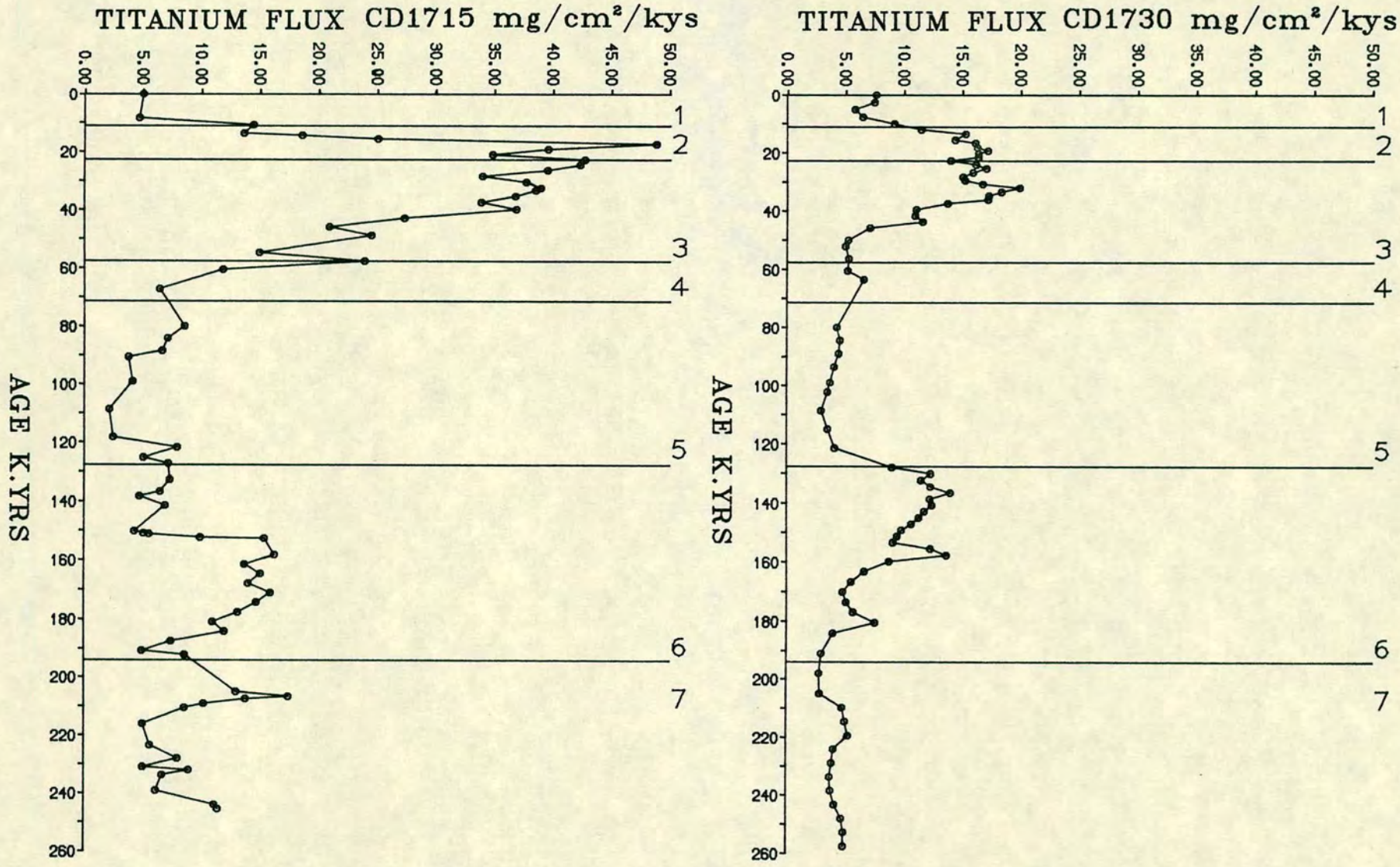

FIGURE 9.8a TITANIUM FLUX PROFILES. CORES CD1715 AND CD1730.

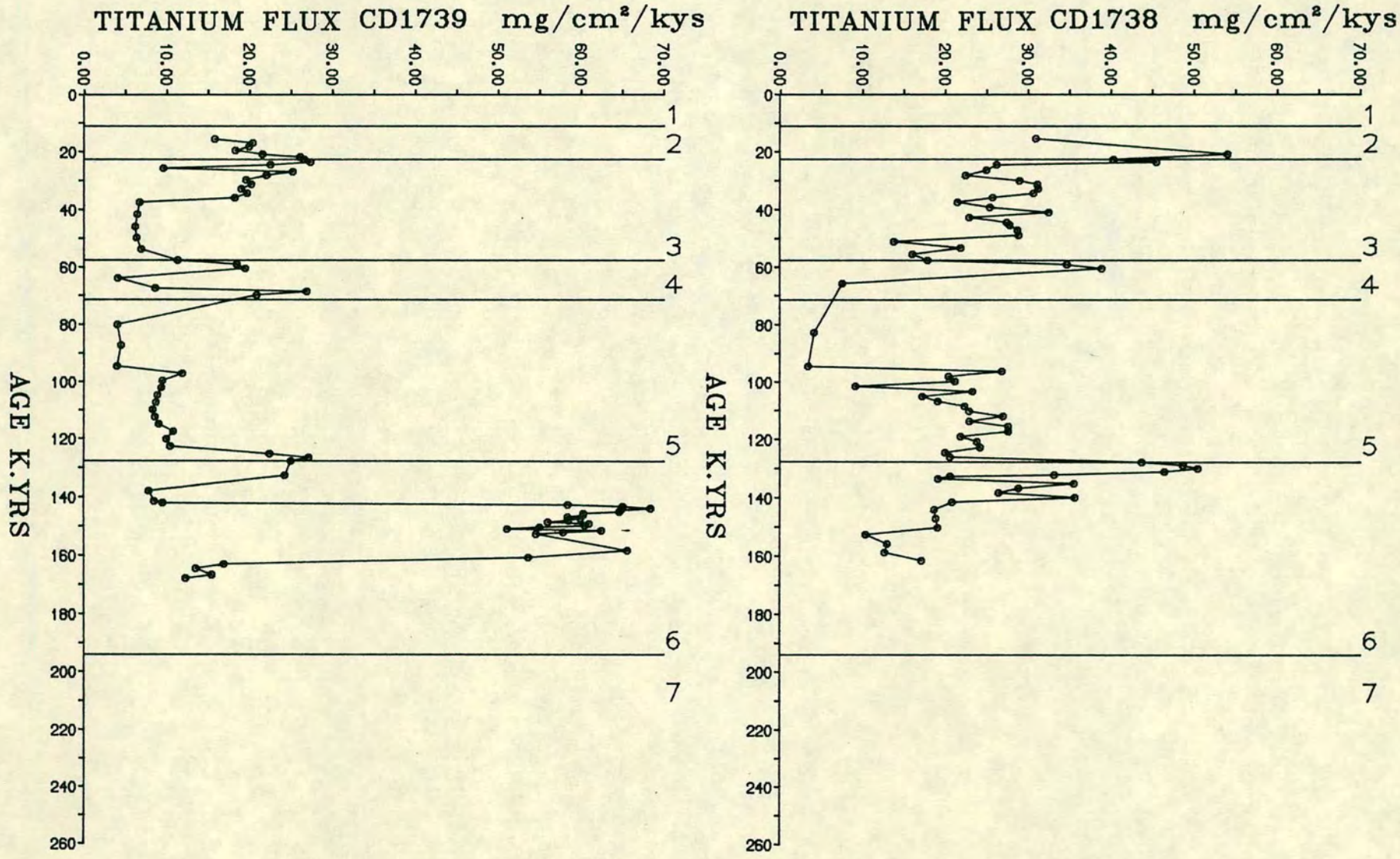

FIGURE 9.8b TITANIUM FLUX PROFILES. CORES CD1739 AND CD1738.

9.5 IMPLICATIONS

9.5:1 Transportation

The Arabian Sea is a repository for the continental derived material originated from the surrounding land masses. Geomorphologically, the neighbouring continents are arid lands where effects of seasonal variation of climate are very severe. The Arabian Peninsula has been identified by Idso (1976) as one of five major world regions where dust storm generation is very intense. Middleton (1986a, b) has noted that prevailing northwesterly winds in the area (Table 9.3) carried this dust load and transport them towards the Arabian Sea. Major dust trajectories and satellite images clearly show that material picked up from the north, in northeast Africa, Mesopotamia, Arabian deserts and Iran, ultimately is transported towards the sea (Grigoryev et al., 1980; Coudie-Gaussen, 1984; Sirocko and Sarnthein, 1988). In Fig. 9.9 which outlines the satellite image of dust raising activity in lower Mesopotamia shows that dust transport is towards the sea. Such consistent trends in transport directions have also been reported from marine aerosol investigation in the area (Aston et al., 1973; Prodi et al., 1983; Chester et al., 1985). Several studies of surface sediments in the area (Emery, 1956; Sugden, 1963; Stewart et al., 1965; Kolla and Biscay, 1977; Kolla et al., 1981a, b; Khalaf and Al-Hashash, 1983; Sirocko and Sarnthein, 1988) have confirmed that prevailing winds are predominant in transporting these sediments. The latest quantitative study (Sirocko and Sarnthein, 1988) using satellite data and sediment cores, has enforced the importance of dust transport in this area. They showed that amount of aerosol discharge in 1979 (115-215) x 10^6t/y broadly equates with the average late Holocene aeolian flux in deep sea sediments of Arabian Sea (80-100) x 10^6t/y.

A comprehensive study of fluxes of various lithogenic elements and their variation with respect to time, undertaken in this thesis strongly confirms the previous published findings. A north-south gradient in the fluxes (Table 9.1) clearly indicates that northwesterly winds from north and northwest moves eastward and shed off their load mainly in northern Arabian Sea. Winds near Oman deflect south and unload the carrying dust preferentially in the area of Gulf of Oman. This is evident from higher average fluxes of lithogenic elements seen in northern cores ie. CD 1739 and CD 1738.

Table 9.3 Dust-bearing winds of the Middle East

Name	Area affected	Season	Direction	Meteorological conditions
Shamal ('North')	Mesopotamia and Arabian Gulf	Regularly: Feb-Oct Peak: June & July	NW	Blows between Azores High and Indian monsoon low
Sad-ou-bist bad ('Wind of 120 days')	SE Iran esp. Sistan	May-Sept	N-NW	Circulates around main Low of Indian monsoon
Belat	SE coast Arabia esp. between Ras Sajar and Masira Island	mid Dec-mid Mar	N-NW	
Simoom ('Poison wind')	Kuwait	summer	NW	Local name for Shamal
Khamsin	Egypt. As generic type over much of area under local names (see below)	spring and winter	varies predom.S	Local wind caused by particular air masses drawn into a region by passage of a cyclone and its associated fronts
Sharav	Israel	Apr-June	SW or SE	
Shlour	Syria and Lebanon	spring and winter	S-SW	Khamsin-type
Shargi	Iraq	spring	SE	

(Table 1. From Middleton, 1986b).

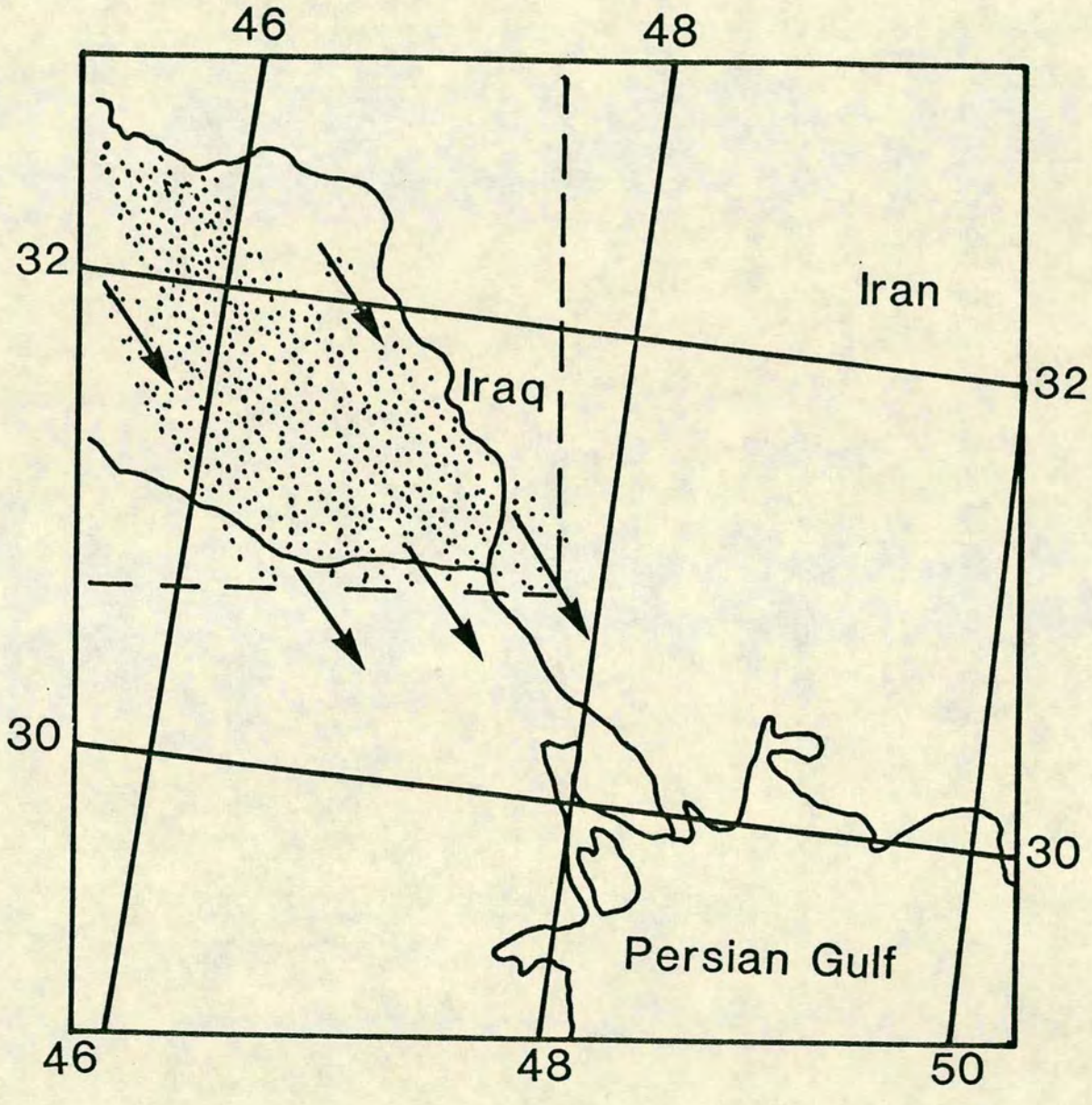

FIGURE 9.9 SKETCH OF SATELLITE IMAGE FROM COSMOS-226 SHOWING DUST TRANSPORT FROM LOWER MESOPOTAMIAN REGION TOWARDS PERSIAN GULF. (GRIGORYEV and KONDRATYEV, 1980).

In core CD 1738 from Gulf of Oman slightly lower fluxes than core CD 1739 are probably a result of dilution by riverine sediments from Makran and Oman or from Persian Gulf outflow. Sirocko and Sarnthein (1988) have noticed the influence of the latter factors and it is likely that site CD 1738 is strongly affected by such a source in addition to aeolian fallout. In chapter 4 discussing the mineralogy of the cores, it was found that core CD 1738 is impoverished in feldspar relative to quartz and shows higher chlorite in the sediments. On the basis of mineralogy it was suggested that high salinity waters flowing out of Persian Gulf transport sediments of this composition in the Gulf of Oman. Thus, it is reasonable to claim that mixing of riverine and aeolian sources in this area may affect a high lithogene flux. Alternatively, the unusually high lithogenic flux of the northern cores may be an artifact of less precise dating, and hence subsequently produced errors in the computation of average fluxes. However, as it can be seen from different isotopic stages, that core CD 1738 in each stage is showing the highest lithogenic flux (Table 9.1) and the dolomite flux is consistent with these findings.

Since the lithogenic fluxes and their variation shown in Figs. 9.4 to 9.8 reflect an aeolian transport, a gradual decrease in flux values toward core CD 1715 signifies a progressive depletion in the dust load. This trend has been consistent during all isotopic stages throughout the last 250,000 years. Irrespective of glacial and interglacial stages, the lowest flux is found in core CD 1715 and highest values occurs in core CD 1738. This suggests that the prevailing patterns of wind, has not changed through time. The changes in the values of fluxes during cold and warm stages could only be explained either by the effectiveness of the transporting agent (ie. winds), or by the climatic conditions of the source areas.

Today the seasonal variation associated with monsoon system of the area shows the extremes of dust load. Major dust haze observed on the Arabian Sea occur during June, July, August (McDonald, 1938; Prospero, 1981). During this season dust outbreaks are common (Foda et al., 1985; Chen, 1986; Ackerman & Cox, 1988), and along both the African and Arabian coasts substantial dust transport, including storms have been reported (Sirocko and Sarnthein, 1988). In cores CD 1739 and CD 1738, especially in their lower and upper parts, anomalously high fluxes probably represent such dust storms. The crude dust estimates off Africa and Oman coast obtained from satellite data (Sirocko and Sarnthein, 1988) show that dust load is 4-5 times higher off Oman than off Africa (Table 9.4b) Fig. 9.10). This indicates that northwesterly winds crossing Oman during the summer dominates the dust input to the northern Arabian Sea. Areal differences reported by Sirocko and Sarnthein (1988) (Fig. 9.10) are similar to the changes in average fluxes of quartz, aluminium

Table 9.4a **Average lithogenic fluxes from NW Arabian Sea for the last 250,000 years BP**

Flux ($mg/cm^2/kys$)	Core CD 1715	Core CD 1739	Core CD 1738
Quartz	130.10	550.1	402.9
Aluminium	89.59	422.3	446.9
Zirconium	0.23	1.21	1.00
Titanium	15.65	26.84	25.42

Table 9.4b **Dust flux along Arabian and African Coast measured from satellite records**

Area	Dust Flux ($x10^6 + y^{-1}$)	Reference
Off Oman	78.4	Sirocko and Sarnthein, 1988
Off Africa	21.3	

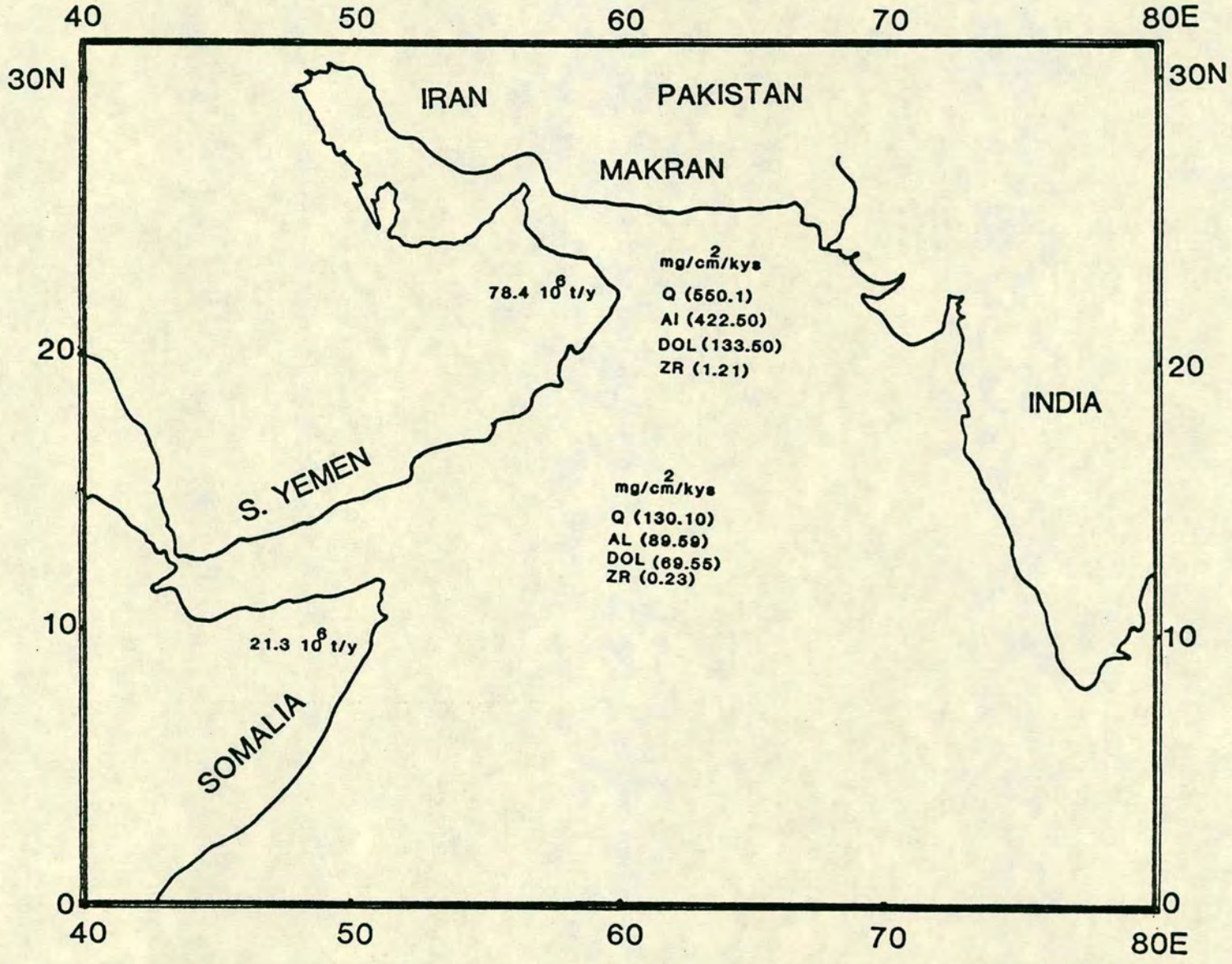

FIGURE 9.10 TODAY'S DUST FLUX (SATELLITE) AND LITHOGENIC FLUXES (OCEANIC SEDIMENTS) RECORD OF 250,000 B.P. OFF THE OMAN AND SOMALIA REGION. DUST FLUX FROM SIROCKO and SARNTHEIN, 1988.

and zirconium in the cores CD 1715 and CD 1738. These two cores lie approximately at the same latitude as those of Sirocko and Sarnthein's (1988) satellite imageries. There is a north-south four to five times decrease in dust flux (Table 9.4a, b; Fig. 9.10) which is remarkably similar to the decrease in lithogenic fluxes observed in cores CD 1715 and CD 1738.

9.5:2 Climatic Significance

In the above discussion, it has been established that prevailing northwesterly winds are the most important factor in controlling the distribution of lithogenic fluxes in Arabian Sea sediments. Depending on their intensity, it may be expected that winds transport varying amount of terrigenous material. The fluxes change with respect to time as shown in Figs. 9.4 to 9.8 and therefore may reflect past changes in the intensity of northwesterly winds relating to the climatic oscillations of the late Pleistocene. A relationship between climate and wind intensity is evident in the winter/summer climatic cycles (Lamb, 1966). During winter, the northern hemisphere is characterized by intensified atmospheric circulation, and the overall zonal circulation is displaced equatorward. In contrast to this, wind belts shift poleward during summer and diminish in intensity. Thus, it is possible to interpret the climate of glacial and interglacial events in a similar fashion.

In the area of study, seasonal variation in wind intensity and the subsequent effect on dust transport is well documented (McDonald, 1938; Prospero, 1981; Middleton, 1986a, b; Sirocko and Sarnthein, 1988). Frequent dust storms (Middleton, 1986b) that raise considerable material from the plains of Arabia, Africa, Mesopotamia and Iran, Makran could profoundly influence the total aeolian flux to marine sediments. A relationship between total aeolian flux and oxygen isotope record shown in Fig. 9.3 from this area implies a climatic influence on the variation of detrital flux. Lithogenic flux profiles of investigated cores (Figs. 9.4 to 9.8), suggest increased supply of continental derived material to Arabian Sea during past cold periods, and decreased supply in warm periods ie. interglacial. From this it can be easily envisaged that during glacial stages, the climate of the source areas was more arid than the intervening interglacial events. Further, the high fluxes in cold stages indicate that winds were more intense at these times. The strength of winds, however, is difficult to discern from the present data.

In Table 9.5 it can be seen that the ratio of quartz and zirconium to aluminium flux shows the reverse of expected trends. The ratio of quartz and zirconium to aluminium flux contrasts a hydraulically heavy to a hydraulically light

Table 9.5 Mean ratio of quartz and zirconium flux to aluminium flux

Stages	Core CD 1715		Core CD 1730	
	Qtz/Al	Zr/Al	Qtz/Al	Zr/Al
		$x10^{-3}$		$x10^{-3}$
1	2.11	2.98	0.67	2.45
2	1.31	2.56	1.10	2.58
3	1.46	2.62	1.16	2.62
4	1.70	2.74	1.08	2.73
5	1.71	3.07	1.08	1.08
6	1.54	2.40	0.97	2.53
7	1.33	2.47	1.04	2.52
Average				
	1.51	2.69	1.03	2.57

terrigenous component. This ratio can show variation in transport energy. During periods of high terrigenous supply, higher quartz/Al and Zr/Al flux ratios may indicate stronger winds. This holds true for glacial Stage 2 periods which shows the high ratios in core CD 1730. In core CD 1715, high ratios of quartz/Al and zirconium/Al probably imply lag sediments enriched in quartz and zirconium. Other stages and especially interglacial stages showing almost equal ratios of quartz/Al and Zr/Al to that of glacial Stage 2 (Table 9.5) as seen in core CD 1730. This is probably due to the residual heavy minerals concentrated after winnowing of fine material during interglacial Stages.

9.5:2a Climatic characters of different isotopic stages

A consistent general trend in the lithogenic fluxes variation is observed in all cores. This coherence is almost isochronous in the investigated area. However, there are some limitations in the precise interpretation of climatic character of different stages. In this study, turbidite identified in core CD 1715 and interglacial erosional events (Shimmield, pers. comm.) seems to pose problems in reconstructing the past climate record. Despite these limitations core CD 1730 is chosen to identify the glacial and interglacial characters of the area. Since this core is free of any coarse turbidite bands, it may represent the complete climatic history of late Quaternary of the area, particularly a period c.40 kys to present. Fig. 9.11 is a summary figure, showing schematically the average fluxes obtained in glacial and interglacial stages of core CD 1730. The fluxes values are given in Table 9.1 for each stage and has been employed to decipher the severity in climate of respective stage.

9.5:2a(i) Holocene (Stage 1)

The values of all lithogenic fluxes at the end of last glacial maximum ie. Stage 2, shows dramatic fall from their maximum. In Figs. 9.4 to 9.8 it is clearly shown that around 9,000 years lithogenic fluxes are very low. Core CD 1730 shows a six times decrease in quartz and dolomite flux, while aluminium, zirconium and trianium decreases by a factor of about 2 to 3. These significant changes in continental input immediately after the most arid last glacial maximum can be simply related to the global climate change that occurred around 11,000-8,000 years ago. The late glacial-early Holocene (Bolling-Alleroid to Boreal) was the most humid period since the last glacial maximum in all equatorial latitude (Rossignol-Strick,

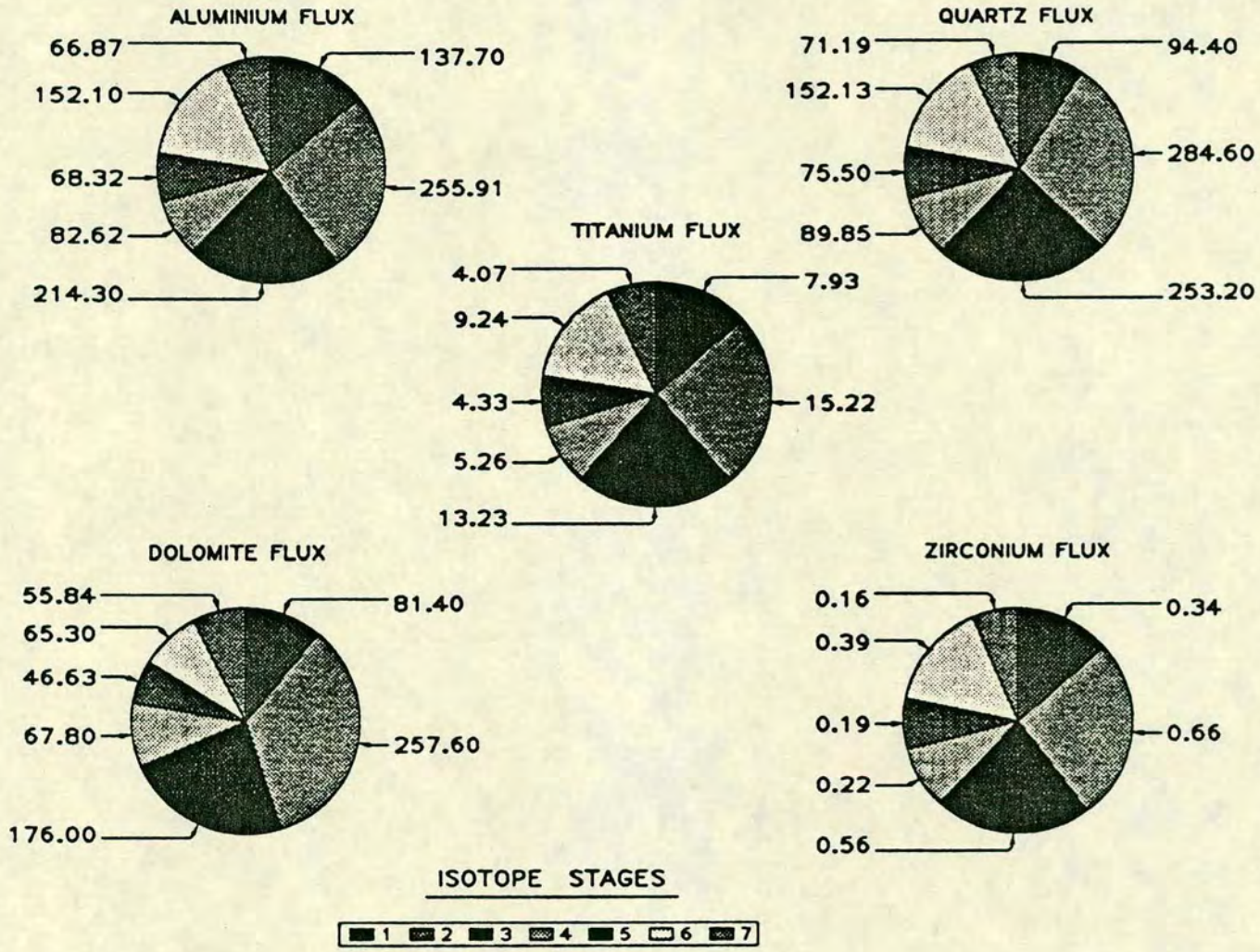

FIGURE 9.11 PIE DIAGRAMS SHOWING THE LITHOGENIC FLUXES (mg/cm²/Kys) IN GLACIAL AND INTERGLACIAL STAGES.
EVEN Nos = GLACIAL STAGES
ODD Nos = INTERGLACIAL STAGES (CD 1730)

Table 9.6 **Simulated surface temperature and precipitation for June to August averages for northern and southern hemisphere. Modern and 9000 years BP values and their difference (Δ).**

Space average	Surface temperature				Precipitation (cm/day)			
	9000 years B.P. (°C)	Modern (°C)	Δ (K)	S.L. %	9000 years B.P.	Modern	Δ	S.L. (%)
			June to August					
Northern Hemisphere, land	24.5	23.8	0.7	1	0.45	0.41	0.04	5
Southern Hemisphere, land	2.0	1.7	0.3		0.47	0.45	0.02	
Global, land and ocean	17.7	17.5	0.2	5	0.35	0.35	0	
			Annual					
Northern Hemisphere, land	13.2	13.4	-0.2		0.39	0.37	0.02	5
Southern Hemisphere, land	7.5	7.3	0.2	5	0.45	0.47	-0.02	
Global, land and ocean	15.9	15.9	0		0.33	0.33	0	

(Table 2. Kutzbach, 1981).

1983). Kutzbach (1981) indicated that global solar radiation was 7% greater than present. As a result of this global increase in temperature (Table 9.6) regional effects are manifested by strong SW monsoon (Kutzbach, 1981; Prell and Kutzbach, 1987). Climatic modelling for 9,000 years BP have documented 50% increase in precipitation over Arabia, India and Southeast Asia (Kutzbach, 1981). This high precipitation over neighbouring continents in a humid phase is evidenced by lake levels, alluvial records, and pollen studies (Butzer and Isaac, 1972; Singh et al., 1972; Street and Grove, 1979; Van Compo, 1982; Swain et al., 1983; Street and Harrison, 1984).

The reduced lithogenic fluxes observed in this study around 9,000 years BP are strongly coherent with the climate of that time and support the published evidence that climate during the Holocene especially the early Holocene time was humid. The continents were probably largely covered by vegetation, winds were not strong, therefore the aeolian fluxes are significantly lowered.

9.5:2a(ii) Glacial Stage 2

The glacial stage 2 which started about 22,000 years ago and ended around 11,000 years BP represents a period of global ice advancement. Compared to other glacial stages, Stage 2 comprises a relatively short interval of time ie. 11,000-18,000 years. The proportion of lithogenic fluxes shown in Fig. 9.11 indicate that more than 25% of total fluxes over the past 250 kys occurred in glacial stage 2. The highest flux (Table 9.1) values observed in this stage clearly imply widespread aridity on the continents bordering the Arabian Sea. Highest quartz flux during Stage 2 (Table 9.1) observed in this study is in close agreement with high quartz content noted by Kolla and Biscay (1977) in the area. Following these workers, high quartz flux in the Arabian Sea sediments suggest increased aridity during last glacial maximum.

Profiles of fluxes shown in Figs. 9.4 to 9.8 display a peak in lithogenic fluxes at 18,000 years BP which steadily decreases upward. There is much information on palaeo-environment for the world for this periods available, which was marked by a global ice volume maximum. A massive ice sheet spread over N. America and there were smaller but still sizeable ice sheets over NW Europe, and Tibet was possibly covered in ice. Due to ice caps over NW Europe, atmospheric high pressures developed. As a result of which the pathway of westerlies was depressed down across N. Africa (Lamb, 1970). A climatic model presented by CLIMAP (1976) and COHMAP (1988) for this period strongly supports the evidence that 18,000 years ago the climate was much drier and atmospheric circulation was more intense than today.

Continental evidence from the area show that at this time the Persian Gulf region (Sarnthein and Diester, 1977) and the Rajasthan (Bryson and Swain, 1981) were dry, the Zagros mountains in the north were drier than they are today (Wright et al., 1967). Vegetation of bordering areas was scanty (Van Compo et al., 1982; Van Compo, 1986) and strong dust storms occurred in the cold sand deserts of Arabia and other parts of Asia (Sarnthein, 1978; Tungshang et al., 1986). The oceanic record presented in this thesis for last glacial maximum shows highly consistent results. Highest lithogenic fluxes in Stage 2 that reach maximum around 18,000 years confirm that climate during this period c. 21,000-12,000 was most severe.

9.5:2a(iii) Interglacial Stages (3, 5 and 7)

Before defining the climatic patterns that prevailed during interglacial stages, it must be pointed out here that from thorium analysis of core CD 1730 (Shimmield, unpublished data) it has been suspected that warm interglacial periods in NW Arabian Sea contain erosive phases (except Holocene). This is shown from the thorium accumulation (Fig. 9.12) in this area that in major interglacial stages (5, 7) the thorium accumulation is less than that predicted from its growth in seawater. Isotopic Stages 5 and 7 are the most affected episodes, whereas Stage 3 appears to be less affected and in later part of this stage, the positive values of thorium suggest a good, and possibly enhanced preservation in the deep sea record. Hence, interpretation of climate using only lithogenic fluxes in NW Arabian Sea sediment seems to be limited.

Although the general decrease in lithogenic fluxes occurs in interglacial stages and may represent a warm humid climate, the quantitative estimates of the fluxes indicated are probably not a complete record, because of losses due to possible erosion. Therefore, the fluxes shown in interglacial stages can not be employed with certainty to show the past climate. The terrestrial record from the surrounding continents is fragmentary, and there is no study which has shown the complete record of environmental changes throughout Pleistocene.

For Stage 3 a paleoclimatic curve has been constructed from pollen record in Europe, Syria and Lebanon (Fig. 9.13, Table 9.7). The latter areas contribute dust to the Arabian Sea and therefore may provide some idea of the regional past climate. Comparison with the present study of quartz in sediment cores reveals a reasonably positive correlation. Widely occurring warm and cold events are largely synchronous. From this it is seen that during the early-middle warm glacial period (60,000-23,000 years BP) the neighbouring continents were warm, but this feature was of relatively

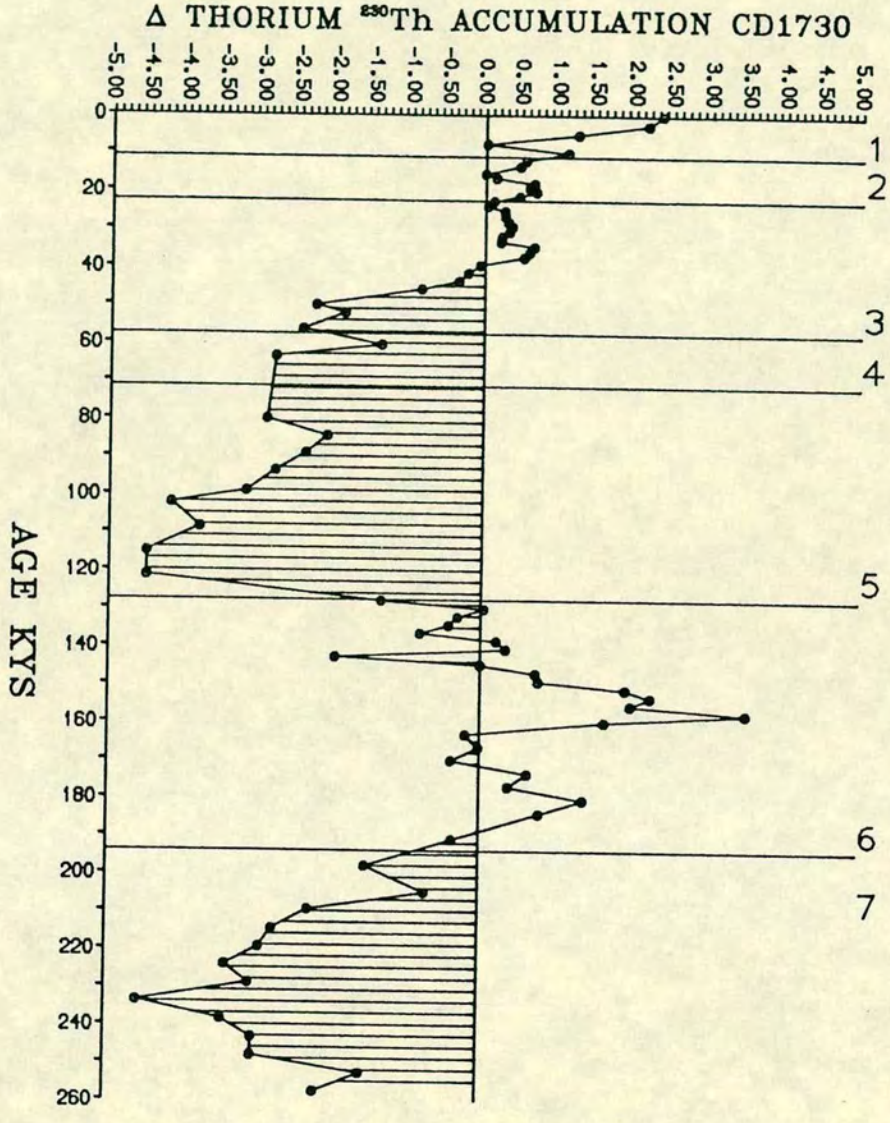

FIGURE 9.12 Δ THORIUM ACCUMULATION PROFILE. CORE CD1730 (UNPUBLISHED DATA FROM C B SHIMMIELD).

ΔThorium = observed excess ^{230}Th - predicted excess ^{230}Th (dpm/g) (predicted excess ^{230}Th is calculated assuming constant U content in seawater and vertical scavenging of ^{230}Th).

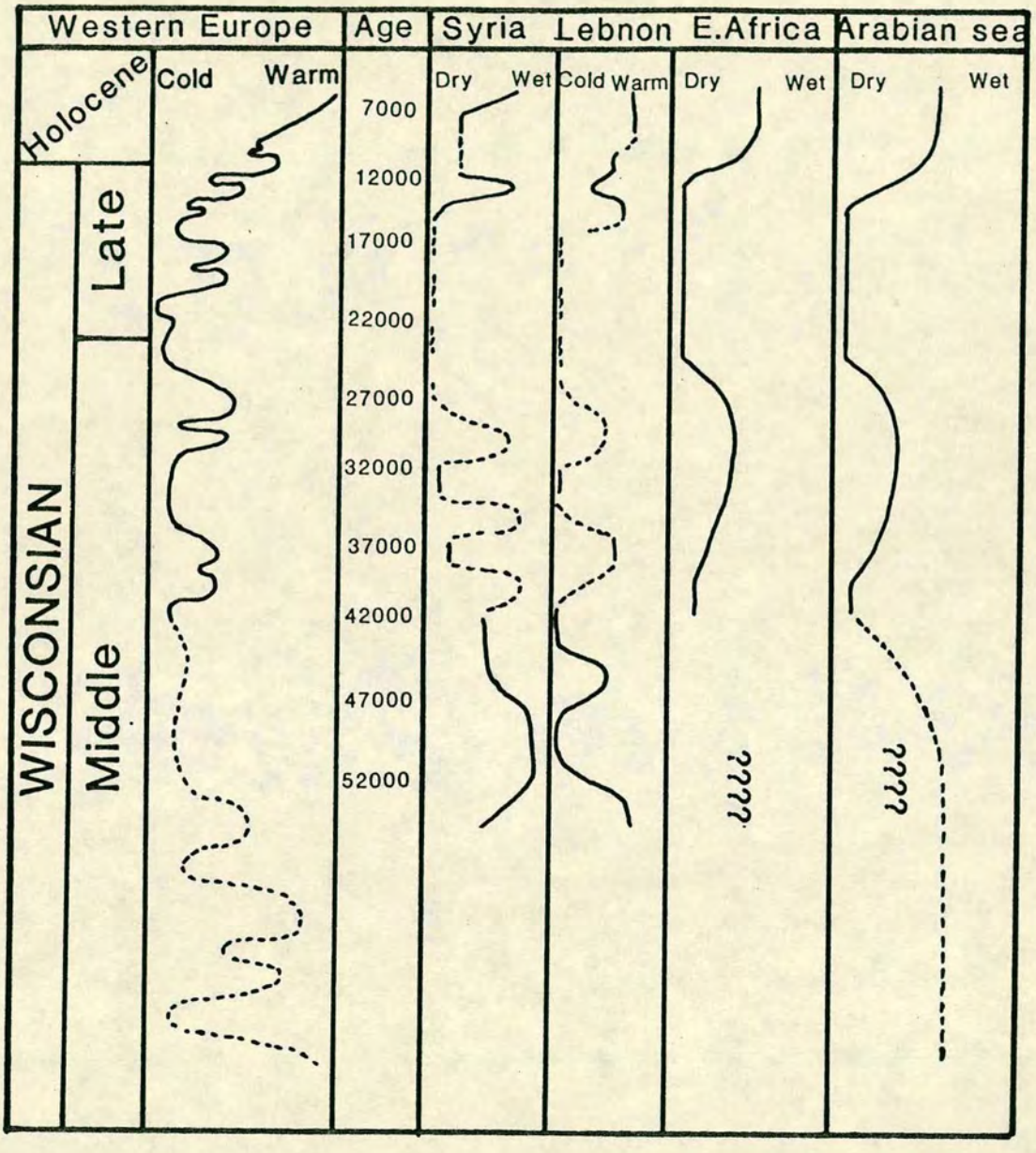

FIGURE 9.13 PALAEOCLIMATIC CURVES FOR THE LAST GLACIAL IN THE NEAR EAST AND WESTERN EUROPE BASED ON POLLEN ANALYSIS (FIG. 1 LEOROI-GROUHAN, 1974) EAST AFRICAN RECORD IS BASED ON LAKE LEVELS (STREET and GROOVE, 1980) AND ARABIAN SEA CURVE IS CONSTRUCTED FROM QUARTZ FLUX OF PRESENT STUDY.

Table 9.7 **Warm, humid periods between 60,000 to 20,000 years BP from published and present work**

Area	Paleotracer	Period	Reference
Arabian Desert	Hydrological	36,000-17,000	Mclure, 1976
East Africa	Hydrological	40,000-20,000	Gasse and Street, 1978
East Africa	Mineralogical	40,000-20,000	Foucault and Stanley, 1989
Arabian Sea	Foraminiferids	59,000-53,000	Prell, 1984
Arabian Sea	Geochemical	60,000-51,000	Present study
Arabian Sea	Geochemical	42,000-39,000	Present study
Arabian Sea	Geochemical	37,000-20,000	Present study

short duration. This particularly occurs during the younger part of Stage 3 (c.40,000-23,000 yrs BP) when lake levels in Africa, Arabia and India were high. However, the overall climatic character of Stage 3 was cold and arid, but not to the extent seen in glacial Stage 2. These trends are also indicated in the core analysis when a higher lithogenic flux is measured relative to other interglacial Stages 5 and 7. The flux is almost as high as in glacial Stage 2, when a massive ice sheet existed over much of the northern hemisphere. The lithogenic fluxes in other warm periods (5 and 7) are very similar. This reflects that climate or erosion, whatever it may be, was essentially the same at these times.

9.5:2a(iv) Glacial Stages (4 and 6)

Glacial Stages 4 and 6 are low in lithogenic fluxes relative to glacial stage 2 (Figs. 9.4 to 9.8). Glacial stage 4 represents a cold period of very short duration; ~10,000 years. The glacial flux values are lowest in this stage (Table 9.1) 70,000-60,000 years BP. The lithogenic fluxes tend to decrease at the stage boundary of 3 and 4, near 60,000 years BP. This refelcts that a period from 70,000 to 60,000 years BP was continuously arid and cold and it is followed by an even more intense climate in Stage 3 and 2 as suggested by steady increase in lithogenic fluxes upward, which terminated at the base of the Holocene.

Stage 6 which encompasses a long time period of about 70,000 years shows intermediate fluxes. This isotopic stage which is equivalent to the late Illinoian of N. America, represent a period of fluctuating fluxes especially in its upper parts (Figs. 9.4 to 9.8). A pronounced decrease in lithogenic fluxes indicated around 150,000 years BP and 170,000 years BP probably imply stadial and interstadial conditions. However, the marked decline in the lithogenic flux in its lower part, at the boundary of preceding interglacial Stage 7, may be related to sediment erosion suspected in Stage 7. Overall the higher fluxes in Stage 6 support the idea that glacial environment was arid like Stage 2, and resulted in higher dust transport in the Arabian Sea.

9.5:3 EFFECTS OF SEA LEVEL CHANGES

In cores CD 1739 and CD 1738 (from Murray ridge and Gulf of Oman) the fluxes seen in late Stage 6 are markedly different from the other two cores, and show an unusually high lithogenic flux ie. CD 1715 and CD 1730. This trend continues to

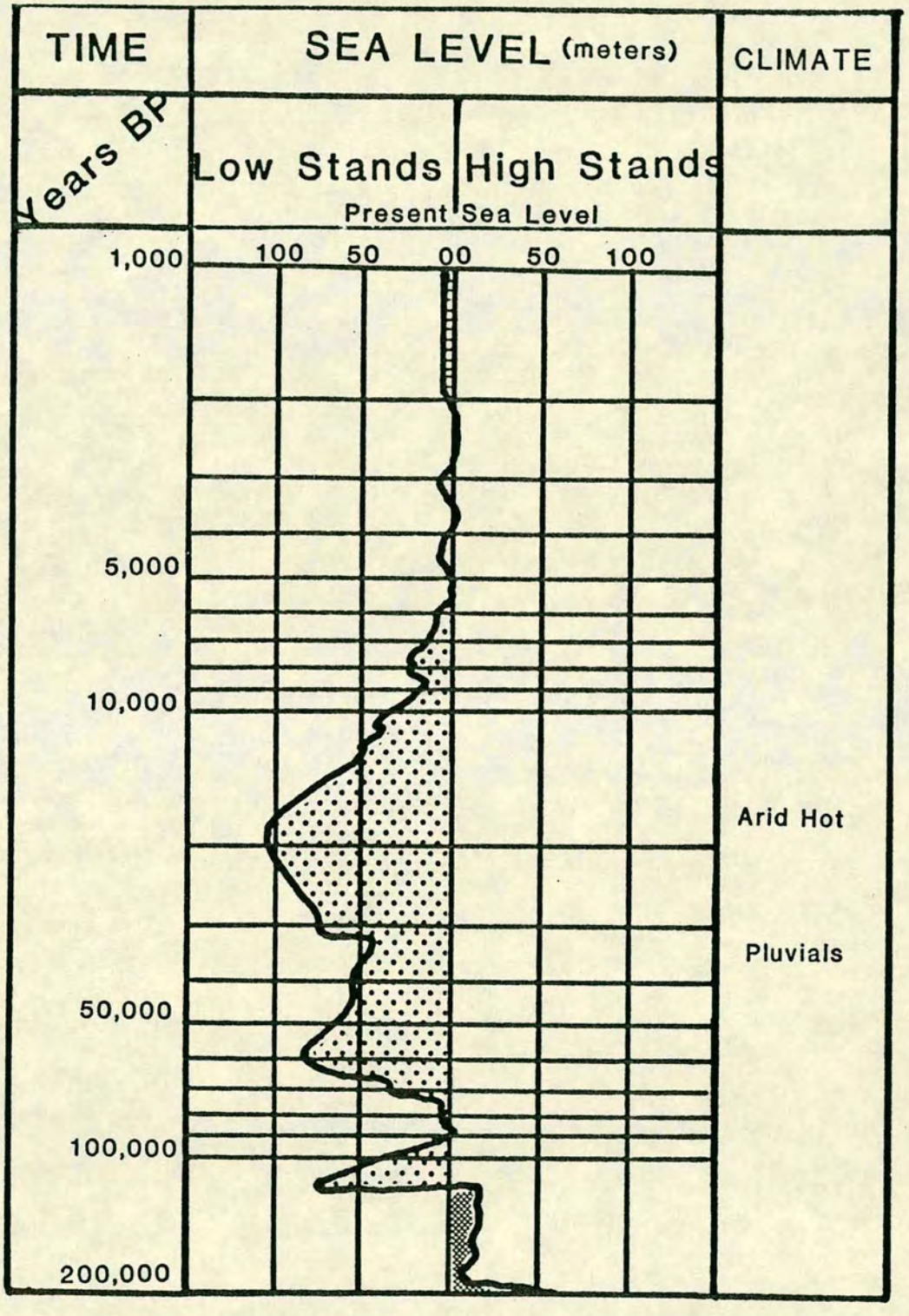

FIGURE 9.14 SEA LEVEL VARIATION IN THE PERSIAN GULF DURING THE LAST 200,000 YEARS B.P. (FAIRBRIDGE, 1961).

some extent in Stage 5 up to the 120,000 years BP. Despite the uncertainty in the dating of these cores, this period (c.140,000-120,000 years BP) has been recognised a time of global high sea level (Turcotte and Bernthal, 1984). Hence, it may be possible to relate such high fluxes during this period to the events of sea level changes at these sites.

Although estimates of sea level history for the late Pleistocene time is lacking in this area, evidences of sea level fluctuations in southern Asia do exist (Pascoe, 1964; Verma and Mathur, 1979; Siddiqui, 1975; Montaggioni and Hoang, 1988). Pascoe (1964) reported the presence of raised beaches along the coast of Pakistan and Makran (Iran). Such coastal deposits on the west coast of India are correlated by Gupta (1972) and Gupta and Amin (1974) with the highs of sea level corresponding to the periods 6,000 yrs BP; 30,000 yrs BP; and 120,000 yrs BP. In the Seychelles area a high stand is assumed to have persisted from about 140,000 to 120,000 years BP, and reached its maximum elevation about 135,000 and 120,000 years ago (Montaggioni and Hoang, 1988).

The sea level curve (Fig. 9.14) constructed by Fairbridge (1961) clearly shows the considerable fluctuation in sea level history of the Persian Gulf. He claims that during the period 70,000-17,000 years BP, Persian Gulf was essentially a river valley. Sea level fell by a maximum of 120 metres during this period and at times sea retreated to the Strait of Hormuz leaving much of the Persian Gulf exposed. The Tigris-Euphrates rivers hence deposited their material directly into the Gulf of Oman (Stoffers amd Ross, 1979).

The lithogenic flux profiles of cores CD 1739 and CD 1738 broadly testify the effects of variation in sea level that occurred. This is particularly seen in core CD 1738 from the Gulf of Oman. The trends of all fluxes are entirely different in the younger section of the core (Figs. 9.4b, 9.5b, 9.6b, 9.7b) compared to other cores examined. A similar feature is also observed in the mineralogy of this core (chapter 3). Thus this core appears to be more influenced by Persian Gulf regressive and transgressive phases.

The high fluxes seen in cores CD 1739 and CD 1738 during late Stage 6, a period between 140,000-120,000 years BP, is synchronous with global sea level rise (Dansgaard and Duplessy, 1981). Thus, they are probably influenced by a Persian Gulf transgression in late Stage 6 which is followed by a regression (100,000 years BP) and this change is reflected by a marked change in flux measurements.

CHAPTER 10

BIOGENIC FLUXES

10.1 INTRODUCTION

The geochemistry of different biomarkers was discussed in chapter **6**. There, it was shown that many profiles of biogenic components (ie. organic carbon, calcite, biog. Si, and Ex.Ba) in sediments from the NW Arabian Sea show a correspondence in trends. However, dissimilar patterns were also observed. Since the contents of these biogenic elements in sediments represent the differential production of overlying water in the form of calcareous and siliceous organisms, the relative input of either is difficult to assess from their absolute contents. There are several other influencing factors that could account for these dissimilar trends. These include alteration (dissolution, oxidation) during settling through the water column, and during deposition on the seafloor.

In this chapter an attempt is made to study these effects using flux calculation; such a study provides better insight into surface production and preservation in sediments than biomarker contents. Accumulation rates described in the preceding chapter are used to compute fluxes of organic carbon, calcite, biog. silica and Ex.Ba. The biogenic fluxes data is listed in appendix C.16 and their vertical variation in four cores is shown in Figs. 10.1 to 10.6.

10.2 CARBON ORGANIC FLUX

The C.org flux changes for the four cores are shown in Fig. 10.1. The highest is found in core CD 1739, up to 150 mg/cm^2-ky (Table 10.1). Cores in the south (CD 1715, CD 1730) show similar trends (except in the lower section of the cores) despite the fact relative input of C.org flux in the two cores is different. Overall, core CD 1730 shows a slightly higher C.org flux than core CD 1715. Such a difference may be attributed to more biological production at site CD 1730, or to less dilution by terrigenous material in the form of turbidites.

In cores CD 1738 and CD 1739 the C.org flux is generally low. Anomalously high values occasionally seen in core CD 1739, are probably a result of unusually high bulk accumulation rates at this site, preserving carbon from oxidation. The general trend for different climatic stages is that glacial stages (ie. 2, 4) tend to have lower fluxes than interglacial stages, except in Stage 6. The high C.org flux seen in Stage 4 of core CD 1730 (Fig. 10.1a) is a result of the abundance of faecal pellets in this stage. The erratic trends in Stage 6 and 7 of core CD 1715 are probably caused by turbidite inputs affecting the sedimentation rate. During the Holocene (Stage 1) low C.org fluxes are seen in both cores CD 1715 and CD 1730. In warm interglacial

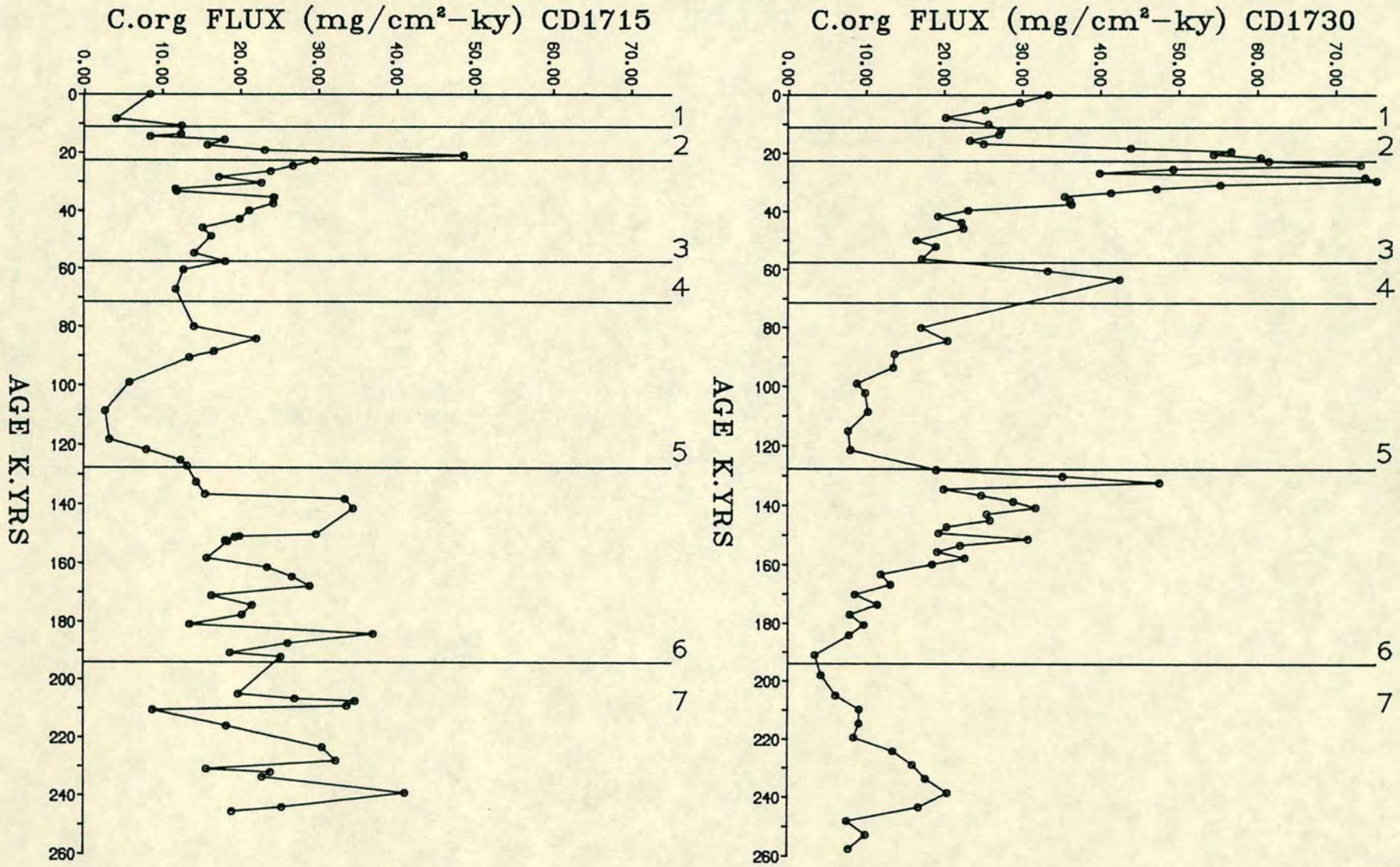

FIGURE 10.1a CARBON ORGANIC FLUX PROFILES. CORES CD1715 AND CD1730.

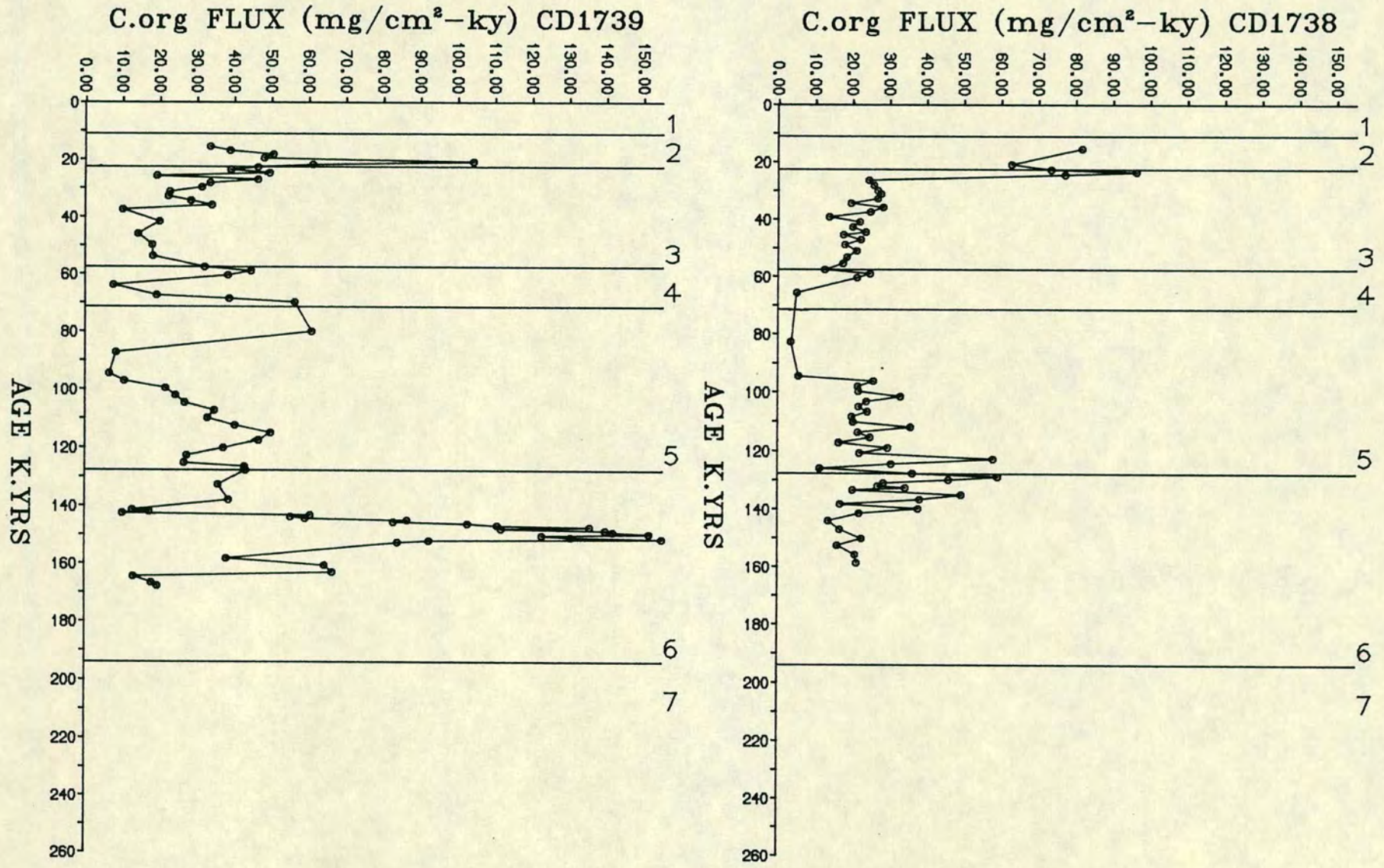

FIGURE 10.1b CARBON ORGANIC FLUX PROFILES. CORES CD1739 AND CD1738.

Table 10.1 Minimum, Maximum and Mean biogenic fluxes in different isotopic stages of NW Arabian Sea Cores.

CORES #	FLUX mg-cm^2/kys	STAGE 1 Range	STAGE 1 Mean	STAGE 2 Range	STAGE 2 Mean	STAGE 3 Range	STAGE 3 Mean	STAGE 4 Range	STAGE 4 Mean	STAGE 5 Range	STAGE 5 Mean	STAGE 6 Range	STAGE 6 Mean	STAGE 7 Range	STAGE 7 Mean	AVERAGE Range	AVERAGE Mean
CD 1715	C.Org	4.03-12.43	8.27	8.38-48.51	20.98	11.63-29.41	19.72	11.68-18.03	14.10	2.66-22.01	11.11	13.18-36.97	22.10	8.78-41.07	24.77	2.66-48.51	19.87
	Biog.Si	15.36-43.24	24.96	24.00-62.13	41.08	20.65-42.21	31.24	17.71 34.61	27.05	5.73-46.37	22.80	15.57-41.57	26.78	9.06-66.90	25.10	5.73-66.91	28.02
	Ex.Ba	0.480-1.00	0.713	0.39-1.42	0.789	0.34-1.00	0.66	0.32-0.70	0.43	0.17-0.99	0.486	0.17-1.61	0.89	0.42-1.56	0.783	0.12-1.61	0.73
	$CaCO_3$	0.510-2.42	1.20	1.93-2.57	2.15	1.18-2.12	1.65	0.55-1.36	0.83	0.42-1.24	0.89	0.27-1.35	1.00	0.27-2.09	1.36	0.27-2.57	1.30
CD 1730	C.Org	20.07-33.17	26.77	23.18-61.40	42.09	16.30-75.15	40.06	16.95-42.31	27.35	7.64-20.38	12.76	3.35-47.53	20.15	3.35-20.41	10.67	3.35-75.15	25.32
	Biog.Si	39.27-67.49	51.79	25.97-57.78	39.13	15.30-62.66	28.58	12.94-36.45	24.24	5.57-31.20	15.51	9.70-61.56	26.20	0.33-22.85	10.53	0.35-67.49	26.20
	Ex.Ba	1.23-2.61	2.26	0.00-1.24	0.81	0.00-0.95	0.44	0.35-1.12	0.758	0.12-0.87	0.46	0.16-2.49	1.05	0.04-1.16	0.46	0.00-2.61	0.81
	$CaCO_3$	0.98-3.21	1.88	2.35-3.21	2.89	0.71-2.93	1.91	0.50-0.95	0.69	0.50-1.24	0.74	0.23-1.83	1.17	0.36-1.00	0.78	0.23-3.21	1.43
CD 1739	C.Org			33.29-104.10	54.43	9.89-42.29	28.36	7.41-56.20	33.71	6.33-60.77	33.07	10.00-154.94	75.77			6.33-155.0	50.19

Table 10.1

CORES #	FLUX mg-cm^2/kys	STAGE 1 Range	STAGE 1 Mean	STAGE 2 Range	STAGE 2 Mean	STAGE 3 Range	STAGE 3 Mean	STAGE 4 Range	STAGE 4 Mean	STAGE 5 Range	STAGE 5 Mean	STAGE 6 Range	STAGE 6 Mean	STAGE 7 Range	STAGE 7 Mean	AVERAGE Range	AVERAGE Mean
	Biog.Si	-	-	na	na	na	na	na	na	na	na	na	na	na	na	na	na
	Ex.Ba	-	-	0.00-0.20	0.49	0.00-0.29	0.047	0.00-0.29	0.095	0.00-0.26	0.085	0.00-1.59	0.22	-	-	0.00-1.59	0.12
	$CaCO_3$	-	-	0.56-1.24	0.79	0.05-1.24	0.45	0.05-0.79	0.43	0.02-0.79	0.26	0.08-3.83	2.24	-	-	0.02-3.8	1.12
CD 1738	C.Org	-	-	62.43-96.06	78.26	12.34-96.06	27.58	4.84-24.58	15.70	3.25-57.90	21.72	11.13-59.16	28.18	-	-	3.25-96.06	27.94
	Biog.Si	-	-	na	na	na	na	na	na	na	na	na	na	na	na	na	na
	Ex.Ba	-	-	0.00-1.71	0.428	0.00-0.57	0.053	0.00-0.05	0.012	0.00-0.020	0.00	-	-	-	-	0.00-1.71	0.05
	$CaCO_3$	-	-	0.52-1.38	0.975	0.55-1.64	0.91	0.42-1.45	1.03	0.22-1.98	1.32	0.65-4.03	1.47	-	-	0.22-4.03	1.21
ODP 722B	C.Org	na	na	na	na	na	na	na	na	na	na	na	na	na	na	na	na
	Biog.Si	na	na	na	na	na	na	na	na	na	na	na	na	na	na	na	na
	Ex.Ba	2.76-7.23	5.79	1.15-2.91	2.1	0.68-2.89	1.76	2.11-3.08	2.52	0.63-8.41	2.14	0.58-5.16	2.13	1.01-3.60	2.32	0.58-8.41	2.21
	$CaCO_3$	3.98-5.23	4.70	3.50-5.72	4.6	2.49-3.50	2.97	0.69-2.35	1.25	1.35-4.40	2.49	1.81-4.79	3.45	1.81-4.09	3.12	1.3-5.72	3.25

*na not analysed.

*ODP 722 (unpublished data, Shimmield).

stages (ie. 3 and 5), although an overall increase in trend is discernable (Fig. 10.1a), very low values in flux of C.org have been noticed in the lower parts of these stages, while the upper parts show high C.org fluxes, especially in cores CD 1715 and CD 1730. In cores located towards the Gulf of Oman (CD 1739 and CD 1738) slightly different patterns are observed. The trends in the latter stages correspond to those seen in cores CD 1715 and CD 1730, but towards the bottom of the cores (Stages 5 and 6) the trends in carbon are very different from CD 1715 and CD 1730.

Since the C.org flux is primarily a measure of productivity, the varying flux within and between cores is implying changes in fertility of the overlying water. The $\delta^{13}C$, $\delta^{15}N$ isotopic data of core CD 1730 (chapter 7) has confirmed that organic matter in the NW Arabian Sea is predominantly marine in origin. Even in glacial Stage 2, ie. 18,000 years BP, when aeolian input was at a maximum (chapter 9) $\delta^{13}C$ values, ie. -21.0, suggest that terrestrial organic input in the NW Arabian Sea sediments was insignificant. Similarly the C/N profile (Fig. 7.1) supports the view that marine organic matter has been dominant throughout the last 250,000 years. Thus it is apparent that C.org flux variations in the cores broadly indicates relative changes in biological productivity between glacial and interglacial stages. Recently, sediment trap data has shown that C.org flux is high during the SW monsoon (Nair et al., 1989). Thus it can be envisaged that the increasing C.org flux during interglacial stages is associated with enhanced upwelling resulting from stronger SW monsoon winds (Prell, 1984). However, the decreased flux at lower stages 3, 5 may be related to other factors affecting the environment of deposition and will be discussed later.

10.3 CALCITE FLUX

The calcite flux records are shown in Fig. 10.2 and it can be seen that they broadly follow the trends of C.org fluxes, especially in CD 1730 (Fig. 10.1). Calcite fluxes tend to show changes between interglacial and glacial stages. The higher carbonate content of Pacific sediments during glacial times has been linked with higher carbonate productivity resulting from increased upwelling (Arrhenius, 1952, 1963; Pederson, 1980). In Atlantic and Pacific Ocean's sediment trap analysis, there is a general correlation between C.organic and calcite fluxes (Fischer, 1983; Dymond and Lyle, 1985; Lyle et al., 1988). Thus any similarity in the trends of C.org flux (Fig. 10.1) and calcite flux (Fig. 10.2) in the NW Arabian sediments may reflect the primary production record. The mean calcite flux of core CD 1715 and CD 1730 is relatively high (ie. 1.30 and 1.4 $g/cm^2/kys$ respectively) and are higher than those seen in cores CD 1738, CD 1739 (~1.20 $g/cm^2/kys$) (Table 10.1). This is probably

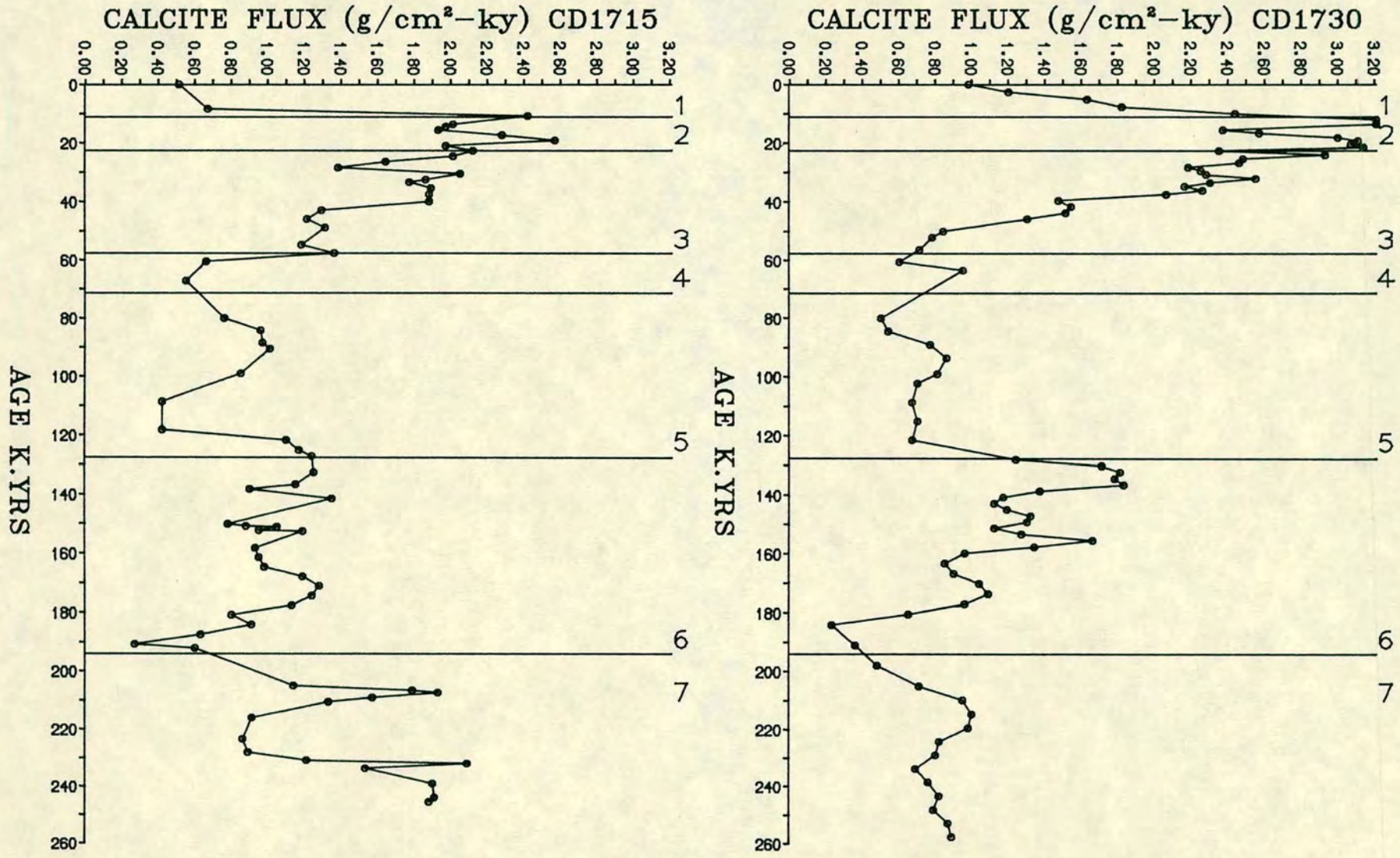

FIGURE 10.2a CALCITE FLUX VARIATIONS DURING GLACIAL AND INTERGLACIAL STAGES IN CORES CD1715 AND CD1730.

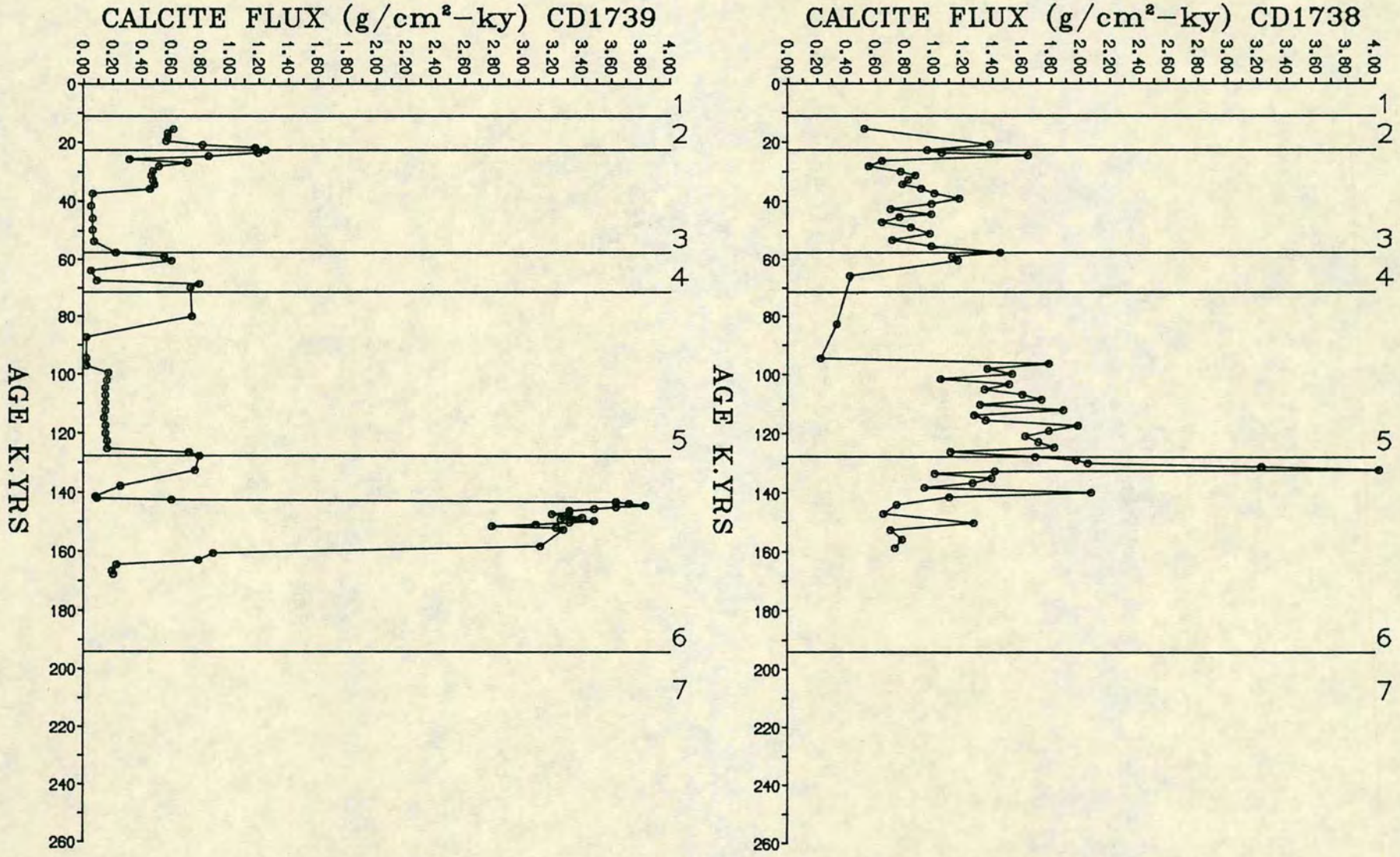

FIGURE 10.2b CALCITE FLUX VARIATIONS DURING GLACIAL AND INTERGLACIAL STAGES IN CORES CD1739 AND CD1738.

due to weaker productivity towards the north. However, the trends of all four cores are similar vertically. From the broad relationship observed between C.org flux and calcite flux, it is clear that calcite flux in the NW Arabian sediments is related in the first instance, to carbonate production in the overlying water.

The vertical changes with time may be a result of either changing biological production or differential dissolution. Prell (1984) noted that foraminiferids are the dominant plankton in the NW Arabian Sea sediments, and during interglacial times of higher upwelling *G. bolloides* is more abundant. Since all the cores occur in deep water, although above the CCD (Kolla et al., 1976), minor dissolution of calcite is likely. This is further evidenced from the ODP core 722 lying on the Owen Ridge (2000 metres water depth, unpublished data, G. Shimmield). This core, where the effects of dissolution are probably minimal, shows a vertical trend of calcite flux similar to the deep sea cores (ie. CD 1715 and CD 1730). Moreover its overall calcite flux is not very much higher than the basin cores, suggesting minimal (10-15%) dissolution of calcite if any. Differences in calcite flux between the cores may relate to productivity changes, rather than dissolution.

In the NW Arabian Sea during periods of high upwelling, ie. the SW monsoon, both fluxes (C.org and calcite) are high (Nair et al., 1989). Similarly, during warm periods, which are characterized by stronger SW monsoon upwelling, a high calcite flux is expected. This is not always seen and the low flux measurements at the lower boundaries of interglacial Stages needs further explanation in addition to possible removal after deposition as suspected from thorium results (Shimmield, pers. comm.). It is possible that many of the anomalous trends in calcite flux may be caused by changes in the total sediment bulk accumulation rates, which are influential in the preservation/dissolution of calcite at the sediment interface.

10.4 BARIUM AND BIOGENIC Si FLUXES

Overall Ex.Ba fluxes shown in Fig. 10.3, tend to follow the trends of C.org flux (Figs. 10.1), but certain distinct negative trends are also observed. This is clearly evidenced in core CD 1730, which shows the highest barium flux in the Holocene and also a substantial flux in the middle of glacial Stage 6; C.org flux shows low trends at these times. Differences are also seen in Stage 3. When these patterns are compared with those of the biog.Si fluxes (Fig. 10.4) a strong correlation is found, suggesting a close affinity in the marine system. However, in core CD 1715, C.org flux and Ba flux patterns show a close similarity to biog.Si fluxes, suggesting that organic carbon is intimately associated with the input of Ba into

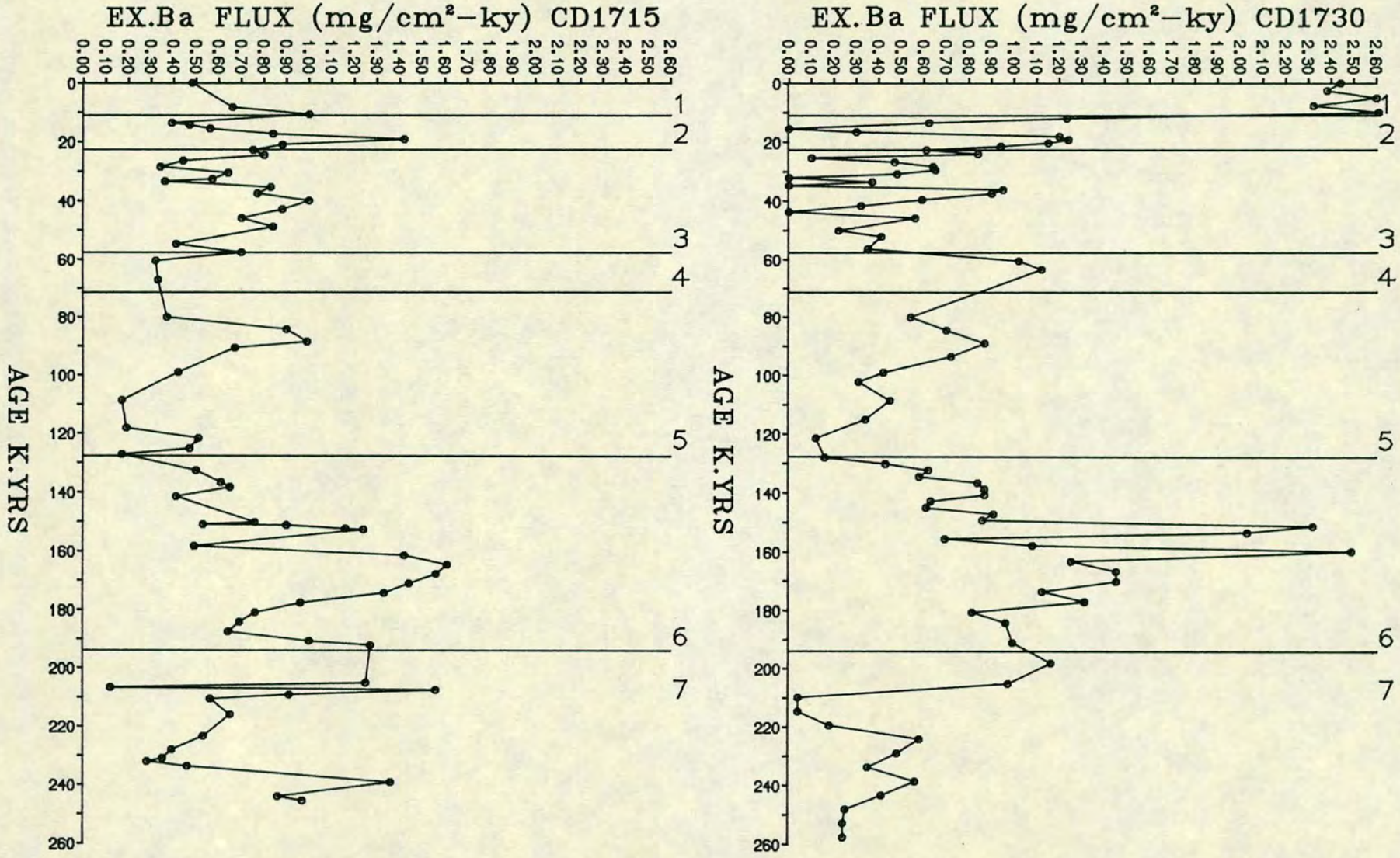

FIGURE 10.3a EXCESS Ba FLUX VARIATIONS DURING GLACIAL AND INTERGLACIAL STAGES IN CORES CD1715 AND CD1730.

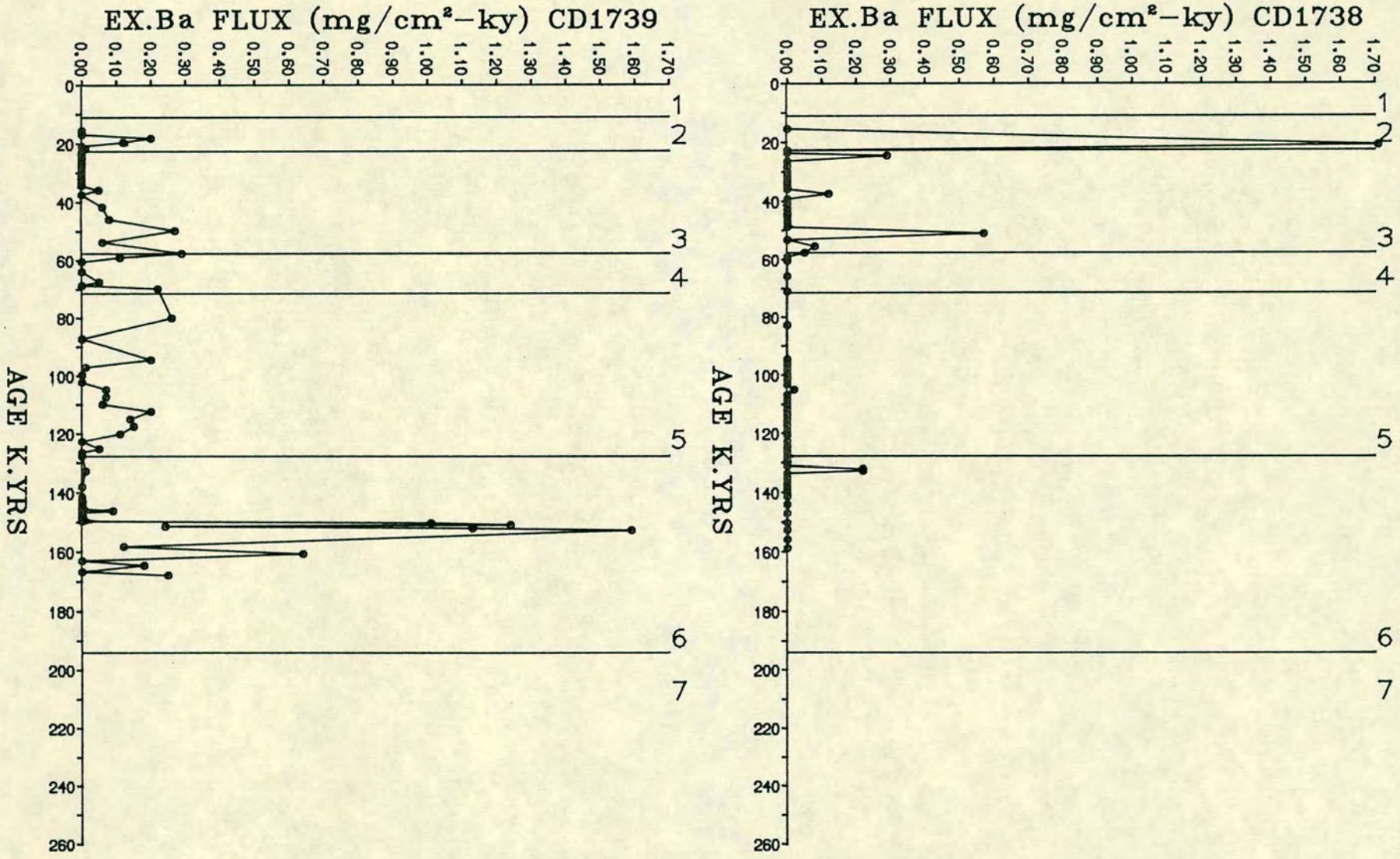

FIGURE 10.3b EXCESS Ba FLUX VARIATIONS DURING GLACIAL AND INTERGLACIAL STAGES IN CORES CD1739 AND CD1738.

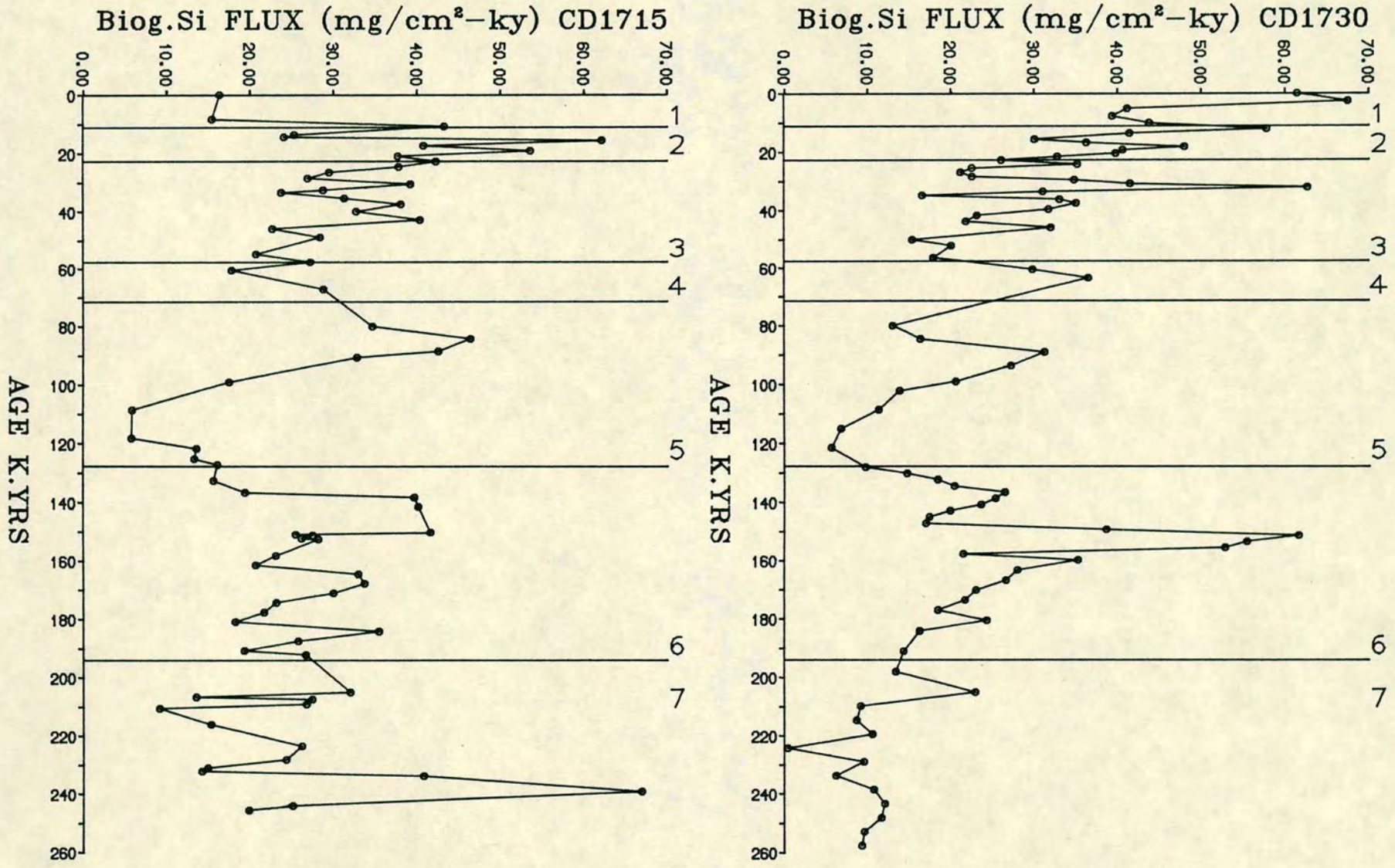

FIGURE 10.4 BIOGENIC SILICA FLUX PROFILES. CORES CD1715 AND CD1730.

sediments. Furthermore, in both cores, Ex.Ba flux is not correlatable with calcite flux (Fig. 10.2) and very different trends are shown in Stage 3 and 5. Since both of these elements are reported to indicate biological processes in the overlying water, and the main occurrence of Ba is related to diatoms (Dehair et al., 1980; Bishop, 1988), their sympathetic patterns in Arabian Sea cores are consistent with these studies. Ex.Ba flux towards the north in cores CD 1739 and CD 1738 is so low as to be hardly significant (Fig. 10.3b), and suggests a considerable decrease in surface biological activity. Even so, isochronous occurrences of Ex.Ba flux in core CD 1739 indicate common episodes of high upwelling in this northern area.

The amplitude of variation of biogenic silica in the two cores CD 1715 and CD 1730 is different, and patterns show an overall disimilarity with that of the calcite flux. Average values of biog.Si flux in these cores are similar (~26 and 28 $mg/cm^2/kys$ respectively), but climatic Stages 1 and 7 show contrasting values (Table 10.1). In the Holocene, (ie. Stage 1) in core CD 1730 (Fig. 10.4) the highest flux is displayed whereas in interglacial Stage 7, a distinct minima is seen. Such differences in the sediments of cores CD 1715 and CD 1730 imply one or more of the following processes have been active; differential production, dissolution, and preservation from erosion.

Ocean waters are known to be undersaturated with respect to silica (Broecker and Peng, 1982), the siliceous shells dissolve in the water column during their fall to the sea floor (Calvert, 1968; Lisitzin, 1972; Berger, 1976; Heath, 1976; Van Bennekom and Berger, 1984). Biog.Si in marine sediments is considered to primarily reflect surface water productivity (Lisitzin, 1972; Molina-Cruz and Price, 1977; Broecker and Peng, 1982; Leinen et al., 1986). In the NW Arabian Sea during the SW monsoon when upwelling is high, the opal flux is considerably higher (Table 10.2). Thus the increasing flux of biogenic silica in interglacial stages suggests a high opal rain rate, which is related to surface water productivity. A very close relationship is observed between C.org flux (Fig. 10.1) and biog.Si flux (Fig. 10.4) profiles, and supports their ultimate link in the overlying waters.

10.5 DIFFERENTIAL PRODUCTION

The relative variation in biog.Si flux and calcite flux down the cores in glacial and interglacial times no doubt indicates differences in primary production rates at different climatic stages (Figs. 10.2, 10.4). Slight differences in the nature of the changes during different climatic stages is probably a result of differential production. For example, the amplitude of biog.Si flux (Fig. 10.4) in Stage 5 and 6

Table 10.2 Biogenic fluxes from sediment trap in the Western Arabian Sea (Nair et al., 1989)

Components <1mm	SW Monsoon $g\ m^{-2}$	NE Monsoon $g\ m^{-2}$
Carbonate	12.10	3.60
Opal	6.08	0.78
C.org	1.18	0.32
N	0.14	0.04

of both cores is greater than calcite flux (Fig. 10.3) whereas calcite flux shows a relatively high amplitude in Stage 3 and Stage 7. This is illustrated when the variation in the ratio of biog.Si flux with respect to calcite flux is recorded in these cores (Fig. 10.5). It is evident here that the Holocene (Stage 1), interglacial Stage 5 and glacial Stage 6 correspond to a high biog.Si/calcite ratio and this possibly implies greater production of diatoms than forams. On the other hand, in interglacial stages 3 and 7, this ratio is suppressed suggesting diatoms are less abundant than forams (calcareous organism).

Moreover, the Ex.Ba and Biog.Si flux (Fig. 10.3 and 10.4) follows the biog.Si/Calcite trend (Fig. 10.5) in a similar manner. Studies have shown the relationship between the distribution of dissolved Si and Ba in the ocean (Chan et al., 1977) and the incorporation of barium in or associated with the skeletons of siliceous plankton (Vinogradora and Kovalskiy, 1962; Brongersma-Sanders, 1967; Li and Chan, 1979; Bischop, 1988). Hence all this evidence suggests that in the Arabian Sea sediments, productivity cycles during interglacial times reflect differential production, not dissolution or dilution.

10.6 ENVIRONMENT OF DEPOSITION

From pronounced upwelling areas like along the Peru Continental Margin, Krissek et al. (1981) have indicated that physical processes such as bottom currents may alter the upwelling signals in sediments. Brockman et al. (1980) have reported that off northern Peru, near-bottom currents are stronger than off central Peru. Krissek et al. (1981) compared the production and preservation of biogenic components in sediments and found that in the northern area the deposition of biogenic fractions was inhibited. Füttener (1981) suspected that off northwest Africa, during upwelling, strong bottom currents prevent the deposition of fine grained material on the shelf. He found that as a result of this potential upwelling, records on shelf sediments are modified. Generally fine grained sediments are found to be rich in opaline silica and organic matter. Workers (Gross et al., 1972; Lisitzin, 1972; Krissek and Scheidegger, 1981) have established a relationship between clay and organic carbon content in marine sediments. Antipathetic trends between C.org and Si/Al and Zr/Al (Figs. 5.2 and 5.12) in this study supports these findings (chapter 6).

In the NW Arabian Sea sediments, warm interglacial stages show relatively low Si/Al and Zr/Al (Table 5.1) (Figs. 5.2 and 5.12). Since Si and Zr in sediments reflect coarser grained sediment, the low Si/Al and Zr/Al ratios suggest fine-grained

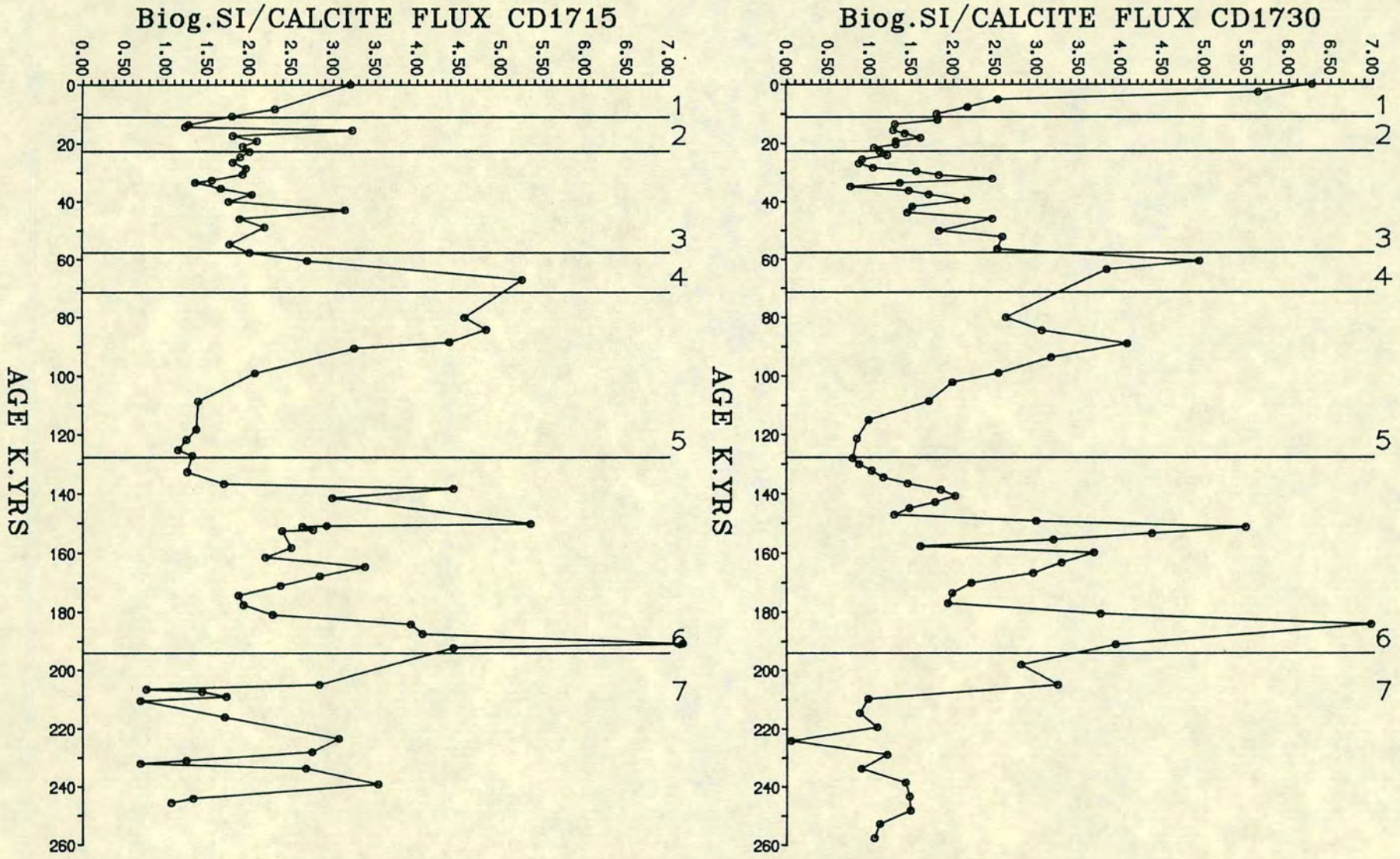

FIGURE 10.5 Biog.Si/CALCITE FLUX PROFILES. CORES CD1715 AND CD1730.

sediments. The ubiquitous low trends seen in both biogenic fluxes (Figs. 10.3 and 10.4) and lithogenic fluxes (Figs. 8.4 and 8.8) at the lower boundaries of interglacial Stages 5 and 7 are difficult to interpret unless erosion is involved.

The association of fine clays and a higher biogenic input may provide a clue to the understanding of the mechanism of removal by strong currents as found in other upwelling areas. Shimmield's unpublished data (1988) on thorium accumulation rates in core CD 1730, suggests that during early interglacial stages, unknown environmental conditions at or after the time of deposition have destroyed the upwelling signatures carried by individual components in the four cores. His data of core CD 1730 shows that isotopic Stages 3, 5, and 7, especially their lower parts, show negative accumulation of thorium in deep sea sediments (Fig. 9.12) and therefore bottom currents may have winnowed away the fine sediments containing the Th and upwelling indicators. This will be discussed further below.

10.7 PALEOPRODUCTIVITY

In the NW Arabian Sea sediments the variation of biogenic fluxes is likely to be associated with upwelling during interglacial times. Since upwelling along the Arabian coast is linked with the strong SW monsoon during warm interglacial periods (Prell, 1984), nutrient rich water will be brought to the surface enhancing the primary productivity and subsequently resulting in a higher organic input to the underlying sediments. Nair et al. (1989) have shown that organic flux from sediment traps is higher during the SW monsoon than the NE monsoon (Table 10.2). Muller and Suess (1981) used the C.org content of marine sediments to estimate variation in the paleoproductivity of water. A similar approach is used here to assess the variation in paleoproductivity using their empirical relation given below:-

$$R = \frac{C.Ps(1-\emptyset)}{0.003.S^{0.3}}$$

R = Paleoproductivity in gC m^2/y
C = Organic carbon content (% dry wt)
Ps = dry densities of solid = ($2.7g/cm^3$)
Ø = Porosity
S = Sedimentation rates = (cm/kys)

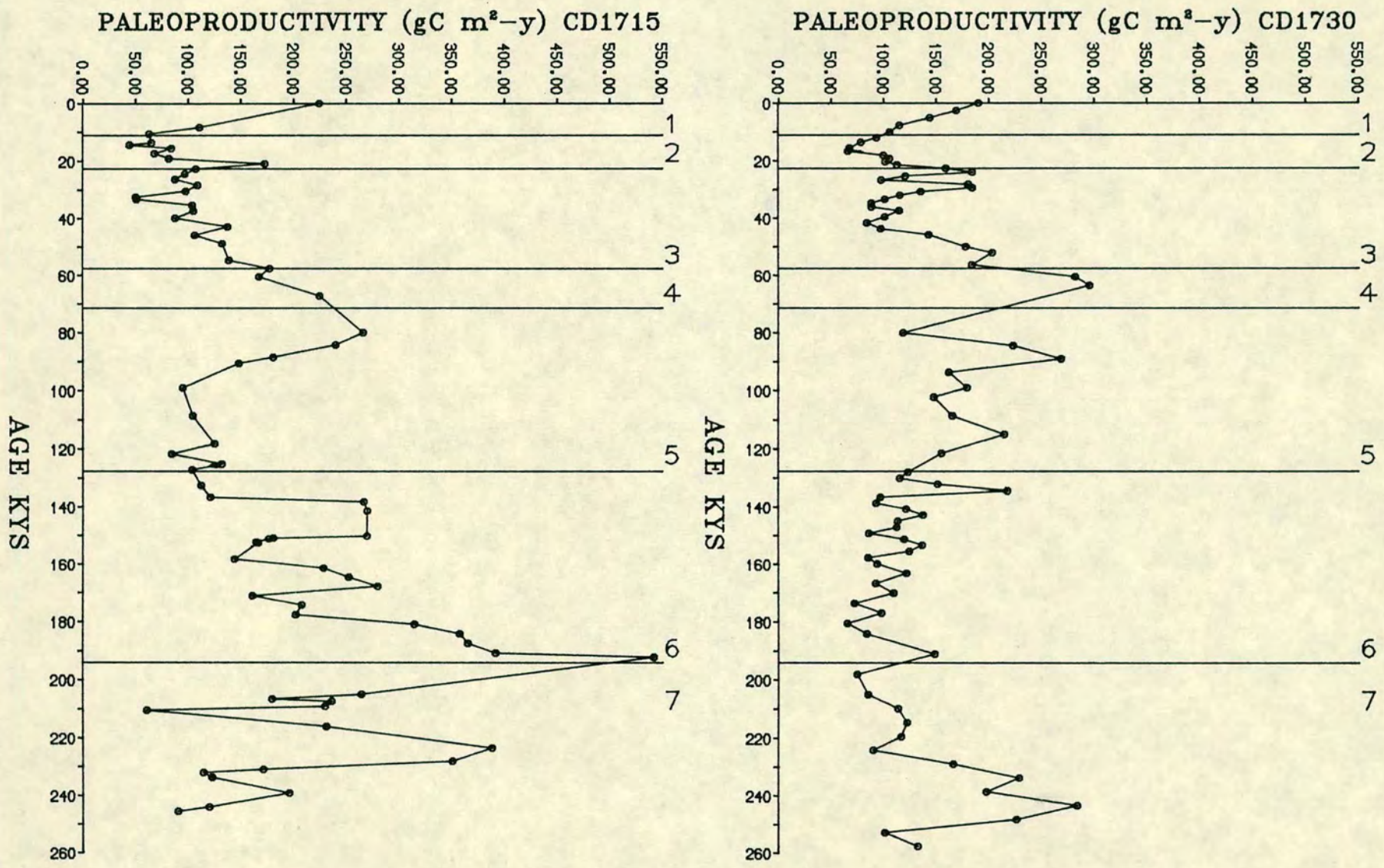

FIGURE 10.6a PALEOPRODUCTIVITY VARIATIONS IN GLACIAL AND INTERGLACIAL STAGES OF CORES CD1715 AND CD1730.

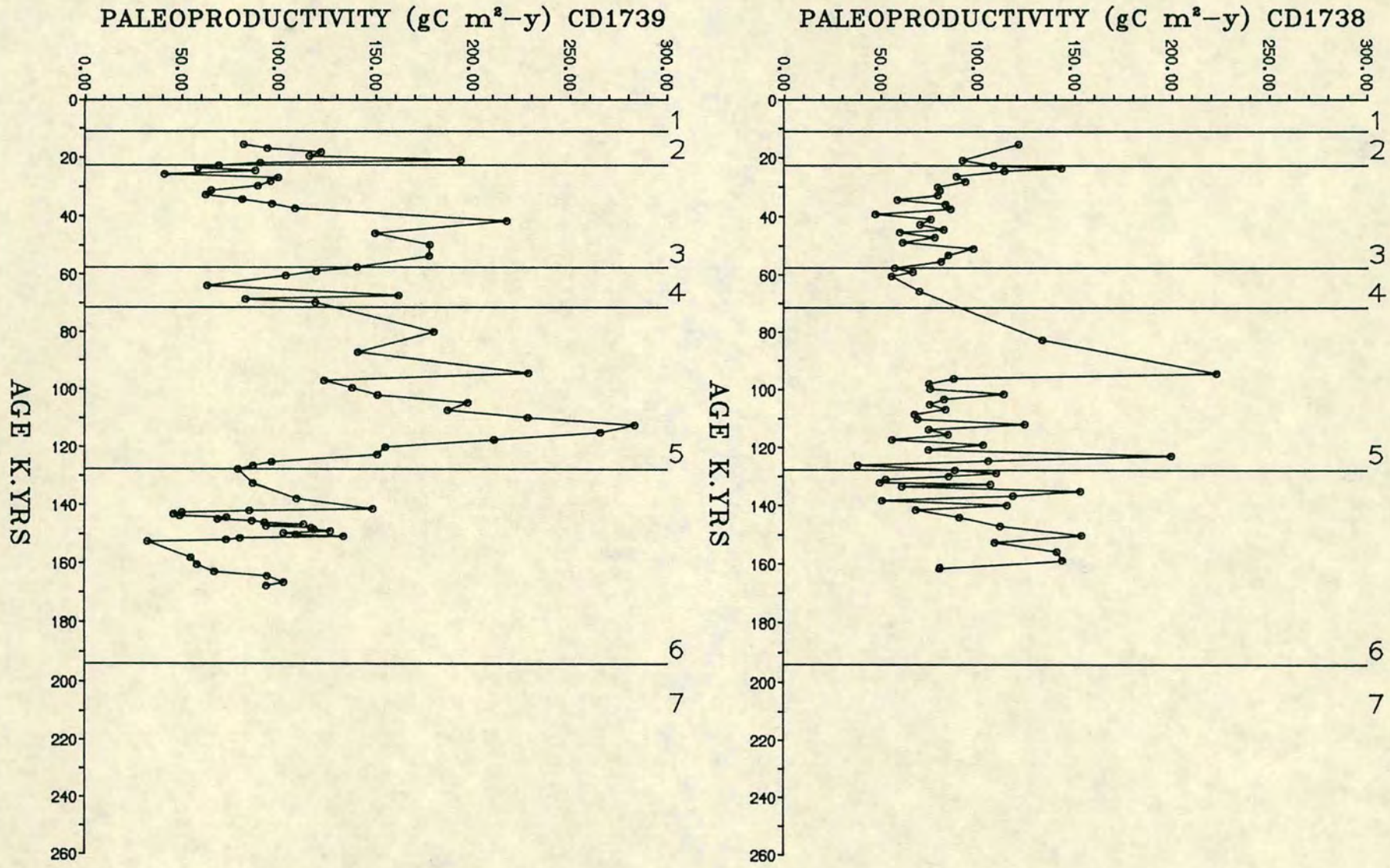

FIGURE 10.6b PALEOPRODUCTIVITY VARIATIONS IN GLACIAL AND INTERGLACIAL STAGES OF CORES CD1739 AND CD1738.

Paleoproductivity data is listed in appendix C.17 and changing patterns with time are shown in Fig. 10.6. Despite the fact that there are certain limitations in quantifying paleoproductivities using this equation (Muller and Suess, 1979), in four cores the patterns of variation (Fig. 10.6) suggest the regional isochronous occurrence of upwelling events.

Cores CD 1715 and CD 1730 show relatively high productivity ie. > 100gC m^2/y, while towards the north in cores CD 1739 and CD 1738, productivity values are low (ie. <100gC m^2/y). It has been noticed that paleoproductivity (Fig. 10.6) in Holocene (Stage 1) and interglacial stages tends to increase whereas glacial stages show a decline in paleoproductivity. A coherent pattern is observed in biogenic fluxes (Fig. 10.1 to 10.4) which tends to support evidence that high upwelling in the NW Arabian Sea occurred in interglacial times. Generally, the biogenic fluxes of biog.Si and Ba and especially the biog.Si/calcite ratio closely follow the trends of paleoproductivity down the cores. However, certain inconsistencies are observed, for example in core CD 1730 the Stage 6 paleoproductivity value is low (ie. 100gC m^2/y) but the relative amplitudes of biog.Si and Ex.Ba fluxes and biog.Si/calcite ratios are high. This lack of correspondence may be a result of rapid preservation due to high sedimentation rates in this stage. C.org flux, which is also a function of sedimentation rates, does not follow the biog.Si and Ex.Ba profile (Fig. 10.1) at this time. This is probably a result of the loss of C.org contents by oxidation/erosion at the sediment/water interface during Stage 6, and low contents of C.org thereby producing low values of paleoproductivity. The low paleoproductivity estimated in northern cores, especially in a core from the Gulf of Oman (< 100gC m^2/y) is consistent with the low biomarker fluxes and productivity patterns in interglacial and glacial stages.

Overall, from these profiles (Fig. 10.1 to 10.6), it is evident that interglacial periods witnessed higher productivity than glacial stages, and confirms Prell (1984). However, the relative production of different organisms appears to differ (Fig. 10.5).

10.8 EROSION OF BIOGENIC FLUXES

Global oxygen isotope records (Imbrie et al., 1984) and $\delta^{18}O$ records from core RC-2761 (Fig. 3.6) show that greater changes in oceanic oxygen isotope record occurred in the Holocene and the beginning of the last interglacial stage. Oxygen isotope records spanning the last 500 k.years indicate that the ice volume was similar to that of today during the early interglacial Stage 5 (Emiliani, 1972; Shackleton and

Opdyke, 1973; Hays et al., 1976). Hence, the last equivalent predecessor to the present interglacial was the isotopic substage 5e, which correlates with the Emian interglacial on the continent (Mangerud et al., 1979). The Emian interglacial lasted only for 10,000 years from 125 to 115 k.years BP. Most low and mid-latitude oceanic areas then experienced climatic conditions similar to the present day (Cline and Hays, 1976). However, in this north Arabian Sea study the biogenic signals recorded in early last interglacial and present Holocene Stage 1 differ in intensity. Records of biomarkers and their flux values in the Holocene (Stage 1) appear to be high, and consistent with the trends of $\delta^{18}O$ records, while the flux values between 125,000 and 110,000 years BP are anomalously low and are lower than observed in the upper Stage 5 or even Stage 4. Since the accumulation of biogenic elements in the North Arabian Sea sediments should generally be associated with the strength of the SW monsoon upwelling, which in turn coincide with the intensity of the interglacial stages, one should expect similar biogenic fluxes in the Holocene and the early Stage 5 interval.

Excess Ba fluxes measured by G.B. Shimmield in the ODP core 722 (16°37.31'N, 59°47.75'E. Water depth 2000m) tend to show a very different profile both in terms of magnitude of flux and vertical distribution (Fig. 10.7). Flux values at some periods are up to an order of magnitude higher than equivalent time horizons in cores CD 1715 and CD 1730 (Fig. 10.3a), particularly during interglacial events. Furthermore, besides the Holocene, a marked increase in flux occurs at or near the base of Stage 5 as well as a more modest increase at the base of Stage 6 and interglacial Stage 3 (Fig. 10.7). Given the more proximal position of this core (ODP 722) relative to the South Arabian shelf, it is possible that the higher overall fluxes may be due to more productive waters. Even so, the difference in geographical position alone is probably not sufficient to explain the discrepancies of flux intensities at certain time intervals, especially near the base of the last interglacial ie. 125,000 years BP.

The relatively elevated position of ODP core 722 (2000m) when compared to cores CD 1715 (4000m) and CD 1730 (3580m) suggests that a higher percentage of Ba production in surface waters will survive fallout dissolution to accumulate within the sediments. Again, while such an explanation could partly account for the higher burial flux of Ba in ODP core 722, it is difficult to explain the contrast in amplitude changes between the cores, especially during interglacial events.

Within the account of lithogenic fluxes it was suggested that periods of active erosion had occurred during the time periods of accumulation of the sediments. As core CD 1715 and CD 1730 lie on the basin floor close to the Owen Ridge, it is possible that intermittent currents on the seafloor have occurred and were of

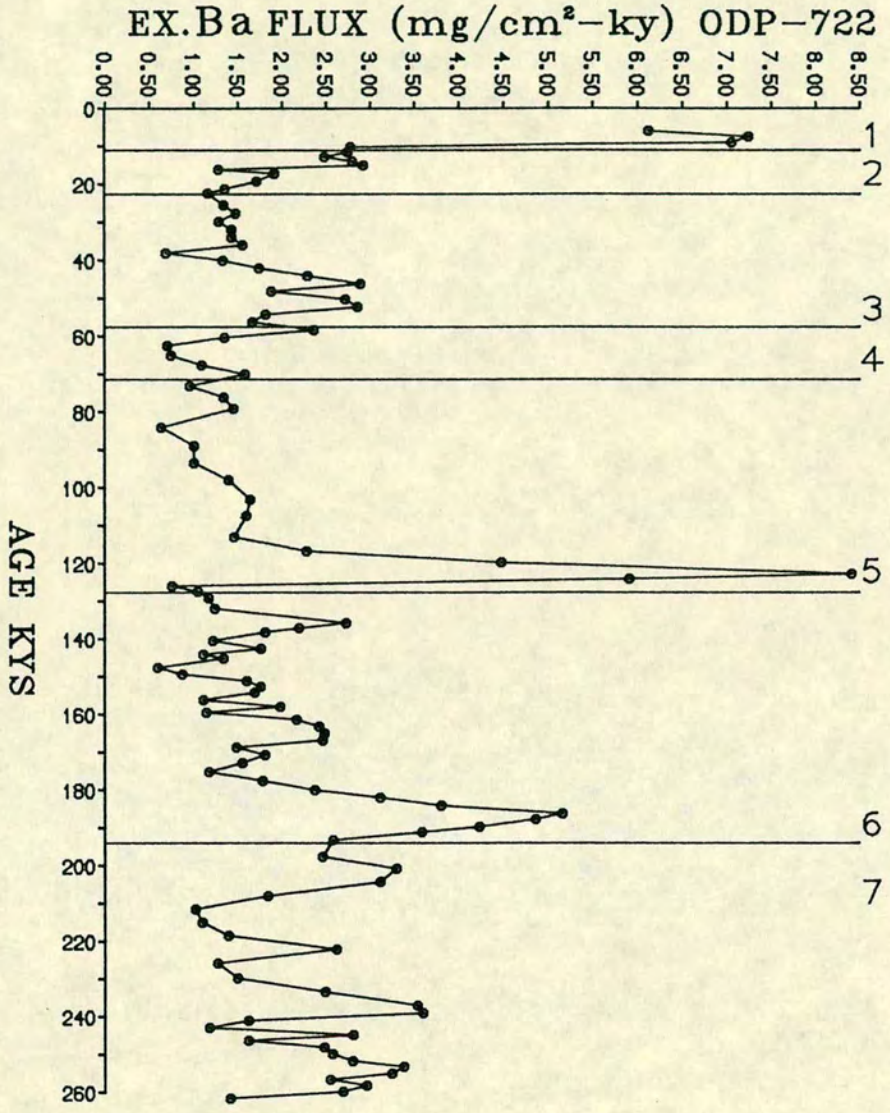

FIGURE 10.7 EXCESS Ba FLUX PROFILE . CORE ODP-722. (UNPUBLISHED DATA G B SHIMMIELD).

sufficient strength to erode surface sediment layer. Core ODP 722 lying at some 1500 metres above the basin floor is not likely to have been subjected to this erosion. The sediments on the Owen Ridge do not appear to have been subjected to disturbance. This is supported by the oxygen isotope stratigraphy of core RC-2761 (Fig. 2.6 Lat. 16°38′N, Long. 59°52′E) which tends to confirm that the history of production, noted by the accumulation of biomarkers, especially Ba, is a true reflection of upwelling activity here over the past 250 kyrs. It follows, therefore, that the difference between the Ba flux record of cores CD 1715 and CD 1730 and that of ODP-722, is due to some erosion factor within the former sediments. Assuming that there has been a constant difference in biological productivity between the two sites over the past 250,000 years, an attempt has been made to identify periods of erosion from the differences in their Ba fluxes. This has been expressed as the percentage loss of excess Ba flux in core CD 1730, ie.

$$\% \text{ loss of } Ex.Ba_F(CD\ 1730) = \frac{Ex.Ba_F(722) - Ex.Ba_F(1730)}{Ex.Ba_F(722)} \times 100$$

$Ex.Ba_F$ = Excess Ba Flux in $mg\text{-}cm^2/kys$

The profile of this loss is shown in Fig. 10.8. Although it expresses erosion in crude terms and must be considered tentative, the greatest loss of Ex.Ba in core CD 1730 occurs at the lower section of Stage 3, Stage 5 and Stage 7. Included in Fig. 10.8 is the record of ^{230}Th accumulation (Shimmield, unpublished data). The thorium profile shows a deficiency in Th input to the sediments at these times, even though there is no reason to assume it is not produced in the waters above. The broad similarity of this thorium and barium loss, especially for sediments from the bottom of Stage 3, supporting the concept of erosion affecting the North Arabian Sea sediments during interglacial periods. The lack of similarity between ^{230}Th accumulation and Ba loss in Stages 1 and 2 is unexplained.

The fact that erosion is more in evidence during the onset of interglacial events is expected in that ice retreat in the North Atlantic and Antarctic could promote high latitude sinking of surface waters, inducing a more rigorous bottom water transport (Duplessy and Shackleton, 1985; Boyle and Keigwin, 1985; Corliss et al., 1986). Deep water of Antarctic origin in the North Arabian Sea has been described in chapter 1. It would appear that the velocity of transport of this water was sufficient in interglacial times to effect erosion of at least the finer grain size material of the sediments, leaving an impoverished biomarker accumulation and an

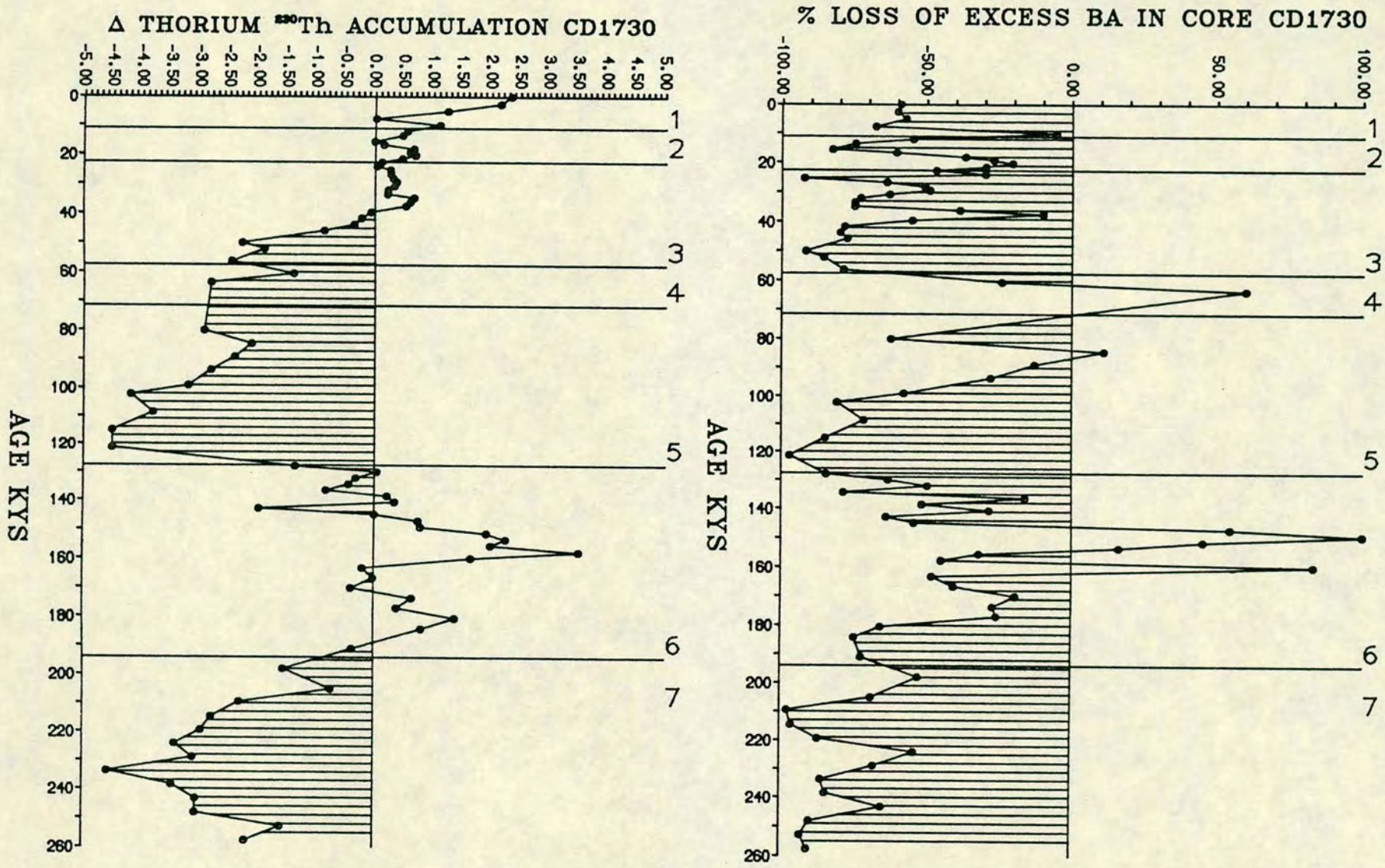

FIGURE 10.8 Δ THORIUM ACCUMULATION AND % LOSSES OF EXCESS Ba IN CORE CD1730.

increased Si(lith)/Al ratio (Fig. 5.2) in the sediments. It would appear that for some of the glacial intervals eg. Stage 4, possibly Stage 2 and the middle part of Stage 6, bottom circulation was non-existant or at least of insufficient velocity to transport much sediment.

CHAPTER 11

SUMMARY AND CONCLUSIONS

SUMMARY AND CONCLUSIONS

Spatial and temporal studies of mineralogical and geochemical changes in sediments of four cores from the north Arabian Sea were undertaken in this thesis. The two suites of piston cores show variable age and sedimentary history. Cores in the south collected in oceanic depths off the Southern Arabian coast extending to 250,000 years BP include CD 1715 and CD 1730 while northern cores collected nearer to the Gulf of Oman and designated as CD 1738 and CD 1739 record a period of accumulation extending to 150,000 years BP.

The oxygen isotope and carbonate records of core RC-2761 supplied by Prell, provide a chronostratigraphic framework for correlation and dating of the four cores investigated in this study. These cores were analysed for their $CaCO_3$ contents, and the carbonate variation is considered to be reliable for a tentative chronostratigraphy to be established. However, in the northern cores ie. CD 1738 and CD 1739, Holocene ie. Stage 1, is not shown because of poor recovery of cores. Cores CD 1715 and CD 1730 extend without major sediment disruption to isotope Stage 7 ~250 kys and cores CD 1738 and CD 1739 have been dated to the base of Stage 5 (120 kys). This age model has been employed to decipher the changing climatic patterns, despite certain limitations, for the last 250,000 years BP.

The study area lies under the influence of both seasonal upwelling, a result of SW monsoon winds, as well as variable dust loads carried by north westerly winds from the neighbouring deserts of Arabia, Mesopotamia and Iran-Makran. Characteristic effects of both atmospheric and oceanic circulation on the mineralogy and chemistry of the northern Arabian Sea sediments are summarised here.

(1) Each core was sampled at 10cm intervals and also at depths where sediments were of an unusual nature, and were optically examined and analysed for mineralogical and geochemical variations. Except for core CD 1715, the cores are essentially free of turbidite layers that are concentrated in the upper and lowest parts of the core. These were sampled separately for a chemical study. The southern cores comprise pale grey and greyish green sediments with some evidence of brownish surfaces. The near surface sediments were collected only in core CD 1730. Occasional green bands occur which contain an abundance of faecal pellets. One of these bands in CD 1730 was identified as an ash band (71 kys). Optical examination of the sediments show an abundance of planktonic and benthic foraminiferids and coccolithoporids, and minor amounts of diatom debris. SEM examination of quartz

shows pitting of rounded grains probably due to aeolian attrition. The dolomite is also detrital and is comprised of weathered grains; only rarely does it occur as subhedral rhombs.

Mineralogical studies by XRD have relied on the peak intensity variations of mineral pairs. However, a more quantitative procedure has been adopted for dolomite analysis and was found to be reliable for dolomite contents in excess of 5% of the sediments. Semiquantitative study of the variation of mineralogy by XRD, has shown that the sediments comprise quartz, dolomite, chlorite, illite, feldspar with minor montmorillonite-illite mixed clays. Towards the Gulf of Oman, the mineralogy of the sediments differ from those in the south in that they show a higher chlorite content in respect to quartz, and feldspar is very low compared to quartz. The cores CD 1715 and CD 1730, are relatively impoverished in quartz and chlorite, but contain more feldspar than cores to the north. From such changes, an attempt has been made to identify the sources of supply. However, down core changes in mineralogy are very variable and it is difficult to identify the changes in source during glacial and interglacial stages.

(2) The chemical analysis of the major elements Si, Al, Fe, Ca, Mg, K, Ti, P and minor elements Sr, Cr, V, Mn, Ni, Cu, Zn, Br, I, Rb, Y, Zr, Ba, La, Ce, Nd were conducted using XRF techniques. The sediments were also analysed for C.org, Nitrogen, $\delta^{13}C$, $\delta^{15}N$ and biogenic silica. These elements are considered in terms of lithogenic and biogenic inputs.

(a) The geochemistry of Si (biogenic free) Fe and K and their relationships to Al have been used to understand the areal and temporal changes of the lithogenous constituents. Their variation relative to Al show covariations with the peak ratios of quartz/feldspar, quartz/chlorite, quartz/illite, chlorite/feldspar. These indicate textural changes as well as variations in aeolian mineralogical input from different sources. Cores in the north are relatively coarser grained than in the south as shown by higher Si/Al ratios, and they also show higher Fe/Al ratios which implies relatively more chlorite relative to other clay minerals. The ratios of element relations to Al is also variable in the different climatic stages. The values of Si/Al and K/Al ratios tend to increase in glacial stages (2, 4 and 6) while low values occur in interglacial stages.

(b) Only Ti, Cr and Zr as minor elements can be used to indicate the provenance of the sediments. Zr is considered to have been introduced from a uniform aeolian source and Zr/Al ratios remain essentially constant over the periods of sediment accumulation. Cr content and Cr/Al ratios are unusually high compared with other oceanic sediments and are thought to have been introduced from local ophiolite sources from the Arabian coast. Ti also shows, as Ti/Al ratio, somewhat higher values than normal oceanic sediments. The spatial and temporal trends of Ti/Al ratios, follows Zr/Al and suggest input from a uniform source. The geochemistry of REEs in the NW Arabian Sea sediments suggests that clay mineral and feldspar content are important in influencing their distribution. The higher La/Ce, Nd/Ce ratios in cores towards the north indicate that in these cores clay minerals are different from southern cores.

(3) The geochemistry of the biogenic constituents calcite, organic carbon, biogenic silica and associated minor elements have been investigated. Positive correlations between carbon organic, aluminosilicate free excess Ba and biogenic silica contents in the southern cores (CD 1715 and CD 1730) indicate a genetic relationship. The contents of these biomarkers are higher in cores CD 1715 and CD 1730 and decrease northwards to cores CD 1738 and CD 1739. Excess Ba contents in the latter cores occur only as traces suggesting that organic productivity inducing $BaSO_4$ precipitation in seawater at these sites was minimal. The higher biogenic contents in cores CD 1715 and CD 1730 are due to their location, that is beneath an area of intense upwelling, a result of SW monsoon which brings nutrients to the surface and subsequently enhances the primary production. Excess Ba contents and excess metals (Ni, Cu, Zn) content, over that held in aluminosilicates, follow organic carbon trends and suggest their causal relationship developed by sorption processes within the sediments.

The changing patterns of all these biomarkers in cold and warm periods are such that during the Holocene (Stage 1), interglacial Stages 3, 5 and 7, they tend to show increasing trends while in glacial Stages (2, 4, and 6) a decrease is noticed. The Holocene (Stage 1) shows the highest content of biomarkers. Profiles of biomarkers when compared with either Si(lith)/Al or K/Al ratios, display an antipathetic trend suggesting an enrichment in finer grain size sediments. The lower boundaries of interglacial stages (3 and 5) tend to show low contents of calcite, organic carbon, excess Ba and biogenic silica. A synchronous increase in Si(lith)/Al and K/Al ratio at these horizons suggests the mechanical removal of fines which consequently resulted in lag sediments containing more quartz and feldspar.

(4) In addition to C/N, the stable isotope analysis of organic carbon and nitrogen in core CD 1730 confirms that most of the organic matter is marine and probably of planktonic origin. The $\delta^{13}C$ values (ie. -19.0 to -21.0) and $\delta^{15}N$ (+7 to +13 are very close to that of marine plankton reported elsewhere, and the changes in $\delta^{15}N$ during glacial/interglacial stages suggest a relative change in productivity with time. During glacial times (Stages 2, 4 and 6), the isotopic values of $\delta^{13}C$ and $\delta^{15}N$ do not indicate enhanced terrigenous organic matter.

(5) The geochemistry of the halides I, Br has been investigated and related to the contents of C.organic, Nitrogen. The I/C.org ratios of sediments in the four cores are intermediate between those of oxic and anoxic sediments. However I/C.org ratios suggest that the Arabian Sea basin has been oxic throughout the last 250,000 years BP. In this oxidising environment, there appears to have been an uptake of I at the sediment/water interface by plankton seston and this accounts for the higher I/C.org ratio than is normally found in plankton. I/Br ratios do not show obvious trends except for an overall fall signifying a preferential loss of I relative to Br during burial diagenesis. The I/C.org ratios generally show contrasting changes in glacial and interglacial stages, similar to that of organic carbon. Ratios of I/C.org and Br/C.org tend to decrease in glacial and increase in interglacial stages in a fashion similar to that seen in profiles of biogenic elements. I/N, though generally follows organic carbon and I/C.org profiles, a dissimilarity seen particularly in Stage 6 (core CD 1730), probably indicating either NH_4^+ absorption on clays or different organic material. Since halogens are biophilic in nature (Vinogradov, 1953; Goldschmidt, 1954), their higher absolute contents and high ratios to C.org in interglacial stages thereby suggests a complex relationship with increased biological productivity and fallout on to the seabed. However, in cores CD 1738 and CD 1739 from the Gulf of Oman, a high halogens/C.org ratio is most likely a result of high sedimentation rates, and lower levels of diagenetic modification of halogens relative to carbon.

(6) Sedimentation rates show a steady increase from the south in cores CD 1715 and CD 1730 to the north in cores CD 1739 and CD 1738. Highest sedimentation rates occur in core CD 1738 from the Gulf of Oman. Major lithogenic fluxes changes down cores (spatial and temporal) of quartz, dolomite, aluminium, zirconium and titanium all show a significant variation and suggest they are linked to both climatic changes and closeness of their source. A marked gradient in overall lithogenic fluxes is seen from north to south, average flux values are four times higher in northern cores (ie. CD 1739 and CD 1738) than in southern cores ie.

CD 1715 and CD 1730. This trend is persistent throughout the climatic history of the last 250,000 years. A north-south change in lithogenic fluxes implies a source in the north and northwest. Northwesterly winds originate from surrounding deserts of Arabia, Mesopotamia, Iran-Makran and transport their dust loads towards the northern Arabian Sea. This study confirms early findings (Sirocko and Sarnthein, 1988) for Holocene sediments that the northern Arabian Sea is a major sink of northwesterly dusts.

(7) Lithogenic flux changes in glacial and interglacial stages indicate a pronounced influence of climatic patterns of neighbouring landmasses. Average values of quartz, aluminium, dolomite, zirconium and titanium fluxes are higher in glacial stages than in interglacial stages. The detrital flux changes of core RC-2761 on the Owen Ridge also indicates an increased lithogenic flux during glacial episodes. Holocene and interglacial stages 3, 5, 6 indicate low values of lithogenic flux, implying that during these times climate was relatively wet and atmospheric circulation was less intensified. A short period from ~41,000 to 23,000 years BP before the inception of last glacial maximum, shows low lithogenic fluxes. This implies a humid period and this trend supports other published evidence on continents.

In contrast, glacial times typify very dry continental conditions and higher lithogenic fluxes in Stages 2, 4, 6 are related to an enhanced atmospheric circulation. The highest lithogenic fluxes in Stage 2 (18,000 years BP) confirms the severity of global climate. During the last glacial maximum desertification of major land areas including the surrounding continents was at a maximum (Sarnthein, 1978). Glacial Stages 4 and 6 show lower values of lithogenic flux than in glacial Stage 2, suggesting the climatic conditions were relatively milder than in glacial stage 2.

(8) Biogenic fluxes of calcite, organic carbon, Excess Ba and biogenic silica have been measured. They all show decreasing values towards the north in cores CD 1739 and CD 1738. The higher fluxes in cores CD 1715 and CD 1730 provide evidence that productivity is more intense in the south. From the contrasting values of lithogenic and biogenic fluxes it seems that whereas in the north atmospheric fallout is important, the southern cores ie. CD 1715 and CD 1730 show greater effects of seasonal upwelling. Down core temporal variations of biogenic flux show higher values in the Holocene and other interglacials. The lower values at the lower boundaries of Stage 3, 5 and in interglacial Stage 7, are ambiguous. Generally, the higher trends in Holocene and upper parts of interglacial stages coincide with increased SW monsoonal upwelling and in fact reflect the higher biological

productivity during these times. The positive correlation of organic carbon, biogenic silica and Excess Ba flux is an evidence of their genetic relationship in the euphotic zone. The calcite flux broadly follows that of organic carbon, which in turn is similar to the biogenic silica profiles. The greatly reduced fluxes of biogenic elements in early interglacial stages ie. 3, 5 and in 7, indicate anomalously low values which may be caused by bottom current erosion. This is seen from a comparison of excess Ba flux in ODP core 722 taken from a ridge (2000m) where erosion from water currents is unlikely. A productivity record as depicted by excess Ba flux in this core shows high measurements at stage boundaries 3/4, 5/6 and 6/7. In deep sea cores they are low. These features together with thorium results (Shimmield, unpublished data) and calculation of the percentage loss of excess Ba in core CD 1730 indicate a substantial removal of sediments involving biomarkers and Th in Stages 5 and 7, possibly due to strong bottom currents.

APPENDICES

APPENDIX A

ANALYTICAL METHODS

A.1 XRD SAMPLE PREPARATION

For X-ray diffraction study the sediment samples were dried and disaggregated in a mortar. The carbonate content of the sediments was removed by attacking the samples with 3M HCL.

Slurry of bulk samples and carbonate free sediments was prepared by mixing with acetone. The oriented slides of both bulk samples and acid digested fraction of the sediments were made by pipetting the dispersed slurry on to glass slides. Slides were dried at room temperature and then subjected to X-ray diffraction.

A.1.1 X-Ray Diffraction Method

Mineral identification work was done on a Philips PW 1011/1050 diffractometer under the following conditions:

Cu k α radiation line source; Ni filter; 40 kV; 20 Ma.

The bulk samples and carbonate free samples both were scanned at 1°2Θ/min scanning speed; CPS 4 x 10^2; 0.1mm detector slit; 5 x 120m/hr chart speed giving 1°2Θ/min on chart.

As no attempt was made to identify mixed-layer species, the unglycolated slides were scanned. All carbonate free samples were scanned from 5°2Θ-30°2Θ while bulk samples slides were scanned from 24°-30°2Θ. The minerals were identified by their characteristics 2Θ values and peak intensities were measured.

A.2 X-RAY FLUORESCENCE SPECTROMETRY

A.2.1 Major Elements

Major elements (Si, Al, Fe, Mg, Ca, K, Ti, Mn, P) were analysed using X-ray fluorescence spectrometry on a Philips PW 1450 sequential automatic X-ray spectrometer. Fused, 45mm diameter glass discs were prepared by a method similar to that of Norrish and Hutton (1969). About 10g of sediment sample was ground in a Tema tungsten carbide mill and dried at 60°C. Approximately 0.8-1.0g of the ground sample was accurately weighed into a platinum crucible. An ultra-pure flux, Spectroflux 105 (Johnson-Matthey Chemicals Ltd), was added in a ratio 5.333:1 (by weight, flux : sample), the crucible recovered and placed in a muffle furnace at 1100°C for 20 minutes.

The flux consists of $Li_2B_4O_2$, La_2O_3 and Li_2CO_3, in which the tetraborate helps to dissolve the sample whilst the La acts as a heavy absorber of the X-rays helping to minimise matrix effects between samples and standards of varying composition. In addition to using La as a heavy absorber, matrix effects for major elements were overcome by use of theoretical absorption coefficients (Theisen and Vollach, 1967) based on a flux : sample ratio of 5.333:1 following the correction procedures of Thirlwall (1979). The crucible was then withdrawn from the furnace, allowed to cool to room temperature and reweighed. Any slight weight loss (from H_2O absorbed by the spectroflux) was made up with further flux and the sample was refused over a Meker burner. On a hot plate at 220°C a disc-shaped, slightly concave graphite mould was placed inside a brass sleeve and the molten glass poured into the centre of the mould. An Al plunger, also at 220°C, was used to press the glass into a ~1mm thick disc, which is later presented directly to the X-ray beam.

International rock and sediment standards (Table A.1) were used for calibration of the samples as these cover the range in composition of the Arabian Sea sediments. For all elements the calibration lines are linear over the range of compositions investigated. The analytical conditions for the XRF major and minor elements are described in Table A.2. Precision and accuracy of the method is given in Table A.3.

A.2.2. Minor Elements

Pressed powder discs, 46mm in diameter were used for minor element analysis. 7gm of sample sediments ground in a Tema Tungsten Carbide mill was placed in a stainless steel sleeve, sitting on a highly polished tungsten carbide disc. Both sleeve and disc were enclosed within a larger stainless steel cylinder. A "perspex" plunger was placed within the inner cylinder and the sediments compacted by hand pressure into a semi compact disc. The "perspex" plunger and sleeve were removed and the semi competent disc was covered by boric acid. A large stainless steel plunger was then lowered onto the powder. A hydraulic ram was used to press the sample at 10 tons for a minute, and gently released over a further half minute. This pressed powder disc was then presented to the X-ray beam.

The standards used for calibration are given in Table A.1. The operating conditions for minor elements are listed in Table A.2. For I, Br, and S, standards were prepared by adding KBr, KI and Na_2SO_4 to a Br, I and S free base and then mixing thoroughly by grinding in Tema WC disc mill. These and other standards show a linear relationship over the range of compositions investigated.

Table A.1 List of Standards used in Calibration of Data Presented in this Thesis

Element	Standard											
Al	G2	GSP1	AGV1	BCR1	PCC1	DTS1	GA	GH	BEN	ANG	MAN	
Ba	G2	GSP1	AGV1	GA	GH	BCR1	PCC1	SY2	JB1	JG1		
Br	GF1	GF2	GF3	GF4	GF5	GF6	SG					
Ca	G2	GSP1	AGV1	BCR1	PCC1	DTS1	GH	BEN	ANG	MAN		
Ce	GA	GH	BR	G2	AGV1	BCR1	JB1	GSN				
Cu	G2	GSP1	AGV1	GA	GH	BR	BCR1	PCC1	SY2	JB1		
Cr	G2	GSP1	AGV1	GA	BR	BCR1	SY2	JB1	GSN	TANZI		
Fe	G2	GSP1	AGV1	BCR1	PCC1	DTS1	GA	GH	BEN	ANG	MAN	
I	GF1	GF2	GF3	GF4	GF5	GF6	SG					
K	G2	GSP1	AGV1	BCR1	PCC1	DTS1	GA	GH	BEN	ANG	MAN	
La	GA	GH	BR	G2	AGV1	BCR1	JB1	GSN				
Mg	G2	GSP1	AGV1	BCR1	PCC1	DTS1	GA	GH	BEN	ANG	MAN	
Mn	G2	GSP1	AGV1	BCR1	PCC1	DTS1	GA	GH	BEN	ANG	MAN	
Na	G2	GSP1	AGV1	BCR1	PCC1	DTS1	GA	GH	BEN	ANG	MAN	
Nd	GA	GH	BR	G2	AGV1	BCR1	SY2	JB1	GSN			
Ni	G2	GH	BR	GA	AGV1	BCR1	PCC1	SY2	SY3	JB1		
P	G2	GSP1	AGV1	BCR1	PCC1	DTS1	GA	GH	BEN	ANG	MAN	
Pb	GSP1	AGV1	GH	BR	BCR1	JB1	JG1	GSN	TANZI			
Rb	G2	GSP1	AGV1	PCC1	GA	GH	BR	SY2	SY3	JB1	JG1	GSN
S	GF1	GF2	GF3	GF4	GF5	GF6	SG					
Si	G2	GSP1	AGV1	BCR1	PCC1	DTS1	GA	GH	BEN	ANG	MAN	
Sr	G2	GSP1	AGV1	GA	GH	BR	BCR1	SY2	SY3	JB1	JG1	GSN
Th	G2	GSP1	AGV1	BCR1	GA	BR	GH					
Ti	G2	GSP1	AGV1	BCR1	PCC1	DTS1	GA	GH	BR	BEN	ANG	MAN
V	G2	GSP1	AGV1	BCR1	PCC1	GH	JB1	JG1	GA	BR		
Y	G2	GSP1	AGV1	BCR1	GA	GH	BR	SY2	JB1			
Zn	G2	GSP1	AGV1	GA	BR	BCR1	PCC1	SY2	SY3	JB1		
Zr	G2	GSP1	AGV1	GA	BCR1	GH	BR	SY2	SY3	JB1		

Standards for Br, I and S are in house synthetic prepared by mixing the following specpure compounds with bulk sediments from core CD 1730.

KB-Br, KI-I, and Na_2So_4-S.

Table A.2 Analytical Conditions for XRF Major and Minor Elements Analysis

Element	Line	Tube	KV	mA	Crystal	Peak °2	Detector	Pulse Height LL	Window	Collimator	Sample
Al	Kα	Cr	50	45	PE	145.13	F*	250	600	c*	Fusion
Ba	Lβ2	Rh	50	45	LIF220	115.44	F	300	500	c	P.D*
Br	Kα	Rh	70	30	LIF220	29.97	F+S	250	500	f	P.D
Ca	Kα	Cr	50	45	LIF220	113.09	F	250	600	c	Fusion
Ce	Lβ1	Rh	50	45	LIF220	71.64	F	300	500	f*	P.D
Cr	Kα	Rh	50	45	LIF220	69.37	F	150	600	f	P.D
Cu	Kα	Rh	50	45	LIF220	45.11	F	400	350	c	P.D
Fe	Kα	Cr	50	45	LIF220	57.52	F	200	500	f	Fusion
I	Kα1	Rh	70	30	LIF220	12.40	F+S	250	500	f	P.D
K	Kα	Cr	50	45	LIF220	136.69	F	250	600	c	Fusion
La	Lα1	Rh	50	45	LIF220	83.01	F	300	500	c	P.D
Mg	Kα	Cr	50	45	TLAP	45.17	F	250	500	c	Fusion
Mn	Kα	Cr	50	45	LIF220	62.97	F	150	700	f	Fusion
Na	Kα	Cr	50	45	TLAP	55.10	F	250	500	c	Fusion
Nd	Lα1	Rh	50	45	LIF220	72.12	F	300	500	f	P.D
Ni	Kα	Rh	50	45	LIF220	48.66	F	400	350	f	P.D
P	Kα	Cr	50	45	GE	141.04	F	370	400	c	Fusion
Pb	Lβ2	Rh	70	30	LIF220	28.23	F+S*	250	500	f	P.D
Rb	Kα	Rh	70	30	LIF220	26.58	F+S	250	600	f	P.D
S	Kα	Rh	40	60	GE	110.69	C	250	600	c	P.D
Si	Kα	Cr	50	45	PE	109.21	F	250	600	c	Fusion
Sr	Kα	Rh	70	30	LIF220	25.11	F+S	250	600	f	P.D
Ti	Kα	Cr	50	45	LIF220	86.14	F	300	500	f	Fusion
Th	Lα1	Rh	70	30	LIF220	27.45	F+S	250	500	f	P.D
V	Kα	Rh	50	45	LIF220	123.40	F	300	500	c	P.D
Y	Kα	Rh	70	30	LIF220	23.76	F+S	250	600	f	P.D
Zn	Kα	Rh	70	30	LIF220	41.77	F+S	250	500	f	P.D
Zr	Kα	Rh	70	30	LIF220	22.51	F+S	250	600	f	P.D

C* = Coarse; f* = fine; F* = Flows; S* = Scintillation; P.D = Pressed disc.

Table A.3 XRF Analytical Precision and Accuracy for Major and Minor Elements

	REPRODUCIBILITY on sample (Core CD 1730)		Estimated total precision (as % relative std. dev. 1σ)	"ACCURACY"
	Mean (n=8)	1σ		
Weight %				
SiO_2	30.85	0.041	0.13	0.23
Al_2O_3	7.02	0.029	0.41	0.14
Fe_2O_3	3.22	0.014	0.43	0.047
MgO	4.18	0.052	1.24	0.069
CaO	25.83	0.038	0.14	0.052
Na_2O	1.68	0.10	5.9	0.093
K_2O	1.37	0.008	0.58	0.010
TiO_2	0.416	0.004	0.96	0.014
MnO	0.123	0.002	1.62	0.005
P_2O_5	0.179	0.005	2.79	0.010
p.p.m.	on sample ST72 (n=5)			
Ni	170.9	0.3		4.3
Cr	380.5	2.9		11.0
V	236.6	3.5		11.5
Sc	18.2	0.3		2.4
Cu	48.4	0.4		5.3
Zn	113.9	1.1		5.0
Pb*	-1.8	1.6		4.0
Sr	1129.7	4.0		9.6
Rb	46.7	0.5		3.5
Zr	366.0	1.0		14.8
Nb	92.2	0.5		2.4
Ba	718.4	5.6		39.0
Th	16.6	1.2		2.8
La	78.9	0.8		5.6
Ce	156.7	1.6		13.5
Nd	66.2	0.6		3.6
Y	33.2	0.4		3.4

1. Total precision includes counting error, disc reproducibility error in regression line and error in matrix mass absorption determination.

2. Accuracy determined from r.m.s.d. of international standards about the regression line.

*Below detection limit. 6 determinations (by MFT) of Pb in andesite MT45 gave a mean concentration of 9.6 p.p.m. with a σ of 0.8 p.p.m.

A.3 CORRECTION FOR THE DILUTION EFFECTS OF RESIDUAL SEA-SALT

Sea salt present in sea water affects considerably element concentration in marine sediments after drying up. Directly affected by this salt are the concentrations of elements like Na, Mg, Ca, K, S and Br; whilst on the whole it dilutes the concentrations of all elements present in sediments.

The concentrations of individual elements are corrected first using the following equations based on the concentration of the element in sea water:

Wt % of Na = T.wt % of Na - 0.306
Wt % of K = T.wt % of K - 0.011
Wt % of Ca = T.wt % of Ca - 0.012
Wt % of Mg = T.wt % of Mg - 0.037
PPm S = T.PPm S - 262
PPm Br = T.PPm Br - 19

Once the individual element concentrations have been adjusted in this manner a subsequent correction for salt dilution is applied using the equation:

(Element) Salt free = (Element) measured x salt.

The salinity of interstitial water is assumed to be constant and the same as that of normal sea water, is 35°/₀₀. The water content given in Table C.1 is employed in order to calculate the salt content in sediments from the relationship.

$$\text{Salt} = \frac{3.513 \times W}{100-W}$$

W = Water content wt %.

A.4 ORGANIC CARBON ANALYSIS

In analysis of organic carbons in sediments which are higher in calcite and dolomite content, decarbonation is necessary without removing organic carbon. Concentrated acid is required to eliminate all the dolomite and calcite in the sediments, which may result in some loss of organic carbon. Further loss can also

occur through hydrolysis if the sediments are washed following acid removal of carbonate carbon. These losses can be avoided by treating samples with 3M HCl (Optimum concentration for dolomite removal) directly in Leco ceramic crucibles. As these are porous, samples are carefully dampened, not wetted, in order to control the removal of soluble organic carbon by perculation of acid through the crucible wall.

Organic carbon was determined in the carbonate-free samples by ignition in an induction furnace in a stream of CO_2-free oxygen followed by potassium hydroxide absorption of the CO_2 produced. A Leco 521-200 induction furnace equipped with dust trap, sulphur trap (SO_2 absorption by MnO_2 powder) and catalyst was used for combustion. This was connected to a Leco 572-100 carbon analyser using a gas burette to measure the change in volume which resulted when the $O\text{-}CO_2$ mixture from the combustion furnace was flushed through CO_2-absorbing KOH. About 500mg of pre-dried ground sediment were weighed into a Leco ceramic crucible. Carbonate elimination was done by dampening the sample with de-ionized water followed by drop wise addition of 3 M HCl (50%). The sample was then placed on a hot plate at 60°C and evaporated to dryness. Acidification was repeated three to four times after the cessation of effervescence to ensure complete decarbonation of samples. Tin and iron accelerators were spread evenly over the surface of dried and carbonate free samples which were then combusted in a furnace.

The organic carbon results obtained by this method are quite satisfactory. However, the induced error by unattacked carbonate in a core higher in calcite and dolomite content, especially in core CD1715 cannot be ignored. Removal of dolomite in samples containing ~5% seems to be incomplete as evidenced by spurious results in this core. The use of more concentrated HCl is a risk as it can effectively wash out labile organic material. Therefore any possible error in the organic carbon analysis of the investigated cores could be due to unattacked carbonate. HCl itself may induce error as $CaCl_2$ formed by adding HCl, may produce HCl fumes during combustion. These HCl vapours are oxidized by MnO_2 in the sulphur trap to chlorine gas which can interfere with KOH absorption giving eraneous results. Nevertheless, the results are largely in agreement with the reported organic carbon content of deep sea sediments (~1.0%) which suggest that overall precision is satisfactory. Analytical precision based on replicates of samples varies between 3% to 14.0% and for each core is as follows:

$$V = \frac{\sqrt{\Sigma x}}{2n}$$

CD 1709 (n = 30)	V = ± 0.099
CD 1715 (n = 20)	V = ± 0.13
CD 1730 (n = 22)	V = ± 0.10
CD 1739 (n = 19)	V = ± 0.045
CD 1738 (n = 10)	V = ± 0.037

A.5 BIOGENIC SILICA DETERMINATION

The method used in this study for biogenic silica determination is developed by Dobbie (1988) following the techniques of Eggiman et al. (1980). Sediment samples digested in PTFE (Polytetrafluorethylene) bomb using 2M Na_2CO_3 and Silica determined calorimetrically. This method is based on the formation of a yellow silicomolybdate acid which is reduced to molybdenum blue and absorption of which is measured at 812 nm in a spectrophotometer.

About 50mg of finely ground sample weight out in PTFE bomb and 20ml of 2M Na_2CO_3 transferred carefully into the bomb. The bomb was then sealed and placed in an oven at 90-100°C for four hours after which it was cooled to room temperature. These optimum conditions were shown by Dobbie (1988) to be very effective for the complete digestion. The leechate obtained filtered in vacuum through 0.4 micron polycarbonate membrane filters using all plastic apparatus. The filtrate and washings were transferred into a 100 ml standard flask, and diluted to the mark with deionised water. The solution was stored in a plastic bottle for Si and Al analysis.

The preparation of different reagents and standards used are described in detail by Dobbie (1988), here the major steps involved for calorimetric analysis are outlined. 5 ml aliquot of solutions, blank and of a standard containing 2 ml of "silica standard" was acidified using 2.2 ml of 50% HCl in a 100 ml glass flask. Before adding the reagents this was diluted by 15ml deionised water. Later 1 ml ammonium molybdate solution was added, the flask shaken to mix and left for 10 minutes which allowed the complete formation of yellow silico molybdate complex. 5 ml oxalic acid

was then added followed immediately by 2 ml of reducing solution and the flask was gently shaken to mix the contents. This solution was then diluted up to the 100 ml mark with deionised water and left for one hour to allow a stable molybdenum blue colour to develop. In spectrophotometer a 2 cm cell is used for the absorbance of Si at a wavelength of 812 nm.

A.5.1 Calculation of biogenic silica

The absorption of the blank was subtracted from the absorption readings of the unknown samples and standard before the silica content of the samples calculated. The silica content computed as follows:

$$\text{App. Silica} = \frac{R-B}{S-B} \times \frac{\text{Factor}}{\text{Wt-samples}}$$

where R = Absorption reading of samples (unknown)

B = Absorption of blank

S = Absorption of standard

Factor = 200.00104

The values obtained are of apparent biogenic silica content because there is a possibility of derivation of non-amporhous silica in solution, thus correction for this is essential. This correction considered only clay derived and ignored quartz silica as it was considered to be a second order correction (Eggimann et al., 1980). The SiO_2/Al_2O_3 ratio of sediments in the north Arabian Sea is assumed to be two and thus biogenic silica content in sediments could be calculated by multiplying the Al_2O_3 content of the solutions by two (giving the clay derived silica) and subtracting this from the apparent silica content. (SiO_2/Al_2O_3 ratio of Mag-1 = 3; Eggimann et al., 1980). (Biog Si% = % apparent silica - (2 X Al_2O_3%)).

A.5.2 Determination of Al_2O_3 content of solutions

The method for Al_2O_3 determination followed here is of Dougen and Wilson (1974) involving the formation of a catechol violet complex. 5ml aliquots of the unknown solution, blank and standard solution was coloured up by adding the following reagents:

1 ml of the 1:10 phenaphtholin solution

2 ml of the catechol violet solutions

10 ml of the hexamine buffer.

The flask was shaken after each addition. The solutions were diluted to the mark with deionised water. After little shaking, these are left for ten minutes to allow the colour to develop. The absorption of the solutions was measured in 1 cm cells at 585 nm. The Al_2O_3 content calculated as follows:

$$Al_2O_3 = \frac{R-B}{S-B} \times \frac{F \times 0.02 \times 20 \times 100}{(\text{Sample. wt})}$$

Factor = 0.9362

A.5.3 Analytical Precision

The precision of the results based on replicate analysis is quite satisfactory. Coefficient of variation estimated as follows:

$$V = \frac{\sqrt{\Sigma p^2}}{2n}$$

is found to be 0.094 for core CD 1730 and 0.143 for core CD 1715. The percentage of variance 4.64% and 7% for 2% Biog. silica in two cores suggest that the analytical error is very small. However in core CD 1715 slightly higher percentage of variance shows that some analytical error is possible.

The results obtained in this study are checked by analysing Mag-1. The biogenic silica content found in Mag-1 (3.2%) is very close to the value (ie. 3.1%) reported by Eggimann et al. (1980). This also confirms that the results of biogenic silica listed in appendix C.10 are very satisfactory.

A.6 NITROGEN AND $\delta^{15}N$ ANALYSIS

Total nitrogen and $\delta^{15}N$ analysis were performed using a Carlo-Erba 1400 nitrogen analyser in the Department of Soil Science. The operations are illustrated in Fig. A6.1. About 20 mg finely ground sediment combusted at 1030°C. The amount of N_2 gas derived is directly related to the amount of N in the sample. A

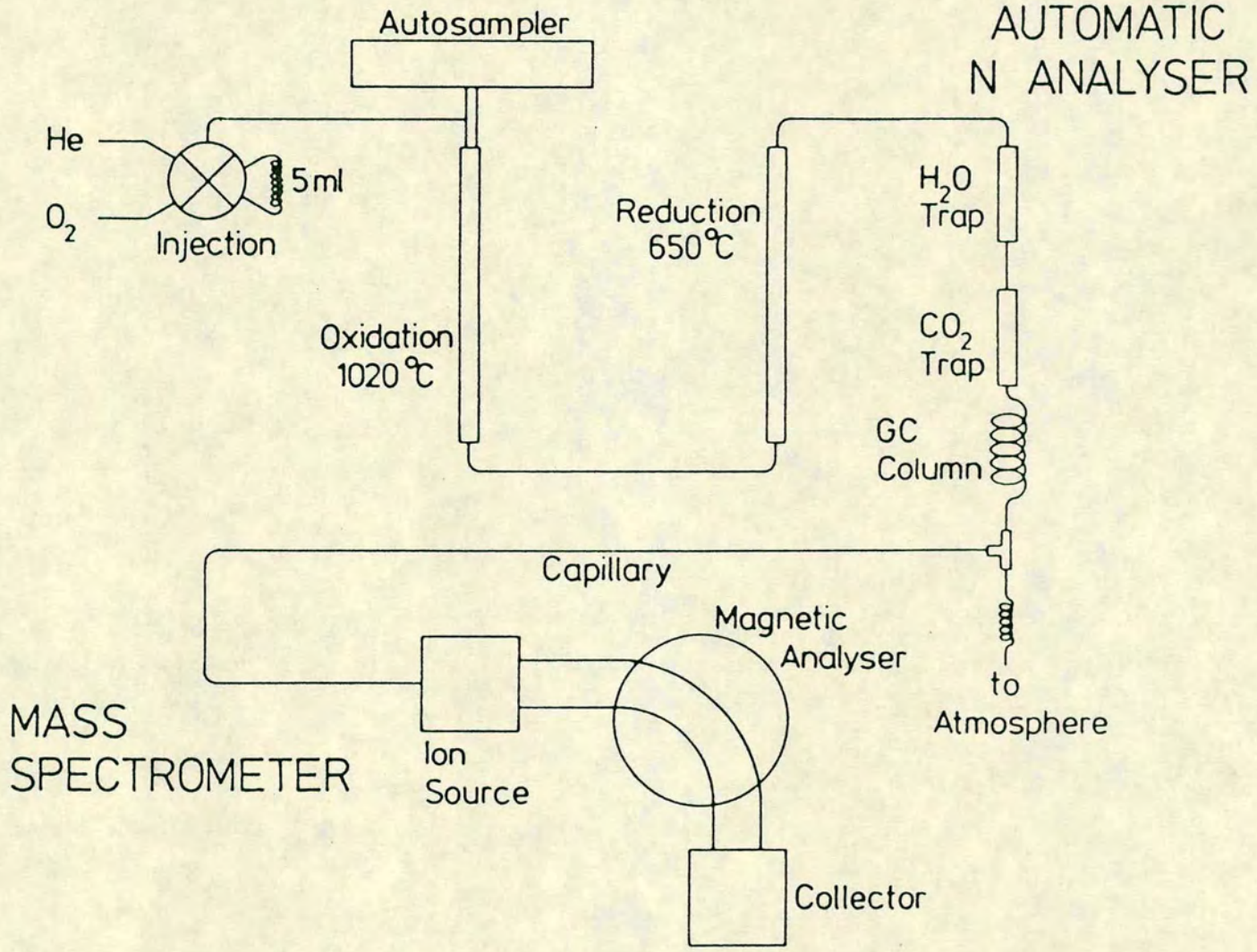

FIGURE A6:1 FLOW DIAGRAM SHOWING THE MAJOR STEPS INVOLVED IN THE OPERATION OF CARLO ERBO 1400N ANALYSER AND VG-MICROMASS 622 MASS SPECTROMETER.

constant proportion of the N_2 produced was then fed into the VG-Micromass 622 mass-spectrometer and the isotopic composition determined by measurements of the ion currents corresponding to mass 28 (N^{14} N^{14}) and mass 29 (N^{15} N^{14}).

The relative abundance of N^{28} and N^{29} is thus obtained on a chart recorder and from their ratio it is possible to calculate the actual abundance of N^{15} in the sample using the equation:

$$\text{atm \% } {}^{15}N = \frac{100}{2R+1}$$

(R is the ratio of N^{28}/N^{29})

After correcting these readings for the machine error the actual $\delta^{15}N$ values relative to atmospheric abundance can be calculated as follows:

$$\delta^{15}N = \frac{(\text{atm \% } {}^{15}N \text{ in sample} - 0.3663)}{0.3663} \times 1000$$

0.3663 at % ^{15}N in atmosphere used as standard.

The quality was continuously observed by running atmospheric standard and acetanilide reference after every 10 runs. The analytical precision in $\delta^{15}N$ based on replicate is of 1.0%.

A.7 $\delta^{13}C$ ANALYSIS

Prior to analysis the sediments were decarbonated using 3M HCl. Complete elimination of calcite and dolomite present in sediment was checked by XRD and no traces of carbonate was found.

The measurements of $\delta^{13}C$ were determined on a VG Prism mass spectrometer, Carlo-Erba 1102 CHN analyser which was attached directly to the prism inlet system, was used to produce the CO_2 by combustion. The CO_2 was trapped cryogenically in a liquid nitrogen trap before being released to the inlet.

The reproducibility of the result is ± 0.1 per mill (1σ), based on replicate measurements of an in-house standard sediment.

APPENDIX B

CALCULATION OF LITHOGENIC AND BIOGENIC CONTENTS IN SEDIMENTS

Calculation of lithogenic and Biogenic contents in sediments.

B.1 CALCULATION OF Fet (IRON TERRIGENOUS)

The Iron terrigenous (Fet) in the sediments calculated using the following equation:

Fet = Total Fe- Fe in Pyrite

The amount of Pyrite determined by the normative relationship is as follows:

Mol. wt. of Pyrite (FeS_2) = 119.8

Amount of Pyrite = % S x $\frac{119.8}{64}$

(% S is sulphur content in sediments analysed by XRF)

Similarly the Fe associated with Pyrite calculated as

Fe in Pyrite (FeS_2) = Pyrite x $\frac{55.8}{119.8}$

B.2 CALCULATION OF Si(Lith) AND QUARTZ (Si) CONTENT

Si(Lith) = T.Si - (Al x Si/Al) (Si/Al = 2.5)

Quartz (Si) content in sediments of core CD1738 and CD1739 computed from the above equation. However in core CD1715 and CD1720 a modified equation is used as follows.

Quartz (Si)% = T.Si - (Al x Si/Al) - Biog. Si.

B.3 CALCULATION OF CALCITE AND DOLOMITE CONTENTS IN SEDIMENTS

From the Ca and Mg analyses performed by XRF method the calcite and dolomite contents are computed using their normative relationship as follows.

Mol. wt. of $CaCO_3$ = 40 + 60 = 100

Mol. wt. of Ca $MgCO_3$ = 40 + 24 + 60 = 124

Calcite % = Ca Total - [Ca (dol) + Ca (Al)] x $\frac{100}{40}$ $\quad Ca(dol) = Dolomite(\%) \times \frac{40}{124}$

Dolomite % = Excess Mg x $\frac{124}{24}$ $\quad Ca(Al) = 0.2$

Excess Mg = T. Mg - (T.Al x Mg/Al)

Mg held in alumino silicates = Total Al x Mg/Al

Total Mg and total Al in sediments and Mg/Al ratio is the average Mg/Al ratio of each core.

B.4 EXCESS Sr CALCULATION

Excess strontium in sediments is the amount of strontium held in excess of aluminosilicates and dolomite and calculated as follows.

Excess Sr = T.Sr - ($Sr_{(clay)}$ + $Sr_{(dol)}$)

Sr (clay) is the Sr content in aluminosilicates and computed from the equation (T.Sr-(T.Al x Sr/Al)) assuming average Sr/Al ratio is deep sea clay is 0.0021 (Turekian and Wedphol, 1964).

$Sr_{(clay)}$ = Al x Sr/Al (Al is Total Aluminium in sediments)

Sr (dol) is Sr associated with dolomite taken 700 ppm average Sr in dolomite (Behren and Land, 1972).

Sr (dol) = 700 x dolomite content in %.

B.5 EXCESS Ba and Metals CALCULATION

Excess Ba is the Ba content in excess of the Ba incorporated in clays. The background ratio of Ba/Al used in these sediments is taken from turbidite (i.e. 0.0066) (See appendix C.9.2). The following relationship is used to compute the excess Ba and metals in sediments:

Excess Ba = T. Ba-(Al x Ba/Al)

Excess Metals = T.metal - (Al x met/Al)

Excess Metals = Ni, Cu and Zn in ppm.

T.metal = Total Ni, Cu and Zn contents in sediments.

met/Al = Average Ni/Al, Cu/Al and Zn/Al ratio in turbidite of core CD 1715.

B.6 CALCULATION OF PALEOPRODUCTIVITY

For the estimation of Paleoproductivity, a relationship given below by Muller et al. (1981) used:

$$R = \frac{C.Ps.(1-\emptyset)}{0.0030 \cdot S^{0.30}}$$

R = Paleoproductivity (g Cm^2/y)

C = Organic Carbon in %

Ps = Dry sediment density g/cm^3 (ie. $2.71 g/cm^3$)

Ø = Porosity

S = Sedimentation rate (ie. cm/Kys)

TABULATED DATA

TABLE C.1:1 WATER CONTENT AND POROSITY DATA OF CORE CD 1709

DEPTH CM	WATER CONTENT (%)	POROSITY	SALT CONTENT (%)
0.00	42.40	0.66	2.57
10.00	52.20	0.74	3.82
20.00	39.80	0.64	2.32
30.00	40.00	0.64	2.33
40.00	43.60	0.67	2.70
50.00	34.83	0.59	1.87
60.00	37.60	0.61	2.10
70.00	38.60	0.62	2.20
80.00	39.20	0.63	2.26
90.00	40.00	0.64	2.33
100.00	50.00	0.73	3.50
110.00	38.70	0.63	2.21
120.00	50.30	0.73	3.54
130.00	40.60	0.64	2.39
140.00	44.20	0.68	2.77
150.00	37.20	0.61	2.08
160.00	42.90	0.67	2.63
170.00	37.90	0.62	2.14
180.00	37.40	0.61	2.09
190.00	36.90	0.61	2.04
200.00	38.50	0.62	2.19
210.00	38.90	0.63	2.23
220.00	39.10	0.63	2.25
230.00	41.90	0.66	2.53
240.00	44.10	0.68	2.76
250.00	41.20	0.65	2.45
260.00	42.00	0.66	2.59
270.00	39.60	0.63	2.30
280.00	32.60	0.56	1.69
290.00	32.70	0.56	1.70
300.00	32.00	0.55	1.47
310.00	32.90	0.56	1.72
320.00	32.90	0.56	1.71
330.00	34.20	0.58	1.82
340.00	32.70	0.56	1.70
350.00	33.70	0.57	1.72
360.00	34.30	0.58	1.82
370.00	35.60	0.59	1.93
380.00	37.50	0.61	2.10
390.00	39.00	0.63	2.23
400.00	38.80	0.63	2.22
410.00	41.00	0.65	2.44
420.00	41.90	0.66	2.52
430.00	38.60	0.62	2.20
440.00	33.10	0.57	1.73
450.00	33.60	0.57	1.77
460.00	37.10	0.61	2.06

TABLE C.1:2 WATER CONTENT AND POROSITY DATA OF CORE CD 1715

DEPTH CM	AGE KYS	W.C (%)	POROSITY (%)	SALT CONTENT (%)
0.00	0.00	42.01	0.66	2.54
10.00	8.31	46.89	0.70	3.10
20.00	10.57	43.90	0.67	2.75
32.00	13.57	42.21	0.66	2.57
35.00	14.28	44.10	0.68	2.77
40.00	15.49	42.33	0.66	2.58
50.00	17.25	42.04	0.66	2.55
60.00	19.05	44.67	0.68	2.84
70.00	20.83	50.64	0.73	3.60
80.00	22.64	45.28	0.69	2.91
90.00	0.00	22.79	0.44	1.04
100.00	24.45	51.32	0.74	3.70
110.00	26.28	54.08	0.76	4.14
120.00	28.33	54.95	0.76	4.29
130.00	0.00	24.68	0.46	1.15
140.00	0.00	22.22	0.43	1.00
150.00	30.38	44.58	0.68	2.83
160.00	32.43	47.65	0.71	3.20
164.00	33.25	45.95	0.69	2.99
174.00	35.30	46.65	0.70	3.07
184.00	37.38	47.50	0.71	3.18
194.00	39.85	47.62	0.71	3.19
204.00	42.85	47.73	0.71	3.21
214.00	45.84	47.52	0.71	3.18
224.00	48.82	46.82	0.70	3.09
234.00	54.70	42.61	0.66	2.61
244.00	57.58	41.56	0.65	2.50
254.00	60.47	50.34	0.73	3.56
264.00	67.14	49.77	0.72	3.48
284.00	80.00	45.36	0.69	2.92
294.00	84.22	51.87	0.74	3.79
304.00	88.44	52.96	0.75	3.96
309.00	90.55	52.73	0.75	3.92
319.00	99.00	48.00	0.71	3.24
329.00	108.60	47.10	0.70	3.13
339.00	118.20	45.50	0.69	2.93
349.00	121.70	48.23	0.71	3.27
359.00	125.20	46.09	0.69	3.00
369.00	127.20	41.56	0.65	2.50
379.00	132.60	42.51	0.66	2.60
390.00	136.60	42.23	0.66	2.57
400.00	138.20	50.59	0.73	3.60
410.00	141.40	34.46	0.58	1.85
420.00	150.20	46.75	0.70	3.08
430.00	150.90	44.14	0.68	2.78
440.00	151.16	46.87	0.70	3.10
450.00	152.30	50.80	0.73	3.63
454.00	152.58	46.45	0.70	3.05
464.00	158.20	44.28	0.68	2.79
474.00	161.40	48.79	0.72	3.35
484.00	164.60	49.55	0.72	3.45
494.00	167.80	49.02	0.72	3.38
504.00	171.06	46.21	0.69	3.02
514.00	174.32	46.67	0.70	3.07
524.00	177.58	46.14	0.69	3.01
534.00	180.84	50.50	0.73	3.58
544.00	184.12	44.65	0.68	2.83
554.00	187.40	49.29	0.72	3.41
564.00	190.70	52.05	0.74	3.81
574.00	192.09	44.27	0.68	2.79
584.00	205.00	44.10	0.68	2.77
594.00	206.61	41.10	0.65	2.45
598.00	207.41	37.88	0.62	2.14
608.00	209.10	42.87	0.66	2.64
618.00	210.50	45.96	0.69	2.99
628.00	216.00	42.81	0.66	2.63
636.00	223.38	42.25	0.66	2.57
643.00	0.00	21.94	0.43	0.99
648.00	228.00	45.93	0.69	2.98
653.00	0.00	20.98	0.41	0.93
663.00	230.90	40.74	0.65	2.42
676.00	0.00	25.64	0.48	1.21
687.00	0.00	21.61	0.42	0.97
682.00	232.00	37.40	0.61	2.10
692.00	0.00	21.74	0.42	0.98
700.00	0.00	20.43	0.40	0.90
706.00	233.70	39.57	0.63	2.30
712.00	239.10	42.81	0.66	2.63
722.00	244.00	42.54	0.66	2.60
733.00	245.50	44.29	0.68	2.79

TABLE C1.3 WATER CONTENT AND POROSITY DATA OF CORE CD 1730

DEPTH CM	AGE KYRS	W.C (%)	POROSITY (%)	SALT CONTENT (%)
0.00	0.00	49.93	0.73	3.50
10.00	2.60	47.74	0.71	3.21
20.00	5.10	45.69	0.69	2.96
30.00	7.70	43.53	0.67	2.71
40.00	10.00	41.90	0.66	2.53
50.00	12.00	36.82	0.61	2.05
60.00	13.50	36.42	0.60	2.01
70.00	15.50	42.24	0.66	2.57
80.00	16.60	42.68	0.66	2.62
90.00	18.10	42.88	0.66	2.64
100.00	19.20	46.48	0.70	3.05
110.00	20.30	46.46	0.70	3.05
120.00	21.40	46.62	0.70	3.07
130.00	22.60	44.99	0.68	2.87
140.00	24.00	39.98	0.64	2.34
150.00	25.30	43.71	0.67	2.73
160.00	26.70	44.91	0.68	2.86
170.00	28.20	47.13	0.70	3.13
180.00	29.40	46.57	0.70	3.06
190.00	30.70	44.62	0.68	2.83
200.00	32.00	39.44	0.63	2.29
210.00	33.40	42.31	0.66	2.58
220.00	34.70	45.01	0.68	2.88
230.00	36.10	44.81	0.68	2.85
240.00	37.40	44.68	0.68	2.84
250.00	39.50	44.90	0.68	2.86
260.00	41.60	43.87	0.67	2.75
270.00	43.70	42.86	0.66	2.64
280.00	45.80	44.66	0.68	2.84
290.00	50.00	44.18	0.68	2.78
295.00	52.10	45.94	0.69	2.99
305.00	56.30	46.86	0.70	3.10
315.00	60.50	52.53	0.75	3.89
325.00	63.50	46.45	0.70	3.05
335.00	71.00	44.16	0.68	2.78
345.00	80.00	49.59	0.72	3.48
355.00	84.50	49.79	0.72	3.48
365.00	89.00	46.32	0.70	3.03
375.00	93.60	46.42	0.70	3.04
385.00	99.00	43.62	0.67	2.72
395.00	102.20	40.61	0.64	2.40
405.00	108.60	44.56	0.68	2.82
415.00	115.00	40.29	0.64	2.37
425.00	121.40	37.21	0.61	2.08
435.00	128.00	36.26	0.60	2.00
450.00	130.10	39.92	0.64	2.33
460.00	132.20	41.46	0.65	2.49
470.00	134.40	40.15	0.64	2.36
480.00	136.50	36.63	0.60	2.03
490.00	138.60	43.21	0.67	2.67
500.00	140.70	45.34	0.69	2.91
510.00	142.80	55.52	0.77	4.38
520.00	144.90	46.38	0.70	3.04
530.00	147.10	47.31	0.70	3.15
540.00	149.20	48.69	0.72	3.33
550.00	151.30	50.44	0.73	3.58
560.00	153.40	50.14	0.73	3.53
570.00	155.50	41.85	0.66	2.53
580.00	157.70	41.80	0.66	2.52
590.00	159.80	46.67	0.70	3.07
600.00	163.20	45.48	0.69	2.93
610.00	166.70	47.89	0.71	3.23
620.00	170.10	48.03	0.71	3.25
630.00	173.60	47.37	0.70	3.16
640.00	177.00	46.51	0.70	3.05
650.00	180.50	47.27	0.70	3.15
660.00	184.10	51.48	0.74	3.73
670.00	191.00	49.67	0.72	3.47
680.00	198.00	47.59	0.71	3.19
690.00	205.00	45.40	0.69	2.92
700.00	209.43	39.01	0.63	2.25
710.00	214.60	37.19	0.61	2.08
720.00	219.40	36.96	0.61	2.06
730.00	224.10	44.14	0.68	2.78
740.00	228.90	45.36	0.69	2.92
750.00	233.70	41.08	0.65	2.45
760.00	238.50	46.24	0.69	3.02
770.00	243.30	43.27	0.67	2.68
780.00	248.10	41.41	0.65	2.48
790.00	252.80	39.72	0.64	2.31
800.00	257.60	38.04	0.62	2.16

TABLE C.1:4 WATER CONTENT AND POROSITY DATA OF CORE CD 1738

DEPTH CM	AGE KYRS	W.C (%)	POROSITY (%)	SALT CONTENT (%)
0.00	0.00	45.95	0.69	2.99
10.00	0.00	45.22	0.69	2.90
20.00	15.40	51.15	0.73	3.68
30.00	20.80	32.34	0.56	1.68
40.00	22.64	39.79	0.64	2.32
50.00	23.55	38.87	0.63	2.23
60.00	24.46	46.86	0.70	3.10
70.00	26.28	36.45	0.60	2.01
80.00	28.10	40.66	0.64	2.41
90.00	29.95	36.18	0.60	1.99
100.00	31.19	32.38	0.56	1.68
110.00	32.73	34.99	0.59	1.89
120.00	34.28	37.40	0.61	2.10
130.00	35.82	39.86	0.64	2.33
140.00	37.38	41.56	0.65	2.50
150.00	39.14	28.68	0.52	1.41
160.00	40.90	27.38	0.50	1.32
170.00	42.66	40.24	0.64	2.37
180.00	44.42	35.04	0.59	1.89
185.00	45.30	35.25	0.59	1.91
195.00	47.06	38.15	0.62	2.17
205.00	48.82	33.10	0.57	1.74
215.00	51.01	41.48	0.65	2.49
225.00	53.20	34.15	0.58	1.82
235.00	55.39	37.06	0.61	2.07
245.00	57.58	31.70	0.55	1.63
255.00	59.05	33.88	0.58	1.80
265.00	60.45	29.55	0.53	1.47
275.00	65.74	35.70	0.59	1.95
285.00	71.00	34.94	0.59	1.89
295.00	82.75	25.94	0.48	1.23
305.00	94.50	29.25	0.52	1.45
315.00	96.24	27.84	0.50	1.36
325.00	97.99	36.52	0.60	2.02
335.00	99.74	34.85	0.59	1.88
345.00	101.48	39.55	0.63	2.30
355.00	103.23	36.71	0.61	2.04
365.00	104.98	39.36	0.63	2.28
375.00	106.73	35.19	0.59	1.91
385.00	108.47	30.21	0.53	1.52
395.00	110.22	29.53	0.53	1.47
405.00	111.97	28.69	0.52	1.41
415.00	113.72	35.50	0.59	1.93
425.00	115.46	28.04	0.51	1.37
435.00	117.21	27.86	0.51	1.36
445.00	118.96	30.00	0.53	1.51
455.00	120.70	29.06	0.52	1.44
465.00	122.70	29.86	0.53	1.50
475.00	124.45	33.61	0.57	1.78
485.00	125.95	29.72	0.53	1.49
495.00	127.70	23.13	0.44	1.06
505.00	128.78	27.40	0.50	1.33
515.00	129.87	27.79	0.50	1.35
525.00	130.96	28.34	0.51	1.39
535.00	132.05	24.92	0.47	1.17
540.00	132.60	30.27	0.53	1.53
545.00	133.40	33.33	0.57	1.76
555.00	135.00	25.62	0.48	1.21
565.00	136.60	33.06	0.57	1.73
575.00	138.20	34.44	0.58	1.85
585.00	139.80	24.40	0.46	1.13
595.00	141.40	36.86	0.61	2.05
605.00	144.00	26.19	0.48	1.25
615.00	146.98	26.70	0.49	1.28
625.00	150.20	28.23	0.51	1.38
635.00	152.60	35.15	0.59	1.90
645.00	155.80	33.92	0.58	1.80
655.00	158.70	36.20	0.60	1.99
665.00	161.60	44.13	0.68	2.77

TABLE C.1:5 WATER CONTENT AND POROSITY DATA OF CORE CD 1739

DEPTH CM	AGE KYRS	W.C (%)	POROSITY (%)	SALT CONTENT (%)
0.00	0.00	48.80	0.72	3.35
10.00	10.00	35.41	0.59	1.93
20.00	15.50	36.15	0.60	1.99
30.00	16.83	38.78	0.63	2.23
40.00	18.16	38.93	0.63	2.24
50.00	19.49	39.76	0.64	2.32
60.00	20.82	41.18	0.65	2.46
70.00	21.73	40.65	0.64	2.41
80.00	22.64	38.36	0.62	2.19
90.00	23.55	39.83	0.64	2.33
100.00	24.46	41.50	0.65	2.49
110.00	25.67	64.86	0.83	6.48
120.00	26.88	37.75	0.62	2.13
130.00	28.10	34.01	0.58	1.81
140.00	29.64	36.59	0.60	2.03
150.00	31.19	37.74	0.62	2.13
160.00	32.74	37.25	0.61	2.09
170.00	34.29	35.53	0.59	1.94
180.00	35.83	38.41	0.62	2.19
190.00	37.38	39.18	0.63	2.26
200.00	41.61	40.16	0.64	2.36
210.00	45.84	40.31	0.64	2.37
220.00	49.76	41.69	0.65	2.51
230.00	53.68	38.53	0.62	2.20
240.00	57.58	40.62	0.64	2.40
250.00	59.01	34.41	0.58	1.84
260.00	60.45	31.23	0.55	1.60
270.00	63.92	60.00	0.80	5.27
280.00	67.40	35.98	0.60	1.97
290.00	68.60	34.23	0.58	1.83
300.00	69.80	37.64	0.61	2.12
310.00	71.00	36.69	0.61	2.04
320.00	80.00	36.25	0.60	2.00
330.00	87.25	32.67	0.56	1.70
340.00	94.50	35.34	0.59	1.92
350.00	97.05	35.29	0.59	1.92
360.00	99.61	36.83	0.61	2.05
370.00	102.17	39.47	0.63	2.29
380.00	104.73	39.47	0.63	2.29
390.00	107.29	40.21	0.64	2.36
400.00	109.85	39.81	0.64	2.32
410.00	112.40	41.76	0.65	2.52
420.00	114.96	39.86	0.64	2.33
430.00	117.52	39.20	0.63	2.26
440.00	120.08	37.91	0.62	2.14
450.00	122.64	36.99	0.61	2.06
460.00	125.20	34.96	0.59	1.89
470.00	126.45	35.82	0.60	1.96
480.00	127.70	32.55	0.56	1.70
490.00	132.60	35.78	0.60	1.96
500.00	137.88	37.67	0.62	2.12
515.00	141.40	33.16	0.57	1.74
525.00	141.98	30.90	0.54	1.57
535.00	142.57	30.61	0.54	1.55
545.00	143.16	29.85	0.53	1.49
555.00	143.74	28.61	0.51	1.41
565.00	144.33	30.57	0.54	1.55
575.00	144.92	32.31	0.56	1.68
585.00	145.50	34.26	0.58	1.83
595.00	146.09	34.35	0.58	1.84
605.00	146.68	35.62	0.59	1.94
615.00	147.26	34.67	0.58	1.86
625.00	147.85	33.33	0.57	1.76
635.00	148.44	34.96	0.59	1.89
645.00	149.00	32.29	0.56	1.68
655.00	149.61	34.34	0.58	1.84
665.00	150.20	37.14	0.61	2.08
675.00	150.80	39.38	0.63	2.28
685.00	151.40	33.58	0.57	1.78
695.00	152.00	32.98	0.57	1.73
705.00	152.60	35.09	0.59	1.90
715.00	158.20	30.20	0.53	1.52
725.00	160.60	35.02	0.59	1.89
735.00	163.00	29.61	0.53	1.48
745.00	164.48	36.32	0.60	2.00
755.00	166.66	34.10	0.58	1.82
765.00	167.80	39.43	0.63	2.29

TABLE C.2:1 XRD MINERALS PEAK RATIO DATA CORE CD1715

DEPTH (CM)	AGE KYRS	QTZ(I)/ FLD(I)	QTZ(I)/ CHL(I)	QTZ(I)/ ILL(I)	FLD(I)/ CHL(I)	DOL* (CFB)	DOL**
0.00	0.00	0.69	1.20	2.66	1.65	5.33	9.39
10.00	8.31	1.10	0.67	1.40	0.61	1.92	5.32
20.00	10.57	0.44	1.15	2.90	0.80	2.81	5.56
32.00	13.57	1.71	2.00	4.80	1.16	4.13	6.60
35.00	14.28	0.67	0.87	2.30	1.29	3.18	7.13
40.00	15.49	1.38	1.20	2.80	0.86	3.00	5.72
50.00	17.25	0.66	1.48	4.00	2.24	3.27	6.80
60.00	19.05	0.82	1.34	4.30	1.63	3.42	6.04
70.00	20.83	0.67	1.45	3.90	2.15	3.85	6.13
80.00	22.64	0.57	1.49	4.00	2.56	3.38	7.64
100.00	24.45	0.52	1.32	3.20	2.58	4.16	6.35
110.00	26.28	1.30	1.47	3.20	1.11	3.39	7.48
120.00	28.33	0.80	0.99	3.50	1.16	4.20	8.19
150.00	30.38	1.19	1.42	4.50	1.35	3.39	4.77
160.00	32.43	0.43	1.42	4.10	3.40	2.62	5.59
164.00	33.25	0.85	1.18	3.40	1.37	4.53	5.65
174.00	35.30	0.92	1.52	4.20	1.58	2.93	4.83
184.00	37.38	0.42	0.92	2.90	1.55	4.40	4.68
194.00	39.85	0.52	0.93	3.00	1.78	4.69	5.30
204.00	42.85	0.94	1.00	4.30	1.03	2.65	4.39
214.00	45.84	0.58	2.00	4.00	3.39	3.38	6.33
224.00	48.82	0.47	1.10	3.70	2.43	4.05	4.65
234.00	54.70	0.84	1.43	3.30	2.21	2.49	4.15
244.00	57.58	0.42	1.46	3.60	3.47	2.49	3.96
254.00	60.47	0.76	1.70	6.60	2.22	1.88	3.45
264.00	67.14	0.48	1.10	4.50	2.28	3.12	4.86
284.00	80.00	0.88	1.44	4.00	1.58	5.22	3.64
294.00	84.22	0.95	1.60	4.90	1.69	2.86	5.25
304.00	88.44	0.80	1.45	3.80	1.83	2.65	4.99
309.00	90.55	0.82	1.32	5.30	1.75	1.72	4.50
319.00	99.00	0.30	0.86	5.00	2.83	1.87	3.13
329.00	108.60	1.10	1.10	4.20	0.97	1.65	3.67
339.00	118.20	0.85	1.08	2.93	1.26	1.67	3.09
349.00	121.70	1.04	1.54	3.70	1.45	2.04	3.79
359.00	125.20	0.47	0.81	2.10	1.72	2.23	2.82
369.00	127.20	0.92	1.76	3.60	1.92	2.81	3.52
379.00	132.60	1.03	1.72	5.10	1.66	3.13	3.38
390.00	136.60	0.82	0.98	3.90	1.19	2.67	3.43
400.00	138.20	0.91	1.05	3.30	1.14	3.40	5.96
410.00	141.40	1.41	3.00	9.00	3.85	10.00	7.70
420.00	150.20	1.16	2.27	6.40	1.91	4.01	3.93
430.00	150.90	1.01	1.75	3.90	1.76	3.11	2.21
440.00	151.16	1.00	1.20	4.60	1.21	2.62	3.06
450.00	152.30	1.60	2.00	7.00	1.25	2.40	3.09
454.00	152.58	0.83	0.90	2.80	1.08	2.12	2.00
464.00	158.20	0.82	1.32	4.30	1.59	3.88	1.51
474.00	161.40	1.02	1.12	4.50	1.10	2.09	2.49
484.00	164.60	0.92	1.22	3.60	1.30	2.48	3.10
494.00	167.80	0.62	1.25	4.30	2.00	2.08	1.96
504.00	171.06	0.88	0.65	2.00	0.74	1.33	2.63
514.00	174.32	1.03	1.57	4.40	1.52	1.51	0.22
524.00	177.58	0.89	1.26	3.60	1.42	1.18	0.44
534.00	180.84	1.00	1.62	6.30	1.94	2.50	6.21
544.00	184.12	1.19	0.71	2.40	0.81	4.00	8.16
554.00	187.40	0.48	1.26	2.86	2.52	3.21	5.29
564.00	190.70	1.00	1.04	3.50	1.05	0.81	0.48
574.00	192.09	0.96	0.85	2.85	0.88	2.82	1.16
584.00	205.00	1.10	1.14	4.50	1.03	3.19	2.57
594.00	206.61	1.23	1.68	4.90	1.36	3.53	5.59
598.00	207.41	1.24	0.94	3.40	0.77	3.22	6.35
608.00	209.10	1.17	0.88	3.70	0.76	4.30	7.35
618.00	210.50	0.88	1.09	2.70	1.12	5.59	8.95
628.00	216.00	1.03	1.60	5.80	1.54	2.79	6.42
636.00	223.38	1.48	0.86	3.36	0.57	3.33	7.90
648.00	228.00	0.72	0.84	3.00	1.16	2.68	6.32
663.00	230.90	0.76	1.42	4.13	1.17	4.26	6.05
682.00	232.00	0.83	1.16	3.60	1.38	3.55	5.17
706.00	233.70	1.19	1.70	6.40	1.42	4.50	4.43
712.00	239.10	0.73	2.04	7.30	2.73	3.03	3.98
722.00	244.00	1.34	1.20	4.72	0.90	3.23	3.53
733.00	245.50	0.75	3.36	10.00	1.50	3.09	3.09

*DOLOMITE % CALCULATED FROM XRD METHOD
**DOLOMITE % CARBONATE FREE BASIS CALCULATED FROM CHEMISTRY

TABLE C.2:2 XRD MINERALS PEAK RATIO DATA CORE CD1730

DEPTH CM	AGE KYRS	QTZ(I)/ FLD(I)	QTZ(I)/ CHL(I)	QTZ(I)/ ILL(I)	FLD(I)/ CHLL(I)	DOL* (CFB)	DOL**
0.00	0.00	1.00	0.70	3.20	0.70	0.49	3.07
10.00	2.60	1.05	1.94	6.60	1.84	0.40	3.22
20.00	5.10	0.86	0.37	1.41	0.42	0.58	3.32
30.00	7.70	1.16	0.32	1.45	0.27	0.99	3.36
40.00	10.00	0.84	0.45	1.78	0.53	0.52	4.82
50.00	12.00	0.94	0.39	1.30	0.41	0.57	5.05
60.00	13.50	1.42	2.18	7.80	1.53	0.77	6.77
70.00	15.50	1.34	2.46	8.40	1.83	0.70	7.10
80.00	16.60	1.04	0.51	1.70	0.48	0.86	6.78
90.00	18.10	1.60	2.18	8.00	1.36	0.56	6.13
100.00	19.20	1.03	2.29	8.40	2.21	0.66	6.62
110.00	20.30	1.28	2.00	5.00	1.56	0.59	6.58
120.00	21.40	1.16	2.94	7.85	2.53	0.62	6.37
130.00	22.60	1.36	1.36	6.70	1.81	0.54	6.21
140.00	24.00	1.09	1.15	3.40	1.05	0.56	5.72
150.00	25.30	1.02	0.54	1.90	0.53	0.67	5.43
160.00	26.70	1.02	2.19	7.84	2.14	0.58	4.81
170.00	28.20	1.20	2.22	4.00	1.14	0.52	4.83
180.00	29.40	1.31	2.67	9.35	2.04	0.59	5.10
190.00	30.70	1.29	2.44	7.80	1.89	0.53	6.40
200.00	32.00	0.92	3.10	10.00	3.36	0.58	6.34
210.00	33.40	1.46	0.85	2.70	0.58	0.57	5.89
220.00	34.70	0.92	0.54	1.70	0.59	0.54	5.28
230.00	36.10	1.11	0.48	1.64	0.43	0.53	4.97
240.00	37.40	1.22	1.16	3.82	0.94	0.56	5.02
250.00	39.50	1.20	1.20	7.20	2.03	0.54	4.66
260.00	41.60	1.14	1.14	5.65	1.67	0.49	5.24
270.00	43.70	0.96	0.96	8.86	2.38	0.52	4.83
280.00	45.80	1.35	2.58	8.00	1.90	0.46	3.47
290.00	50.00	0.91	0.91	2.80	0.99	0.50	3.52
295.00	52.10	1.30	2.69	9.40	2.06	0.77	4.23
305.00	56.30	1.16	2.70	7.85	2.32	0.69	4.64
315.00	60.50	1.33	2.60	6.80	1.95	0.35	5.99
325.00	63.50	0.64	2.32	5.10	3.62	0.52	5.11
345.00	80.00	0.98	2.78	6.62	2.84	0.53	3.96
355.00	84.50	1.27	1.56	5.87	1.23	0.49	4.79
365.00	89.00	1.34	1.93	6.80	1.43	0.59	4.95
375.00	93.60	1.11	1.81	5.70	1.63	0.56	5.15
385.00	99.00	1.15	1.71	5.20	1.48	0.48	3.99
395.00	102.20	0.90	1.07	3.50	1.10	0.67	4.60
405.00	108.60	0.96	2.30	6.70	2.38	0.54	2.92
415.00	115.00	1.02	2.46	8.00	2.40	0.57	4.02
425.00	121.40	1.28	2.91	10.00	2.72	0.53	4.87
435.00	128.00	0.53	2.43	8.75	1.87	0.49	4.41
450.00	130.10	1.46	0.79	2.60	0.54	0.67	3.87
460.00	132.20	1.18	2.32	5.50	1.96	0.61	3.34
470.00	134.40	1.61	2.46	8.00	1.52	0.42	3.45
480.00	136.50	1.25	0.68	2.00	0.54	0.51	3.04
490.00	138.60	0.88	0.60	2.00	0.68	0.58	3.27
500.00	140.70	0.64	1.11	2.20	1.73	0.53	3.49
510.00	142.80	1.35	0.95	3.80	0.70	0.49	3.72
520.00	144.90	1.43	0.69	2.26	0.48	0.50	2.80
530.00	147.10	0.92	0.46	1.68	0.50	0.47	3.52
540.00	149.20	1.09	0.56	2.00	0.51	0.48	2.86
550.00	151.30	1.27	2.00	6.75	1.57	0.47	2.92
560.00	153.40	1.26	0.55	1.78	0.44	0.40	2.05
570.00	155.50	1.48	2.57	7.00	1.73	0.52	1.40
580.00	157.70	1.25	0.91	3.46	0.73	0.47	1.44
590.00	159.80	1.02	0.76	2.48	0.74	0.54	3.25
600.00	163.20	0.93	0.79	2.54	0.84	0.47	3.22
610.00	166.70	1.31	1.86	7.70	1.41	0.51	3.93
620.00	170.10	1.17	0.46	1.69	0.39	0.45	6.35
630.00	173.60	1.13	0.26	0.98	0.23	0.47	2.43
640.00	177.00	1.19	0.49	1.76	0.41	0.44	1.65
650.00	180.50	0.79	0.40	1.36	0.51	0.33	0.07
660.00	184.10	0.73	1.39	4.33	1.89	0.51	0.90
670.00	191.00	0.83	2.03	6.93	2.43	0.50	3.16
680.00	198.00	1.12	0.84	1.75	0.75	0.48	1.61
690.00	205.00	1.20	1.90	6.00	1.58	0.64	1.85
700.00	209.80	1.28	1.44	4.45	1.11	0.58	4.10
710.00	214.60	1.06	0.50	1.83	0.47	0.77	5.95
720.00	219.40	0.67	1.78	5.36	1.48	0.75	6.30
730.00	224.10	1.12	2.00	6.45	1.77	0.58	5.94
740.00	228.90	1.36	1.58	4.90	1.16	0.69	6.31
750.00	233.70	1.36	2.77	7.15	2.04	0.53	6.14
760.00	238.50	1.12	1.12	5.30	1.42	0.55	5.96
770.00	243.30	1.28	1.28	3.96	1.00	0.57	5.94
780.00	248.10	1.42	3.00	10.00	2.14	0.52	5.29
790.00	252.80	0.85	2.26	6.18	2.66	0.59	5.98
800.00	257.60	1.15	2.94	7.50	2.54	0.60	6.25

* DOLOMITE % CALCULATED FROM XRD METHOD
** DOLOMITE % CARBONATE FREE BASIS CALCULATED FROM CHEMISTRY

TABLE C.2:3 XRD MINERALS PEAK RATIO DATA CORE CD1738

DEPTH CM	AGE KYRS	QTZ(I)/ FLD(I)	QTZ(I) CHL(I)	QTZ(I)/ ILL(I)	FLD(I)/ CHL(I)	DOL* (CFB)	DOL**
0.00	0.00	1.16	0.50	1.89	0.43	0.14	1.75
10.00	0.00	1.26	0.52	1.85	0.41	0.17	1.34
20.00	15.40	0.81	0.64	2.14	0.78	0.16	4.17
30.00	20.80	1.62	0.44	1.88	0.27	0.25	0.15
40.00	22.64	1.15	0.67	2.91	0.46	0.24	2.55
50.00	23.55	1.75	0.41	1.64	0.23	0.24	1.18
60.00	24.46	1.29	1.06	3.50	0.81	0.32	8.38
70.00	26.28	1.41	0.45	1.36	0.32	0.19	0.64
80.00	28.10	1.40	0.48	1.70	0.34	0.22	2.22
90.00	29.95	1.45	0.39	1.61	0.27	0.23	1.17
100.00	31.19	2.33	0.47	1.84	0.20	0.33	1.26
110.00	32.73	1.87	0.41	1.42	0.22	0.19	0.87
120.00	34.28	1.48	0.55	1.60	0.37	0.24	0.18
130.00	35.82	1.77	0.39	1.18	0.21	0.19	2.00
140.00	37.38	1.15	0.27	1.57	0.23	0.24	4.16
150.00	39.14	1.13	0.77	2.32	0.68	0.17	1.83
160.00	40.90	2.00	0.65	2.24	0.32	0.23	0.46
170.00	42.66	2.09	0.34	1.04	0.16	0.19	1.24
180.00	44.42	1.96	0.43	1.28	0.22	0.20	0.09
185.00	45.30	2.03	0.53	1.72	0.26	0.26	2.42
195.00	47.06	2.18	0.41	1.37	0.18	0.16	5.55
205.00	48.82	1.53	0.56	1.85	0.36	0.27	0.11
215.00	51.01	1.32	0.61	1.94	0.46	0.32	6.92
225.00	53.20	1.75	0.52	1.61	0.30	0.30	0.95
235.00	55.39	1.29	0.56	1.84	0.45	0.39	6.97
245.00	57.58	1.36	0.62	1.76	0.45	0.91	8.73
255.00	59.05	2.06	0.53	1.58	0.25	0.24	0.93
265.00	60.45	1.91	0.55	1.75	0.29	0.24	0.02
275.00	65.74	1.65	0.53	1.55	0.32	0.31	3.82
285.00	71.00	1.36	0.46	1.66	0.34	0.25	0.69
295.00	82.75	2.30	0.50	1.53	0.21	0.39	4.18
305.00	94.50	1.75	0.84	3.11	0.48	0.43	7.35
315.00	96.24	1.78	0.37	1.32	0.20	0.30	3.47
325.00	97.99	1.22	0.44	1.57	0.36	0.39	5.12
335.00	99.74	1.06	0.57	2.04	0.53	0.30	5.03
345.00	101.48	0.87	2.30	7.00	2.66	0.41	7.53
355.00	103.23	1.75	0.48	1.55	0.27	0.34	2.15
365.00	104.98	1.27	0.56	2.00	0.43	0.40	6.24
375.00	106.73	1.37	0.41	1.44	0.30	0.37	7.81
385.00	108.47	1.04	0.44	1.51	0.42	0.42	6.41
395.00	110.22	1.13	0.65	2.00	0.57	0.44	6.98
405.00	111.97	1.19	0.60	2.70	0.51	0.30	3.38
415.00	113.72	1.45	0.47	1.70	0.32	0.58	2.56
425.00	115.46	1.63	0.60	2.58	0.37	0.02	4.86
435.00	117.21	1.27	0.76	3.60	0.60	0.26	4.36
445.00	118.96	1.37	1.70	6.80	1.29	0.57	8.08
455.00	120.70	1.00	0.57	1.70	0.57	0.48	6.67
465.00	122.70	1.50	2.50	9.40	1.69	0.33	6.07
475.00	124.45	0.75	0.96	2.60	1.28	0.36	7.87
485.00	125.95	0.96	1.30	3.57	1.36	0.52	9.20
495.00	127.70	1.18	0.83	3.18	0.70	0.26	1.38
505.00	128.78	1.36	0.55	1.80	0.40	0.33	2.39
515.00	129.87	1.64	0.52	1.80	0.32	0.26	1.56
525.00	130.96	1.29	0.77	2.58	0.60	0.23	1.40
535.00	132.05	1.10	1.90	5.16	1.75	0.51	9.03
540.00	132.60	1.01	2.40	9.50	2.43	0.52	10.00
545.00	133.40	1.14	0.18	0.66	0.17	0.36	3.94
555.00	135.00	1.30	0.24	1.04	0.18	0.27	1.37
565.00	136.60	0.63	0.41	1.60	0.66	0.27	2.52
575.00	138.20	1.50	0.23	0.85	0.15	0.39	3.79
585.00	139.80	1.08	0.26	1.18	0.24	0.27	1.92
595.00	141.40	1.01	1.10	3.30	1.08	0.48	7.05
605.00	144.00	1.35	0.50	1.70	0.37	0.26	1.57
615.00	146.98	1.46	0.73	2.10	0.50	0.25	1.49
625.00	150.20	1.55	0.50	1.58	0.33	0.25	1.59
635.00	152.60	1.08	1.60	4.00	1.50	0.51	9.78
645.00	155.80	1.15	3.30	8.20	2.90	0.33	4.78
655.00	158.70	1.27	1.12	3.50	0.88	0.27	5.28
665.00	161.60	1.07	1.15	3.70	1.07	0.39	9.93

* DOLOMITE % CALCULATED FROM XRD METHOD
** DOLOMITE % CARBONATE FREE BASIS CALCULATED FROM CHEMISTRY

TABLE C.2:4 XRD MINERALS PEAK RATIO DATA OF CORE CD1739

DEPTH CM	AGE KYRS	QTZ(I)/ FLD(I)	QTZ(I)/ CHL(I)	QTZ(I)/ ILL(I)	FLD(I)/ CHL(I)	DOL* (CFB)	DOL**
0.00	0.00	1.50	0.38	1.44	0.26	0.45	2.31
10.00	10.00	2.63	0.63	2.20	0.24	0.72	3.90
20.00	15.50	2.90	0.28	1.00	0.09	0.53	2.79
30.00	16.83	2.75	1.13	3.66	0.41	0.60	3.26
40.00	18.16	2.88	0.73	2.88	0.25	0.57	3.06
50.00	19.49	0.87	0.76	2.87	0.26	0.68	3.01
60.00	20.82	3.30	0.87	3.00	0.25	0.50	2.90
70.00	21.73	2.40	0.54	2.00	0.22	0.40	2.84
80.00	22.64	0.43	0.80	2.66	0.32	0.46	2.15
90.00	23.55	2.82	0.72	2.66	0.20	0.67	1.45
100.00	24.46	2.75	1.10	3.23	0.40	0.75	2.57
110.00	25.67	3.16	2.17	6.90	0.68	0.52	1.59
120.00	26.88	2.30	0.71	2.50	0.31	0.46	3.12
130.00	28.10	2.50	0.62	2.10	0.25	0.71	2.21
140.00	29.64	2.27	0.89	2.77	0.39	0.45	2.18
150.00	31.19	2.00	0.57	2.00	0.29	0.49	2.29
160.00	32.74	2.20	0.66	2.00	0.30	0.54	2.21
170.00	34.29	2.33	0.84	2.90	0.36	0.47	2.74
180.00	35.83	1.66	0.89	2.77	0.53	0.47	1.95
190.00	37.38	4.28	2.10	7.27	0.31	0.34	1.51
200.00	41.61	2.88	0.96	3.12	0.46	0.48	2.19
210.00	45.84	2.36	1.23	4.00	0.52	0.44	2.34
220.00	49.76	2.18	1.14	3.69	0.52	0.55	2.61
230.00	53.68	2.58	1.55	4.10	0.62	0.42	1.24
240.00	57.58	0.33	1.42	4.60	0.28	0.50	2.50
250.00	59.01	2.00	0.58	2.00	0.29	0.40	1.94
260.00	60.45	2.17	0.54	1.72	0.25	0.48	1.93
270.00	63.92	2.69	0.46	1.46	0.17	0.54	0.49
280.00	67.40	5.00	1.20	3.68	0.44	0.43	0.90
290.00	68.60	2.31	0.87	2.55	0.38	0.44	0.50
300.00	69.80	2.00	2.40	4.84	0.93	0.50	0.91
310.00	71.00	2.12	2.42	4.85	1.14	0.37	1.57
320.00	80.00	2.95	1.03	4.00	0.35	0.40	0.24
330.00	87.25	2.73	0.70	2.30	0.25	0.38	0.13
340.00	94.50	2.50	0.37	1.25	0.15	0.46	0.56
350.00	97.05	2.30	0.28	0.90	0.12	0.63	1.68
360.00	99.61	0.73	0.97	2.10	0.42	0.58	3.58
370.00	102.17	0.90	0.73	2.20	0.38	0.49	3.73
380.00	104.73	1.92	1.00	2.52	0.52	0.44	3.44
390.00	107.29	1.23	1.50	3.50	1.21	0.55	3.87
400.00	109.85	2.46	2.05	4.60	0.83	0.45	3.57
410.00	112.40	2.46	2.20	4.50	0.90	0.47	2.69
420.00	114.96	1.80	1.36	2.97	0.75	0.42	1.69
430.00	117.52	3.28	2.10	5.30	0.65	0.42	1.83
440.00	120.08	1.46	1.09	3.10	0.74	0.46	2.87
450.00	122.64	1.73	0.95	3.00	0.54	0.49	2.18
460.00	125.20	1.85	0.92	2.60	0.50	0.47	2.62
470.00	126.45	2.26	0.89	2.30	0.39	0.49	2.41
480.00	127.70	1.96	0.82	2.30	0.41	0.63	5.79
490.00	132.60	3.30	1.15	3.50	0.34	0.49	2.23
500.00	137.88	1.86	0.87	2.50	0.46	0.52	2.29
515.00	141.40	0.87	1.00	3.20	0.53	0.49	2.29
525.00	141.98	2.37	0.44	1.35	0.18	0.59	1.95
535.00	142.57	2.54	1.27	3.73	0.50	0.57	2.09
545.00	143.16	1.83	0.91	2.29	0.50	0.52	2.67
555.00	143.74	3.42	0.66	1.92	0.27	0.55	1.87
565.00	144.33	1.40	0.28	1.00	0.12	0.47	1.64
575.00	144.92	2.48	0.61	2.10	0.29	0.45	1.65
585.00	145.50	2.55	0.85	2.55	0.33	0.45	2.79
595.00	146.09	2.15	0.74	2.38	0.34	0.52	3.11
605.00	146.68	2.47	0.91	3.00	0.36	0.54	3.28
615.00	147.26	1.61	1.00	2.80	0.62	0.54	2.97
625.00	147.85	2.68	0.67	2.15	0.25	0.78	2.60
635.00	148.44	2.10	0.95	3.60	0.45	0.52	2.75
645.00	149.00	2.42	0.48	1.60	0.20	0.42	2.49
655.00	149.61	2.33	0.58	2.30	0.25	0.52	1.39
665.00	150.20	1.80	0.81	3.00	0.23	0.43	2.19
675.00	150.80	2.50	1.00	3.60	0.38	0.34	2.71
685.00	151.40	2.00	0.39	1.20	0.19	0.42	1.23
695.00	152.00	1.90	0.54	1.68	0.28	0.38	1.55
705.00	152.60	2.53	0.43	1.58	0.17	0.39	1.80
715.00	158.20	1.34	0.38	1.25	0.28	0.58	1.51
725.00	160.60	2.25	0.38	1.20	0.17	0.36	0.76
735.00	163.00	2.40	0.39	1.38	0.16	0.46	1.36
745.00	164.48	2.57	0.42	1.50	0.16	0.33	0.20
755.00	166.66	2.50	0.54	1.66	0.22	0.41	1.29
765.00	167.80	0.61	0.88	2.53	0.33	0.43	1.27

* DOLOMITE % CALCULATED FROM XRD METHOD
** DOLOMITE % CARBONATE FREE BASIS CALCULATED FROM CHEMISTRY

TABLE C.3:1 SALT FREE MAJOR ELEMENTS DATA OF CORE CD1709

DEPTH (CM)	Si %	Al %	Fe %	Mg %	Ca %	K %	Ti %	Mn %	P %
00.00	11.87	2.48	1.31	2.25	21.55	0.67	0.195	0.0306	0.114
10.00	10.22	1.96	0.93	1.70	24.22	0.50	0.160	0.0310	0.167
20.00	11.35	2.43	1.27	2.31	21.58	0.68	0.19	0.0306	0.114
30.00	12.39	2.68	1.44	2.56	19.92	0.74	0.21	0.0306	0.092
40.00	12.07	2.59	1.43	2.41	20.88	0.71	0.21	0.0306	0.100
50.00	12.48	2.75	1.50	2.57	19.70	0.78	0.218	0.0380	0.091
60.00	12.68	2.78	1.57	2.66	19.65	0.79	0.220	0.0387	0.092
70.00	12.57	2.74	1.53	2.56	20.06	0.78	0.220	0.0387	0.096
80.00	12.89	2.83	1.61	2.67	19.63	0.79	0.220	0.0387	0.087
90.00	12.88	2.86	1.66	2.66	19.26	0.81	0.220	0.0306	0.096
100.00	12.98	2.88	1.65	2.61	19.48	0.80	0.222	0.0309	0.100
110.00	12.82	2.88	1.54	2.62	19.87	0.79	0.224	0.0326	0.097
120.00	13.00	2.94	1.68	2.67	19.21	0.80	0.230	0.0298	0.095
130.00	12.86	2.90	1.61	2.64	19.37	0.81	0.229	0.0336	0.095
140.00	12.93	2.90	1.67	2.67	19.39	0.80	0.230	0.0306	0.095
150.00	12.85	2.87	1.62	2.63	19.41	0.80	0.226	0.0326	0.099
160.00	12.85	2.92	1.64	2.68	19.37	0.81	0.232	0.0316	0.097
170.00	12.68	2.83	1.62	2.59	19.79	0.79	0.224	0.0306	0.100
180.00	12.62	2.80	1.52	2.55	19.85	0.79	0.225	0.0265	0.147
190.00	12.80	2.85	1.58	2.60	19.11	0.79	0.223	0.0306	0.106
200.00	12.52	2.78	1.59	2.53	19.91	0.78	0.223	0.0265	0.130
210.00	13.14	2.93	1.65	2.64	18.88	0.82	0.223	0.0316	0.137
220.00	13.00	2.90	1.63	2.60	19.16	0.81	0.233	0.0336	0.108
230.00	13.10	2.94	1.53	2.70	18.61	0.82	0.229	0.0316	0.120
240.00	13.31	2.95	1.69	2.61	18.37	0.82	0.233	0.0336	0.110
250.00	12.85	2.80	1.53	2.50	20.22	0.76	0.233	0.0336	0.097
260.00	12.91	2.95	1.73	2.55	19.01	0.81	0.229	0.0306	0.093
270.00	12.53	2.81	1.66	2.51	19.92	0.78	0.231	0.0360	0.108
280.00	12.76	2.75	1.56	2.49	19.85	0.77	0.226	0.0303	0.105
290.00	12.82	2.76	1.55	2.55	19.90	0.77	0.225	0.0290	0.097
300.00	12.74	2.76	1.51	2.53	19.94	0.77	0.227	0.0310	0.093
310.00	12.80	2.89	1.69	2.58	18.51	0.81	0.226	0.0303	0.141
320.00	12.41	2.76	1.53	2.48	19.99	0.77	0.224	0.0320	0.121
330.00	12.65	2.80	1.56	2.51	20.01	0.77	0.229	0.0333	0.104
340.00	12.40	2.73	1.48	2.42	20.11	0.75	0.220	0.0279	0.095
350.00	12.46	2.73	1.49	2.49	20.22	0.76	0.224	0.0294	0.099
360.00	12.80	2.84	1.56	2.51	19.66	0.79	0.228	0.0310	0.108
370.00	12.84	2.87	1.61	2.53	19.58	0.79	0.230	0.0333	0.113
380.00	12.95	2.91	1.65	2.55	19.50	0.81	0.231	0.0326	0.109
390.00	12.85	2.97	1.68	2.60	18.97	0.82	0.232	0.0316	0.120
400.00	12.94	2.94	1.65	2.67	18.80	0.80	0.232	0.0285	0.129
410.00	12.87	2.99	1.73	2.67	18.32	0.82	0.232	0.0275	0.165
420.00	12.98	3.02	1.84	2.73	18.30	0.83	0.231	0.0314	0.131
430.00	12.04	2.77	1.59	2.52	20.14	0.77	0.220	0.0275	0.12
440.00	12.75	2.82	1.57	2.61	19.72	0.79	0.225	0.031	0.119
450.00	12.49	2.75	1.53	2.57	19.84	0.78	0.221	0.0323	0.120
460.00	12.57	2.77	1.54	2.57	20.03	0.77	0.222	0.0329	0.116

TABLE C.3:2 SALT FREE MAJOR ELEMENTS DATA OF CORE CD1715

DEPTH (CM)	Si %	Al %	Fe %	Mg %	Ca %	K %	Ti %	Mn %	P %
0.000	12.500	2.740	1.660	2.400	20.380	0.750	0.235	0.246	0.061
10.000	6.560	1.790	1.300	1.240	28.720	0.530	0.154	0.092	0.041
20.000	7.980	2.330	1.420	1.600	26.420	0.680	0.215	0.061	0.041
32.000	11.110	3.160	2.010	2.260	21.920	0.990	0.277	0.051	0.041
35.000	10.560	2.890	2.270	2.150	22.530	0.960	0.257	0.061	0.041
40.000	12.890	3.700	2.240	2.530	19.710	1.100	0.297	0.061	0.041
50.000	11.730	3.290	2.110	2.320	21.180	1.100	0.266	0.051	0.051
60.000	10.750	3.090	1.960	2.160	22.200	0.910	0.257	0.061	0.051
70.000	11.600	3.310	2.210	2.450	20.500	0.950	0.270	0.083	0.052
80.000	12.460	3.320	2.110	2.540	19.610	0.980	0.277	0.092	0.061
90.000	15.370	2.900	1.480	2.710	18.290	0.800	0.333	0.060	0.060
100.000	11.440	3.200	2.050	2.270	21.530	0.990	0.290	0.062	0.051
110.000	11.760	3.450	2.430	2.590	19.620	1.030	0.302	0.128	0.062
120.000	11.790	3.410	2.290	2.660	19.380	1.010	0.302	0.177	0.073
130.000	15.680	2.470	0.940	1.940	19.930	0.750	0.192	0.300	0.050
140.000	18.050	2.450	0.800	1.750	18.030	0.820	0.191	0.300	0.040
150.000	12.540	3.410	2.160	2.250	20.390	1.020	0.277	0.082	0.051
160.000	12.500	3.390	2.110	2.330	20.230	1.010	0.278	0.082	0.051
164.000	13.610	3.720	2.350	2.560	18.510	1.120	0.298	0.072	0.051
174.000	12.690	3.490	2.120	2.310	19.970	1.040	0.278	0.072	0.051
184.000	12.200	3.360	2.300	2.210	20.580	1.010	0.268	0.072	0.051
194.000	12.660	3.430	2.080	2.330	19.900	1.040	0.268	0.072	0.051
204.000	12.120	3.460	2.180	2.240	20.230	1.010	0.258	0.144	0.051
214.000	13.370	3.280	2.040	2.380	19.390	0.940	0.268	0.154	0.061
224.000	10.880	2.970	1.880	1.960	22.500	0.860	0.268	0.132	0.051
234.000	12.050	3.280	2.260	2.110	20.850	0.980	0.266	0.071	0.051
244.000	9.920	2.780	1.810	1.780	23.420	0.810	0.246	0.082	0.051
254.000	14.470	3.830	2.470	2.370	18.350	1.140	0.321	0.062	0.051
264.000	11.960	2.980	2.180	2.040	20.250	0.860	0.269	0.093	0.051
274.000	11.730	3.160	2.010	2.670	21.510	0.900	0.271	0.083	0.052
284.000	9.720	2.680	1.670	1.690	23.940	0.770	0.247	0.072	0.051
294.000	9.390	2.380	1.750	1.670	23.880	0.690	0.218	0.218	0.052
304.000	8.640	2.150	1.540	1.500	25.010	0.610	0.208	0.104	0.052
309.000	8.100	2.170	1.390	1.460	25.780	0.590	0.196	0.103	0.041
319.000	8.890	2.420	1.460	1.480	25.580	0.690	0.227	0.103	0.041
329.000	9.640	2.620	1.860	1.650	24.290	0.800	0.237	0.082	0.051
339.000	9.430	2.630	1.630	1.200	24.560	0.770	0.236	0.082	0.041
349.000	9.930	2.710	1.820	1.700	24.030	0.820	0.237	0.082	0.041
359.000	10.050	2.790	1.580	1.670	24.070	0.830	0.247	0.133	0.051
369.000	14.660	3.900	2.420	2.410	18.170	1.170	0.317	0.071	0.041
379.000	13.890	3.820	2.560	2.350	18.690	1.170	0.307	0.071	0.051
390.000	14.700	4.050	2.640	2.500	17.310	1.210	0.318	0.061	0.061
400.000	13.470	3.650	2.470	2.590	17.490	1.020	0.279	0.062	0.082
410.000	15.070	3.520	2.020	2.740	17.400	1.390	0.274	0.061	0.061
420.000	15.970	4.350	2.950	2.760	15.000	1.270	0.340	0.092	0.051
430.000	16.230	4.340	2.780	2.530	15.320	1.330	0.318	0.102	0.051
440.000	13.700	3.720	2.500	2.270	18.270	1.060	0.298	0.134	0.061
450.000	12.570	3.400	2.420	2.080	19.930	0.980	0.279	0.144	0.062
454.000	11.360	3.150	2.010	1.820	21.800	0.950	0.257	0.134	0.061
464.000	15.710	4.370	2.970	2.450	16.020	1.320	0.349	0.092	0.061
474.000	13.090	3.590	2.560	2.120	19.250	1.050	0.299	0.133	0.062
484.000	12.240	3.320	2.240	2.030	20.560	0.910	0.279	0.124	0.062
494.000	10.050	2.780	1.870	1.600	24.610	0.780	0.242	0.116	0.063
504.000	9.410	2.600	1.770	1.560	24.270	0.760	0.226	0.113	0.061
514.000	9.630	2.850	1.890	1.500	23.600	0.850	0.226	0.082	0.061
524.000	11.880	3.560	2.270	1.810	21.060	1.040	0.268	0.082	0.061
534.000	12.730	3.490	2.290	2.510	18.330	1.010	0.259	0.114	0.062
544.000	13.620	3.360	2.150	2.700	17.820	0.960	0.277	0.164	0.092
547.000	14.270	3.830	2.460	2.440	17.440	1.140	0.300	0.372	0.093
554.000	12.970	3.560	2.310	2.440	18.220	1.210	0.289	0.207	0.082
564.000	18.990	5.310	3.520	2.830	11.060	1.620	0.394	0.145	0.072
574.000	12.880	3.600	2.340	1.990	19.550	1.070	0.277	0.092	0.061
584.000	8.460	2.500	1.430	1.480	26.060	0.750	0.215	0.092	0.051
594.000	10.580	3.010	1.960	2.060	22.810	0.910	0.256	0.061	0.041
598.000	10.590	3.000	1.870	2.120	23.020	0.910	0.265	0.061	0.051
508.000	10.910	2.990	1.930	2.260	21.640	0.940	0.256	0.051	0.061
618.000	11.050	3.060	2.110	2.520	20.390	0.940	0.257	0.051	0.061
628.000	12.130	3.280	2.260	2.360	20.270	1.010	0.287	0.051	0.051
636.000	12.280	3.320	2.250	2.580	19.410	0.990	0.277	0.061	0.061
643.000	15.810	2.930	1.400	2.680	18.210	0.790	0.322	0.020	0.050
648.000	12.250	3.730	2.390	2.620	19.220	1.060	0.278	0.061	0.061
653.000	16.700	2.830	1.280	2.340	18.050	0.780	0.322	0.020	0.050
663.000	10.950	3.020	1.840	2.120	22.460	0.910	0.235	0.071	0.051
668.000	15.750	3.120	1.530	2.580	17.940	0.890	0.222	0.030	0.040
676.000	16.890	2.950	1.240	2.330	17.800	0.830	0.211	0.030	0.040
682.000	13.560	3.710	2.140	2.490	18.890	1.130	0.316	0.061	0.051
687.000	14.440	3.860	2.790	2.900	16.670	1.210	0.319	0.051	0.061
692.000	15.830	3.070	1.610	2.740	17.650	0.860	0.353	0.030	0.060
700.000	16.210	2.670	1.250	2.200	18.700	0.760	0.272	0.030	0.060
706.000	16.140	4.410	2.930	2.860	14.990	1.330	0.347	0.061	0.051
712.000	13.060	3.610	2.190	2.290	19.590	1.070	0.287	0.061	0.051
722.000	13.290	3.690	2.350	2.290	19.330	1.110	0.297	0.051	0.051
733.000	13.100	3.640	2.350	2.210	19.780	1.050	0.298	0.061	0.051

TABLE C.3:3 SALT FREE MAJOR ELEMENTS DATA CORE CD1730

DEPTH (CM)	Si %	Al %	Fe %	Mg %	Ca %	K %	Ti %	Mn %	P %
0.000	15.630	4.350	2.840	2.480	14.330	1.170	0.259	1.118	0.082
10.000	14.900	4.160	2.730	2.383	16.260	1.110	0.238	0.621	0.072
20.000	11.500	3.350	2.230	1.930	21.570	0.920	0.176	0.342	0.051
30.000	11.270	3.190	2.230	1.970	21.720	0.920	0.185	0.144	0.061
40.000	11.350	3.190	2.180	1.980	21.900	0.930	0.196	0.041	0.051
50.000	11.680	3.270	1.950	2.040	21.580	0.950	0.185	0.061	0.051
60.000	13.300	3.610	2.140	2.450	19.550	1.070	0.215	0.051	0.051
70.000	14.940	3.950	2.490	2.740	17.120	1.220	0.235	0.051	0.051
80.000	14.820	3.910	2.410	2.680	17.220	1.200	0.245	0.051	0.051
90.000	14.000	3.760	2.350	2.500	18.090	1.160	0.226	0.051	0.051
100.000	14.110	3.710	2.400	2.540	17.920	1.130	0.227	0.051	0.015
110.000	14.310	3.770	2.380	2.570	17.700	1.140	0.216	0.061	0.051
120.000	13.900	3.660	2.330	2.480	18.060	1.100	0.216	0.061	0.051
130.000	14.740	3.860	2.480	2.600	16.600	1.150	0.227	0.072	0.062
140.000	13.810	3.660	2.370	2.410	17.770	1.100	0.227	0.061	0.051
150.000	15.560	4.140	2.480	2.650	16.250	1.250	0.256	0.071	0.051
160.000	15.390	4.050	2.460	2.520	16.520	1.210	0.247	0.061	0.051
170.000	15.450	4.080	2.710	2.560	15.650	1.210	0.248	0.072	0.062
180.000	15.410	4.030	2.590	2.560	15.960	1.200	0.248	0.082	0.062
190.000	15.750	4.070	2.530	2.760	15.600	1.240	0.257	0.072	0.061
200.000	16.280	4.180	2.730	2.820	15.200	1.290	0.266	0.071	0.051
210.000	16.560	4.310	2.660	2.830	14.860	1.320	0.266	0.071	0.061
220.000	16.660	4.270	2.770	2.780	14.780	1.300	0.268	0.061	0.061
230.000	16.170	4.300	2.610	2.690	15.360	1.290	0.267	0.082	0.061
240.000	15.460	4.130	2.450	2.580	16.730	1.210	0.257	0.061	0.072
250.000	16.220	4.210	2.780	2.600	15.580	1.260	0.268	0.061	0.061
260.000	15.950	4.150	2.670	2.640	15.850	1.260	0.257	0.061	0.061
270.000	16.500	4.390	2.610	2.720	15.180	1.320	0.266	0.082	0.051
280.000	14.430	3.870	2.440	2.250	17.610	1.140	0.226	0.072	0.072
290.000	15.130	3.980	2.590	2.320	16.970	1.200	0.247	0.072	0.061
295.000	15.370	3.990	2.500	2.420	16.550	1.190	0.247	0.082	0.061
305.000	15.800	4.130	2.580	2.560	15.680	1.240	0.267	0.102	0.061
315.000	15.850	4.050	2.880	2.750	13.790	1.890	0.260	0.072	0.072
325.000	15.170	3.860	2.760	2.500	15.250	1.120	0.239	0.104	0.073
335.000	17.750	4.670	2.810	2.730	13.620	1.400	0.288	0.072	0.061
345.000	16.320	4.320	2.880	2.590	14.310	1.270	0.280	0.083	0.072
355.000	16.000	4.140	2.880	2.620	14.190	1.220	0.269	0.103	0.082
365.000	14.150	3.650	2.400	2.310	17.900	1.090	0.238	0.103	0.062
375.000	12.700	3.270	2.060	2.100	19.870	0.970	0.217	0.175	0.062
385.000	12.880	3.370	2.170	2.020	20.210	0.990	0.216	0.134	0.051
395.000	13.320	3.450	2.290	2.140	19.520	1.010	0.226	0.103	0.051
405.000	13.120	3.710	2.260	2.070	20.340	1.010	0.211	0.105	0.063
415.000	13.780	3.610	2.260	2.160	19.110	1.120	0.225	0.102	0.051
425.000	15.010	3.890	2.480	2.430	17.340	1.190	0.245	0.091	0.051
435.000	16.150	4.260	2.680	2.590	15.710	1.310	0.265	0.081	0.051
450.000	16.280	4.300	2.670	2.540	15.790	1.350	0.266	0.081	0.051
460.000	15.320	4.130	2.510	2.370	17.000	1.240	0.256	0.102	0.051
470.000	15.750	4.200	2.620	2.430	16.270	1.290	0.266	0.092	0.051
480.000	16.410	4.440	2.790	2.510	15.350	1.350	0.277	0.082	0.061
490.000	17.210	4.660	3.010	2.670	13.880	1.410	0.288	0.082	0.061
500.000	17.850	4.810	3.290	2.790	12.710	1.470	0.309	0.113	0.072
510.000	17.630	4.780	3.240	2.810	12.490	1.400	0.300	0.124	0.062
520.000	18.070	4.770	2.920	2.670	12.980	1.460	0.288	0.092	0.061
530.000	16.410	4.460	2.910	2.590	14.780	1.310	0.278	0.113	0.061
540.000	15.990	4.420	2.830	2.480	15.110	1.280	0.269	0.124	0.072
550.000	16.880	4.570	3.060	2.580	13.720	1.380	0.269	0.186	0.083
560.000	16.090	4.450	2.910	2.390	15.160	1.310	0.259	0.165	0.082
570.000	16.430	4.540	2.680	2.350	15.490	1.350	0.277	0.123	0.061
580.000	18.300	5.030	3.230	2.610	12.640	1.530	0.308	0.092	0.071
590.000	17.380	4.690	3.180	2.690	13.220	1.360	0.279	0.186	0.093
600.000	16.620	4.520	2.860	2.580	14.690	1.340	0.267	0.154	0.082
610.000	14.840	4.050	2.770	2.410	16.690	1.150	0.238	0.217	0.082
620.000	12.970	3.620	2.500	2.410	19.480	1.100	0.207	0.155	0.082
630.000	13.780	3.830	2.360	2.090	19.460	1.100	0.217	0.144	0.072
640.000	15.070	4.400	2.790	1.920	16.650	1.310	0.237	0.124	0.072
650.000	19.330	5.470	3.470	2.630	11.210	1.640	0.319	0.092	0.072
660.000	20.790	5.830	3.880	2.940	8.350	1.720	0.333	0.062	0.093
670.000	16.780	4.500	3.040	2.570	14.320	1.310	0.269	0.124	0.072
680.000	14.850	4.180	2.570	2.190	17.060	1.210	0.238	0.124	0.072
690.000	12.500	3.640	2.240	1.930	20.130	1.110	0.194	0.112	0.061
700.000	13.530	3.690	2.160	2.210	18.860	1.140	0.224	0.102	0.051
710.000	13.220	3.510	2.160	2.320	19.470	1.090	0.225	0.092	0.051
720.000	13.820	3.690	2.150	2.450	19.140	1.120	0.237	0.257	0.160
730.000	12.950	3.480	2.240	2.310	19.160	1.050	0.217	0.082	0.062
740.000	12.520	3.410	2.290	2.310	19.370	1.770	0.216	0.082	0.061
750.000	11.870	3.200	2.220	2.310	15.530	1.080	0.185	0.075	0.051
760.000	13.850	3.620	2.300	2.390	18.810	1.090	0.216	0.092	0.051
770.000	13.830	3.600	2.290	2.380	18.810	1.100	0.216	0.092	0.051
780.000	14.320	3.860	2.540	2.470	17.130	1.270	0.236	0.092	0.051
790.000	14.370	3.720	2.320	2.460	18.110	1.120	0.235	0.092	0.051
800.000	14.070	3.660	2.250	2.470	17.950	1.140	0.225	0.092	0.051

TABLE C.3:4 SALT FREE MAJOR ELEMENTS DATA OF CORE CD1738

DEPTH (CM)	Si %	Al %	Fe %	Mg %	Ca %	K %	Ti %	Mn %	P %
0.000	24.360	7.550	4.270	2.470	4.230	2.210	0.400	0.055	0.079
10.000	24.140	7.890	4.640	2.500	3.870	2.350	0.400	0.063	0.079
20.000	23.940	7.040	4.370	2.750	4.160	2.020	0.390	0.063	0.084
30.000	25.070	7.380	4.170	2.180	4.470	2.100	0.410	0.062	0.073
40.000	24.310	6.920	4.100	2.450	4.990	1.940	0.370	0.070	0.083
50.000	23.660	7.840	4.600	2.470	4.370	2.860	0.410	0.070	0.079
60.000	19.460	5.440	3.410	2.880	9.960	1.580	0.290	0.095	0.088
70.000	23.640	7.720	4.530	2.350	4.770	2.310	0.420	0.070	0.074
80.000	23.230	7.510	4.590	2.560	5.050	2.270	0.420	0.070	0.079
90.000	24.910	7.070	4.920	2.250	4.970	2.060	0.410	0.062	0.074
100.000	24.900	6.830	5.030	2.210	5.090	1.930	0.400	0.070	0.074
110.000	23.400	7.800	4.540	2.420	5.030	2.320	0.430	0.067	0.073
120.000	23.180	8.190	4.720	2.410	4.930	2.430	0.450	0.069	0.068
130.000	22.020	7.910	4.240	2.410	6.570	2.130	0.400	0.087	0.070
140.000	20.420	6.430	3.810	2.500	8.990	2.130	0.400	0.072	0.064
150.000	24.950	5.870	3.200	2.010	8.940	1.920	0.340	0.058	0.072
160.000	25.010	6.890	3.930	2.100	5.450	1.940	0.420	0.065	0.073
170.000	23.130	7.400	4.350	2.350	5.580	2.200	0.410	0.064	0.070
180.000	22.370	7.600	4.390	2.220	5.550	2.270	0.430	0.069	0.067
185.000	23.830	7.830	4.490	2.240	5.080	2.330	0.440	0.078	0.069
195.000	26.000	8.900	4.590	3.210	6.300	2.700	0.490	0.080	0.077
205.000	24.010	7.550	4.350	2.220	5.340	2.200	0.430	0.066	0.066
215.000	18.850	5.610	3.600	2.650	11.210	1.690	0.320	0.061	0.069
225.000	22.940	7.370	4.340	2.300	5.990	2.220	0.420	0.063	0.067
235.000	19.920	5.840	3.610	2.770	10.310	1.710	0.330	0.066	0.064
245.000	18.700	4.760	3.130	2.630	12.810	1.340	0.320	0.071	0.060
255.000	22.880	7.470	4.500	2.330	6.080	2.230	0.430	0.066	0.070
265.000	23.670	7.710	4.450	2.310	5.370	2.290	0.430	0.060	0.068
275.000	20.260	6.510	4.100	2.480	9.450	1.950	0.360	0.070	0.066
285.000	23.170	7.360	4.280	2.250	6.400	2.170	0.420	0.055	0.069
295.000	20.090	6.060	3.820	2.410	10.140	1.850	0.340	0.065	0.060
305.000	17.730	5.130	3.120	2.530	13.220	1.530	0.300	0.060	0.067
315.000	19.770	6.490	3.740	2.430	9.260	1.980	0.350	0.061	0.061
325.000	18.930	6.100	3.670	2.530	10.970	1.850	0.330	0.059	0.061
335.000	20.080	5.940	3.500	2.480	10.480	1.730	0.330	0.063	0.065
345.000	12.160	3.660	2.170	2.140	11.810	0.910	0.160	0.040	0.053
355.000	20.700	7.300	4.280	2.460	8.270	2.220	0.380	0.064	0.065
365.000	17.220	5.210	3.280	2.410	13.600	1.570	0.300	0.066	0.059
375.000	18.870	5.450	3.160	2.750	11.720	1.660	0.300	0.062	0.062
385.000	18.760	5.600	3.240	2.570	11.980	1.700	0.310	0.057	0.057
395.000	19.360	5.330	3.200	2.590	11.670	1.610	0.310	0.064	0.058
405.000	22.320	6.240	3.590	2.370	8.280	1.810	0.360	0.056	0.071
415.000	18.790	6.440	3.720	2.240	11.040	1.960	0.360	0.059	0.068
425.000	20.550	6.230	3.620	2.580	9.520	1.890	0.360	0.060	0.062
435.000	21.680	6.280	3.730	2.540	8.530	1.820	0.360	0.060	0.069
445.000	18.550	5.110	3.160	2.660	12.630	1.540	0.300	0.078	0.060
455.000	19.050	5.410	3.250	2.550	11.730	1.640	0.320	0.063	0.059
465.000	19.990	5.790	3.410	2.620	10.570	1.780	0.330	0.063	0.062
475.000	18.740	5.380	3.150	2.740	11.690	1.670	0.300	0.059	0.063
485.000	18.010	4.490	2.770	2.610	13.510	1.280	0.280	0.062	0.065
495.000	25.820	5.750	3.130	1.920	6.680	1.500	0.390	0.063	0.076
505.000	23.170	6.600	3.820	2.330	6.960	1.920	0.390	0.073	0.068
515.000	21.510	7.340	4.290	2.410	7.010	2.230	0.410	0.061	0.066
525.000	24.010	6.270	3.550	2.050	7.300	1.760	0.380	0.056	0.069
535.000	19.630	4.360	2.380	2.570	13.040	1.230	0.250	0.052	0.057
540.000	18.770	3.690	2.020	2.550	15.050	0.950	0.260	0.046	0.059
545.000	20.770	6.570	3.890	2.540	8.530	2.010	0.260	0.046	0.062
555.000	24.610	6.600	3.710	2.170	6.100	1.880	0.400	0.060	0.068
565.000	21.660	7.710	4.180	2.500	7.260	2.180	0.390	0.077	0.065
575.000	21.060	6.810	4.010	2.590	8.160	2.070	0.370	0.069	0.068
585.000	24.640	6.720	3.770	2.300	6.040	1.920	0.390	0.062	0.067
595.000	19.200	5.300	3.380	2.570	11.240	1.620	0.310	0.069	0.065
605.000	23.340	6.760	3.780	2.240	7.270	1.930	0.390	0.066	0.073
615.000	23.310	6.790	3.850	2.240	6.940	1.960	0.400	0.061	0.072
625.000	23.150	7.270	4.130	2.400	6.270	2.170	0.420	0.063	0.071
635.000	17.700	4.300	2.710	2.600	13.960	1.250	0.270	0.071	0.069
645.000	22.280	5.560	3.220	2.370	8.960	1.560	0.330	0.085	0.065
655.000	20.690	5.860	3.510	2.520	9.670	1.700	0.340	0.077	0.068
665.000	20.390	5.350	3.780	2.500	8.820	1.520	0.320	0.072	0.072
675.000	19.700	5.060	3.090	3.300	11.280	1.430	0.300	0.071	0.065

TABLE C.3:5 SALT FREE MAJOR ELEMENTS DATA OF CORE CD1739

DEPTH (CM)	Si %	Al %	Fe %	Mg %	Ca %	K %	Ti %	Mn %	P %
0.000	10.800	2.970	1.780	1.380	23.260	0.835	0.192	0.040	0.048
10.000	16.180	4.290	2.380	2.170	16.590	1.273	0.268	0.047	0.055
20.000	17.040	4.420	2.430	2.110	15.540	1.316	0.262	0.039	0.061
30.000	15.770	4.160	2.370	2.040	16.810	1.230	0.245	0.039	0.061
40.000	15.510	4.030	2.360	1.960	17.080	1.198	0.245	0.039	0.056
50.000	15.540	4.090	2.360	1.980	17.060	1.214	0.245	0.039	0.056
60.000	15.100	3.980	2.420	1.910	17.510	1.157	0.235	0.039	0.056
70.000	15.650	4.150	2.480	1.990	16.860	1.222	0.251	0.039	0.056
80.000	16.590	4.330	2.480	1.990	16.060	1.291	0.251	0.039	0.061
90.000	16.810	4.390	2.440	1.930	15.920	1.298	0.251	0.039	0.061
100.000	19.640	5.070	3.070	2.300	18.830	1.484	0.294	0.047	0.079
110.000	17.360	4.510	2.620	1.990	16.500	1.290	0.288	0.041	0.064
120.000	16.320	4.240	2.470	2.070	16.240	1.264	0.275	0.039	0.061
130.000	18.090	4.640	2.620	2.140	14.300	1.398	0.292	0.039	0.061
140.000	17.300	4.510	2.630	2.070	14.980	1.339	0.269	0.039	0.065
150.000	17.190	4.530	2.570	2.090	15.300	1.347	0.269	0.039	0.065
160.000	17.040	4.490	2.620	2.060	15.440	1.339	0.268	0.039	0.065
170.000	17.130	4.520	2.490	2.140	15.330	1.357	0.281	0.039	0.069
180.000	16.800	4.460	2.500	2.020	15.700	1.332	0.275	0.047	0.061
190.000	16.220	4.330	2.580	1.910	16.390	1.290	0.263	0.039	0.061
200.000	16.270	4.290	2.510	1.980	15.880	1.264	0.263	0.039	0.065
210.000	16.420	4.270	2.540	1.990	15.880	1.222	0.263	0.039	0.069
220.000	15.220	4.050	2.530	1.920	17.120	1.190	0.245	0.039	0.074
230.000	14.900	3.990	2.250	1.730	18.210	1.164	0.232	0.094	0.061
240.000	14.200	3.770	2.210	1.770	19.020	1.097	0.227	0.039	0.061
250.000	16.260	4.240	2.330	1.920	16.770	1.256	0.256	0.047	0.065
260.000	17.900	4.570	2.470	2.070	14.850	1.380	0.274	0.047	0.060
270.000	18.530	4.770	2.640	1.940	15.390	1.382	0.283	0.040	0.063
280.000	15.740	4.250	2.450	1.800	16.260	1.240	0.238	0.039	0.060
290.000	17.110	4.550	2.420	1.880	15.850	1.330	0.268	0.047	0.065
300.000	16.920	4.570	2.800	1.940	15.230	1.348	0.269	0.039	0.074
310.000	16.780	4.470	2.710	1.980	15.690	1.250	0.269	0.038	0.065
320.000	15.600	4.300	4.430	1.750	17.460	1.220	0.256	0.038	0.065
330.000	17.020	4.690	2.590	1.860	15.790	1.372	0.274	0.038	0.069
340.000	13.620	3.760	2.220	1.560	19.820	1.080	0.226	0.038	0.074
350.000	15.120	4.140	2.280	1.840	18.020	1.220	0.238	0.038	0.069
360.000	14.390	3.890	2.120	1.940	18.780	1.470	0.226	0.038	0.069
370.000	14.460	3.890	2.120	1.960	18.570	1.148	0.226	0.038	0.065
380.000	13.870	3.630	2.120	1.840	19.380	1.047	0.214	0.038	0.065
390.000	14.930	3.840	2.280	1.980	17.340	1.113	0.233	0.038	0.074
400.000	14.780	3.800	2.250	1.920	17.870	1.109	0.233	0.038	0.074
410.000	15.660	4.120	2.520	1.970	16.080	1.206	0.276	0.038	0.078
420.000	14.780	3.850	2.430	1.730	17.500	1.139	0.245	0.030	0.074
430.000	15.230	3.910	2.320	1.770	17.330	1.164	0.251	0.038	0.061
440.000	14.960	3.850	2.380	1.860	17.750	1.156	0.250	0.038	0.061
450.000	15.970	4.100	2.290	1.890	17.040	1.240	0.275	0.038	0.057
460.000	14.880	3.840	2.510	1.830	17.760	1.164	0.262	0.030	0.055
470.000	15.530	3.990	2.300	1.870	17.360	1.190	0.275	0.038	0.061
480.000	17.460	4.260	2.310	1.980	16.410	1.281	0.264	0.046	0.061
490.000	15.460	4.120	2.430	1.900	17.390	1.223	0.254	0.038	0.061
500.000	15.980	4.190	2.390	1.960	16.800	1.239	0.269	0.038	0.061
515.000	16.320	4.250	2.380	1.970	16.430	1.273	0.274	0.038	0.061
525.000	17.750	4.590	2.560	2.080	14.860	1.368	0.298	0.046	0.065
535.000	18.070	4.610	2.480	2.110	14.500	1.364	0.304	0.046	0.061
545.000	17.850	4.530	2.550	2.150	14.890	1.355	0.304	0.046	0.056
555.000	18.510	4.720	2.610	2.130	14.040	1.429	0.316	0.046	0.060
565.000	18.140	4.700	2.550	2.090	14.380	1.414	0.310	0.046	0.061
575.000	17.650	4.460	2.550	1.990	14.950	1.347	0.310	0.039	0.065
585.000	17.610	4.510	2.740	2.160	14.480	1.373	0.311	0.046	0.065
595.000	17.630	4.570	2.750	2.230	14.300	1.407	0.311	0.039	0.065
605.000	17.360	4.490	2.820	2.220	14.370	1.335	0.293	0.039	0.065
615.000	17.080	4.420	2.620	2.140	15.060	1.338	0.293	0.039	0.065
625.000	17.690	4.610	2.680	2.180	14.210	1.339	0.298	0.039	0.065
635.000	17.620	4.600	2.830	2.200	13.830	1.389	0.311	0.039	0.065
645.000	17.710	4.630	2.520	2.170	14.530	1.398	0.304	0.039	0.061
655.000	18.350	4.840	2.780	2.120	13.350	1.407	0.306	0.039	0.065
665.000	18.510	4.920	3.100	2.270	12.420	1.457	0.323	0.039	0.069
675.000	16.460	4.470	2.980	2.130	14.790	1.483	0.294	0.039	0.065
685.000	16.760	4.480	2.620	1.940	15.710	1.323	0.292	0.039	0.055
695.000	16.810	4.550	2.670	2.010	15.490	1.346	0.310	0.039	0.056
705.000	15.480	4.200	2.480	1.880	17.140	1.345	0.287	0.039	0.056
715.000	17.360	4.680	2.640	2.060	14.940	1.246	0.316	0.039	0.056
725.000	16.960	4.690	2.670	1.970	15.190	1.406	0.299	0.047	0.061
735.000	18.760	5.370	2.620	1.970	13.650	1.388	0.322	0.039	0.061
745.000	16.380	4.590	2.530	1.860	15.980	1.498	0.293	0.039	0.065
755.000	16.920	4.530	2.500	1.970	15.460	1.330	0.335	0.030	0.061
765.000	15.730	4.300	2.570	1.870	16.210	1.348	0.318	0.023	0.069
775.000	15.170	4.120	2.080	1.770	16.930	1.248	0.312	0.030	0.065
785.000	15.770	4.500	2.730	1.880	16.320	1.181	0.312	0.030	0.069

TABLE C.4:1 SALT FREE MINOR ELEMENTS DATA (in ppm) CORE CD1709

DEPTH (CM)	Ni	Cr	V	Cu	Zn	Sr	Rb	Zr	Ba	Nb	Pb	Th
0.000	62.580	225.720	47.190	13.330	45.140	681.260	27.700	102.600	147.740	6.150	7.180	1.020
10.000	49.870	205.720	34.280	12.460	27.010	777.170	22.850	110.130	157.920	4.150	2.070	0.000
20.000	63.420	216.870	46.030	12.270	35.800	691.540	26.590	97.180	155.490	6.130	7.160	1.020
30.000	70.580	199.480	52.170	12.270	34.780	621.980	30.690	100.250	137.080	7.160	7.160	1.020
40.000	66.750	202.310	49.290	15.400	34.910	650.090	29.780	101.670	166.370	7.160	7.180	1.020
50.000	77.440	238.440	59.100	14.260	36.680	604.260	30.570	103.930	137.560	6.110	7.130	0.000
60.000	80.650	215.430	63.300	13.270	39.810	586.050	31.650	100.050	180.710	6.110	6.120	2.040
70.000	76.200	209.290	54.860	15.240	38.600	607.560	30.480	99.560	151.380	7.110	7.110	2.030
80.000	78.770	238.350	56.260	14.320	39.890	593.340	31.710	105.360	180.040	7.110	1.020	6.130
90.000	83.880	230.170	63.420	16.360	40.920	575.940	32.730	105.360	187.200	7.160	6.130	0.000
100.000	82.880	235.170	63.190	14.500	41.440	590.520	33.150	103.600	188.550	6.210	8.280	3.100
110.000	79.150	204.510	56.400	14.890	37.740	604.650	28.960	120.760	156.260	5.710	5.100	2.040
120.000	83.010	208.980	63.440	13.490	39.550	573.710	31.210	121.430	165.100	6.070	5.560	4.220
130.000	90.780	223.170	63.340	14.380	38.250	588.540	30.600	119.740	184.410	5.810	3.160	1.830
140.000	82.310	223.680	64.620	14.680	38.350	586.290	30.490	121.170	174.620	6.120	4.380	1.120
150.000	81.600	237.450	63.440	13.970	36.720	592.920	29.780	120.360	196.350	5.910	5.610	2.140
160.000	81.800	223.170	63.030	14.480	38.350	588.740	30.800	122.400	194.510	5.810	3.970	2.340
170.000	81.390	221.340	63.750	13.560	40.800	613.940	30.090	117.910	167.070	6.320	4.990	1.530
180.000	78.330	206.550	61.910	12.030	36.920	608.940	29.580	120.870	202.770	5.710	3.870	2.340
190.000	79.450	211.140	59.970	12.440	36.510	590.070	30.800	118.110	175.640	6.010	4.690	2.140
200.000	78.840	217.360	59.670	12.850	37.020	615.060	29.070	129.130	197.260	5.610	3.160	2.240
210.000	82.310	225.210	62.420	14.170	38.450	579.560	31.410	120.970	212.360	5.910	6.120	2.950
220.000	81.190	219.090	63.540	13.050	36.920	588.640	31.600	122.090	211.540	6.220	4.600	2.750
230.000	85.170	206.750	60.690	14.070	38.140	579.640	31.000	117.700	205.730	6.010	5.710	2.850
240.000	86.900	221.640	65.480	15.090	38.960	565.590	30.800	116.990	221.030	6.010	4.890	2.340
250.000	90.670	208.180	60.180	18.150	42.020	607.410	32.740	120.870	210.420	5.810	4.990	3.060

DEPTH (CM)	Ni	Cr	V	Cu	Zn	Sr	Rb	Zr	Ba	Nb	Pb	Th
260.000	87.000	205.220	59.360	14.070	39.780	611.890	31.410	113.930	220.210	6.120	6.010	2.240
270.000	81.290	210.010	57.010	12.140	37.430	664.830	29.270	116.280	172.070	5.910	4.990	1.630
280.000	71.910	219.370	51.510	10.700	32.920	628.520	27.970	118.060	162.810	5.350	4.740	2.520
290.000	72.920	236.940	52.720	11.510	33.020	622.960	28.780	120.690	142.500	5.650	3.130	2.020
300.000	73.730	228.050	51.000	10.100	33.020	628.120	28.070	124.330	158.870	5.650	3.430	0.707
310.000	70.800	216.840	50.290	9.690	31.100	615.390	27.160	116.950	137.000	6.060	3.530	2.220
320.000	73.120	210.880	53.830	19.790	51.200	641.450	28.480	115.740	137.460	5.750	4.040	1.410
330.000	76.250	215.730	53.830	12.500	33.830	630.440	29.180	123.720	138.870	5.850	3.830	2.220
340.000	73.620	224.490	51.200	11.710	33.930	647.140	27.670	124.930	144.730	5.950	2.820	2.520
350.000	73.730	231.290	50.800	11.210	33.630	643.970	27.670	120.490	149.480	5.350	3.670	1.010
360.000	77.360	229.770	55.340	12.120	34.840	620.840	29.080	118.870	133.320	5.950	2.220	1.510
370.000	79.080	227.450	55.240	12.420	34.440	614.680	29.890	117.160	135.740	6.060	4.890	2.220
380.000	83.740	220.320	57.220	15.300	36.720	605.160	30.900	121.680	167.890	5.910	3.770	2.850
390.000	86.590	204.400	62.620	15.700	41.100	589.450	31.920	117.400	199.100	6.630	4.890	2.650
400.000	89.650	219.090	63.030	15.090	38.450	568.850	31.310	117.090	138.610	6.220	4.790	3.160
410.000	96.390	205.930	66.700	15.700	41.310	567.220	32.530	115.970	198.180	6.120	3.970	3.460
420.000	96.390	219.910	63.850	14.790	43.650	557.630	32.840	120.660	204.710	6.520	5.300	2.460
430.000	86.630	193.290	62.620	15.300	38.960	651.880	29.470	114.440	115.660	6.010	1.730	1.420
440.000	79.790	201.590	55.040	13.530	34.540	609.630	29.180	114.020	151.360	6.060	3.830	1.410
450.000	77.260	207.250	55.040	14.170	34.640	622.360	29.580	118.970	144.730	5.960	3.830	2.220
460.000	77.010	209.500	55.890	12.240	34.780	633.520	28.960	110.670	139.330	6.010	4.080	2.240

TABLE C.4:2 SALT FREE MINOR ELEMENTS DATA (in ppm) CORE CD1715

DEPTH (CM)	Ni	Cr	V	Cu	Zn	Sr	Rb	Zr	Ba	Nb	Pb	Th
0.00	124.46	138.46	68.74	46.17	71.82	773.60	28.72	115.93	613.54	6.15	7.18	1.02
10.00	122.68	56.70	112.00	79.30	118.56	124.76	24.74	48.45	802.11	4.12	6.18	0.00
20.00	88.40	71.96	58.59	33.92	58.59	1090.70	32.89	60.65	417.36	5.14	7.19	0.00
32.00	105.67	111.83	85.15	34.88	72.84	835.16	45.14	76.95	309.85	7.18	8.20	1.02
35.00	105.88	113.08	100.74	44.20	82.24	852.21	47.28	80.18	318.68	7.19	10.28	1.02
40.00	108.75	128.23	79.00	30.78	67.71	738.72	53.35	89.26	279.07	8.20	11.28	2.05
50.00	103.62	108.75	84.13	38.98	71.82	829.00	46.17	88.23	403.21	7.18	8.20	1.02
60.00	108.04	105.98	93.63	36.01	73.05	873.62	42.19	84.37	493.90	7.20	8.23	0.00
70.00	139.49	125.96	89.52	34.35	74.95	859.86	46.84	77.03	433.05	7.28	8.32	0.00
80.00	121.42	136.85	76.14	29.84	61.74	778.95	42.18	85.40	379.70	7.20	8.23	0.00
90.00	83.83	390.87	54.54	10.10	33.33	543.38	30.30	181.80	203.01	8.08	7.07	2.02
100.00	98.61	112.10	94.45	33.21	72.66	859.46	44.63	84.07	414.16	7.26	9.34	0.00
110.00	131.41	124.11	99.08	33.37	75.09	866.73	46.93	74.05	349.40	7.30	8.34	1.04
120.00	125.28	128.41	84.56	30.27	69.94	863.38	45.93	75.16	334.08	7.30	8.35	1.04
130.00	57.62	166.81	32.35	6.06	18.19	783.52	24.26	71.78	161.76	5.05	4.04	0.00
140.00	46.46	233.31	29.29	4.04	14.14	732.25	25.25	89.89	190.89	4.04	5.05	0.00
150.00	109.07	125.53	101.87	37.04	83.34	807.76	46.30	93.63	376.61	8.23	10.29	2.05
160.00	115.69	117.76	83.67	34.08	82.64	799.54	46.48	96.06	370.84	8.26	8.26	2.06
164.00	117.42	125.66	93.73	52.53	135.90	714.82	51.50	98.88	332.69	9.27	11.33	3.09
174.00	97.94	107.22	97.94	37.11	87.63	797.99	47.42	91.75	437.14	7.21	9.27	0.00
184.00	111.45	107.32	90.81	38.18	83.59	811.15	48.50	94.94	421.05	9.28	10.32	2.06
194.00	110.63	101.33	119.94	41.36	86.85	828.23	46.53	85.82	475.64	7.23	9.30	1.03
204.00	107.43	99.16	104.33	38.22	83.67	857.39	49.58	77.47	557.82	6.19	9.29	2.06
214.00	111.45	146.54	82.50	31.99	72.24	711.24	43.34	104.23	479.88	7.22	8.25	1.03
224.00	107.22	103.10	67.01	36.08	67.01	927.90	40.20	83.51	542.30	6.18	9.27	1.03

DEPTH (CM)	Ni	Cr	V	Cu	Zn	Sr	Rb	Zr	Ba	Nb	Pb	Th
234.00	97.47	110.80	99.52	40.01	75.92	827.98	46.17	89.26	390.90	8.20	12.31	3.07
244.00	100.45	90.20	93.27	37.92	101.47	1003.47	37.92	77.90	473.55	6.15	8.20	0.00
254.00	142.96	84.95	83.91	32.11	93.24	963.48	35.22	75.62	467.23	5.18	9.32	0.00
264.00	121.21	97.38	109.81	38.33	104.63	855.73	42.47	87.02	485.88	7.25	9.32	1.03
274.00	150.33	115.88	97.09	45.93	115.88	936.46	43.84	92.91	751.68	7.30	8.35	1.04
284.00	118.45	129.78	104.03	38.11	85.49	736.45	51.50	100.94	463.50	8.24	9.27	2.06
294.00	138.18	108.05	98.70	43.63	105.97	931.98	43.63	87.27	694.05	6.23	8.31	0.00
304.00	121.79	84.32	84.32	38.51	108.26	1081.59	32.27	71.82	755.76	5.20	5.20	0.00
309.00	98.42	68.37	74.59	35.22	91.16	1167.57	26.93	69.41	584.30	4.14	5.18	0.00
319.00	104.33	74.37	76.44	32.02	75.40	1147.66	33.05	77.47	467.94	6.19	5.16	0.00
329.00	92.88	80.49	75.33	29.29	69.14	1052.64	36.12	79.46	414.86	6.19	6.19	0.00
339.00	88.58	88.58	73.13	31.93	71.07	1081.50	35.02	80.34	445.99	6.18	8.24	0.00
349.00	99.16	91.93	88.83	34.08	78.50	1016.47	39.25	82.64	450.38	5.16	6.19	0.00
359.00	185.40	91.67	73.13	32.96	76.22	1031.03	38.11	81.37	421.27	6.18	5.15	0.00
369.00	102.50	125.05	92.25	35.87	76.87	692.90	54.32	101.47	317.75	8.20	12.30	4.10
379.00	105.67	120.04	95.41	38.98	81.05	741.79	54.37	96.44	431.94	8.20	10.26	4.10
390.00	110.80	126.19	110.80	47.19	101.57	689.47	59.50	102.60	486.32	9.23	12.31	5.10
400.00	158.66	127.55	100.58	41.48	85.03	766.34	45.62	94.36	534.05	6.23	0.00	0.00
410.00	128.26	150.66	71.26	23.41	52.93	641.34	33.59	99.76	353.24	7.12	0.00	0.00
420.00	163.92	161.86	140.21	75.73	130.93	571.17	53.60	119.51	629.94	7.21	4.12	0.00
430.00	129.52	131.58	104.85	52.42	109.99	623.99	64.76	99.71	506.80	9.25	13.36	6.16
440.00	137.12	110.31	154.65	61.82	152.58	801.08	49.48	87.63	654.48	8.24	12.37	2.06
450.00	143.10	105.77	130.66	59.10	150.36	836.86	47.70	83.99	810.93	7.25	11.40	4.14
454.00	183.51	90.72	109.28	61.86	145.37	933.05	44.33	68.04	766.03	7.21	12.37	2.06
464.00	147.00	129.52	104.85	58.59	105.88	625.02	63.73	98.68	493.44	9.25	15.42	5.14
474.00	142.69	123.04	127.18	57.90	151.99	805.48	52.73	90.99	933.70	8.27	14.47	5.17
484.00	217.35	117.99	146.97	68.31	176.98	877.68	44.50	83.83	1032.93	7.24	13.45	2.07

DEPTH (CM)	Ni	Cr	V	Cu	Zn	Sr	Rb	Zr	Ba	Nb	Pb	Th
494.00	156.14	104.44	121.32	56.97	147.70	1007.52	42.20	77.01	963.21	7.38	11.60	1.05
504.00	150.52	74.23	71.13	50.51	89.69	1076.36	35.05	58.76	843.35	5.15	10.31	0.00
514.00	106.26	76.34	82.53	57.77	105.23	1018.28	40.23	58.80	812.97	6.19	10.31	0.00
524.00	115.47	93.82	87.63	62.89	100.07	894.90	53.61	68.04	678.39	7.21	12.37	2.06
534.00	144.14	123.40	96.44	49.77	98.51	809.89	48.73	64.29	633.60	7.25	11.40	2.07
544.00	144.06	151.26	83.34	41.16	74.08	719.27	44.24	74.08	527.87	7.20	9.26	3.08
547.00	142.96	154.36	95.31	61.12	118.10	720.02	53.87	128.46	897.17	8.28	14.50	3.10
554.00	174.91	121.09	101.43	57.96	106.60	783.49	49.68	71.41	668.61	7.24	11.38	4.14
564.00	195.33	169.35	121.56	89.35	157.92	491.44	74.80	123.64	1349.66	10.39	21.81	8.31
574.00	141.86	101.77	106.91	79.15	128.50	840.90	48.31	84.29	1247.99	7.19	13.36	3.08
584.00	123.36	70.93	81.21	92.52	81.21	1063.98	37.00	57.56	867.63	5.14	11.30	1.02
594.00	90.20	97.37	73.80	39.97	60.47	906.10	41.00	74.82	233.70	7.17	8.20	0.00
598.00	89.84	101.07	71.47	28.58	57.17	914.81	40.84	77.59	244.01	6.12	7.14	0.00
608.00	99.61	113.99	94.48	33.89	75.99	900.67	41.88	82.16	490.90	7.18	9.24	1.02
618.00	151.44	115.36	79.31	32.96	70.04	876.53	41.20	66.95	397.58	6.18	8.24	1.03
628.00	107.83	125.29	99.61	35.94	82.16	837.00	45.18	87.29	556.63	7.18	9.24	0.00
636.00	114.91	125.17	89.26	32.83	69.76	819.77	45.14	76.95	422.71	7.18	9.23	2.05
643.00	70.63	298.66	50.45	9.08	30.27	502.48	28.25	128.14	159.42	8.07	5.04	2.01
648.00	117.42	116.39	90.64	31.93	73.13	847.69	48.41	75.19	440.84	7.21	11.33	3.09
653.00	72.64	422.77	49.44	6.05	28.25	576.13	27.24	196.75	193.72	7.06	7.06	2.01
663.00	81.92	102.40	74.75	28.67	62.46	872.44	40.90	80.89	352.25	7.16	8.19	2.04
668.00	99.17	132.57	55.66	15.18	37.44	563.68	33.39	60.72	181.14	6.07	8.09	2.02
676.00	81.73	279.49	48.43	9.08	30.27	515.59	28.25	113.00	166.48	7.06	7.06	3.02
682.00	86.78	122.52	74.53	27.56	61.26	685.09	52.07	94.95	304.25	8.16	10.21	4.08
687.00	120.51	158.62	107.12	38.11	75.19	646.84	54.59	99.91	360.50	8.24	11.33	5.15
692.00	84.75	247.20	56.50	11.09	35.31	543.85	32.28	102.91	189.69	8.07	8.07	2.01
700.00	76.68	457.07	52.46	8.07	28.25	714.37	26.23	175.56	214.95	7.06	6.05	2.01
706.00	141.17	166.74	101.27	36.82	84.90	543.21	61.38	108.43	395.90	9.20	12.27	6.13
712.00	122.21	130.42	84.21	41.08	91.40	802.08	47.24	87.29	572.03	8.21	11.29	4.10
722.00	119.01	132.35	87.21	43.09	87.21	741.79	52.32	89.26	453.49	8.20	11.28	4.10
733.00	113.08	133.64	90.46	44.20	88.40	752.49	53.45	96.63	487.27	8.22	12.33	3.08

TABLE C.4:3 SALT FREE MINOR ELEMENTS DATA (in ppm) CORE CD1730

DEPTH (CM)	Ni	Cr	V	Cu	Zn	Sr	Rb	Zr	Ba	Nb	Pb	Th
0.00	235.17	153.32	99.45	108.78	250.71	618.49	56.98	100.49	1124.06	9.32	21.75	6.21
10.00	188.55	153.32	96.34	77.70	134.68	681.68	53.87	110.85	1240.00	7.25	15.54	3.10
20.00	129.87	117.40	91.43	76.88	140.26	870.68	46.75	93.51	1019.25	6.23	11.42	1.04
30.00	124.87	101.13	77.40	41.28	89.78	925.70	45.40	66.04	882.36	6.19	11.35	2.06
40.00	111.56	106.39	84.70	48.55	76.44	893.54	44.41	78.50	672.48	7.23	8.26	0.00
50.00	99.71	96.63	70.93	31.86	67.84	833.70	44.20	79.15	415.31	7.19	8.22	0.00
60.00	104.55	152.72	77.90	29.72	68.67	714.42	50.22	94.30	325.95	8.20	10.25	3.07
70.00	100.35	133.12	69.63	26.62	59.39	587.77	54.27	100.35	100.35	8.19	11.26	3.07
80.00	99.23	129.92	78.77	30.69	65.47	607.66	54.21	101.27	303.81	8.18	11.25	3.07
90.00	112.05	126.44	78.12	25.70	71.96	666.14	50.37	94.57	415.31	8.22	9.25	1.03
100.00	122.92	141.52	90.90	29.95	82.64	667.31	51.65	95.03	409.06	8.26	12.39	2.06
110.00	108.46	144.62	86.77	27.89	78.50	666.28	52.68	97.10	400.80	8.26	11.36	2.06
120.00	110.53	144.62	86.77	27.89	76.44	680.74	51.65	96.06	366.71	8.26	11.36	4.13
130.00	125.11	145.79	95.12	28.95	86.85	625.57	53.76	106.50	354.66	7.23	11.37	3.10
140.00	126.93	141.38	88.75	31.99	82.56	698.66	50.56	99.07	360.16	7.22	9.20	3.09
150.00	103.62	141.58	81.05	28.72	71.82	592.00	56.43	106.70	288.30	8.20	12.31	4.10
160.00	114.33	143.17	93.73	31.93	84.46	631.39	56.65	109.18	340.93	8.24	12.36	4.12
170.00	128.34	145.93	106.60	36.22	95.22	594.09	56.92	108.67	375.07	8.28	11.38	5.17
180.00	140.89	150.22	103.60	33.15	92.20	615.38	55.94	108.78	371.92	8.28	11.39	4.14
190.00	128.75	157.59	94.76	29.87	87.55	565.47	55.62	106.09	341.96	8.24	12.36	5.15
200.00	98.40	104.55	64.57	17.42	62.52	478.67	51.25	99.42	207.05	8.20	11.27	4.10
210.00	111.83	146.71	91.31	32.83	76.95	528.39	59.50	113.88	338.58	9.23	11.28	5.13
220.00	91.75	98.97	61.86	31.96	74.23	534.05	58.76	114.44	257.75	9.27	14.43	5.15
230.00	116.39	154.50	106.09	35.02	85.49	565.47	60.77	112.27	432.60	9.27	13.39	5.15
240.00	111.34	147.43	96.91	34.02	87.63	617.56	57.73	109.28	443.33	9.27	12.37	4.12

DEPTH (CM)	Ni	Cr	V	Cu	Zn	Sr	Rb	Zr	Ba	Nb	Pb	Th
250.00	106.29	136.22	91.84	36.12	78.43	572.76	58.88	111.45	421.05	8.25	14.44	5.16
260.00	113.19	154.35	89.52	32.92	78.20	565.95	57.62	109.07	349.86	9.26	13.37	4.11
270.00	87.21	97.47	56.43	27.70	64.63	518.13	57.45	109.78	206.22	9.23	13.33	4.10
280.00	122.68	130.93	84.54	32.99	84.54	705.20	54.64	103.10	436.11	8.24	10.31	3.09
290.00	101.03	111.34	83.51	34.02	79.38	675.30	54.64	102.06	368.06	9.28	12.37	5.15
295.00	122.80	147.57	106.29	62.95	151.70	663.57	55.72	108.36	467.49	8.25	14.44	3.09
305.00	123.12	150.82	105.67	33.85	89.26	595.00	58.48	109.78	451.44	8.20	12.31	3.07
315.00	163.43	170.72	122.83	51.00	119.71	542.36	56.21	112.42	782.83	8.32	12.49	4.16
325.00	163.75	154.36	105.34	43.80	112.64	624.75	53.19	107.42	664.39	8.34	12.51	5.21
335.00	116.27	162.58	105.98	31.89	82.32	476.42	63.79	119.36	363.23	9.26	11.31	4.11
345.00	141.30	163.12	116.36	42.59	111.17	576.64	61.30	116.36	642.10	9.35	12.46	4.15
355.00	146.97	153.18	103.50	43.47	106.60	566.14	57.96	110.74	694.48	8.28	13.45	5.17
365.00	117.99	141.79	95.22	37.26	96.25	747.27	49.68	100.39	717.25	7.24	10.35	2.07
375.00	121.89	126.02	83.67	33.05	81.60	848.09	44.41	91.93	606.37	7.23	9.29	1.03
385.00	102.06	126.81	83.51	27.83	70.10	852.63	46.39	93.82	470.13	8.24	8.24	0.00
395.00	96.82	129.78	81.37	23.69	70.04	788.98	45.32	95.79	430.54	7.21	9.27	0.00
405.00	113.09	142.69	89.84	34.88	87.73	862.51	47.56	95.13	573.95	7.39	11.62	1.05
415.00	102.70	137.61	82.16	30.81	73.94	775.38	50.32	98.59	459.06	8.21	10.27	3.08
425.00	107.31	148.19	93.00	29.63	72.56	654.08	54.16	109.35	328.06	8.17	9.19	2.04
435.00	106.28	146.14	97.09	29.38	73.58	564.14	58.25	116.50	327.04	9.19	12.26	4.08
450.00	114.68	148.48	101.37	29.69	75.77	585.72	60.41	115.71	375.80	9.21	11.26	5.12
460.00	124.58	152.14	105.84	35.28	88.20	719.93	61.74	117.96	411.23	8.82	12.12	3.30
470.00	115.02	144.80	98.59	33.89	80.10	628.52	60.59	111.94	403.61	9.24	12.32	4.10
480.00	119.13	150.96	112.97	39.02	91.40	598.74	63.67	116.05	460.09	9.24	13.35	4.10
490.00	140.97	164.64	126.56	46.30	108.04	525.81	66.68	119.36	512.44	9.26	15.43	5.14
500.00	169.08	184.54	136.09	51.55	116.50	485.60	69.07	123.72	534.05	10.31	14.43	6.18
510.00	166.79	175.08	128.46	49.72	112.92	471.38	66.30	117.06	476.56	10.36	16.57	6.21

DEPTH (CM)	Ni	Cr	V	Cu	Zn	Sr	Rb	Zr	Ba	Nb	Pb	Th
520.00	142.41	156.86	166.15	55.72	117.64	508.77	71.20	116.61	469.56	9.28	15.48	6.19
530.00	142.55	152.88	131.19	51.65	110.53	607.40	61.98	111.56	531.99	9.29	13.42	4.13
540.00	143.86	146.97	149.04	57.96	153.18	643.77	62.10	109.71	736.92	9.31	14.49	4.14
550.00	183.72	142.20	143.24	64.35	160.89	572.97	64.35	111.06	965.34	8.30	13.49	4.15
560.00	163.84	141.03	130.66	65.33	145.18	637.75	64.29	108.88	874.19	8.29	16.59	5.18
570.00	125.29	153.02	106.80	49.29	101.67	609.01	64.70	115.02	455.98	9.24	13.35	5.13
580.00	131.45	165.34	135.56	45.18	110.91	484.74	72.91	123.24	575.12	10.27	13.35	7.18
590.00	223.34	169.57	166.47	100.29	203.69	553.19	66.17	117.87	1107.41	9.30	16.54	6.20
600.00	181.28	159.65	141.11	64.89	134.93	603.58	63.86	116.39	805.46	9.27	13.39	5.15
610.00	188.37	143.86	120.00	58.99	130.41	704.83	54.85	108.67	902.52	8.28	10.35	2.07
620.00	141.03	129.62	108.80	54.96	110.95	828.56	48.73	96.44	874.19	7.25	9.33	0.00
630.00	120.97	112.70	109.60	58.93	112.70	817.89	54.80	98.23	737.24	8.27	12.40	1.03
640.00	148.89	123.04	130.28	68.24	133.38	709.32	64.10	104.43	844.77	8.27	14.47	4.13
650.00	163.05	172.34	148.60	68.11	141.38	476.78	81.52	118.68	706.92	11.35	21.67	9.28
660.00	341.77	189.64	190.68	181.30	333.44	394.91	87.52	125.04	1206.63	11.46	25.00	8.34
670.00	155.55	175.25	123.40	70.51	128.58	612.86	61.18	108.88	1212.25	9.33	17.62	5.18
680.00	203.89	128.34	121.09	77.62	131.44	728.64	58.99	91.08	1284.43	8.28	16.56	4.14
690.00	126.97	106.49	104.44	73.72	119.80	826.36	54.27	77.82	911.36	6.14	13.31	4.09
700.00	95.04	126.72	82.78	34.74	74.60	737.88	51.10	86.87	258.56	7.15	10.22	2.04
710.00	95.13	130.94	83.88	27.62	62.40	755.99	49.10	85.93	248.58	7.16	9.20	4.09
720.00	98.13	130.15	88.83	29.95	67.14	728.26	51.65	88.83	325.39	8.26	10.33	4.13
730.00	117.99	142.83	87.97	37.26	79.69	775.21	48.64	86.94	544.41	7.24	11.38	4.14
740.00	115.47	137.12	80.41	32.99	70.10	781.49	45.36	87.63	493.84	7.21	7.21	2.06
750.00	90.81	127.96	83.59	20.64	61.92	602.68	45.40	86.68	389.06	7.22	10.32	3.09
760.00	126.69	150.38	94.76	36.05	84.46	722.03	53.56	98.88	560.32	8.24	10.30	3.09
770.00	116.39	155.53	96.82	30.90	81.37	665.38	53.56	101.97	453.20	8.24	11.33	3.09
780.00	104.75	131.45	89.34	27.72	73.94	720.95	49.29	94.48	381.01	8.21	11.29	3.08
790.00	96.25	131.07	83.96	27.64	68.60	664.57	51.20	95.23	359.42	9.21	12.28	4.09
800.00	98.20	137.08	85.93	26.59	68.54	657.78	49.10	105.36	354.98	7.16	8.18	1.023

TABLE C.4:4 SALT FREE MINOR ELEMENTS DATA (in ppm) CORE CD1738

DEPTH (CM)	Ni	Cr	V	Cu	Zn	Sr	Rb	Zr	Ba	Nb	Pb	Th
0.00	135.90	174.40	151.76	31.71	115.51	204.60	123.82	135.90	424.31	12.36	20.60	14.42
10.00	142.02	182.26	161.74	34.72	119.14	192.52	132.55	138.86	441.05	13.37	21.60	15.43
20.00	162.62	192.19	168.26	47.87	157.70	205.57	114.05	146.43	594.88	11.41	21.79	13.49
30.00	123.98	155.72	135.05	23.62	98.89	166.79	120.29	148.34	264.20	13.22	19.32	13.22
40.00	132.17	173.69	141.17	33.91	112.80	234.59	105.18	148.09	434.58	11.25	16.36	10.23
50.00	130.93	170.91	156.80	32.93	111.33	194.43	130.93	138.77	409.25	13.29	17.38	12.27
60.00	136.00	174.62	174.62	34.27	84.86	497.22	73.44	104.45	391.14	9.28	10.31	4.12
70.00	132.78	164.44	146.68	29.34	105.76	203.04	130.47	140.50	325.01	13.26	20.40	14.28
80.00	144.19	183.99	157.71	37.55	118.66	234.31	126.17	141.19	441.59	12.28	20.40	13.74
90.00	122.31	168.27	130.80	24.74	96.15	195.13	114.53	147.06	325.22	13.26	19.38	13.26
100.00	122.26	159.82	124.99	27.32	98.35	200.12	108.60	159.82	336.72	13.22	20.34	13.22
110.00	134.94	171.60	159.90	29.64	104.52	202.80	125.58	141.96	369.72	12.43	16.30	14.16
120.00	130.22	171.17	158.07	29.48	102.37	208.84	136.77	143.32	284.19	13.77	17.64	15.70
130.00	131.31	166.11	147.92	33.22	106.79	288.71	114.69	135.26	457.99	11.22	17.03	11.83
140.00	127.96	160.11	133.74	30.22	96.45	380.01	98.38	127.31	447.53	9.07	13.77	8.97
150.00	93.92	210.15	99.20	19.96	68.09	308.17	77.48	248.30	217.19	10.40	11.41	10.10
160.00	109.55	155.71	121.95	16.54	83.37	182.58	106.11	158.47	202.57	13.02	16.76	13.83
170.00	125.06	165.76	150.96	30.34	103.60	251.60	118.40	142.08	395.16	12.13	15.09	12.64
180.00	117.04	158.84	145.92	30.40	98.04	445.36	125.40	148.96	307.80	13.05	17.03	13.05
185.00	118.23	162.86	148.77	31.32	114.32	241.95	129.98	152.68	293.62	13.15	16.42	14.79
195.00	145.96	192.24	168.21	41.83	115.70	262.55	145.96	157.53	443.22	14.17	19.27	16.62
205.00	121.55	163.08	141.94	25.67	95.13	203.85	123.07	150.24	317.10	13.01	18.30	14.54
215.00	122.86	172.23	120.05	34.78	87.52	444.87	84.15	120.61	503.78	9.18	12.44	8.16
225.00	119.39	165.09	140.77	28.74	93.60	236.58	121.60	142.98	319.12	12.42	16.26	13.83
235.00	127.90	171.11	113.30	29.20	85.26	453.18	85.26	148.34	401.79	9.48	12.64	8.77

DEPTH (CM)	Ni	Cr	V	Cu	Zn	Sr	Rb	Zr	Ba	Nb	Pb	Th
245.00	124.71	227.05	102.34	30.94	66.16	486.95	66.16	157.08	323.68	8.68	11.00	7.17
255.00	123.25	162.85	153.14	29.88	99.35	248.00	122.51	141.93	318.97	12.31	16.79	14.25
265.00	121.82	170.39	148.80	26.21	94.83	205.09	126.44	144.95	289.90	12.47	15.71	13.28
275.00	120.44	160.80	130.85	27.99	90.49	388.00	102.86	131.50	335.92	10.30	14.68	11.32
285.00	119.97	161.92	137.63	24.29	90.53	290.72	119.23	148.67	265.70	12.54	14.89	12.24
295.00	107.26	157.56	122.41	27.88	80.60	401.78	90.29	133.32	299.36	9.61	12.75	8.39
305.00	110.81	173.39	104.14	25.65	68.23	592.00	73.87	126.71	292.92	8.72	8.72	4.36
315.00	113.57	155.76	126.55	24.01	85.67	387.45	101.89	130.45	336.18	10.13	12.46	8.20
325.00	120.17	157.38	119.56	23.79	79.91	539.85	93.94	128.10	295.85	9.48	9.58	6.83
335.00	118.80	153.25	110.48	21.98	76.63	455.00	86.72	127.12	273.83	9.18	11.83	6.12
345.00	114.92	169.09	83.81	21.23	58.19	793.49	56.36	113.09	211.18	7.44	7.75	2.95
355.00	125.56	170.09	143.81	24.82	90.52	376.68	118.99	135.05	277.40	11.42	14.28	10.71
365.00	111.49	149.53	107.33	24.49	75.54	523.08	76.59	122.44	348.55	8.77	11.73	5.46
375.00	114.45	154.78	129.71	25.61	82.29	465.97	83.38	129.71	287.21	9.07	11.11	6.52
385.00	103.04	153.44	114.24	21.84	73.92	496.16	82.88	135.52	234.08	9.33	9.90	4.66
395.00	99.14	156.17	101.80	20.25	68.22	453.58	76.22	133.25	214.27	9.22	9.83	5.47
405.00	105.46	155.38	114.19	17.47	73.01	604.03	90.48	147.89	171.60	9.50	9.93	7.60
415.00	97.24	135.88	123.00	23.18	77.92	1455.44	103.68	161.00	258.24	10.60	9.38	5.91
425.00	109.65	168.21	118.99	22.43	76.63	517.09	93.45	148.90	239.23	10.01	10.40	6.76
435.00	106.13	151.98	115.55	20.72	74.10	632.40	89.18	140.67	159.51	9.11	10.73	6.18
445.00	101.18	159.43	97.60	21.97	66.43	467.05	71.54	132.86	231.99	8.52	11.46	5.48
455.00	99.54	163.38	105.49	24.89	70.87	126.05	78.44	135.25	239.66	9.32	10.64	5.98
465.00	104.22	166.75	112.90	25.48	81.64	376.93	86.85	137.80	237.97	9.32	11.06	7.91
475.00	119.97	152.25	105.45	23.67	71.55	471.29	77.47	120.51	347.01	8.45	9.06	4.78
485.00	102.37	177.80	82.62	17.06	56.12	515.00	58.82	129.31	248.30	7.91	8.12	3.55
495.00	88.55	152.37	94.30	12.65	66.70	226.55	77.63	181.12	223.67	11.81	12.72	11.21
505.00	110.22	155.10	124.74	19.80	81.18	269.94	100.32	143.88	322.08	11.91	13.73	11.21

DEPTH (CM)	Ni	Cr	V	Cu	Zn	Sr	Rb	Zr	Ba	Nb	Pb	Th
515.00	111.57	160.01	143.13	25.69	91.02	411.77	120.38	143.86	318.56	12.72	15.75	13.43
525.00	92.80	145.46	108.47	18.81	73.99	362.41	94.05	165.53	341.09	11.71	14.03	11.31
535.00	105.08	145.19	68.45	13.08	50.58	487.01	53.19	100.28	304.33	7.27	5.35	3.13
540.00	101.84	230.99	75.28	10.70	38.01	541.69	38.38	145.75	271.21	7.41	6.19	3.04
545.00	113.66	163.59	128.77	23.65	84.10	329.81	104.46	137.97	298.93	10.67	14.23	10.06
555.00	103.62	163.02	120.12	17.16	78.54	215.16	100.32	164.34	234.30	12.04	12.44	10.12
565.00	121.05	164.99	141.09	24.67	90.21	303.00	114.88	141.86	285.27	11.49	16.06	12.71
575.00	121.22	172.97	132.79	23.15	85.12	306.45	106.24	137.56	268.99	10.89	12.72	10.99
585.00	106.18	157.92	119.62	19.49	78.62	242.59	100.13	153.89	247.30	11.52	13.14	12.23
595.00	106.53	164.83	108.65	24.91	74.73	414.46	75.79	136.74	247.51	8.46	11.32	6.22
605.00	106.13	153.45	120.33	20.28	82.47	488.75	102.75	155.48	398.16	11.94	13.15	10.42
615.00	109.32	152.77	122.90	18.33	82.16	418.26	103.21	152.77	349.01	12.04	13.56	11.03
625.00	116.32	162.12	137.40	21.81	88.69	252.27	114.87	162.12	287.89	12.76	15.19	12.35
635.00	105.78	192.64	82.99	19.35	55.04	587.38	55.04	133.30	273.05	7.43	8.35	4.28
645.00	102.86	162.35	100.64	23.35	73.95	329.15	76.73	144.00	257.43	9.26	12.11	7.73
655.00	111.34	164.08	115.44	23.44	76.77	366.25	84.97	145.33	285.38	9.69	12.34	7.95
665.00	112.35	177.08	120.37	32.10	82.39	318.32	72.23	141.77	243.96	8.94	12.13	7.60

TABLE C.4:5 SALT FREE MINOR ELEMENTS DATA (in ppm) CORE CD1739

DEPTH (CM)	Ni	Cr	V	Cu	Zn	Sr	Rb	Zr	Ba	Nb	Pb	Th
0.00	58.88	96.06	66.11	32.02	121.89	770.61	43.38	95.03	286.14	5.16	9.29	1.03
10.00	80.42	122.16	91.62	21.37	55.99	711.58	59.04	127.25	211.74	8.14	8.14	1.01
20.00	74.38	115.14	82.53	19.36	55.02	649.10	62.15	130.43	229.27	8.15	10.19	4.07
30.00	77.59	120.47	81.68	21.44	55.13	681.00	60.23	122.52	257.29	8.16	9.18	3.06
40.00	74.53	122.52	79.63	21.44	55.13	717.76	58.19	124.56	292.00	9.18	8.16	3.06
50.00	73.58	125.70	81.76	20.44	56.21	665.32	59.27	119.50	286.16	9.19	8.17	3.06
60.00	73.72	117.76	80.89	20.48	57.34	664.57	58.36	118.78	260.00	8.19	9.21	3.07
70.00	75.62	120.59	82.78	20.44	56.21	706.20	60.29	122.64	274.91	8.17	9.19	3.06
80.00	74.60	116.50	82.78	20.44	56.21	686.78	62.34	128.77	247.32	9.19	8.17	1.02
90.00	71.54	119.57	87.89	21.46	55.18	690.87	62.34	132.86	255.50	8.17	8.17	2.04
100.00	90.11	147.45	102.40	31.74	66.56	726.01	72.70	143.36	338.94	9.21	10.24	4.09
110.00	80.02	125.90	87.49	22.40	59.75	658.33	64.92	134.44	266.75	9.60	9.60	3.20
120.00	76.50	121.38	86.70	19.38	58.14	672.18	60.18	126.48	274.38	8.16	9.18	4.08
130.00	78.30	135.76	92.54	20.34	62.03	564.43	66.10	138.31	260.35	10.17	10.17	3.05
140.00	76.42	124.31	90.69	20.38	62.15	595.09	65.21	137.56	293.47	10.19	10.19	5.09
150.00	77.52	125.46	94.86	21.42	60.18	567.12	65.28	127.50	257.04	10.20	11.22	4.08
160.00	75.33	127.25	94.67	21.37	61.08	600.62	65.15	129.28	277.91	8.14	10.18	5.09
170.00	77.44	128.39	92.72	23.43	59.10	596.11	64.19	131.45	261.88	8.15	11.20	4.07
180.00	77.59	123.54	88.82	22.46	57.17	601.36	65.34	127.62	302.21	8.16	9.18	3.06
190.00	73.58	113.44	87.89	23.50	59.27	638.75	63.36	122.64	272.85	8.17	8.17	3.06
200.00	78.69	123.66	85.84	22.48	60.29	586.62	62.34	126.72	309.66	8.17	8.17	4.08
210.00	77.67	133.88	86.87	22.48	61.32	591.73	62.34	128.77	315.79	8.17	8.17	3.06
220.00	80.89	129.02	95.23	25.60	62.46	637.95	59.39	119.80	378.88	8.19	10.24	4.09
230.00	70.49	113.33	79.63	22.46	54.11	709.59	56.15	119.45	285.88	8.16	9.18	3.06
240.00	74.67	113.55	76.72	21.48	51.15	735.53	53.19	117.64	310.99	7.16	9.20	2.04

DEPTH (CM)	Ni	Cr	V	Cu	Zn	Sr	Rb	Zr	Ba	Nb	Pb	Th
250.00	73.29	115.03	81.44	21.37	57.00	679.00	60.00	128.26	294.20	8.14	10.18	3.05
260.00	72.06	119.77	88.30	19.28	59.88	620.16	63.94	140.07	201.98	8.12	11.16	4.06
270.00	76.72	127.17	93.53	24.17	68.31	645.31	68.31	143.98	295.33	9.45	12.61	4.20
280.00	73.36	105.97	80.50	19.36	56.04	669.48	61.14	124.31	296.52	8.45	11.20	3.05
290.00	73.29	126.23	93.65	23.41	60.06	595.53	65.15	133.35	287.07	9.16	11.19	5.09
300.00	88.82	128.64	91.89	27.56	64.32	578.90	67.38	130.68	326.72	9.18	12.25	3.06
310.00	84.59	135.52	91.71	27.51	64.19	593.05	65.21	127.37	324.04	9.17	12.22	6.11
320.00	76.42	118.20	92.72	21.45	62.15	648.08	63.17	118.20	313.85	8.15	11.20	5.09
330.00	77.21	122.93	97.53	26.41	66.04	575.05	70.10	125.98	309.88	9.14	13.20	6.09
340.00	70.31	115.14	83.55	25.47	66.23	692.92	57.06	103.93	367.78	7.13	11.20	5.09
350.00	78.38	114.01	88.56	25.45	58.02	688.16	62.09	112.99	283.00	8.14	10.18	4.07
360.00	74.46	113.22	82.62	21.42	53.04	737.46	57.12	107.10	236.64	8.16	10.20	3.06
370.00	74.60	115.48	77.67	21.46	52.12	754.23	56.21	106.28	190.09	8.17	7.15	2.04
380.00	72.56	118.55	69.49	22.48	50.07	751.17	52.12	110.37	257.54	7.15	10.22	4.08
390.00	78.77	128.89	69.56	21.48	54.21	662.90	54.21	115.59	272.11	8.18	8.18	4.09
400.00	79.71	127.75	72.56	21.46	54.16	679.63	54.16	118.55	265.72	7.15	8.17	5.11
410.00	84.99	133.12	80.89	23.55	62.46	630.78	59.39	116.73	322.56	8.19	9.21	5.12
420.00	76.70	126.81	71.58	22.49	57.27	661.68	56.24	113.51	293.51	7.15	10.22	4.09
430.00	74.65	113.51	72.61	20.45	55.22	658.61	55.22	117.61	297.60	7.15	8.18	3.06
440.00	75.48	115.26	73.44	19.38	55.08	679.32	55.08	114.24	283.56	8.16	9.18	3.06
450.00	77.52	115.26	72.42	18.36	53.04	682.38	53.04	111.18	248.88	7.14	8.16	2.04
460.00	70.24	116.05	79.40	21.37	53.95	667.80	58.02	124.19	264.68	8.14	9.16	4.07
470.00	69.29	113.10	77.44	19.30	54.00	669.48	56.04	118.20	263.92	7.13	8.15	2.03
480.00	75.18	119.88	88.39	23.30	59.94	670.56	62.99	135.12	289.56	9.14	9.14	4.06
490.00	74.38	121.20	79.48	21.39	73.36	690.88	56.04	119.22	376.01	7.13	89.67	5.09
500.00	72.42	110.16	79.56	20.40	57.12	684.42	59.16	122.40	237.66	8.16	9.18	4.08
515.00	74.24	120.00	83.39	20.34	56.95	669.18	60.00	125.09	224.75	8.13	11.18	3.05

DEPTH (CM)	Ni	Cr	V	Cu	Zn	Sr	Rb	Zr	Ba	Nb	Pb	Th
525.00	75.11	120.78	86.27	20.30	60.90	616.10	64.96	133.98	232.43	9.13	11.16	5.07
535.00	77.14	132.96	89.32	20.30	59.88	574.49	65.97	133.98	258.82	9.13	11.16	6.09
545.00	79.09	130.80	89.23	20.28	59.82	572.91	64.88	134.86	247.41	9.12	11.15	5.07
555.00	76.98	129.66	92.18	22.28	62.80	544.99	68.88	139.79	250.21	10.13	14.18	6.07
565.00	81.20	127.89	93.38	28.42	113.68	547.08	66.99	133.98	286.23	9.13	13.19	5.07
575.00	79.09	130.80	88.21	20.28	58.81	539.44	63.88	135.87	272.76	9.12	11.15	5.07
585.00	86.53	141.50	90.60	21.37	60.08	529.36	66.17	128.26	291.14	9.16	12.21	7.12
595.00	87.54	139.46	93.65	21.37	62.09	520.19	65.15	127.25	306.41	9.16	12.21	5.09
605.00	93.74	144.69	88.65	22.41	64.19	530.89	64.19	126.35	290.41	9.17	12.22	6.11
615.00	90.60	137.43	86.53	21.37	61.08	563.97	63.11	124.19	238.21	9.16	12.21	5.09
625.00	84.49	141.36	89.49	22.37	62.03	528.84	66.10	129.15	277.64	10.17	12.20	5.08
635.00	97.72	153.71	87.54	24.43	68.20	516.12	67.18	128.26	297.25	10.18	12.21	7.12
645.00	84.32	137.16	90.42	21.33	61.97	555.75	67.05	130.04	246.88	9.14	12.19	5.08
655.00	89.58	142.52	96.71	24.43	68.20	513.07	70.24	135.39	311.50	10.18	15.27	6.10
665.00	106.89	151.68	102.81	29.52	73.29	463.19	72.27	133.35	376.66	10.18	14.25	8.14
675.00	104.24	150.23	99.13	28.61	70.51	544.72	65.40	118.55	363.83	9.19	12.26	7.15
685.00	85.42	137.29	92.54	23.39	64.07	606.13	66.10	123.05	310.18	9.15	12.20	6.10
695.00	87.37	138.17	95.50	22.35	65.02	589.28	67.05	124.96	358.64	9.14	12.19	6.09
705.00	83.47	127.25	92.63	21.37	60.06	626.07	60.06	116.05	358.33	8.14	11.19	6.10
715.00	85.17	135.87	98.35	21.29	67.93	584.06	68.95	127.76	315.35	10.14	15.21	6.08
725.00	87.54	128.26	99.76	23.41	64.13	574.15	69.22	124.19	340.01	9.16	13.23	5.09
735.00	78.07	130.80	99.37	20.28	64.89	533.36	71.99	141.96	315.35	9.12	15.21	6.08
745.00	83.55	126.35	95.78	22.41	61.14	591.00	66.23	118.20	337.28	9.17	13.24	7.13
755.00	78.30	132.21	91.53	22.37	58.98	591.89	66.10	127.12	295.94	9.15	12.20	6.10
765.00	88.91	129.79	86.87	27.59	61.32	609.11	63.36	112.42	335.21	8.17	12.26	6.13

TABLE C.5:1 MAJOR ELEMENTS TO Al RATIO DATA OF CORE CD1709

DEPTH (CM)	Si/Al	Fe/Al	Mg/Al	Ca/Al	K/Al	Ti/Al	Mn/Al	P/Al
0.00	4.79	0.53	0.91	8.69	0.27	0.08	0.01	0.05
10.00	5.21	0.47	0.87	12.36	0.26	0.08	0.02	0.09
20.00	4.67	0.52	0.95	8.88	0.28	0.08	0.01	0.05
30.00	4.62	0.54	0.96	7.43	0.28	0.08	0.01	0.03
40.00	4.66	0.55	0.93	8.06	0.27	0.08	0.01	0.04
50.00	4.54	0.55	0.93	7.16	0.28	0.08	0.01	0.03
60.00	4.56	0.56	0.96	7.07	0.28	0.08	0.01	0.03
70.00	4.59	0.56	0.93	7.32	0.28	0.08	0.01	0.04
80.00	4.55	0.57	0.94	6.94	0.28	0.08	0.01	0.03
90.00	4.50	0.58	0.93	6.73	0.28	0.08	0.01	0.03
100.00	4.51	0.57	0.91	6.76	0.28	0.08	0.01	0.03
110.00	4.45	0.53	0.91	6.90	0.27	0.08	0.01	0.03
120.00	4.42	0.57	0.91	6.53	0.27	0.08	0.01	0.03
130.00	4.43	0.56	0.91	6.68	0.28	0.08	0.01	0.03
140.00	4.46	0.58	0.92	6.69	0.28	0.08	0.01	0.03
150.00	4.48	0.56	0.92	6.76	0.28	0.08	0.01	0.03
160.00	4.40	0.56	0.92	6.63	0.28	0.08	0.01	0.03
170.00	4.48	0.57	0.92	6.99	0.28	0.08	0.01	0.04
180.00	4.51	0.54	0.91	7.09	0.28	0.08	0.01	0.05
190.00	4.49	0.55	0.91	6.71	0.28	0.08	0.01	0.04
200.00	4.50	0.57	0.91	7.16	0.28	0.08	0.01	0.05
210.00	4.48	0.56	0.90	6.44	0.28	0.08	0.01	0.05
220.00	4.48	0.56	0.90	6.61	0.28	0.08	0.01	0.04
230.00	4.46	0.52	0.92	6.33	0.28	0.08	0.01	0.04
240.00	4.51	0.57	0.88	6.23	0.28	0.08	0.01	0.04
250.00	4.59	0.55	0.89	7.22	0.27	0.08	0.01	0.03
260.00	4.38	0.59	0.86	6.44	0.27	0.08	0.01	0.03
270.00	4.46	0.59	0.89	7.09	0.28	0.08	0.01	0.04
280.00	4.64	0.57	0.91	7.22	0.28	0.08	0.01	0.04
290.00	4.64	0.56	0.92	7.21	0.28	0.08	0.01	0.04
300.00	4.62	0.55	0.92	7.22	0.28	0.08	0.01	0.03
310.00	4.43	0.58	0.89	6.40	0.28	0.08	0.01	0.05
320.00	4.50	0.55	0.90	7.24	0.28	0.08	0.01	0.04
330.00	4.52	0.56	0.90	7.15	0.27	0.08	0.01	0.04
340.00	4.54	0.54	0.89	7.37	0.27	0.08	0.01	0.03
350.00	4.56	0.55	0.91	7.41	0.28	0.08	0.01	0.04
360.00	4.51	0.55	0.88	6.92	0.28	0.08	0.01	0.04
370.00	4.47	0.56	0.88	6.82	0.28	0.08	0.01	0.04
380.00	4.45	0.57	0.88	6.70	0.28	0.08	0.01	0.04
390.00	4.33	0.57	0.88	6.39	0.28	0.08	0.01	0.04
400.00	4.40	0.56	0.91	6.39	0.27	0.08	0.01	0.04
410.00	4.30	0.58	0.89	6.13	0.27	0.08	0.01	0.06
420.00	4.30	0.61	0.90	6.06	0.27	0.08	0.01	0.04
430.00	4.35	0.57	0.91	7.27	0.28	0.08	0.01	0.04
440.00	4.52	0.56	0.93	6.99	0.28	0.08	0.01	0.04
450.00	4.54	0.56	0.93	7.21	0.28	0.08	0.01	0.04
460.00	4.54	0.56	0.93	7.23	0.28	0.08	0.01	0.04

TABLE C.5:2 MAJOR ELEMENTS TO Al RATIO DATA OF CORE CD1715

DEPTH (CM)	AGE (KYRS)	Si/Al	Fe/Al	Mg/Al	Ca/Al	K/Al	Ti/Al	Mn/Al	P/Al
0.000	0.000	4.560	0.606	0.875	7.430	0.273	0.085	0.089	0.022
10.000	8.310	3.660	0.726	0.692	16.040	0.296	0.086	0.051	0.229
20.000	10.570	3.420	0.609	0.686	11.330	0.291	0.092	0.026	0.017
32.000	13.570	3.510	0.636	0.715	6.930	0.314	0.087	0.016	0.012
35.000	14.280	3.650	0.785	0.743	7.790	0.334	0.088	0.021	0.014
40.000	15.490	3.480	0.605	0.681	5.320	0.299	0.080	0.016	0.011
50.000	17.250	3.560	0.641	0.705	6.430	0.309	0.080	0.015	0.015
60.000	19.050	3.470	0.634	0.699	7.180	0.295	0.083	0.019	0.016
70.000	20.830	3.500	0.667	0.740	6.190	0.287	0.081	0.025	0.015
80.000	22.640	3.750	0.635	0.765	5.900	0.296	0.083	0.027	0.018
100.000	24.450	3.570	0.640	0.709	6.720	0.310	0.090	0.019	0.016
110.000	26.280	3.400	0.704	0.750	5.686	0.300	0.087	0.037	0.018
120.000	28.330	3.450	0.671	0.780	5.680	0.297	0.088	0.052	0.021
150.000	30.380	3.670	0.633	0.659	5.970	0.301	0.081	0.024	0.015
160.000	32.430	3.680	0.622	0.687	5.960	0.300	0.082	0.024	0.015
164.000	33.250	3.650	0.631	0.688	4.970	0.300	0.080	0.019	0.013
174.000	35.300	3.630	0.607	0.661	5.720	0.300	0.079	0.020	0.014
184.000	37.380	3.630	0.684	0.657	6.120	0.302	0.079	0.021	0.015
194.000	39.850	3.690	0.606	0.679	5.800	0.305	0.078	0.021	0.014
204.000	42.850	3.500	0.630	0.647	5.840	0.293	0.074	0.041	0.014
214.000	45.840	4.070	0.621	0.725	5.910	0.287	0.081	0.047	0.018
224.000	48.820	3.660	0.632	0.659	7.570	0.290	0.090	0.414	0.017
234.000	54.700	3.670	0.689	0.643	6.350	0.300	0.081	0.021	0.015
244.000	57.580	3.560	0.651	0.640	8.420	0.292	0.088	0.029	0.018
254.000	60.470	3.770	0.644	0.618	4.790	0.297	0.083	0.016	0.013
264.000	67.140	4.010	1.360	0.684	6.790	0.288	0.090	0.031	0.017
284.000	80.000	3.620	0.623	0.630	8.930	0.287	0.092	0.026	0.019
294.000	84.220	3.940	0.735	0.702	10.030	0.291	0.091	0.043	0.021
304.000	88.440	4.010	0.716	0.698	11.630	0.283	0.096	0.048	0.024
309.000	90.550	3.730	0.640	0.672	11.880	0.272	0.090	0.047	0.018
319.000	99.000	3.670	0.603	0.614	10.570	0.287	0.093	0.042	0.017
229.000	108.600	3.670	0.709	0.631	9.270	0.305	0.090	0.031	0.019
339.000	118.200	3.580	0.619	0.611	9.330	0.292	0.089	0.031	0.015
349.000	121.700	3.660	0.671	0.628	8.860	0.302	0.087	0.030	0.015
359.000	125.200	3.600	0.566	0.601	8.620	0.297	0.088	0.047	0.018
369.000	127.200	3.750	0.620	0.619	4.650	0.300	0.081	0.018	0.010
379.000	132.600	3.630	0.654	0.615	4.890	0.306	0.080	0.018	0.013
390.000	136.600	3.620	0.651	0.617	4.270	0.298	0.078	0.015	0.015
400.000	138.200	3.690	0.676	0.709	4.790	0.280	0.076	0.017	0.022
410.000	141.400	4.280	0.573	0.778	4.940	0.350	0.077	0.017	0.017
420.000	150.200	3.670	0.678	0.634	0.291	0.291	0.078	0.021	0.011
430.000	150.900	3.730	0.640	0.582	3.520	0.306	0.073	0.023	0.011
440.000	151.160	3.680	0.672	0.610	4.910	0.284	0.080	0.036	0.016
450.000	152.300	3.690	0.711	0.611	5.860	0.289	0.082	0.033	0.018
454.000	152.580	3.600	0.638	0.577	6.920	0.301	0.081	0.042	0.019
464.000	158.200	3.590	0.679	0.561	3.660	0.303	0.080	0.021	0.014
474.000	161.400	3.640	0.713	0.592	5.360	0.292	0.083	0.031	0.017
484.000	164.600	3.680	0.674	0.611	6.190	0.275	0.084	0.037	0.018
494.000	167.800	3.610	0.672	0.575	8.850	0.281	0.087	0.041	0.022
504.000	171.060	3.610	0.680	0.600	9.330	0.291	0.087	0.043	0.023
514.000	174.320	3.370	0.663	0.526	8.280	0.298	0.079	0.028	0.021
524.000	177.580	3.330	0.637	0.508	5.910	0.294	0.075	0.023	0.017
534.000	180.840	3.640	0.656	0.719	5.250	0.291	0.074	0.032	0.017
544.000	184.120	4.050	0.639	0.803	5.300	0.287	0.082	0.048	0.027
554.000	187.400	3.640	0.648	0.685	5.110	0.339	0.081	0.058	0.023
564.000	190.700	3.570	0.662	0.532	2.080	0.305	0.074	0.027	0.013
574.000	192.090	3.570	0.650	0.552	5.430	0.299	0.076	0.025	0.017
584.000	205.000	3.380	0.572	0.5921	0.420	0.299	0.086	0.036	0.020
594.000	206.610	3.510	0.651	0.684	7.570	0.303	0.085	0.020	0.013
598.000	207.410	3.530	0.623	0.706	7.670	0.305	0.088	0.020	0.017
608.000	209.100	3.640	0.645	0.755	7.230	0.316	0.085	0.017	0.020
618.000	210.500	3.610	0.689	0.823	6.660	0.308	0.084	0.016	0.020
628.000	216.000	3.690	0.689	0.719	6.170	0.310	0.087	0.015	0.015
636.000	223.380	3.690	0.677	0.777	5.840	0.300	0.083	0.018	0.018
648.000	228.000	3.280	0.640	0.702	5.150	0.284	0.074	0.016	0.016
663.000	230.900	3.620	0.609	0.701	7.430	0.302	0.077	0.023	0.016
682.000	232.000	3.650	0.576	0.671	5.090	0.304	0.085	0.016	0.013
706.000	233.700	3.650	0.664	0.648	3.390	0.301	0.078	0.013	0.011
712.000	239.100	3.610	0.606	0.634	5.420	0.298	0.079	0.016	0.014
722.000	244.000	3.600	0.636	0.620	5.230	0.303	0.075	0.014	0.014
733.000	245.500	3.590	0.645	0.607	5.430	0.290	0.081	0.016	0.014

TABLE C.5:3 MAJOR ELEMENTS TO Al RATIO DATA OF CORE CD1730

AGE (KYRS)	DEPTH (CM)	Si/Al	Fe/Al	Mg/Al	Ca/Al	K/Al	Ti/Al	Mn/Al	P/Al
0.000	0.000	3.590	0.652	0.571	3.290	0.268	0.059	0.257	0.018
2.600	10.000	3.580	0.656	0.572	3.900	0.266	0.057	0.149	0.017
5.100	20.000	3.430	0.665	0.576	6.430	0.274	0.052	0.102	0.015
7.700	30.000	3.530	0.699	0.617	6.800	0.288	0.057	0.045	0.019
10.000	40.000	3.550	0.683	0.620	6.860	0.291	0.061	0.012	0.015
12.000	50.000	3.570	0.596	0.623	6.600	0.290	0.056	0.018	0.015
13.500	60.000	3.680	0.592	0.678	5.410	0.298	0.059	0.014	0.014
15.500	70.000	3.780	0.630	0.693	4.330	0.308	0.059	0.012	0.012
16.600	80.000	3.790	0.616	0.685	4.400	0.306	0.062	0.013	0.013
18.100	90.000	3.720	0.625	0.664	4.810	0.308	0.060	0.013	0.013
19.200	100.000	3.800	0.646	0.684	4.830	0.304	0.061	0.013	0.013
20.300	110.000	3.790	0.631	0.681	4.690	0.302	0.057	0.016	0.013
21.400	120.000	3.790	0.636	0.677	4.930	0.300	0.059	0.016	0.013
22.600	130.000	3.810	0.642	0.673	4.330	0.297	0.058	0.018	0.016
24.000	140.000	3.830	0.658	0.669	4.930	0.305	0.063	0.016	0.014
25.300	150.000	3.750	0.599	0.640	3.920	0.301	0.061	0.017	0.012
26.700	160.000	3.800	0.607	0.622	4.070	0.298	0.060	0.015	0.012
28.200	170.000	3.780	0.664	0.627	3.830	0.296	0.060	0.017	0.015
29.400	180.000	3.820	0.642	0.635	3.960	0.297	0.061	0.020	0.015
30.700	190.000	3.860	0.621	0.678	3.830	0.304	0.063	0.017	0.014
32.000	200.000	3.890	0.653	0.674	3.630	0.308	0.063	0.016	0.012
33.400	210.000	3.840	0.617	0.656	3.440	0.306	0.061	0.016	0.014
34.700	220.000	3.810	0.633	0.636	3.380	0.297	0.061	0.013	0.013
36.100	230.000	3.760	0.606	0.625	3.570	0.300	0.062	0.019	0.014
37.400	240.000	3.740	0.593	0.624	4.050	0.292	0.062	0.014	0.017
39.500	250.000	3.850	0.660	0.617	3.700	0.299	0.063	0.014	0.014
41.600	260.000	3.840	0.643	0.636	3.810	0.303	0.061	0.014	0.014
43.700	270.000	3.750	0.594	0.601	3.450	0.300	0.060	0.018	0.011
45.800	280.000	3.720	0.630	0.581	4.550	0.294	0.058	0.018	0.018
50.000	290.000	3.800	0.650	0.582	4.260	0.301	0.062	0.018	0.015
52.100	295.000	3.900	0.634	0.614	4.200	0.302	0.062	0.020	0.015
56.300	305.000	3.820	0.624	0.619	3.790	0.300	0.064	0.249	0.014
60.500	315.000	3.910	0.711	0.679	3.400	0.346	0.064	0.017	0.017
63.500	325.000	3.930	0.715	0.647	3.950	0.290	0.061	0.269	0.018
80.000	345.000	3.770	0.666	0.599	3.310	0.293	0.064	0.019	0.016
84.500	355.000	3.860	0.695	0.632	3.420	0.294	0.064	0.024	0.019
89.000	365.000	3.870	0.657	0.632	4.900	0.298	0.065	0.028	0.016
93.600	375.000	3.900	0.629	0.642	6.070	0.296	0.066	0.053	0.018
99.000	385.000	3.820	0.643	0.599	5.990	0.293	0.064	0.039	0.015
102.200	395.000	3.860	0.663	0.620	5.650	0.292	0.065	0.029	0.014
108.600	405.000	3.530	0.609	0.557	5.480	0.272	0.056	0.028	0.016
115.000	415.000	3.810	0.626	0.598	5.290	0.310	0.062	0.028	0.014
121.400	425.000	3.850	0.637	0.624	4.450	0.305	0.062	0.023	0.013
128.000	435.000	3.800	0.630	0.609	3.690	0.308	0.062	0.019	0.012
130.100	450.000	3.780	0.620	0.590	3.670	0.313	0.061	0.018	0.011
132.200	460.000	3.700	0.607	0.573	4.110	0.300	0.061	0.024	0.012
134.400	470.000	3.750	0.523	0.578	3.870	0.307	0.063	0.022	0.012
136.500	480.000	3.690	0.628	0.565	3.450	0.304	0.062	0.018	0.013
138.600	490.000	3.710	0.645	0.572	2.970	0.302	0.061	0.017	0.013
140.700	500.000	3.710	0.683	0.580	2.640	0.305	0.064	0.023	0.014
142.800	510.000	3.680	0.677	0.587	2.610	0.292	0.062	0.026	0.012
144.900	520.000	3.780	0.612	0.559	2.720	0.306	0.060	0.019	0.012
147.100	530.000	3.670	0.652	0.580	3.310	0.293	0.062	0.025	0.013
149.200	540.000	3.610	0.640	0.561	3.410	0.289	0.060	0.029	0.016
151.300	550.000	3.640	0.669	0.564	3.000	0.301	0.058	0.040	0.018
153.400	560.000	3.610	0.653	0.537	3.400	0.294	0.058	0.037	0.018
155.500	570.000	3.610	0.590	0.517	3.410	0.297	0.061	0.027	0.013
157.700	580.000	3.630	0.642	0.518	2.510	0.304	0.061	0.018	0.014
159.800	590.000	3.700	0.678	0.573	2.810	0.289	0.059	0.039	0.019
163.200	600.000	3.670	0.632	0.570	3.250	0.296	0.059	0.034	0.018
166.700	610.000	3.660	0.683	0.595	4.120	0.283	0.058	0.053	0.020
170.100	620.000	3.580	0.690	0.665	5.380	0.303	0.057	0.042	0.022
173.600	630.000	3.590	0.616	0.545	5.080	0.287	0.056	0.037	0.018
177.000	640.000	3.420	0.634	0.456	3.780	0.297	0.053	0.028	0.016
180.500	650.000	3.530	0.634	0.480	2.040	0.299	0.058	0.016	0.013
184.100	660.000	3.560	0.665	0.504	1.430	0.295	0.057	0.010	0.016
191.000	670.000	3.720	0.675	0.571	3.180	0.291	0.059	0.275	0.016
198.000	680.000	3.550	0.614	0.523	4.080	0.289	0.057	0.029	0.017
205.000	690.000	3.430	0.615	0.530	5.530	0.304	0.053	0.030	0.016
209.800	700.000	3.660	0.585	0.598	5.110	0.308	0.060	0.027	0.013
214.600	710.000	3.760	0.615	0.660	5.540	0.310	0.064	0.026	0.014
219.400	720.000	3.740	0.582	0.663	5.180	0.303	0.064	0.069	0.043
224.100	730.000	3.720	0.643	0.663	5.500	0.301	0.062	0.023	0.017
228.900	740.000	3.670	0.671	0.677	5.680	0.284	0.063	0.024	0.017
233.700	750.000	3.700	0.693	0.721	4.850	0.337	0.057	0.023	0.016
238.500	760.000	3.820	0.635	0.660	5.190	0.301	0.059	0.025	0.014
243.300	770.000	3.840	0.636	0.661	5.220	0.305	0.060	0.025	0.014
248.100	780.000	3.700	0.658	0.639	4.430	0.329	0.061	0.023	0.013
252.800	790.000	3.860	0.623	0.661	4.860	0.301	0.063	0.024	0.013
257.600	800.000	3.840	0.614	0.674	4.900	0.311	0.061	0.025	0.013

TABLE C.5:4 MAJOR ELEMENTS TO Al RATIO DATA OF CORE CD1738

DEPTH (CM)	Si/Al	Fe/Al	Mg/Al	Ca/Al	K/Al	Ti/Al	Mn/Al	P/Al
0.000	3.226	0.566	0.327	0.560	0.293	0.053	0.073	0.105
10.000	3.060	0.588	0.317	0.490	0.298	0.051	0.080	0.100
20.000	3.401	0.621	0.391	0.591	0.287	0.055	0.089	0.119
30.000	3.397	0.565	0.295	0.606	0.285	0.056	0.084	0.099
40.000	3.513	0.592	0.354	0.721	0.280	0.053	0.101	0.120
50.000	3.018	0.587	0.315	0.557	0.365	0.052	0.089	0.101
60.000	3.577	0.627	0.529	1.831	0.290	0.053	0.175	0.162
70.000	3.062	0.587	0.304	0.618	0.299	0.054	0.091	0.096
80.000	3.093	0.611	0.341	0.672	0.302	0.056	0.093	0.105
90.000	3.523	0.696	0.318	0.703	0.291	0.058	0.088	0.105
100.000	3.646	0.736	0.324	0.745	0.283	0.059	0.102	0.108
110.000	3.000	0.582	0.310	0.645	0.297	0.055	0.086	0.094
120.000	2.830	0.576	0.294	0.602	0.297	0.055	0.084	0.083
130.000	2.784	0.536	0.305	0.831	0.269	0.051	0.110	0.088
140.000	3.176	0.593	0.389	1.398	0.331	0.062	0.112	0.100
150.000	4.250	0.545	0.342	1.523	0.327	0.058	0.099	0.123
160.000	3.630	0.570	0.305	0.791	0.282	0.061	0.094	0.106
170.000	3.126	0.588	0.318	0.754	0.297	0.055	0.086	0.095
180.000	2.943	0.578	0.292	0.730	0.299	0.057	0.091	0.088
185.000	3.043	0.573	0.286	0.649	0.298	0.056	0.100	0.088
195.000	2.921	0.516	0.361	0.708	0.303	0.055	0.090	0.087
205.000	3.180	0.576	0.294	0.707	0.291	0.057	0.087	0.087
215.000	3.360	0.642	0.472	1.998	0.301	0.057	0.109	0.123
225.000	3.113	0.589	0.312	0.813	0.301	0.057	0.085	0.091
235.000	3.411	0.618	0.474	1.765	0.293	0.057	0.113	0.110
245.000	3.929	0.658	0.553	2.691	0.282	0.067	0.149	0.126
255.000	3.063	0.602	0.312	0.814	0.299	0.058	0.088	0.094
265.000	3.070	0.577	0.300	0.696	0.297	0.056	0.078	0.088
275.000	3.112	0.630	0.381	1.452	0.300	0.055	0.108	0.101
285.000	3.148	0.582	0.306	0.870	0.295	0.057	0.075	0.094
295.000	3.315	0.630	0.398	1.673	0.305	0.056	0.107	0.099
305.000	3.456	0.608	0.493	2.577	0.298	0.058	0.117	0.131
315.000	3.046	0.576	0.374	1.427	0.305	0.054	0.094	0.094
325.000	3.103	0.602	0.415	1.798	0.303	0.054	0.097	0.100
335.000	3.380	0.589	0.418	1.764	0.291	0.056	0.106	0.109
345.000	3.322	0.593	0.585	3.227	0.249	0.044	0.109	0.145
355.000	2.836	0.586	0.337	1.133	0.304	0.052	0.088	0.089
365.000	3.305	0.630	0.463	2.610	0.301	0.058	0.127	0.113
375.000	3.462	0.580	0.505	2.150	0.305	0.055	0.114	0.114
385.000	3.350	0.579	0.459	2.139	0.304	0.055	0.102	0.102
395.000	3.632	0.600	0.486	2.189	0.302	0.058	0.120	0.109
405.000	3.577	0.575	0.380	1.327	0.290	0.058	0.090	0.114
415.000	2.918	0.578	0.348	1.714	0.304	0.056	0.092	0.106
425.000	3.299	0.581	0.414	1.528	0.303	0.058	0.096	0.100
435.000	3.452	0.594	0.404	1.358	0.290	0.057	0.096	0.110
445.000	3.630	0.618	0.521	2.472	0.301	0.059	0.153	0.117
455.000	3.521	0.601	0.471	2.168	0.303	0.059	0.116	0.109
465.000	3.453	0.589	0.453	1.826	0.307	0.057	0.109	0.107
475.000	3.483	0.586	0.509	2.173	0.310	0.056	0.110	0.117
485.000	4.011	0.617	0.581	3.009	0.285	0.062	0.138	0.145
495.000	4.490	0.544	0.334	1.162	0.261	0.068	0.110	0.132
505.000	3.511	0.579	0.353	1.055	0.291	0.059	0.111	0.103
515.000	2.931	0.584	0.328	0.955	0.304	0.056	0.083	0.090
525.000	3.829	0.566	0.327	1.164	0.281	0.061	0.089	0.110
535.000	4.502	0.546	0.589	2.991	0.282	0.057	0.119	0.131
540.000	5.087	0.547	0.691	4.079	0.257	0.070	0.125	0.160
545.000	3.161	0.592	0.387	1.298	0.306	0.040	0.070	0.094
555.000	3.729	0.562	0.329	0.924	0.285	0.061	0.091	0.103
565.000	2.809	0.542	0.324	0.942	0.283	0.051	0.100	0.084
575.000	3.093	0.589	0.380	1.198	0.304	0.054	0.101	0.100
585.000	3.667	0.561	0.342	0.899	0.286	0.058	0.092	0.100
595.000	3.623	0.638	0.485	2.121	0.306	0.058	0.130	0.123
605.000	3.453	0.559	0.331	1.075	0.286	0.058	0.098	0.108
615.000	3.433	0.567	0.330	1.022	0.289	0.059	0.090	0.106
625.000	3.184	0.568	0.330	0.862	0.298	0.058	0.087	0.098
635.000	4.116	0.630	0.605	3.247	0.291	0.063	0.165	0.160
645.000	4.007	0.579	0.426	1.612	0.281	0.059	0.153	0.117
655.000	3.531	0.599	0.430	1.650	0.290	0.058	0.131	0.116
665.000	3.811	0.707	0.467	1.649	0.284	0.060	0.135	0.135
675.000	3.893	0.611	0.652	2.229	0.283	0.059	0.140	0.128

TABLE C.5:5 MAJOR ELEMENTS TO Al RATIO DATA OF CORE CD1739

DEPTH (CM)	Si/Al	Fe/Al	Mg/Al	Ca/Al	K/Al	Ti/Al	Mn/Al	P/Al
0.000	3.636	0.599	0.465	7.832	0.281	0.065	0.135	0.162
10.000	3.772	0.555	0.506	3.867	0.297	0.062	0.110	0.128
20.000	3.855	0.550	0.477	3.516	0.298	0.059	0.088	0.138
30.000	3.791	0.570	0.490	4.041	0.296	0.059	0.094	0.147
40.000	3.849	0.586	0.486	4.238	0.297	0.061	0.097	0.139
50.000	3.800	0.577	0.484	4.171	0.297	0.060	0.095	0.137
60.000	3.794	0.608	0.480	4.399	0.291	0.059	0.098	0.141
70.000	3.771	0.598	0.480	4.063	0.294	0.060	0.094	0.135
80.000	3.831	0.573	0.460	3.709	0.298	0.058	0.090	0.141
90.000	3.829	0.556	0.440	3.626	0.296	0.057	0.089	0.139
100.000	3.874	0.606	0.454	3.714	0.293	0.058	0.093	0.156
110.000	3.849	0.581	0.441	3.659	0.286	0.064	0.091	0.142
120.000	3.849	0.583	0.488	3.830	0.298	0.065	0.092	0.144
130.000	3.899	0.565	0.461	3.082	0.301	0.063	0.084	0.131
140.000	3.836	0.583	0.459	3.322	0.297	0.060	0.086	0.144
150.000	3.795	0.567	0.461	3.377	0.297	0.059	0.086	0.143
160.000	3.795	0.584	0.459	3.439	0.298	0.060	0.087	0.145
170.000	3.790	0.551	0.473	3.392	0.300	0.062	0.086	0.153
180.000	3.767	0.561	0.453	3.520	0.299	0.062	0.105	0.137
190.000	3.746	0.596	0.441	3.785	0.298	0.061	0.090	0.141
200.000	3.793	0.585	0.462	3.702	0.295	0.061	0.091	0.152
210.000	3.845	0.595	0.466	3.719	0.286	0.062	0.091	0.162
220.000	3.758	0.625	0.474	4.227	0.294	0.060	0.096	0.183
230.000	3.734	0.564	0.434	4.564	0.292	0.058	0.236	0.153
240.000	3.767	0.586	0.469	5.045	0.291	0.060	0.103	0.162
250.000	3.835	0.550	0.453	3.955	0.296	0.060	0.111	0.153
260.000	3.917	0.540	0.453	3.249	0.302	0.060	0.103	0.131
270.000	3.885	0.553	0.407	3.226	0.290	0.059	0.084	0.132
280.000	3.704	0.576	0.424	3.826	0.292	0.056	0.092	0.141
290.000	3.760	0.532	0.413	3.484	0.292	0.059	0.103	0.143
300.000	3.702	0.613	0.425	3.333	0.295	0.059	0.085	0.162
310.000	3.754	0.606	0.443	3.510	0.280	0.060	0.085	0.145
320.000	3.628	1.030	0.407	4.060	0.284	0.060	0.088	0.151
330.000	3.629	0.552	0.397	3.367	0.293	0.058	0.081	0.147
340.000	3.622	0.590	0.415	5.271	0.287	0.060	0.101	0.197
350.000	3.652	0.551	0.444	4.353	0.295	0.057	0.092	0.167
360.000	3.699	0.545	0.499	4.828	0.378	0.058	0.098	0.177
370.000	3.717	0.545	0.504	4.774	0.295	0.058	0.098	0.167
380.000	3.821	0.584	0.507	5.339	0.288	0.059	0.105	0.179
390.000	3.888	0.594	0.516	4.516	0.290	0.061	0.099	0.193
400.000	3.889	0.592	0.505	4.703	0.292	0.061	0.100	0.195
410.000	3.801	0.612	0.478	3.903	0.293	0.067	0.092	0.189
420.000	3.839	0.631	0.449	4.545	0.296	0.064	0.078	0.192
430.000	3.895	0.593	0.453	4.432	0.298	0.064	0.097	0.156
440.000	3.886	0.618	0.483	4.610	0.300	0.065	0.099	0.158
450.000	3.895	0.559	0.461	4.156	0.302	0.067	0.093	0.139
460.000	3.875	0.654	0.477	4.625	0.303	0.068	0.078	0.143
470.000	3.892	0.576	0.469	4.351	0.298	0.069	0.095	0.153
480.000	4.099	0.542	0.465	3.852	0.301	0.062	0.108	0.143
490.000	3.752	0.590	0.461	4.221	0.297	0.062	0.092	0.148
500.000	3.814	0.570	0.468	4.010	0.296	0.064	0.091	0.146
515.000	3.840	0.560	0.464	3.866	0.300	0.064	0.089	0.144
525.000	3.867	0.558	0.453	3.237	0.298	0.065	0.100	0.142
535.000	3.920	0.538	0.458	3.145	0.296	0.066	0.100	0.132
545.000	3.940	0.563	0.475	3.287	0.299	0.067	0.102	0.124
555.000	3.922	0.553	0.451	2.975	0.303	0.067	0.097	0.127
565.000	3.860	0.543	0.445	3.060	0.301	0.066	0.098	0.130
575.000	3.957	0.572	0.446	3.352	0.302	0.070	0.087	0.146
585.000	3.905	0.608	0.479	3.211	0.304	0.069	0.102	0.144
595.000	3.858	0.602	0.488	3.129	0.308	0.068	0.085	0.142
605.000	3.866	0.628	0.494	3.200	0.297	0.065	0.087	0.145
615.000	3.864	0.593	0.484	3.407	0.303	0.066	0.088	0.147
625.000	3.837	0.581	0.473	3.082	0.290	0.065	0.085	0.141
635.000	3.830	0.615	0.478	3.007	0.302	0.068	0.085	0.141
645.000	3.825	0.544	0.469	3.138	0.302	0.066	0.084	0.132
655.000	3.791	0.574	0.438	2.758	0.291	0.063	0.081	0.134
665.000	3.762	0.630	0.461	2.524	0.296	0.066	0.079	0.140
675.000	3.682	0.667	0.477	3.309	0.332	0.066	0.087	0.145
685.000	3.741	0.585	0.433	3.507	0.295	0.065	0.087	0.123
695.000	3.695	0.587	0.442	3.404	0.296	0.068	0.086	0.123
705.000	3.686	0.590	0.448	4.081	0.320	0.068	0.093	0.133
715.000	3.709	0.564	0.440	3.192	0.266	0.068	0.083	0.120
725.000	3.616	0.569	0.420	3.239	0.300	0.064	0.100	0.130
735.000	3.493	0.488	0.367	2.542	0.258	0.060	0.073	0.114
745.000	3.569	0.551	0.405	3.481	0.326	0.064	0.085	0.142
755.000	3.735	0.552	0.435	3.413	0.294	0.074	0.066	0.135
765.000	3.658	0.598	0.435	3.770	0.313	0.074	0.053	0.160
775.000	3.682	0.505	0.430	4.109	0.303	0.076	0.073	0.158
785.000	3.504	0.607	0.418	3.627	0.262	0.069	0.067	0.153

TABLE C.6:1 LITHOGENIC ELEMENTS AND THEIR RATIOS CORE CD1715

DEPTH (CM)	AGE (KYRS)	Si/Al (Si.lith)	Fe/Al (FEt)	K/Al	Ti/Al $x10^{-2}$	Fe/Ti	Zr/Al $x10^{-3}$	Cr/Al $x10^{-3}$	Zr/Qtz $x10^{-3}$	Cr/Zr	Ti/Qtz $x10^{-2}$	Cr/Qtz $x10^{-3}$
0.000	0.000	4.000	0.547	0.273	8.500	6.380	4.231	2.509	1.640	1.190	3.310	1.950
10.000	8.308	2.770	0.670	0.296	8.600	7.790	2.707	6.257	1.310	1.170	4.160	1.530
20.000	10.700	2.660	0.523	0.291	9.200	5.670	2.603	2.515	1.550	1.190	5.500	1.840
32.000	13.570	3.310	0.623	0.314	8.700	7.110	2.435	2.695	1.990	1.450	7.180	2.900
35.000	14.280	3.430	0.700	0.334	8.800	7.870	2.774	3.486	2.020	1.410	6.490	2.860
40.000	15.490	3.330	0.594	0.299	8.000	7.400	2.412	2.135	2.980	1.440	9.900	4.270
50.000	17.270	3.290	0.626	0.309	8.000	7.740	2.682	2.557	2.010	1.230	6.070	2.480
60.000	19.050	3.220	0.614	0.295	8.300	7.380	2.730	3.030	2.070	1.260	6.300	2.600
70.000	20.830	3.230	0.613	0.287	8.100	7.510	2.327	2.705	1.830	1.640	6.430	3.000
80.000	22.640	3.500	0.578	0.296	8.300	6.930	2.572	2.293	1.720	1.600	5.560	2.750
100.000	24.460	3.350	0.606	0.310	9.000	6.690	2.627	2.952	2.020	1.330	6.970	2.690
110.000	26.280	3.180	0.628	0.300	8.700	7.170	2.146	2.872	1.890	1.680	7.720	3.170
120.000	28.330	3.210	0.601	0.297	8.800	6.790	2.204	2.480	1.840	1.710	7.400	3.150
150.000	30.380	3.470	0.592	0.301	8.100	7.290	2.746	2.987	1.990	1.340	5.880	2.660
160.000	32.430	3.430	0.589	0.300	8.200	7.180	2.834	2.468	0.970	1.230	2.820	1.190
164.000	33.250	3.470	0.604	0.300	8.000	7.540	2.658	2.520	1.990	1.270	5.980	2.520
174.000	35.300	3.410	0.581	0.300	7.900	7.290	2.629	2.806	1.940	1.170	5.890	2.270
184.000	37.380	3.340	0.663	0.302	7.900	8.310	2.826	2.703	1.990	1.130	5.630	2.260
194.000	39.860	3.460	0.583	0.305	7.800	7.460	2.502	3.497	1.760	1.180	5.500	2.080
204.000	42.850	3.080	0.592	0.293	7.400	7.940	2.239	3.015	1.570	1.280	5.230	2.010
214.000	45.840	3.760	0.612	0.287	8.100	7.490	3.178	2.515	1.680	1.410	4.320	2.360
224.000	48.820	3.280	0.585	0.289	9.000	6.480	2.812	2.256	3.660	1.230	11.750	4.520
234.000	54.700	3.410	0.652	0.300	8.100	8.040	2.721	3.034	1.900	1.240	5.660	2.360
244.000	57.580	3.170	0.602	0.292	8.400	6.800	2.802	3.355	1.910	1.160	6.040	2.220
254.000	60.470	3.510	0.600	0.297	8.300	7.160	1.974	2.191	1.280	1.120	5.420	1.440
264.000	67.140	3.190	0.684	0.288	9.000	7.580	2.920	3.685	1.250	1.120	3.870	1.400

DEPTH (CM)	AGE (KYRS)	Si/Al (Si.lith)	Fe/Al (FEt)	K/Al	Ti/Al $x10^{-2}$	Fe/Ti	Zr/Al $x10^{-3}$	Cr/Al $x10^{-3}$	Zr/Qtz $x10^{-3}$	Cr/Zr	Ti/Qtz $x10^{-2}$	Cr/Qtz $x10^{-3}$
284.000	80.000	3.260	0.555	0.287	9.200	6.020	3.766	3.882	2.540	1.290	6.210	3.260
294.000	84.220	3.080	0.647	0.291	9.100	7.060	3.667	4.147	1.590	1.240	3.970	1.970
304.000	88.440	3.360	0.618	0.283	9.600	6.390	3.340	3.922	1.540	1.170	4.460	1.810
309.000	90.550	2.830	0.566	0.272	9.000	6.270	3.199	3.437	1.500	0.990	4.240	1.480
319.000	99.000	3.100	0.570	0.287	9.300	6.080	3.201	3.159	1.840	0.960	5.380	1.760
329.000	108.600	3.370	0.671	0.305	9.000	7.420	3.033	2.875	2.050	1.010	6.110	2.070
339.000	118.200	3.310	0.589	0.292	8.900	6.560	3.055	2.781	2.260	1.100	6.630	2.490
349.000	121.700	3.400	0.645	0.302	8.700	7.380	3.049	3.278	2.150	1.110	6.170	2.390
359.000	125.200	3.010	0.537	0.297	8.800	6.070	2.916	2.621	1.720	1.130	5.230	1.940
369.000	127.200	3.610	0.597	0.300	8.100	7.340	2.602	2.365	1.860	1.230	5.810	2.290
379.000	132.600	3.410	0.633	0.306	8.000	7.880	2.525	2.498	1.860	1.240	5.930	2.320
390.000	136.600	3.410	0.632	0.298	7.800	8.050	2.533	2.736	1.890	1.230	5.850	2.320
400.000	138.200	3.220	0.600	0.280	7.600	7.850	2.585	2.756	1.560	1.350	4.600	2.100
410.000	141.400	3.950	0.500	0.350	7.700	6.420	2.834	2.024	1.350	1.510	3.700	2.030
420.000	150.200	3.250	0.639	0.291	7.800	8.180	2.747	3.223	1.740	1.350	4.940	2.350
430.000	150.900	3.500	0.610	0.306	7.300	8.330	2.297	2.416	1.560	1.320	4.960	2.050
440.000	151.160	3.300	0.629	0.284	8.000	7.850	2.356	4.157	1.510	1.260	5.130	1.900
450.000	152.300	3.230	0.655	0.289	8.200	7.980	2.470	3.843	1.490	1.260	4.950	1.870
454.000	152.580	3.090	0.603	0.301	8.100	7.390	2.160	3.469	1.330	1.330	5.040	1.780
464.000	158.200	3.350	0.654	0.303	8.000	8.190	2.258	2.399	2.060	1.310	7.300	2.710
474.000	161.400	3.370	0.682	0.292	8.300	8.190	2.535	3.543	1.790	1.350	5.890	2.420
484.000	164.600	3.200	0.641	0.275	8.400	7.630	2.525	4.427	1.510	1.410	5.040	2.130
494.000	167.800	3.050	0.625	0.281	8.700	7.180	2.770	4.364	1.660	1.360	5.200	2.250
504.000	171.060	3.100	0.646	0.291	8.700	7.430	2.260	2.736	1.380	1.260	5.310	1.740
514.000	174.320	3.030	0.628	0.298	7.900	7.920	2.063	2.896	1.690	1.300	6.480	2.190
524.000	177.580	3.040	0.601	0.294	7.500	7.980	1.911	2.462	1.690	1.380	6.650	2.330
534.000	180.840	3.090	0.567	0.291	7.400	7.640	1.842	2.763	1.080	1.920	4.370	2.080
544.000	184.120	3.440	0.541	0.287	8.200	6.560	2.205	2.480	1.050	2.040	3.920	2.140

DEPTH (CM)	AGE (KYRS)	Si/Al (Si.lith)	Fe/Al (FEt)	K/Al	Ti/Al $x10^{-2}$	Fe/Ti	Zr/Al $x10^{-3}$	Cr/Al $x10^{-3}$	Zr/Qtz $x10^{-3}$	Cr/Zr	Ti/Qtz $x10^{-2}$	Cr/Qtz $x10^{-3}$
554.000	187.400	3.090	0.561	0.339	8.100	6.910	2.006	2.849	1.180	1.700	4.790	2.010
564.000	190.700	3.260	0.630	0.305	7.400	8.490	2.328	2.289	1.680	1.370	5.340	2.300
574.000	192.090	3.150	0.616	0.299	7.600	8.010	2.341	2.970	1.560	1.210	5.130	1.890
584.000	205.000	2.680	0.540	0.299	8.600	6.280	2.302	3.248	1.450	1.230	5.430	1.790
594.000	206.610	3.380	0.630	0.303	8.500	7.410	2.486	2.452	2.180	1.300	7.440	2.830
598.000	207.410	3.370	0.600	0.305	8.800	6.790	2.586	2.382	2.160	1.300	7.380	2.810
608.000	209.030	3.360	0.615	0.316	8.500	7.180	2.748	3.160	1.920	1.390	5.990	2.670
618.000	210.500	3.510	0.598	0.308	8.400	7.120	2.188	2.592	1.810	1.720	6.950	3.120
628.000	216.000	3.590	0.634	0.310	8.700	7.250	2.661	3.037	2.050	1.440	6.740	2.940
636.000	223.380	3.330	0.590	0.300	8.300	7.070	2.318	2.689	1.480	1.630	5.330	2.410
648.000	228.000	2.970	0.579	0.284	7.400	7.770	2.016	2.430	1.840	1.550	6.810	2.850
663.000	230.900	3.410	0.576	0.302	7.700	7.400	2.678	2.475	2.010	1.270	5.830	2.540
682.000	232.000	3.340	0.560	0.304	8.500	6.570	2.559	2.009	2.030	1.290	6.770	2.620
706.000	233.700	4.000	0.619	0.301	7.800	7.870	2.459	2.296	1.810	1.540	5.780	2.780
712.000	239.100	3.450	0.573	0.298	7.900	7.210	2.418	2.333	1.550	1.490	5.090	2.310
722.000	244.000	3.170	0.604	0.303	8.000	7.500	2.419	2.363	1.920	1.480	6.390	2.850
733.000	245.500	3.440	0.615	0.290	8.100	7.510	2.655	2.485	2.150	1.380	6.640	2.980

TABLE C.6:2 LITHOGENIC ELEMENTS AND THEIR RATIOS CORE CD1730

DEPTH (CM)	AGE (KYRS)	Si/Al (Si.lith)	Fe/Al (FEt)	K/Al	Ti/Al $x10^{-2}$	Fe/Ti	Zr/Al $x10^{-3}$	Cr/Al $x10^{-3}$	Zr/Qtz $x10^{-3}$	Cr/Zr	Ti/Qtz $x10^{-2}$	Cr/Qtz $x10^{-3}$
0.000	0.000	3.120	0.634	0.268	5.900	10.650	2.000	3.500	3.722	1.526	9.593	5.679
10.000	2.600	3.070	0.637	0.266	5.700	11.130	2.600	3.600	4.619	1.383	9.917	6.388
20.000	5.100	3.060	0.644	0.274	5.200	12.260	2.800	3.100	4.922	1.255	9.263	6.179
30.000	7.700	3.180	0.680	0.288	5.700	11.730	2.000	3.300	3.002	1.531	8.409	4.597
40.000	10.000	3.270	0.664	0.291	6.100	10.810	2.400	2.900	3.191	1.355	7.967	4.325
50.000	12.000	3.290	0.581	0.290	5.600	10.270	2.400	4.200	3.044	1.221	7.115	3.717
60.000	13.500	3.520	0.581	0.298	5.900	9.760	2.600	3.300	2.549	1.620	5.811	4.128
70.000	15.500	3.660	0.625	0.308	5.900	10.510	2.500	3.300	2.191	1.327	5.131	2.907
80.000	16.600	3.650	0.608	0.306	6.200	9.700	2.600	3.300	2.250	1.283	5.444	2.887
90.000	18.100	3.550	0.606	0.308	6.000	10.080	2.500	3.300	2.394	1.337	5.722	3.201
100.000	19.200	3.660	0.609	0.304	6.100	9.950	2.500	3.800	2.205	1.489	5.267	3.284
110.000	20.300	3.660	0.599	0.302	5.700	10.450	2.500	3.900	2.222	1.489	4.943	3.309
120.000	21.400	3.680	0.595	0.300	5.900	10.080	2.600	3.700	2.218	1.506	4.988	3.340
130.000	22.600	3.710	0.593	0.297	5.800	10.080	2.700	3.800	2.191	1.369	4.671	3.000
140.000	24.000	3.640	0.598	0.305	6.300	9.640	2.700	3.400	2.370	1.427	5.431	3.382
150.000	25.300	3.670	0.584	0.301	6.100	9.440	2.500	3.500	2.186	1.327	5.246	2.901
160.000	26.700	3.720	0.572	0.298	6.000	9.380	2.700	3.500	2.210	1.311	5.000	2.898
170.000	28.200	3.690	0.620	0.296	6.000	10.200	2.600	3.700	2.222	1.343	5.072	2.984
180.000	29.400	3.680	0.583	0.297	6.100	9.470	2.700	3.800	2.276	1.381	5.188	3.143
190.000	30.700	3.710	0.582	0.304	6.300	9.220	2.600	2.500	2.143	1.485	5.192	3.184
200.000	32.000	3.690	0.636	0.308	6.300	9.990	2.300	3.400	1.984	1.052	5.309	2.087
210.000	33.400	3.740	0.596	0.306	6.100	9.660	2.600	2.200	2.133	1.288	4.981	2.747
220.000	34.700	3.750	0.613	0.297	6.100	9.770	2.600	3.500	2.088	0.865	4.891	1.806
230.000	36.100	3.640	0.576	0.300	6.200	9.280	2.600	3.500	2.282	1.376	5.427	3.140
240.000	37.400	3.580	0.566	0.292	6.200	9.100	2.600	3.200	2.428	1.349	5.711	3.276
250.000	39.500	3.670	0.641	0.299	6.300	10.070	2.600	3.700	2.256	1.222	5.425	2.757

DEPTH (CM)	AGE (KYRS)	Si/Al (Si.lith)	Fe/Al (FEt)	K/Al	Ti/Al $x10^{-2}$	Fe/Ti	Zr/Al $x10^{-3}$	Cr/Al $x10^{-3}$	Zr/Qtz $x10^{-3}$	Cr/Zr	Ti/Qtz $x10^{-2}$	Cr/Qtz $x10^{-3}$
260.000	41.600	3.950	0.621	0.303	6.100	10.030	2.600	2.200	2.164	1.415	5.099	3.062
270.000	43.700	3.640	0.571	0.300	6.000	9.420	2.500	3.300	2.183	0.888	5.288	1.938
280.000	45.800	3.470	0.576	0.294	5.800	9.860	2.600	2.800	2.749	1.270	6.027	3.491
290.000	50.000	3.620	0.615	0.301	6.200	9.910	2.500	3.700	2.283	1.091	5.526	2.491
295.000	52.100	3.610	0.576	0.302	6.200	9.300	2.700	3.600	2.452	1.362	5.588	3.339
305.000	56.300	3.610	0.564	0.300	6.400	8.720	2.600	4.200	2.397	1.374	5.830	3.293
315.000	60.500	3.550	0.565	0.346	6.400	8.800	2.700	4.000	2.633	1.519	6.089	3.998
325.000	63.500	3.590	0.582	0.290	6.100	9.400	2.700	3.400	2.533	1.437	5.637	3.641
335.000	71.000	3.630	0.565	0.299	6.100	9.160	2.500	3.400	2.265	1.362	5.465	3.085
345.000	80.000	3.580	0.590	0.293	6.400	9.100	2.700	3.200	2.486	1.402	5.983	3.485
355.000	84.500	3.630	0.613	0.294	6.400	9.430	2.600	3.800	2.356	1.383	5.723	3.259
365.000	89.000	3.530	0.600	0.298	6.500	9.200	2.700	3.700	2.670	1.412	6.330	3.771
375.000	93.600	3.460	0.571	0.296	6.600	8.600	2.800	3.700	2.909	1.371	6.867	3.988
385.000	99.000	3.490	0.602	0.293	6.400	9.390	2.700	3.800	2.792	1.352	6.429	3.774
395.000	102.200	3.600	0.611	0.292	6.500	9.330	2.700	3.800	2.521	1.355	5.947	3.415
405.000	108.600	3.320	0.571	0.272	5.600	10.040	2.600	3.800	3.119	1.500	6.918	4.678
415.000	115.000	3.690	0.595	0.310	6.200	9.550	2.700	3.400	2.282	1.396	5.208	3.185
425.000	121.400	3.770	0.611	0.305	6.200	9.700	2.800	3.400	2.209	1.355	4.949	2.994
435.000	128.000	3.720	0.610	0.308	6.200	9.810	2.700	3.700	2.232	1.254	5.077	2.800
450.000	130.100	3.710	0.597	0.313	6.100	9.650	2.700	3.400	2.212	1.283	5.086	2.839
460.000	132.200	3.610	0.583	0.300	6.100	9.410	2.800	3.400	2.383	1.290	5.172	3.074
470.000	134.400	3.640	0.602	0.307	6.300	9.510	2.600	3.500	2.322	1.294	5.519	3.004
480.000	136.500	3.580	0.599	0.304	6.200	9.600	2.600	3.800	2.418	1.301	5.771	3.145
490.000	138.600	3.580	0.613	0.302	6.100	9.920	2.560	3.600	2.359	1.379	5.692	3.254
500.000	140.700	3.590	0.634	0.305	6.400	9.870	2.570	3.200	2.357	1.492	5.886	3.515
510.000	142.800	3.580	0.606	0.292	6.200	9.660	2.400	3.200	2.255	1.496	5.780	3.373
520.000	144.900	3.690	0.566	0.306	6.000	9.370	2.400	3.400	2.042	1.345	5.044	2.747
530.000	147.100	3.440	0.605	0.293	6.200	9.710	2.500	3.300	2.637	1.370	6.572	3.614

DEPTH (CM)	AGE (KYRS)	Si/Al (Si.lith)	Fe/Al (FEt)	K/Al	Ti/Al $x10^{-2}$	Fe/Ti	Zr/Al $x10^{-3}$	Cr/Al $x10^{-3}$	Zr/Qtz $x10^{-3}$	Cr/Zr	Ti/Qtz $x10^{-2}$	Cr/Qtz $x10^{-3}$
540.000	149.200	3.330	0.599	0.289	6.000	9.840	2.480	3.100	2.989	1.340	7.330	4.005
550.000	151.300	3.270	0.612	0.301	5.800	10.400	2.400	3.100	3.128	1.280	7.577	4.006
560.000	153.400	3.270	0.615	0.294	5.800	10.570	2.400	3.300	3.174	1.295	7.551	4.112
570.000	155.500	3.360	0.568	0.297	6.100	9.310	2.500	3.200	2.934	1.330	7.066	3.904
580.000	157.700	3.540	0.616	0.304	6.100	10.060	2.400	3.600	2.347	1.342	5.867	3.149
590.000	159.800	3.470	0.633	0.289	5.900	10.640	2.500	3.500	2.585	1.439	6.118	3.719
600.000	163.200	3.430	0.606	0.296	5.900	10.260	2.500	3.500	2.758	1.372	6.327	3.783
610.000	166.700	3.280	0.627	0.283	5.800	10.670	2.680	3.500	3.407	1.324	7.461	4.510
620.000	170.100	3.310	0.640	0.303	5.700	11.190	2.600	2.900	3.269	1.344	7.017	4.394
630.000	173.600	3.360	0.590	0.287	5.600	10.410	2.500	2.800	2.977	1.147	6.576	3.415
640.000	177.000	3.250	0.602	0.297	5.300	11.180	2.300	3.100	3.145	1.178	7.139	3.706
650.000	180.500	3.350	0.612	0.299	5.800	10.490	2.160	3.200	2.547	1.452	6.845	3.698
660.000	184.100	3.330	0.626	0.295	5.700	10.960	2.100	3.800	2.562	1.517	6.824	3.886
670.000	191.000	3.440	0.651	0.291	5.900	10.890	2.400	3.000	2.556	1.610	6.315	4.114
680.000	198.000	3.190	0.576	0.289	5.700	10.120	2.100	2.900	3.141	1.409	8.207	4.426
690.000	205.000	3.000	0.593	0.304	5.300	11.130	2.100	3.400	4.206	1.368	10.486	5.756
700.000	209.430	3.550	0.569	0.308	6.000	9.370	2.300	3.700	2.239	1.459	5.773	3.266
710.000	214.600	3.650	0.592	0.310	6.400	9.240	2.400	3.500	2.117	1.524	5.542	3.225
720.000	219.400	3.620	0.566	0.303	6.400	8.810	2.400	4.100	2.151	1.465	5.738	3.151
730.000	224.100	3.590	0.568	0.301	6.200	9.110	2.500	4.000	2.276	1.643	5.681	3.739
740.000	228.900	3.510	0.560	0.284	6.300	8.840	2.500	3.900	2.525	1.565	6.225	3.952
750.000	233.700	3.610	0.615	0.337	5.700	10.640	2.700	4.100	2.428	1.476	5.182	3.584
760.000	238.500	3.660	0.535	0.301	5.900	8.970	2.700	4.300	2.354	1.521	5.143	3.580
770.000	243.300	3.670	0.552	0.305	6.000	9.200	2.800	3.400	2.422	1.525	5.131	3.694
780.000	248.100	3.560	0.603	0.329	6.100	9.860	2.400	3.500	2.304	1.391	5.756	3.206
790.000	252.800	3.740	0.583	0.301	6.300	9.230	2.500	3.700	2.061	1.376	5.087	2.837
800.000	257.000	3.730	0.584	0.311	6.100	9.510	2.870	3.740	2.061	1.301	5.000	3.046

TABLE C.6:3 LITHOGENIC ELEMENTS AND THEIR RATIOS CORE CD1738

DEPTH (CM)	AGE (KYRS)	Si/Al (Si.lith)	Fe/Al (FEt)	K/Al	Ti/Al $x10^{-2}$	Fe/Ti	Zr/Al $x10^{-3}$	Cr/Al $x10^{-3}$	Zr/Qtz $x10^{-3}$	Cr/Zr	Ti/Qtz $x10^{-2}$	Cr/Qtz $x10^{-3}$
0.000	0.000	3.226	0.558	0.293	5.300	10.530	1.800	2.310	2.481	1.280	7.299	3.176
00.000	0.000	3.060	0.581	0.298	5.100	11.460	1.760	2.310	3.150	1.311	9.070	4.130
20.000	15.400	3.401	0.606	0.287	5.500	10.940	2.080	2.730	2.308	1.312	6.151	3.029
30.000	20.800	3.397	0.558	0.285	5.600	10.040	2.010	2.110	2.243	1.048	6.193	2.350
40.000	22.640	3.513	0.576	0.280	5.300	10.770	2.140	2.510	2.116	1.172	5.278	2.481
50.000	23.550	3.018	0.580	0.365	5.200	11.090	1.770	2.180	3.426	1.228	10.010	4.207
60.000	24.460	3.577	0.582	0.290	5.300	10.920	1.920	3.210	1.778	1.673	4.949	2.976
70.000	26.280	3.062	0.557	0.299	5.400	10.240	1.820	2.130	3.243	1.171	9.677	3.796
80.000	28.100	3.093	0.601	0.302	5.600	10.750	1.880	2.450	3.176	1.304	9.438	4.142
90.000	29.950	3.523	0.687	0.291	5.800	11.850	2.080	2.380	2.032	1.146	5.671	2.328
100.000	31.190	3.646	0.700	0.283	5.900	11.950	2.340	2.340	2.042	1.000	5.115	2.042
110.000	32.730	3.000	0.575	0.297	5.500	10.430	1.820	2.200	3.634	1.210	11.020	4.397
120.000	34.280	2.830	0.571	0.297	5.500	10.390	1.750	2.090	5.323	1.192	16.660	6.343
130.000	35.820	2.784	0.577	0.269	5.100	11.410	1.710	2.100	3.340	1.228	9.901	4.103
140.000	37.380	3.176	0.575	0.331	6.200	9.240	1.980	2.490	2.928	1.258	9.217	3.683
150.000	39.140	4.250	0.526	0.327	5.800	9.080	4.230	3.580	2.416	0.847	3.311	2.046
160.000	40.900	3.630	0.566	0.282	6.100	9.290	2.300	2.260	2.041	0.981	5.398	2.002
170.000	42.660	3.126	0.577	0.297	5.500	10.410	1.920	2.240	3.064	1.167	8.855	3.578
180.000	44.420	2.943	0.571	0.299	5.700	10.090	1.960	2.090	4.425	1.067	12.760	4.722
185.000	45.300	3.043	0.569	0.298	5.600	10.130	1.950	2.080	3.593	1.068	10.350	3.837
195.000	47.060	2.921	0.510	0.303	5.500	9.260	1.770	2.160	4.208	1.219	13.060	5.130
205.000	48.820	3.180	0.572	0.291	5.700	10.040	1.990	2.160	2.922	1.087	8.382	3.176
215.000	51.010	3.360	0.620	0.301	5.700	10.870	2.150	3.070	2.505	1.427	6.639	3.574
225.000	53.200	3.113	0.584	0.301	5.700	10.250	1.940	2.240	3.164	1.156	9.313	3.659
235.000	55.390	3.411	0.607	0.293	5.700	10.740	2.540	2.930	3.171	1.153	7.051	3.655
245.000	57.580	3.929	0.632	0.282	6.700	9.400	3.300	4.770	2.307	1.446	4.706	3.336

DEPTH (CM)	AGE (KYRS)	Si/Al (Si.lith)	Fe/Al (FEt)	K/Al	Ti/Al $x10^{-2}$	Fe/Ti	Zr/Al $x10^{-3}$	Cr/Al $x10^{-3}$	Zr/Qtz $x10^{-3}$	Cr/Zr	Ti/Qtz $x10^{-2}$	Cr/Qtz $x10^{-3}$
255.000	59.050	3.063	0.597	0.299	5.800	10.370	1.900	2.180	3.374	1.149	10.230	3.878
265.000	60.450	3.070	0.574	0.297	5.600	10.290	1.880	2.210	3.308	1.175	9.795	3.885
275.000	65.740	3.112	0.623	0.300	5.500	11.270	2.020	2.470	3.303	1.221	9.045	4.034
285.000	71.000	3.148	0.577	0.295	5.700	10.110	2.020	2.200	3.155	1.092	8.917	3.445
295.000	82.750	3.315	0.623	0.305	5.600	11.100	2.200	2.600	2.664	1.197	6.883	3.187
305.000	94.500	3.456	0.592	0.298	5.800	10.120	2.470	3.380	2.589	1.366	6.122	3.537
315.000	96.240	3.046	0.570	0.305	5.400	10.570	2.010	2.400	3.680	1.196	9.887	4.401
325.000	97.990	3.103	0.586	0.303	5.400	10.830	2.100	2.580	3.484	1.228	8.967	4.277
335.000	99.740	3.380	0.570	0.291	5.600	10.260	2.140	2.580	2.430	1.206	6.310	2.931
345.000	101.480	3.322	0.527	0.249	4.400	12.060	3.090	4.620	3.758	1.496	5.316	5.622
355.000	103.230	2.836	0.575	0.304	5.200	11.050	1.850	2.330	5.520	1.259	15.510	6.953
365.000	104.980	3.305	0.606	0.301	5.800	10.520	2.350	2.870	2.924	1.221	7.160	3.569
375.000	106.730	3.462	0.565	0.305	5.500	10.260	2.380	2.840	2.474	1.194	5.725	2.955
385.000	108.470	3.350	0.564	0.304	5.500	10.190	2.420	2.740	2.842	1.135	6.513	3.226
395.000	110.220	3.632	0.575	0.302	5.800	9.890	2.500	2.930	2.206	1.173	5.141	2.588
405.000	111.970	3.577	0.552	0.290	5.800	9.570	2.370	2.490	2.204	1.048	5.357	2.310
415.000	113.720	2.918	0.562	0.304	5.600	10.050	2.500	2.110	5.980	0.847	13.380	5.062
425.000	115.460	3.299	0.565	0.303	5.800	9.780	2.390	2.700	2.991	1.133	7.243	3.390
435.000	117.210	3.452	0.571	0.290	5.700	9.960	2.240	2.420	2.355	1.080	6.020	2.543
445.000	118.960	3.630	0.589	0.301	5.900	10.030	2.600	3.120	2.306	1.198	5.199	2.762
455.000	120.700	3.521	0.573	0.303	5.900	9.690	2.500	3.020	2.434	1.211	5.766	2.947
465.000	122.700	3.453	0.566	0.307	5.700	9.930	2.380	2.880	2.498	1.212	5.989	3.028
475.000	124.450	3.483	0.548	0.310	5.600	9.830	2.240	2.830	2.280	1.264	5.671	2.883
485.000	125.950	4.011	0.556	0.285	6.200	8.920	2.880	3.960	1.906	1.375	4.130	2.620
495.000	127.700	4.490	0.530	0.261	6.800	7.810	3.150	2.650	1.588	0.837	3.409	1.330
505.000	128.780	3.511	0.562	0.291	5.900	9.510	2.180	2.350	2.156	1.077	5.847	2.321
515.000	129.870	2.931	0.568	0.304	5.600	10.170	1.960	2.180	4.551	1.112	12.970	5.063
525.000	130.960	3.829	0.548	0.281	6.100	9.040	2.640	2.320	1.988	0.879	4.562	1.748

DEPTH (CM)	AGE (KYRS)	Si/Al (Si.lith)	Fe/Al (FEt)	K/Al	Ti/Al $x10^{-2}$	Fe/Ti	Zr/Al $x10^{-3}$	Cr/Al $x10^{-3}$	Zr/Qtz $x10^{-3}$	Cr/Zr	Ti/Qtz $x10^{-2}$	Cr/Qtz $x10^{-3}$
535.000	132.050	4.502	0.510	0.282	5.700	8.890	2.300	3.330	1.149	1.449	2.864	1.665
540.000	132.600	5.087	0.501	0.257	7.000	7.110	3.950	6.260	1.527	1.585	2.725	2.419
545.000	133.400	3.161	0.569	0.306	4.000	14.380	2.100	2.490	3.177	1.185	5.991	3.766
555.000	135.000	3.729	0.551	0.285	6.100	9.090	2.490	2.470	2.028	0.992	4.932	2.011
565.000	136.600	2.809	0.566	0.283	5.100	11.190	1.840	2.140	3.803	1.162	10.450	4.420
575.000	138.200	3.093	0.568	0.304	5.400	10.450	2.020	2.540	3.405	1.259	9.181	4.287
585.000	139.800	3.667	0.550	0.286	5.800	9.480	2.290	2.350	1.959	1.028	4.974	2.013
595.000	141.400	3.623	0.586	0.306	5.800	10.020	2.580	3.110	2.382	1.202	5.391	2.863
605.000	144.000	3.453	0.548	0.286	5.800	9.500	2.300	2.270	2.418	0.987	6.056	2.387
615.000	146.980	3.433	0.556	0.289	5.900	9.440	2.250	2.250	2.409	1.001	6.319	2.412
625.000	150.200	3.184	0.558	0.298	5.800	9.660	2.230	2.230	3.049	1.068	8.451	3.255
635.000	152.600	4.116	0.560	0.291	6.300	8.920	3.100	4.480	1.918	1.447	3.885	2.774
645.000	155.800	4.007	0.552	0.281	5.900	9.300	2.590	2.920	1.720	1.126	3.938	1.936
655.000	158.700	3.531	0.573	0.290	5.800	9.880	2.480	2.800	2.410	1.125	5.629	2.712
665.000	161.600	3.811	0.557	0.284	6.000	9.310	2.650	3.310	2.021	1.250	4.565	2.527

NOTE: FE is FEt

TABLE C.6:4 LITHOGENIC ELEMENTS AND THEIR RATIOS CORE CD1739

DEPTH (CM)	AGE (KYRS)	Si/Al (Si.lith)	Fe/Al (FEt)	K/Al	Ti/Al $x10^{-2}$	Fe/Ti	Zr/Al $x10^{-3}$	Cr/Al $x10^{-3}$	Zr/Qtz $x10^{-3}$	Cr/Zr	Ti/Qtz $x10^{-2}$	Cr/Qtz $x10^{-3}$
0.000	0.000	3.636	0.575	0.281	6.500	8.890	3.200	3.230	2.820	1.011	5.697	2.850
10.000	10.000	3.772	0.545	0.297	6.200	8.720	2.970	2.850	2.335	0.960	4.917	2.241
20.000	15.500	3.855	0.538	0.298	5.900	9.080	2.950	2.600	2.177	0.883	4.374	1.922
30.000	16.830	3.791	0.550	0.296	5.900	9.340	2.950	2.900	2.282	0.983	4.562	2.243
40.000	18.160	3.849	0.555	0.297	6.100	9.130	3.090	3.040	2.294	0.984	4.512	2.256
50.000	19.490	3.800	0.547	0.297	6.000	9.130	2.920	3.070	2.250	1.052	4.614	2.367
60.000	20.820	3.794	0.557	0.291	5.900	9.430	2.980	2.960	2.306	0.991	4.563	2.287
70.000	21.730	3.771	0.554	0.294	6.000	9.160	2.960	2.910	2.327	0.983	4.763	2.288
80.000	22.640	3.831	0.542	0.298	5.800	9.350	2.970	2.690	2.236	0.905	4.358	2.023
90.000	23.550	3.829	0.530	0.296	5.700	9.270	3.030	2.720	2.279	0.900	4.305	2.051
100.000	24.460	3.874	0.560	0.293	5.800	9.660	2.830	2.910	2.060	1.029	4.224	2.119
110.000	25.670	3.849	0.543	0.286	6.400	8.500	2.980	2.790	2.211	0.936	4.737	2.071
120.000	26.880	3.849	0.544	0.298	6.500	8.390	2.980	2.860	2.211	0.960	4.808	2.122
130.000	28.100	3.899	0.540	0.301	6.300	8.580	2.980	2.930	2.131	0.982	4.499	2.092
140.000	29.640	3.836	0.549	0.297	6.000	9.200	3.050	2.760	2.285	0.904	4.468	2.065
150.000	31.190	3.795	0.540	0.297	5.900	9.090	2.810	2.770	2.176	0.984	4.590	2.141
160.000	32.740	3.795	0.561	0.298	6.000	9.400	2.880	2.830	2.225	0.984	4.613	2.190
170.000	34.290	3.790	0.530	0.300	6.200	8.530	2.910	2.840	2.255	0.977	4.820	2.202
180.000	35.830	3.767	0.535	0.299	6.200	8.680	2.860	2.770	2.259	0.968	4.867	2.187
190.000	37.380	3.746	0.535	0.298	6.100	8.810	2.830	2.620	2.275	0.925	4.879	2.105
200.000	41.610	3.793	0.526	0.295	6.100	8.580	2.950	2.880	2.287	0.976	4.747	2.232
210.000	45.840	3.845	0.538	0.286	6.200	8.730	3.020	3.140	2.243	1.040	4.582	2.332
220.000	49.760	3.758	0.558	0.294	6.000	9.220	2.960	3.190	2.354	1.077	4.813	2.535
230.000	53.680	3.734	0.531	0.292	5.800	9.130	2.990	2.840	2.428	0.949	4.715	2.303
240.000	57.580	3.767	0.546	0.291	6.000	9.070	3.120	3.010	2.466	0.965	4.759	2.381

DEPTH (CM)	AGE (KYRS)	Si/Al (Si.lith)	Fe/Al (FEt)	K/Al	Ti/Al $x10^{-2}$	Fe/Ti	Zr/Al $x10^{-3}$	Cr/Al $x10^{-3}$	Zr/Qtz $x10^{-3}$	Cr/Zr	Ti/Qtz $x10^{-2}$	Cr/Qtz $x10^{-3}$
250.000	59.010	3.835	0.528	0.296	6.000	8.740	3.020	2.710	2.266	0.897	4.523	2.032
260.000	60.450	3.917	0.522	0.302	6.000	8.710	3.060	2.620	2.165	0.855	4.235	1.851
270.000	63.920	3.885	0.532	0.290	5.900	8.970	3.020	2.670	2.182	0.883	4.288	1.927
280.000	67.400	3.704	0.536	0.292	5.600	9.570	2.920	2.490	2.433	0.852	4.658	2.074
290.000	68.600	3.760	0.514	0.292	5.900	8.730	2.930	2.770	2.327	0.947	4.677	2.203
300.000	69.800	3.702	0.560	0.295	5.900	9.510	2.860	2.810	2.380	0.984	4.900	2.343
310.000	71.000	3.754	0.574	0.280	6.000	9.540	2.850	3.030	2.283	1.064	4.821	2.429
320.000	80.000	3.628	0.503	0.284	6.000	8.450	2.750	2.750	2.447	1.000	5.300	2.447
330.000	87.250	3.629	0.540	0.293	5.800	9.240	2.690	2.620	2.381	0.976	5.180	2.324
340.000	94.500	3.622	0.569	0.287	6.000	9.470	2.760	3.060	2.463	1.108	5.355	2.728
350.000	97.050	3.652	0.533	0.295	5.700	9.270	2.730	2.750	2.369	1.009	4.990	2.390
360.000	99.610	3.699	0.521	0.378	5.800	8.970	2.750	2.910	2.298	1.057	4.850	2.430
370.000	102.170	3.717	0.514	0.295	5.800	8.850	2.730	2.970	2.247	1.087	4.778	2.441
380.000	104.730	3.821	0.528	0.288	5.900	8.960	3.040	3.270	2.304	1.074	4.468	2.475
390.000	107.290	3.888	0.505	0.290	6.100	8.320	3.010	3.360	2.169	1.115	4.371	2.418
400.000	109.850	3.889	0.507	0.292	6.100	8.270	3.120	3.360	2.245	1.078	4.413	2.420
410.000	112.400	3.801	0.516	0.293	6.700	7.700	2.830	3.230	2.178	1.140	5.149	2.484
420.000	114.960	3.839	0.524	0.296	6.400	8.230	2.950	3.290	2.204	1.117	4.757	2.462
430.000	117.520	3.895	0.506	0.298	6.400	7.880	3.010	2.900	2.158	0.965	4.606	2.083
440.000	120.080	3.886	0.535	0.300	6.500	8.240	2.970	2.990	2.143	1.009	4.690	2.162
450.000	122.640	3.895	0.508	0.302	6.700	7.570	2.710	2.810	1.944	1.037	4.808	2.015
460.000	125.200	3.875	0.614	0.303	6.800	9.000	3.230	3.020	2.352	0.934	4.962	2.198
470.000	126.450	3.892	0.531	0.298	6.900	7.700	2.960	2.830	2.130	0.957	4.955	2.038
480.000	127.700	4.099	0.507	0.301	6.200	8.180	3.170	2.810	1.984	0.887	3.877	1.760
490.000	132.600	3.752	0.543	0.297	6.200	8.810	2.890	2.940	2.310	1.017	4.922	2.349
500.000	137.880	3.814	0.539	0.296	6.400	8.400	2.920	2.630	2.225	0.900	4.891	2.003

DEPTH (CM)	AGE (KYRS)	Si/Al (Si.lith)	Fe/Al (FEt)	K/Al	Ti/Al $x10^{-2}$	Fe/Ti	Zr/Al $x10^{-3}$	Cr/Al $x10^{-3}$	Zr/Qtz $x10^{-3}$	Cr/Zr	Ti/Qtz $x10^{-2}$	Cr/Qtz $x10^{-3}$
515.000	141.400	3.840	0.534	0.300	6.400	8.280	2.940	2.820	2.195	0.959	4.807	2.105
525.000	141.980	3.867	0.540	0.298	6.500	8.320	2.920	2.630	2.137	0.901	4.753	1.926
535.000	142.570	3.920	0.520	0.296	6.600	7.890	2.910	2.880	2.049	0.992	4.648	2.033
545.000	143.160	3.940	0.540	0.299	6.700	8.050	2.980	2.890	2.068	0.970	4.663	2.006
555.000	143.740	3.922	0.540	0.303	6.700	8.070	2.960	2.750	2.188	0.928	4.945	2.029
565.000	144.330	3.860	0.519	0.301	6.600	7.870	2.850	2.720	2.061	0.955	4.769	1.968
575.000	144.920	3.957	0.533	0.302	7.000	7.670	3.050	2.930	2.146	0.963	4.897	2.066
585.000	145.500	3.905	0.552	0.304	6.900	8.000	2.840	3.140	2.069	1.103	5.016	2.282
595.000	146.090	3.858	0.553	0.308	6.800	8.130	2.780	3.050	2.096	1.096	5.124	2.298
605.000	146.680	3.866	0.559	0.297	6.500	8.570	2.810	3.220	2.095	1.145	4.859	2.400
615.000	147.260	3.864	0.540	0.303	6.600	8.150	2.810	3.110	2.016	1.107	4.756	2.231
625.000	147.850	3.837	0.537	0.290	6.500	8.310	2.800	3.070	2.110	1.095	4.869	2.310
635.000	148.440	3.830	0.545	0.302	6.800	8.060	2.790	3.340	2.092	1.198	5.073	2.508
645.000	149.000	3.825	0.511	0.302	6.600	7.780	2.810	2.960	2.081	1.055	4.864	2.195
655.000	149.610	3.791	0.537	0.291	6.300	8.490	2.800	2.940	2.180	1.053	4.928	2.295
665.000	150.200	3.762	0.552	0.296	6.600	8.410	2.710	3.080	2.526	1.137	6.117	2.873
675.000	150.800	3.682	0.581	0.332	6.600	8.830	2.650	3.360	2.132	1.267	5.288	2.702
685.000	151.400	3.741	0.549	0.295	6.500	8.420	2.750	3.060	2.266	1.116	5.378	2.528
695.000	152.000	3.695	0.547	0.296	6.800	8.030	2.750	3.040	2.509	1.106	6.225	2.774
705.000	152.600	3.686	0.542	0.320	6.800	7.930	2.760	3.030	2.050	1.097	5.071	2.248
715.000	158.200	3.709	0.547	0.266	6.800	8.100	2.730	2.900	2.443	1.063	6.042	2.598
725.000	160.600	3.616	0.541	0.300	6.400	8.490	2.650	2.730	2.330	1.033	5.610	2.406
735.000	163.000	3.493	0.506	0.258	6.000	8.440	2.640	2.440	2.897	0.921	6.571	2.669
745.000	164.480	3.569	0.518	0.326	6.400	8.110	2.580	2.750	2.114	1.069	5.242	2.260
755.000	166.660	3.735	0.529	0.294	7.400	7.150	2.810	2.920	2.553	1.040	6.727	2.655
765.000	167.800	3.658	0.541	0.313	7.400	7.320	2.610	3.020	2.308	1.155	6.530	2.665

TABLE C.7:1 REEs CONTENTS AND THEIR RATIOS CORE CD1709

DEPTH (CM)	La (ppm)	Ce (ppm)	Nd (ppm)	Y (ppm)	La/Ce	Nd/Ce	La/Nd	Ce/Nd
0.000	0.000	21.540	13.330	14.360	0.000	0.619	0.000	1.616
10.000	3.110	25.110	17.660	13.500	0.124	0.703	0.176	1.422
20.000	2.040	30.970	13.290	15.340	0.066	0.429	0.153	2.330
30.000	7.160	27.620	11.250	15.400	0.259	0.407	0.636	2.455
40.000	0.000	21.560	15.400	15.400	0.000	0.714	0.000	1.400
50.000	8.150	23.430	15.280	15.280	0.348	0.652	0.533	1.533
60.000	4.080	31.650	9.180	15.310	0.129	0.290	0.444	3.448
70.000	1.010	28.440	13.200	16.250	0.036	0.464	0.077	2.155
80.000	27.620	17.390	16.360	4.230	1.588	0.941	1.688	1.063
90.000	13.290	29.660	15.340	16.360	0.448	0.517	0.866	1.934
100.000	8.280	34.180	17.610	16.570	0.242	0.515	0.470	1.941
110.000	1.730	32.020	17.950	14.280	0.054	0.561	0.096	1.784
120.000	3.400	26.570	15.860	15.650	0.128	0.597	0.214	1.675
130.000	5.500	21.210	14.680	14.790	0.259	0.692	0.375	1.445
140.000	4.890	38.450	18.760	15.090	0.127	0.488	0.261	2.050
150.000	0.000	29.070	17.640	15.090	0.000	0.607	0.000	1.648
160.000	0.000	24.780	14.790	14.790	0.000	0.597	0.000	1.675
170.000	10.500	23.400	11.520	15.300	0.449	0.492	0.911	2.031
180.000	8.050	16.620	8.670	14.580	0.484	0.522	0.928	1.917
190.000	9.070	27.840	17.130	14.480	0.326	0.615	0.529	1.625
200.000	3.770	26.620	16.320	14.990	0.142	0.613	0.231	1.631
210.000	1.930	24.580	15.090	15.300	0.079	0.614	0.128	1.629
220.000	2.750	31.920	14.890	3.440	0.086	0.466	0.185	2.144
230.000	4.080	24.680	16.320	15.700	0.165	0.661	0.250	1.512
240.000	0.000	28.860	14.480	15.480	0.000	0.502	0.000	1.993
250.000	0.710	33.550	17.130	16.110	0.021	0.511	0.041	1.959
260.000	0.000	32.130	15.600	14.890	0.000	0.486	0.000	2.060
270.000	2.240	25.800	11.620	15.400	0.087	0.450	0.193	2.220
280.000	8.280	25.150	17.870	15.150	0.329	0.711	0.463	1.407
290.000	6.960	23.930	15.550	14.540	0.291	0.650	0.448	1.539
300.000	0.000	23.830	15.250	14.840	0.000	0.640	0.000	1.563
310.000	0.000	22.640	11.510	14.540	0.000	0.508	0.000	1.967
320.000	4.640	25.800	15.350	15.150	0.180	0.595	0.302	1.681
330.000	0.000	26.410	15.250	15.450	0.000	0.577	0.000	1.732
340.000	2.720	17.440	14.640	14.640	0.156	0.839	0.186	1.191
350.000	1.610	28.350	13.330	14.240	0.057	0.470	0.121	2.127
360.000	2.020	23.200	15.750	15.750	0.087	0.679	0.128	1.473
370.000	8.850	22.970	12.320	15.350	0.385	0.536	0.718	1.864
380.000	4.380	25.190	16.420	15.500	0.174	0.652	0.267	1.534
390.000	1.830	38.650	22.130	15.900	0.047	0.573	0.083	1.746
400.000	4.380	27.330	17.340	15.340	0.160	0.634	0.253	1.576
410.000	2.650	25.600	16.110	16.320	0.104	0.629	0.164	1.589
420.000	3.900	29.470	17.540	15.910	0.132	0.595	0.222	1.680
430.000	8.160	21.110	14.480	15.400	0.387	0.686	0.564	1.458
440.000	3.230	28.280	15.850	15.750	0.114	0.560	0.204	1.784
450.000	0.800	29.080	15.950	15.550	0.028	0.548	0.050	1.823
460.000	1.320	31.620	15.810	15.400	0.042	0.500	0.083	2.000

TABLE C.7:2 REEs CONTENTS AND THEIR RATIOS CORE CD1715

AGE (KYRS)	DEPTH (CM)	La (ppm)	Ce (ppm)	Nd (ppm)	Y (ppm)	La/Ce	Nd/Ce	La/Nd	Ce/Nd
0.000	0.000	20.520	29.750	15.390	18.460	0.690	0.520	1.330	1.930
8.300	10.000	8.240	20.620	15.460	14.430	0.400	0.750	0.530	1.330
10.700	20.000	14.390	24.670	14.390	14.390	0.580	0.580	1.000	1.710
13.570	32.000	10.260	35.910	14.360	16.410	0.290	0.400	0.710	2.500
14.280	35.000	14.390	41.120	19.530	17.470	0.350	0.470	0.740	2.110
15.490	40.000	13.330	44.110	20.520	17.440	0.300	0.470	0.650	2.150
17.270	50.000	16.410	46.170	21.540	17.440	0.360	0.470	0.760	2.140
19.050	60.000	11.320	31.890	15.430	16.460	0.360	0.480	0.730	2.070
20.830	70.000	9.360	42.680	15.610	15.610	0.220	0.370	0.600	2.730
22.640	80.000	13.370	30.870	16.460	15.430	0.430	0.530	0.810	1.870
24.460	100.000	7.260	38.400	19.720	17.640	0.190	0.510	0.370	1.950
26.280	110.000	8.340	27.110	18.770	16.680	0.310	0.690	0.440	1.440
28.330	120.000	2.080	35.490	16.700	16.700	0.060	0.470	0.120	2.130
30.380	150.000	9.260	36.010	17.490	19.550	0.260	0.490	0.530	2.060
32.430	160.000	5.160	37.180	20.660	18.590	0.140	0.560	0.250	1.800
33.250	164.000	12.360	37.080	14.420	19.570	0.330	0.390	0.860	2.570
35.300	174.000	15.460	19.590	14.430	18.550	0.790	0.740	1.070	1.360
37.380	184.000	12.380	26.830	13.410	18.570	0.460	0.500	0.920	2.000
39.860	194.000	11.370	31.020	17.570	17.570	0.370	0.570	0.650	1.770
42.850	204.000	16.520	16.520	14.460	16.520	1.000	0.880	1.140	1.140
45.840	214.000	18.570	27.860	13.410	17.540	0.670	0.480	1.390	2.080
48.820	224.000	9.560	34.020	10.310	17.520	0.280	0.300	0.930	3.300
54.700	234.000	11.280	29.750	19.490	17.440	0.380	0.660	0.580	1.530
57.580	244.000	3.070	34.850	15.370	17.420	0.090	0.440	0.200	2.270
60.470	254.000	2.070	23.820	13.460	15.540	0.090	0.570	0.150	1.770
67.140	264.000	9.320	33.150	20.720	16.570	0.280	0.630	0.450	1.600
80.000	284.000	16.480	38.110	18.540	18.540	0.430	0.490	0.890	2.060
84.220	294.000	12.460	36.360	18.700	17.660	0.340	0.510	0.670	1.940
88.440	304.000	9.360	26.020	14.410	15.610	0.360	0.550	0.650	1.810
90.550	309.000	2.072	30.040	16.570	13.460	0.070	0.550	0.130	1.810
99.000	319.000	0.000	25.820	16.520	15.490	0.000	0.640	0.000	1.560
108.600	329.000	7.220	21.670	15.480	15.480	0.330	0.710	0.470	1.400
118.200	339.000	0.000	21.630	16.480	15.450	0.000	0.760	0.000	1.310
121.700	349.000	4.130	27.890	18.590	15.490	0.150	0.670	0.220	1.500
125.200	359.000	1.030	27.810	20.600	15.450	0.040	0.740	0.050	1.350
127.200	369.000	9.220	33.820	19.470	19.470	0.270	0.580	0.470	1.740
132.600	379.000	5.130	33.850	23.590	20.520	0.150	0.700	0.220	1.440
136.600	390.000	5.130	34.880	17.440	22.570	0.150	0.500	0.290	2.000
138.200	400.000	10.370	36.290	21.770	16.590	0.290	0.600	0.480	1.670
141.400	410.000	9.160	33.590	14.250	15.270	0.270	0.420	0.640	2.360
150.200	420.000	18.550	37.110	16.490	20.620	0.500	0.440	1.120	2.250
150.900	430.000	18.500	15.420	12.330	23.640	1.200	0.800	1.500	1.250
151.160	440.000	6.180	24.740	13.400	22.680	0.250	0.540	0.460	1.850
152.300	450.000	9.330	26.960	15.550	21.770	0.350	0.580	0.600	1.730
152.580	454.000	4.120	28.860	20.620	20.620	0.140	0.710	0.200	1.400
158.200	464.000	14.390	28.780	21.580	23.640	0.500	0.750	0.670	1.330
161.400	474.000	16.540	37.220	21.710	25.850	0.440	0.580	0.760	1.720
164.600	484.000	11.380	30.110	19.660	22.770	0.380	0.650	0.580	1.530
167.800	494.000	6.330	30.590	22.150	22.150	0.210	0.720	0.290	1.380
171.060	504.000	2.060	27.830	15.460	18.550	0.070	0.560	0.130	1.800
174.320	514.000	9.280	41.260	20.630	19.600	0.220	0.500	0.450	2.000
177.580	524.000	5.150	30.930	20.620	19.580	0.170	0.670	0.250	1.500
180.840	534.000	8.290	34.220	16.590	18.660	0.240	0.480	0.500	2.060
184.100	544.000	15.430	27.780	12.340	18.520	0.560	0.440	1.250	2.250
187.400	554.000	10.350	43.470	15.520	19.660	0.240	0.360	0.670	2.800
190.700	564.000	24.930	48.830	24.930	32.200	0.510	0.510	1.000	1.960
192.090	574.000	9.250	40.090	22.600	22.610	0.230	0.560	0.410	1.770
205.000	584.000	0.000	29.810	18.500	18.500	0.000	0.620	0.000	1.610
206.610	594.000	7.175	31.770	13.320	15.370	0.230	0.420	0.540	2.390
207.410	598.000	6.120	25.520	13.270	16.330	0.240	0.520	0.460	1.920
209.030	508.000	6.160	32.860	17.450	17.450	0.190	0.530	0.350	1.880
210.500	618.000	0.000	41.200	17.510	14.420	0.000	0.430	0.000	2.350
216.000	628.000	4.100	32.860	18.480	18.480	0.120	0.560	0.220	1.780
223.380	636.000	13.330	30.780	17.440	17.440	0.430	0.570	0.770	1.770
228.000	648.000	15.450	26.780	15.450	17.510	0.580	0.580	1.000	1.730
230.900	663.000	5.120	35.840	16.380	16.380	0.140	0.460	0.310	2.190
232.000	682.000	11.230	35.730	21.440	19.390	0.310	0.600	0.520	1.670
233.700	706.000	13.290	42.960	16.360	21.480	0.310	0.380	0.810	2.630
239.100	712.000	8.210	31.830	18.480	20.540	0.260	0.580	0.440	1.720
244.000	722.000	7.180	38.980	22.570	19.490	0.180	0.580	0.320	1.730
245.500	733.000	17.470	29.810	15.420	19.530	0.590	0.520	1.130	1.930

TABLE C.7:3 REEs CONTENTS AND THEIR RATIOS CORE CD1730

AGE (KYRS)	DEPTH (CM)	La (ppm)	Ce (ppm)	Nd (ppm)	Y (ppm)	La/Ce	Nd/Ce	La/Nd	Ce/Nd
0.000	0.000	10.360	42.470	17.610	22.790	0.240	0.410	0.590	2.410
2.600	10.000	14.500	30.040	17.610	21.750	0.480	0.590	0.820	1.710
5.100	20.000	11.420	33.240	20.780	18.700	0.340	0.630	0.550	1.600
7.700	30.000	5.160	36.120	17.540	16.510	0.140	0.490	0.290	2.060
10.000	40.000	6.190	22.720	14.460	16.520	0.270	0.640	0.430	1.570
12.000	50.000	4.110	41.120	18.500	15.420	0.100	0.450	0.220	2.220
13.500	60.000	8.200	33.820	16.400	16.400	0.240	0.480	0.500	2.060
15.500	70.000	10.240	27.240	17.400	16.380	0.380	0.640	0.590	1.570
16.600	80.000	13.290	39.890	17.390	17.390	0.330	0.440	0.760	2.290
18.100	90.000	10.280	31.860	19.530	17.470	0.320	0.610	0.530	1.630
19.200	100.000	5.160	33.050	11.360	17.560	0.160	0.340	0.450	2.910
20.300	110.000	7.230	27.890	12.390	17.560	0.260	0.440	0.580	2.250
21.400	120.000	11.360	38.220	20.660	17.560	0.300	0.540	0.550	1.850
22.600	130.000	14.470	38.250	16.540	17.570	0.380	0.430	0.870	2.310
24.000	140.000	14.440	38.180	16.510	17.540	0.380	0.430	0.870	2.310
25.300	150.000	17.440	28.720	11.280	18.460	0.610	0.390	1.550	2.550
26.700	160.000	19.570	32.960	17.510	19.570	0.590	0.530	1.120	1.880
28.200	170.000	13.450	33.120	14.490	18.630	0.410	0.440	0.930	2.290
29.400	180.000	11.390	37.290	20.720	18.640	0.310	0.560	0.550	1.800
30.700	190.000	12.360	35.020	16.480	19.570	0.350	0.470	0.750	2.120
32.000	200.000	13.320	29.720	14.350	18.450	0.450	0.480	0.930	2.070
33.400	210.000	11.280	35.910	16.410	19.490	0.310	0.460	0.690	2.190
34.700	220.000	16.490	26.800	16.490	19.580	0.620	0.620	1.000	1.630
36.100	230.000	12.360	41.200	15.450	19.570	0.300	0.370	0.800	2.670
37.400	240.000	20.620	37.110	17.520	19.580	0.560	0.470	1.180	2.120
39.500	250.000	8.250	29.920	15.480	18.570	0.280	0.520	0.530	1.930
41.600	260.000	10.290	30.870	17.490	18.520	0.330	0.570	0.590	1.770
43.700	270.000	0.000	22.570	11.280	17.440	0.000	0.500	0.000	2.000
45.800	280.000	13.400	26.800	9.270	18.550	0.500	0.350	1.450	2.890
50.000	290.000	6.180	27.830	13.400	18.550	0.220	0.480	0.460	2.080
52.100	295.000	8.250	41.280	15.480	19.600	0.200	0.370	0.530	2.670
56.300	305.000	7.180	28.720	13.330	18.460	0.250	0.460	0.540	2.150
60.500	315.000	12.490	30.180	15.610	19.770	0.410	0.520	0.800	1.930
63.500	325.000	10.430	30.240	11.470	18.770	0.340	0.380	0.910	2.640
80.000	345.000	12.460	29.090	11.420	20.780	0.430	0.390	1.090	2.550
84.500	355.000	12.420	32.080	11.380	18.630	0.390	0.350	1.090	2.820
89.000	365.000	3.100	22.770	13.450	18.630	0.140	0.590	0.230	1.690
93.600	375.000	1.030	27.890	11.360	16.520	0.040	0.410	0.090	2.460
99.900	385.000	0.000	29.890	19.580	16.490	0.000	0.660	0.000	1.530
102.200	395.000	9.270	28.840	21.630	17.510	0.320	0.750	0.430	1.330
108.600	405.000	8.450	36.990	19.020	17.960	0.230	0.510	0.440	1.940
115.000	415.000	8.210	33.890	18.480	17.450	0.240	0.550	0.440	1.830
121.400	425.000	3.060	28.610	17.370	18.390	0.110	0.610	0.180	1.650
128.000	435.000	7.150	32.700	18.390	17.370	0.220	0.560	0.390	1.780
130.100	450.000	8.190	40.960	18.430	19.450	0.200	0.450	0.440	2.220
132.200	460.000	4.410	36.380	19.840	20.940	0.120	0.550	0.220	1.830
134.400	470.000	4.100	40.050	15.400	20.540	0.100	0.380	0.270	2.600
136.500	480.000	7.180	42.100	22.590	21.560	0.170	0.540	0.320	1.860
138.600	490.000	27.780	41.160	22.630	22.630	0.670	0.550	1.230	1.820
140.700	500.000	19.580	42.270	16.490	23.710	0.460	0.390	1.190	2.560
142.800	510.000	20.720	38.330	19.680	22.790	0.540	0.510	1.050	1.950
144.900	520.000	21.670	39.210	20.640	21.670	0.550	0.530	1.050	1.900
147.100	530.000	12.390	40.280	20.660	20.660	0.310	0.510	0.600	1.950
149.200	540.000	13.450	31.050	15.520	21.730	0.430	0.500	0.870	2.000
151.300	550.000	13.490	48.780	18.680	21.790	0.280	0.380	0.720	2.610
153.400	560.000	7.250	40.440	21.770	20.740	0.180	0.540	0.330	1.860
155.500	570.000	12.320	40.050	18.480	20.540	0.310	0.460	0.670	2.170
157.700	580.000	5.130	52.370	23.620	23.620	0.100	0.450	0.220	2.220
159.800	590.000	9.300	53.760	23.780	24.810	0.170	0.440	0.390	2.260
163.200	600.000	7.210	42.230	21.630	22.620	0.170	0.510	0.330	1.950
166.700	610.000	15.520	26.910	13.450	20.700	0.580	0.500	1.150	2.000
170.100	620.000	12.440	34.220	16.590	18.660	0.360	0.480	0.750	2.060
173.600	630.000	9.300	34.120	18.610	19.640	0.270	0.550	0.500	1.830
177.000	640.000	18.610	31.020	19.640	21.710	0.600	0.630	0.950	1.580
180.500	650.000	24.760	41.280	17.540	25.800	0.600	0.420	1.410	2.350
184.100	660.000	29.170	63.560	25.000	30.210	0.460	0.390	1.170	2.540
191.000	670.000	15.550	35.250	26.960	22.810	0.440	0.760	0.580	1.310
198.000	680.000	10.350	34.150	20.700	20.700	0.300	0.610	0.500	1.650
205.000	690.000	7.160	41.980	23.550	18.430	0.170	0.560	0.300	1.780
209.800	700.000	8.170	32.700	14.300	16.350	0.250	0.440	0.570	2.290
214.600	710.000	3.060	33.750	14.320	15.340	0.090	0.420	0.210	2.360
219.400	720.000	9.290	44.410	15.490	16.520	0.210	0.350	0.600	2.870
224.100	730.000	12.420	30.010	16.560	17.590	0.410	0.550	0.750	1.810
228.900	740.000	10.310	29.890	13.400	16.490	0.340	0.450	0.770	2.230
233.700	750.000	7.220	33.000	18.570	14.440	0.220	0.560	0.390	1.780
238.500	760.000	10.300	35.020	20.600	17.510	0.290	0.590	0.500	1.700
243.300	770.000	13.390	36.050	20.600	18.540	0.370	0.570	0.650	1.750
248.100	780.000	8.210	25.670	15.400	17.450	0.320	0.600	0.530	1.670
252.800	790.000	12.280	29.690	13.310	13.310	0.410	0.450	0.920	2.230
257.600	800.000	11.250	35.800	20.460	16.360	0.310	0.570	0.550	1.750

TABLE C.7:4 REEs CONTENTS AND THEIR RATIO CORE CD1738

AGE (KYRS)	DEPTH (CM)	La (ppm)	Ce (ppm)	Nd (ppm)	Y (ppm)	Sc (ppm)	La/Ce	Nd/Ce	La/Nd	Ce/Nd
--	0.000	27.810	60.770	21.630	23.690	17.510	0.458	0.356	1.286	2.810
--	10.000	25.720	67.910	26.750	25.720	17.510	0.379	0.394	0.961	2.539
15.400	20.000	23.870	51.900	21.790	22.830	18.540	0.460	0.420	1.095	2.382
20.800	30.000	28.470	72.240	25.420	25.420	9.090	0.394	0.352	1.120	2.842
22.640	40.000	22.500	52.170	17.390	21.480	15.150	0.431	0.333	1.294	3.000
23.550	50.000	28.630	66.470	24.540	22.490	18.360	0.431	0.369	1.167	2.709
24.460	60.000	18.570	36.110	18.570	17.540	8.240	0.514	0.514	1.000	1.945
26.280	70.000	30.600	70.380	23.460	24.480	12.240	0.435	0.333	1.304	3.000
28.100	80.000	60.410	20.480	20.480	24.570	13.260	2.950	1.000	2.950	1.000
29.950	90.000	30.600	61.200	26.520	24.480	10.200	0.500	0.433	1.154	2.308
31.190	100.000	26.440	52.880	20.340	25.420	10.100	0.500	0.385	1.300	2.600
32.730	110.000	33.520	61.240	25.160	24.760	18.850	0.547	0.411	1.332	2.434
34.280	120.000	34.570	82.000	31.000	25.290	20.290	0.422	0.378	1.115	2.645
35.820	130.000	33.250	53.040	21.420	23.350	14.480	0.627	0.404	1.552	2.476
37.380	140.000	19.680	58.850	24.270	20.400	17.740	0.334	0.412	0.811	2.425
39.140	150.000	17.370	51.710	22.820	24.130	10.500	0.336	0.441	0.761	2.266
40.900	160.000	28.880	65.850	26.760	25.550	15.950	0.439	0.406	1.079	2.461
42.660	170.000	26.310	56.500	25.290	23.760	17.640	0.466	0.448	1.040	2.234
44.420	180.000	30.900	76.290	31.820	24.370	18.970	0.405	0.417	0.971	2.398
45.300	185.000	30.490	69.760	25.500	24.580	18.250	0.437	0.366	1.196	2.736
47.060	195.000	30.700	69.760	29.070	27.130	20.290	0.440	0.417	1.056	2.400
48.820	205.000	33.560	69.760	31.010	25.220	16.980	0.481	0.445	1.082	2.250
51.010	215.000	16.720	42.730	21.420	19.990	13.050	0.391	0.501	0.781	1.995
53.200	225.000	30.800	66.450	29.080	24.740	17.670	0.464	0.438	1.059	2.285
55.390	235.000	15.600	33.860	15.090	20.700	15.190	0.461	0.446	1.034	2.244
57.580	245.000	17.570	43.120	20.500	19.690	8.380	0.407	0.475	0.857	2.103
59.050	255.000	31.960	68.200	23.720	24.330	18.220	0.469	0.348	1.347	2.875
60.450	265.000	26.360	67.630	27.070	25.240	19.670	0.390	0.400	0.974	2.498
65.740	275.000	20.700	55.480	22.740	21.820	15.400	0.373	0.410	0.910	2.440
71.000	285.000	27.640	63.640	22.230	27.780	15.400	0.434	0.349	1.243	2.863
82.750	295.000	15.070	49.380	19.730	20.540	11.730	0.305	0.400	0.764	2.503
94.500	305.000	14.190	44.000	19.770	19.060	9.730	0.322	0.449	0.718	2.226
96.240	315.000	21.570	46.490	22.580	20.460	14.280	0.464	0.486	0.955	2.059
97.990	325.000	18.870	50.180	21.210	20.090	14.070	0.376	0.423	0.890	2.366
99.740	335.000	18.250	53.440	17.640	20.090	16.210	0.342	0.330	1.035	3.029
101.480	345.000	10.300	31.720	15.600	16.620	5.500	0.325	0.492	0.660	2.033
103.230	355.000	23.970	59.870	24.780	22.950	13.970	0.400	0.414	0.967	2.416
104.980	365.000	15.910	38.860	17.230	19.270	8.770	0.409	0.443	0.923	2.255
106.730	375.000	21.270	38.860	20.290	19.680	11.110	0.547	0.522	1.048	1.915
108.470	385.000	18.980	48.210	19.180	19.690	8.620	0.394	0.398	0.990	2.514
110.220	395.000	15.810	39.950	18.250	19.770	4.960	0.396	0.457	0.866	2.189
111.970	405.000	12.970	47.960	16.520	22.380	13.050	0.270	0.344	0.785	2.903
113.720	415.000	14.890	53.850	22.950	21.620	13.770	0.277	0.426	0.649	2.346
115.460	425.000	21.770	49.790	22.620	21.090	12.320	0.437	0.454	0.962	2.201
117.210	435.000	20.360	47.200	19.040	21.980	16.000	0.431	0.403	1.069	2.479
118.960	445.000	10.150	45.770	18.570	19.380	9.200	0.222	0.406	0.547	2.465
120.700	455.000	13.380	42.080	19.160	20.070	13.890	0.318	0.455	0.698	2.196
122.700	465.000	23.440	49.120	21.110	20.300	12.480	0.477	0.430	1.110	2.327
124.450	475.000	13.940	35.220	16.890	18.520	9.200	0.396	0.480	0.825	2.085
125.950	485.000	10.040	43.840	19.690	18.270	3.550	0.229	0.449	0.510	2.227
127.700	495.000	22.520	55.850	24.130	24.540	15.040	0.403	0.432	0.933	2.315
128.780	505.000	21.000	52.110	22.420	23.750	10.700	0.403	0.430	0.937	2.324
129.870	515.000	19.080	67.570	26.760	23.630	15.950	0.282	0.396	0.713	2.525
130.960	525.000	21.510	61.910	23.630	24.140	12.420	0.347	0.382	0.910	2.620
132.050	535.000	9.390	41.610	15.950	16.260	3.430	0.226	0.383	0.589	2.609
132.600	540.000	4.060	41.000	17.960	18.570	0.000	0.099	0.438	0.226	2.283
133.400	545.000	27.960	57.560	23.080	21.500	15.250	0.486	0.401	1.211	2.494
135.000	555.000	31.770	62.540	25.190	24.490	11.940	0.508	0.403	1.261	2.483
136.600	565.000	32.540	69.860	31.520	23.280	19.010	0.466	0.451	1.032	2.216
138.200	575.000	20.050	58.940	24.530	21.980	18.010	0.340	0.416	0.817	2.403
139.800	585.000	23.050	56.710	22.740	24.060	14.760	0.406	0.401	1.014	2.494
141.400	595.000	16.930	47.530	19.170	20.090	9.580	0.356	0.403	0.883	2.479
144.000	605.000	24.790	57.170	24.280	24.590	19.120	0.434	0.425	1.021	2.355
146.980	615.000	25.700	45.740	19.530	23.880	15.680	0.562	0.427	1.316	2.342
150.200	625.000	31.400	56.520	24.410	25.020	16.510	0.556	0.432	1.286	2.315
152.600	635.000	6.820	35.150	16.810	17.520	6.310	0.194	0.478	0.406	2.091
155.800	645.000	14.860	45.810	17.710	20.250	12.520	0.324	0.387	0.839	2.587
158.700	655.000	18.870	53.750	22.130	21.520	11.110	0.351	0.412	0.853	2.429
161.600	665.000	13.560	44.820	19.220	21.170	11.200	0.303	0.429	0.706	2.332

TABLE C.7:5 REEs CONTENTS AND THEIR RATIOS CORE CD1739

AGE (KYRS)	DEPTH (CM)	La (ppm)	Ce (ppm)	Nd (ppm)	Y (ppm)	La/Ce	Nd/Ce	La/Nd	Ce/Nd
--	0.000	6.190	28.920	14.460	13.420	0.214	0.500	0.428	2.000
--	10.000	5.090	31.550	18.320	18.320	0.161	0.581	0.278	1.722
15.500	20.000	13.240	31.580	16.300	17.320	0.419	0.516	0.812	1.937
16.830	30.000	13.270	37.770	20.420	16.330	0.351	0.541	0.650	1.850
18.160	40.000	8.160	33.690	22.460	16.330	0.242	0.667	0.363	1.500
19.490	50.000	7.150	23.500	16.350	15.330	0.304	0.696	0.437	1.437
20.820	60.000	14.330	38.910	17.400	16.380	0.368	0.447	0.824	2.236
21.730	70.000	10.220	31.680	16.350	16.350	0.323	0.516	0.625	1.938
22.640	80.000	12.260	23.500	12.260	17.370	0.522	0.522	1.000	1.917
23.550	90.000	16.350	35.770	16.350	17.370	0.457	0.457	1.000	2.188
24.460	100.000	13.310	40.960	18.430	19.450	0.325	0.450	0.722	2.222
25.670	110.000	11.730	30.940	18.130	18.130	0.379	0.586	0.647	1.707
26.880	120.000	14.280	34.680	18.360	17.340	0.412	0.529	0.778	1.889
28.100	130.000	15.250	32.540	14.230	19.320	0.469	0.437	1.072	2.287
29.640	140.000	15.280	34.640	18.340	18.340	0.441	0.529	0.833	1.889
31.190	150.000	21.420	40.800	17.340	18.360	0.525	0.425	1.235	2.353
32.740	160.000	18.320	37.660	18.320	18.320	0.486	0.486	1.000	2.056
34.290	170.000	10.190	46.870	17.320	17.320	0.217	0.370	0.588	2.706
35.830	180.000	13.270	37.770	19.390	17.370	0.351	0.513	0.684	1.948
37.380	190.000	17.370	37.810	18.390	17.370	0.459	0.486	0.945	2.056
41.610	200.000	17.370	34.740	18.390	17.370	0.500	0.529	0.945	1.889
45.840	210.000	17.370	35.770	18.390	18.390	0.486	0.514	0.945	1.945
49.760	220.000	24.570	37.880	16.380	17.400	0.649	0.432	1.500	2.313
53.680	230.000	16.330	34.710	15.310	16.330	0.470	0.441	1.067	2.267
57.580	240.000	14.320	31.710	12.270	16.360	0.452	0.387	1.167	2.584
59.010	250.000	14.250	38.680	18.320	17.300	0.368	0.474	0.778	2.111
60.450	260.000	8.120	35.520	20.300	18.270	0.229	0.572	0.400	1.750
63.920	270.000	17.860	39.930	17.860	19.960	0.447	0.447	1.000	2.236
67.400	280.000	12.220	36.680	18.340	18.340	0.333	0.500	0.666	2.000
68.600	290.000	16.280	35.630	19.340	19.340	0.457	0.543	0.842	1.842
69.800	300.000	13.270	34.710	17.350	20.420	0.382	0.500	0.765	2.001
71.000	310.000	21.390	47.890	22.410	19.360	0.447	0.468	0.954	2.137
80.000	320.000	19.360	30.570	17.320	18.340	0.633	0.567	1.118	1.765
87.250	330.000	18.280	43.680	22.350	19.300	0.418	0.512	0.818	1.954
94.500	340.000	8.150	36.680	18.340	18.340	0.222	0.500	0.444	2.000
97.050	350.000	10.180	32.570	14.250	18.320	0.313	0.438	0.714	2.286
99.610	360.000	16.320	30.600	17.340	16.320	0.533	0.567	0.941	1.765
102.170	370.000	13.280	38.830	18.390	16.350	0.342	0.474	0.722	2.111
104.730	380.000	12.260	33.720	18.390	16.350	0.364	0.545	0.667	1.834
107.290	390.000	10.230	31.710	21.480	17.390	0.323	0.677	0.476	1.476
109.850	400.000	10.220	33.720	14.300	17.370	0.303	0.424	0.715	2.358
112.400	410.000	9.210	37.880	15.360	17.400	0.243	0.405	0.600	2.466
114.960	420.000	5.110	32.720	14.310	17.380	0.156	0.437	0.357	2.287
117.520	430.000	13.290	36.810	18.400	17.380	0.361	0.500	0.722	2.001
120.080	440.000	15.300	40.800	17.340	17.340	0.375	0.425	0.882	2.353
122.640	450.000	14.280	34.680	14.280	16.320	0.412	0.412	1.000	2.429
125.200	460.000	11.190	37.660	17.300	18.320	0.297	0.459	0.647	2.177
126.450	470.000	13.240	38.720	20.380	17.320	0.342	0.526	0.650	1.900
127.700	480.000	15.240	29.460	16.250	20.320	0.517	0.552	0.938	1.813
132.600	490.000	17.320	38.720	18.340	17.320	0.447	0.474	0.944	2.111
137.880	500.000	14.280	40.800	17.340	17.340	0.350	0.425	0.824	2.353
141.400	515.000	10.170	37.620	20.340	18.300	0.270	0.541	0.500	1.850
141.980	525.000	19.280	34.510	17.250	20.300	0.559	0.500	1.118	2.001
142.570	535.000	16.240	36.540	21.310	19.280	0.444	0.583	0.762	1.715
143.160	545.000	14.190	41.570	22.300	19.260	0.341	0.536	0.636	1.864
143.740	555.000	17.220	39.500	18.230	20.200	0.436	0.462	0.945	2.167
144.330	565.000	10.150	41.610	18.270	20.300	0.244	0.439	0.556	2.278
144.920	575.000	10.140	38.530	19.260	19.260	0.263	0.500	0.526	2.001
145.500	585.000	15.270	42.750	19.340	19.340	0.357	0.452	0.790	2.210
146.090	595.000	15.270	43.770	23.410	19.340	0.349	0.535	0.652	1.870
146.680	605.000	15.280	41.770	16.300	19.360	0.366	0.390	0.937	2.563
147.260	615.000	24.430	34.610	17.300	19.340	0.706	0.500	1.412	2.001
147.850	625.000	27.450	45.760	25.420	19.320	0.600	0.556	1.080	1.800
148.440	635.000	24.430	47.840	20.360	19.340	0.511	0.426	1.200	2.350
149.000	645.000	15.240	48.760	18.280	20.320	0.313	0.375	0.834	2.667
149.610	655.000	16.280	38.680	19.340	20.360	0.421	0.500	0.842	2.000
150.200	665.000	17.300	48.860	19.340	20.360	0.354	0.396	0.895	2.526
150.800	675.000	18.390	47.010	22.480	20.440	0.391	0.478	0.818	2.091
151.400	685.000	17.280	49.830	16.270	20.340	0.347	0.327	1.062	3.063
152.000	695.000	20.320	42.670	21.330	20.320	0.476	0.500	0.953	2.000
152.600	705.000	22.390	46.820	17.300	19.340	0.478	0.370	1.294	2.706
158.200	715.000	22.300	37.510	20.200	21.290	0.595	0.539	1.104	1.857
160.600	725.000	21.370	41.730	20.360	20.360	0.512	0.488	1.050	2.050
163.000	735.000	22.300	44.610	17.230	21.290	0.500	0.386	1.294	2.589
164.480	745.000	23.430	46.870	22.410	18.340	0.500	0.478	1.046	2.091
166.660	755.000	21.350	45.760	25.420	20.340	0.467	0.556	0.840	1.800
167.800	765.000	24.520	43.940	18.390	19.410	0.558	0.419	1.333	2.389

TABLE C.8:1 QUARTZ, DOLOMITE, TERRIGENOUS SILICA (Si.lith) AND IRON (FEt). CORE CD1715

DEPTH (CM)	AGE (KYS)	QUARTZ (%)	DOLMITE (%)	Si(lith) (%)	FEt (%)
0.00	0.00	7.09	5.03	10.96	1.50
10.00	8.31	3.70	1.54	4.96	1.20
20.00	10.70	3.91	2.00	6.20	1.22
32.00	13.57	3.86	3.18	10.46	1.97
35.00	14.28	3.96	3.34	9.91	2.02
40.00	15.49	3.00	3.07	12.32	2.20
50.00	17.27	4.38	3.14	10.82	2.06
60.00	19.05	4.08	2.85	9.95	1.90
70.00	20.83	4.20	3.17	10.69	2.03
80.00	22.64	4.98	4.20	11.62	1.92
100.00	24.46	4.16	3.13	10.72	1.94
110.00	26.28	3.91	4.11	10.97	2.17
120.00	28.33	4.08	4.58	10.95	2.05
150.00	30.38	4.71	2.46	11.83	2.02
160.00	32.43	9.87	2.93	11.63	2.00
164.00	33.25	4.98	3.23	12.91	2.25
174.00	35.30	4.72	2.55	11.90	2.03
184.00	37.38	4.76	2.39	11.22	2.23
194.00	39.86	4.87	2.82	11.87	2.00
204.00	42.85	4.93	2.27	10.66	2.05
214.00	45.84	6.20	3.48	12.33	2.01
224.00	48.82	2.28	2.14	9.74	1.74
234.00	54.70	4.70	2.08	11.18	2.14
244.00	57.58	4.07	1.72	8.81	1.67
254.00	60.47	5.92	1.95	13.44	2.30
264.00	67.14	6.95	2.53	9.51	2.04
284.00	80.00	3.98	1.53	8.74	1.49
294.00	84.22	5.49	2.24	7.33	1.54
304.00	88.44	4.66	1.98	7.22	1.33
309.00	90.55	4.62	1.71	6.14	1.23
319.00	99.00	4.22	1.18	7.50	1.38
329.00	108.60	3.88	1.51	8.83	1.76
339.00	118.20	3.56	1.24	8.71	1.55
349.00	121.70	3.84	1.51	9.21	1.75
359.00	125.20	4.72	1.16	8.40	1.50
369.00	127.20	5.46	2.00	14.08	2.33
379.00	132.60	5.18	1.87	12.96	2.41
390.00	136.60	5.44	2.03	13.81	2.56
400.00	138.20	6.06	3.57	11.75	2.19
410.00	141.40	7.41	4.69	13.90	1.76
420.00	150.20	6.89	2.57	14.14	2.78
430.00	150.90	6.41	1.41	15.19	2.65
440.00	151.16	5.81	1.73	12.28	2.34
450.00	152.30	5.64	1.61	10.98	2.23
454.00	152.58	5.10	0.94	9.73	1.90
464.00	158.20	4.78	0.93	14.64	2.86
474.00	161.40	5.08	1.34	12.10	2.45
484.00	164.60	5.54	1.56	10.62	2.13
494.00	167.80	4.65	0.79	8.48	1.74
504.00	171.06	4.26	1.07	8.06	1.68
514.00	174.32	3.49	0.09	8.64	1.79
524.00	177.58	4.03	0.21	10.82	2.14
534.00	180.84	5.93	3.59	10.78	1.98
544.00	184.12	7.07	4.92	11.56	1.82
554.00	187.40	6.03	3.04	11.00	2.00
564.00	190.70	7.38	0.35	17.31	3.35
574.00	192.09	5.40	0.61	11.34	2.22
584.00	205.00	3.96	0.93	6.70	1.35
594.00	206.61	3.44	2.55	10.17	1.90
598.00	207.41	3.59	2.89	10.11	1.80
608.00	209.03	4.27	3.64	10.05	1.84
618.00	210.50	3.70	4.79	10.74	1.83
628.00	216.00	4.26	3.38	11.78	2.08
636.00	223.38	5.20	4.39	11.06	1.96
648.00	228.00	4.08	3.51	11.08	2.16
663.00	230.90	4.03	2.83	10.30	1.74
682.00	232.00	4.67	2.89	12.39	2.08
706.00	233.70	6.00	2.92	17.64	2.73
712.00	239.10	5.64	2.13	12.45	2.07
722.00	244.00	4.65	1.91	11.70	2.23
733.00	245.50	4.49	1.63	12.52	2.24

TABLE C.8:2 QUARTZ, DOLOMITE, TERRIGENOUS SILICA (Si.lith) AND IRON (FEt). CORE CD1730

DEPTH (CM)	AGE (KYS)	QUARTZ (%)	DOLOMITE (%)	Si(lith) (%)	FEt (%)
0.00	0.00	2.70	2.05	13.57	2.76
10.00	2.60	2.40	1.99	12.77	2.65
20.00	5.10	1.90	1.66	10.25	2.16
30.00	7.70	2.20	1.60	10.14	2.17
40.00	10.00	2.46	2.31	10.43	2.12
50.00	12.00	2.60	2.43	10.76	1.90
60.00	13.50	3.70	3.70	12.71	2.10
70.00	15.50	4.58	4.36	14.46	2.47
80.00	16.60	4.50	4.14	14.27	2.38
90.00	18.10	3.95	3.59	13.35	2.28
100.00	19.20	4.31	3.92	13.58	2.26
110.00	20.30	4.37	3.92	13.80	2.26
120.00	21.40	4.33	3.73	13.47	2.18
130.00	22.60	4.86	3.86	14.32	2.29
140.00	24.00	4.18	3.37	13.32	2.19
150.00	25.30	4.88	3.42	15.19	2.42
160.00	26.70	4.94	2.97	15.07	2.32
170.00	28.20	4.89	3.10	15.06	2.53
180.00	29.40	4.78	3.23	14.83	2.35
190.00	30.70	4.95	4.16	15.10	2.37
200.00	32.00	5.01	4.20	15.42	2.66
210.00	33.40	5.34	3.93	16.12	2.57
220.00	34.70	5.48	3.52	16.39	2.68
230.00	36.10	4.92	3.23	15.65	2.48
240.00	37.40	4.50	3.08	14.79	2.34
250.00	39.50	4.94	2.99	15.45	2.70
260.00	41.60	5.04	3.34	16.39	2.58
270.00	43.70	5.03	3.16	15.98	2.51
280.00	45.80	3.75	2.02	13.43	2.23
290.00	50.00	4.47	2.11	14.41	2.45
295.00	52.10	4.42	2.60	14.40	2.30
305.00	56.30	4.58	2.98	14.91	2.33
315.00	60.50	4.27	4.16	14.38	2.29
325.00	63.50	4.24	3.34	13.86	2.25
335.00	71.00	5.27	2.52	16.95	2.64
345.00	80.00	4.68	2.66	15.47	2.55
355.00	84.50	4.70	3.26	15.03	2.54
365.00	89.00	3.76	2.88	12.88	2.19
375.00	93.60	3.16	2.74	11.31	1.87
385.00	99.00	3.36	2.07	11.76	2.03
395.00	102.20	3.80	2.49	12.42	2.11
405.00	108.60	3.05	1.49	12.32	2.12
415.00	115.00	4.32	2.20	13.32	2.15
425.00	121.40	4.95	2.90	14.67	2.38
435.00	128.00	5.22	2.81	15.85	2.60
450.00	130.10	5.23	2.45	15.95	2.57
460.00	132.20	4.95	2.00	14.91	2.41
470.00	134.40	4.82	2.13	15.29	2.53
480.00	136.50	4.80	1.95	15.90	2.66
490.00	138.60	5.06	2.23	16.68	2.86
500.00	140.70	5.25	2.48	17.27	3.05
510.00	142.80	5.19	2.66	17.11	2.90
520.00	144.90	5.71	1.96	17.60	2.70
530.00	147.10	4.23	2.32	15.34	2.70
540.00	149.20	3.67	1.85	14.72	2.65
550.00	151.30	3.55	1.99	14.94	2.80
560.00	153.40	3.43	1.31	14.55	2.74
570.00	155.50	3.92	0.88	15.25	2.58
580.00	157.70	5.25	1.01	17.81	3.10
590.00	159.80	4.56	2.26	16.27	2.97
600.00	163.20	4.22	2.12	15.50	2.74
610.00	166.70	3.19	2.40	13.28	2.54
620.00	170.10	2.95	3.47	11.98	2.32
630.00	173.60	3.30	1.29	12.87	2.26
640.00	177.00	3.32	0.99	14.30	2.65
650.00	180.50	4.66	0.05	18.32	3.35
660.00	184.10	4.88	0.73	19.41	3.65
670.00	191.00	4.26	2.11	15.48	2.93
680.00	198.00	2.90	0.95	13.33	2.41
690.00	205.00	1.85	0.94	10.92	2.16
700.00	209.43	3.88	2.27	13.10	2.10
710.00	214.60	4.06	3.28	12.81	2.08
720.00	219.40	4.13	3.50	13.36	2.09
730.00	224.10	3.82	3.30	12.49	1.98
740.00	228.90	3.47	3.47	11.97	1.91
750.00	233.70	3.57	3.99	11.55	1.97
760.00	238.50	4.20	3.37	13.25	1.94
770.00	243.30	4.21	3.36	13.21	1.99
780.00	248.10	4.10	3.18	13.74	2.33
790.00	252.80	4.62	3.48	13.91	2.17
800.00	257.00	4.50	3.68	13.65	2.14

TABLE C.8:3 QUARTZ, DOLOMITE, TERRIGENOUS SILICA (Si.lith) AND IRON (FEt). CORE CD1738

DEPTH (CM)	AGE (KYS)	QUARTZ (%)	DOLOMITE (%)	Si(lith) (%)	FEt (%)
0.00	0.00	5.48	1.60	24.36	4.21
0.00	0.00	4.41	1.24	24.14	4.58
20.00	15.40	6.34	3.90	23.94	4.27
30.00	20.80	6.62	0.14	25.07	4.12
40.00	22.64	7.01	2.34	24.31	3.99
50.00	23.55	4.06	1.03	23.66	4.55
60.00	24.46	5.86	6.87	19.46	3.17
70.00	26.28	4.34	0.57	23.64	4.30
80.00	28.10	4.45	2.00	23.23	4.51
90.00	29.95	7.23	1.05	24.91	4.86
100.00	31.19	7.82	1.15	23.70	4.55
110.00	32.73	3.90	0.78	23.40	4.48
120.00	34.28	2.70	0.16	23.18	4.68
130.00	35.82	4.04	1.73	20.02	4.15
140.00	37.38	4.34	3.29	20.42	3.70
150.00	39.14	10.27	1.55	24.95	3.09
160.00	40.90	7.78	0.41	25.01	3.90
170.00	42.66	4.63	1.09	23.13	4.27
180.00	44.42	3.37	0.07	22.37	4.34
185.00	45.30	4.25	0.00	23.83	4.46
195.00	47.06	3.75	4.96	26.00	4.54
205.00	48.82	5.13	0.10	24.01	4.32
215.00	51.01	4.82	5.37	18.85	3.48
225.00	53.20	4.51	0.82	22.94	4.30
235.00	55.39	4.68	5.58	19.92	3.54
245.00	57.58	6.80	6.47	18.70	3.01
255.00	59.05	4.20	0.81	22.88	4.46
265.00	60.45	4.39	0.01	23.67	4.43
275.00	65.74	3.98	3.06	20.26	4.06
285.00	71.00	4.71	0.59	23.17	4.25
295.00	82.75	4.94	3.27	20.09	3.78
305.00	94.50	4.90	5.33	17.73	3.04
315.00	96.24	3.54	2.72	19.77	3.70
325.00	97.99	3.68	3.94	18.93	3.57
335.00	99.74	5.23	3.93	20.08	3.39
345.00	101.48	3.01	5.75	12.16	1.93
355.00	103.23	2.45	1.76	20.70	4.20
365.00	104.98	4.19	4.73	17.22	3.16
375.00	106.73	5.24	6.01	18.87	3.08
385.00	108.47	4.76	4.82	18.76	3.16
395.00	110.22	6.03	5.33	19.36	3.06
405.00	111.97	6.72	2.80	22.32	3.44
415.00	113.72	2.69	1.93	18.79	3.62
425.00	115.46	4.97	3.92	20.55	3.52
435.00	117.21	5.98	3.61	21.68	3.59
445.00	118.96	5.77	6.03	18.55	3.01
455.00	120.70	5.55	5.00	19.05	3.10
465.00	122.70	5.51	4.78	19.99	3.28
475.00	124.45	5.29	6.06	18.74	2.95
485.00	125.95	6.78	6.72	18.01	2.50
495.00	127.70	11.44	1.18	25.82	3.05
505.00	128.78	6.67	2.05	23.17	3.71
515.00	129.87	3.16	1.33	21.51	4.17
525.00	130.96	8.33	1.17	24.01	3.44
535.00	132.05	8.73	6.68	19.63	2.22
540.00	132.60	9.54	7.63	18.77	1.85
545.00	133.40	4.34	3.26	20.77	3.74
555.00	135.00	8.11	1.19	24.61	3.64
565.00	136.60	3.73	2.14	20.14	4.06
575.00	138.20	4.03	3.16	21.06	3.87
585.00	139.80	7.84	1.67	24.64	3.70
595.00	141.40	5.75	5.47	19.20	3.11
605.00	144.00	6.44	1.32	23.34	3.70
615.00	146.98	6.33	1.27	22.97	3.72
625.00	150.20	4.97	1.37	23.15	4.06
635.00	152.60	6.95	7.04	17.70	2.41
645.00	155.80	8.38	3.92	22.28	3.07
655.00	158.70	6.04	4.26	20.69	3.36
665.00	161.60	7.01	9.45	20.39	2.98

TABLE C.8:4 QUARTZ, DOLOMITE, TERRIGENOUS SILICA (Si.lith) AND IRON (FEt). CORE CD1739

DEPTH (CM)	AGE (KYS)	QUARTZ (%)	DOLOMITE (%)	Si(lith) (%)	FEt (%)
0.00	00.00	3.37	1.00	10.80	1.71
10.00	00.00	5.45	2.38	16.18	2.34
20.00	15.50	5.99	1.77	17.04	2.38
30.00	16.83	5.37	1.97	15.77	2.29
40.00	18.16	5.43	1.82	15.51	2.24
50.00	19.49	5.31	1.79	15.54	2.24
60.00	20.82	5.15	1.69	15.10	2.22
70.00	21.73	5.27	1.70	15.65	2.30
80.00	22.64	5.76	1.33	16.59	2.35
90.00	23.55	5.83	0.90	16.81	2.33
100.00	24.46	6.96	1.40	19.64	2.84
110.00	25.67	6.08	0.96	17.36	2.45
120.00	26.88	5.72	1.93	16.32	2.31
130.00	28.10	6.49	1.47	18.09	2.51
140.00	29.64	6.02	1.41	17.30	2.48
150.00	31.19	5.86	1.46	17.19	2.45
160.00	32.74	5.81	1.40	17.04	2.52
170.00	34.29	5.83	1.75	17.13	2.40
180.00	35.83	5.65	1.22	16.80	2.39
190.00	37.38	5.39	0.92	16.22	2.32
200.00	41.61	5.54	1.36	16.27	2.26
210.00	45.84	5.74	1.46	16.42	2.30
220.00	49.76	5.09	1.55	15.22	2.26
230.00	53.68	4.92	0.69	14.90	2.12
240.00	57.58	4.77	1.35	14.20	2.06
250.00	59.01	5.66	1.16	16.26	2.24
260.00	60.45	6.47	1.25	17.90	2.39
270.00	63.92	6.60	0.31	18.53	2.54
280.00	67.40	5.11	0.55	15.74	2.28
290.00	68.60	5.73	0.31	17.11	2.34
300.00	69.80	5.49	0.58	16.92	2.56
310.00	71.00	5.58	0.98	16.78	2.57
320.00	80.00	4.83	0.14	15.60	2.16
330.00	87.25	5.29	0.08	17.02	2.53
340.00	94.50	4.22	0.29	13.62	2.14
350.00	97.05	4.77	0.95	15.12	2.21
360.00	99.61	4.66	1.98	14.39	2.03
370.00	102.17	4.73	2.09	14.46	2.00
380.00	104.73	4.79	2.00	13.87	1.92
390.00	107.29	5.33	2.29	14.93	1.94
400.00	109.85	5.28	2.07	14.78	1.93
410.00	112.40	5.36	1.66	15.66	2.13
420.00	114.96	5.15	0.98	14.78	2.02
430.00	117.52	5.45	1.06	15.23	1.98
440.00	120.08	5.33	1.65	14.96	2.06
450.00	122.64	5.72	1.29	15.97	2.08
460.00	125.20	5.28	1.51	14.88	2.36
470.00	126.45	5.55	1.41	15.53	2.12
480.00	127.70	6.81	3.62	17.46	2.16
490.00	132.60	5.16	1.30	15.46	2.24
500.00	137.88	5.50	1.46	15.98	2.26
515.00	141.40	5.70	1.39	16.32	2.27
525.00	141.98	6.27	1.26	17.75	2.48
535.00	142.57	6.54	1.37	18.07	2.40
545.00	143.16	6.52	1.74	17.85	2.45
555.00	143.74	6.39	1.25	18.51	2.55
565.00	144.33	6.50	1.08	18.14	2.44
575.00	144.92	6.33	1.06	17.65	2.38
585.00	145.50	6.20	1.84	17.61	2.49
595.00	146.09	6.07	2.08	17.63	2.53
605.00	146.68	6.03	2.19	17.36	2.51
615.00	147.26	6.16	1.92	17.08	2.39
625.00	147.85	6.12	1.73	17.69	2.48
635.00	148.44	6.13	1.86	17.62	2.51
645.00	149.00	6.25	1.64	17.71	2.37
655.00	149.61	6.21	0.95	18.35	2.60
665.00	150.20	5.28	1.56	18.51	2.72
675.00	150.80	5.56	1.77	16.46	2.60
685.00	151.40	5.43	0.76	16.76	2.46
695.00	152.00	4.98	0.98	16.81	2.49
705.00	152.60	5.66	1.06	15.48	2.28
715.00	158.20	5.23	0.97	17.36	2.56
725.00	160.60	5.33	0.49	16.96	2.54
735.00	163.00	4.90	0.92	18.76	2.72
745.00	164.48	5.59	0.12	16.38	2.38
755.00	166.66	4.98	0.82	16.92	2.40
765.00	167.80	4.87	0.77	15.73	2.33

TABLE C.9:1 MAJOR ELEMENTS DATA OF TURBIDITES IN CORE CD1715

No	Depth (cm)	Si (%)	Al (%)	Fe (%)	Mg (%)	Ca (%)	K (%)	Ti (%)	Mn (%)	P (%)
1.	90.0	15.37	2.90	1.48	2.71	18.29	0.806	0.333	0.060	0.060
2.	130.0	15.68	2.47	0.94	1.94	19.93	0.755	0.192	0.030	0.050
3.	140.0	18.05	2.45	0.80	1.75	18.03	0.827	0.191	0.030	0.040
4.	643.0	15.81	2.93	1.40	2.68	18.21	0.796	0.322	0.020	0.050
5.	653.0	16.70	2.83	1.28	2.34	18.05	0.786	0.322	0.020	0.050
6.	668.0	15.75	3.12	1.53	2.58	17.94	0.897	0.222	0.030	0.040
7.	676.0	16.89	2.95	1.24	2.33	17.80	0.836	0.211	0.030	0.040
8.	687.0	14.44	3.86	2.79	2.90	16.67	1.21	0.319	0.051	0.061
9.	692.0	15.83	3.07	1.61	2.74	17.65	0.867	0.353	0.030	0.060
10.	700.0	16.21	2.67	1.25	2.20	18.70	0.766	0.272	0.030	0.060

TABLE C.9:2 MINOR ELEMENTS DATA OF TURBIDITES (in ppm) IN CORE CD1715

NO	DEPTH CM	Ni	Cr	V	Cu	Zn	Sr	Rb	Zr	Ba	Nb	Pb	Th
1.00	90.00	83.83	390.87	54.54	10.10	33.33	543.38	30.30	181.80	203.01	8.08	7.07	2.02
2.00	130.00	57.62	166.81	32.35	6.06	18.19	783.52	24.26	71.78	161.76	7.30	8.35	1.04
3.00	140.00	46.46	233.31	29.29	4.04	14.14	732.25	25.25	89.89	190.89	5.05	4.04	0.00
4.00	643.00	70.63	298.66	50.45	9.08	30.27	502.48	28.25	128.14	159.42	8.07	5.04	2.01
5.00	653.00	72.64	422.77	49.44	6.05	28.25	576.13	27.24	196.75	193.72	7.06	7.06	2.01
6.00	668.00	99.17	132.57	55.66	15.18	37.44	563.68	33.39	60.72	181.14	6.07	8.09	2.02
7.00	676.00	81.73	279.49	48.43	9.08	30.27	515.59	28.25	113.00	166.48	7.06	7.06	3.02
8.00	687.00	120.51	158.62	107.12	38.11	75.10	646.84	54.59	99.91	360.50	8.24	11.33	5.15
9.00	692.00	84.75	247.20	56.50	11.09	35.31	543.85	32.28	102.91	189.69	8.07	8.07	2.01
10.00	700.00	76.68	457.07	52.46	8.07	28.25	714.37	26.23	175.56	214.91	7.06	6.05	2.01

TABLE C.9:3 REEs DATA OF TURBIDITE IN CORE CD1715

No	DEPTH CM	La (ppm)	Ce (ppm)	Nd (ppm)	Y (ppm)
1.	90.0	10.10	41.41	19.19	17.17
2.	130.0	2.088	35.49	16.70	16.70
3.	140.0	0.00	13.14	8.08	12.13
4.	643.0	7.06	29.26	17.15	17.15
5.	653.0	11.09	27.24	12.10	17.15
6.	668.0	13.15	18.21	16.19	14.16
7.	676.0	14.12	23.20	11.09	16.14
8.	687.0	14.42	33.99	19.57	18.54
9.	692.0	15.13	36.32	14.42	17.15
10.	700.0	7.060	34.30	16.14	17.15

TABLE C.10:1 BIOGENIC ELEMENTS DATA (SALT FREE) OF CORE CD1715

DEPTH CM	AGE KYS	CALCITE (%)	Ex.Sr/Ca (x10 3)	C.Org (%)	Biog.Si (%)	Ex.Ba (ppm)
0.00	0.00	46.39	3.60	0.76	1.48	432.70
10.00	8.31	70.01	4.26	0.42	1.60	683.97
20.00	10.70	63.93	4.01	0.33	1.14	263.58
32.00	13.57	51.73	3.60	0.32	0.65	101.12
35.00	14.28	53.13	3.61	0.23	0.65	127.94
40.00	15.49	46.27	3.45	0.43	1.49	134.87
50.00	17.27	50.41	3.66	0.35	0.90	186.07
60.00	19.05	52.70	3.74	0.47	1.10	289.98
70.00	20.83	48.19	3.98	1.19	0.92	214.59
80.00	22.64	45.14	3.76	0.63	0.90	160.58
100.00	24.46	50.80	3.79	0.67	0.95	202.96
110.00	26.28	45.24	4.23	0.66	0.81	121.70
120.00	28.33	44.23	4.29	0.55	0.86	109.02
150.00	30.38	48.49	3.70	0.54	0.93	151.55
160.00	32.43	47.71	3.70	0.30	0.74	147.10
164.00	33.25	43.17	3.55	0.29	0.58	87.10
174.00	35.30	47.36	3.73	0.61	0.78	206.80
184.00	37.38	49.02	3.69	0.63	0.99	199.29
194.00	39.86	46.97	3.91	0.53	0.82	249.26
204.00	42.85	48.24	3.99	0.74	1.51	328.46
214.00	45.84	45.17	3.42	0.57	0.85	263.40
224.00	48.82	54.02	3.93	0.67	1.17	346.28
234.00	54.70	49.94	3.80	0.60	0.87	174.42
244.00	57.58	56.62	4.11	0.75	1.13	290.07
254.00	60.47	43.80	4.96	0.84	1.17	214.45
264.00	67.14	48.08	4.03	1.02	2.52	289.20
284.00	80.00	58.11	2.88	1.07	2.64	286.12
294.00	84.22	57.39	3.77	1.31	2.76	536.97
304.00	88.44	60.43	4.23	1.03	2.64	613.86
309.00	90.55	62.56	4.43	0.83	2.02	414.08
319.00	99.00	62.50	4.35	0.42	1.28	308.22
329.00	108.60	59.01	4.18	0.37	0.81	242.02
339.00	118.20	59.90	4.24	0.45	0.81	272.41
349.00	121.70	58.35	4.06	0.42	0.72	271.52
359.00	125.20	58.73	4.10	0.62	0.66	237.13
369.00	127.20	43.32	3.44	0.46	0.56	60.13
379.00	132.60	44.72	3.22	0.51	0.56	179.82
390.00	136.60	41.15	3.58	0.55	0.69	219.02
400.00	138.20	40.34	4.12	1.50	1.78	293.15
410.00	141.40	39.21	3.40	1.00	1.17	120.15
420.00	150.20	34.93	3.30	1.33	1.86	342.84
430.00	150.90	36.66	3.56	0.83	1.06	220.84
440.00	151.16	47.78	4.06	0.88	1.25	409.16
450.00	152.30	48.03	3.92	0.91	1.32	586.53
454.00	152.58	53.24	4.04	0.82	1.26	558.13
464.00	158.20	38.80	3.39	0.66	0.96	205.13
474.00	161.40	46.50	3.87	1.15	1.01	696.76
484.00	164.60	49.53	4.01	1.35	1.66	813.81
494.00	167.80	59.63	3.95	1.44	1.68	779.73
504.00	171.06	59.31	4.27	0.76	1.39	671.75
514.00	174.32	58.42	4.09	1.01	1.08	624.87
524.00	177.58	52.58	3.89	0.94	1.00	447.43
534.00	180.84	42.43	4.19	0.71	0.96	403.26
544.00	184.12	40.09	3.81	1.64	1.57	306.11
554.00	187.40	42.85	4.01	1.76	1.74	433.65
564.00	190.70	26.87	3.51	1.87	1.92	999.20
574.00	192.09	47.88	3.97	2.00	2.11	1010.39
584.00	205.00	63.90	3.93	1.11	1.80	702.63
594.00	206.61	54.46	3.78	0.82	0.41	35.04
598.00	207.41	54.67	3.85	0.98	0.78	441.99
608.00	209.03	50.66	4.00	1.09	0.86	293.56
618.00	210.50	46.62	4.17	0.31	0.32	195.62
628.00	216.00	47.45	3.92	0.95	0.80	340.15
636.00	223.38	44.49	4.04	1.58	1.36	274.21
648.00	228.00	44.72	4.16	1.62	1.22	194.66
663.00	230.90	53.36	3.69	0.69	0.65	152.93
682.00	232.00	44.39	3.30	0.51	0.30	59.39
706.00	233.70	34.62	3.10	0.51	0.92	104.84
712.00	239.10	46.76	3.80	1.01	1.64	333.77
722.00	244.00	46.28	3.51	0.61	0.61	209.95
733.00	245.50	47.63	3.48	0.48	0.50	247.03

TABLE C.10:2 BIOGENIC ELEMENTS DATA (SALT FREE) OF CORE CD1730

DEPTH CM	AGE KYS	CALCITE (%)	Ex.Sr/Ca (x10 3)	C.org (%)	Biog.Si (%)	Ex.Ba (ppm)
0.00	0.00	33.67	3.80	1.14	2.11	836.96
10.00	2.60	38.54	3.76	0.95	2.17	765.44
20.00	5.10	50.08	3.78	0.77	1.26	798.15
30.00	7.70	52.50	4.03	0.58	1.14	671.82
40.00	10.00	52.38	3.86	0.55	0.94	561.94
50.00	12.00	51.99	3.59	0.44	0.94	199.49
60.00	13.50	45.39	3.37	0.38	0.58	87.69
70.00	15.50	38.80	3.05	0.38	0.49	0.00
80.00	16.60	39.22	3.16	0.38	0.55	45.77
90.00	18.10	41.85	3.35	0.61	0.67	167.15
100.00	19.20	41.15	3.41	0.75	0.54	164.20
110.00	20.30	40.60	3.44	0.72	0.53	151.98
120.00	21.40	41.65	3.46	0.80	0.43	125.15
130.00	22.60	38.27	3.38	1.00	0.42	99.90
140.00	24.00	41.25	3.62	1.03	0.50	118.60
150.00	25.30	37.37	3.21	0.74	0.34	15.06
160.00	26.70	38.42	3.42	0.62	0.33	73.63
170.00	28.20	36.12	3.36	1.22	0.37	105.79
180.00	29.40	36.80	3.45	1.23	0.57	105.94
190.00	30.70	35.15	3.20	0.85	0.64	73.34
200.00	32.00	34.12	2.64	0.63	0.84	0.00
210.00	33.40	33.50	3.06	0.60	0.45	54.12
220.00	34.70	33.62	3.10	0.55	0.26	0.00
230.00	36.10	35.30	3.20	0.56	0.51	148.80
240.00	37.40	38.84	3.27	0.68	0.66	170.15
250.00	39.50	36.04	3.21	0.56	0.77	143.19
260.00	41.60	36.43	3.12	0.45	0.55	75.96
270.00	43.70	34.90	2.89	0.51	0.50	0.00
280.00	45.80	41.89	3.64	0.72	1.03	180.69
290.00	50.00	40.22	3.58	0.78	0.73	105.38
295.00	52.10	38.77	3.62	0.94	1.00	204.15
305.00	56.30	36.30	3.35	0.87	0.91	178.86
315.00	60.50	30.62	3.49	1.68	1.51	515.53
325.00	63.50	34.95	3.72	1.55	1.34	409.63
345.00	80.00	33.12	3.59	1.13	0.86	356.98
355.00	84.50	32.34	3.53	1.23	0.98	421.24
365.00	89.00	41.93	3.87	0.74	1.70	476.35
375.00	93.60	46.97	4.05	0.73	1.48	390.55
385.00	99.00	48.35	3.96	0.52	1.22	247.71
395.00	102.20	46.20	3.78	0.65	0.91	202.84
405.00	108.60	49.15	3.93	0.75	0.83	329.84
415.00	115.00	45.52	3.75	0.50	0.44	220.80
425.00	121.40	40.52	3.40	0.48	0.34	71.32
435.00	128.00	36.52	3.11	0.56	0.29	45.88
450.00	130.10	37.00	3.23	0.76	0.32	92.08
460.00	132.20	40.40	3.83	1.06	0.41	138.65
470.00	134.40	38.40	3.41	0.43	0.44	126.41
480.00	136.50	36.30	3.38	0.49	0.52	167.05
490.00	138.60	32.40	3.18	0.68	0.60	204.88
500.00	140.70	29.27	3.13	0.79	0.59	216.59
510.00	142.80	28.60	3.08	0.65	0.51	161.08
520.00	144.90	30.37	3.25	0.66	0.44	154.74
530.00	147.10	34.60	3.62	0.53	0.44	237.74
540.00	149.20	35.70	3.75	0.53	1.06	237.63
550.00	151.30	32.19	3.59	0.88	1.76	663.72
560.00	153.40	36.34	3.68	0.63	1.59	580.49
570.00	155.50	37.51	3.38	0.43	1.19	156.34
580.00	157.70	30.28	3.07	0.51	0.48	243.14
590.00	159.80	30.75	3.56	0.59	1.13	797.87
600.00	163.20	34.52	3.57	0.48	1.13	507.14
610.00	166.70	39.30	3.83	0.57	1.16	635.22
620.00	170.10	45.42	4.00	0.37	1.00	635.27
630.00	173.60	47.12	3.80	0.49	0.93	484.46
640.00	177.00	40.35	3.78	0.33	0.77	554.37
650.00	180.50	27.48	3.29	0.41	1.03	345.90
660.00	184.10	19.78	3.38	0.66	1.38	821.85
670.00	191.00	33.59	3.45	0.31	1.32	915.25
680.00	198.00	41.38	3.83	0.36	1.16	1008.55
690.00	205.00	49.06	3.78	0.42	1.59	671.12
700.00	209.43	44.82	3.59	0.43	0.43	18.32
710.00	214.60	45.35	3.61	0.41	0.39	16.92
720.00	219.40	44.53	3.51	0.38	0.48	81.85
730.00	224.10	44.74	3.79	0.73	0.02	314.73
740.00	228.90	45.12	3.79	0.90	0.54	268.78
750.00	233.70	35.10	3.61	0.89	0.31	177.86
760.00	238.50	43.81	3.54	1.18	0.62	321.40
770.00	243.30	43.81	3.18	0.89	0.64	215.60
780.00	248.10	39.76	3.88	0.38	0.58	126.25
790.00	252.80	41.97	3.34	0.48	0.46	113.90
800.00	257.60	41.42	3.34	0.36	0.43	113.42

TABLE C.10:3 BIOGENIC ELEMENTS DATA (SALT FREE) OF CORE CD1738

DEPTH CM	AGE KYRS	CALCITE (%)	Ex.Sr/Ca (x10 3)	C.org (%)	Ex.Ba (ppm)
00.00	00.00	8.58	1.02	0.84	0.00
10.00	00.00	7.98	0.56	0.78	0.00
20.00	15.40	6.57	1.15	1.03	0.00
30.00	20.80	10.51	0.27	0.47	130.13
40.00	22.64	8.74	2.07	0.67	0.00
50.00	23.55	9.45	0.59	0.87	0.00
60.00	24.46	18.26	4.58	0.85	32.01
70.00	26.28	10.78	0.85	0.41	0.00
80.00	28.10	10.35	1.51	0.48	0.00
90.00	29.95	10.89	0.89	0.38	0.00
100.00	31.19	11.26	1.23	0.35	0.00
110.00	32.73	11.26	0.75	0.37	0.00
120.00	34.28	11.52	0.78	0.29	0.00
130.00	35.82	14.28	2.20	0.44	0.00
140.00	37.38	18.76	2.94	0.46	23.19
150.00	39.14	15.77	2.76	0.18	0.00
160.00	40.90	12.71	0.68	0.28	0.00
170.00	42.66	12.51	1.67	0.36	0.00
180.00	44.42	15.46	4.60	0.37	0.00
185.00	45.30	12.00	1.61	0.27	0.00
195.00	47.06	11.00	0.93	0.38	0.00
205.00	48.82	12.61	0.88	0.26	0.00
215.00	51.01	22.72	3.18	0.49	133.41
225.00	53.20	13.73	5.31	0.35	0.00
235.00	55.39	20.35	4.19	0.36	16.13
245.00	57.58	26.06	3.27	0.22	9.44
255.00	59.05	13.84	1.54	0.31	0.00
265.00	60.45	12.78	0.83	0.23	0.00
275.00	65.74	20.25	2.84	0.23	0.00
285.00	71.00	14.77	2.23	0.25	0.00
295.00	82.75	21.96	2.86	0.27	0.00
305.00	94.50	27.85	4.01	0.49	0.00
315.00	96.24	20.21	2.87	0.33	0.00
325.00	97.99	23.27	4.12	0.35	0.00
335.00	99.74	22.10	3.42	0.34	0.00
345.00	101.48	23.89	0.33	0.58	0.00
355.00	103.23	18.40	2.87	0.39	0.00
365.00	104.98	24.61	3.86	0.38	4.14
375.00	106.73	23.45	3.29	0.38	0.00
385.00	108.47	25.16	3.43	0.27	0.00
395.00	110.22	24.03	3.16	0.27	0.00
405.00	111.97	17.72	6.40	0.48	0.00
415.00	113.72	25.06	3.05	0.34	0.00
425.00	115.46	19.96	4.49	0.32	0.00
435.00	117.21	17.68	6.72	0.21	0.00
445.00	118.96	25.81	3.07	0.41	0.00
455.00	120.70	24.45	2.83	0.29	0.00
465.00	122.70	21.74	2.50	0.79	0.00
475.00	124.45	23.39	3.37	0.46	0.00
485.00	125.95	27.41	3.40	0.15	0.00
495.00	127.70	15.11	1.61	0.32	0.00
505.00	128.78	15.11	1.93	0.47	0.00
515.00	129.87	15.82	3.92	0.37	0.00
525.00	130.96	16.68	3.33	0.23	0.00
535.00	132.05	26.44	3.29	0.20	16.55
540.00	132.60	30.47	3.70	0.44	27.77
545.00	133.40	17.89	2.36	0.27	0.00
555.00	135.00	13.66	1.24	0.56	0.00
565.00	136.60	15.67	2.19	0.52	0.00
575.00	138.20	17.05	2.07	0.23	0.00
585.00	139.80	13.12	1.71	0.41	0.00
595.00	141.40	22.71	2.91	0.33	0.00
605.00	144.00	16.43	5.13	0.28	0.00
615.00	146.98	15.64	4.26	0.35	0.00
625.00	150.20	13.81	1.63	0.50	0.00
635.00	152.60	28.15	3.97	0.42	0.00
645.00	155.80	18.41	2.51	0.53	0.00
655.00	158.70	19.84	2.68	0.57	0.00
665.00	161.60	19.76	1.77	0.43	0.00

TABLE C.10:4 BIOGENIC ELEMENTS DATA (SALT FREE) CORE CD1739

DEPTH CM	AGE KYRS	CALCITE (%)	Ex.Sr/Ca (x10 3)	C.org (%)	Ex.Ba (ppm)
00.00	00.00	56.84	3.08	0.57	9.12
10.00	00.00	39.05	3.85	0.31	0.00
20.00	15.50	36.93	3.68	0.41	0.00
30.00	16.83	39.94	3.63	0.51	0.00
40.00	18.16	40.73	3.80	0.66	26.02
50.00	19.49	40.70	3.48	0.64	16.22
60.00	20.82	41.91	3.39	1.19	0.00
70.00	21.73	40.28	3.76	0.57	1.01
80.00	22.64	38.57	3.80	0.41	0.00
90.00	23.55	38.57	3.83	0.36	0.00
100.00	24.66	45.44	3.35	0.55	0.00
110.00	25.67	39.97	3.48	0.50	0.00
120.00	26.88	38.54	3.69	0.54	0.00
130.00	28.10	34.07	3.35	0.44	0.00
140.00	29.64	35.81	3.42	0.44	0.00
150.00	31.19	36.57	3.15	0.33	0.00
160.00	32.74	36.97	3.35	0.31	0.00
170.00	34.29	36.41	3.35	0.39	0.00
180.00	35.83	37.76	3.30	0.50	7.85
190.00	37.38	39.73	3.21	0.42	0.00
200.00	41.61	38.10	3.19	0.86	26.52
210.00	45.84	38.02	3.23	0.60	33.97
220.00	49.76	41.05	3.30	0.75	111.58
230.00	53.68	44.47	3.49	0.69	22.54
240.00	57.58	45.96	3.52	0.69	62.17
250.00	59.01	40.49	3.59	0.56	14.36
260.00	60.45	35.62	3.62	0.45	0.00
270.00	63.92	37.72	3.59	0.47	0.00
280.00	67.40	39.71	3.63	0.61	16.02
290.00	68.60	38.87	3.20	0.41	0.00
300.00	69.80	37.11	3.22	0.64	25.10
310.00	71.00	37.94	3.23	0.68	0.00
320.00	80.00	43.03	3.23	0.55	29.58
330.00	87.25	38.91	3.06	0.39	0.34
340.00	94.50	48.81	3.13	0.68	119.62
350.00	97.05	43.78	3.39	0.50	9.76
360.00	99.61	44.88	3.57	0.58	0.00
370.00	102.17	44.24	3.72	0.68	0.00
380.00	104.73	42.11	3.24	0.89	17.96
390.00	107.29	41.00	3.39	0.86	18.67
400.00	109.85	42.51	3.44	1.04	14.92
410.00	112.40	38.31	3.47	1.36	50.64
420.00	114.96	42.46	3.38	1.21	39.41
430.00	117.52	41.97	3.39	0.95	39.54
440.00	120.08	42.54	3.45	0.67	29.46
450.00	122.64	41.05	3.51	0.64	0.00
460.00	125.20	42.67	3.37	0.48	11.24
470.00	126.45	41.76	3.44	0.44	0.00
480.00	127.70	36.00	3.69	0.37	0.00
490.00	132.60	41.92	3.54	0.44	0.58
505.00	137.88	36.60	4.13	0.43	0.00
515.00	141.40	39.45	3.61	0.52	0.00
525.00	141.98	35.63	3.58	0.28	0.00
535.00	142.57	34.64	3.37	0.28	0.00
545.00	143.16	35.32	3.29	0.25	0.00
555.00	143.74	33.59	3.25	0.26	0.00
565.00	144.33	34.57	3.18	0.41	0.00
575.00	144.92	36.02	3.01	0.40	0.00
585.00	145.50	34.47	3.06	0.53	0.00
595.00	146.09	33.58	3.05	0.57	4.79
605.00	146.68	33.66	3.13	0.72	0.00
615.00	147.26	35.60	3.02	0.58	0.00
625.00	147.25	33.63	3.12	0.70	0.00
635.00	148.44	32.58	3.12	0.74	0.00
645.00	149.00	34.50	3.24	0.74	0.00
655.00	149.61	32.11	3.15	0.63	0.00
665.00	150.20	30.00	3.07	0.72	51.94
675.00	150.80	35.05	3.12	0.93	68.81
685.00	151.40	38.16	3.32	0.48	14.50
695.00	152.00	37.43	3.25	0.43	58.34
705.00	152.60	41.49	3.19	0.20	81.13
715.00	158.20	36.07	3.32	0.30	6.47
725.00	160.60	37.08	3.18	0.36	30.47
735.00	163.00	32.88	3.15	0.24	0.00
745.00	164.48	39.35	3.13	0.40	34.34
755.00	166.66	37.49	3.27	0.41	0.00
765.00	167.80	39.40	3.22	0.43	51.41

TABLE C.11:1 EXCESS METAL CONTENTS OF CORE CD 1715

DEPTH CM	AGE KYS	Ni (ppm)	Cu (ppm)	Zn (ppm)
0.000	0.000	52.900	37.400	44.420
10.000	8.310	76.150	73.560	100.660
20.000	10.700	27.820	26.460	35.290
32.000	13.570	23.510	24.760	41.240
35.000	14.280	30.740	34.950	53.340
40.000	15.490	12.550	18.940	30.710
50.000	17.270	18.080	28.450	38.920
60.000	19.050	27.700	26.120	42.150
70.000	20.830	53.430	23.750	41.850
80.000	22.640	35.100	19.210	28.540
100.000	24.460	15.410	22.970	40.660
110.000	26.280	41.710	22.370	40.590
120.000	28.330	36.750	19.350	35.840
150.000	30.380	20.410	26.120	49.240
160.000	32.430	27.500	23.230	48.740
164.000	33.250	20.700	40.620	98.760
174.000	35.300	7.200	25.940	52.730
184.000	37.380	24.090	27.420	50.000
194.000	39.860	21.250	30.380	52.550
204.000	42.850	17.410	27.140	49.070
214.000	45.840	26.170	21.490	39.440
224.000	48.820	30.210	26.570	37.310
234.000	54.700	12.190	29.510	43.120
244.000	57.580	28.170	29.020	43.670
254.000	60.470	43.380	19.850	54.940
264.000	67.140	43.730	28.790	74.830
284.000	80.000	48.770	29.530	58.690
294.000	84.220	76.970	36.490	82.170
304.000	88.440	65.890	32.060	86.760
309.000	90.550	42.000	28.710	69.460
319.000	99.000	41.410	24.760	51.200
329.000	108.600	24.760	22.060	42.990
339.000	118.200	20.200	24.040	44.770
349.000	121.700	28.700	25.950	51.400
359.000	125.200	112.860	24.590	48.320
369.000	127.200	1.100	24.170	37.870
379.000	132.600	6.350	27.520	42.850
390.000	136.600	5.500	35.040	61.070
400.000	138.200	63.760	30.530	48.530
410.000	141.400	36.740	12.850	17.730
420.000	150.200	50.820	44.680	87.430
430.000	150.900	16.680	39.400	66.590
440.000	151.160	40.400	50.660	115.380
450.000	152.300	54.700	48.900	116.360
454.000	152.580	101.610	52.410	113.870
464.000	158.200	33.380	45.480	62.180
474.000	161.400	49.350	47.130	116.090
484.000	164.600	131.030	58.350	143.780
494.000	167.800	83.860	48.630	119.900
504.000	171.060	82.920	42.710	63.690
514.000	174.320	32.160	49.220	76.730
524.000	177.580	22.910	52.210	64.400
534.000	180.840	53.400	39.300	63.610
544.000	184.120	56.700	31.080	40.480
554.000	187.400	82.350	47.280	71.000
564.000	190.700	57.270	73.420	104.820
574.000	192.090	48.260	68.350	92.500
584.000	205.000	58.360	85.020	56.000
594.000	206.610	11.940	30.940	30.370
598.000	207.410	11.840	19.580	27.170
608.000	209.030	21.810	24.920	46.090
618.000	210.500	71.880	23.780	39.440
628.000	216.000	22.550	26.100	49.360
636.000	223.380	28.590	22.870	36.560
648.000	228.000	20.440	20.740	35.830
663.000	230.900	3.400	19.610	32.260
682.000	232.000	9.680	16.430	24.160
706.000	233.700	26.510	23.590	40.800
712.000	239.100	28.250	30.250	55.300
722.000	244.000	23.070	32.020	50.310
733.000	245.500	18.440	33.280	52.000

TABLE C.11:2 EXCESS METAL CONTENTS OF CORE CD 1730

DEPTH CM	AGE KYS	Ni (ppm)	Cu (ppm)	Zn (ppm)
0.000	0.000	122.070	94.860	207.210
10.000	2.600	80.390	64.380	93.080
20.000	5.100	42.770	66.160	106.760
30.000	7.700	41.930	31.070	57.880
40.000	10.000	28.620	38.340	44.540
50.000	12.000	14.690	21.390	35.140
60.000	13.500	10.690	18.160	32.570
70.000	15.500	0.000	13.980	19.890
80.000	16.600	0.000	18.170	26.370
90.000	18.100	14.290	13.660	34.360
100.000	19.200	26.460	18.070	45.540
110.000	20.300	10.290	15.820	40.800
120.000	21.400	15.370	16.170	39.840
130.000	22.600	24.750	16.590	48.250
140.000	24.000	31.770	20.270	45.960
150.000	25.300	4.020	15.470	30.420
160.000	26.700	9.030	18.970	43.960
170.000	28.200	22.260	23.160	54.420
180.000	29.400	36.110	20.250	51.900
190.000	30.700	22.930	16.840	46.850
200.000	32.000	10.280	4.050	20.720
210.000	33.400	0.230	19.030	33.850
220.000	34.700	0.000	17.970	30.530
230.000	36.100	21.870	21.260	42.490
240.000	37.400	4.590	20.800	46.330
250.000	39.500	3.960	22.640	36.330
260.000	41.600	3.170	19.640	36.700
270.000	43.700	0.000	13.650	20.730
280.000	45.800	22.060	32.980	45.840
290.000	50.000	0.000	21.280	39.580
295.000	52.100	19.060	50.180	111.800
305.000	56.300	15.740	20.630	47.960
315.000	60.500	58.130	38.040	79.210
325.000	63.500	63.390	31.440	74.040
335.000	71.000	5.150	16.940	35.620
345.000	80.000	28.980	28.760	67.970
355.000	84.500	39.330	30.220	65.200
365.000	89.000	23.090	25.580	59.750
375.000	93.600	36.870	22.580	48.900
385.000	99.000	14.440	17.040	36.400
395.000	102.200	7.120	12.650	35.540
405.000	108.600	16.630	23.000	50.630
415.000	115.000	8.840	19.250	37.840
425.000	121.400	6.170	17.180	33.660
435.000	128.000	2.920	15.740	30.980
450.000	130.100	2.880	15.930	32.770
460.000	132.200	17.200	22.060	46.900
470.000	134.400	5.820	20.450	38.100
480.000	136.500	3.690	24.810	47.000
490.000	138.600	19.810	31.380	61.440
500.000	140.700	44.020	36.150	68.400
510.000	142.800	42.510	34.420	65.120
520.000	144.900	18.390	40.450	69.940
530.000	147.100	26.590	37.370	65.930
540.000	149.200	28.940	43.810	108.980
550.000	151.300	64.900	49.720	115.190
560.000	153.400	48.140	51.090	100.680
570.000	155.500	7.250	34.760	56.270
580.000	157.700	0.670	29.080	60.610
590.000	159.800	101.400	85.280	156.790
600.000	163.200	63.760	50.420	89.730
610.000	166.700	83.070	46.030	89.910
620.000	170.100	46.910	43.370	74.750
630.000	173.600	21.390	46.670	74.400
640.000	177.000	34.490	54.160	89.380
650.000	180.500	20.830	50.600	86.680
660.000	184.100	190.190	162.640	275.140
670.000	191.000	38.550	56.110	83.580
680.000	198.000	95.210	64.240	89.640
690.000	205.000	32.330	62.070	83.400
700.000	209.430	0.000	22.930	37.700
710.000	214.600	3.870	16.380	27.300
720.000	219.400	2.190	18.140	30.240
730.000	224.100	27.510	26.120	44.890
740.000	228.900	26.810	22.070	36.000
750.000	233.700	7.610	10.400	29.920
760.000	238.500	32.570	24.460	48.260
770.000	243.300	22.790	19.380	45.370
780.000	248.100	4.390	15.360	35.340
790.000	252.800	0.000	15.730	31.400
800.000	257.600	3.040	14.870	31.940

TABLE C.12:1 CARBON AND NITROGEN ISOTOPE DATA OF CORE CD1730

DEPTH	AGE	T.N (%)	at.N (%)	$\delta^{15}N$	Nm* (%)	Nt** (%)	$\delta^{13}C$
00.00	0.00	0.15	0.37	15.81	0.26	-0.11	-19.71
10.00	2.60	0.15	0.37	12.64	0.20	-0.05	-21.61
20.00	5.10	0.09	0.37	13.90	0.13	-0.04	-18.90
30.00	7.70	0.09	0.37	11.44	0.11	-0.02	-19.62
40.00	10.00	0.07	0.37	14.50	0.11	-0.04	-20.36
50.00	12.00	0.08	0.37	13.32	0.11	-0.03	-20.32
60.00	13.50	0.07	0.37	12.99	0.10	-0.03	-20.94
70.00	15.50	0.06	0.37	11.96	0.07	-0.01	-21.13
80.00	16.60	0.07	0.37	13.68	0.10	-0.03	-20.78
90.00	18.10	0.11	0.37	11.36	0.13	-0.02	-19.61
100.00	19.20	0.11	0.37	11.06	0.12	-0.01	-19.27
110.00	20.30	0.10	0.37	11.00	0.11	-0.01	n.a
120.00	21.40	0.13	0.37	8.11	0.10	0.03	n.a
130.00	22.60	0.15	0.37	10.40	0.16	-0.01	n.a
140.00	24.00	0.15	0.37	14.03	0.23	-0.08	n.a
150.00	25.30	0.08	0.37	13.95	0.12	-0.04	n.a
160.00	26.70	0.10	0.37	16.71	0.18	-0.08	n.a
170.00	28.20	0.17	0.37	12.64	0.23	-0.06	n.a
180.00	29.40	0.17	0.37	12.31	0.22	-0.05	n.a
190.00	30.70	0.11	0.37	10.70	0.12	-0.01	n.a
200.00	32.00	0.08	0.37	10.76	0.09	-0.01	n.a
210.00	33.40	0.09	0.37	11.36	0.11	-0.02	n.a
220.00	34.70	0.09	0.37	10.48	0.10	-0.01	n.a
230.00	36.10	0.09	0.37	8.33	0.07	0.02	n.a
240.00	37.40	0.10	0.37	7.34	0.07	0.03	n.a
250.00	39.50	0.09	0.37	7.10	0.06	0.03	n.a
260.00	41.60	0.08	0.37	8.38	0.06	0.02	n.a
270.00	43.70	0.08	0.37	7.75	0.06	0.02	n.a
280.00	45.80	0.12	0.37	7.04	0.08	0.04	n.a
290.00	50.00	0.10	0.37	10.21	0.10	0.00	n.a
295.00	52.10	0.12	0.37	8.52	0.10	0.02	-19.40
305.00	56.30	0.12	0.37	9.91	0.12	0.00	-19.88
315.00	60.50	0.22	0.37	10.35	0.23	-0.01	-19.21
325.00	63.50	0.17	0.37	9.04	0.15	0.02	-19.31
335.00	71.00	0.09	0.37	5.79	0.04	0.05	-19.30
345.00	80.00	0.21	0.37	10.57	0.22	-0.01	-19.23
355.00	84.50	0.23	0.37	9.96	0.23	0.00	-19.23
365.00	89.00	0.14	0.37	10.59	0.15	-0.01	-19.92
375.00	93.60	0.11	0.37	9.77	0.11	0.00	-20.63
385.00	99.00	0.08	0.37	13.87	0.12	-0.04	-20.34
395.00	102.20	0.08	0.37	8.68	0.07	0.01	-19.80
405.00	108.60	0.10	0.37	14.47	0.16	-0.06	-20.06
415.00	115.00	0.07	0.37	12.56	0.09	-0.02	-20.64
425.00	121.40	0.07	0.37	10.92	0.08	-0.01	-20.65
435.00	128.00	0.07	0.37	12.83	0.09	-0.02	n.a
450.00	130.10	0.07	0.37	12.01	0.09	-0.02	n.a
460.00	132.20	0.09	0.37	12.29	0.12	-0.03	n.a
470.00	134.40	0.08	0.37	9.58	0.08	0.00	n.a
480.00	136.50	0.09	0.37	6.47	0.05	0.04	m.a
490.00	138.60	0.11	0.37	7.81	0.08	0.03	n.a
500.00	140.70	0.17	0.37	7.84	0.12	0.05	n.a
510.00	142.80	0.17	0.37	10.51	0.18	-0.01	n.a
520.00	144.90	0.13	0.37	9.80	0.13	0.00	n.a
530.00	147.10	0.10	0.37	9.50	0.09	0.01	n.a
540.00	149.20	0.14	0.37	10.02	0.14	0.00	n.a
550.00	151.30	0.13	0.37	9.77	0.13	0.00	n.a
560.00	153.40	0.12	0.37	11.36	0.14	-0.02	n.a
570.00	155.50	0.09	0.37	14.96	0.15	-0.06	n.a
580.00	157.70	0.09	0.37	10.76	0.10	-0.01	n.a
590.00	159.80	0.13	0.37	13.08	0.18	-0.05	n.a
600.00	163.20	0.11	0.37	12.23	0.14	-0.03	n.a
610.00	166.70	0.12	0.37	12.48	0.16	-0.04	n.a
620.00	170.10	0.11	0.37	10.54	0.12	-0.01	n.a
630.00	173.60	0.08	0.37	9.28	0.07	0.01	n.a
640.00	177.00	0.09	0.37	8.79	0.08	0.01	n.a
650.00	180.50	0.10	0.37	8.49	0.08	0.02	n.a
660.00	184.10	0.14	0.37	12.31	0.18	-0.04	n.a
670.00	191.00	0.09	0.37	9.96	0.09	0.00	n.a
680.00	198.00	0.09	0.37	6.77	0.05	0.04	n.a
690.00	205.00	0.07	0.37	7.02	0.04	0.03	n.a
700.00	209.80	0.05	0.37	5.02	0.02	0.03	n.a
710.00	214.60	0.06	0.37	7.32	0.04	0.02	n.a
720.00	219.40	0.07	0.37	8.03	0.05	0.02	n.a
730.00	224.10	0.17	0.37	9.75	0.16	0.01	n.a
740.00	228.90	0.18	0.37	9.36	0.17	0.01	n.a
750.00	233.70	0.13	0.37	8.63	0.11	0.02	n.a
760.00	238.50	0.21	0.37	9.36	0.19	0.02	n.a
770.00	243.30	0.12	0.37	8.74	0.10	0.02	n.a
780.00	248.10	0.08	0.37	8.19	0.06	0.02	n.a
790.00	252.80	0.06	0.37	8.27	0.05	0.01	n.a
800.00	257.60	0.06	0.37	8.90	0.05	0.01	n.a

TABLE C.13:1 HALOGENS (SALT FREE) AND THEIR RATIOS TO CARBON ORGANIC DATA OF CORE CD1709

DEPTH CM	C.org (%)	I (ppm)	Br (ppm)	I/C.org ($x10^{-4}$)	Br/C.org ($x10^{-4}$)	I/Br	S (%)
0.00	0.71	54.72	45.04	76.64	63.08	1.21	0.348
10.00	1.05	120.69	82.26	114.94	78.34	1.47	0.290
20.00	1.16	60.58	63.78	52.14	54.89	0.95	0.380
30.00	0.97	26.09	30.98	26.92	31.97	0.84	0.437
40.00	1.20	39.43	40.46	32.77	33.63	0.97	0.360
50.00	1.22	27.68	48.49	22.65	39.68	0.57	0.498
60.00	1.17	22.35	53.02	19.06	45.20	0.42	0.531
70.00	0.98	23.93	49.64	24.44	50.70	0.48	0.510
80.00	1.07	25.10	41.97	23.43	39.19	0.60	0.509
90.00	1.45	27.72	52.83	19.14	36.48	0.52	0.555
100.00	1.51	30.08	30.83	19.87	20.36	0.98	0.588
110.00	1.31	28.37	53.28	21.57	40.52	0.53	0.516
120.00	1.71	35.09	47.94	20.53	28.05	0.73	0.601
130.00	1.28	24.85	34.47	19.33	26.82	0.72	0.547
140.00	1.26	35.15	50.50	27.81	39.95	0.70	0.573
150.00	1.60	31.81	61.49	19.87	38.41	0.52	0.587
160.00	1.50	30.20	41.20	20.14	27.48	0.73	0.573
170.00	1.23	21.02	58.53	17.03	47.43	0.36	0.566
180.00	1.27	27.46	60.29	21.54	47.29	0.46	0.544
190.00	1.25	25.83	59.54	20.60	47.48	0.43	0.552
200.00	1.58	31.56	64.69	19.96	40.92	0.49	0.558
210.00	1.77	31.27	66.15	17.62	37.29	0.47	0.624
220.00	1.49	26.00	63.20	17.46	42.44	0.41	0.612
230.00	1.94	25.61	76.47	13.22	39.46	0.33	0.615
240.00	1.70	30.89	78.16	18.14	45.90	0.40	0.707
250.00	1.94	30.72	71.00	15.85	36.64	0.43	0.685
260.00	1.87	29.23	59.98	15.67	32.14	0.49	0.643
270.00	1.60	23.04	54.35	14.39	33.95	0.42	0.553
280.00	1.04	16.63	36.96	15.99	35.54	0.45	0.473
290.00	0.88	19.52	39.21	22.23	44.66	0.50	0.455
300.00	0.96	16.62	40.21	17.33	41.93	0.41	0.444
310.00	1.07	19.64	51.80	18.35	48.41	0.38	0.420
320.00	1.98	16.79	49.75	8.48	25.14	0.34	0.503
330.00	1.28	23.37	45.07	18.23	35.16	0.52	0.496
340.00	1.19	20.27	47.12	17.02	39.56	0.43	0.470
350.00	1.18	17.80	48.39	15.07	40.97	0.37	0.506
360.00	0.98	24.47	49.30	25.00	50.36	0.50	0.504
370.00	1.01	24.10	52.17	23.86	51.65	0.46	0.535
380.00	0.99	24.82	55.87	25.10	56.49	0.44	0.553
390.00	1.46	28.07	78.10	19.26	53.57	0.36	0.636
400.00	1.45	29.45	76.73	20.33	52.99	0.38	0.643
410.00	1.98	32.45	98.39	16.40	49.74	0.33	0.767
420.00	1.14	36.01	75.99	31.53	66.54	0.47	0.781
430.00	0.87	26.72	62.83	30.82	72.47	0.43	0.628
440.00	0.69	21.16	43.25	30.85	63.05	0.49	0.548
450.00	0.63	17.56	48.08	28.05	76.81	0.37	0.544
460.00	0.77	19.33	40.72	25.21	53.09	0.47	0.524

TABLE C.13:2 HALOGENS (SALT FREE) AND THEIR RATIOS TO CARBON ORGANIC DATA OF CORE CD1715

DEPTH (CM)	AGE KYS	C.org (%)	I (ppm)	Br (ppm)	I/C.org ($x10^{-4}$)	Br/C.org ($x10^{-4}$)	I/Br	S (%)
00.00	0.00	0.76	61.50	25.07	80	33	2.45	0.190
10.00	8.303	0.42	42.56	32.41	101	77	1.31	0.075
20.00	10.70	0.328	26.31	16.47	80	50	1.59	0.067
32.00	13.57	0.318	27.56	09.92	86	30	2.77	0.047
35.00	14.28	0.226	32.74	10.92	144	50	2.99	0.060
40.00	15.49	0.43	27.11	02.86	63	6.65	9.48	0.039
50.00	17.27	0.348	47.66	11.06	136	31	4.30	0.050
60.00	19.05	0.473	77.34	32.02	163	67	2.41	0.069
70.00	20.83	1.186	89.11	46.70	75	39	1.90	0.208
80.00	22.64	0.627	63.76	39.30	101	62	1.60	0.224
100.00	24.45	0.674	87.31	31.78	129	47	2.74	0.124
110.00	26.28	0.657	71.70	53.79	109	81	1.33	0.308
120.00	28.33	0.822	72.28	46.21	138	88	1.56	0.284
150.00	30.38	0.535	59.40	05.68	111	10	10.45	0.164
160.00	33.243	0.299	55.20	05.95	184	19	09.27	0.130
164.00	33.25	0.288	41.97	14.58	145	50	02.87	0.119
174.00	35.30	0.608	59.77	32.23	98	53	01.85	0.113
184.00	37.38	0.629	48.64	21.00	77	33	02.31	0.082
194.00	39.85	0.527	70.00	15.95	134	30	04.38	0.096
204.00	42.85	0.743	61.04	36.05	82	48	01.69	0.158
214.00	45.84	0.567	54.10	14.54	95	25	03.72	0.173
224.00	48.82	0.670	61.23	20.56	91	30	02.97	0.164
234.00	54.70	0.595	49.01	21.07	82	35	02.32	0.145
244.00	57.58	0.748	77.41	58.46	103	78	01.32	0.156
254.00	60.47	0.839	79.15	11.64	94	13	06.79	0.188
264.00	67.14	1.025	77.46	35.29	75	34	02.19	0.165
284.00	80.00	1.071	46.67	21.15	43	19	02.20	0.214
294.00	84.22	1.31	86.25	62.54	65	47	01.38	0.240
304.00	88.44	1.03	82.25	66.75	79	64	01.23	0.241
309.00	90.55	0.828	71.24	56.35	86	68	01.26	0.181
319.00	99.00	0.423	47.56	16.64	112	39	02.85	0.091
329.00	108.6	0.371	41.46	04.35	111	11	09.53	0.120
339.00	118.2	0.453	49.96	14.89	110	32	03.35	0.094
349.00	121.7	0.423	35.57	02.53	84	5	14.06	0.088
359.00	125.2	0.618	52.56	14.76	85	23	03.56	0.091
369.00	127.2	0.461	26.70	01.25	56	2	21.36	0.096
379.00	132.6	0.513	30.77	05.48	59	10	05.61	0.085
390.00	136.6	0.554	47.70	17.13	86	31	02.78	0.089
400.00	138.2	1.53	77.93	75.80	51	50	01.02	0.327
410.00	141.4	1.00	30.82	22.81	30	22	01.35	0.340
420.00	150.2	1.33	65.00	36.61	48	27	01.77	0.200
430.00	150.9	0.832	47.80	15.73	57	19	03.03	0.156
440.00	151.16	0.876	55.82	38.60	63	44	01.44	0.191
450.00	152.3	0.912	66.27	44.03	72	48	01.50	0.220
454.00	152.58	0.824	62.72	40.74	76	49	01.49	0.122
464.00	158.2	0.657	19.63	15.78	29	24	01.24	0.131
474.00	161.4	1.189	59.85	30.88	50	26	01.93	0.129
484.00	164.6	1.345	81.81	47.45	60	35	01.72	0.130
494.00	167.8	1.455	79.00	41.59	54	28.58	1.90	0.149
504.00	171.06	0.783	42.67	19.83	54	25	02.15	0.093
514.00	174.32	1.011	49.03	12.25	48	12	04.00	0.119
524.00	177.58	0.969	43.42	09.19	44	9	04.72	0.122
534.00	180.84	1.715	68.23	71.25	39	41	00.95	0.366
544.00	184.12	1.636	61.31	57.82	37	35	01.06	0.385
554.00	187.4	1.76	63.63	71.01	36	40	00.89	0.357
564.00	190.7	1.870	57.05	34.96	30	18	01.63	0.202
574.00	192.09	2.06	41.76	38.52	20	18	01.03	0.147
584.00	205.0	1.108	12.12	29.56	10	26	00.41	0.090
594.00	206.61	0.82	10.58	1.92	12	2.34	5.51	0.069
598.00	207.41	0.98	10.10	08.38	10	8	01.20	0.063
608.00	209.03	1.088	61.85	78.51	56	76	00.78	0.100
618.00	210.5	0.308	56.02	65.69	181	213	00.85	0.313
628.00	216.0	0.955	59.04	94.80	61	99	00.62	0.205
636.00	223.38	1.58	54.56	65.40	34	41	00.83	0.341
648.00	228.00	1.62	51.45	69.14	31	42.67	00.74	0.262
663.00	230.90	0.694	36.95	15.22	53	21.93	02.42	0.119
682.00	232.00	0.508	11.74	9.89	23	19.46	01.18	0.070
706.00	233.7	0.58	24.47	15.80	42.18	27.20	01.54	0.221
712.00	239.1	1.009	49.70	39.18	49	38	01.26	0.140
722.00	244.0	0.611	28.17	09.66	46	15.81	02.91	0.133
733.00	245.5	0.48	28.57	21.69	59	45	01.31	0.117

TABLE C.13:3 HALOGENS (SALT FREE) AND THEIR RATIOS TO CARBON ORGANIC DATA OF CORE CD1730

DEPTH (CM)	AGE KYS	C.org (%)	I (ppm)	Br (ppm)	I/N x10 4	I/C x10 4	Br/C (%)	I/Br	S
0.00	0.00	1.14	204.47	96.20	136.31	179.00	84.00	2.12	0.093
10.00	2.60	0.95	167.72	76.36	111.81	176.00	80.00	2.19	0.083
20.00	5.10	0.77	87.80	46.24	97.56	114.00	60.00	1.89	0.072
30.00	7.70	0.58	55.86	34.65	62.07	96.00	59.00	1.61	0.062
40.00	10.00	0.55	55.77	24.66	79.67	101.00	44.00	2.26	0.062
50.00	12.00	0.44	52.34	25.01	65.43	118.00	56.00	2.09	0.058
60.00	13.50	0.38	43.36	12.41	61.94	114.00	32.00	3.49	0.049
70.00	15.50	0.38	34.93	24.00	58.22	91.00	63.00	1.45	0.018
80.00	16.60	0.38	43.03	29.25	61.47	113.00	76.00	1.47	0.027
90.00	18.10	0.61	77.45	42.18	70.41	127.00	69.00	1.83	0.079
100.00	19.20	0.75	81.79	50.58	74.35	109.00	61.00	1.61	0.164
110.00	20.30	0.72	81.82	52.55	81.82	113.00	72.00	1.55	0.132
120.00	21.40	0.80	81.55	60.23	62.73	101.00	75.00	1.35	0.176
130.00	22.60	1.00	74.82	72.81	49.88	74.00	72.00	1.02	0.227
140.00	24.00	1.02	74.31	77.89	49.54	72.00	76.00	0.95	0.213
150.00	25.30	0.74	53.75	32.99	67.19	72.00	44.00	1.62	0.062
160.00	26.70	0.62	64.01	48.95	64.01	103.00	78.00	1.30	0.156
170.00	28.20	1.22	97.35	94.73	57.26	79.00	77.00	1.02	0.204
180.00	29.40	1.23	97.16	91.38	57.15	79.00	74.00	1.06	0.275
190.00	30.70	0.85	70.10	56.03	63.73	82.00	65.00	1.25	0.185
200.00	32.00	0.63	51.81	30.80	64.76	82.00	48.00	1.68	0.072
210.00	33.40	0.60	62.39	28.58	69.32	103.00	47.00	2.18	0.104
220.00	34.70	0.56	78.91	46.66	87.68	140.00	83.00	1.69	0.103
230.00	36.10	0.56	74.44	39.64	82.71	132.00	70.00	1.87	0.154
240.00	37.40	0.68	81.05	39.67	81.05	119.00	58.00	2.04	0.131
250.00	39.50	0.56	73.52	30.86	81.69	131.00	55.00	2.38	0.093
260.00	41.60	0.45	58.14	21.73	72.68	129.00	48.00	2.67	0.114
270.00	43.70	0.51	41.40	23.78	51.75	81.00	46.00	1.78	0.112
280.00	45.80	0.72	97.25	48.90	81.04	135.00	68.00	1.98	0.236
290.00	50.00	0.78	84.54	47.72	84.54	108.00	61.00	1.77	0.157
295.00	52.10	0.94	111.33	62.04	92.77	118.00	66.00	1.79	0.226
305.00	56.30	0.87	109.47	66.64	91.22	125.00	76.00	1.88	0.284
315.00	60.50	1.68	191.63	168.90	87.10	114.00	100.00	1.13	0.683
325.00	63.50	1.55	146.05	127.20	85.91	94.00	82.00	1.14	0.595
345.00	80.00	0.58	55.67	27.57	26.51	96.00	47.00	2.01	0.387
355.00	84.50	1.13	121.43	94.91	52.80	107.00	83.00	1.28	0.396
365.00	89.00	1.23	152.62	120.80	109.01	124.00	98.00	1.26	0.249
375.00	93.60	0.74	122.49	53.25	111.35	65.00	72.00	2.30	0.227
385.00	99.00	0.73	86.16	49.89	107.70	118.00	68.00	1.72	0.165
395.00	102.20	0.52	61.96	21.49	77.45	119.00	41.00	2.88	0.214
405.00	108.60	0.65	64.44	29.75	64.44	99.00	45.00	2.16	0.167
415.00	115.00	0.75	76.24	18.98	108.92	101.00	25.30	4.01	0.134
425.00	121.40	0.50	54.00	15.26	77.14	108.00	30.00	3.53	0.117
435.00	128.00	0.48	29.96	13.15	42.80	62.00	27.00	2.27	0.088
450.00	130.10	0.56	19.62	15.96	28.03	35.00	28.00	1.22	0.119
460.00	132.20	0.76	38.49	14.82	42.77	50.00	19.00	2.59	0.119
470.00	134.40	1.06	47.73	19.43	59.66	45.00	18.00	2.45	0.097
480.00	136.50	0.43	46.08	19.00	51.20	107.00	44.00	2.42	0.147
490.00	138.60	0.49	51.77	29.79	47.06	105.00	60.00	1.73	0.174
500.00	140.70	0.68	58.39	14.33	34.35	85.00	21.00	4.07	0.279
510.00	142.80	0.79	62.42	93.83	36.72	79.00	118.00	0.66	0.397
520.00	144.90	0.65	71.24	90.08	54.80	109.00	138.00	0.79	0.257
530.00	147.10	0.66	69.53	41.06	69.53	105.00	62.00	1.69	0.240
540.00	149.20	0.53	75.12	49.37	53.66	141.00	93.00	1.52	0.211
550.00	151.30	0.77	91.91	65.60	70.70	119.00	85.00	1.40	0.306
560.00	153.40	0.88	109.06	99.22	90.88	123.00	112.00	1.09	0.198
570.00	155.50	0.63	95.27	55.52	105.86	151.00	88.00	1.71	0.116
580.00	157.70	0.43	42.81	12.05	47.57	99.00	28.02	3.55	0.151
590.00	159.80	0.51	42.45	18.21	32.65	83.00	35.00	2.30	0.247
600.00	163.20	0.59	107.60	68.87	97.82	182.00	116.00	1.56	0.138
610.00	166.70	0.48	96.37	39.32	80.31	200.00	82.00	2.45	0.263
620.00	170.10	0.57	100.14	62.91	91.04	175.00	110.00	1.59	0.205
630.00	173.60	0.37	74.80	37.54	93.50	202.00	101.00	1.99	0.111
640.00	177.00	0.49	54.67	19.73	60.74	111.00	44.00	2.77	0.154
650.00	180.50	0.33	73.07	22.53	73.07	221.00	68.00	3.24	0.140
660.00	184.10	0.41	54.86	26.34	39.19	133.00	64.00	2.08	0.264
670.00	191.00	0.66	106.17	59.80	117.97	160.00	90.00	1.77	0.127
680.00	198.00	0.31	55.30	32.95	61.44	178.00	106.00	1.67	0.188
690.00	205.00	0.35	66.86	57.95	95.51	191.00	165.00	1.15	0.090
700.00	209.80	0.42	37.44	39.41	74.88	89.00	93.00	0.95	0.062
710.00	214.60	0.43	21.43	18.86	35.72	49.00	43.00	1.13	0.088
720.00	219.40	0.41	34.78	13.98	49.69	84.00	34.00	2.48	0.064
730.00	224.10	0.38	36.78	5.63	21.64	96.00	14.00	6.53	0.301
740.00	228.90	0.73	76.64	95.24	42.58	104.00	130.00	0.80	0.445
750.00	233.70	0.90	59.25	89.21	45.58	65.00	99.00	0.66	0.287
760.00	238.50	0.89	59.70	51.16	28.43	67.00	57.00	1.16	0.420
770.00	243.30	1.18	63.16	110.20	52.63	53.00	93.00	0.57	0.354
780.00	248.10	0.89	59.40	62.47	74.25	66.00	70.00	0.95	0.240
790.00	252.80	0.38	53.98	34.12	89.97	142.00	90.00	1.58	0.175
800.00	257.60	0.48	41.76	18.73	69.60	87.00	40.00	2.22	0.129

TABLE C.13:4 HALOGENS (SALT FREE) AND THEIR RATIOS TO CARBON ORGANIC DATA OF CORE CD1738

DEPTH CM	AGE KYRS	C.org (%)	I (ppm)	Br (ppm)	I/O.C ($x10^{-4}$)	Br/O.C $x(10^{-4})$	I/Br	S (%)
0.00	0.00	0.84	167.85	114.01	198.87	135.08	1.47	0.0525
10.00	10.00	0.78	133.41	77.41	170.61	99.00	1.72	0.0519
20.00	15.40	1.03	227.67	129.98	221.04	126.19	1.75	0.1152
30.00	20.80	0.47	40.57	34.63	85.59	73.07	1.17	0.0533
40.00	22.64	0.67	122.98	66.87	182.74	99.37	1.84	0.1194
50.00	23.55	0.87	87.63	55.50	101.07	64.01	1.58	0.0494
60.00	24.46	0.85	143.66	108.04	168.23	126.50	1.33	0.2670
70.00	26.28	0.41	65.38	43.49	160.25	106.59	1.50	0.0814
80.00	28.10	0.48	123.55	53.18	257.93	111.03	2.32	0.0824
90.00	29.95	0.38	67.09	28.56	178.42	75.97	2.35	0.0640
100.00	31.19	0.35	60.51	33.02	171.41	93.53	1.83	0.0567
110.00	32.73	0.37	64.55	35.00	176.37	95.62	1.84	0.0586
120.00	34.28	0.29	43.90	30.84	154.03	108.21	1.42	0.0464
130.00	35.82	0.44	96.88	61.94	221.19	141.42	1.56	0.1034
140.00	37.38	0.46	98.26	57.84	214.08	126.02	1.70	0.1264
150.00	39.14	0.18	27.37	10.72	151.23	59.20	2.55	0.1177
160.00	40.90	0.28	137.27	8.01	486.77	28.39	17.15	0.0317
170.00	42.66	0.36	96.76	44.15	271.03	123.68	2.19	0.0834
180.00	44.42	0.37	36.26	16.23	98.79	44.23	2.23	0.0564
185.00	45.30	0.27	14.06	19.34	51.13	70.33	0.73	0.0331
195.00	47.06	0.38	63.77	24.06	169.16	63.83	2.65	0.0493
205.00	48.82	0.26	37.57	13.73	142.30	52.02	2.74	0.0275
215.00	51.01	0.49	97.85	36.70	200.11	75.06	2.67	0.1304
225.00	53.20	0.35	35.88	14.27	101.92	40.53	2.51	0.0337
235.00	55.39	0.36	32.78	14.78	91.82	41.40	2.22	0.0694
245.00	57.58	0.22	30.33	6.52	136.64	29.38	4.65	0.1337
255.00	59.05	0.31	52.59	19.10	172.42	62.61	2.75	0.0255
265.00	60.45	0.23	21.29	10.31	91.36	44.23	2.07	0.0156
275.00	65.74	0.23	51.20	14.53	218.80	62.10	3.52	0.0364
285.00	71.00	0.25	29.29	2.20	114.86	8.62	13.33	0.0254
295.00	82.75	0.27	50.35	19.17	184.43	70.22	2.63	0.0386
305.00	94.50	0.49	51.76	30.68	106.50	63.14	1.69	0.0876
315.00	96.24	0.33	40.90	57.57	122.44	172.35	0.71	0.0436
325.00	97.99	0.35	60.35	29.06	174.43	83.99	2.08	0.1014
335.00	99.74	0.34	54.95	14.15	163.53	42.10	3.88	0.1214
345.00	101.48	0.58	63.13	49.23	108.66	84.73	1.28	0.2724
355.00	103.23	0.39	49.13	20.28	126.95	52.41	2.42	0.0884
365.00	104.98	0.38	62.72	29.29	166.37	77.71	2.14	0.1424
375.00	106.73	0.38	48.84	23.17	129.54	61.47	2.11	0.0824
385.00	108.47	0.27	37.31	16.88	136.17	61.59	2.21	0.0936
395.00	110.22	0.27	37.49	13.77	137.31	50.44	2.72	0.1496
405.00	111.97	0.48	16.89	15.82	35.48	33.23	1.07	0.1536
415.00	113.72	0.34	25.26	14.57	75.18	43.36	1.73	0.1084
425.00	115.46	0.32	27.40	12.79	84.81	39.61	2.14	0.1057
435.00	117.21	0.21	20.02	13.27	94.44	62.60	1.51	0.1516
445.00	118.96	0.41	28.14	14.63	69.31	36.03	1.92	0.1630
455.00	120.70	0.29	30.73	21.21	104.54	72.15	1.45	0.1656
465.00	122.70	0.79	34.33	19.85	43.40	25.09	1.73	0.1416
475.00	124.45	0.46	48.40	41.32	105.69	90.22	1.17	0.2245
485.00	125.95	0.15	36.13	36.39	237.73	239.40	0.99	0.3046
495.00	127.70	0.32	13.92	7.83	43.10	24.25	1.78	0.0907
505.00	128.78	0.47	22.70	21.30	47.89	44.93	1.07	0.1197
515.00	129.87	0.37	26.90	28.46	72.11	76.31	0.94	0.1327
525.00	130.96	0.23	23.04	8.68	99.32	37.40	2.66	0.1257
535.00	132.05	0.20	14.56	10.96	72.05	54.27	1.33	0.2720
540.00	132.60	0.44	9.84	40.25	22.57	92.31	0.24	0.3196
545.00	133.40	0.27	40.01	36.05	146.00	131.55	1.11	0.1725
555.00	135.00	0.56	12.97	15.28	23.33	27.48	0.85	0.0726
565.00	136.60	0.52	30.82	25.81	59.62	49.93	1.19	0.1395
575.00	138.20	0.23	40.49	35.24	173.03	150.62	1.15	0.1515
585.00	139.80	0.41	7.93	11.79	19.16	28.48	0.67	0.0807
595.00	141.40	0.33	53.82	56.75	165.11	174.08	0.95	0.3014
605.00	144.00	0.28	18.39	12.67	64.98	44.78	1.45	0.0756
615.00	146.98	0.35	17.38	15.36	49.08	43.39	1.13	0.0726
625.00	150.20	0.50	22.00	20.78	44.36	41.90	1.06	0.0796
635.00	152.60	0.42	42.99	50.54	103.10	121.19	0.85	0.3485
645.00	155.80	0.53	39.09	30.48	73.90	57.61	1.28	0.1725
655.00	158.70	0.57	54.52	48.23	95.48	84.46	1.13	0.1634
665.00	161.60	0.43	82.73	114.80	191.95	266.36	0.72	0.9162

TABLE C.13:5 HALOGENS (SALT FREE) AND THEIR RATIOS TO CARBON ORGANIC DATA OF CORE CD1739

DEPTH CM	AGE KYS	C.org (%)	I (ppm)	Br (ppm)	I/O.C ($\times 10^{-4}$)	Br/O.C ($\times 10^{-4}$)	I/Br	S (%)
0.00	0.00	0.57	105.74	42.68	186.17	75.14	2.48	0.079
10.00	10.00	0.31	33.25	14.02	109.01	45.96	2.37	0.046
20.00	15.50	0.41	49.90	21.99	122.61	54.03	2.27	0.052
30.00	16.83	0.51	77.15	44.39	151.26	87.04	1.74	0.086
40.00	18.16	0.66	77.71	44.88	117.21	67.69	1.73	0.137
50.00	19.49	0.64	74.13	45.40	115.29	70.61	1.63	0.148
60.00	20.82	1.19	70.04	54.16	59.00	45.63	1.29	0.226
70.00	21.73	0.57	73.28	52.67	128.11	92.08	1.39	0.213
80.00	22.64	0.41	61.99	40.04	151.94	98.13	1.55	0.159
90.00	23.55	0.36	68.16	37.35	190.92	104.62	1.82	0.136
100.00	24.66	0.55	90.42	63.16	163.80	114.43	1.43	0.275
110.00	25.67	0.50	68.77	61.04	137.28	122.08	1.12	0.202
120.00	26.88	0.54	50.18	36.78	92.93	68.11	1.36	0.192
130.00	28.10	0.44	57.60	30.01	131.82	68.68	1.92	0.134
140.00	29.64	0.44	70.12	41.48	160.10	94.69	1.69	0.179
150.00	31.19	0.33	58.84	29.96	180.48	91.90	1.96	0.145
160.00	32.74	0.31	65.00	33.39	206.34	106.01	1.95	0.120
170.00	34.29	0.39	56.42	25.58	145.78	66.10	2.21	0.101
180.00	35.83	0.50	66.44	38.92	132.87	77.85	1.71	0.134
190.00	37.38	0.42	82.59	50.87	197.11	121.42	1.62	0.181
200.00	41.61	0.86	96.97	71.81	113.01	83.70	1.35	0.287
210.00	45.84	0.60	103.72	63.80	172.30	105.98	1.63	0.269
220.00	49.76	0.75	116.26	65.67	155.63	87.91	1.77	0.312
230.00	53.68	0.69	74.72	37.10	107.67	53.46	2.01	0.156
240.00	57.58	0.69	77.14	38.21	110.99	54.98	2.02	0.176
250.00	59.01	0.56	52.94	21.92	94.54	39.14	2.42	0.103
260.00	60.45	0.45	16.89	11.50	37.87	25.79	1.47	0.087
270.00	63.92	0.47	35.42	47.68	75.04	101.01	0.74	0.107
280.00	67.40	0.61	60.24	31.26	98.60	51.17	1.93	0.196
290.00	68.60	0.41	54.96	3.01	135.05	7.38	18.29	0.083
300.00	69.80	0.64	99.66	53.60	155.00	83.35	1.86	0.273
310.00	71.00	0.68	86.29	45.15	126.53	66.20	1.91	0.154
320.00	80.00	0.55	64.20	27.13	116.73	49.33	2.37	0.090
330.00	87.25	0.39	43.60	31.67	112.95	82.04	1.38	0.065
340.00	94.50	0.68	82.40	25.58	120.83	37.51	3.22	0.087
350.00	97.05	0.50	56.18	25.68	112.81	51.57	2.19	0.074
360.00	99.61	0.58	36.69	28.76	63.15	49.50	1.28	0.095
370.00	102.17	0.68	34.57	32.10	50.55	46.94	1.08	0.136
380.00	104.73	0.89	44.42	49.39	49.97	55.56	0.90	0.225
390.00	107.29	0.86	48.27	77.53	56.19	90.25	0.62	0.390
400.00	109.85	1.04	54.13	65.15	51.94	62.53	0.83	0.369
410.00	112.40	1.36	56.52	88.53	41.53	65.05	0.64	0.448
420.00	114.96	1.21	76.70	78.41	63.60	65.02	0.98	0.466
430.00	117.52	0.95	64.14	67.59	67.44	71.07	0.95	0.390
440.00	120.08	0.67	49.18	56.44	73.07	83.86	0.87	0.370
450.00	122.64	0.64	43.78	44.50	68.20	69.31	0.98	0.425
460.00	125.20	0.48	41.70	22.80	87.24	47.70	1.83	0.173
470.00	126.45	0.44	44.02	20.65	100.51	47.15	2.13	0.202
480.00	127.70	0.37	26.75	11.18	71.34	29.82	2.39	0.169
490.00	132.60	0.44	40.96	20.65	93.52	47.13	1.98	0.209
505.00	137.88	0.43	42.30	13.63	98.84	31.85	3.10	0.151
515.00	141.40	0.52	30.67	12.82	59.20	24.75	2.39	0.134
525.00	141.98	0.28	18.33	6.47	64.53	22.79	2.83	0.089
535.00	142.57	0.28	20.26	6.27	71.33	22.07	3.23	0.091
545.00	143.16	0.25	20.87	8.55	82.47	33.80	2.44	0.112
555.00	143.74	0.26	24.35	4.68	92.60	17.78	5.21	0.068
565.00	144.33	0.41	35.00	11.06	86.21	27.25	3.16	0.125
575.00	144.92	0.40	45.41	22.68	112.12	56.00	2.00	0.190
585.00	145.50	0.53	55.14	24.24	104.23	45.82	2.27	0.287
595.00	146.09	0.57	52.80	29.44	92.64	51.65	1.79	0.244
605.00	146.68	0.72	58.75	45.74	81.25	63.27	1.28	0.355
615.00	147.26	0.58	53.52	28.03	92.27	48.32	1.91	0.273
625.00	147.25	0.70	38.83	29.35	55.40	41.88	1.32	0.226
635.00	148.44	0.74	55.44	56.58	74.62	76.16	0.98	0.368
645.00	149.00	0.74	37.24	23.81	50.26	32.13	1.56	0.170
655.00	149.61	0.63	66.22	41.78	104.94	66.21	1.59	0.227
665.00	150.20	0.72	106.59	84.87	147.63	117.56	1.26	0.438
675.00	150.80	0.93	105.33	80.05	113.25	86.08	1.32	0.443
685.00	151.40	0.48	50.04	25.09	104.91	52.60	1.99	0.193
695.00	152.00	0.43	44.70	21.57	104.92	50.62	2.07	0.200
705.00	152.60	0.20	47.74	17.12	235.19	84.32	2.79	0.228
715.00	158.20	0.30	24.19	5.12	79.57	16.85	4.72	0.084
725.00	160.60	0.36	45.40	19.96	127.52	56.06	2.27	0.149
735.00	163.00	0.24	29.29	17.63	120.55	72.55	1.66	0.067
745.00	164.48	0.40	56.44	28.84	142.17	72.64	1.96	0.174
755.00	166.66	0.41	28.51	25.16	70.23	61.97	1.13	0.106
765.00	167.80	0.43	72.04	70.54	167.93	164.43	1.02	0.269

TABLE C.14:1 SEDIMENTATION RATES AND ACCUMULATION RATES OF CORE CD1715

DEPTH CM	AGE KYRS	W.C (%)	DBD*	S.Rates cm^2/kys	A.Rates g-cm^2/kys
0.00	0.00	42.01	0.93	1.19	1.10
10.00	8.31	46.89	0.83	1.19	0.96
20.00	10.57	43.90	0.88	4.31	3.79
32.00	13.57	42.21	0.93	4.18	3.88
35.00	14.28	44.10	0.88	4.22	3.71
40.00	15.49	42.33	0.92	4.54	4.17
50.00	17.25	42.04	0.93	4.87	4.52
60.00	19.05	44.67	0.87	5.61	4.88
70.00	20.83	50.64	0.73	5.61	4.09
80.00	22.64	45.28	0.85	5.52	4.69
100.00	24.45	51.32	0.72	5.49	3.95
110.00	26.28	54.08	0.66	5.49	3.62
120.00	28.33	54.95	0.64	4.87	3.11
150.00	30.38	44.58	0.87	4.87	4.23
160.00	32.43	47.65	0.80	4.87	3.89
164.00	33.25	45.95	0.84	4.87	4.09
174.00	35.30	46.65	0.82	4.87	3.99
184.00	37.38	47.50	0.80	4.80	3.84
194.00	39.85	47.62	0.80	5.00	4.00
204.00	42.85	47.73	0.80	3.34	2.67
214.00	45.84	47.52	0.80	3.34	2.67
224.00	48.82	46.82	0.82	2.96	2.42
234.00	54.70	42.61	0.92	2.57	2.36
244.00	57.58	41.56	0.94	2.57	2.41
254.00	60.47	50.34	0.74	2.05	1.51
264.00	67.14	49.77	0.75	1.53	1.14
284.00	80.00	45.36	0.85	1.55	1.31
294.00	84.22	51.87	0.71	2.37	1.68
304.00	88.44	52.96	0.68	2.37	1.61
309.00	90.55	52.73	0.69	2.36	1.62
319.00	99.00	48.00	0.80	1.77	1.36
329.00	108.60	47.10	0.81	0.88	0.72
339.00	118.20	45.50	0.80	0.88	0.71
349.00	121.70	48.23	0.78	2.42	1.88
359.00	125.20	46.09	0.83	2.42	2.00
369.00	127.20	41.56	0.94	3.05	2.86
379.00	132.60	42.51	0.92	3.05	2.80
390.00	136.60	42.23	0.92	3.05	2.80
400.00	138.20	50.59	0.73	3.05	2.22
410.00	141.40	34.46	1.13	3.05	3.44
420.00	150.20	46.75	0.82	2.72	2.23
430.00	150.90	44.14	0.88	2.72	2.39
440.00	151.16	46.87	0.81	2.72	2.20
450.00	152.30	50.80	0.73	2.72	1.98
454.00	152.58	46.45	0.82	2.72	2.23
464.00	158.20	44.28	0.88	2.72	2.39
474.00	161.40	48.79	0.77	2.65	2.04
484.00	164.60	49.55	0.75	2.65	1.98
494.00	167.80	49.02	0.77	2.60	2.00
504.00	171.06	46.21	0.83	2.69	2.15
514.00	174.32	46.67	0.82	2.60	2.13
524.00	177.58	46.14	0.83	2.60	2.15
534.00	180.84	50.50	0.73	2.60	1.89
544.00	184.12	44.65	0.87	2.60	2.26
554.00	187.40	49.29	0.76	1.95	1.48
564.00	190.70	52.05	0.70	1.44	1.00
574.00	192.09	44.27	0.88	1.44	1.26
584.00	205.00	44.10	0.88	2.03	1.78
594.00	206.61	41.10	0.95	3.47	3.29
598.00	207.41	37.88	1.04	3.40	3.53
608.00	209.10	42.87	0.91	3.40	3.09
618.00	210.50	45.96	0.84	3.40	2.85
628.00	216.00	42.81	0.91	2.10	1.91
636.00	223.38	42.25	0.92	2.10	1.93
648.00	228.00	45.93	0.84	2.37	1.99
663.00	230.90	40.74	0.96	2.37	2.27
682.00	232.00	37.40	1.05	4.48	4.70
706.00	233.70	39.57	0.99	4.48	4.43
712.00	239.10	42.81	0.91	4.48	4.07
722.00	244.00	42.54	0.92	4.48	4.12
733.00	245.50	44.29	0.88	4.48	3.94

*DBD = DRY BULK DENSITY

TABLE C.14:2 SEDIMENTATION RATES AND ACCUMULATION RATES OF CORE CD1730

DEPTH CM	AGE KYS	W.C (%)	DBD*	S.Rates cm^2/kys	A.Rates g-cm^2/kys
00.00	0.00	49.93	0.75	3.89	2.92
10.00	2.60	47.74	0.80	3.89	3.11
20.00	5.10	45.69	0.84	3.89	3.27
30.00	7.70	43.53	0.89	3.89	3.46
40.00	10.00	41.90	0.93	5.00	4.65
50.00	12.00	36.82	1.07	5.78	6.18
60.00	13.50	36.42	1.08	6.56	7.08
70.00	15.50	42.24	0.93	6.56	6.10
80.00	16.60	42.68	0.91	6.56	5.97
90.00	18.10	42.88	0.91	7.89	7.18
100.00	19.20	46.48	0.82	9.21	7.55
110.00	20.30	46.46	0.82	9.21	7.55
120.00	21.40	46.62	0.82	9.21	7.55
130.00	22.60	44.99	0.86	7.14	6.14
140.00	24.00	39.98	0.98	7.25	7.10
150.00	25.30	43.71	0.89	7.46	6.64
160.00	26.70	44.91	0.86	7.46	6.42
170.00	28.20	47.13	0.81	7.46	6.04
180.00	29.40	46.57	0.82	7.46	6.12
190.00	30.70	44.62	0.87	7.46	6.49
200.00	32.00	39.44	1.00	7.46	7.46
210.00	33.40	42.31	0.92	7.46	6.86
220.00	34.70	45.01	0.86	7.46	6.42
230.00	36.10	44.81	0.86	7.46	6.42
240.00	37.40	44.68	0.87	6.11	5.32
250.00	39.50	44.90	0.86	4.76	4.09
260.00	41.60	43.87	0.89	4.76	4.24
270.00	43.70	42.86	0.91	4.76	4.33
280.00	45.80	44.66	0.87	3.57	3.11
290.00	50.00	44.18	0.88	2.32	2.04
295.00	52.10	45.94	0.84	2.38	2.00
305.00	56.30	46.86	0.82	2.38	1.95
315.00	60.50	52.53	0.69	2.86	1.97
325.00	63.50	46.45	0.82	3.33	2.73
355.00	80.00	49.59	0.75	2.00	1.50
365.00	84.50	49.79	0.75	2.21	1.66
375.00	89.00	46.32	2.21	0.83	1.83
385.00	93.60	46.42	2.21	0.83	1.83
395.00	99.00	43.62	1.89	0.89	1.68
405.00	102.20	40.61	0.97	1.56	1.51
415.00	108.60	44.56	0.87	1.56	1.36
425.00	115.00	40.29	0.98	1.56	1.53
435.00	121.40	37.21	1.06	1.56	1.65
450.00	128.00	36.26	1.08	3.14	3.39
460.00	130.10	39.92	0.98	4.72	4.63
470.00	132.20	41.46	0.95	4.72	4.48
480.00	134.40	40.15	0.98	4.72	4.63
490.00	136.50	36.63	1.07	4.72	5.05
500.00	138.60	43.21	0.90	4.72	4.25
510.00	140.70	45.34	0.85	4.72	4.01
520.00	142.80	55.52	0.83	4.72	3.92
510.00	144.90	46.38	0.83	4.72	3.92
530.00	147.10	47.31	0.81	4.72	3.82
540.00	149.20	48.69	0.77	4.72	3.63
550.00	151.30	50.44	0.74	4.72	3.49
560.00	153.40	50.14	0.74	4.72	3.49
570.00	155.50	41.85	0.94	4.72	4.44
580.00	157.70	41.80	0.94	4.72	4.44
590.00	159.80	46.67	0.82	3.81	3.12
600.00	163.20	45.48	0.85	2.90	2.46
610.00	166.70	47.89	0.79	2.90	2.29
620.00	170.10	48.03	0.79	2.90	2.29
630.00	173.60	47.37	0.80	2.90	2.32
640.00	177.00	46.51	0.82	2.90	2.38
650.00	180.50	47.27	0.81	2.90	2.35
660.00	184.10	51.48	0.71	1.65	1.17
670.00	191.00	49.67	0.75	1.44	1.08
680.00	198.00	47.59	0.80	1.44	1.15
690.00	205.00	45.40	0.85	1.70	1.44
700.00	209.43	39.01	1.01	2.09	2.11
710.00	214.60	37.19	1.06	2.09	2.22
720.00	219.40	36.96	1.06	2.09	2.22
730.00	224.10	44.14	0.88	2.09	1.84
740.00	228.90	45.36	0.85	2.09	1.78
750.00	233.70	41.08	0.95	2.09	1.99
760.00	238.50	46.24	0.83	2.09	1.73
770.00	243.30	43.27	0.90	2.09	1.88
780.00	248.10	41.41	0.95	2.09	1.99
790.00	252.80	39.72	0.99	2.09	2.07
800.00	257.60	38.04	1.03	2.09	2.15

*DBD = DRY BULK DENSITY

TABLE C.14:3 SEDIMENTATION AND ACCUMULATION RATES OF CORE CD1738

DEPTH CM	AGE KYS	W.C (%)	DBD*	S.Rates cm^2/kys	A.Rates g-cm^2/kys
20.00	15.40	51.15	0.72	10.98	7.90
30.00	20.80	32.34	1.20	10.98	13.17
40.00	22.64	39.79	0.99	10.98	10.87
50.00	23.55	38.87	1.01	10.98	11.08
60.00	24.46	46.86	0.82	10.98	9.00
70.00	26.28	36.45	1.08	5.49	5.92
80.00	28.10	40.66	0.97	5.49	5.32
90.00	29.95	36.18	1.09	6.47	7.05
100.00	31.19	32.38	1.20	6.47	7.76
110.00	32.73	34.99	1.12	6.47	7.24
120.00	34.28	37.40	1.05	6.47	6.79
130.00	35.82	39.86	0.99	6.47	6.40
140.00	37.38	41.56	0.94	5.68	5.34
150.00	39.14	28.68	1.31	5.68	7.44
160.00	40.90	27.38	1.36	5.68	7.72
170.00	42.66	40.24	0.98	5.68	5.56
180.00	44.42	35.04	1.12	5.68	6.36
185.00	45.30	35.25	1.11	5.68	6.30
195.00	47.06	38.15	1.03	5.68	5.85
205.00	48.82	33.10	1.18	5.68	6.70
215.00	51.01	41.48	0.94	4.56	4.28
225.00	53.20	34.15	1.14	4.56	5.19
235.00	55.39	37.06	1.06	4.56	4.83
245.00	57.58	31.70	1.22	4.56	5.56
255.00	59.05	33.88	1.15	7.01	8.06
265.00	60.45	29.55	1.29	7.01	9.04
275.00	65.74	35.70	1.10	1.89	2.07
285.00	71.00	34.94	1.12	1.89	2.11
295.00	82.75	25.94	1.41	0.85	1.19
305.00	94.50	29.25	1.30	0.85	1.10
315.00	96.24	27.84	1.34	5.72	7.66
325.00	97.99	36.52	1.08	5.72	6.17
335.00	99.74	34.85	1.12	5.72	6.40
345.00	101.48	39.55	0.99	5.72	5.66
355.00	103.23	36.71	1.07	5.72	6.12
365.00	104.98	39.36	1.00	5.72	5.72
375.00	106.73	35.19	1.11	5.72	6.35
385.00	108.47	30.21	1.26	5.72	7.20
395.00	110.22	29.53	1.29	5.72	7.37
405.00	111.97	28.69	1.31	5.72	7.49
415.00	113.72	35.50	1.11	5.72	6.35
425.00	115.46	28.04	1.34	5.72	7.66
435.00	117.21	27.86	1.34	5.72	7.66
445.00	118.96	30.00	1.27	5.72	7.26
455.00	120.70	29.06	1.30	5.72	7.43
465.00	122.70	29.86	1.28	5.72	7.32
475.00	124.45	33.61	1.16	5.72	6.63
485.00	125.95	29.72	1.28	5.72	7.32
495.00	127.70	23.13	1.51	7.42	11.20
505.00	128.78	27.40	1.36	9.18	12.48
515.00	129.87	27.79	1.34	9.18	12.30
525.00	130.96	28.34	1.33	9.18	12.21
535.00	132.05	24.92	1.44	9.18	13.22
540.00	132.60	30.27	1.26	6.25	7.87
545.00	133.40	33.33	1.17	6.25	7.31
555.00	135.00	25.62	1.42	6.25	8.87
565.00	136.60	33.06	1.18	6.25	7.37
575.00	138.20	34.44	1.14	6.25	7.12
585.00	139.80	24.40	1.46	6.25	9.12
595.00	141.40	36.86	1.07	6.25	6.68
605.00	144.00	26.19	1.40	3.40	4.76
615.00	146.98	26.70	1.38	3.40	4.69
625.00	150.20	28.23	1.33	3.40	4.52
635.00	152.60	35.15	1.12	3.40	3.80
645.00	155.80	33.92	1.15	3.40	3.91
655.00	158.70	36.20	1.09	3.40	3.70
665.00	161.60	44.13	1.57	3.40	5.33

*DBD = DRY BULK DENSITY

TABLE C.14:4 SEDIMENTATION AND ACCUMULATION RATES OF CORE CD1739

DEPTH CM	AGE KYS	W.C (%)	DBD*	S.Rates cm^2/kys	A.Rates g-cm^2/kys
20.00	15.50	36.15	1.09	7.51	8.18
30.00	16.83	38.78	1.01	7.51	7.58
40.00	18.16	38.93	1.01	7.51	7.58
50.00	19.49	39.76	0.99	7.51	7.43
60.00	20.82	41.18	0.95	9.24	8.77
70.00	21.73	40.65	0.97	10.90	10.63
80.00	22.64	38.36	1.03	10.98	11.30
90.00	23.55	39.83	0.99	10.98	10.87
100.00	24.46	41.50	0.94	9.50	8.93
110.00	25.67	64.86	0.46	8.24	3.79
120.00	26.88	37.75	1.04	8.24	8.56
130.00	28.10	34.01	1.15	6.64	7.63
140.00	29.64	36.59	1.07	6.64	7.10
150.00	31.19	37.74	1.04	6.64	6.90
160.00	32.74	37.25	1.06	6.64	7.03
170.00	34.29	35.53	1.10	6.64	7.30
180.00	35.83	38.41	1.02	6.64	6.77
190.00	37.38	39.18	1.00	2.36	2.36
200.00	41.61	40.16	0.98	2.36	2.31
210.00	45.84	40.31	0.97	2.40	2.32
220.00	49.76	41.69	0.94	2.55	2.39
230.00	53.68	38.53	1.02	2.55	2.60
240.00	57.58	40.62	0.97	4.75	4.60
250.00	59.01	34.41	1.14	6.96	7.94
260.00	60.45	31.23	1.23	6.96	8.57
270.00	63.92	60.00	0.55	2.87	1.57
280.00	67.40	35.98	1.09	2.87	3.12
290.00	68.60	34.23	1.14	8.33	9.49
300.00	69.80	37.64	1.05	8.33	8.74
310.00	71.00	36.69	1.07	8.33	8.91
320.00	80.00	36.25	1.08	1.38	1.48
330.00	87.25	32.67	1.19	1.38	1.64
340.00	94.50	35.34	1.11	1.38	1.53
350.00	97.05	35.29	1.11	3.90	4.32
360.00	99.61	36.83	1.07	3.90	4.17
370.00	102.17	39.47	1.00	3.90	3.90
380.00	104.73	39.47	1.00	3.90	3.90
390.00	107.29	40.21	0.98	3.90	3.82
400.00	109.85	39.81	0.99	3.90	3.86
410.00	112.40	41.76	0.94	3.90	3.66
420.00	114.96	39.86	0.99	3.90	3.86
430.00	117.52	39.20	1.00	3.90	3.90
440.00	120.08	37.91	1.04	3.90	4.05
450.00	122.64	36.99	1.06	3.90	4.13
460.00	125.20	34.96	1.12	8.00	8.96
470.00	126.45	35.82	1.10	8.00	9.85
480.00	127.70	32.55	1.19	8.00	9.52
490.00	132.60	35.78	1.10	8.00	8.80
500.00	137.88	37.67	1.04	2.84	2.95
515.00	141.40	33.16	1.17	2.84	3.32
525.00	141.98	30.90	1.24	2.84	3.52
535.00	142.57	30.61	1.25	17.04	21.30
545.00	143.16	29.85	1.28	17.04	21.81
555.00	143.74	28.61	1.32	17.04	22.49
565.00	144.33	30.57	1.25	17.04	21.30
575.00	144.92	32.31	1.20	17.04	20.44
585.00	145.50	34.26	1.14	17.04	19.42
595.00	146.09	34.35	1.14	17.04	19.42
605.00	146.68	35.62	1.10	17.04	18.74
615.00	147.26	34.67	1.13	17.04	19.25
625.00	147.85	33.33	1.17	17.04	19.93
635.00	148.44	34.96	1.12	17.04	19.08
645.00	149.00	32.29	1.20	17.04	20.44
655.00	149.61	34.34	1.14	17.04	19.42
665.00	150.20	37.14	1.06	17.04	18.06
675.00	150.80	39.38	1.00	16.66	16.66
685.00	151.40	33.58	1.16	16.66	19.32
695.00	152.00	32.98	1.18	16.66	19.65
705.00	152.60	35.09	1.12	16.66	18.65
715.00	158.20	30.20	1.27	16.66	21.15
725.00	160.60	35.02	1.12	16.66	18.65
735.00	163.00	29.61	1.28	4.16	5.32
745.00	164.48	36.32	1.08	4.16	4.49
755.00	166.66	34.10	1.15	4.16	4.78
765.00	167.80	39.43	1.00	4.16	4.16

DBD* = DRY BULK DENSITY

TABLE C.15:1 LITHOGENIC FLUXES DATA (in mg-cm^2/kyrs) OF CORE CD1715

DEPTH CM	AGE KYS	ALUMINIUM FLUX	QUARTZ FLUX	DOLOMITE FLUX	ZIRCONIUM FLUX	TITANIUM FLUX
0.00	0.00	30.14	77.99	55.33	0.13	4.95
10.00	8.31	17.18	35.52	14.78	0.05	4.61
20.00	10.70	88.31	148.19	75.80	0.23	14.40
32.00	13.57	122.61	149.77	123.38	0.30	13.58
35.00	14.28	107.22	146.92	123.91	0.30	18.55
40.00	15.49	154.29	125.10	128.02	0.37	25.02
50.00	17.27	148.71	197.98	141.93	0.40	48.82
60.00	19.05	150.79	199.10	139.08	0.41	39.53
70.00	20.83	135.38	171.78	129.65	0.31	34.76
80.00	22.64	155.71	233.56	196.98	0.40	42.68
100.00	24.46	126.40	164.32	123.63	0.33	42.26
110.00	26.28	124.89	141.54	148.78	0.27	39.46
120.00	28.33	106.05	126.89	142.44	0.23	33.90
150.00	30.38	144.24	199.23	104.06	0.40	37.65
160.00	32.43	131.87	383.94	113.98	0.37	38.90
164.00	33.25	152.15	203.68	132.11	0.40	38.45
174.00	35.30	139.25	188.33	101.74	0.37	36.71
184.00	37.38	129.02	182.78	91.78	0.37	33.79
194.00	39.86	137.20	194.80	112.80	0.34	36.80
204.00	42.85	92.38	131.63	60.61	0.21	27.23
214.00	45.84	87.58	165.54	92.92	0.28	20.83
224.00	48.82	71.87	55.18	51.79	0.20	24.44
234.00	54.70	77.41	110.92	49.09	0.21	14.87
244.00	57.58	67.00	98.09	41.45	0.19	23.86
254.00	60.47	57.83	89.39	29.45	0.11	11.78
264.00	67.14	33.97	79.23	28.84	0.10	6.38
284.00	80.00	35.11	52.14	20.04	0.13	8.52
294.00	84.22	39.98	92.23	37.63	0.15	7.06
304.00	88.44	34.62	75.03	31.88	0.12	6.60
309.00	90.55	35.15	74.84	27.70	0.11	3.73
319.00	99.00	32.91	57.39	16.05	0.11	4.08
329.00	108.60	18.86	27.94	10.87	0.06	2.09
339.00	118.20	18.67	25.28	8.80	0.06	2.41
349.00	121.70	50.95	72.19	28.39	0.15	7.90
359.00	125.20	55.80	94.40	23.20	0.16	5.00
369.00	127.20	111.54	156.16	57.20	0.29	7.15
379.00	132.60	106.40	145.04	52.36	0.27	7.28
390.00	136.60	113.40	152.32	56.84	0.29	6.44
400.00	138.20	81.03	134.53	79.25	0.21	4.66
410.00	141.40	121.09	254.90	161.34	0.34	6.88
420.00	150.20	97.01	153.65	57.31	0.27	4.24
430.00	150.90	103.73	153.20	33.70	0.24	5.02
440.00	151.16	81.84	127.82	38.06	0.19	5.50
450.00	152.30	67.32	111.67	31.88	0.17	9.90
454.00	152.58	70.24	113.73	20.96	0.15	15.39
464.00	158.20	104.44	114.24	22.23	0.24	16.25
474.00	161.40	73.24	103.63	27.34	0.19	13.67
484.00	164.60	65.74	109.69	30.89	0.17	15.05
494.00	167.80	55.60	93.00	15.80	0.15	14.00
504.00	171.06	55.90	91.59	23.01	0.13	15.91
514.00	174.32	60.71	74.34	1.92	0.12	14.70
524.00	177.58	76.54	86.65	4.52	0.15	13.11
534.00	180.84	65.96	112.08	67.85	0.12	10.96
544.00	184.12	75.94	159.78	111.19	0.17	11.98
554.00	187.40	52.69	89.24	44.99	0.11	7.40
564.00	190.70	53.10	73.80	3.50	0.12	4.90
574.00	192.09	45.36	68.04	7.69	0.11	8.57
584.00	205.00	44.50	70.49	16.55	0.10	12.99
594.00	206.61	99.03	113.18	83.90	0.25	17.44
598.00	207.41	105.90	126.73	102.02	0.27	13.77
608.00	209.03	92.39	131.94	112.48	0.25	10.20
618.00	210.50	87.21	105.45	136.51	0.19	8.55
628.00	216.00	62.65	81.37	64.56	0.17	4.97
636.00	223.38	64.08	100.36	84.73	0.15	5.60
648.00	228.00	74.23	81.19	69.85	0.15	7.96
663.00	230.90	68.55	91.48	64.24	0.18	4.99
682.00	232.00	174.37	219.49	135.83	0.45	8.93
706.00	233.70	195.36	265.80	129.36	0.48	6.64
712.00	239.10	146.93	229.55	86.69	0.36	6.10
722.00	244.00	152.03	191.58	78.69	0.37	11.12
733.00	245.50	143.42	176.91	64.22	0.38	11.43

TABLE C.15:2 LITHOGENIC FLUXES DATA (in mg-cm^2/kys) OF CORE CD1730

DEPTH CM	AGE KYS	ALUMINIUM FLUX	QUARTZ FLUX	DOLOMITE FLUX	ZIRCONIUM FLUX	TITANIUM FLUX
00.00	0.00	126.59	78.57	59.65	0.29	7.54
10.00	2.60	129.38	74.64	61.89	0.35	7.40
20.00	5.10	109.21	61.94	54.12	0.31	5.74
30.00	7.70	110.37	76.12	55.36	0.23	6.40
40.00	10.00	148.34	114.39	107.41	0.37	9.11
50.00	12.00	202.09	160.68	150.17	0.49	11.43
60.00	13.50	255.59	261.96	261.96	0.67	15.22
70.00	15.50	240.95	279.38	265.96	0.61	14.33
80.00	16.60	256.50	295.20	271.58	0.66	16.07
90.00	18.10	269.97	283.61	257.76	0.68	16.23
100.00	19.20	280.10	325.41	295.96	0.72	17.14
110.00	20.30	284.64	329.94	295.96	0.73	16.31
120.00	21.40	276.33	326.92	281.61	0.73	16.31
130.00	22.60	237.00	298.40	237.00	0.65	13.94
140.00	24.00	259.86	296.78	239.27	0.70	16.12
150.00	25.30	274.90	324.03	227.09	0.71	17.00
160.00	26.70	259.60	316.65	190.38	0.70	15.83
170.00	28.20	246.43	295.36	187.24	0.66	14.98
180.00	29.40	246.23	292.06	197.35	0.67	15.15
190.00	30.70	264.14	321.25	269.98	0.69	16.68
200.00	32.00	311.83	373.75	313.32	0.74	19.84
210.00	33.40	295.67	366.32	269.60	0.78	18.25
220.00	34.70	280.12	351.27	225.63	0.73	17.18
230.00	36.10	275.63	315.37	207.04	0.72	17.11
240.00	37.40	219.30	238.95	163.55	0.58	13.65
250.00	39.50	172.19	202.05	122.29	0.46	10.96
260.00	41.60	175.54	213.19	141.28	0.46	10.87
270.00	43.70	190.09	217.80	136.83	0.48	11.52
280.00	45.80	119.97	116.25	62.62	0.32	7.01
290.00	50.00	83.18	93.42	44.10	0.21	5.16
295.00	52.10	79.80	88.40	52.00	0.22	4.94
305.00	56.30	80.54	89.31	58.11	0.21	5.21
315.00	60.50	79.79	84.12	81.95	0.22	5.12
325.00	63.50	105.38	115.75	91.18	0.29	6.52
345.00	80.00	64.80	70.20	39.90	0.18	4.20
355.00	84.50	68.72	78.02	54.12	0.18	4.47
365.00	89.00	66.79	68.81	52.70	0.18	4.36
375.00	93.60	59.84	57.83	50.14	0.17	3.97
385.00	99.00	56.62	56.45	34.78	0.16	3.63
395.00	102.20	52.10	57.38	37.60	0.14	3.41
405.00	108.60	50.46	41.48	20.26	0.13	2.87
415.00	115.00	55.23	66.10	33.66	0.15	3.44
425.00	121.40	64.18	81.68	47.85	0.18	4.04
435.00	128.00	144.41	176.96	95.26	0.39	8.98
450.00	130.10	198.66	241.63	113.19	0.54	12.29
460.00	132.20	185.02	221.76	89.60	0.53	11.47
470.00	134.40	194.04	222.68	98.41	0.52	12.29
480.00	136.50	224.22	242.40	98.48	0.59	13.99
490.00	138.60	197.58	214.54	94.55	0.51	12.21
500.00	140.70	192.88	210.52	99.45	0.50	12.39
510.00	142.80	186.90	202.93	104.01	0.46	11.73
520.00	144.90	186.51	223.26	76.64	0.46	11.26
530.00	147.10	170.37	161.59	88.62	0.43	10.62
540.00	149.20	160.45	133.22	67.15	0.40	9.76
550.00	151.30	159.49	123.90	69.45	0.39	9.39
560.00	153.40	155.30	119.71	45.72	0.38	9.04
570.00	155.50	201.12	173.66	38.98	0.51	12.27
580.00	157.70	222.83	232.57	44.74	0.55	13.64
590.00	159.80	146.33	142.27	70.51	0.37	8.70
600.00	163.20	111.19	103.81	52.15	0.29	6.57
610.00	166.70	92.74	73.05	54.96	0.25	5.45
620.00	170.10	82.90	67.55	79.46	0.22	4.74
630.00	173.60	88.86	76.56	29.93	0.23	5.03
640.00	177.00	104.28	78.68	23.46	0.25	5.62
650.00	180.50	128.54	109.51	1.18	0.28	7.50
660.00	184.10	68.21	57.10	8.54	0.15	3.90
670.00	191.00	48.60	46.01	22.79	0.12	2.91
680.00	198.00	48.07	33.35	10.93	0.11	2.74
690.00	205.00	52.42	26.64	13.54	0.11	2.79
700.00	209.80	77.86	81.87	47.90	0.18	4.73
710.00	214.60	77.57	89.73	72.49	0.19	4.97
720.00	219.40	81.55	91.27	77.35	0.20	5.24
730.00	224.10	64.03	70.29	60.72	0.16	3.99
740.00	228.90	60.36	61.42	61.42	0.15	3.82
750.00	233.70	63.36	70.69	79.00	0.17	3.66
760.00	238.50	62.63	72.66	58.30	0.17	3.74
770.00	243.30	67.68	79.15	63.17	0.19	4.06
780.00	248.10	76.43	81.18	62.96	0.19	4.67
790.00	252.80	77.00	95.63	72.04	0.20	4.86
800.00	257.60	78.69	96.75	79.12	0.23	4.84

TABLE C.15:3 LITHOGENIC FLUXES DATA (in mg-cm^2/kys) OF CORE CD1738

DEPTH CM	AGE KYS	ALUMINIUM FLUX	QUARTZ FLUX	DOLOMITE FLUX	ZIRCONIUM FLUX	TITANIUM FLUX
20.00	15.40	556.16	500.86	308.10	1.16	30.81
30.00	20.80	971.95	871.85	18.44	1.95	54.00
40.00	22.64	752.20	761.99	254.36	1.61	40.22
50.00	23.55	868.67	449.85	114.12	1.54	45.43
60.00	24.46	489.60	527.40	618.30	0.94	26.10
70.00	26.28	457.02	256.93	33.74	0.83	24.86
80.00	28.10	399.53	236.74	106.40	0.75	22.34
90.00	29.95	498.44	509.72	74.02	1.04	28.90
100.00	31.19	504.40	606.83	89.24	1.24	31.04
110.00	32.73	564.72	282.36	56.47	1.03	31.13
120.00	34.28	556.10	183.33	10.86	0.98	30.55
130.00	35.82	460.16	258.56	110.72	0.86	25.60
140.00	37.38	343.36	231.76	175.69	0.68	21.36
150.00	39.14	436.73	764.09	115.32	1.85	25.30
160.00	40.90	531.91	600.62	31.65	1.23	32.42
170.00	42.66	411.44	257.43	60.60	0.79	22.80
180.00	44.42	483.36	214.33	4.45	0.95	27.35
185.00	45.30	493.29	267.75	0.00	0.96	27.72
195.00	47.06	520.65	219.37	290.16	0.92	28.66
205.00	48.82	505.85	343.71	6.70	1.00	28.81
215.00	51.01	240.11	206.30	229.84	0.52	13.70
225.00	53.20	382.50	234.07	42.56	0.74	21.80
235.00	55.39	282.07	226.04	269.51	0.72	15.94
245.00	57.58	264.66	378.08	359.73	0.87	17.79
255.00	59.05	602.08	338.52	65.29	1.14	34.66
265.00	60.45	696.98	396.86	0.90	1.31	38.87
275.00	65.74	134.76	82.39	63.34	0.27	7.45
295.00	82.75	72.11	58.79	38.91	0.16	4.05
305.00	94.50	56.43	53.90	58.63	0.14	3.30
315.00	96.24	497.13	271.16	208.35	1.00	26.81
325.00	97.99	376.37	227.06	243.10	0.79	20.36
335.00	99.74	380.16	334.72	251.52	0.81	21.12
345.00	101.48	207.16	170.37	325.45	0.64	9.06
355.00	103.23	446.76	149.94	107.71	0.83	23.26
365.00	104.98	298.01	239.67	270.56	0.70	17.16
375.00	106.73	346.07	332.74	381.64	0.82	19.05
385.00	108.47	403.20	342.72	347.04	0.97	22.32
395.00	110.22	392.82	444.41	392.82	0.98	22.85
405.00	111.97	467.38	503.33	209.72	1.11	26.96
415.00	113.72	408.94	170.82	122.55	1.02	22.86
425.00	115.46	477.22	380.70	300.27	1.14	27.58
435.00	117.21	481.05	458.07	276.53	1.08	27.58
445.00	118.96	370.99	418.90	437.78	0.97	21.78
455.00	120.70	401.96	412.36	371.50	1.00	23.78
465.00	122.70	423.83	403.33	349.90	1.01	24.16
475.00	124.45	356.69	350.73	401.78	0.80	19.89
485.00	125.95	328.67	496.30	491.90	0.95	20.50
495.00	127.70	644.00	1281.28	132.16	2.03	43.68
505.00	128.78	823.68	832.42	255.84	1.80	48.67
515.00	129.87	902.82	388.68	163.59	1.77	50.43
525.00	130.96	765.57	1017.09	142.86	2.02	46.40
535.00	132.05	576.39	1154.11	883.10	1.33	33.05
540.00	132.60	290.40	750.80	600.48	1.15	20.46
545.00	133.40	480.27	317.25	238.31	1.01	19.01
555.00	135.00	585.42	719.36	105.55	1.46	35.48
565.00	136.60	528.43	274.90	157.72	1.05	28.74
575.00	138.20	484.87	286.94	224.99	0.98	26.34
585.00	139.80	612.86	715.01	152.30	1.40	35.57
595.00	141.40	354.04	384.10	365.40	0.92	20.71
605.00	144.00	321.78	306.54	62.83	0.74	18.56
615.00	146.98	313.76	296.88	59.56	0.71	18.76
625.00	150.20	328.60	224.64	61.92	0.69	18.98
635.00	152.60	163.40	264.10	267.52	0.51	10.26
645.00	155.80	217.40	327.66	153.27	0.56	12.90
655.00	158.70	216.82	223.48	157.62	0.54	12.58
665.00	161.60	285.16	373.63	503.69	0.75	17.06

TABLE C.15:4 LITHOGENIC FLUXES DATA (in mg-cm^2/kys) OF CORE CD1739

DEPTH CM	AGE KYS	ALUMINIUM FLUX	QUARTZ FLUX	DOLOMITE FLUX	ZIRCONIUM FLUX	TITANIUM FLUX
20.00	15.50	361.56	489.98	144.79	1.07	15.71
30.00	16.83	315.33	407.05	149.33	0.93	20.31
40.00	18.16	305.47	411.59	137.96	0.94	19.86
50.00	19.49	303.89	394.53	133.00	0.89	18.20
60.00	20.82	349.05	451.66	148.21	1.04	21.49
70.00	21.73	441.15	560.20	180.71	1.30	26.04
80.00	22.64	489.29	650.88	150.29	1.45	26.55
90.00	23.55	477.19	633.72	97.83	1.44	27.28
100.00	24.46	452.75	621.53	125.02	1.28	22.41
110.00	25.67	170.93	230.43	36.38	0.51	9.51
120.00	26.88	362.94	489.63	165.21	1.08	25.17
130.00	28.10	354.03	495.19	112.16	1.06	21.97
140.00	29.64	320.21	427.42	100.11	0.98	19.52
150.00	31.19	312.57	404.34	100.74	0.88	20.15
160.00	32.74	315.65	408.44	98.42	0.91	18.91
170.00	34.29	329.96	425.59	127.75	0.96	19.64
180.00	35.83	301.94	382.50	82.59	0.86	18.14
190.00	37.38	102.19	127.20	21.71	0.29	6.63
200.00	41.61	99.10	127.97	31.42	0.29	6.35
210.00	45.84	99.06	133.17	33.87	0.30	6.10
220.00	49.76	96.79	121.65	37.04	0.29	6.29
230.00	53.68	103.74	127.92	17.94	0.31	6.84
240.00	57.58	173.42	219.42	62.10	0.54	11.27
250.00	59.01	336.66	449.40	92.10	1.02	18.42
260.00	60.45	391.65	554.48	107.12	1.20	19.45
270.00	63.92	74.89	103.62	4.87	0.23	4.02
280.00	67.40	132.60	159.43	17.16	0.39	8.55
290.00	68.60	431.79	543.78	29.42	1.27	26.86
300.00	69.80	399.42	479.83	50.69	1.14	20.80
320.00	80.00	63.64	71.48	2.07	0.18	3.97
330.00	87.25	76.92	86.76	1.31	0.21	4.41
340.00	94.50	57.53	64.57	4.44	0.16	3.92
350.00	97.05	178.85	206.06	41.04	0.49	11.84
360.00	99.61	162.21	194.32	82.57	0.45	9.42
370.00	102.17	151.71	184.47	81.51	0.41	9.28
380.00	104.73	141.57	186.81	78.00	0.43	8.81
390.00	107.29	146.69	203.61	87.48	0.44	8.63
400.00	109.85	146.68	203.81	79.90	0.46	8.26
410.00	112.40	150.79	196.18	60.76	0.43	8.53
420.00	114.96	148.61	198.79	37.83	0.44	8.99
430.00	117.52	152.49	212.55	41.34	0.46	10.76
440.00	120.08	155.93	215.87	66.82	0.46	9.92
450.00	122.64	169.33	236.24	53.28	0.46	10.37
460.00	125.20	344.06	473.09	135.30	1.11	22.40
470.00	126.45	393.01	546.68	138.88	1.16	27.09
480.00	127.70	405.55	648.31	344.62	1.29	24.94
490.00	132.60	362.56	454.08	114.40	1.05	24.20
500.00	137.88	123.60	162.25	43.07	0.36	7.79
515.00	141.40	141.10	189.24	46.15	0.42	8.43
525.00	141.98	161.57	220.70	44.35	0.47	9.47
535.00	142.57	981.93	1393.02	291.81	2.85	58.36
545.00	143.16	987.99	1422.01	379.49	2.94	64.99
555.00	143.74	1061.53	1437.11	281.12	3.14	68.37
565.00	144.33	1001.10	1384.50	230.04	2.85	64.75
575.00	144.92	911.62	1293.85	216.66	2.78	64.59
585.00	145.50	875.84	1204.04	357.33	2.50	60.20
595.00	146.09	887.49	1178.79	403.94	2.47	60.20
605.00	146.68	841.43	1130.02	410.41	2.37	58.28
615.00	147.26	850.85	1185.80	369.60	2.39	59.87
625.00	147.85	918.77	1219.72	344.79	2.57	58.39
635.00	148.44	877.68	1169.60	354.89	2.45	55.90
645.00	149.00	946.37	1277.50	335.22	2.66	60.91
655.00	149.61	939.93	1205.98	184.49	2.63	60.40
665.00	150.20	888.55	953.57	281.74	2.41	54.90
675.00	150.80	744.70	926.30	294.88	1.98	50.98
685.00	151.40	865.54	1049.08	146.83	2.38	62.40
695.00	152.00	894.07	978.57	192.57	2.45	57.77
705.00	152.60	783.30	1055.59	197.69	2.16	54.46
715.00	158.20	989.82	1106.15	205.15	2.70	65.56
725.00	160.60	874.69	994.04	91.38	2.32	53.53
735.00	163.00	285.68	260.68	48.94	0.75	16.81
745.00	164.48	206.09	250.99	5.39	0.53	13.43
755.00	166.66	216.53	238.04	39.20	0.61	15.39
765.00	167.80	178.88	202.59	32.03	0.47	12.19

TABLE C.16:1 BIOGENIC FLUXES DATA OF CORE CD1715

DEPTH CM	AGE KYS	Calcite (g-cm^2/kys)	C.org (mg-cm^2/kys)	Ex.Ba (mg-cm^2/kys)	Biog.Si (mg-cm^2/kys)	Biog.Si/ Calcite
0.00	0.00	0.51	8.36	0.48	16.28	3.19
10.00	8.31	0.67	4.03	0.66	15.36	2.29
20.00	10.70	2.42	12.43	1.00	43.24	1.78
32.00	13.57	2.01	12.34	0.39	25.22	1.26
35.00	14.28	1.97	8.38	0.47	24.00	1.22
40.00	15.49	1.93	17.93	0.56	62.13	3.22
50.00	17.27	2.28	15.73	0.84	40.68	1.79
60.00	19.05	2.57	23.08	1.42	53.53	2.08
70.00	20.83	1.97	48.51	0.88	37.63	1.91
80.00	22.64	2.12	29.41	0.75	42.21	1.99
100.00	24.46	2.01	26.62	0.80	37.72	1.88
110.00	26.28	1.64	23.78	0.44	29.39	1.79
120.00	28.33	1.38	17.17	0.34	26.81	1.95
150.00	30.38	2.05	22.63	0.64	39.17	1.91
160.00	32.43	1.86	11.63	0.57	28.67	1.54
164.00	33.25	1.77	11.78	0.36	23.64	1.34
174.00	35.30	1.89	24.26	0.83	31.24	1.65
184.00	37.38	1.88	24.15	0.77	38.02	2.02
194.00	39.86	1.88	21.08	1.00	32.64	1.74
204.00	42.85	1.29	19.84	0.88	40.32	3.13
214.00	45.84	1.21	15.14	0.70	22.59	1.87
224.00	48.82	1.31	16.21	0.84	28.34	2.17
234.00	54.70	1.18	14.04	0.41	20.65	1.75
244.00	57.58	1.36	18.03	0.70	27.16	1.99
254.00	60.47	0.66	12.67	0.32	17.71	2.68
264.00	67.14	0.55	11.68	0.33	28.73	5.24
284.00	80.00	0.76	14.03	0.37	34.61	4.55
294.00	84.22	0.96	22.01	0.90	46.37	4.81
304.00	88.44	0.97	16.58	0.99	42.50	4.37
309.00	90.55	1.01	13.41	0.67	32.72	3.23
319.00	99.00	0.85	5.75	0.42	17.41	2.05
329.00	108.60	0.42	2.66	0.17	5.80	1.37
339.00	118.20	0.42	3.20	0.19	5.73	1.35
349.00	121.70	1.10	7.95	0.51	13.54	1.23
359.00	125.20	1.17	12.36	0.47	13.28	1.13
369.00	127.20	1.24	13.18	0.17	16.04	1.30
379.00	132.60	1.25	14.36	0.50	15.57	1.24
390.00	136.60	1.15	15.51	0.61	19.35	1.68
400.00	138.20	0.90	33.37	0.65	39.63	4.42
410.00	141.40	1.35	34.40	0.41	40.11	2.97
420.00	150.20	0.78	29.66	0.76	41.57	5.34
430.00	150.90	0.88	19.88	0.53	25.38	2.90
440.00	151.16	1.05	19.27	0.90	27.43	2.61
450.00	152.30	0.95	18.06	1.16	26.08	2.74
454.00	152.58	1.19	18.38	1.24	28.10	2.37
464.00	158.20	0.93	15.70	0.49	22.99	2.48
474.00	161.40	0.95	23.46	1.42	20.58	2.17
484.00	164.60	0.98	26.63	1.61	32.91	3.36
494.00	167.80	1.19	28.90	1.56	33.66	2.82
504.00	171.06	1.28	16.34	1.44	29.91	2.35
514.00	174.32	1.24	21.53	1.33	23.07	1.85
524.00	177.58	1.13	20.21	0.96	21.59	1.91
534.00	180.84	0.80	13.51	0.76	18.14	2.26
544.00	184.12	0.91	36.97	0.69	35.39	3.91
554.00	187.40	0.63	26.05	0.64	25.69	4.05
564.00	190.70	0.27	18.70	1.00	19.24	7.16
574.00	192.09	0.60	25.20	1.27	26.62	4.41
584.00	205.00	1.14	19.72	1.25	31.95	2.81
594.00	206.61	1.79	26.98	0.12	13.46	0.75
598.00	207.41	1.93	34.66	1.56	27.39	1.42
608.00	209.03	1.57	33.62	0.91	26.70	1.71
618.00	210.50	1.33	8.78	0.56	9.06	0.68
628.00	216.00	0.91	18.24	0.65	15.28	1.69
636.00	223.38	0.86	30.49	0.53	26.17	3.05
648.00	228.00	0.89	32.24	0.39	24.28	2.73
663.00	230.90	1.21	15.66	0.35	14.85	1.23
682.00	232.00	2.09	23.88	0.28	14.15	0.68
706.00	233.70	1.53	22.81	0.46	40.76	2.66
712.00	239.10	1.90	41.07	1.36	66.91	3.52
722.00	244.00	1.91	25.30	0.86	24.97	1.31
733.00	245.50	1.88	18.91	0.97	19.74	1.05

TABLE C.16:2 BIOGENIC FLUXES DATA OF CORE CD1730

DEPTH CM	AGE KYS	Calcite ($g\text{-}cm^2/kys$)	C.org ($mg\text{-}cm^2/kys$)	Ex.Ba ($mg\text{-}cm^2/kys$)	Biog.Si ($mg\text{-}cm^2/kys$)	Biog.Si/ Calcite
0.00	0.00	0.98	33.17	2.44	61.40	6.27
10.00	2.60	1.20	29.54	2.38	67.49	5.63
20.00	5.10	1.63	25.10	2.60	41.08	2.52
30.00	7.70	1.82	20.07	2.32	39.27	2.16
40.00	10.00	2.44	25.57	2.61	43.71	1.79
50.00	12.00	3.21	27.19	1.23	57.78	1.80
60.00	13.50	3.21	26.90	0.62	41.35	1.29
70.00	15.50	2.37	23.18	0.00	29.95	1.27
80.00	16.60	2.57	24.93	0.30	36.21	1.41
90.00	18.10	3.00	43.80	1.20	47.96	1.60
100.00	19.20	3.11	56.62	1.24	40.54	1.30
110.00	20.30	3.07	54.36	1.15	39.71	1.30
120.00	21.40	3.14	60.40	0.94	32.69	1.04
130.00	22.60	2.35	61.40	0.61	25.97	1.11
140.00	24.00	2.93	73.13	0.84	35.14	1.20
150.00	25.30	2.48	49.14	0.10	22.44	0.90
160.00	26.70	2.46	39.74	0.47	21.09	0.86
170.00	28.20	2.18	73.69	0.64	22.47	1.03
180.00	29.40	2.25	75.15	0.65	34.77	1.55
190.00	30.70	2.28	55.16	0.48	41.47	1.82
200.00	32.00	2.55	47.00	0.00	62.66	2.46
210.00	33.40	2.30	41.16	0.37	30.94	1.35
220.00	34.70	2.16	35.25	0.00	16.47	0.76
230.00	36.10	2.26	35.90	0.95	33.01	1.46
240.00	37.40	2.06	36.11	0.90	34.99	1.70
250.00	39.50	1.47	22.90	0.59	31.66	2.15
260.00	41.60	1.54	19.03	0.32	23.05	1.50
270.00	43.70	1.51	22.08	0.00	21.74	1.44
280.00	45.80	1.30	22.32	0.56	31.96	2.46
290.00	50.00	0.84	16.30	0.22	15.30	1.82
295.00	52.10	0.78	18.80	0.41	20.00	2.58
305.00	56.30	0.71	16.97	0.35	17.81	2.52
315.00	60.50	0.60	33.15	1.02	29.77	4.93
325.00	63.50	0.95	42.31	1.12	36.45	3.82
345.00	80.00	0.50	16.95	0.54	12.94	2.61
355.00	84.50	0.54	20.38	0.70	16.29	3.04
365.00	89.00	0.77	13.57	0.87	31.20	4.06
375.00	93.60	0.86	13.39	0.72	27.16	3.15
385.00	99.00	0.81	8.75	0.42	20.52	2.52
395.00	102.20	0.70	9.83	0.31	13.77	1.97
405.00	108.60	0.67	10.18	0.45	11.26	1.69
415.00	115.00	0.70	7.64	0.34	6.72	0.97
425.00	121.40	0.67	7.93	0.12	5.57	0.83
435.00	128.00	1.24	18.98	0.16	9.70	0.78
450.00	130.10	1.71	35.15	0.43	14.66	0.86
460.00	132.20	1.81	47.53	0.62	18.38	1.01
470.00	134.40	1.78	19.89	0.58	20.35	1.15
480.00	136.50	1.83	24.74	0.84	26.41	1.44
490.00	138.60	1.37	28.83	0.87	25.27	1.84
500.00	140.70	1.17	31.68	0.87	23.54	2.01
510.00	142.80	1.12	25.41	0.63	19.82	1.77
520.00	144.90	1.19	25.81	0.61	17.32	1.46
530.00	147.10	1.32	20.25	0.91	16.92	1.28
540.00	149.20	1.30	19.24	0.86	38.59	2.98
550.00	151.30	1.12	30.71	2.32	61.56	5.48
560.00	153.40	1.27	21.99	2.03	55.35	4.36
570.00	155.50	1.66	19.05	0.69	52.76	3.18
580.00	157.70	1.34	22.59	1.08	21.35	1.59
590.00	159.80	0.96	18.41	2.49	35.16	3.67
600.00	163.20	0.85	11.81	1.25	27.87	3.28
610.00	166.70	0.90	13.05	1.45	26.50	2.94
620.00	170.10	1.04	8.47	1.45	22.90	2.20
630.00	173.60	1.09	11.37	1.12	21.58	1.97
640.00	177.00	0.96	7.82	1.31	18.34	1.92
650.00	180.50	0.65	9.63	0.81	24.22	3.75
660.00	184.10	0.23	7.72	0.96	16.13	6.97
670.00	191.00	0.36	3.35	0.99	14.22	3.92
680.00	198.00	0.48	4.14	1.16	13.29	2.79
690.00	205.00	0.71	6.05	0.97	22.85	3.23
700.00	209.80	0.95	9.07	0.04	9.05	0.96
710.00	214.60	1.00	9.06	0.04	8.57	0.86
720.00	219.40	0.98	8.40	0.18	10.50	1.07
730.00	224.10	0.82	13.42	0.58	0.33	0.04
740.00	228.90	0.80	15.93	0.48	9.49	1.19
750.00	233.70	0.69	17.62	0.35	6.12	0.88
760.00	238.50	0.76	20.41	0.56	10.69	1.41
770.00	243.30	0.82	16.73	0.41	11.99	1.46
780.00	248.10	0.79	7.52	0.25	11.58	1.47
790.00	252.80	0.87	9.94	0.24	9.52	1.10
800.00	257.60	0.89	7.74	0.24	9.22	1.04

TABLE C.16:3 BIOGENIC FLUXES DATA OF CORE CD1738

DEPTH CM	AGE KYS	Calcite ($g\text{-}cm^2/kys$)	C.org ($mg\text{-}cm^2/kys$)	Ex.Ba ($mg\text{-}cm^2/kys$)
0.00	0.00	n.a	n.a	n.a
10.00	0.00	n.a	n.a	n.a
20.00	15.40	0.52	81.37	0.00
30.00	20.80	1.38	62.43	1.71
40.00	22.64	0.95	73.16	0.00
50.00	23.55	1.05	96.06	0.00
60.00	24.46	1.64	76.86	0.29
70.00	26.28	0.64	24.15	0.00
80.00	28.10	0.55	25.48	0.00
90.00	29.95	0.77	26.51	0.00
100.00	31.19	0.87	27.39	0.00
110.00	32.73	0.82	26.50	0.00
120.00	34.28	0.78	19.35	0.00
130.00	35.82	0.91	28.03	0.00
140.00	37.38	1.00	24.51	0.12
150.00	39.14	1.17	13.47	0.00
160.00	40.90	0.98	21.77	0.00
170.00	42.66	0.70	19.85	0.00
180.00	44.42	0.98	23.34	0.00
185.00	45.30	0.76	17.32	0.00
195.00	47.06	0.64	22.05	0.00
205.00	48.82	0.84	17.69	0.00
215.00	51.01	0.97	20.93	0.57
225.00	53.20	0.71	18.27	0.00
235.00	55.39	0.98	17.24	0.08
245.00	57.58	1.45	12.34	0.05
255.00	59.05	1.12	24.58	0.00
265.00	60.45	1.16	21.06	0.00
275.00	65.74	0.42	4.84	0.00
285.00	71.00	0.46	5.38	0.00
295.00	82.75	0.33	3.25	0.00
305.00	94.50	0.22	5.35	0.00
315.00	96.24	1.78	25.58	0.00
325.00	97.99	1.36	21.35	0.00
335.00	99.74	1.53	21.50	0.00
345.00	101.48	1.04	32.88	0.00
355.00	103.23	1.51	23.68	0.00
365.00	104.98	1.34	21.56	0.02
375.00	106.73	1.60	23.94	0.00
385.00	108.47	1.73	19.73	0.00
395.00	110.22	1.31	20.12	0.00
405.00	111.97	1.88	35.65	0.00
415.00	113.72	1.27	21.34	0.00
425.00	115.46	1.35	24.74	0.00
435.00	117.21	1.98	16.24	0.00
445.00	118.96	1.78	29.48	0.00
455.00	120.70	1.62	21.84	0.00
465.00	122.70	1.71	57.90	0.00
475.00	124.45	1.82	30.37	0.00
485.00	125.95	1.11	11.13	0.00
495.00	127.70	1.69	36.18	0.00
505.00	128.78	1.97	59.16	0.00
515.00	129.87	2.05	45.88	0.00
525.00	130.96	3.23	28.33	0.00
535.00	132.05	4.03	26.70	0.22
540.00	132.60	1.41	34.31	0.22
545.00	133.40	1.00	20.03	0.00
555.00	135.00	1.39	49.32	0.00
565.00	136.60	1.26	38.10	0.00
575.00	138.20	0.93	16.66	0.00
585.00	139.80	2.07	37.76	0.00
595.00	141.40	1.10	21.78	0.00
605.00	144.00	0.74	13.47	0.00
615.00	146.98	0.65	16.60	0.00
625.00	150.20	1.27	22.42	0.00
635.00	152.60	0.70	15.85	0.00
645.00	155.80	0.78	20.68	0.00
665.00	161.60	0.73	21.13	0.00

n.a = not analysed

TABLE C.16:4 BIOGENIC FLUXES DATA OF CORE CD1739

DEPTH CM	AGE KYS	Calcite (g-cm^2/kys)	C.org (mg-cm^2/kys)	Ex.Ba (mg-cm^2/kys)
00.00	0.00	n.a	n.a	n.a
10.00	0.00	0.00	n.a	n.a
20.00	15.50	0.61	33.29	0.00
30.00	16.83	0.57	38.66	0.00
40.00	18.16	0.57	50.26	0.20
50.00	19.49	0.56	47.77	0.12
60.00	20.82	0.81	104.10	0.00
70.00	21.73	1.17	60.80	0.01
80.00	22.64	1.24	46.10	0.00
90.00	23.55	1.19	38.81	0.00
100.00	24.66	0.85	49.29	0.00
110.00	25.67	0.31	18.99	0.00
120.00	26.88	0.71	46.22	0.00
130.00	28.10	0.51	33.34	0.00
140.00	29.64	0.47	31.10	0.00
150.00	31.19	0.46	22.49	0.00
160.00	32.74	0.47	22.14	0.00
170.00	34.29	0.48	28.25	0.00
180.00	35.83	0.45	33.85	0.05
190.00	37.38	0.06	9.89	0.00
200.00	41.61	0.05	19.82	0.06
210.00	45.84	0.06	13.97	0.08
220.00	49.76	0.06	17.85	0.27
230.00	53.68	0.07	18.04	0.06
240.00	57.58	0.22	31.97	0.29
250.00	59.01	0.55	44.46	0.11
260.00	60.45	0.60	38.22	0.00
270.00	63.92	0.05	7.41	0.00
280.00	67.40	0.09	19.06	0.05
290.00	68.60	0.79	38.62	0.00
300.00	69.80	0.73	56.20	0.22
320.00	80.00	0.74	60.77	0.26
330.00	87.25	0.02	8.14	0.00
340.00	94.50	0.02	6.33	0.20
350.00	97.05	0.02	10.43	0.01
360.00	99.61	0.17	21.51	0.00
370.00	102.17	0.16	24.23	0.00
380.00	104.73	0.15	26.68	0.07
390.00	107.29	0.15	34.67	0.07
400.00	109.85	0.15	32.81	0.06
410.00	112.40	0.15	40.22	0.20
420.00	114.96	0.14	49.81	0.14
430.00	117.52	0.15	46.55	0.15
440.00	120.08	0.15	37.09	0.11
450.00	122.64	0.16	27.26	0.00
460.00	125.20	0.16	26.51	0.05
470.00	126.45	0.72	42.83	0.00
480.00	127.70	0.79	43.14	0.00
490.00	132.60	0.76	35.70	0.01
505.00	137.88	0.25	38.54	0.00
515.00	141.40	0.08	12.63	0.00
525.00	141.98	0.09	17.20	0.00
535.00	142.57	0.60	10.00	0.00
545.00	143.16	3.63	60.49	0.00
555.00	143.74	3.72	55.18	0.00
565.00	144.33	3.83	59.15	0.00
575.00	144.92	3.63	86.48	0.00
585.00	145.50	3.48	82.78	0.00
595.00	146.09	3.31	102.73	0.09
605.00	146.68	3.31	110.69	0.00
615.00	147.26	3.19	135.49	0.00
625.00	147.85	3.28	111.65	0.00
635.00	148.44	3.40	139.71	0.00
645.00	149.00	3.25	141.76	0.00
655.00	149.61	3.48	151.46	0.00
665.00	150.20	3.31	122.54	1.01
675.00	150.80	3.08	130.39	1.24
685.00	151.40	2.78	154.94	0.24
695.00	152.00	3.22	92.16	1.13
705.00	152.60	3.27	83.71	1.59
715.00	158.20	3.11	37.86	0.12
725.00	160.60	0.88	64.30	0.64
735.00	163.00	0.78	66.39	0.00
745.00	164.48	0.22	12.93	0.18
755.00	166.66	0.19	17.83	0.00
765.00	167.80	0.20	19.41	0.25

n.a = not analysed

TABLE C.17:1 PALEOPRODUCTIVITY DATA OF CORE CD1715

AGE KYS	C.org (%)	DBD*	S.Rates** cm/kys	PALEOPRODUCTIVITY gC-m^2/y
0.00	0.76	0.93	1.19	223.62
8.31	0.42	0.83	1.19	110.29
10.57	0.33	0.88	4.31	62.45
13.57	0.32	0.93	4.18	64.59
14.28	0.23	0.88	4.22	43.80
15.49	0.43	0.92	4.54	83.76
17.25	0.35	0.93	4.87	67.48
19.05	0.47	0.87	5.61	81.25
20.83	1.19	0.73	5.61	172.61
22.64	0.63	0.85	5.52	106.92
24.45	0.67	0.72	5.49	96.47
26.28	0.66	0.66	5.49	87.12
28.33	0.82	0.64	4.87	108.80
30.38	0.54	0.87	4.87	97.39
32.43	0.30	0.80	4.87	49.75
33.25	0.29	0.84	4.87	50.50
35.30	0.61	0.82	4.87	103.70
37.38	0.63	0.80	4.80	104.94
39.85	0.53	0.80	5.00	87.21
42.85	0.74	0.80	3.34	137.43
45.84	0.57	0.80	3.34	105.86
48.82	0.67	0.82	2.96	132.25
54.70	0.60	0.92	2.57	138.62
57.58	0.75	0.94	2.57	177.05
60.47	0.84	0.74	2.05	167.06
67.14	1.02	0.75	1.53	224.46
80.00	1.07	0.85	1.55	265.82
84.22	1.31	0.71	2.37	239.32
88.44	1.03	0.68	2.37	180.22
90.55	0.83	0.69	2.36	147.55
99.00	0.42	0.80	1.77	94.37
108.60	0.37	0.81	0.88	103.81
118.20	0.45	0.80	0.88	124.69
121.70	0.42	0.78	2.42	83.77
125.20	0.62	0.83	2.42	131.58
127.20	0.46	0.94	3.05	103.15
132.60	0.51	0.92	3.05	111.93
136.60	0.55	0.92	3.05	120.71
138.20	1.53	0.73	3.05	266.44
141.40	1.00	1.13	3.05	269.57
150.20	1.33	0.82	2.72	269.26
150.90	0.83	0.88	2.72	180.33
151.16	0.88	0.81	2.72	175.99
152.30	0.91	0.73	2.72	164.01
152.58	0.82	0.82	2.72	166.01
158.20	0.66	0.88	2.72	143.40
161.40	1.19	0.77	2.65	228.00
164.60	1.35	0.75	2.65	251.94
167.80	1.45	0.77	2.60	279.41
171.06	0.78	0.83	2.69	160.37
174.32	1.01	0.82	2.60	207.26
177.58	0.97	0.83	2.60	201.48
180.84	1.72	0.73	2.60	314.22
184.12	1.64	0.87	2.60	357.07
187.40	1.76	0.76	1.95	364.92
190.70	1.87	0.70	1.44	391.12
192.09	2.06	0.88	1.44	541.65
205.00	1.11	0.88	2.03	263.29
206.61	0.82	0.95	3.47	178.78
207.41	0.98	1.04	3.40	235.34
209.10	1.09	0.91	3.40	229.04
210.50	0.31	0.84	3.40	60.13
216.00	0.95	0.91	2.10	230.66
223.38	1.58	0.92	2.10	387.84
228.00	1.62	0.84	2.37	350.15
230.90	0.69	0.96	2.37	170.44
232.00	0.51	1.05	4.48	113.83
233.70	0.58	0.99	4.48	122.06
239.10	1.01	0.91	4.48	195.37
244.00	0.61	0.92	4.48	119.29
245.50	0.48	0.88	4.48	89.79

DBD* = DRY BULK DENSITY
S.Rates** = Sed. rates

TABLE C.17:2 PALEOPRODUCTIVITY DATA OF CORE CD1730

DEPTH CM	AGE KYS	C.org (%)	DBD*	S.Rates** cm/kys	PALEOPRODUCTIVITY gC-m^2/y
0.00	0.00	1.14	0.75	3.89	189.61
10.00	2.60	0.95	0.80	3.89	168.54
20.00	5.10	0.77	0.84	3.89	143.44
30.00	7.70	0.58	0.89	3.89	114.48
40.00	10.00	0.55	0.93	5.00	105.20
50.00	12.00	0.44	1.07	5.78	92.71
60.00	13.50	0.38	1.08	6.56	77.81
70.00	15.50	0.38	0.93	6.56	67.00
80.00	16.60	0.38	0.91	6.56	65.56
90.00	18.10	0.61	0.91	7.89	99.57
100.00	19.20	0.75	0.82	9.21	105.31
110.00	20.30	0.72	0.82	9.21	101.10
120.00	21.40	0.80	0.82	9.21	112.33
130.00	22.60	1.00	0.86	7.14	158.95
140.00	24.00	1.02	0.98	7.25	183.91
150.00	25.30	0.74	0.89	7.46	120.14
160.00	26.70	0.62	0.86	7.46	97.26
170.00	28.20	1.22	0.81	7.46	180.26
180.00	29.40	1.23	0.82	7.46	183.98
190.00	30.70	0.85	0.87	7.46	134.89
200.00	32.00	0.63	1.00	7.46	114.92
210.00	33.40	0.60	0.92	7.46	100.69
220.00	34.70	0.56	0.86	7.46	87.85
230.00	36.10	0.56	0.86	7.46	87.85
240.00	37.40	0.68	0.87	6.11	114.58
250.00	39.50	0.56	0.86	4.76	100.53
260.00	41.60	0.45	0.89	4.76	83.60
270.00	43.70	0.51	0.91	4.76	96.87
280.00	45.80	0.72	0.87	3.57	142.54
290.00	50.00	0.78	0.88	2.32	177.75
295.00	52.10	0.94	0.84	2.38	202.91
305.00	56.30	0.87	0.82	2.38	183.33
315.00	60.50	1.68	0.69	2.86	281.92
325.00	63.50	1.55	0.82	3.33	295.32
345.00	80.00	0.58	0.75	2.00	117.78
355.00	84.50	1.13	0.75	2.21	222.69
365.00	89.00	1.23	0.83	2.21	268.25
375.00	93.60	0.74	0.83	2.21	161.39
385.00	99.00	0.73	0.89	1.89	178.92
395.00	102.20	0.52	0.97	1.56	147.14
405.00	108.60	0.65	0.87	1.56	164.96
415.00	115.00	0.75	0.98	1.56	214.40
425.00	121.40	0.50	1.06	1.56	154.60
435.00	128.00	0.48	1.08	3.14	122.59
450.00	130.10	0.56	0.98	4.72	114.84
460.00	132.20	0.76	0.95	4.72	151.09
470.00	134.40	1.06	0.98	4.72	217.38
480.00	136.50	0.43	1.07	4.72	96.28
490.00	138.60	0.49	0.90	4.72	92.29
500.00	140.70	0.68	0.85	4.72	120.96
510.00	142.80	0.79	0.83	4.72	137.21
520.00	144.90	0.65	0.83	4.72	112.90
530.00	147.10	0.66	0.81	4.72	111.87
540.00	149.20	0.53	0.77	4.72	85.40
550.00	151.30	0.77	0.74	4.72	119.24
560.00	153.40	0.88	0.74	4.72	136.27
570.00	155.50	0.63	0.94	4.72	123.93
580.00	157.70	0.43	0.94	4.72	84.58
590.00	159.80	0.51	0.82	3.81	93.32
600.00	163.20	0.59	0.85	2.90	121.46
610.00	166.70	0.48	0.79	2.90	91.84
620.00	170.10	0.57	0.79	2.90	109.06
630.00	173.60	0.37	0.80	2.90	71.69
640.00	177.00	0.49	0.82	2.90	97.31
650.00	180.50	0.33	0.81	2.90	64.74
660.00	184.10	0.41	0.71	1.65	83.50
670.00	191.00	0.66	0.75	1.44	147.90
680.00	198.00	0.31	0.80	1.44	74.10
690.00	205.00	0.35	0.85	1.70	84.57
700.00	209.80	0.42	1.01	2.09	113.35
710.00	214.60	0.43	1.06	2.09	121.79
720.00	219.40	0.41	1.06	2.09	116.12
730.00	224.10	0.38	0.88	2.09	89.35
740.00	228.90	0.73	0.85	2.09	165.80
750.00	233.70	0.90	0.95	2.09	228.46
760.00	238.50	0.89	0.83	2.09	197.38
770.00	243.30	1.18	0.90	2.09	283.77
780.00	248.10	0.89	0.95	2.09	225.92
790.00	252.80	0.38	0.99	2.09	100.52
800.00	257.60	0.48	1.03	2.09	132.10

DBD* = DRY BULK DENSITY
S.Rates** = Sed.rates

TABLE C.17:3 PALEOPRODUCTIVITY DATA OF CORE CD1738

DEPTH CM	AGE KYS	C.org (%)	DBD*	S.Rates** cm/kys	PALEOPRODUCTIVITY gC-m^2/y
20.00	15.40	1.03	0.72	10.98	120.47
30.00	20.80	0.47	1.20	10.98	91.62
40.00	22.64	0.67	0.99	10.98	107.75
50.00	23.55	0.87	1.01	10.98	142.74
60.00	24.46	0.85	0.82	10.98	113.22
70.00	26.28	0.41	1.08	5.49	88.56
80.00	28.10	0.48	0.97	5.49	93.12
90.00	29.95	0.38	1.09	6.47	78.85
100.00	31.19	0.35	1.20	6.47	79.96
110.00	32.73	0.37	1.12	6.47	78.89
120.00	34.28	0.29	1.05	6.47	57.97
130.00	35.82	0.44	0.99	6.47	82.93
140.00	37.38	0.46	0.94	5.68	85.60
150.00	39.14	0.18	1.31	5.68	46.68
160.00	40.90	0.28	1.36	5.68	75.38
170.00	42.66	0.36	0.98	5.68	69.84
180.00	44.42	0.37	1.12	5.68	82.03
185.00	45.30	0.27	1.11	5.68	59.33
195.00	47.06	0.38	1.03	5.68	77.48
205.00	48.82	0.26	1.18	5.68	60.73
215.00	51.01	0.49	0.94	4.56	97.39
225.00	53.20	0.35	1.14	4.56	84.37
235.00	55.39	0.36	1.06	4.56	80.69
245.00	57.58	0.22	1.22	4.56	56.75
255.00	59.05	0.31	1.15	7.01	66.26
265.00	60.45	0.23	1.29	7.01	55.14
275.00	65.74	0.23	1.10	1.89	69.67
285.00	71.00	0.25	1.12	1.89	77.11
295.00	82.75	0.27	1.41	0.85	133.24
305.00	94.50	0.49	1.30	0.85	222.94
315.00	96.24	0.33	1.34	5.72	87.35
325.00	97.99	0.35	1.08	5.72	74.67
335.00	99.74	0.34	1.12	5.72	75.22
345.00	101.48	0.58	0.99	5.72	113.43
355.00	103.23	0.39	1.07	5.72	82.43
365.00	104.98	0.38	1.00	5.72	75.07
375.00	106.73	0.38	1.11	5.72	83.32
385.00	108.47	0.27	1.26	5.72	67.20
395.00	110.22	0.27	1.29	5.72	68.80
405.00	111.97	0.48	1.31	5.72	124.21
415.00	113.72	0.34	1.11	5.72	74.55
425.00	115.46	0.32	1.34	5.72	84.71
435.00	117.21	0.21	1.34	5.72	55.59
445.00	118.96	0.41	1.27	5.72	102.86
455.00	120.70	0.29	1.30	5.72	74.47
465.00	122.70	0.79	1.28	5.72	199.75
475.00	124.45	0.46	1.16	5.72	105.41
485.00	125.95	0.15	1.28	5.72	37.93
495.00	127.70	0.32	1.51	7.42	88.28
505.00	128.78	0.47	1.36	9.18	109.56
515.00	129.87	0.37	1.34	9.18	84.98
525.00	130.96	0.23	1.33	9.18	52.43
535.00	132.05	0.20	1.44	9.18	49.36
540.00	132.60	0.44	1.26	6.25	106.64
545.00	133.40	0.27	1.17	6.25	60.77
555.00	135.00	0.56	1.42	6.25	152.96
565.00	136.60	0.52	1.18	6.25	118.03
575.00	138.20	0.23	1.14	6.25	50.44
585.00	139.80	0.41	1.46	6.25	115.15
595.00	141.40	0.33	1.07	6.25	67.92
605.00	144.00	0.28	1.40	3.40	90.52
615.00	146.98	0.35	1.38	3.40	111.53
625.00	150.20	0.50	1.33	3.40	153.55
635.00	152.60	0.42	1.12	3.40	108.62
645.00	155.80	0.53	1.15	3.40	140.74
655.00	158.70	0.57	1.09	3.40	143.46
665.00	161.60	0.43	1.57	3.40	86.10

DBD* = DRY BULK DENSITY
S.Rates** = Sed.Rates

TABLE C.17:4 PALEOPRODUCTIVITY DATA OF CORE CD1739

DEPTH CM	AGE KY	C.org (%)	DBD*	S.Rates** cm/kys	PALEOPRODUCTIVITY $gC-m^2/y$
20.00	15.50	0.41	1.09	7.51	81.36
30.00	16.83	0.51	1.01	7.51	93.77
40.00	18.16	0.66	1.01	7.51	121.35
50.00	19.49	0.64	0.99	7.51	115.35
60.00	20.82	1.19	0.95	9.24	193.40
70.00	21.73	0.57	0.97	10.90	90.01
80.00	22.64	0.41	1.03	10.98	68.60
90.00	23.55	0.36	0.99	10.98	57.89
100.00	24.46	0.55	0.94	9.50	87.71
110.00	25.67	0.50	0.46	8.24	40.72
120.00	26.88	0.54	1.04	8.24	99.43
130.00	28.10	0.44	1.15	6.64	95.58
140.00	29.64	0.44	1.07	6.64	88.93
150.00	31.19	0.33	1.04	6.64	64.83
160.00	32.74	0.31	1.06	6.64	62.07
170.00	34.29	0.39	1.10	6.64	81.04
180.00	35.83	0.50	1.02	6.64	96.34
190.00	37.38	0.42	1.00	2.36	108.21
200.00	41.61	0.86	0.98	2.36	217.14
210.00	45.84	0.60	0.97	2.40	149.19
220.00	49.76	0.75	0.94	2.55	177.46
230.00	53.68	0.69	1.02	2.55	177.16
240.00	57.58	0.69	0.97	4.75	139.79
250.00	59.01	0.56	1.14	6.96	118.90
260.00	60.45	0.45	1.23	6.96	103.09
270.00	63.92	0.47	0.55	2.87	62.80
280.00	67.40	0.61	1.09	2.87	161.54
290.00	68.60	0.41	1.14	8.33	82.48
300.00	69.80	0.64	1.05	8.33	118.59
320.00	80.00	0.55	1.08	1.38	179.76
330.00	87.25	0.39	1.19	1.38	140.45
340.00	94.50	0.68	1.11	1.38	228.43
350.00	97.05	0.50	1.11	3.90	122.99
360.00	99.61	0.58	1.07	3.90	137.52
370.00	102.17	0.68	1.00	3.90	150.68
380.00	104.73	0.89	1.00	3.90	197.22
390.00	107.29	0.86	0.98	3.90	186.76
400.00	109.85	1.04	0.99	3.90	228.15
410.00	112.40	1.36	0.94	3.90	283.29
420.00	114.96	1.21	0.99	3.90	265.45
430.00	117.52	0.95	1.00	3.90	210.52
440.00	120.08	0.67	1.04	3.90	154.41
450.00	122.64	0.64	1.06	3.90	150.33
460.00	125.20	0.48	1.12	8.00	96.03
470.00	126.45	0.44	1.10	8.00	86.46
480.00	127.70	0.37	1.19	8.00	78.65
490.00	132.60	0.44	1.10	8.00	86.46
500.00	137.88	0.43	1.04	2.84	108.99
515.00	141.40	0.52	1.17	2.84	148.28
525.00	141.98	0.28	1.24	2.84	84.62
535.00	142.57	0.28	1.25	17.04	49.83
545.00	143.16	0.25	1.28	17.04	45.56
555.00	143.74	0.26	1.32	17.04	48.86
565.00	144.33	0.41	1.25	17.04	72.97
575.00	144.92	0.40	1.20	17.04	68.34
585.00	145.50	0.53	1.14	17.04	86.02
595.00	146.09	0.57	1.14	17.04	92.52
605.00	146.68	0.72	1.10	17.04	112.76
615.00	147.26	0.58	1.13	17.04	93.31
625.00	147.85	0.70	1.17	17.04	116.61
635.00	148.44	0.74	1.12	17.04	118.00
645.00	149.00	0.74	1.20	17.04	126.43
655.00	149.61	0.63	1.14	17.04	102.25
665.00	150.20	0.72	1.06	17.04	108.66
675.00	150.80	0.93	1.00	16.66	133.31
685.00	151.40	0.48	1.16	16.66	79.81
695.00	152.00	0.43	1.18	16.66	72.73
705.00	152.60	0.20	1.12	16.66	32.11
715.00	158.20	0.30	1.27	16.66	54.61
725.00	160.60	0.36	1.12	16.66	57.80
735.00	163.00	0.24	1.28	4.16	66.77
745.00	164.48	0.40	1.08	4.16	93.89
755.00	166.66	0.41	1.15	4.16	102.48
765.00	167.80	0.43	1.00	4.16	93.46

DBD* = DRY BULK DENSITY
S.Rates** = Sed.Rates

ACKNOWLEDGEMENTS

I take this opportunity to thank all those numerous well wishers and friends who have been a source of encouragement during the last three years. It is God Almighty who has bestowed his special kindness and given strength and health to complete this work.

It is impossible in a few words to describe the debt I owe to Dr N B Price. This work is in fact a result of his conscientious supervision and enormous encouragement, at every turn. I particularly acknowledge his comments during writing and long discussions.

Frequently, I have benefited from the advice and discussion of Dr G B Shimmield and I wish to express my gratitude for kindly allowing me to use his data of ODP Cores.

I am fortunate enough to carry out my research work at the Grant Institute of Geology, Edinburgh, where I had the best time of my life. During this period I had a great help at various stages from various people. Thanks are due to Dr Godfrey Fitton and Mrs Doreen James for XRF analysis. I would like to thank Mr G R Angell for XRD analysis and Mr Mike Saunders for wet chemical analysis.

I am very grateful to Dr T F Pederson of the Department of Oceanography, U.B.C. Canada for $\delta^{13}C$ analyses. Thanks are due to the technical staff of the Soil Science Department in the School of Agriculture for Nitrogen analysis.

I am thankful to Dr G S Quraishee, Director General, NIO Pakistan, without whose active inspiration I would never have got the chance to continue this work.

The British Council is gratefully acknowledged for the grant and support in completing this research work.

I enjoyed the great company of my research colleagues and I am highly obliged to my Attic friends for their reading and comments to improve the style of writing. I am especially grateful to Miss Claire Linklater, who has been reading the manuscript. Thanks are also due to Dr Shi Ping and Mr Jon Bull for their help in using the computer.

I am indebted to Mr Gregory Jones for the arduous task of proof reading. I highly acknowledge the efficiency and patience of Mrs Helena Jack and Mrs Denise Wilson, who typed this thesis with great care.

I acknowledge my debt to my brothers Mr Mazhar Ali Khan and Mr Azhar Ali Khan for their early support in making my career.

BIBLIOGRAPHY

Ackerman, F; 1980. A procedure for correcting the grain size effect in heavy metal analysis of esturine and coastal sediments. Technol.Lett;1. pp.518-527.

Ackermann, S.A; Cox, S.K; 1982. The Saudi Arabian heat low: aerosol distribution and thermodynamics structure . Journal of Geophys.Res. Vol.87:No.C11. pp 8991-9002.

Ackermann, S.A; Cox, S.K; 1988. Dust outbreaks associated with the southwest monsoon region. Meteorology and Atmospheric Physics. In press.

Ahmed, S.S; 1969. Tertiary Geology of Part of south Makran, Baluchistan . West Pakistan . Bull.Am.Assoc.Petrol.Geol. Vol. 53. pp.1480-1499.

Aller, R.C. 1980. Diagenetic processes near the sediment water interface of LIS. I decomposition and nutrient element geochemistry (S.N.P). Adv.geophys. 22, pp.237-350.

Altabet, M.A; Deuser, W.G; 1985. Seasonal variation in natural abundance of $\delta^{15}N$ in particles sinking to the deep Sargasso sea. Nature. Vol.315. pp.218-219.

Altabet, M.A; MaCarthy, J.J; 1985. Temporal and spatial variations in the natural abundance of $\delta^{15}N$ in PON from a warm core ring. Deep Sea Res. Vol.32. pp.755-772.

Altabet, M.A; MaCarthy, J.J; 1986. Vertical patterns in $\delta^{15}N$ natural abundance in PON from the surface waters of warm-core rings. J.Mar.Res. Vol.44. pp.185-201.

Anderson, J.J; Okubo, A; Robbins; A.S; Richards, F.A; 1982. A model for nitrite distributions in oceanic Oxygen minimum zones. Deep Sea Res. Vol. 29A: pp.1113-1140.

Arrhenius, G; 1952. Sediment cores from the East Pacific. Swedish Deep Sea Expedition Report. No.5, Gotenberg, pp. 227.

Arrhenius, G; 1963. Pelagic sediments . in: M.N.Hill.(ed), The Sea. Vol.3. pp.655-727. Wiley.London.

Aston, S.R; Chester, R; Johnson, L.R; Padgham, R.C; 1973. Eolian dust from the lower atmosphere of the eastern Atlantic and Indian ocean, China sea and the sea of Japan . Marine Geology. Vol.14. pp.15-28.

Bader, R.G; 1955. Carbon and Nitrogen relations . In: surface and subsurface marine sediments. Geochim.Cosmochim.Acta. Vol.7. pp.205-211.

Baily, E.H; 1981. Geological map of Muscat-Ibra area ,Sultanate of Oman .Pocket map, J.Geophys.Res. Vol.86. No.B4.

Barker, P.F; 1966. A reconnaissance survey of the Murray ridge. Philosophical Transactions of the Royal Society of London, Series A, 259. pp.187-197.

Beer, J.R; 1966. Studies in the chemical composition of major zooplankton groups in the Sargasso sea off Bermuda. Limnology.Oceanography. Vol.11. pp.520-528.

Behrens, E.W.; Land, L.S.; 1972. Subtidal Holocene dolomite, Baffin Bay, Texas. J.Sediment.Petrol. Vol.42. pp.155.

Berger, W.H; 1970. Planktonic foraminifera : Selective solution and the lysocline . Marine Geology. Vol.8. pp.111-138.

Berger, W.H; 1976. Biogenous deep_sea sediments : production, preservation and interpretation . In: J.P.Riley and R.Chestre (eds), Chemical Oceanogragrphy. Vol.5. Academic press, New york, pp.265-374.

Berner, R.A; 1971. Principles of Chemical Sedimentology. McGraw-Hill, New York, p.240.

Berner, R.A; 1975. Diagenetic models of dissolved species in the interstitial waters of compacting sediments . Am.Journal of Science. Vol.275. pp.88-96.

Berner, R.A; 1979. A new look at biogenous material in deep sea sediments. Ambio. Sp.Rep. Vol.6. pp.5-10.

Biscay, P.E; 1965. Mineralogy and sedimentation of recent deep sea clay in the Atlantic Ocean and adjacent seas and Oceans. Geol.Soc.Amer.Bull. Vol.76. pp.803-832.

Bischoff, J.L; Heath, G.R; Leinen, M; 1979. Geochemistry of deep sea sediments from the Pacific manganese nodule province: Domes sites A,B,and C. Bischoff and Piper;(eds). in Marine Geology and oceanography of the Pacific Manganese Nodule Province. Plenum. New York. pp.397-473.

Bishop, J.K.B; 1988. The barite-opal-organic carbon association in oceanic particulate matter. Nature. Vol.332. pp.341-343.

Blank, M; Leinen, M; Prospero, J.M; 1985. Major Asian eolian inputs indicated by the mineralogy of aerosols and sediments in the western North Pacific: Nature. Vol. 314. pp.84

Bordovskiy, O.K; 1965a. Sources of organic matter in marine basins. Marine Geol. Vol.3. pp.5-31.

Bordovskiy, O.K; 1965b. Transformation and diagenesis of organic matter in sediments. Marine Geol. Vol.3. pp.83-114.

Bordovskiy, O.K; 1965c. Accumulation of Organic matter in bottom sediments. Marine Geol. Vol.3. pp.33-82

Bostrom, K; Peterson, M.N.A; Joenssu, O; Fisher, D.E; 1969. Aluminium-poor ferromanganoan sediments on active ocean ridges. J.Geophys.Res. Vol.74. pp.3261-3270.

Bostrom, K; Joenssu, O; Valdes, S; Riera, M; 1972. Geochemical history of South Atlantic ocean sediments since late cretaceous . Marine Geology. Vol.12. pp.85-121.

Bostrom, K; Jonessu, O; Moore, C; Bostrom, B; Dalziel, M; Horowitz, A; 1973. Geochemistry of barium in pelagic sediments. Lithos. Vol.6. pp.159-174.

Bostrom, K; Joenssu, O; Brohm, I; 1974. Plankton: its chemical composition and its significance as a source of pelagic sediments. Chemical Geology. Vol.14. pp.255-271.

Bowen, H.J.M; 1966. Trace elements in biochemistry. Academic Press, pp.241.

Bowles, F.A; 1975. Paleoclimatic significance of Quartz/Illite variation in cores from the Eastern Equatorial North Atlantic. Quaternary Research. Vol.5. pp.225-235.

Boyle, E.A; 1983. Chemical accumulation variations under the Peru Current during the past 130,000 years. J.Geophys.Res. Vol.88. pp.7667-7680.

Boyle, E.A; Keigwin, L.D; 1985. Comparison of Atlantic and Pacific paleochemical records for the last 215,000 years: changes in deep ocean circulation and chemical inventories. Earth and Planetary Science Letters. Vol.76. pp.135-150.

Bremner, J.M; Tabatabai, M.A; 1973. Nitrogen-15 enrichment of soils and soil derived nitrate. J.Environ.Qual. Vol.2. pp.363-365.

Brockman, C; Fahrabach, E; Huyer, A; Smith, R.L; 1980. The poleward undercurrent along the Peru coast: 5° to 15°S. Deep sea Research. Vol.27A. pp.847-856.

Broecker, W.S; Turekian, K.K; Hazeen, B.C; 1958. The relations of deep sea sedimentation rates to variations in climate. Am.J.Sci. Vol.256. pp.503-517.

Broecker, W.S; VanDok, J; 1970. Insolation changes, ice volumes and the $\delta^{18}O$ record in deep Sea sediments. Review.Geoph.Space Phys. 8, 169-191.

Broecker, W.S; Peng, T.H; 1982. Tracers in the Sea. Eldigio, Palisades, 690 pp.

Bromberger, S.H; Hayes, J.B; 1956. Quantitative determination of calcite-dolomite-apatite mixtures by X-ray diffraction. Journal of sedimentary Petrology. Vol.36. pp.358-361.

Brongersma-Sanders, M; 1965. Metals of Kupferschiefer supplied by normal seawater. Geol.Rund. Vol.55. pp.365-375.

Brongersma-Sanders, M; 1966. Origin of trace metal enrichment in bituminous shales. In: G.D.Hobson and G.C.Spears (eds); Advances in organic geochemistry . Pergman Press. London. pp. 231-236.

Brongersma-Sanders, M; 1967. Barium in pelagic sediments and in diatoms, Koninklijke Nederlandsche Akademie Van WetenSchappen, Series B, 70, pp.93-99.

Bruce, J.G; 1974. Some details of upwelling off the Somali and Arabian Coasts. Journal of Marine Research. Vol.32. pp.419-423.

Brumsack, H.J; 1980. Geochemistry of cretaceous black shales from the Atlantic ocean (DSDP legs 11,14,36,41). Chemical Geology. Vol.31. pp.1-25.

Bryson, R.A; Swain, A.M; 1981. Holocene Variations of Monsoon rainfall in Rajasthan. Quat.Res. Vol.16. pp.135-145.

Bush, W.H; Keller, G.H; 1981. The physical properties of Peru-Chile continental margin sediments : the influence of coastal upwelling on sediment properties. Journal of Sedimentary Petrology. Vol.51. pp.705-719.

Butzer, K.W; Isacc, G.L; Richardson, J.L; Wash-Bourn-Kamau, C; 1972. Radiocarbon dating of East African lake levels. Science. Vol.175. pp.1069-1076.

Calvert, S.E; 1966. Accumulation of diatomaceous silica in the sediments of the Gulf of California. Geol.Soc.Am.Bull. Vol.77. pp.569-596.

Calvert, S.E; 1968. Silica balance in the ocean and diagenesis. Nature. Vol.219. pp.919-920.

Calvert, S.E; 1976. The minearlogy and Geochemisrty of nearshore sediments, in: Chemical Oceanography, 2nd ed, J.P.Riley and R. Chester, (eds) Academic Press, London, 6: pp.187-280.

Calvert, S.E; Morris, A.J; 1977. Geochemical studies of organic rich sediments from the Namibian shelf. II. Metal-organic associations. in: M.Angel.(ed). A Vovage of Discovery . Pergman Press. London . pp.580-667.

Calvert, S.E; Mukherjee, S; Morris, R.J; 1985. Trace metals in humic and fulvic acids from modern organic rich sediments. Oceanol.Acta. Vol.8. pp.167-173.

Calvert, S.E; Price, N.B; 1970. Minor metal contents of recent Organic rich sediments off South West Africa, Nature. Vol.227. pp.593-595.

Calvert, S.E; Price, N.B; 1971 . Recent sediments of the South West African Shelf, in: F.M. Delany, (ed); Geology of the East Atlantic Continental Margin . Institute of Geological Science Report 70/16, pp.171-185.

Calvert, S.E; Price, N.B; 1983. Geochemistry of Namibian shelf sediments. Suess, E and Theide, J; (eds). in: Coastal upwelling (Part A), Pleneum Publishing corporation.

Carroll, D; 1958. Role of clay minerals in the transportation of iron. Geochim.Cosmocim.Acta. Vol.14. pp.1-27.

Chan, L.H; Drummond, D; Edmond, J.M; Grant, B; 1977. On the barium data of the Atlantic Geosecs expedition. Deep sea Research. Vol.24. pp.613.

Chaudhuri, S; Cullers, R.L; 1979. The distribution of rare earth elements in deeply burried Gulf coast sediments. Chem.Geol. Vol.24. pp.327-338.

Chen, F.H; 1986. Analysis of a major dust outbreak over the Arabian Sea during Monex. Thesis at the University of Wisconsin- Madison. Unpublished

Chester, R; Aston, S.R; 1976. The geochemistry of deep sea sediments. in: J.P.Riley and R.Chester (eds). Chemical Oceanography. Vol.6. Academic Press. London. pp.281-390.

Chester, R; Sharples, E.J; Sanders, G.S; 1985. The concentrations of particulate Aluminium and clay minerals in Aerosols from the northern Arabian sea. J.Sed.Pet. Vol.55. No.1. pp.37-41.

Chmelik, F.B; 1967. Electro-Osmotic core cutting. Marine Geology. Vol.5. pp.321-325.

Church, T.M; 1970. Marine Barite . Unpublished. Ph.D.Thesis. University of California.

Church, T.M; 1979. Marine Barite. Marine Minerals, Min. Soc. Am. Short Course Notes. Vol.6

Clemens, S.C; Prell, W.L; Howard, W.R; 1987. Retrospective dry bulk density estimates from southeast Indian ocean sediments- Comparison of water loss and Chloride-ion methods. Marine Geology. Vol.76. pp.57-69.

CLIMAP Project Members; 1976. Seasonal reconstruction of the earth Science. Vol.191. pp.1131-1137.

Cline, J.D; Kaplan, I.R; 1975. Isotopic fractionation of dissolved nitrate during denitrification in the eastern tropical north Pacific ocean. Marine.Chemistry. Vol.3. pp.271-299.

Cline, R.M; Hays, J.D; 1976. Investigation of Late Quaternary paleooceanography and paleoclimatology. Geol.Soc.Am. Mem.145.

COHMAP; 1988. Climatic changes of the last 18,000 years: observations and model simulations. Science. Vol.241. pp.1043-1052.

Corliss, B.H; Martinson, G.D; Keffer, T; 1986. Late Quaternary deep ocean circulation. Geol.Soc.Am.Bull. Vol.97. pp.1106-1121.

Coude-Gaussen, G; 1984. Le cycle des poussieres eoliennes desertiques actualles et la sedimentation des loess peridesertiques quarternaires. Bull.Centre Rech. Explor. Product. Elf-Aquitaine 8, pp.167-182.

Cullers, R.L; Chaudhuri, S; Arnold, B; Lee, M; Wolf, C.W; 1975. Rare earth distribution in clays minerals and in the clay-sized fraction of the Lower Permian Havensville and Eskridge shale of Kansas and Oklahoma. Geochim.Cosmochim.Acta. Vol.39. pp.1691-1703.

Curtis, C.D; 1966. The incorporation of soluble Organic matter in to sediments and its effect on trace element assemblage, in: G.D. Hobson and M.C. Louis, (eds); Advances in Organic Geochemistry, ; Pergaman Press, 1-13.

Curry, W.B; Lohman, G.P; 1985. Carbon deposition rates and deep water residence time in the equatorial Atlantic ocean throughout the last 160,000 years . In: E.T.Sundquist and W.S.Broecker (eds) The Carbon cycle and Atmospheric Co2: Natural variations Archean to Present. Am.Geophys.Union. Washington.

Dansgaard, W; Duplessy, J.C; 1981. The Emian interglacial and its termination. Boreas. vol.10. pp.219-229.

Degens, E.T; 1969. Biogeochemistry of stable carbon isotopes, in: G.Eglinton and M.T.J.Murphy (eds); Organic geochemistry. Speringer-Verlag. New York. pp.304-328.

Degens, E.T; Ross; D.A; 1974. The Black sea- Geology,Chemistry and Biology. (eds). Am.Ass.Pet.Geol. Mem.No.20. pp.633.

Dehairs, F; Chesselt, R; Jedwab, J; 1980. Discrete suspended particles of barite and the barium cycle in the open ocean. Earth Planet.Sci.Lett. Vol.61. pp.257-271.

Demaster, D; 1981. The supply and accumulation of silica in the marine environment. Geochimica Cosmochimica Acta. Vol.45. pp.1715-1732.

Deuser, W.G; Ross, E.H; Mlodzinska, Z.J; 1978. Evidence for and rate of denitrification in the Arabian sea. Deep-sea Res. Vol.25. pp.431-445.

Dobbie, K.E; 1988. The determination of the biogenic silica content of sediments from the Arabian sea off the coast of southern Oman. B.sc(Hons) . Unpublished report. Edinburgh University.

Dougen, W.K; Wilson, A.L; 1974. The absorptiometric determination of Aluminium in Water. Analyst. Vol.99. pp.413-430.

Dugdale, R.C; Geoering, J.J; Ryther, J.H; 1964. High nitrogen fixation rates in the Sargasso sea and the Arabian Sea. Limnolgy and Oceanography. Vol.9. pp.507-510.

Duing, W; Schnwill; 1967. Ausbreitung and Vermischung des Salzeseiche Wassers aus dem Roten Meer und aus dem Persischen Golf."Meteor" Forschungsergebniss, A,3: pp.44-66. Borntrager,Berlin.

Duplessy, J.C; 1982. Glacial to Interglacial contrasts in the northern Indian Ocean. Nature. London. Vol.295. pp.494-498.

Duplessy, J.C; Shackleton, N.J; 1985. Response of global deep water circulation to Earths climatic change 135,000-107,000 years ago. Nature. Vol.316. pp.500-506.

Dymond, J; Lyle, M; 1985. Flux Comparisions between sediments and sediment traps in the eastern tropical Pacific: Implications for atmospheric Co2 variations in the Pleistocene . Limnology Oceanography. Vol.30. pp.699-712.

Dypvik, H.; Brunfelt, A.O; 1976. Rare-earth elements in lower Palaeozoic epicontinental and eugeosynclinal sediments from the Oslo and Tronheim regions. Sedimentology. Vol.23. pp.363-378.

Eggiman, D.W; Manheim, F.T; Betzer, P.R; 1980. Dissolution and analysis of amorphous silica in marine sediments. J.Sed.Pet. Vol.50.no 1. pp.215-225.

Elderfield, H; Trusedale, V; 1980. On the nature of Iodine in seawater. Earth Planet.Sci.Lett. Vol.50. pp.105-114.

Elderfield, H; McCaffrey, R.J; Luedke, N; Bender, M; Truesdale, V.M; 1981. Chemical diagenesis in Narragasett Bay sediments. Am.Journal.Science. Vol.281. pp.1021-1053.

El-Wakeel, S.K; Riley, J.P; 1961. Chemical and mineralogical studies of deep sea sediments. Geochim.Cosmochim.Acta. Vol.25. pp.110-146.

Emery, K.O; 1956. Sediments and water of the Persian Gulf. A.A.P.G.Bull. Vol.40. pp.2354-2383.

Emery, K.O; 1960. The sea off southern california, John Wiley, New York. 366 pp.

Emiliani, C; 1955a. Pleistocene temperatures, Journal of Geology. Vol.63. pp.538-578.

Emiliani, C; 1955b. Mineralogical and chemical composition of the tests of certain pelagic Foraminifera. Micropalentology. Vol.1.No.4. pp.377-380.

Emiliani, C; 1972. Quaternary paleotemperatures and the duration of the high temperature intervals. Science. Vol.178. pp.398-401.

Erlank, A.J; Smith, H,S; Marchant, J.N; Cardoso, M.P; Ahrens; L.H; 1978. Zirconium abundance in common sediments and sedimentary rocks. In: Wedepohl etal.(eds). Handbook of Geochemistry II/4. Springer Verlag. Heidelberg. New York.

Fairbridge, R.W; 1961. Eustatic changes in sea level. In: Physics and Chemistry of the earth. vol.4.

Farhaudi, G; Karig, D.E; 1977. Makran of Iran and Pakistan as an active arc system. Geology. Vol.5. pp.664-668.

Finney, B.P; 1986. Paeoclimatic influence on sedimentation and manganse nodule growth during the past 400,000 years at MANOP site H (Eastern equatorial Pacific) . Ph.D. Thesis, Oregon state University.

Fischer, K; 1983. Particle fluxes in the eastern tropical pacific ocean -source and processes. Ph.D. Thesis, Oregon state University.

Fleming, R.H; 1940. The composition of plankton and units for reporting population and production. Proc. Sixth Pacific Sci. Cong. Calif. 3. pp.535-540.

Foda, M.A; Khalaf, F.I; Kadi-Al, A.S; 1985. Estimation of dust fallout rates in the northern Arabian Gulf. Sedimentology. Vol.32. pp.595-603.

Folger, D.W; 1970. Wind transport of land-derived minerogenic,biogenic and industrial matter over the north Atlantic. Deep sea Research. Vol.17. pp.337-352.

Fontugne, M.N; Duplessy, J.C; 1978. Carbon isotope ratio of marine plankton related to surface water masses. Earth Planet.Sci.Lett. Vol.41. pp.365-371.

Fontugne, M.N; Duplessy, J.C; 1981. Organic isotope fractionation by marine plankton in the temperature range -1° to 31° C. Oceanol. Acta. Vol.4. pp.85-90.

Fontugne, M.N; Duplessy, J.C; 1986. Variation of the monsoon regime during the upper Quaternary: Evidence from Carbon isotopic records of Organic matter in North Indian Ocean sediment core. Paleogeography. Paleoclimatology. paleoecology. Vol.56. pp.69-88.

Fontugne, M.N; Jouanneau, J.M; 1981. La composition isotopique du carbon organique des matieres en suspension dans lestuaire de la Gironde. Application a letude de la distribution du plomb et du Zinc particulaire. C.R.Accad.Sci. Paris. II, 293 (5). pp.389-392.

Food and Agriculture Organisation Department of Fisheries, 1972. Atlas of the living resources of the sea. Food and Agricultural Organisation of the United Nations, Rome.

Foucault, A; Stanley; D.J; 1989. Late Quaternary Paleoclimatic oscillations in East Africa recorded by heavy minerals in the Nile delta. Nature. Vol.339.pp.44-46.

Fowler, S.W.; 1977. Trace elements in zooplankton particulate products. Nature. Vol.269. pp.51-53.

Füchtbauer, H; Reineck, H.E; 1963. Porositt und verdichtung rezenter, mariner sedimente. Sedimentology. Vol.2. pp.294-306.

Fütterer, D.K; 1981. The modern upwelling record off northwest Africa. In: Thiede and Suess (eds). Coastal upwelling. Part B: sedimentary records of Ancient coastal upwelling. Plenum Pres. New york.

Gardner, R.M; Hays, J.D; 1976. Response of sea surface temperature and circulation to global climatic cahnges during the past 200,000 years in the Eastern equatorial Atlantic ocean. in Late Quaternary Palaeooceanography and Palaeoclimatology . Geol.Soc.Am. Memoir.145.

Gasse, F; Street; F.A; 1978. Late Quaternary lake level fluctuations and environments of the Northeastern Rift Valley and Afar Region (Ethiopia and Djibouti). Palaeogeography.paleoclimatol.paleoecol. Vol.24. pp.279-325.

Gearing, P; Plucker, F.E; Parker, P.L; 1977. Organic carbon stable isotope ratios of continental margin sediments. Marine Chemistry. Vol.5. pp.251-266.

Goldberg, E.D; Arrhenius, G.O.S; 1958. Chemistry of Pacific Pelagic sediments. Geochem. Cosm.Acta. Vol.13. pp.153-212.

Goldberg, E.D; Griffin, J.J; 1969. The sediments of the northern Indian Ocean. Deep sea Res. Vol.17. pp.513-537.

Goldschmidt, V.M; 1954. Geochemistry. Muir,A. (ed). Claredon Press. Oxford. pp.730.

Gordon, D.C; 1971. Distribution of organic carbon and nitrogen at an oceanic station in central Pacific. Deep Sea Research. Vol.18. pp.1127-1134.

Grigoryev, A.A; Kondratyev, K.J; 1980. Atmospheric dust observed from space . Part I- analysis of pictures. WMO BULLETIN. Vol.29. pp.250-255.

Gross, M.G; Carey, A.G; Fowler, G.A; Kulm, L.D; 1972. Distribution of organic carbon in surface sediment, northeast Pacific ocean. in: Pruter and Alverson (eds), Bioenvironmental studies. University of Washington Press. Seattle. pp.254-264.

Grundmanis, V; Murray, J.W; 1982. Aerobic respiration in pelagic marine sediments . Geochim.Cosmochim.Acta. Vol.46. pp.1101-1120.

Gupta, S.K; 1972. Chronology of the raised beaches and inland coral reefs of the Saurashtra coast. Jour.Geol. vol.84. pp.357-361.

Gupta, S.k; and Amin, B.S; 1974. IO/U ages of corals from Saurashtra coast. Marine Geology. Vol.16. pp.M79-M83.

Harvey, A; 1980. A study of the chemistry of I and Br in marine sediments. Marine Chemistry. Vol.8. pp.237-332.

Hastenrath, S; Lamb, P.J; 1980. On the heat budget of hydrosphere and atmosphere in the indian Ocean. J.Physical Oceanography. Vol.10. pp.694-708.

Haskin, M.A ; Haskin, L.A; 1966. Rare earth elements in European shales : a redetermination. Science. Vol.154. pp.507-509.

Haskin, L.A; Wildeman, T.R, Frey, F.A; Collns, K.A; Keedy, C.R; Haskin, M.A; 1966. Rare earths in sediments. J.Geophys.Res. Vol.71. pp.6091-6105.

Hays, J.D; Saito, T; Opdyke, N.D; Burkle, L.M; 1969. Pliocene-Pleistocene sediments of the equatorial Pacific : their palaeomagnetic,biostratigraphic and climatic record . Geol.Soc.Am.Bull. Vol.80. pp.1481-1514.

Hays, J.D; Imbrie, J; Shackleton, N.J; 1976. Variations in the Earths orbit: pacemaker of the ice ages. Science. Vol.194. pp.1121-1132.

Heath, G.R; 1969. Mineralogy of Cenozoic deep sea sediments from the equatorial Pacific ocean. Geol.Soc.Am.Bull. Vol.80. pp.1997-2018.

Heath, G.R; 1976. Dissolved silicaa in deep sea sediments. Soc.Econ.Paleontol.Mineral. Spec. Publ. No.20. pp.77-93.

Hedges, J.I; Clark, W.A; Quay, P.D; Richey, J.E; Devol, A.H; Sautos, U.M; 1986a. Composition and fluxes of particulate organic material in the Amazon River. Limnol.Oceanogr. Vol.31. pp.717-738.

Hedges, J.I; Ertel, J.R; Quay, P.D; Grootes, P.M; Richey, J.E; Devol, A.H; Farewell, G.W; Schmidt, F.W; Salati, E; 1986b. Organic Carbon^{14} in the Amazon River system. Science. Vol.231. pp.1129-1131.

Hedges, J.I; Parker, P.L; 1976. Land derived organic matter in surface sediments from the Gulf of Mexico. Geochim.Cosmochim.Acta. Vol.40. pp.1019-1029.

Hill, P.A; Parker, A; 1970. Tin and Zirconium in the sediments around the British Isles: A preliminary reconnaissance. Econ.Geol. Vol.65. pp.409-416.

Hirst, D.M; 1962. The geochemistry of modern sediments from the Gulf of Paria- II The location and distribution of trace elements. Geochim.Cosmochim.Acta. Vol.26. pp.1147-1187.

Hoering, T.C; 1955. Variations of nitrogen-15 abundance in naturally occuring substances. Science. Vol.122. pp.1233-1234.

Hunt, C.D; 1981. Regulation of sedimentary cation exchange capacity by organic matter. Chem.Geology. Vol.34. pp.131-149.

Hunt, J.M; 1970. The significance of carbon isotope variations in marine sediments. in: Hobson and Speers (eds). Advances in Organic Chemistry. Pergmon,Oxford. pp.27-35.

Hurd, D.C; 1973. Interactions of biogenic opal, sediment and seawater in the central equatorial Pacific. Geochim.Cosmochim.Acta. Vol.37. pp.2257-2282.

Idso, S.B; 1976. Dust storms . Scientific American. Vol.235.(4) pp.108-114.

Imbrie, J; Hayes, J.D; Martinson, D.G; McIntyre, A; Mix, A.C; Morley, J.J; Pisias, N.G; Prell, W.L; Shackleton, N.J; 1984. The Orbital theory of PleistoceneClimate : Support from a revised chronology of the Marine $\delta^{18}O$ record . In: Milankovitch and Climate (I). Berger, A; etal (eds).

Invanenkov, V.N; Gubin, F.A; 1960. Water masses and hydrochemistry of the northern parts of the Indian ocean. Trudy Instituta Okeanologii Akademiya nauk USSR. 64.pp.28-143.

Jansen, J.H.F; Van Der Gasst, S.J; 1988. Accumulation of opal in quaternary sediments of the Zair Deep Sea Fan (Northeastern Angola basin). Marine Geology. Vol.83. pp.1-7.

Jipa, D; Kidd, R.B; 1974. Sedimentation of coarser grained interbeds in the Arabian Sea and sedimentation process of the Indus Cone. In: Whitmarsh, R.B; etal; (eds), Initial reports of the Deep Sea Drilling ProJect. Vol.23. pp.471-495.

Jones, A.G; 1961. Reconnaissance geology of part of west Pakistn: a Colombo plan cooperative Project. Report by Govt of Canada for govt of Pakistan . Toronto. 550 pp.

Keeny, D.R; Bremner, J.M; 1967. Determination and isotope ratio analysis of different forms of nitrogen in soils 7-urea. Soil.Sci.Soc.Amer.Proc. Vol.31. pp.317-321.

Khalaf, F; Al-Hashash, M.Z; 1983. Aeolian sedimentation in the north-western part of the Arabian Gulf . Journal of Arid Environments. Vol.6. pp.319-332.

Koblentz-Mishke, O,J; Volkovinsky, V.V; Kabonova, J.G; 1970. Plankton primary production of the world ocean. in: W.S. Wooster (ed) . Scientific Exploration of the south Pacific . Washington.

Koczy, F.F; 1951. Factor determining the elemet concentration in sediments . Geochim.Cosmochim.Acta. Vol.1. pp.73-85.

Kohl, D.H; Shearer, G; Commoner, B; 1971. Fertiliser nitrogen: contribution of No3 in surface waters in a corn belt watershed. Science. Vol.174. pp.1331-1334.

Kolla. V; Be, A.W.H; Biscay, P.E; 1976. Calcium carbonate distribution in the surface sediments of the Indian Ocean. Journal of Geophysical Research. Vol.3. pp.279-288

Kolla, V; Biscay, P.E; 1977. Distribution and origin of quartz in the sediments of the Indian Ocean. Journal of Sed.Pet. Vol.47.N0.2, pp.642-649.

Kolla, V; Coumes, F; 1984. Indus Fan, Indian Ocean. In: Bouma, A.H and etal; Submarine fans and related turbidite systems. Springer Verlag.

Kolla, V; Kostecki, J.A; Robinson, F; Biscay, P.E; Ray, P.K; 1981a. Distributions and origins of clay minerals and Quartz in surface sediments of the Arabian sea. J.Sed.Pet. Vol.51. pp.563-569.

Kolla, V; Ray, P.K; Kostecki, J.A; 1981b. Surfacial sediments of the Arabian sea. Marine Geology. Vol.41. pp.183-204.

Krauskopf, K.B; 1979. Introduction to Geochemistry. McGraw-Hill. pp.617

Krey, J; Babenerd, B ; 1976. Phytoplankton production. Atlas of the International Indian Ocean Expedition. University of Kiel, Institute of fur Meereskunde.

Krinsley, D. 1960. Trace elements in the tests of planktonic forimineferа. Micropaleontology. Vol.6. pp.297-300.

Krinsley, D. 1960. Trace elements in the tests of planktonic forimineferа. Micropaleontology. Vol.6. pp.297-300.

Krishnamurti, T.N; Greiman, P; Ramanathan, Y; Pasch, R; Ardany, P; 1980. Quick look summer monex atlas, Part 1,2,3, FSU Report, No.80-4.

Krissek, L.A; Scheidegger, K.F; Kulm, L.D ; 1980. Surface sediments of the Peru-Chile continental margin and the Nazca plate. Geol.Soc.Amer.Bull. Vol.91. pp.321-331.

Krissek, L.A; Scheidegger, K.F; 1981. Environmental controls on sediment texture and composition in low oxygen zone off Peru and oregon. in: Theide and Suess (eds). Coastal Upwelling. Pelenum. New york.

Kutzbach, J.E; 1981. Monsoon climate of the Early Holocene; Climate Experiment with the earths Orbital Parameters for 9000 year ago. Science. Vol.214. pp.59-61.

Kutzbach, J.E; Guetter, P.J; 1986. The influence of cahanging orbital parameters and surface boundary conditions on climate simulation for the past 18000 years . Journal of Atmospheric science. Vol.39.No.6. pp.1177-1187.

Kutzbach, J.E; Street, F.A; 1985. Milinkovitch forcing of fluctuations in the level of tropical lakes from 18 to zero kyr BP, Nature. Vol.317. pp.130-134.

Kuzmenko, L.V; 1973. Primary production of the northern Arabian Sea. Oceanology. Vol.13. pp.251-256.

Lamb, H.H; 1966. The changing climate, Methven; London.

Lamb, H.H; Woodroffe; 1970. Atmospheric circulation during the last Ice Age . Quat.Research. Vol.1. pp.29-58.

Landergren, S; 1964. On the geochemistry of deep sea sediments . In Reports of the Swedish Deep sea Expidition. Vol.X.Special investigations. No.5. pp.154.

Lee, C; Wakeham, S.G; 1988. Organic matter in seawater. In: J.P.Riley and R.Chester (eds). Chemical Oceanography. Vol.9.

Leinen, M; Cwienk, D; Heath, G.R; 1986. Distribution of biogenic silica and quartz in recent deep sea sediments. Geology. Vol.1 (3). pp.199-203.

Leinen, M; Heath, R; 1981. Sedimentary indicators of atmospheric activity in the northern hemisphere during the cenozoic . Palaeoecology. Vol.36. pp.1-21.

Leroi-Gourhan, A; 1974. Analysis Polliniques, Pre-Historie et variations Climatiques Quaternaires. Colloques Internationaux du CRNS 219. pp.66.

Li, Y.H; Chan; L.H; 1979; Desorption of Ba and 266 Ra from river-borne sediments in the Hudson estury. Earth Planet.Sci.Lett. Vol.43. pp.343-350.

Listizin, A.P; 1972. Sedimentation in the world ocean. Soc.Econ.Paleontol.Mineral. Spec.Publ.No.17. pp.218 pp.

Longhurst, A.R; 1981. Analysis of marine ecosystem, Academic press. London. pp.741.

Lumsden, D.N; 1979. Discrepency between thin section and X-ray estimates of dolomite in limestone. J.Sed.Petrol. Vol.49. pp.429-436.

Luz, B; Shackleton, N.J; 1975. CaCo3 solution in the tropical east Pacific during the past 130,000 years . In: W.V. Silter, A.W.H. Be and W.H.Berger (eds) Dissolution of deep sea carbonates. Cushman Found.Foraminifer.Res. Spec.Publ.No.13. pp.142-150.

Lyle, M.W; Dymond, J; 1976. Metal accumulation rates in the south east Pacific - errors introduced from assumed bulk densities. Earth and Planetary Sci.Letters. Vol.30. pp.164-168.

Lyle, M; Murray, D.W; Finney, B.P; Dymond, J; Robbins, J.M; Brooksforce, K; 1988. The records of late Pleistocene biogenic sedimentation in the eastern tropical pacific ocean. Paleooceanography. Vol.E3.No.1. pp.39-59.

Macko, S.A; Entzeroth, L; Parker, P.L; 1984. Regional Differences in Nitrogen and Carbon Isotopes on the continental shelf of the Gulf of Mexico. Naturwissanschaften. Vol.71. pp.374-375.

Malcolm, S.J; Price, N.B; 1984. The behaviour of iodine and bromine in esturine surface sediments. Marine Chemistry. Vol.15. pp.263-271.

Mangerud, J; Sonstegaard, E; Sejrup, H.P; 1979. Correlation of the Emian (interglacial) stage and the deep sea Oxygen isotope stratigraphy. Nature. Vol.277. pp.189-192.

Marching, V; 1974. Zur Geochemie rezenter sedimente des Indischen Ozeans II, Arabisches Meer, afrikanischer Kontinentalrand und Vergleich mit dem indisch-pakistanischen Kontinentalrand. Meteor Forsch. Erg. Reihe C. No.18. pp.1-34.

Marlett, E.M; Erdman, J.B; 1959. Carbon-nitrogen distribution and nitrogen type relationships in recent and ancient sediments. Div.Petroleum Chemistry . Am.Chem.Soc. 135th meeting. p.107-119.

Martens, C.S; Kulmp, J.V; 1980. Biogeochemical cycling in an organic-rich coastal marine basin . I. methane sediment water exchange processes. Geochim.Cosmochim.Acta. Vol.44. pp.471-490.

Martin, J.H; Knauer, G.A; 1973. The elemental composition of plankton . Geochim.Cosmochim.Acta. Vol.37. pp.1639-1653.

Mattiat, B; Peters, J; Eckhardt, F.J; 1973. Ergebnisse petrographischer Untersuchungen an Sedimenten des indisch-pakistanischen Kontinentalrands (Arabian see). Meteor Forsch. Erg.Reihe C, No.14. pp.1-50.

Margalef, R; Estrada, M; 1981. On upwelling, eutrophic lakes,the primitive biosphere and biological membranes. In: F.A.Richards,ed. Coastal upwelling. AGU publication.

Mariotti, A; 1983. Atmospheric nitrogen is a reliable standard for natural $\delta^{15}N$ abundance measurements. Nature. Vol.303. pp.605-617.

Mayer, L.M; Macks, S.A; Mook, W.H; Murray, S; 1981. The distribution of bromine in coastal sediments and its use as a source indicator for organic matter. Organic. Geochem. 3. p.37-42.

McClure, H.A; 1976. Radiocarbon chronology of late Quaternary lakes in the Arabian desert. Nature. Vol.263. pp.755-756.

McDonald, W.F; 1938. Atlas of climatic charts of the ocean. U.S. Dept.Agr. Weather Bur. No.1. Vol.247. charts 59-62.

McGill, D.A; 1973. Light and nutrients in the Indian Ocean. In: The Biology of the Indian Ocean, B.Zeitzschel,(ed). Springer-Verlag. pp.53-102.

McHargue, T.R; Webb, J.E; 1986. Internal geometry,seismic facies,and petroleum potential of canyons and fan channels of the Indus submarine fan. A.A.P.G Bulletin. Vol.70.NO.2. pp.161-180

McIntyre, A; Kipp, N.G; Be, A.W.H; Crowley, T; Kellog, T; Gardner, J.V; Prell, W.L; Ruddiman, W.F; 1976. Glacial north Atlantic 18,000 years ago: A climap reconstruction . Geol.Soc.Am. Mem.145. pp.43-76.

Middleton, N.J; 1986a. A geography of dust storms in Soutwest Asia. Journal of Climatology. Vol.6. pp.183-196.

Middleton, N.J; 1986b. Dust storms in the Middle East. Journal of Arid Environments. Vol.10. pp.83-96.

Minagawa, M; Wada, E; 1984. Stepwise enrichment of $\delta^{15}N$ along food chains : Further eveidence and the realtion between $\delta^{15}N$ and animal age. Geochim. Cosmochim. Acta. Vol.48. pp.1135-1140.

Miyakie, Y; Wada, E; 1967. The abundance ratio of 15 N/14 N in marine environments. Records of oceanographic works in Japan, 9, pp.37-53.

Molina-Cruz, A; Price, P; 1977. Distribution of opal and quartz on the ocean floor of the subtropical southern Pacific . Geology. Vol. 5(2). pp.81-84.

Montaggioni, L.F; Hoang, C.T; 1988. The Last interglacial high sea level in the Granitic Seychelles, Indian Ocean. Palaeogeo,Palaeoclim,Palaeoecol. Vol.64. pp.79-91.

Moore, C; Bostrom, K; 1978. The elemental composition of lower marine organisms. Chemical Geology. Vol.23. pp.1-9.

Muller, P.J; 1977. C/N ratio in Pacific Deep Sea sediments: Effect of inorganic ammonium and organic nitrogen compounds sorbed by clays. Geochim.Cosmochim.Acta. Vol.41. pp.765-776.

Muller, P.J; Erlankeuser, H; Von Grerfenstein, R; 1981. Glacial-intergalcial cycles in oceanic productivity inferred from organic carbon contents in eastern north Atlantic sediment cores. in: Theide and Suess (eds). Coastal upwelling . Part B: sedimentary records of ancient coastal upwelling. Plenum Press. New york.

Muller, P.J; Suess, 1979. Productivity, sedimentation rate and sedimentary organic matter in the oceans. I. Organic Carbon presrvation. Deep-Sea Res. Vol.26. pp.1347-1362.

Nair ,R.R; Ittekkot, V; Manganini, S.J; Ramaswamy, V; Haake, B; Degens, E.T; Desai, B.N; 1989. Increased particle flux to the deep ocean related to monsoons. Nature. Vol.338. pp.749-752.

Narayanan, M.S; Rao, B.M; 1981. Detection of monsoon inversion by Trios-N Satellite. Nature. Vol.294. pp.546-548.

Newman, J.W; Parker, P.L; Behrens, E.W; 1973. Organic carbon isotope ratio in Quaternary cores from the Gulf of Maxico. Geochim. Cosmochim.Acta. Vol.37. pp.225-238.

Nicholls, G.D; Curl, H.C; Bowen, V.T; 1959. Spectrographic analysis of marine plankton. Limnol.Oceanogr. Vol.4. pp.472.

Nissenbaum, A; Swaine, D.J; 1976. Organic matter-metal interactions in recent sediments. The role of humic substances. Geochim.Cosmochim.Acta. Vol.40. pp.809-816.

Norish, K; Hutton, J.T; 1969. An accurate X-ray spectrographic method for the analysis of a wide range of geological samples. Geochim.Cosmochim.Acta. Vol.33. pp.431-453.

O'Donnell, D; 1987. The geochemical association of metals and organic matter in west coast of Scottish sediments. Ph.D. Thesis. Unpublish. University of Edinburgh.

Odum, H.T; 1957. Biogeochemical deposition of Strontium. Publ.Inst.Mar.Sci. 4. pp.38-114. University of Texas.

Olaussen, E; 1961. Remarks on some Cenozoic core sequences from the Central Pacific , With a discission of the role of coccolithophorids and foraminifera in carbonate deposition. Medd. Oceanograf.Inst. Goteborg, No.29. pp.1-35.

Olaussen, E; 1966. Sediments of the Atlantic Ocean. In: R.W.Fairbridge (ed). The Encyclopedia of Oceanography , Reinhold, New york.

Olaussen, E; Olsson, I.V; 1968. Varve stratigraphy in a core from the Gulf of Aden. Paleogeography,Paleoclimatology,Paleoecology. Vol.6. pp.87-103.

Olaussen, E; Haq, B.U; Karlsson, G.B; Olsson, I.U; 1971. Evidence in indian ocean cores of late pleistocene changes in oceanic and atmospheric circulation . Geologiske Foreningens I Stockholm Forhandilnger. Vol.93. pp.51-84.

Pant, M.C; 1978. Vertical structure of the planetary layer in the West Indian Ocean during the Indian summer monsoon as revealed by ISMEX data. Indian J.Met.Hydrol.Geophys. Vol.29.No.1&2. pp.88-98.

Pascoe, E.H; 1964. A manual of the Geology of India and Burma, vol.3. pp.1878-1939.

Pavlova, G.A; Shishkina, O.V; 1973. Accumulation of iodine in interstitial water during metamorphism in relation to the iodine distribution in Pacific sediments. Geochem.Int. Vol.10. pp.804-813.

Pederson, T.F; 1979. The geochimistry of sediments of the Panama Basin . Eastern Equatorial Pacific ocean. Ph.D. Thesis. Unpublished. University of Edinburgh. pp.235.

Pederson, T.F; 1983. Increased productivity in the eastern equatorial Pacific during the last glacial maximum. Geology. Vol.11. pp.16-19.

Pederson, T.F; Price, N.B; 1980. The geochemistry of iodine and bromine in sediments of the Panama Basin. J.Mar.Res. Vol.38. pp. 397-411.

Peterson, M.N.A; Goldberg, E.D; 1962. Feldspar distribution in south Pacific Pelagic sediments. J.Geophys.Res. Vol.67. PP.3477-3492.

Peters, K.E; Sweeny, R.E; Kaplan, I.R; 1978. Correlation of C and N stable isotope ratios in sedimentary organic matter. Limnol.Oceanogr. Vol.23. pp.598-604.

Pettijohn, F.J; 1975. Sedimentary rocks. 3rd edition. Harper & Rpw, New york, 628.

Pocklington, R; Leonard, J.D. 1979. Terrigenous organic matter in sediments of the St lawrence estuary and Saguenay Fjord. J.Fish.Res.Board can. Vol.36. p.1250-1255.

Prell, W.L; 1984. Monsoon climate of the Arabian sea during the late Quaternary : A response to Changing solar radiatioin. In: Milankovitch and climate , Part 1. Berger,A. etal(eds). pp.349-366.

Prell, W.L; Curry, W.B; 1981. Faunal and isotopic indicies of monsoonal upwelling : western Arabian Sea. Oceanologica Acta. Vol.4.N0.1. pp.91-98.

Prell, W.L; Hutson, W.H; 1979. Zonal temperature anamoly maps of Indian Ocean surface waters: Moderen and ice age patterns. Science. Vol.206. pp.454-456.

Prell, W.L; Kutzbach, J.E; 1987. Monsoon variability over the past 150000 years. J.Geophysical Research. Vol.92. pp.8411-8425.

Prell, W.L; Streeter; 1981. Temporal and Spatial patterns of monsoonal upwelling along Arabia: A modern analogue for the interpretation of Quaternary SST anomalies. J.Mar.Research. Vol.40. pp.143-155.

Prell, W.L; Van Campo, E; 1986. Coherent response of Arabian Sea upwelling and pollen transport to late Quaternary monsoonal winds. Nature. Vol.323. pp.526-528.

Premuzic, E.T; Benkovitz, C.M; Gattney, J.S; Walsh, J.J; 1982. The nature and distribution of organic matter in the surface sediments of world oceans and sea. Org.Geochem. Vol.4. pp.63-77.

Presley, B.J; Kolodny, Y; Nissenbaum, A; Kaplan, I.R; 1972. Early diagenesis in a reducing fjord, Saanich inlet, British Columbia- II. Trace element distribution in interstital water and sediments. Geochim.Cosmocim.Acta. Vol.36. pp.1073-1090.

Price , N.B; 1976. Chemical diagenesis in sediments. In: Chemical Ocaenography .Vol 6. 2nd ed. J.P.Riley and R.Chester (eds). Academic Press, London.

Price, N.B; Calvert, S.E; 1973. The geochemistry of Iodine in oxidized and reduced recent marine sediments. Geochim.Cosmochim.Acta. Vol.37. pp.2149-2158.

Price, N.B; Calvert, S.E; 1977. The contrasting geochemical behaviors of iodine and bromine in recent sediments from the Namibian shelf. Geochim. Cosmochim. Acta. Vol.41. pp.1769-1775.

Price, N.B; Calvert, S.E; Jones, P.G.W; 1970. The distribution of Iodine and Bromine in the sediments of southwest Barnet sea. Journal of Marine Research. Vol.28. pp.22-34.

Prodi, F; Santachiara, G; Oliosi, F; 1983. Characterisation of aerosols in marine environments (Mediterranean, Red sea and Indian ocean) Journal of Geophysical Research. Vol.88 C: No.10. pp.957-968.

Prospero, J.M; 1981. Arid regions as sources of mineral aerosols in the marine atmosphere. in: Peive, T.L (ed). Desert dust origin,characteristics and effect on man. Geological society of America Special paper. Vol.186. pp.71-86.

Prospero, J.M; Bonatti, E; 1969. Continental dust in the atmosphere of the eastern equatorial Pacific: Journal of Geophysical Research Vol.74. pp.3362-3371.

Prospero, J.M; Carlson,T.N; 1972. Vertical and areal distribution of Saharan dust over the western equatorial North Atlantic Ocean: Journal of Geophysical Research. Vol.77. pp.5255-5265.

Qasim, S.Z; 1970. Some characteristics of a Tricodesmium bloom in the Laccadives. Deep Sea Research. Vol.17. pp.655-660.

Qasim, S.Z; 1982. Oceanography of the northern Arabian sea. Deep sea Rsearch. Vol.29. pp.1041-1068.

Quinn, W.H; 1971. Late Quaternary meteorological and oceanic development in the equatorial Pacific . Nature. Vol.229. pp.330-331.

Rajendron, A; Rajagopal, M.D; Reddy, C.V; 1980. Distribution of dissolved silicate in the Arabian sea and bay of Bengal. Indian journal of marine sciences. Vol.9. pp.172-178.

Ramage, C.S; 1969. Indian Ocean surface meteorology. Oceanogr. Mar. Biol. Ann. Rev; 7. pp.11-30.

Ramage, C.S; Miller, F.R; Jefferies, C; 1972. Meteorological atlas of the international Indian ocean expedition. U.S.National Science Foundation and India Metreological Department.

Ramesbabu, V; Varkey, M.J; Kesava, Das; Govveia, A.D; 1980. Deep water masses and general hydrography along the west coast of India during early March. Indian journal of marine sciences. Vol.9. pp.82-89.

Rankama, k; Sahama, T.G; 1950. Geochemistry. Univ.of Chicago Press. pp.912.

Rea, D.k; Harrsch, E; 1981. Mass accumulation rates of the non authigenic inorganic crystalline (eolian) component of deep sea sediments from Hess Rise. Deep sea Drilling project sites 464, 465,466. In: J.Thiede; T.L. Vallier etal.(eds) Initial Reports of the Deep sea Drilling Project . Vol. 62.

Rea, D.K; Janecek, T.R; 1982. Late Cenozoic changes in atmospheric circulation deduced from north Pacific eolian sediments. Marine Geology. Vol.49. pp.149-168.

Redfield, A,C; Ketchum, B.H; Richards, F.A; 1963. The influence of organisms on the composition of sea water. in: M.N.Hill (ed). The Sea. Vol.2. pp.26-77. J.Willey.

Reedy, C.V; Shnkaranavayanan; 1968. Distribution of Phosphates and Silicates in the central western north Indian Ocean in relation to some hydrographical factors. Bulletin of the national institute of sciences of India. Vol.38. pp.103-122

Reimmers, C.E; 1982. Organic matter in anoxic sediments off central Peru: relations of porosity,microbial decomposition and deformation properties. Marine Geology. Vol.46. pp.175-197.

Reimmers, C.E; Suess, E; 1981. Spatial and temporal patterns of organic matter accumulation on the Peru continental margin . in: Theide and Sues (eds). Coastal upwelling Part B: sedimentary records of ancient coastal upwelling. Plenum Press. New york.

Revelle, R.R; Bramlette, M; Arrhenius, G; Goldberg, E.D; 1955. Pelagic sediments of Pacific . Geol.Soc.Amm.Spec.Paper.62. pp.221-236.

Richard, F.A; 1981. Coastal Upwelling, Coastal and Estuarine science 1, American Geophysical Union, Washington, 529.pp.

Riga, A; Van Praag, H.J; Brigode, N; 1971. Rapport isotopique natural de lazote dans quelques sols forestiers et agricoles de Belgique soumis a divers traitements culturaux. Geoderma. Vol.6. pp.213-222.

Rochford, D.J; 1964. Salinity maxima in the upper 1000 meters of the north indian ocean . Australian Journal of marine and freshwater Research. Vol.15. pp.1-24.

Rosenfled, J.K; 1979. Ammonium adsorption in nearshore anoxic sediments. Limnol.Oceanogr. Vol.24. pp.356-364.

Rossignol-Strick, M; 1983. African monsoons, an immediate climate response to orbital insolation. Nature. Vol.304. pp.46-49.

Royse, C.F; Waddael, J.S; Petersen, L.E; 1971. X-ray determination of calcite - dolomite: an evolution. J.Sed.Petrol. Vol.41. pp.483-488.

Ruddiman, W.F; McIntyre, A; 1977. Late quaternary surface ocean kinematics and climatic change in the High-latitude north Atlantic. J.Geophys.Res. Vol.82. pp.3877-3887.

Ryther, J.H and Menzel; 1965. On the Production,Composition,and distribution of organic matter in the western Arabian sea. Deep sea Research. Vol.12. pp.199-209.

Ryther, J.H; Hall, J.R; Pease, A.K; Bakun, A; Jones, M.M; 1966. Primary production in relation to the chemistry and hydrography of the Western Indian Ocean. Limnology and Oceanography. Vol.11. pp.371-380.

Sackett, W.M; 1964. The depositional history and isotopic organic carbon composition of marine sediments. Marine Geology. Vol.2. pp.173-185.

Sackett, W.M; Eadie, B.J; Exner, M.E; 1973. Stable isotope composition of organic carbon in recent Antartic Sediments. In: Advances in Organic Chemistry.

Sackett, W.M; Rankin, J.G; 1970. Brief report. Paleotemperature for the Gulf of Mexico. J.Geophys.Research. Vol.75. pp.4557-4560.

Sackett, W.M; Thompson, R.R; 1963. Isotopic organic Carbon composition of recent continental derived clastic sediment of eastern gulf coast,Gulf of Mexico. Bull.Am.Assoc.Pet.Geol. Vol.47. pp.525-531.

Saino, T; Hattori, A; 1980. $\delta^{15}N$ natural abundance in chemistry of two cores from Florida Bay. J.Sed.Pet. Vol.283. pp.752-754.

Salomons, W; Forstner, U; 1983. Metals in the Hydrocycle.Springer, Berlin. pp.348.

Sanders, G.S; 1983. Metals in marine atmospheric particles. PhD. Thesis. University of Liverpool. Unpublished

Sarnthein, M; 1978. Sand deserts during glacial maximum and climatic optimum. Nature. Vol.272. pp.43-46.

Sarnthein, M; Diestre-Hass; 1977. Eolian-sand turbidites. J.Sedimentary Petrology. Vol.47. pp.868-889.

Sarnthein, M; Winn, K; Zahn, R; 1987. Paleoproductivity of oceanic upwelling and the effect on atmospheric CO2 and climate change during deglaciation times. In: W.H.Berger, L.Labeyrie; D.Reidel (eds) . Abrupt climate change. Hangham. pp.311-377.

Sastry, J.S; DeSouza, R.S; 1970. Oceanography of the Arabian sea during s.w monsoon season. Parrt I. Thermal structure . Indian Journal of Meteorology and Geophysics. Vol.21.No.3. pp.367-382.

Sastry, J.S; De Souza, R.S; 1971. Oceanography of the Arabian Sea during s.w monsoon . Part II. Stratification and circulation. Indian Journal of Meteorology and Geophys. Vol.22.No.1. pp.23-34.

Sastry, J.S; De Souza, R.S; 1972. Upwelling and upward mixing in the Arabian Sea. Indian Journal Of Marine Science. Vol.1. pp.17-27.

Scharde, H.J; 1972. Kiedelsaure-Skelette in sedimenten des ibro-marokkanischen Kontinentalrandes und angrenzender Tiefsee-Ebenen. Meteor. Forschungsergeb; Reihe C. 8: 10-36.

Schnetzler, C.C; Philpotts, J.A; 1970. Partition coefficients of rare earth between igneous matrix material and rock forming mineral phenocrysts. II. Geochim. Cosmochim. Acta. Vol.34. pp.331-340.

Schüette, G; Schrader, H; 1981. Diatoms in surface sediments : A reflection of coastal upwelling , in: "Coastal upwelling " F.A. Richards, ed; Coastal and Estuarine Science 1, American Geophysical Union, Washington, 372-380.

Sen-Gupta, R; Fondekar, S.P; Sankaranayanan; De Souza, S.N; 1975. Chemical Oceanography of the Arabian Sea: Part I- hydrochemical and hydrographical features of the northern basin. Indian Journal of Marine Sciences. Vol.4. pp.136-140.

Sen-Gupta, R; Naqvi, S.W.A; 1984. Chemical Oceanography of the Indian Ocean , north of Equator. Deep sea Research. Vol.31. pp.671-706.

Sen-Gupta, R; Rajagopal, M.D; Qasim, S.Z; 1976. Relationships between dissolved Oxygen and nutrients in the north-western Indian Ocean. Indian Journal of Marine Sciences. Vol.5. pp.201-211.

Shackleton, N.J; Opdyke, N; 1973. Oxygen isotope and paleomagnetic stratgraphy of equatorial Pacific core V28-238: Oxygen isotope temperatures and ice volume on a 10^5 and 10^6, 10^4 year scale. Quaternary Research. Vol.3. pp.39-55.

Shanker, R; Subbaro, R; Kolla, K.V; 1987. Geochemistry of surface sediments from the Arabian Sea. Marine Geology. Vol.76. pp.253-279.

Shaw, T.I; 1959. The mechanism of iodide accumulation by the brown seaweed Laminaria digitata. The uptake of 131 I. Proc.R.Soc.London, Ser. B, 150: pp.356-371.

Shearer, G; Kohl, D.H; Commoner, B; 1973. Variation of $\delta^{15}N$ in corn and soil following application of fertiliser Nitrogen. Soil.Sci.Am.Proc. Vol.37. pp.888-892.

Shearer, G; Kohl, D.H; Commoner, B; 1979. Nitrogen-15 abundance in N-fixing and non N-fixing plants. 4 Int.Symposium on Mass Spectrometry in Biochem. and Madicine. Riva del Garda, Italy. 20-22 June 1979.

Shimmield, G.B; Price, N.B; Pederson, F.B; 1988. The influence of hydrography,bathymetry and productivity on sediment type and composition on the Oman margin and in the northwest Arabian sea. In Press.

Shishkina, O.V; Pavlova, G.A; 1965. Iodine distribution in marine and oceanic bottom muds and their pore fluids. Geochim. Int. Vol. 2. pp.559-565.

Siddiquie, H.N; 1975. Submerged Terraces in the Laccadive Islands, India. Marine Geology. Vol.18. M95-M101.

Singh, G; Joshi, R.D; Singh, A.B; 1972. Stratigraphic and radiocarbon evidence for the age and development of three salt lake deposits in Rajasthan,India. Quart.Res. Vol.2. pp.496-505.

Sirocko, F; Sarnthein, M; 1988. Wind borne deposits in the Northwestern Indian Ocean: record of Holocne sediments versus modern satellite data. In Press.

Smith, S.L; Codispoti; 1980. Southwest monsoon of 1979 : Chemical and Biological response of Somali coastal waters. Science. Vol.209. pp.597-600.

Spears, D.A; Amin, M.A; 1981. Geochemistry and mineralogy of marine and non marine Namurian black shales from the Transley Borehole, Derbyshire. Sedimentology. Vol.28. pp.407-417.

Spencer, D.W; Brewer, P.G; Fleer, A; Honjo, S; Krinsnaswami, S; Nozaky; 1978. Chemical fluxes from a sediment trap experiment in the deep Sargasso Sea. J.Mar.Res. Vol.36. pp.493-523.

Stevenson, F.J; Cheng, C.N; 1972. Organic geochemistry of the Argentine Basin sediments: C/N relationship and Quaternary correlations. Geochim. Cosmochim.Acta. Vol.36. pp.653-671.

Stevenson, F.J; Dhariwal, A.P.S; 1959. Distribution of fixed ammonium in soils. Soil Sci.Soc.Am. Proc.23. pp.121-125.

Stevenson, F.J; Kidder, G; Tilo, S.N; 1967. Extraction of organic nitrogen and ammonium from soil with hydroflouric acid. Soil.Sci.Soc.Amer.Proc. Vol.31. pp.71-76.

Stewart, R.A; Pilkey, O.H; Nelson, B.W; 1965. Sediments of the northern Arabian Sea. Marine Geology. Vol.3. pp.411-427.

Stoffers, P; Ross, D.A; 1979. Late Pleistocene and Holocene sedimentation in the Persian Gulf and Gulf of Oman. Sedimentary Geology. Vol.23. pp.181-208.

Street, F.A; Grove, A.T; 1979. Global maps of lake-level fluctations since 30,000 yr BP. Quat.Research. Vol.12. pp.83-118.

Street, F.A; Harrison, S.P; 1984. Temporal variations in lake levels since 30,000 yr BP an index of the global hydrological cycle. in Climate Processes and Climate Sensitivity , Geophys.Monogr.Ser; vol.29. pp.118-129.

Suess, E; Muller, P.J; 1980. Productivity,Sedimentation rate and sedimentary organic matter in the oceans II. Elemental fractionation. Proceedings CRNS Symposium on the benthic boundary layer. Marsielle, France. pp.17-26.

Sugden, W; 1963. Some aspects of Sedimentation in the Persian Gulf. J.Sedimentary Petrology. Vol.33. pp.355-364.

Swain, A.M; Kutzbach, J.E; Hastenrath, S; 1983. Monsoon climate of Rajasthan for the Holocene ; Estimates of precipitation based on pollen and lake levels. Quaternary Reaearch. Vol.19. pp.1-17.

Swallow, J.C; 1980. The Indian Ocean Experiment : Introduction. Science. Vol. 209.

Sweeny, R.E; Liu, K.K; Kaplan, I.R; 1978. Oceanic nitrogen isotope and their uses in determining the source of sedimentary nitrogen. In: Stable isotope in the earth science. DSIR BUll. pp.9-26.

Sweeny, R.E; Kaplan, I.R; 1980. Natural abundances of $\delta^{15}N$ as a source indicator for near shore marine sedimentary and dissolved nitrogen. Marine chemistry. Vol.9. pp.81-94.

Szekielda, K.H; 1970. The liberated energy potential available from oxidation processes in the Arabian sea . Deep sea Research. Vol.17. pp.641-646.

Tchernia, P; 1980. Descriptive regional Oceanography . Pergamon press.

Tennant, C.B; Berger, R.W; 1957. X-ray derterminatin of dolomite calcite ratio of a carbonate rock. Am.Miner. Vol.42. pp.23-29.

Theide, J; 1973. Plankonic foraminifera in hemipelagic sediments: shell preservation off Portugal and Morocco. Geol.Soc.Am.Bull. Vol.84. pp.2749-2754.

Theide, J; Suess, E; Muller, P; 1982. late quaternary fluxes of major sediment components to the sea floor at the Northwest African continental slope . In: Von Rad, U; Hinz, K; etal (eds) Geology of the Northwest African continental margin, Springer Verlag Berlin. pp.505-631.

Theisen, R; Vollach, D; 1967. Tables of X-ray Mass Absorption coefficients. Verlag Stahleisen M.B.H; Dusseldorf.

Thirlwall, M.F; 1979. The Petrochemistry of the British old Red sandstone Volcanic province. unpublish. Phd. Thesis, Edinburgh University.

Thompson, T.G; Bowen; 1969. Analysis of coccolith ooze from the deep tropical Atlantic. Journal of Marine research. Vol.27. pp.32-37.

Thompson T.G; Chow T.J; 1956. The Strontium-calcium atom ratio in carbonate secreting marine organisms. Pap.Mar.Biol.Oceanogr; Deep Sea Res. Supplement to Vol.3. pp.20-39.

Thunnel, R.C; 1976. Calcium Carbonate dissolution history in late Quaternary deep sea sediments. Western Gulf of Mexico. Quaternary Research. Vol.6. pp.281-297.

Thurman, E.M; 1985. Organic geochemistry of natural waters. Dr.W.Junk Publishers. Dordrecht. Netherland. pp.497.

Trask, P.D; 1953. Chemical studies of the Western Gulf of Mexico, Part 2 , papers in Physical Oceanography and Meteorology; Mass. Inst. Tech. and Woods Hole Oceanogr. Inst. 12, pp. 49-120.

Tungshang, Liu; Shouxin, Zhang; Jiaomao, Han; 1986. Stratigraphy and paleoenvironmental changes in the loess of central China. In: Sibrova, V; Bowen, D.Q; Richmond, G.M (eds). Quaternary glaciations in the Northern hemisphere. Quaternary Science Reviews. Vol.5. pp.489-497.

Turcotte, D.L; Bernthal, M.J; 1984. Synthetic coral reef terraces and variations of quaternary sea level. Earth Planet. Sci.Lett. Vol.70. pp.121-128.

Turekian, K.K; 1957. The significance of variations in the strontium content of deep sea cores. Limnol.Oceanogr. Vol.2. pp.309-314.

Turekian, K.K; 1964. The marine geochemistry of strontium. Geochim.Cosmochim.Acta. Vol.28. pp.1479-1496.

Turekian, K.K; Kulp, J.L; 1956. The geochemistry of strontium. Geochoim.Cosmochim.Acta. Vol.10. pp.245-296.

Turekian, K.K; Tausch, E.H; 1964. Barium in deep sea sediments of the Atlantic ocean. Nature. Vol.201. pp.696-697.

Turekian, K.K; Wedepohl, K.H; 1961. Distribution of the elements in some major units of the Earths crust. Geol.Soc.Am.Bull. Vol.72. pp.175-192.

Ullman, W.J; Aller, R.C; 1980. Dissolved I flux from estuarine sediments and implications for enrichment at the sediment/water interface . Geochim.Cosmochim.Acta. Vol.44. pp.1177-1184.

Ullman, W.J; Aller, R.C; 1983. Rates of iodine remineralisation in terrigenous near shore sediments. Geochim.Cosmochim.Acta. Vol.47. pp.1423-1432.

Valencia, M.J; 1977. Pleistocene stratigraphy of the western equatorial Pacific . Geol. Soc. Am. Bull. Vol.88. pp.143-150.

Van Andel, Tj.H; 1964. Recent marine sediments of the Gulf of California. Van Andel, T.H. and Shar, G.D.(eds). J. Am. Assoc.Petrol.Geol. Memoir.3. pp.216-310.

Van Andel, Tj.H; Heath, G.R; Moore, T.C; 1975. Cenozoic history and paleocenography of the central Equatorial Pacific ocean. Geol. Soc. Amer. Memoir 143.

Van Bennnekom, A.J; Jansen, J.H.F; Van der Gasst, S.J; Van Iperen, J ; 1988. Aluminium-rich opal: an intermediate in the preservation of biogenic silica in the Zaire (Congo). Deep-Sea Res. in press.

Van Campo, E; 1986. Monsoon fluctuations in two 20,000 years B.P. Oxygen isotope/pollen records off Southwest India. Quaternary Res. Vol.26, pp.376-388.

Van Campo, E; Duplessy, J.C; Rossignol-Strick, M; 1982. Climatic conditions deduced from a 150 K.Yr Oxygen isotope pollen record from the Arabian sea. Nature. Vol.296. pp.56-59.

Van der Gaast, S.J; Jansen, A.H.F; 1984. Mineralogy,opal and manganese of Middle and Late Quaternary sediments of the Zaire (Congo) deep-sae fan: Origin and climatic variation . Neth.J.Sea Research. Vol.17 (2-4). pp.313-341.

Verma, K.K; Mathur, U.B; 1979. Quaternary sea level changes along west coast of india . Geological survey of India. Misc.Publication No.45. pp.263-272.

Vinogradov, A.P; 1953. The elementary composition of marine organisms . Sears Found. Mar.Res. Vol.2. pp.647.

Vinogradova, Z.A; Kovalskiy, V.V; 1962. Elemental composition of Black sea plankton. Dokl.Acd.Nauk.SSSR. No.147. pp.1458-1460.(English. p.217.).

Volat, J.L; Pastouret ,L; Vergnaud-Grazzini, C; 1980. Dissolution and carbonate fluctuations in Pleistocene deep sea cores : a review. Marine Geology. Vol.34. pp.1-28.

Volkov, I.I; Fomina, L.S; 1971. Dispersed elements in sapropel of the Black Sea and their interrelationship with organic matter. Litologiya i poleznye Iskopaemye, 6, pp.3-15.

Volkov, I.I; Fomina, L.S; 1974. Influence of organic material and processes of sulphide formation of the distribution of some trace elements in deep water sediments of the black sea. In: D.A.Ross and E.T.Degens (eds); The Black sea. Geology,Chemistry and Biology. Am. Ass. Petrol. Geol. Memoir. Vol.20. pp.456-476.

Von-Stackelberg, U; 1972. Faziesverteilung in Sedimenten des indisch- pakistanischen Kontinentalrandes. Meteor Forsch. Erg; Reihe C, No.9. pp.1-73.

Waber, J.N; Smith, F.G; 1961. Rapid dtermination of calcite-dolomite ratio in sedimentary rocks. Journal of Sedimentary Petrology. Vol.51. pp.130-131.

Wada, E; Hattori, A; 1978. Nitrogen isotope effects in the assimilation of inorganic nitrogenous compounds in marine diatoms. Geomicrobiol. J. Vol.1. pp.85-101.

Wakefield, S.J; 1981. Aspect of geochemistry and early burial diagenesis of metalliferous deep sea sediments. Ph.D thesis. Leeds University. U.K.

Wakeham, S.G; Lee, J.W; Gagosian, R.B; 1984. Biogeochemistry of particulate organic matter in the oceans. Results from sediments trap experiments. Deep sea Research. Vol.31. pp.509-528.

Warren, B.A; 1978. Bottom Water transport through the southwest Indian Ridge. Deep Sea Research. Vol.25. pp.315-322.

Warren, B.A; 1981. Transindian hydrographic section of Lat. 18°S. Property distribution and circulation in the South Indian Ocean. Deep Sea Research. Vol.28. pp.751-788.

Weaver, C.E; Pollard, L.D; 1973. The Chemistry of Clay minerals. Elsevier. Amsrerdam. pp.213.

Wedepohl, K.H; 1960. Spurenanalytische Untersuchungen an Tiefseetonen aus dem Atlantik. Geochim.Cosmochim.Acta. Vol.18. pp.200-231.

White, R.S; 1982. Deformation of the Makran Accretionary sediment prism in the Gulf of Oman (north-west Indian Ocean). In Trench and Fore-arc geology: Sedimentation and tectonics on modern and ancient active Plate margins. (J.K Legget, ed). Geological Society of London 88. pp.69-84.

White, R.S; 1984. Active and Passive Plate Boundries around the Gulf of Oman, n.w Indian Ocean. Deep sea Res. Vol.31(A).pp.731-745.

Wong, G.T.F; Brewer, P.G; Spencer, D.W; 1976. The distribution of particulate iodine in the Atlantic Ocean, Earth Planet.Sci.Lett. Vol.32. pp.441-450.

Wright, H.E; McAndrews, J.H; Zeist, W.V; 1967. Modern pollen rain in Iran, and its relation to plant geography and Quaternary vegetational history. The Journal Of Ecology. Vol.55. pp.415-443.

Wyrtki, K; 1971. Oceanographic Atlas of the International Indian Ocean. U.S. Govt. Printing Office, Washington, D.C; 531 pp.

Wyrtki, K; 1973. Physical Oceanography of the Indian Ocean In: B. Zeitzschel (ed), The Biology of the Indian Ocean. Springer-verlag.

Young, E; 1954. Trace elements in recent marine sediments. Bull.Geol.Soc.Amm. Vol.65. pp.1329.